Cardiff University

Cardiff School of Chemistry

Synthesis and characterization of borazine-doped polyphenylenes: towards the construction of boron-nitrogen-carbon hybrid polycyclic aromatic hydrocarbons

Davide MARINELLI

PhD Thesis

December 2017

Supervisor: Prof. Dr. Davide BONIFAZI

Doctoral commission:

Prof. Emilio M. Pérez

Dr. Louis Morrill

Table of Contents

Abstract

Figure 1. Representation of general polyphenylene structures differentiating in doping dosage or doping orientations.

This thesis manuscript focuses on the synthesis and characterization of branched polyphenylene derivatives in which one or more aryl units are replaced by borazines (B_3N_3), the isosteric and isoelectronic inorganic analogue of benzene. In particular, the divergent bottom-up synthesis of hexa-branched borazine-doped polyphenylene derivatives is carried out taking advantage of the decarbonylative [4 + 2] Diels-Alder cycloaddition reaction. Given the possibility to graft different functional groups on the aryl substituents at the B and N atoms, borazine-doped polyphenylene frameworks with different doping dosages, topology, and orientations were prepared. The generation of the series of star-shaped borazine-polyphenylene hybrids was possible through the use of borazine-doped or full-carbon core and branching building blocks bearing ethynyl or tetraphenylcyclopentadienone functionalities. Thanks to this synthetic strategy, depending on the chemical nature of the building blocks chosen, it was possible to precisely control the formation of different doping patterns. The photophysical investigation of the synthesized series of hexa-branched BNC hybrid derivatives revealed a progressive reduction of luminescence upon increasing the doping dosage, while the effect of the doping orientation has revealed to be minor. Secondarily, thanks to the Cu-catalyzed cycloaddition reaction a suitable chromophore was covalently grafted to a three-branched BNC hybrid polyphenylene scaffold. Photophysical studies assessed the possibility for the borazine-doped polyphenylene backbone to harvest and transfer energy to the chromophore. Finally, the synthesis of borazine-doped graphene sub-structures and large polycyclic aromatic hydrocarbons (PAHs) was envisaged through planarization of

suitable borazine-doped polyphenylene derivatives. In this study, the development of a synthetic methodology for the production of these precursors was addressed.

List of abbreviations

Å	Angstrom
Abs	Absorption
AFM	Atomic force microscopy
aq.	Aqueous
ASU	Asymmetric unit
BNC	Boron-nitrogen-carbon
ºC	Degree centigrade (0 ºC = 273.16 K)
calc.	Calculated
Cm	Centimetre
CPD	Tetraphenylcyclopentadienone
CHX	Cyclohexane
d_i	Doping vector
D	Doping descriptor
D.A.	Diels-Alder
DIPEA	N,N-Diisopropylethylamine
DMF	N,N-Dimethylformamide
DMSO	Dimethylsulfoxide
eq.	Equivalent
ESI	Electrospray ionisation
eV	Electronvolt (1eV = 1.602 x 10^{-19} J)
FPT	Freeze-pump-thaw
h	Hour
HBBNC	Hexa-*peri*-hexabenzoborazinocoronene
h-BN	Hexagonal boron nitride
HRMS	High resolution mass spectrometry
HOMO	Highest occupied molecular orbital
HOPG	Highly oriented pyrolytic graphite
Hz	Hertz (s^{-1})
IR	Infrared
K	Kelvin
LEC	Light-emitting electrochemical cell

LRMS	Low resolution mass spectrometry
LUMO	Lowest unoccupied molecular orbital
MALDI	Matrix-assisted laser desorption ionisation
min	Minutes
MS	Mass spectrometry
mw	Microwave irradiation
nm	Nanometer
NMR	Nuclear magnetic resonance
o	Doping orientation
OLED	Organic-light emitting diode
OFET	Organic field-effect transistor
ORTEP	Oak ridge thermal ellipsoid plot
PAH	Polycyclic aromatic hydrocarbon
PPh	Polyphenylene
NDI	Naphtalene diimide
PDI	Perylene diimide
PMI	Perylenemonoimide
ppm	Parts per million
r.t.	Room temperature
SEM	Scanning electron microscopy
TDI	Terrylene diimide
TEM	Transmission electronic microscopy
TIPS	Triisopropylsilyl
TIPSA	Triisopropylsilylacetylene
TFA	Trifluoroacetic acid
TGA	Thermogravimetric analysis
THF	Tetrahydrofuran
TLC	Thin layer chromatography
TMS	Trimethylsilyl
TMSA	Trimethylsilylacetylene
TPA	Triphenylamine
UHV	Ultra-high vacuum
UV-Vis	Ultraviolet-visible

WCI	Weakly coordinating ion
λ	Wavelength (nm)
ε	Molar extinction coefficient
Φ_n	Fluorescence quantum yield
ρ	Doping dosage
τ	Fluorescence lifetimes

Chapter 1: Introduction

1.1 Borazine-doped carbon structures: synthesis and applications

Borazine (H$_3$B$_3$N$_3$H$_3$, **1**, Scheme 1) was first isolated by *Stock* and *Polhand* in 1926.[1] It is often called "inorganic benzene" due to its similarities with the popular hydrocarbon. Both compounds are liquid at room temperature, have a planar hexagonal structure and show equalized bond lengths of 1.40 Å and 1.44 Å for benzene[2] and borazine,[3] respectively. In particular, the latter value stands between the B-N single bond (1.51 Å) and the B=N double bond (1.31 Å). However, borazine displays only a weak aromaticity[4,5] and has a great tendency to undergo hydrolysis forming boric acid and ammonia when in the presence of water.
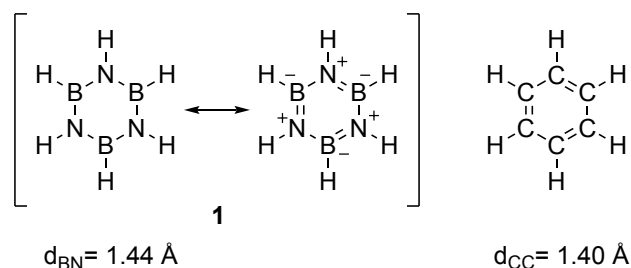
Scheme 1. Resonance forms of borazine **1** and structural comparison with benzene.

Furthermore, the electron donation of the nitrogen lone pair to the empty p orbital of the boron results in the strong polar character of the B-N couple.[6,7] This imparts peculiar properties to borazine such as a wider HOMO-LUMO gap of 6.2 eV compared with that of benzene (6.0 eV). The ionization potentials measured by photoelectron spectroscopy (10.1 eV for borazine, 9.25 eV for benzene) show a much lower energy of the HOMO for the inorganic counterpart compared to the carbon analogue.[8–10] Borazine and its derivatives display absorption spectra which are blue-shifted respect to those of polyphenylenes, thus making these species good UV emitters.[11] However, due to the different electronic density distribution, the reactivity of this class of compounds is substantially different from that of the all-carbon congeners.[12] The first studies on the reactivity of borazines appeared in the '60s and '70s,[13–15] but only after 1990 the interest of the scientific community focused on substituted borazines mostly for its potential use as precursor for BN ceramics, in particular for hexagonal boron nitride (*h*-BN), the graphene analogue with insulating properties.[16–18] Borazine derivatives were investigated

as active materials in optoelectronic devices starting from 2005.[19] In this respect, the substitution of sp^2 carbon atoms with heteroatoms[20–23] has gained value as one of the most versatile ways to finely tune the optoelectronic properties of graphitic materials. This task has gained a renewed importance, especially given the strong development in the synthesis of polycyclic aromatic hydrocarbons (PAHs),[24] graphene[25–27] and its substructures.[28–34] The use of boron and nitrogen as doping agents has been widely exploited for tailoring the optoelectronic properties[35–40] of conjugated hybrid BNC monolayers.[32,37,41–45] In this context, the attention of the scientific community has been attracted by borazine derivatives and BN-doped PAHs such as azaborines,[46,47] borazapyrenes,[48,49] borazaphenantrenes,[50,51] and borazanaphtalenes.[52–56] Borazine and its derivatives were the object of a recent rise in number of publications concerning UV-emitting OLEDs, materials for H_2 storage, coatings, ceramics, and in supramolecular chemistry for the devising of functional assemblies in solution and at interfaces. In the following paragraphs of this introduction a general overview will be given about the synthesis, reactivity and applications of borazine derivatives. The broadening of the synthetic scope and the knowledge in the chemistry of borazines have been boosted despite the intrinsic sensitivity of the BN six-membered ring towards hydrolysis. A large variety of functional groups can in fact be grafted through nucleophilic addition/substitution, electrophilic substitution, metal-catalyzed cross coupling, photocyclization, and thermal dehydrogenation. Owing to this, borazine derivatives have shown remarkable compatibility with a vast range of conditions employed in the protection/deprotection of functional groups (basic conditions, fluoride, metal-based reductions, and hydrogenolysis) allowing for the broadening of the spectrum of application for these BN doped materials. For a smoother understanding of the functionalization pattern around the borazine core, the nomenclature introduced in Figure 2 will be used throughout this chapter. Since the central unit of the molecule is composed of a substituted B_3N_3 moiety, different functionalities can be grafted on the B or N atom, and depending on their nature can form an *inner* shell, directly attached to the BN core, or an *outer* shell which will constitute the external decoration of the molecule. To complete the definition, a labelling nomenclature is proposed: $(ACD)B_3N_3(EFG)$, where A, C, and D are the boron substituents, E, F, and G are the nitrogen ones, while the B letter is kept only as the boron atom label for clarity. In the presence of the same substituents, the letters with higher grade in the alphabet will be used to describe the

substitution pattern. For example, when the substituents at the B and N are the same the $A_3B_3N_3E_3$ notation will be used (with A = E or A ≠ E).
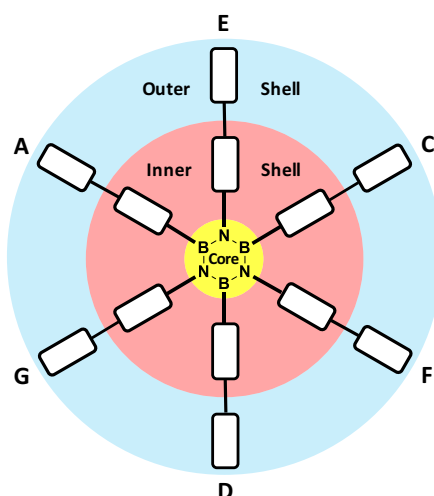
Figure 2. Schematic representation of a general borazine derivative. The different substitution regions and their labelling is displayed.

1.1.1 Synthesis of the borazine core

Two cyclization approaches can be used for the preparation of the borazine core (Figure 3). Using an amine precursor and a borane (hydride or halide), the BN ring can be formed through a (1+1'+1+1'+1+1') hexamerization. When using a pre-formed imino- or aminoborane derivative, the borazine ring will be formed following a (2+2+2) trimerization strategy. When a boron halide (BX_3) is chosen, a condensation reaction is required, but when boron hydrides are employed, the product is obtained through thermal or metal-catalyzed dehydrogenation.
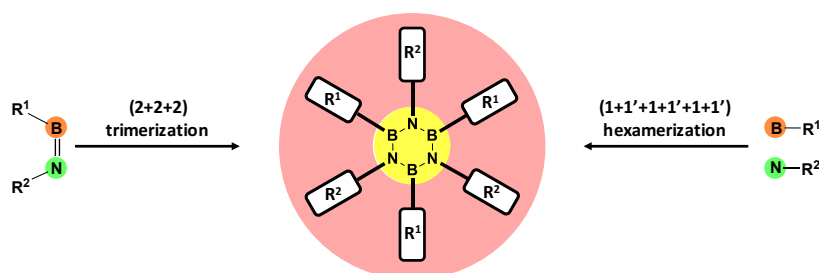
Figure 3. Strategies for the synthesis of the borazine core. Where $R^1 = R^2$ or $R^1 \neq R^2$ are alkyl, aryl, or hydrogen substituents.

1.1.1.1 (1+1'+1+1'+1+1') hexamerization *via* dehydrogenation reactions

Thermal dehydrogenation of ammonia-borane complexes was the very first method used by *Stock* and *Pohland* for the synthesis of borazine ($H_3B_3N_3H_3$). In this reaction ammonia and borane form a $NH_3 \cdot BH_3$ adduct which releases H_2 upon heating at 200 °C, leading to the formation of **1**.[1] Even being of difficult operability, this pioneering protocol did not fail to inspire further developments (Scheme 2). Some following methodologies employed lower temperatures (140-160 °C),[57,58] higher pressures (11 atm),[59] or different precursors like mixtures of $(NH_4)_2SO_4$ and $NaBH_4$,[57] or NH_4Cl and $LiBH_4$.[60]
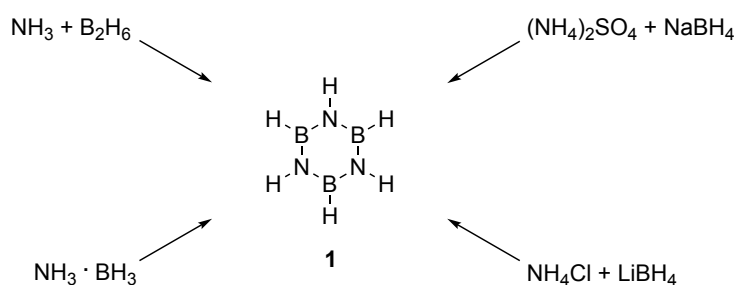
Scheme 2. Different precursors for the production of borazine **1** by thermal dehydrogenation of ammonia-borane adducts.

Using similar methodologies, *N*-aryl as well as *N*-alkyl borazines were also synthesized (Scheme 3). Thermolysis of aromatic amino-borane adducts yielded tri-*N*-arylborazines in solvent free conditions.[58] Notably, heating these adducts at 120 °C led to a mixture of substituted borazine and cyclotriborazane. This latter could be completely dehydrogenated by further heating at 200 °C.[58] Rather, starting from $^tBuNH_2 \cdot BH_3$, tri-*N*-tertbutylborazine could be obtained in quantitative yield after heating at 360 °C in a sealed vial.[61] Taken all together, these studies show an increased tendency for the more hindered amines to undergo dehydrogenation, resulting in the formation of substituted borazines in milder conditions. Starting from an aromatic tris(amino)-borane precursor, the formation of a polyborazine structure was additionally favoured by the reduced pressure which facilitated the H_2 elimination.[62] By treating 2-aminobiphenyl with an $Et_3N \cdot BH_3$ adduct at 205 °C tri-*N*-(2-biphenylyl)borazine could be prepared in 80% yield. Employing alkylammonium chloride salts and $LiBH_4$ as nitrogen and boron source, respectively, tri-*N*-methylborazine could be quantitatively synthesised.[63] The same approach led also to the preparation of tri-*N*-ethyl-, tri-*N*-propyl-, and tri-*N*-isopropylborazine in 94%, 92%, and 84% yield respectively.[64] Alkyl-borazines were also produced by reaction of nitriles with diborane. Heating a dimethoxyethane solution of trichloroacetonitrile and B_2H_6 gave

N-(2,2,2-trichloroethyl)borazine in 54% yield.[15] Similarly, starting from methyl cyanide or ethyl cyanide the corresponding borazines could be obtained at room temperature upon reaction with diborane.[65] Alkylamino-borane complexes were also produced using the $Me_2S \cdot BH_3$ adduct as source of boron.[66] From these, a mixture of *N*-alkylcycloborazanes ($H_6B_3N_3R_3$) and *N*-alkylborazines was produced upon heating at 120 °C. The loss of hydrogen could be completed after further heating at 200 °C to give the relative *N*-alkylborazine.

$R^{2,3,12}$ + B_2H_6 $R^{1,4,5,7,10,13}$–$NH_2 \cdot BH_3$

R^{1-8}–NH_2 + $Me_2SH \cdot BH_3$ R^{1-4}–NH_3Cl + MBH_4
                                                          M= Li, Na

R^1= Me; R^2= Et; R^3= ^{n}Pr; R_4= ^{i}Pr; R^5= ^{n}Bu; R^6= ^{s}Bu; R^7= ^{t}Bu; R^8= neo-Pen; R^9= Hex; R^{10}= Hept; R^{11}= -CH_2Ph; R^{12}= -CH_2CCl_3; R^{13}= Ph.
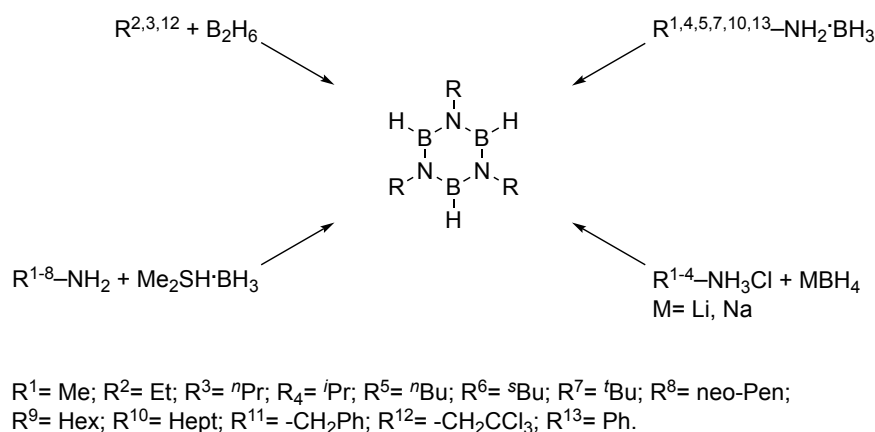
Scheme 3. Strategies for the synthesis of alkyl- and aryl-*N*-substituted borazines

A relationship between the bulkiness of the alkyl substituents and the rates of dehydrogenation has been found in this case. Additionally, methylamino-borane could be readily produced when methylamine and sodium borohydride were mixed in THF in the presence of $BF_3 \cdot OEt_2$. Thermolysis of the isolated adduct gave tri-*N*-methylborazine in nearly quantitative yield.[66] The same boron precursor was also used to produce borazine-based polymeric networks **2** and **3** through reaction with *para*-phenylenediamine or tetrakis(4-aminophenyl)methane, respectively, in glyme at 120 °C for 3 days (Scheme 4).[67] Furthermore, lowering of the reaction temperatures for the dehydrogenation process was possible thanks to the use of a rhodium catalyst.[68] Investigation of the reaction kinetics related to the formation of borazines from $NH_3 \cdot BH_3$ or $CH_3NH_2 \cdot BH_3$ at 45 °C revealed the loss of the last H_2 to be the rate determining step. Remarkably, aniline-borane adduct led to the formation of tri-*N*-phenylborazine in 56% yield after just 16 h at r.t. As for the previously reported examples,[58,61] also for the metal-catalyzed reaction, the loss of H_2 seems to be prompted by the steric bulkiness of the substituents, to give substituted borazines in milder conditions.
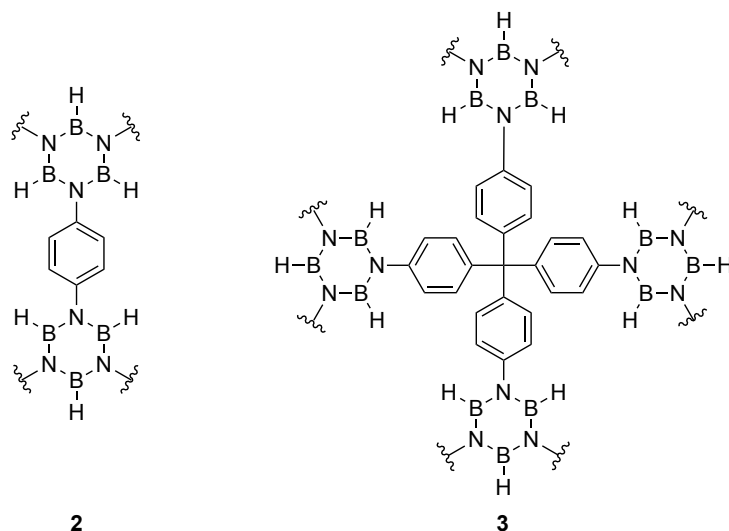
Scheme 4. Amorphous aryl-borazine polymers **2** and **3**, obtained via dehydrogenation route.

In a recent study,[69] complexes of Mo(III), W(IV), and Cr(IV) were employed in the dehydrogenation of ammonia-borane and ^{t}BuNH$_2$·BH$_3$, with the latter metal displaying the best performances. Similarly, *N*-alkylborazines were obtained using hexacarbonyl complexes of such metals, with Cr(0) showing once again the best activities.[70] In this case, the metal catalyst and the amino-borane adducts were dissolved in benzene, irradiated using a Hg lamp and then left to react in the dark. While tri-*N*-methyl- and tri-*N*-ethylborazine were obtained in good yields, tri-*N*-tertbutylborazine was produced only in 19% yield.[70] Also nickel nanoparticles catalyzed the formation of borazine with a reasonable 53% yield when ammonia-borane was heated at 80 °C in tetraglyme.[71] Finally, borazine formation was achieved also by Lewis-acid catalysis. Reaction between (NH$_4$)$_2$SO$_4$ and NaBH$_4$ in tetraglyme gave borazine in 30% yield, which could be boosted to a 67% yield when a catalytic amount of AlCl$_3$ was added to the reaction mixture.[72]

1.1.1.2 (1+1'+1+1'+1+1') hexamerization *via* condensation reactions

Concerning the B source, starting from the 50's boron halides were used as valid alternative to hydrides. Tri-*B*-chloroborazine **4** could be prepared by reacting NH$_4$Cl and BCl$_3$ in either refluxing chlorobenzene or in neat conditions at 165 °C.[73] In a similar fashion, tri-*B*-chloro-tri-*N*-phenylborazine **5** could be prepared refluxing aniline in dry toluene in the presence of BCl$_3$ (Scheme 5).[74] Besides aniline, other aromatic amines were employed for this purpose.
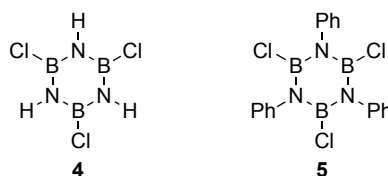
Scheme 5. Structures of tri-*B*-chloroborazines **4** and **5**.

The reaction between phenylenediamine,[75] benzidine, and 1,3,5-tris-(4-aminophenyl)benzene[76] with boron trihalides led to the formation of amorphous *B*-halo-borazine polymeric networks **6-10** (Scheme 6). With BCl$_3$ the reaction gave higher yields compared to those obtained using BBr$_3$. In section 1.1.3 the further functionalization of *B*-haloborazines at the boron sites using nucleophiles will be discussed.
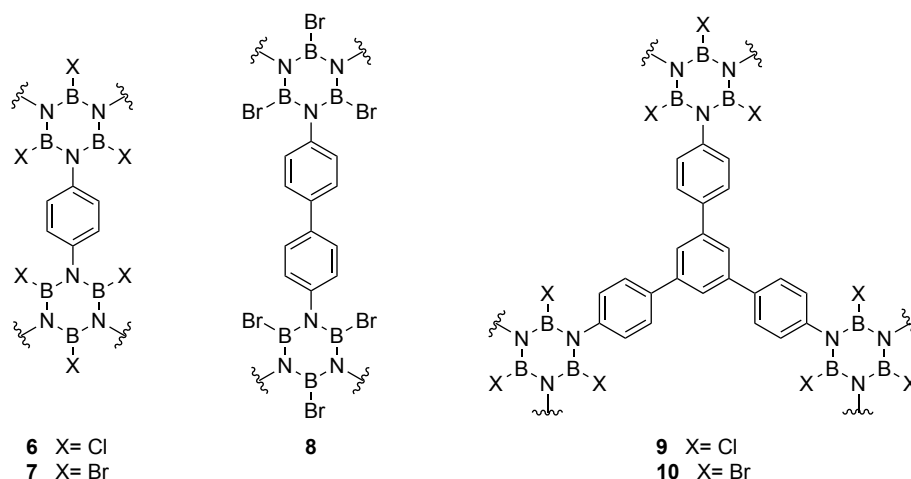
Scheme 6. Amorphous aryl-borazine polymers **6-10** via BX$_3$ route.

1.1.1.3 (2+2+2) trimerization and 'inner shell' fusion

Alternatively to the hexamerization approach, one can think of using pre-organized cyclic BN-precursors. Heating the six-membered cyclic amino-borane **11** in toluene resulted in the formation of the corresponding borazine **12** in quantitative yield (Scheme 7).[77] Borazine **14** could be quantitatively obtained from the five-membered BN-doped analogue **13** starting from the same reaction conditions.[78] Such reaction could be also conducted at lower temperature (80 °C) and in the absence of solvent, thanks to the use of metal chlorides as catalysts. In particular, between Cu, Co, Ni, and Fe, the latter displayed the best activity (Scheme 7).[78]
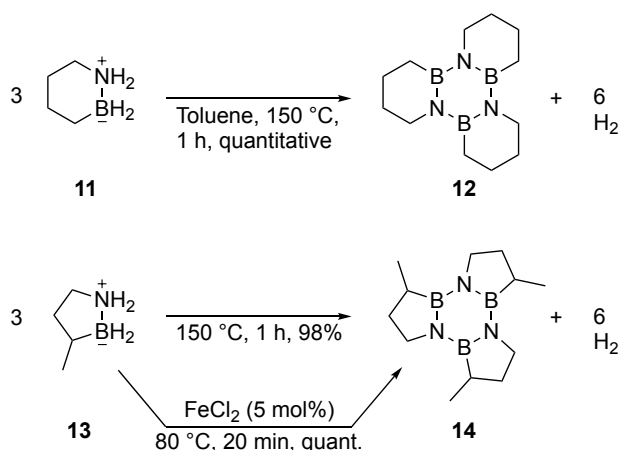
Scheme 7. Trimerization of cyclic amino-borane adducts to form borazines **12** and **14**.

The mild conditions used for the dehydrogenation reaction made this cyclic amino-boranes good candidates for hydrogen storage applications. This aspect will be furtherly discussed in section 1.1.5.2. An alternative trimerization procedure was developed by the group of *Bettinger* (Scheme 8).[79] The microwave-assisted reaction of 2-aminobiphenyl **15** with BCl_3 in the presence of $AlCl_3$, led to 9,10-BN-phenanthrene **16**,[51] subsequently transformed into triflate derivative **17**. Treatment of the latter with potassium bis(trimethylsilyl)amide (KHMDS) gave molecule **18** (43% yield), in which the borazine core is composed of three 9,10-BN-phenanthrene moieties linked together. Partial planarization of **18** was observed after photocyclization in the presence of iodine.[80] Notably, total planarization of derivative **18** to obtain hexa-*peri*-hexabenzoborazinocoronene (HBBNC) **21** was never achieved even upon extension of the reaction time. To understand why full planarization could not be obtained using this method, the same group studied the photochemistry of hexaphenylbenzene and hexaphenylborazine.[81,82] These molecules were studied by fs, ns, and µs time-resolved spectroscopy to understand the effects of the BN doping on the photoinduced 6π electrocyclization reaction and on the stability of the resulting planar BN-doped structures. It was found that the relaxation from the excited state for hexaphenylborazine (τ= 3 ps) is faster with respect to its full-carbon analogue (τ= 428 ps) by more than 2 orders of magnitude.[81] The fast decay of the excited state introduced by BN-doping is therefore considered to be the main resistance to the photoinduced cyclization. Moreover, by combining experimental and computational findings, a decrease in the predicted stability of the cyclized BN-doped products with respect to the non-doped one, was found. Taking advantage of an alternative methodology, BN-embedded coronene **21** was

obtained in low yield (3-5%) by pyrolysis of tris-*N*-(2-biphenyl)borazine **20** (Scheme 8).[83] Precursor **20** was obtained following the procedure by *Köster et al.*,[84] including thermal dehydrogenation of 2-aminobiphenyl **15** and $BH_3 \cdot NEt_3$.
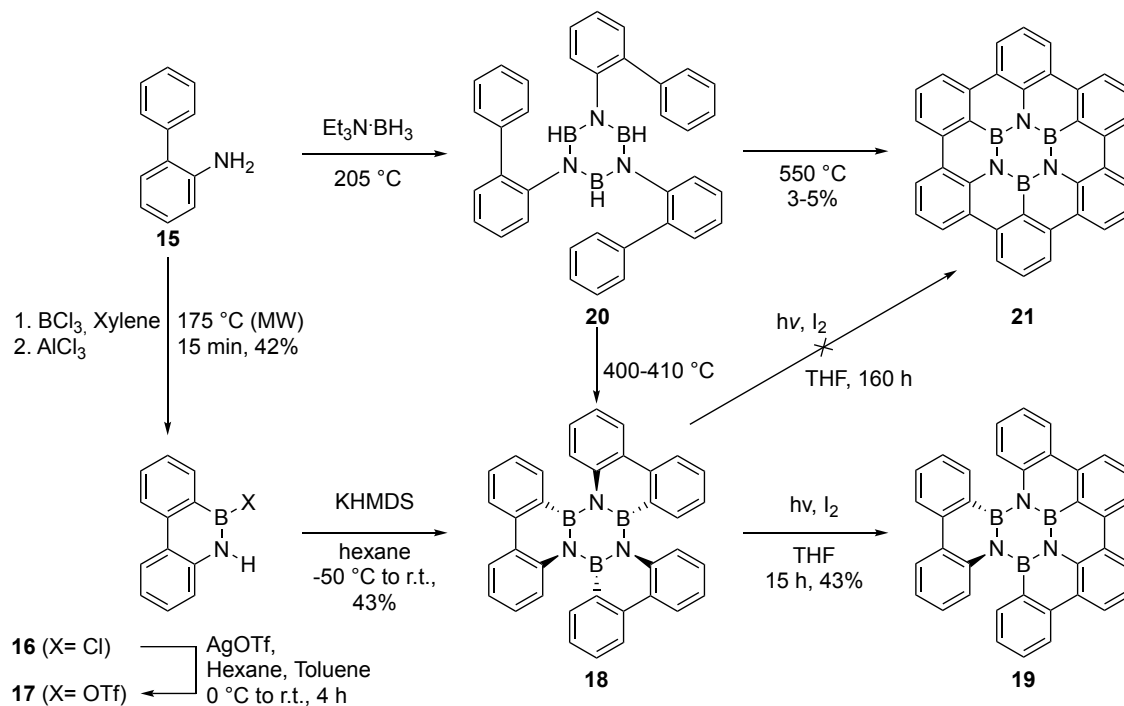
Scheme 8. Synthetic strategies towards borazines **18** and **20**, and planarization attempts to give borazines **19** and **21**.

1.1.2 Reactivity of the B_3N_3 core

1.1.2.1 Chemical stability and reactivity of the B_3N_3 core

Rather predictably, borazine and its derivatives are very susceptible towards nucleophilic attack at the *B*-sites. As an example, species such as water, alcohols,[78] urea and pyrazole,[85,86] can attack borazines prompting a ring opening reaction and leading to degradation to form the corresponding amine and the boric or boronic acid. Borazine itself (**1**, $H_3B_3N_3H_3$) generates boric acid, ammonia, and H_2 when in the presence of moisture. As one can foretell, this major drawback weakened and slowed down the scientific progress towards the study and exploitation of BN-doped polycyclic aromatic hydrocarbons. By either introducing electron-donating groups on the *N*-sites, or protecting the *B*-sites with bulky substituents, the reactivity of borazine derivatives can be significantly reduced. In the first case, upon introduction of electron-donating groups on the N, the electronic delocalization on B is favoured. This makes the latter less electrophilic, as the aromaticity of the borazine ring is enhanced.[87–89] The same effect on

the reactivity can also be obtained by placing electron-withdrawing groups at the boron sites.[90] By using this second approach, the empty p orbital of B is sterically shielded by the presence of bulky groups grafted to the N[87] or B.[91] As shown by X-ray crystal structures, 2,6-dimethylphenyl,[14] 2-mesityl,[14,91] and 9-anthryl[92] substituents are reported to be the best protective groups. Oxidants are also capable of destroying the borazine ring. However, no detailed information about the products obtained by oxidation has been described in the literature. Despite being weakly aromatic, borazine displays a similar ability to benzene for the complexation of metallic centres. η^6-type complexes of alkyl-borazine derivatives with Cr(0) have been characterized and crystallized (Scheme 9).[93,94] Further studies on phenyl-substituted borazines showed that the weak borazine-metal interaction can favour protodeborylation of the phenyl substituents, leading to the formation of $C_6H_6 \cdot Cr(CO)_3$ complex as major product.[95]

Scheme 9. Formation of borazine-Cr complexes **24** and **25**.

Formation of lithium complexes have also been described.[96] Depending on the reagents and equivalent used, different type of complexes could be prepared and characterized by X-ray diffraction.

1.1.2.2 Electrophilic additions at the B₃N₃ core

In the presence of hydracids, such as HCl or HBr, borazine can undergo addition at low temperatures and, therefore, it can assume a non-planar and non-aromatic conformation.[97–99] Addition of HCl to borazine led quantitatively to the $H_3B_3N_3H_3 \cdot 3HCl$ adduct **26**, breaking the partial double bond character on each BN bond and forcing the system to adopt a chair-like conformation (Scheme 10). The weakly aromatic borazine **1** could be re-obtained upon heating at 130 °C. While saturation of the BN ring was rather straightforward, the formation of a mono-protonated borazinium ion could not be achieved by direct HX addition.

Scheme 10. Reaction of electrophilic addition of HCl on **1**, and AlBr$_3$ to **27**.

Mono-addition was however observed when hexamethylborazine **27** was treated with AlBr$_3$ in benzene, leading to compound **28** in 85% yield (Scheme 10).[100,101] Computational investigations and theoretical modelling were performed to shine light on the aromaticity of borazine in comparison with that of benzene,[4] and on the peculiar reactivity of the B$_3$N$_3$ core. From this study, the energy for the resonance stabilization were quantified as 9.6 kcal/mol for H$_3$B$_3$N$_3$H$_3$. Although being significantly lower than that of benzene (21.9 kcal/mol), this value confirms the weak aromaticity of the BN ring and explain the observed chemical behaviour.[102] Thanks to the electrophilicity of the B atoms, several borazine derivatives were employed as CF$_3^-$ transfer reagents.[103] In particular, the CF$_3$·hexamethylborazine derivative exhibited the best efficiency in promoting trifluoromethylation reactions. Moreover, Me$_3$B$_3$N$_3$Me$_3$ could be quantitatively recovered after the reaction.

1.1.2.3 Exchange reactions at the boron site
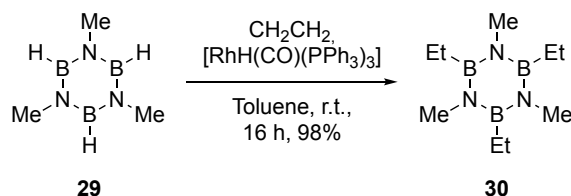
Scheme 11. Rh-catalyzed hydroboration of ethylene of tri-*N*-methylborazine **29**.

The first example of halogenation at the *B*-site was reported in 1951 by *Schlesinger*.[57] The reaction between borazine and BCl$_3$ and BBr$_3$ gave a mixture of mono- and dihalogenoborazine. Using a revised procedure, the group of *Niedenzu* isolated *B*-mono

and *B*-dihaloborazines in yields between 25% and 35%.[104] Mono-, di-, and tri-*B*-haloborazines were also prepared using HCl, HBr,[13] or Br$_2$.[105] Thanks to a Rh-catalyzed hydroboration of alkenes, functionalization of H$_3$B$_3$N$_3$E$_3$ derivative **29** afforded mono-, bi-, and tri-*B*-alkylborazines in 70-98% yield (Scheme 11).[66] Moreover, since the first report from *Groszos* and *Stafiej* in 1958,[106] the use of aryl/alkyllithium species and Grignard reagents emerged as a versatile approach to graft substituents at the B positions. In particular, after reaction of an amine with BCl$_3$ (see section 1.2), the produced tri-*B*-chloroborazine intermediate could be further functionalized using the organometallic species of choice. The versatility of this methodology allowed the formation of differently *B*-substituted products. When tri-*B*-chloro-*N*-triphenylborazine **5** was treated with LiAlH$_4$, tri-*B*-hydro-tri-*N*-triphenylborazine **31** was obtained in 85% yield. Upon further treatment with either RMgBr or PhMgBr the intermediate borazine could be converted into its A$_3$B$_3$N$_3$E$_3$, A$_2$CB$_3$N$_3$E$_3$, or ACDB$_3$N$_3$E$_3$ type derivatives **32** (Scheme 12). In particular, the selectivity towards the different derivatives could be controlled depending on the addition sequence and stoichiometry of the carbon nucleophiles.[106] Tri-*B*-chloroborazine derivative **5** could also be directly attacked by Grignard reagents to yield differently substituted derivative **32** depending on the nature of the reagent implied (Scheme 12).[91,92,106–110]
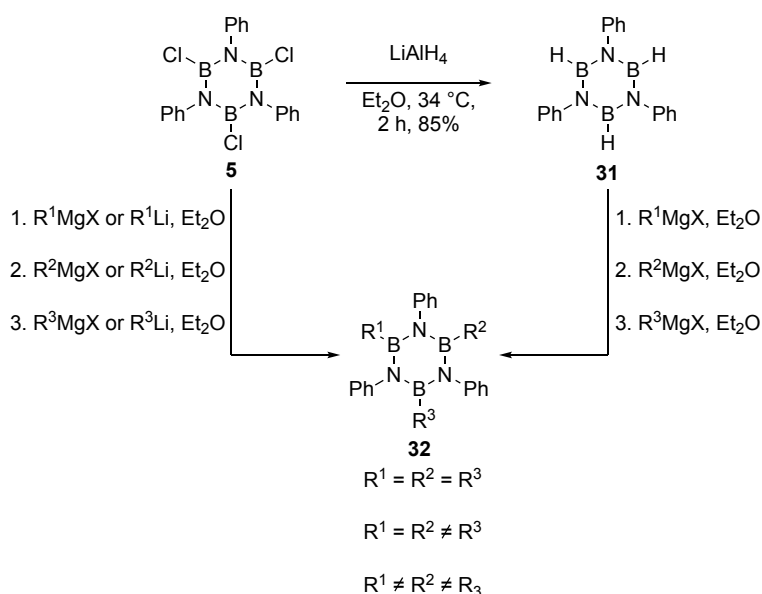
Scheme 12. Approaches towards the synthesis of *B*-substituted borazines using organometallic reagents.

However, in the latter case, acid-free and anhydrous conditions are essential to have high yields. Substitution of the *B*-halogen groups have been exploited also by *Helten* et al. for

the construction of a borazine-based inorganic-organic hybrid polymer.[111] Different crosslinked borazine polymers (**36a-c**) were obtained through either condensation between a tri-*N*-methyl-tri-*B*-chloroborazine precursor (**33**) and diamines **34a-c** (Route A), or by Si/B exchange between **33** and *N*-sylilated diamine crosslinkers **35a-c** (Route B, Scheme 13).
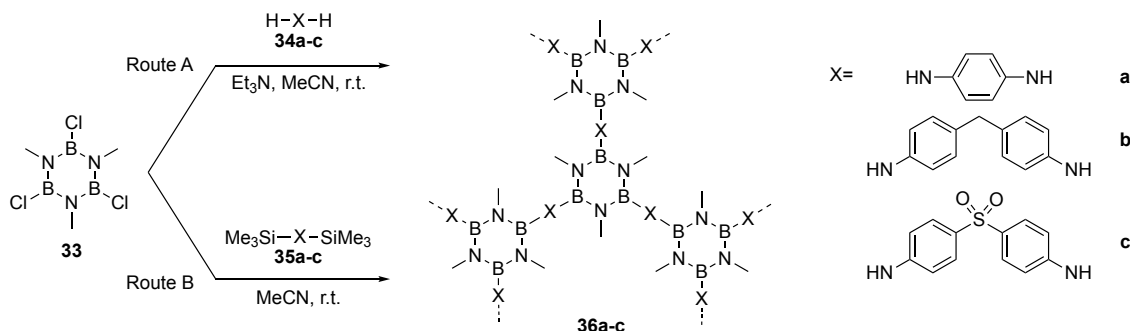
Scheme 13. Synthesis of hybrid borazine-based polymers **36a-c** *via* condensation reaction (Route A) or by silicon/boron exchange condensation (Route B).

Thanks to the controlled precipitation of the polymeric product, microparticles with different morphology and size distribution were obtained. Notably, the cyclomatrix architecture conferred a remarkable thermal stability, with a major weight loss detected at 450 ˚C by TGA.

1.1.3 Functionalization of the inner shell
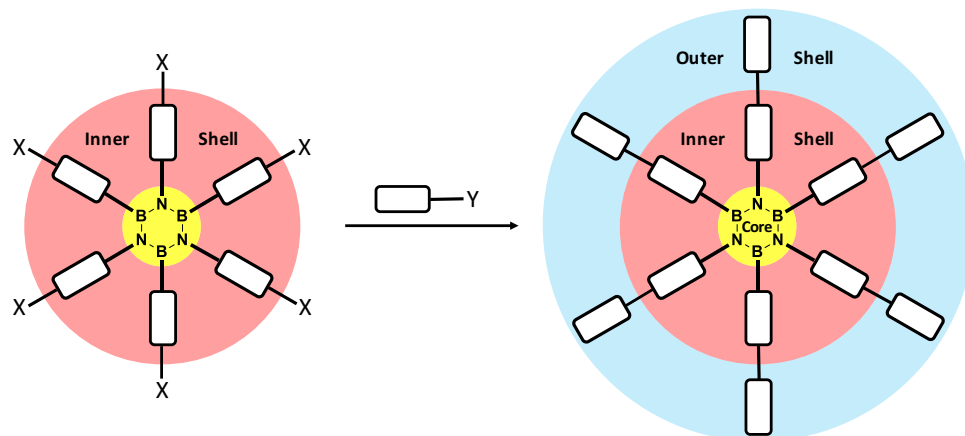
Figure 4. Construction of the "outer shell" using reactive functional groups (X, Y).

The substituents directly attached to the central B_3N_3 ring constitute the 'inner shell'. Functionalization of this through different strategies can lead to the building of an 'outer shell' (Figure 4). In this respect, the hydrosilylation of tri-*B*-ethynylborazine **37** was achieved after 36-48 h using Pt as catalyst in toluene at 120 °C (Scheme 14).[112]
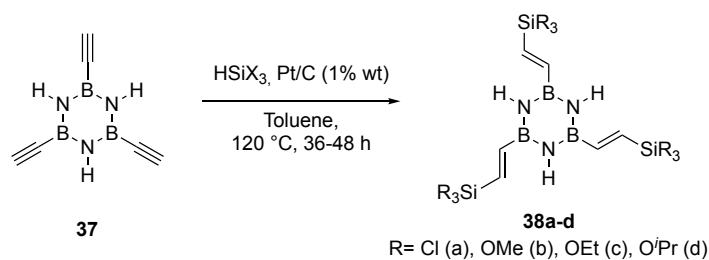
Scheme 14. Platinum-catalyzed hydrosilylation of tri-*B*-ethynylborazine **37**.

The addition of trichlorosilane (HSiCl$_3$), or trialkoxysilane (HSi(OR)$_3$; R= Me, Et, ^{i}Pr) led to *cis*-stereoselectivity and in all the cases tri-*β-trans* isomers were observed as major products. However, when alkoxysilanes were employed, the regioselectivity of the reaction was reduced and complex mixtures containing *α-* and *β*-silylated products were obtained. Notably, the hydrolysis of the trichlorosilane groups appears to be faster than that of the borazine core, making these derivatives suitable precursors for the preparation of amorphous silica gel.[112] Following the same BCl$_3$ route, 10-bromoanthryl borazine **39** bearing bromine substituents as anchor units, was prepared by the group of *Yamaguchi* and subsequently functionalized with different substituents (Scheme 15).[92]
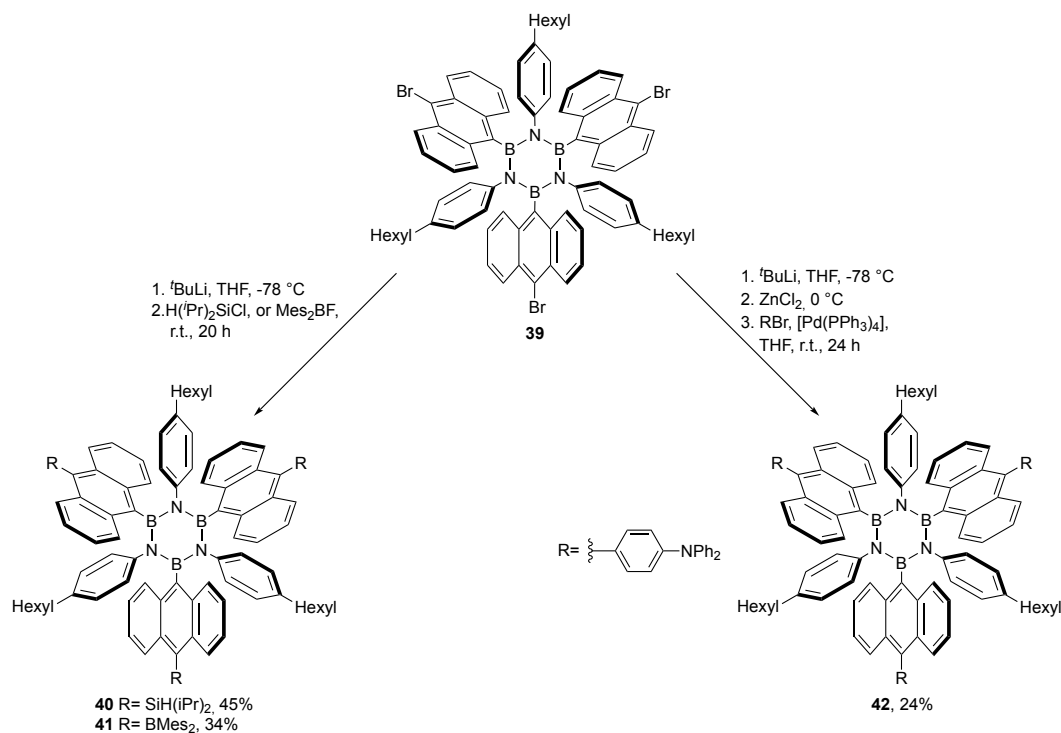
Scheme 15. Strategies for the peripheral functionalization of tri-N-anthrylborazine **39**.

More in detail, treatment of **39** with ^{t}BuLi at -78 °C in THF followed by the addition of diisopropylsilyl chloride (H(^{i}Pr$_2$)SiCl) or dimesitylboryl fluoride (Mes$_2$BF) afforded

derivatives **40** and **41** in 45% and 34% yields, respectively. In this case the borazine ring was protected by the anthryl hydrogens which, standing on top of the B centres, did not allow the attack of strong carbon nucleophiles such as ^{t}BuLi. Additionally, the tri-lithiated derivative of **39** could undergo Negishi cross-coupling with aryl halides in the presence of [Pd(PPh$_3$)$_4$] as catalyst, to give tri-phenylamine derivative **42** in moderate 24% yield (Scheme 15).[92]
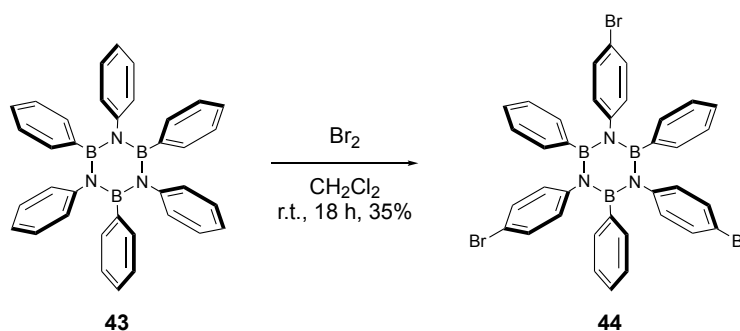
Scheme 16. Electrophilic aromatic bromination of hexaphenylborazine **43**.

Finally, the selective electrophilic aromatic bromination of hexaphenylborazine **43** to give tri-*N*-(*p*-bromophenyl)-tri-*B*-phenylborazine **44** with a moderate 35% yield, was recently reported by the group of *Bettinger* (Scheme 16).[113]

1.1.4 Compatibility of borazine derivatives towards reagents and conditions

Looking ahead to further derivatization, the fundamental knowledge about the reactivity of borazines is of obvious importance, since it will allow for the design of suitable synthetic pathways and hence, drive the choice of reagents and conditions which are compatible with the BN core. As pointed out in section 1.1.2.1, many borazine derivatives are very sensitive to nucleophiles. Regarding aryl-borazines, the resistance towards such conditions can be obtained upon shielding the empty B orbital with bulky aryl-groups (mesityl-, 2,6-dimethylphenyl-, 2,6-difluorophenyl, or anthryl-substituents).[14,91,92,114] With the intent of constructing a list of compatible reagents, and to furtherly elucidate the chemical behaviour of aryl-substituted borazines, the known reactions involving these derivatives must be reviewed. Table 1 contains all the experimental conditions explored so far on aryl-borazines with protected *B*-sites (*B*-mesityl-, *B*-2,6-dimethylphenyl-, *B*-2,6-difluorophenyl-, or *B*-anthryl-). More in detail, stability of *ortho*-substituted hexaarylborazines were tested towards hydrolysis in the presence of organometallics, oxidants, reductants, bases, electrophiles and under UV light irradiation.

Table 1. Experimental conditions tested for hydrolysis-stable *ortho*-substituted hexaarylborazines.

	Reagents	Reactivity	Reference
Organometallics	RLi	S	91,106,115–117
	RMgX	S	14,91,106,116,118
	RZnX	S	115
	Pd-catalized reactions	S	115,117 b.u.
Oxidants	Aniline, NaI, ^{t}BuOCl, MeCN, r.t.	D	b.u.
	Trfluorobenzaldehyde, MeCN, r.t.	S	b.u.
	Dimethoxyphenol, ^{t}BuONO, BF$_3$·OEt$_2$, CH$_2$Cl$_2$, 0 C°-r.t.	D	b.u.
	MAD^a, nitrosobenzene, MeCN, r.t.	D	b.u.
	Nitrosobenzene, KOH, DMF, 150 °C	D	b.u.
	Aniline, CuBr, Pyridine, 65 °C	D	b.u.
	O$_3$, Me$_2$S, CH$_2$Cl$_2$, -84 °C	D	b.u.
	m-CPBA, CH$_2$Cl$_2$, r.t.	SD	b.u.
	FeCl$_3$, MeNO$_2$, 90 °C	S	b.u.
	FeCl$_3$, MeNO$_2$, TFA, r.t.	S	b.u.
	CAN^b, CH$_2$Cl$_2$, or THF, r.t.	S	b.u.
Reductants	NaBH$_4$, CHCl$_3$, r.t.	S	b.u.
	Fe, CH$_2$Cl$_2$, r.t.	S	b.u.
	H$_2$, Pd/C	S	b.u.
Bases	TBAF, THF, r.t.	S	117, b.u.
	K$_2$CO$_3$, THF, MeOH, r.t.	S	117, b.u.
Electrophiles	BnBr, NaH, DMF, r.t.	S	b.u.
	Ac$_2$O, pyridine, r.t.	S	b.u.
	Me$_2$NSO$_2$Cl, DBU, MeCN, r.t.	S	b.u.
Irradiation	I$_2$, hv, cyclohexane/or THF, r.t.	D	80
	I$_2$, hv, toluene/heptane, r.t.	D	80, b.u.

^{a}MAD: methylaluminium bis(2,6-di-tertbutyl-4-methylphenoxide). ^{b}CAN: cerium ammonium nitrate. b.u.: by us, these conditions were tested in our group. "S": stable, "SD": slow degradation. "D": degradation.

These experimental evidences derive partially from the literature, and partially from the knowledge developed in the group of Prof. *Bonifazi*, where this thesis work was carried out. In particular, test reactions were conducted by our group using tri-*B*-mesityl-tri-*N*-phenylborazine **45** (Scheme 17) as a test molecule and, together with the data summarized from scientific reports, a three-level reactivity chart has been used to express the extent of the reactivity: "D" indicates "degradation" of the borazine, "SD" indicates instead that a "slow degradation" is happening over a prolonged amount of time (≥8 h), and "S" stands

for "stable" towards the tested conditions. These tests, show a clear susceptibility for molecule **45** in the presence of oxidants and when irradiated with UV light. On the contrary, the resistance of the borazine core towards strong organometallic nucleophiles, bases and reducing agents, is disclosed.

45
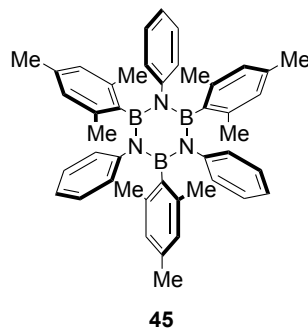
Scheme 17. Structure of tri-*B*-mesityl-tri-*N*-phenylborazine **45**, used for the compatibility and stability tests.

1.1.5 Applications
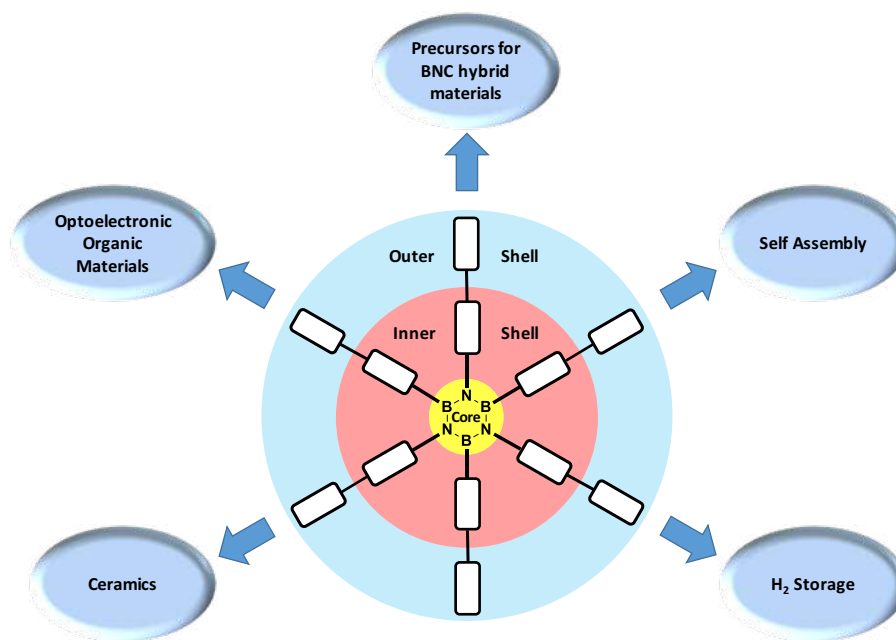
Figure 5. Applications of borazines and its derivatives.

During the past few years, a number of various applications has involved borazine and its derivatives. These applications are mostly related to the development of materials for organic optoelectronics, H_2 storage, and supramolecular self-assembly systems, as shown in Figure 5. This chapter will review the examples and the main achievements in the field. The employment of borazine and its derivatives as precursors for polymers,[111] ceramic materials,[116,118] coatings,[119−121] BN nanomeshes,[122] 2D[123−125] and 3D[126] crystalline boron

nitrides are thoroughly treated in focused reviews[127,128] and will not be furtherly discussed in this manuscript.

1.1.5.1 On-surface self-assembled architectures

The study of interactions between molecules and the formation of supramolecular self-assemblies has gained a new impetus due to the rapid development of molecular-based technologies. This is essential for the understanding of the interactions occurring within thin films of organic compounds composing organic electronic devices or interfaces that are exposed to metal electrodes.[129–132] The mastering of the formation of molecular layers and molecular assemblies could provide the key for the engineering of functional supramolecular materials.[133–136] Concerning borazines however, the interactions with solid surfaces have not been extensively explored. The very first bottom-up preparation of supramolecular architectures based on borazines have been reported.[137] Low temperature scanning tunnelling microscopy (LT-STM) revealed that borazines **45** and **46** form assemblies of different nature when deposited on Cu(111) surfaces. Tri-*B*-phenyl-tri-*N*-mesitylborazine **45** self-organizes in monolayers mostly thanks to van der Waals interactions to form large islands.
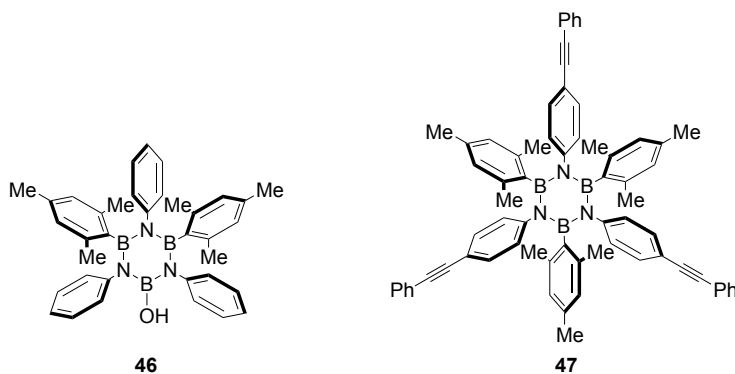
Scheme 18. Chemical structures of borazines **46** and **47**.

Mono-hydroxyborazine **46** (Scheme 18) displays a different behaviour forming peculiar clusters of 7, 10, 11, 12, and 13 molecules (Figure 6). These results can be explained in terms of a delicate interplay between the long-range Coulombic repulsion of deprotonated charged molecules and short-range van der Waals attractions between neighbouring molecules.
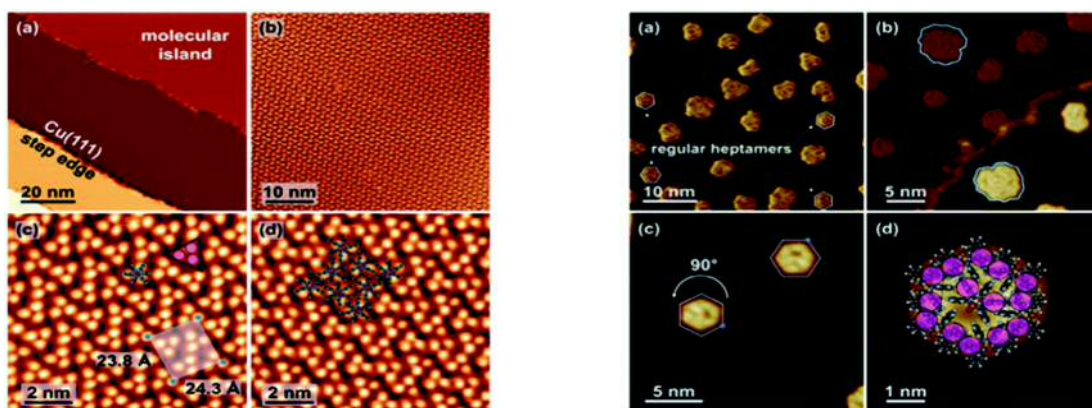
Figure 6. Left: STM of **45** on Cu(111), deposited at 300 K, scan performed at 77 K. a) Large area of Cu(111) surface. b) and c) Large molecular islands (expanded views). d) Calculated structure superimposed on the image. Right: STM images of **51** on Cu(111). a) Isolated molecular clusters, the 7-mers are highlighted. b) Cu(111) step edge (expanded view), revealing two enantiomers of an irregular cluster. c) 90° rotated 7-mers (expanded view). d) Calculated molecular model superimposed on 7-mer. Reprinted with permission from Kervyn, S.; Kalashnyk, N.; Riello, M.; Moreton, B.; Tasseroul, J.; Wouters, J.; Jones, T. S.; De Vita, A.; Costantini, G.; Bonifazi, D. *Angew. Chem., Int. Ed.* 2013, *52* (29), 7410–7414. Copyright (2014) John Wiley and Sons.

In a following endeavour,[138] the role of the "outer shell" functionalization on the self-assembly has been investigated. The study showed that borazine derivative **45** formed identical van der Waals-driven closely-packed networks on either Au(111) or Cu(111).
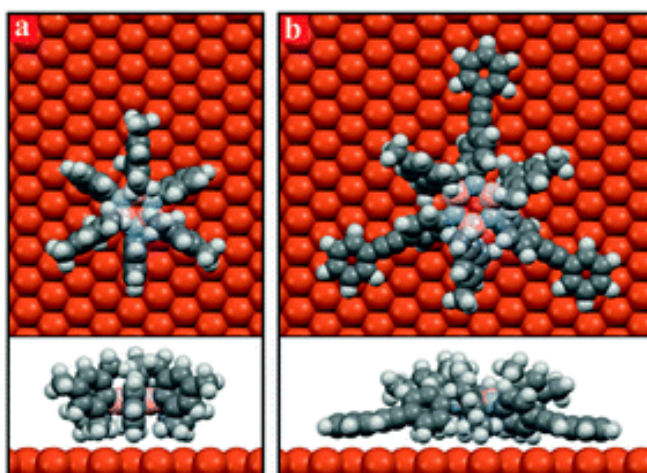
Figure 7. MD simulations showing minimum energy adsorption configuration for borazines **45** (a) and **47** (b) on Cu(111). Steric repulsion between phenyl- and mesityl-substituents originate effective decoupling of the borazine cores from the metal surface. Reprinted with permission from Kalashnyk, N.; Ganesh Nagaswaran, P.; Kervyn, S.; Riello, M.; Moreton, B.; Jones, T. S.; De Vita, A.; Bonifazi, D.; Costantini, G. *Chem. Eur. J.* 2014, *20* (37), 11856–11862. Copyright (2014) John Wiley and Sons.

Rather differently, molecule **46** (Scheme 18) revealed an interaction of the peripheral substituents with the metallic surfaces which drives the assembly and, ultimately, leads to the formation of networks whose porosity was closely dependent on the nature of the metallic surface and therefore with the affinity of the outer rim with the surface.[138] Thanks

to molecular dynamics simulations, it was possible to confirm that the different behaviour of the BN-doped derivatives on metal surfaces derives only from the peripheral substituents. Therefore, a contribution from the central borazine core to the interaction with the surface can be excluded. In the future, one can expect that the combination of full-carbon and boron-nitrogen doped materials can lead to peculiar self-assemblies on surfaces for the development of electronic devices (Figure 7). The surface-assisted polymerization and cyclodehydrogenation reaction of tri-*B*-phenyl-tri-*N*-(4-bromophenyl)borazine **44** and 2,12,22-tribromo-tri(o,o′-biphenylyl)borazine **48** led to the formation of interlinked hexa-*peri*-hexabenzoborazinocoronene (HBBNC) domains on a Ag(111) surface under ultra-high vacuum (UHV) conditions.[139] As depicted in Figure 8, the thermal deposition of **48** on the Ag(111) surface at 425 K gave flower-like assemblies (Figure 8a). Cleavage of the C-Br bonds occurred upon increasing the temperature at 475 K giving Ag-catalyzed cross coupling reactions to form phenyl-phenyl linkages and, therefore, covalent networks (Figure 8b).
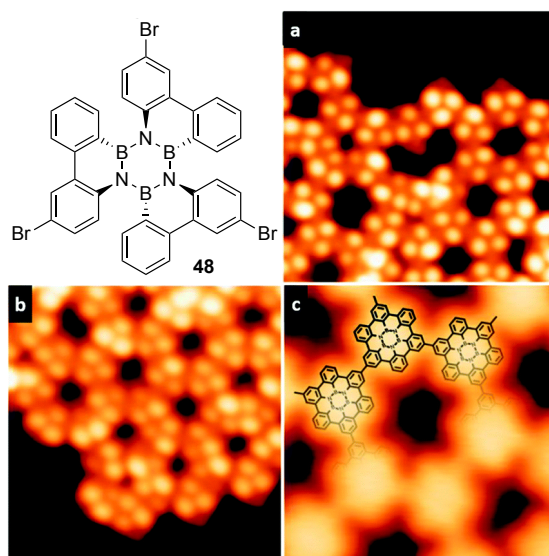
Figure 8. Structure of **48**. a) STM image following deposition at 425 K. b) Covalently-linked network after treatment at 475 K. c) High resolution STM images of the planar network after treatment at 575 K. Reprinted with permission from Sánchez-Sánchez, C.; Sachdev, H.; Brüller, S.; Müllen, K.; Krieg, M.; Bettinger, H. F.; Nicolaï, A.; Meunier, V.; Talirz, L.; Fasel, R.; Ruffieux, P. *ACS Nano* **2015**, *9* (9), 9228-9235. Copyright (2015) American Chemical Society.

Planarization to the final covalently linked borazino-coronene network was achieved by complete cyclodehydrogenation at a temperature of 575 K (Figure 8c). Following the very first assembly study on metallic surfaces, this work clearly represents the first step towards the implementation of BN-doped conjugated carbon materials and the study of

their electronic properties and their potential application in optoelectronics and molecular devices. Apart from surface-driven self-assemblies, solid-state arrangement can also be affected by the presence of different substituents in the "inner shell" of the borazine derivatives. For example, the crystal structure of tri-*B*-anthryl-tri-*N*-(4-trifluoromethylphenyl)borazine **49** shows peculiar gear-shaped crystalline architectures with C_3 symmetry (Figure 9).[92] Characteristic honeycomb-like networks, consisting of intermolecular face-to-face π-stacks between the anthracene moieties, were formed. Having high degree of solid-state ordering, these peculiar structures are regarded as good candidates for the employment in optoelectronic devices. In particular, the recurrent π-π interactions might potentially confer high carrier transport mobility. Molecule **49** displays a quantum yield (Φ_F) of 0.63 from a solution of THF, a double value with respect to anthracene (Φ_F= 0.27).
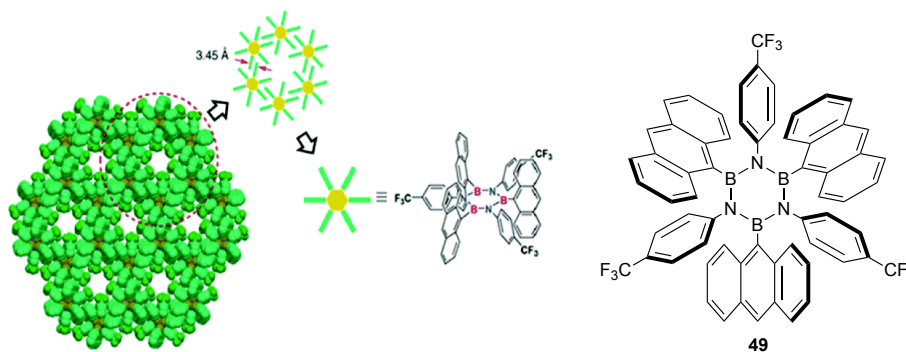
Figure 9. Structure of borazine **54** and gear-shaped honeycomb arrangement in the solid-state. Reprinted with permission from Wakamiya, A.; Ide, T.; Yamaguchi, S. *J. Am. Chem. Soc.* 2005, *127* (42), 14859–14866. Copyright (2005) American Chemical Society.

This can be explained in terms of the rigidity imparted by the molecular architecture at the solid-state, in which the bundled structure can disfavour non-radiative decays of the excited states. An investigation on a single layer of HBBNC **21** (Scheme 8) deposited on a Au(111) surface has been performed by the group of *Casu*.[140] The experimental study, assisted by computational findings, investigated the electronic structure of occupied and unoccupied states of BN-HBC and revealed similar features to those of hexagonal boron nitride-doped graphene. This makes borazine-doped PAH potential good candidates for the fabrication of 2D materials, hot topic in the field of organic electronics.

1.1.5.2 Materials for storage of H_2

Due to an increasing attention to the preservation of the environment, sustainability of production processes has become a key focus of modern science. The development of clean sources of energy is one of the most important challenges of the future, since it can soften, or possibly eliminate, the dependence of mankind from fossil fuels. In this context, H_2 has become an important candidate as a reliable long-term solution to such problem.[141,142] Although being possibly recognized as the cleanest energy source, its implementation in everyday life is prevented by technical issues related to its safe and economical storage.[143] The physical storage of H_2 inside porous materials or its chemical storage as product that can be released by a simple reaction, have arisen as possible solutions to solve this problem. The preparation of organic polymers with a defined porosity and high surface areas is considered of great potential for gas separation and storage.[144] More in detail, six polymeric species (Scheme 4, Scheme 6), containing the borazinic polar cores to improve H_2 absorption, have been recently synthesized by *El Kaderi*.[67,75,76]

Table 2. Morphological properties of borazine-doped polymers and their gas uptake performances.

Polymer	$SA_{BET}{}^a$ (m^2 g^{-1})	$P_{vol}{}^b$ (cm^3 g^{-1})	H_2 77 K (wt%)
2 (H)	1360	0.69	1.33
3 (H)	2244	1.08	1.93
6 (Cl)	1364	0.75	1.10
7 (Br)	503	0.30	0.68
8 (Cl)	924	0.67	1.30
9 (Cl)	1174	0.65	1.30
10 (Br)	849	0.57	0.98

a: Calculated by Brunauer-Emmett-Teller (BET) method. *b*: Calculated from nitrogen adsorption at $P/P_0 = 0.9$.

Their performances in terms of surface and gas uptake capability, are reported in Table 2. The hydrogen-bearing (**2** (H): 1360 m^2 g^{-1}; **3** (H): 2244 m^2 g^{-1}) and chloride-bearing polymers (**6** (Cl): 1364 m^2 g^{-1}; **8** (Cl): 924 m^2 g^{-1}; **9** (Cl): 1174 m^2 g^{-1}) displayed higher BET (Brunauer-Emmett-Teller) surface areas with respect to the bromo-borazine networks (**7** (Br): 503 m^2 g^{-1}; **10** (Br): 849 m^2 g^{-1}). At a first glance these results might seem controversial and surprising since, for instance, one would expect polymer **9** (Cl) to exhibit higher surface area respect to **6** (Cl). Most probably however, the trend is not

followed due to the amorphous nature of such species. Regarding the pore volumes (P_{vol}), the values (calculated at $P/P_0 = 0.9$) seem to be depending on the size of the substituents on the borazine cores as the H-bearing networks display the best results while Br-functionalized polymers give lower outcomes.

1.1.5.3 Materials for optoelectronic devices

Obtaining highly energetic emission from organic materials has been a major challenge. To obtain organic UV emitters, chemists relied on the principle of the "conjugation breaking".[41] In fact, shortening of the delocalization in conjugated molecules can lead to a HOMO-LUMO gap widening, resulting in an increase of the energy related to the electronic transition. A way to decrease the conjugation of all-carbon scaffolds is to replace carbon atoms with heteroatoms. In particular, doping with B-N couples has revealed to be very effective for the purpose, conferring an increased polarity whilst leaving the geometry of the structure unaffected.[41,49,51,145] Besides the insertion of BN couples, conjugated carbonaceous structures can be doped with borazines to obtain similar effects.[91,114,146–148] Having a large band gap (> 4 eV),[19,149] borazine-based organic molecules assume a certain importance as UV-emitting scaffolds. They represent nowadays highly valuable materials for the construction of organic light emitting devices (OLEDs) for the emission of UV and deep-UV light. *Bonifazi* and co-workers employed a borazine-based UV-emitter as active component in a light-emitting electrochemical cell (LEC).[91] When tri-*B*-phenyl-tri-*N*-mesitylborazine **45** was characterized in solution it displayed quantum yields of photoluminescence (Φ_{em}) of 6.6-7.7%, with little dependence on the solvent used. On the contrary, the solid-state emission spectra of **45** changed in relation to its crystalline structure (Figure 10). At high voltages, a weak emission was observed when aryl-borazine **45** was employed as emissive layer in the light-emitting electrochemical cell. Charge injection was also observed, and the current density J was found to be non-linearly dependent on the applied voltage V. With high voltages (~15 V) current densities of >100 mA·cm^{-2} were achieved. Encouraging results were also obtained when a LEC was fabricated. Although the device gave a rather weak electroluminescence (EL) quantum yield of ~10^{-4}%, it represented the first example of the use of borazine-based materials for the development of UV-emitting devices.
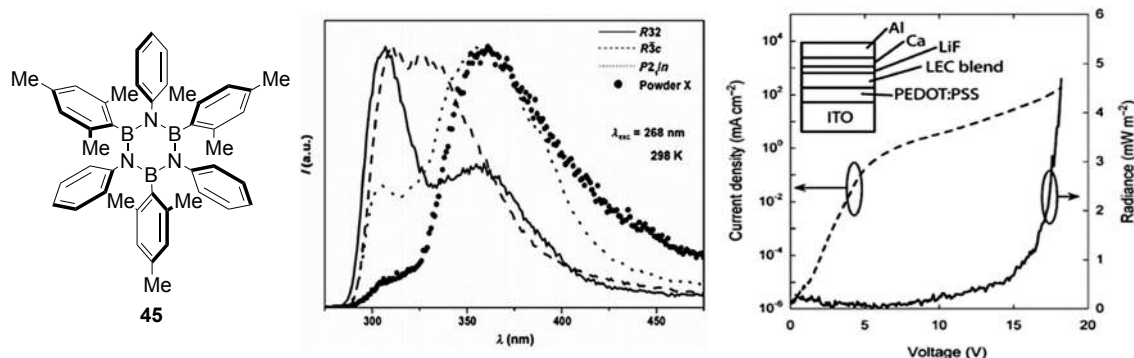
Figure 10. Left: Chemical structure of borazine **45**. Centre: Normalized emission spectra of the different polymorphs from molecule **45**. Space group R32 (solid line), R3c (dashed line), P2$_{1/n}$ (dotted line), and ground powder (full circles). Right: Current and radiance *vs.* light characteristics of the LEC incorporating borazine **45** as active layer, blended with polyethylene oxide (PEO, ion transporter), and LiOTf as mobile ions source. Device fabricated with vertical architecture ITO/PEDOT:PSS (poly(3,4-ethylenedioxythiophene):polydosium styrene sulphonate) (80 nm)/active layer/LiF (6nm)/Ca (30 nm)/Al(150 nm). Reprinted with permission from Kervyn, S.; Fenwick, O.; Di Stasio, F.; Shin, Y. S.; Wouters, J.; Accorsi, G.; Osella, S.; Beljonne, D.; Cacialli, F.; Bonifazi, D. *Chem. Eur. J.* 2013, *19* (24), 7771−7779. Copyright (2005) American Chemical Society.

The electronic properties of substituted borazine have been finely tuned by *Che* and co-workers introducing different substituents into the 'inner shell'.[19] This work describes the preparation of the five different derivatives **31** and **50-53** (Scheme 19) which, due to the encouraging values of hole and electron mobility displayed (10^{-6}-10^{-4} and 10^{-6}-10^{-3} cm^2 V^{-1} s^{-1} respectively), resulted suitable for the construction of optoelectronic devices.

31 R^1 = R^3 = R^5 = Ph; R^2 = R^4 = R^6 = H
50 R^1 = R^3 = R^5 = H; R^2 = R^4 = R^6 = Ph
51 R^1 = R^3 = R^5 = H; R^2 = R^4 = R^6 = Diphenylamino
52 R^1 = R^3 = R^5 = ^{t}BuPh; R^2 = R^4 = R^6 = Ph
53 R^1 = R^3 = R^5 = 1-Naphtyl; R^2 = R^4 = R^6 = H
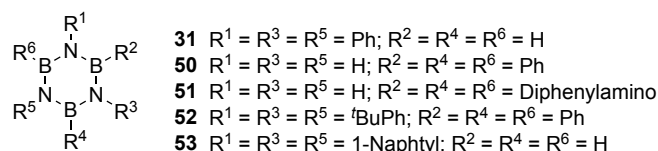
Scheme 19. Borazine derivatives tested for optoelectronic applications by *Che* and co-workers.[19]

When borazine **52** was employed as hole transporting material, the OLED device gave the characteristic yellow emission from Alq$_3$ (tris-(8-hydroxyquinoline)) and a luminance of 290 cd m^{-2} at 11 V, which can be increased up to 6200 cd m^{-2} at a higher voltage (21 V). In particular, the authors linked the high luminance at high voltage to the thermal stability of the borazine-based compounds.

1.1.5.4 Towards BN-doped carbon nanostructures

In modern applied science, graphene has emerged as one of the most studied materials.[26,27] The lack of a band gap is however impeding its use as semiconductor for the construction of optoelectronic devices.[24,26,150] The replacement of C=C units with B-N couples in fully planar structures is of great interest since it can provide an enlargement

of the HOMO-LUMO gap, while leaving the geometric features unaffected.[35,47,147,148,151–154] Before applying this strategy to graphene itself, many synthetic procedures for the doping of polymers[155–157] and small PAH derivatives with BN motifs were developed over the years.[46,83,158,159] In particular, BN-doped naphtalenes, anthracenes, and phenanthrenes were synthesized using different synthetic strategies such as cyclization-dehydrogenation,[160] $AlCl_3$-promoted electrophilic borylation,[48] or by reaction between bis-borabiphenyl and pyridazine precursors.[161] The first example of BN-doping of graphene was published by *Ajayan*.[41] In his report, embedding of hexagonal BN domains on sp^2 carbon monolayers was possible by chemical vapour deposition (CVD) of a mixture of methane and $BH_3 \cdot NH_3$ on a Cu surface. Different samples were analysed by UV-Vis absorption to evaluate the optical bandgap. A first sample having a C content of 65% showed a bandgap value of 4.48 eV, while in a second one where the C percentage increased to 84%, the measured bandgap decreased to 3.85 eV.
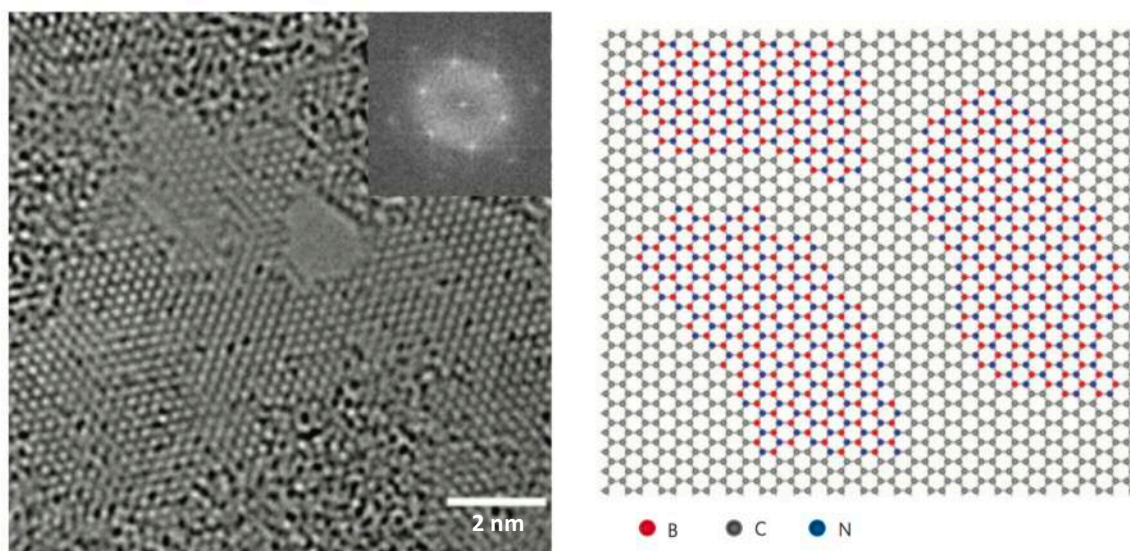
Figure 11. Left: HR-TEM image of a single layer portion of BN-graphene film. Inset: FFT pattern of the single layer region. Right: Atomic model of the *h*-BNC layer showing hybridized *h*-BN and graphene domains. Reprinted with permission from Ci, L.; Song, L.; Jin, C.; Jariwala, D.; Wu, D.; Li, Y.; Srivastava, A.; Wang, Z. F.; Storr, K.; Balicas, L.; Liu, F.; Ajayan, P. M. *Nat. Mater.* 2010, *9* (5), 430–435. Copyright (2010) Springer Nature.

Since pure hexagonal boron nitride (*h*-BN) shows a bandgap of 5.69 eV, this is a clear indication of the effectiveness of BN-doping for the bandgap opening of graphene. Despite being the first seed towards the construction of a BN-containing graphene sheet, the fact that different values of bandgap are observed means that different BN-graphene subspecies were formed, and no homogeneous blending of BN and carbon domains occurred. Other attempts aiming to obtain 2D-BNC hybrids featuring controlled blending

of BN and carbon domains by means of lithographical patterning,[162] patching growth,[163] and patterned regrowth[164] were reported. However, a perfect BNC "alloy" could not be obtained using either of these techniques. More recently, *Wang* et al. prepared BNC hybrid layers by pyrolysis of boron oxide, urea, and glucose at 1250 °C.[42] These BN-doped graphene sheets showed band gap values of 2-3 eV, and were used as photocatalysts for the water splitting under visible irradiation when coupled to a layered Ni-Co co-catalyst. Using a similar approach, the same group reported the synthesis of porous BNC nanosheets and their use for the oxidative dehydrogenation of alkanes such as ethylbenzene.[45] Using bis-BN cyclohexane as sole precursor, the growth of BNC monolayers on Ir(111) by annealing under ultrahigh vacuum, was reported by *Enders* and co-workers.[165] Undoubtedly, this last example represents the only report concerning the synthesis of a graphene monolayer featuring ordered BN-doping. However, the use of top-down approaches to form graphene substructures with defined and controllable shape and BN content has still to be perfected.

A recent breakthrough in this field came from a report published by our group.[114] In this, the bottom-up synthesis and characterization of HBBNC derivative **57** was described. Its synthesis started by formation of *B*-tri(2,6-diflurophenyl)-*N*-tri(4-xylylphenyl)borazine (**56**). This was prepared with 42% yield by reaction of *p*-xylylaniline **54** with BCl$_3$, and by following treatment with the lithium derivative of 2,6-difluorobenzene bromide **55**. Molecule **56** was then submitted to stepwise Friedel-Crafts-type reaction[166] in the presence of [*i*Pr$_3$Si·CB$_{11}$H$_6$Cl$_6$] and Me$_2$SiMes$_2$ in PhCl at 110 °C, yielding **57** in 5% yield (Scheme 20). Notably, the formation of side product **58** in 17% yield suggests that the planarization reaction proceeds in a stepwise manner, with the last aryl-aryl bond formation being the slow step. Therefore, HBBNC **57** was characterized by UV-Vis absorption and emission measurements in solution of CH$_2$Cl$_2$ at r.t., and compared to its full carbon congener **59** in the same conditions. As expected, molecule **57** showed an intense singlet emission (λ_{max}= 404 nm, Φ_F= 43%) and a high hypsochromic shift with respect to the much weaker emission from **59** (λ_{max}= 485 nm, Φ_F= 3%) . Notably, in the absence of O$_2$ the Φ_F value for **57** increased to 77%, while for **59** the Φ_F only increased at 5%. Moreover, molecule **57** displays solid-state fluorescence emission in the violet-blue region. As expected, a widening of the HOMO-LUMO gap by 0.53 eV was observed going from full-carbon **59** to molecule **57**.
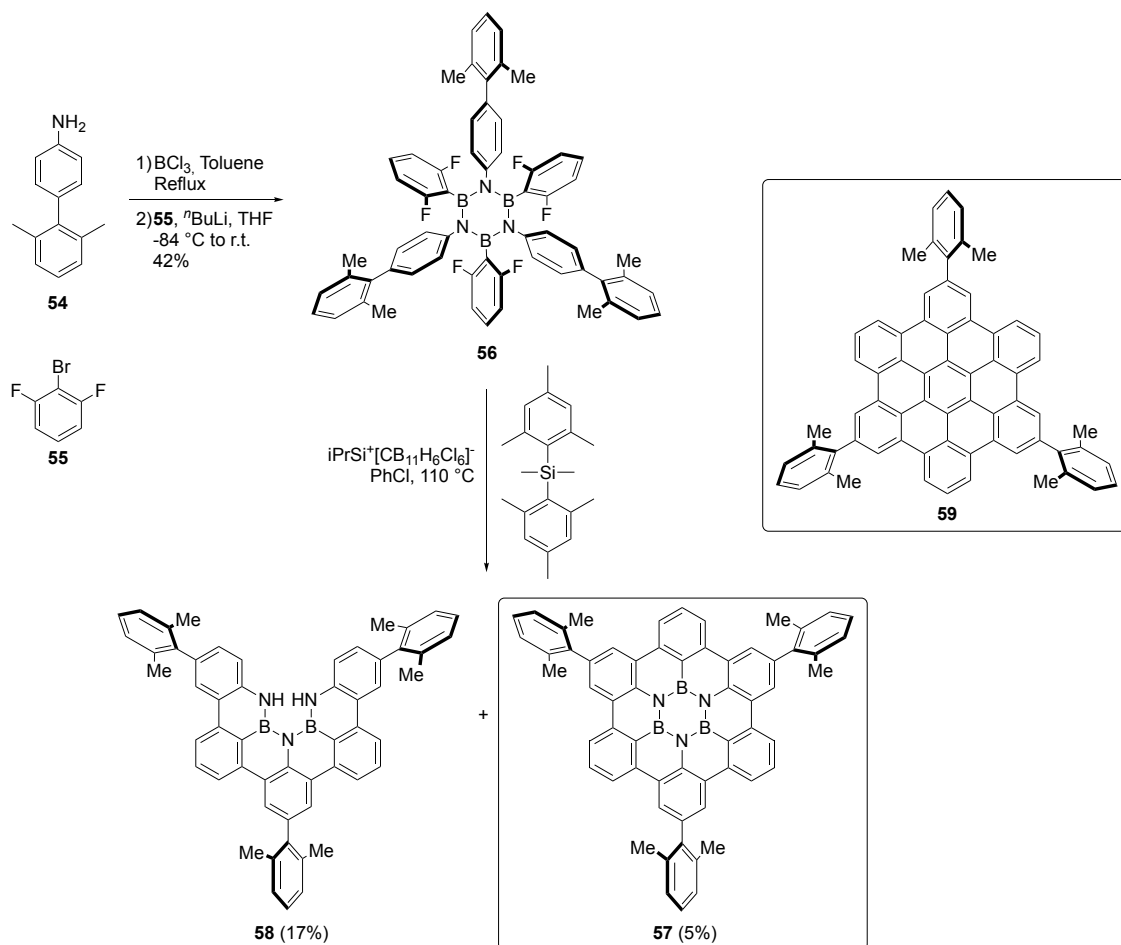
Scheme 20. Synthesis of aryl-borazine **56** and its planarization to give HBBNC **57**. Bottom-left: full carbon congener **59**.

This work represents the first in-solution synthesis of a borazine-doped PAH, and the first step towards the construction of 2D structures featuring embedded borazine units. Thanks to the development of a scalable methodology, this report will undoubtedly prompt future discoveries and developments in material science, particularly regarding the synthesis of borazine-doped graphenoid molecules.

1.1.6 General considerations on borazine and its derivatives

During the first part of the introduction of this thesis manuscript, the synthetic methodologies for the production and functionalization of borazine were explored. Along with these, the examples in the literature concerning the main applications of borazine derivatives were discussed. Regarding these examples, the use of the B_3N_3 moiety to modify the electronic features of carbon structures is of great importance. Indeed, it can allow the access to novel organic materials with tailored properties and to their use for optoelectronic applications. In this context, however, only the borazine-doping of small

molecules have been object of study. An investigation on the effects of borazine-doping of extended carbon-based polyarenes and polyaromatic structures is nowadays missing. This is rather surprising considering that branched polyphenylene-based nanoparticles possess a key role in material science, mainly being used for the construction of functional molecules and as precursors for nanographenes. Therefore, the borazine-doping of these structures would be of great interest as they would give important insights into the effects of heteroatom doping of large conjugated structures. In light of this, this thesis work focuses exactly on the doping of polyphenylenes with borazines. The objectives of this project, will be explained in detail after an introduction regarding the synthesis, properties, and applications of branched polyphenylenes.

1.2 Branched polyphenylenes

In the following section, the preparation and use of polyphenylenes (PPh) for the scalable and reproducible bottom-up synthesis of small-to-large functional nanostructures and PAH will be reviewed. Initially, an overview of the main synthetic methodologies used for the construction of full-carbon branched arene nanoparticles will be given. Following this, the main applications of functionalized PPhs will be detailed, with a particular focus on the studies concerning the effects of size and shape on the photophysical properties of dendrimeric systems. In the final part, the same consideration will be done also for PAHs, that can be synthesised with precise control starting from PPh precursors.

1.2.1 Overview and synthesis

Benzene rings can be connected in different ways to form a vast library of conjugated compounds[167] in which different sizes and degrees of branching are explored.[168] The term polyphenylene (PPh) indicates the class of chemicals composed by the repetition of benzene units. Of the mono-dimensional PPhs (Scheme 21), poly(*para*-phenylenes) are the most common. They are formed when phenyl groups are repeatedly connected at the -1 and -4 positions.

poly-(***para***-phenylene)   poly-(***meta***-phenylene)   poly-(***ortho***-phenylene)
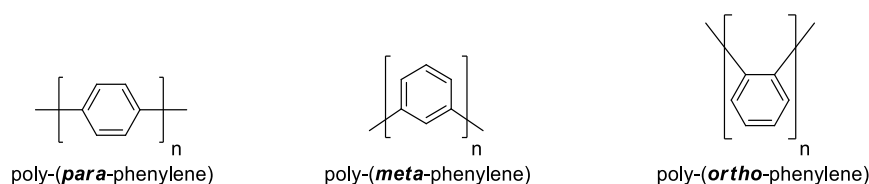
Scheme 21. Polyhenylenes with *para*, *meta*, or *ortho* connections.

These rod-like structures have a limited use due to their low solubility in the common organic solvents.[168] Introduction of alkyl chains as solubilizing groups avoided this problem, however they lead to an increase in the torsion angles in the phenylenic backbone.[169] As a main drawback, the disruption of the π-electron overlap results in an electronic localization and, therefore, in a decrease of the conjugation through the polymeric chain.[170] Oligo(*para*-phenylenes) and poly(*para*-phenylenes) were employed as chromophores, redox systems,[171−173] as luminescent materials in OLEDs,[174,175] or to study the effects of substituents and chain length on the electronic properties.[176] An early report from Kovacic showed the synthesis of poly-(*para*-phenylene) from benzene itself in presence of $AlCl_3$ and $CuCl_2$.[177] The process used was already known from the beginning of the century as "Scholl reaction".[178] In the following years, the explosion in the use of transition metals in organic synthesis led to the development of a series of novel reactions for the preparation of oligo- and poly-phenylenes.[179−186] Use of metal-catalyzed cross-couplings such as the Ullmann, Stille, Kumada, Yamamoto, and Suzuki reaction led to broadening in the synthetic scope for polyphenylenes. These reactions were employed in the production of poly-(*para*-phenylenes), and *ortho*-phenylenes with foldable architectures.[187,188] Moreover, *meta*-phenylenes were synthesised and used as blue and green phosphorescent materials,[23] or as amorphous polymers with high glass transition temperature.[24] Having briefly pointed out the main strategies to connect benzene rings to form mono-dimensional wires, the attention will now be focused on the main strategies towards the formation of branched oligomers and three-dimensional phenylenic dendritic networks. Radial growth from a central benzene can result in the formation of 2D networks.[191−193] In the early 90's the Co-[194−196] and Pd-catalyzed[191,197] cyclotrimerization of substituted acetylenes was revealed to be a rather versatile tool for the synthesis of hexaaryl benzenes. Acetylene and diphenylacetylene derivatives can be used as starting materials even bearing different functional groups such as aryl, alkyl or alkylsilyl groups, ethers, esters, and halides.[194] For this reason the cyclotrimerization reaction paved the way for the production of oligophenylenes which are soluble and open for further derivatizations. Another useful way of synthesising hexaarylbenzenes has been found in the decarbonylative Diels-Alder cycloaddition (Scheme 22).[198−200] The reaction is a inverse electron demand type cycloaddition with final extrusion of carbon monoxide and takes place between an acetynyl moiety (donor, dienophile) and a tetraphenylcyclopentadienone (CPD) derivative (diene, acceptor). This latter can be

easily prepared by base-catalyzed Knoevenagel reaction between benzil derivatives and substituted diphenylacetones.[200–202]
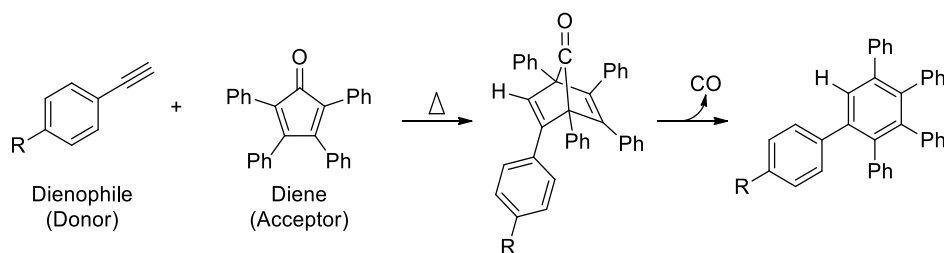
Scheme 22. General scheme of the inverse demand decarbonylative Diels-Alder reaction.

The reaction presents important advantages when performed in all-carbon scaffolds. The formation of the aromatic product is therefore promoted by the irreversible loss of CO from the bridged bicyclic intermediate, which makes this reaction quick and clean. Early reports show the use of this versatile and efficient tool for the production of a set of branched oligophenylenes and soluble polymeric phenylenes.[173,198,199,203–208] From the late 90's *Müllen* and co-workers took advantage of the D.A. reaction to build a series of PPh with a large variety of shapes and dimensions.[167,168,209,210] The strategy appears to be advantageous in comparison to the metal-catalyzed (2+2+2) cyclotrimerization since it allowed the synthesis of a vast library of monodispersed oligo- and poly-phenylenes with different and controllable sizes (1-6 nm) and branching degrees. Performing multiple cycloaddition reactions, different small oligophenylenes bearing solubilizing groups could be prepared in high yields (90-100% yields).[173,211–213] These molecules formed by the repetition of 2, 3 or 6 pentaphenylbenzene segments,[214] were only the starting point for a further study on the size growth of such species. Starting from central carbon cores bearing different branching units and by sequential peripheral coupling of small phenylene units to form extended architectures, the introduction of this class of chemicals in the world of dendrimers was possible. In particular, the role of the central carbon core in the dendrimer growth was studied (Scheme 23).[215]
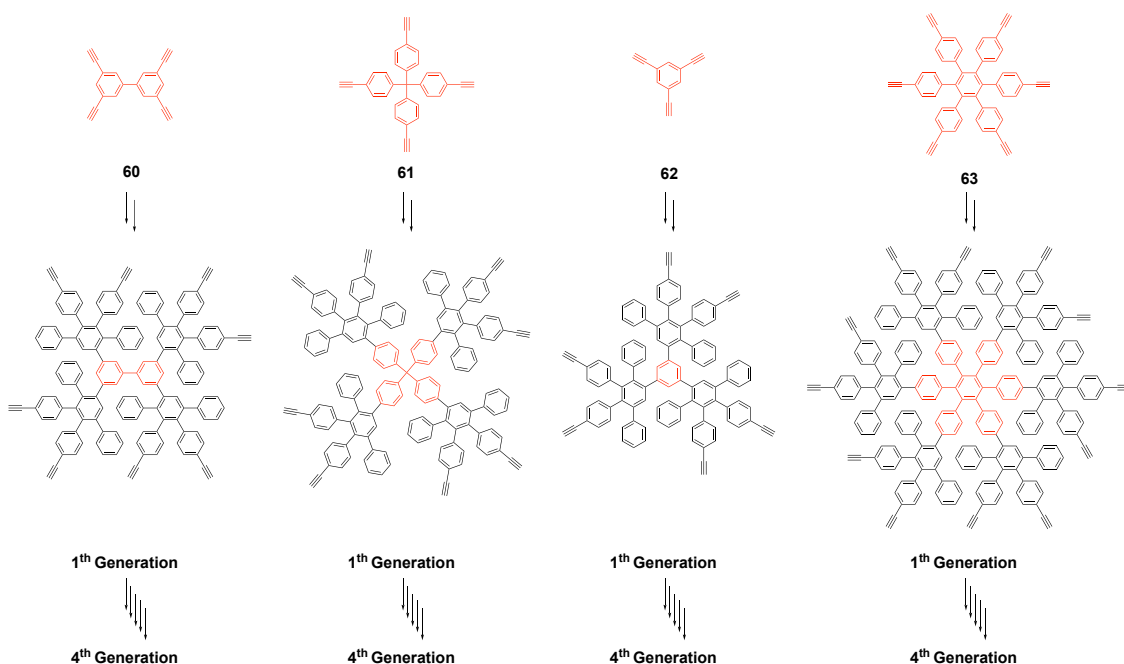
Scheme 23 Dendrimeric step-growth from biphenyl **60**, tetraphenylmethane **61**, phenyl **62**, and hexaphenylbenzene **63**.

Four different aromatic groups, differing in geometry and number of ethynyl functionalities were used as starting a starting point for dendrimer formation and submitted to sequential growth using CPD derivatives bearing protected ethynyl groups. The bulky protecting groups grafted to the CPD were then removed to leave ethynyl groups free of the steric hindrance and ready to react in the second growth step. Starting from 3,3',5,5'-tetraethynylbiphenyl (**60**), growth of a polyphenylenic dendrimer has been successfully achieved until the 4th generation.[215] The complete formation of the fifth-generation polymer was prevented by the very high degree of crowding reached in the outer shell of the structure. The study was furthermore enriched by using tetrakis(4-ethynylphenyl)-methane (**61**), 1,3,5-triethynylbenzene (**62**), and hexakis(4-ethynylphenyl)benzene) (**63**) as the central core. As for the first example, also starting from tetrahedral core **61**, triangular core **62**, and hexagonal core **63,** the synthesis of the 4th generation dendrimer was possible in a straightforward and efficient manner, but the prohibitive steric hindrance prevented further enlargement of the aromatic structure. This result proved that, for branched polyphenylenes, growth limitations are independent from the geometry of the core.[215] These defect-free polyphenylene nanoparticles have shown high chemical and thermal stability, with degradation observed at T> 500˚C according to TGA analysis under N_2.[209,215] Furthermore, by comparison with the linear poly-*para*-

phenylenes, branched polyphenylenes show increasing solubility upon growth as the branching prevents aggregation phenomena.[215–217]
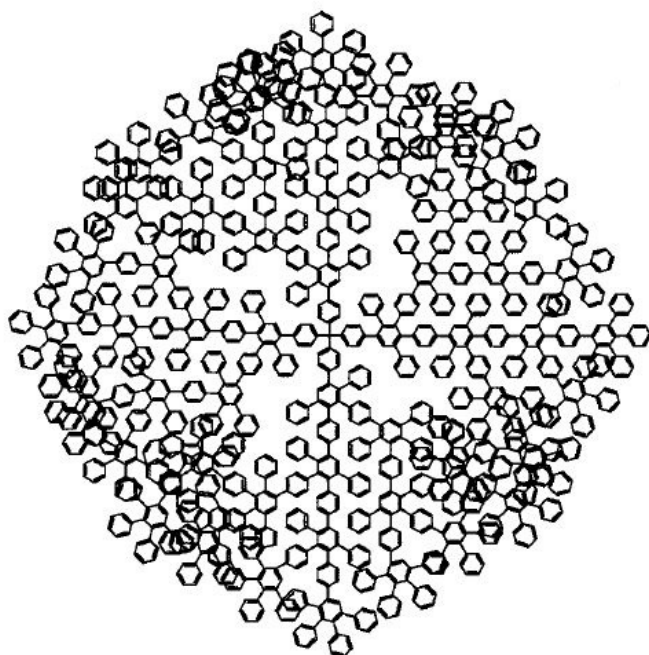
Scheme 24. 4th generation polyphenylenic dendrimer from tetraphenylmethane core **61**. Reprinted with permission from Zhang, H.; Grim, P. C. M.; Foubert, P.; Vosch, T.; Vanoppen, P.; Wiesler, U. M.; Berresheim, A. J.; Müllen, K.; De Schryver, F. C. *Langmuir* 2000, *16* (23), 9009-9014. Copyright (2005) American Chemical Society.

Atomic force microscopy (AFM) measurements shown diameters of 2.5, 3.8, 5.1, and 6.4 nm respectively for the 1st, 2nd, 3rd, and 4th generation of the dendritic molecule obtained starting from the tetrahedral core **61** (Scheme 24).[218,219] Deposition on highly oriented pyrolytic graphite (HOPG) of second generation dendrimer from tetrahedral core **61** led to the formation of parallel rods. A 2D crystalline monolayer was instead observed when depositing 2nd generation dendrimer from triangular core **62**.

The ease and reliability of the synthetic methodologies for the production of 3D PPh structures made these molecular modules of great interest in material science and in the development of functional macromolecular species. In particular, thanks to their structural features, PPh made from repeating pentaphenylbenzene units have proven their utility in a wide range of applications: from catalysis, to host-guest chemistry and optoelectronics. The use and application of 3D PPh molecules will be reviewed in the next section.

1.2.2 Applications and bottom-up construction of functional systems

The crowded outer shell of PPh nanoparticles, made from the repetition of pentaphenylbenzene units, forces the system to assume a persistent globular shape.[220] As a major effect, the intrinsic rigidity of the *para*-phenylene backbone and the hampered rotation of the phenyl groups, prevented complete and unhindered mobility of the branches. Pure PPh dendrimers can be produced with exceptionally precise size and shape control, yet functional moieties can be introduced in the inner part of the bulky structure. In this respect, the methodology using the Diels-Alder cycloaddition has been revealed to be an optimal strategy for the bottom-up connection of different molecular synthons bearing a wide range of functionalities.

1.2.2.1 Weakly coordinating ions

The exploration of the most representative literature examples starts with the field of weakly coordinating ions (WCIs), where ions shielded by bulky groups can display different properties with respect to the unshielded charged species.
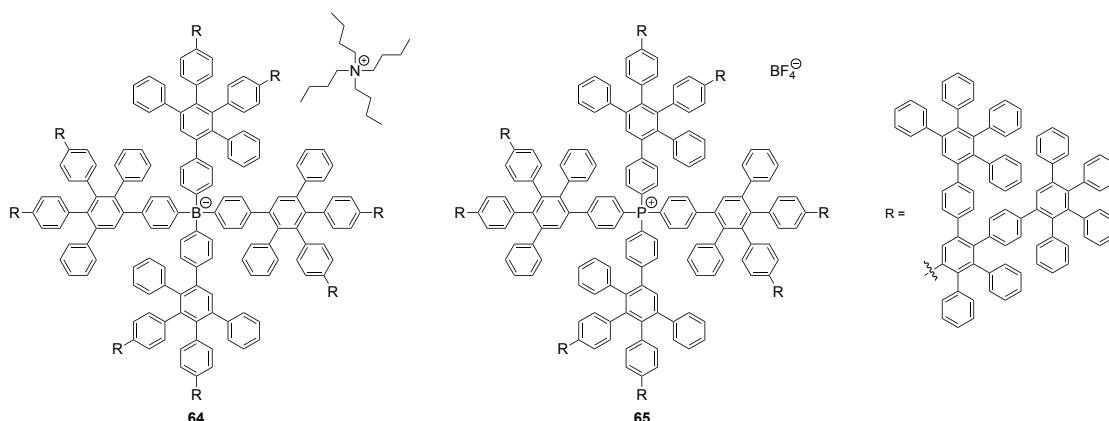
Scheme 25. Weakly coordinating tetraphenylboronate anion **64** and tetraphenylphosphonium cation **65**.

When a tetraphenylborate anion[221] or a tetraphenylphosphonium cation[222] were incorporated into a polyphenylenic dendrimer to produce derivatives **64** and **65** respectively (Scheme 25), ion dissociation and conductivity properties could be finely tuned. As result, the Coulombic interaction with the counterion decreased upon dimensional growth of the PPh periphery. Ultimately, the presence of the bulky organic shield made it possible to synthesise non-coordinating ionic species in low polarity environments. On weakly coordinating anion **66**, bearing photo-switchable azobenzene

moieties within the shielding scaffold, it could be possible to modify the hydrodynamic radius of the charged particle.[223]
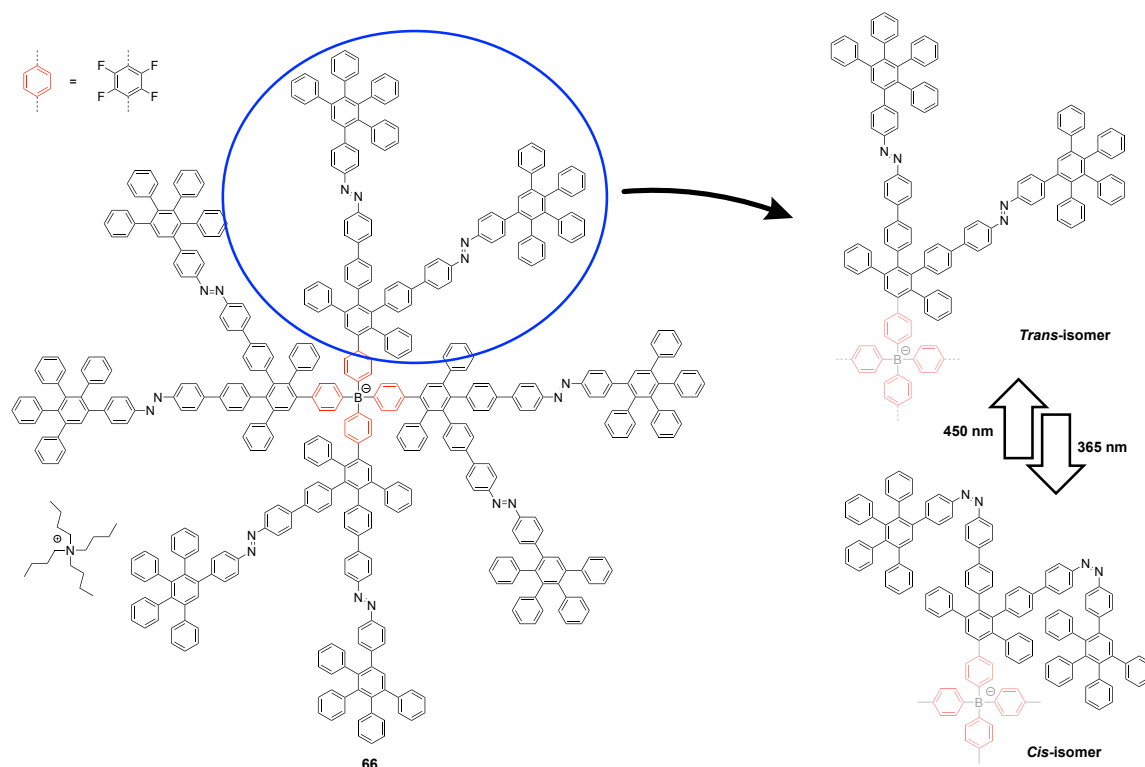
Scheme 26. Photoisomerization of azobenzene-branched dendrimeric PPh **66**.

After irradiation at 365 nm the azobenzene linkages assumed a *cis* configuration reducing the particle radius to 1.6 nm. Further irradiation at 450 nm restored the *trans* configuration, with a radius of 1.9 nm (Scheme 26). In this case, by controlling the size of the charged particle it was possible to influence ion-dissociation properties and conductivity.[223]

1.2.2.2 Bulky ligands for transition metals

Benzyl ethers and polyamide-based dendritic species with charged metallic cores of ruthenium were reported showing similar dendritic effects to polyphenylenes.[224,225] In particular, when 2,2-bipyridyl dendritic ligands were used, a more intense emission and longer excited state lifetimes were achieved although leaving the absorption and emission spectra unaffected. As a further effect of the steric protection, it was possible to observe a decrease in efficiency of the luminescence quenching by O_2.[224,225] A late version of these Ru-cored dendrimers bearing pure polyphenylene branching units was synthesized thanks to the Diels-Alder approach either by convergent or divergent strategy.[226]
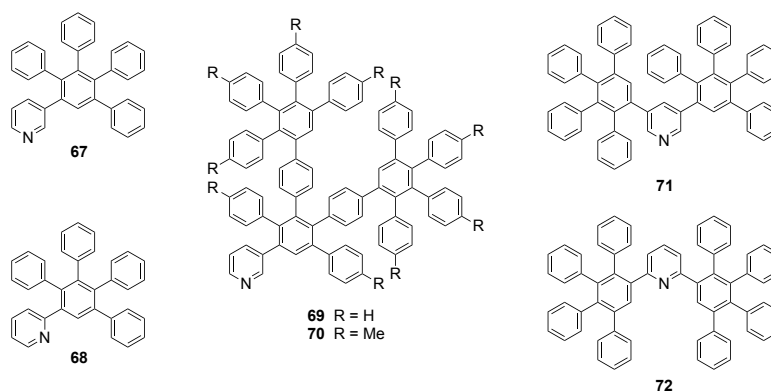
Scheme 27. PPh-based bulky ligands used to prevent Pd-black formation.

Other than Ru, also Pd, Rh, and Co complexes were also functionalized with PPh not only to prevent aggregation and oxidation but also to increase their solubility. When pyridyl ligands **67-72** (Scheme 27), bearing polyphenyl units were used to complex a Pd centre, the formation of Pd black through aggregation was completely suppressed while the catalytic activity towards alcohol oxidation remained unaltered.[227,228] Similarly, N-heterocyclic carbene ligands featuring 2,3,4,5-tetraphenylphenyl groups were used to improve the solubility of a Rh catalyst for the selective 1,4-hydrosilylation α,β-unsaturated ketones.[229] Starting from a (tetraphenylcyclobutadiene)-cyclopentadienyl Co centre it was possible to link pentaphenylbenzene units with different geometries (Scheme 28a), generating complexes **73**, **74**, and **75** with different sizes and properties. In-solution voltammetry studies showed that the oxidation potentials changed depending on the geometry of the outskirt of the complex, with a small but significant increase in the oxidation potentials (0.80-0.83 eV) going from the least to the most encumbered species.[230] For Co-phthalocyanine derivatives **76** and **77**, the functionalization with polyphenylene moieties resulted in the partial steric isolation of the metallic centre conferring selectivity towards binding of different pyridine-like ligands (Scheme 28, b).[231] Ligation of polyphenylenyl dendritic species with different sizes to an Ir(III) core resulted in the production of a red-emitting (λ_{em}= 621 nm) complexes which displayed electroluminescence in thin films. The shielding polyphenylene shell prevented aggregation-induced triplet-triplet annihilation. As a result, by increasing the size of the PPh branches, an enhancement of the photoluminescence quantum yield was detected, with Φ_{PL} values ranging from 6% to 9% going from the 1st to the 3rd generation complex.[232,233]
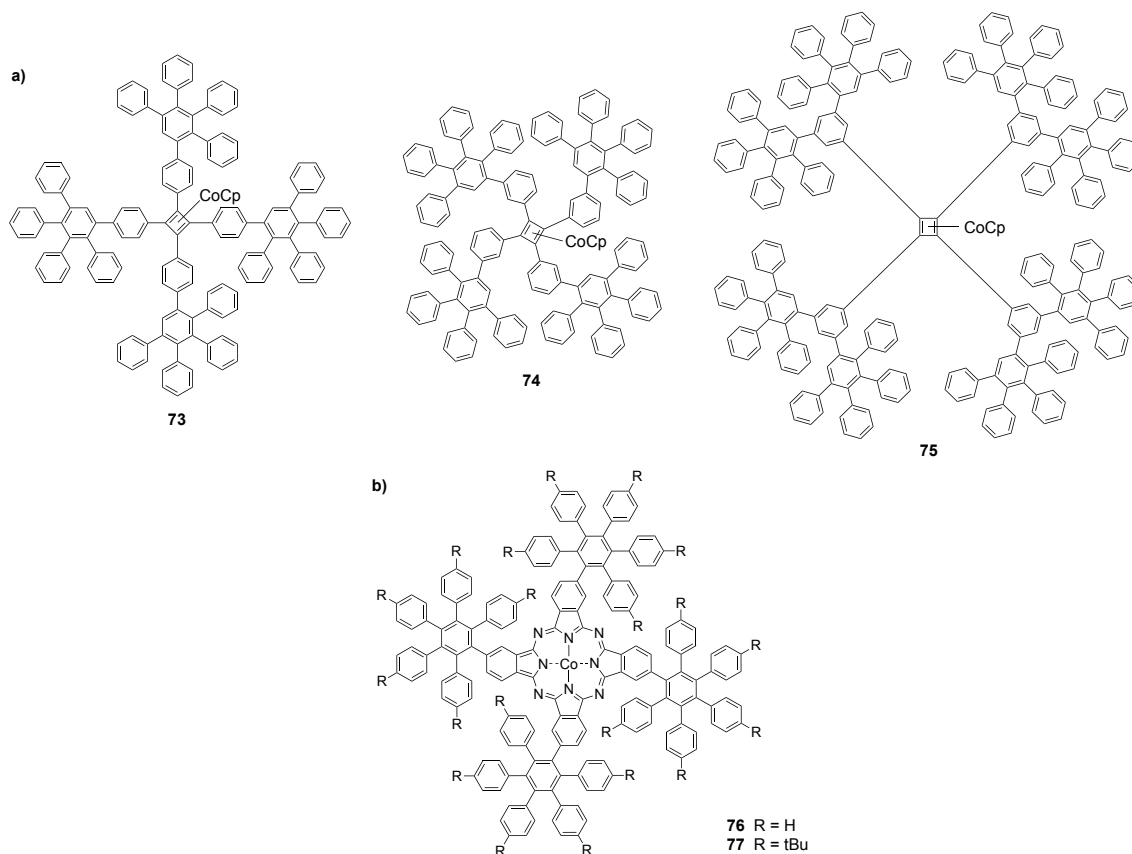
Scheme 28. Cyclobutadiene-cyclopentadienyl Co complexes **73-75** (a) and phtalocyanine-Co complexes **76** and **77** (b) centred dendrimeric PPhs.

1.2.2.3 Photophysical study of branched polyphenylenes

Despite being studied for their potential use in a wide range of applications, on only one occasion the rational interpretation of the relationship between the photophysical properties of such species and their morphological features has been discussed in detail. In 2003, *De Schryver* and co-workers have shown the dependence of the fluorescence on the size and steric congestion of the phenyl rings in the molecular periphery of these species.[234] Having prepared second- (**78**), and third-generation (**79**) dendrimers starting from a biphenyl core (Scheme 29, top), and second- (**80**), third- (**81**, Scheme 29, bottom) and fourth-generation (**82**, Scheme 30) dendrimers possessing a tetraphenylmethane core, absorption and emission measurements were carried out in CH_2Cl_2 and THF. Not surprisingly, in all the molecules investigated, the molar extinction coefficients increased in relation to the number of phenyl rings composing the structure (Figure 12). In fact, for **81** the extinction coefficient ($\varepsilon = 1 \times 10^6$ $cm^{-1}M^{-1}$) was double with respect to that of **80** ($\varepsilon = 5 \times 10^5$ $cm^{-1}M^{-1}$), while **82** displayed the highest value ($\varepsilon = 2 \times 10^6$ $cm^{-1}M^{-1}$).
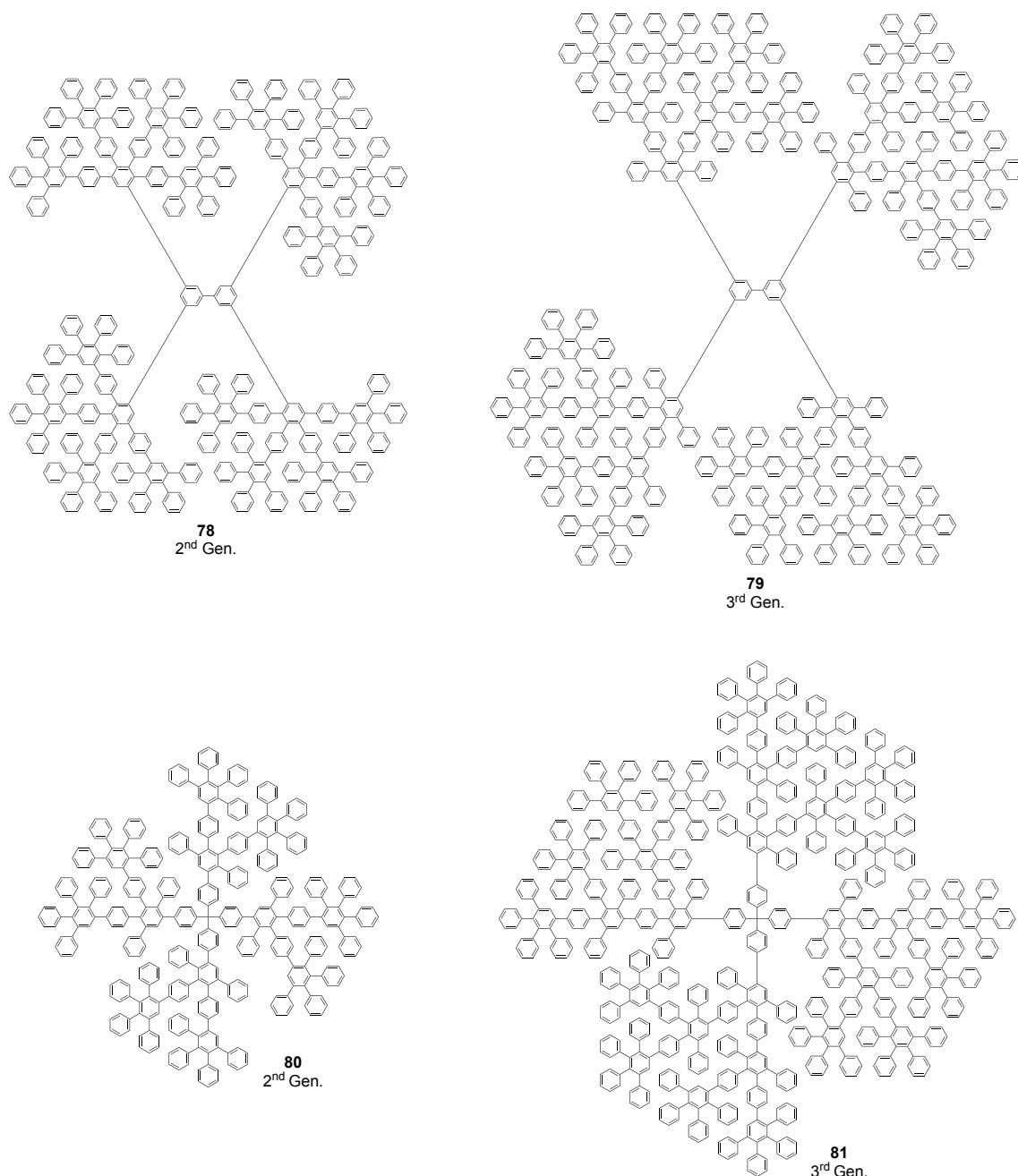
Scheme 29. Molecular structures of biphenyl-cored 2nd generation PPh **78** and 3rd generation PPh **79** (top), and molecular structures of tetraphenylmethane-cored 2nd generation PPh **80**, and 3rd generation PPh **81** (bottom).

Dendritic molecules **79** and **81**, with similar branching degree but different cores (biphenyl or tetraphenylmethane) show almost overlapping normalized absorption profiles, suggesting a negligible role of the core geometry on the phenyl-phenyl interactions (Figure 12b, inset). Indeed, the degree of branching seems to have an important effect on the absorption. When this parameter is increased to 4 (when four new oligophenylene units are added at every generation), the dendrimeric structure becomes more crowded.

82
4th Gen.
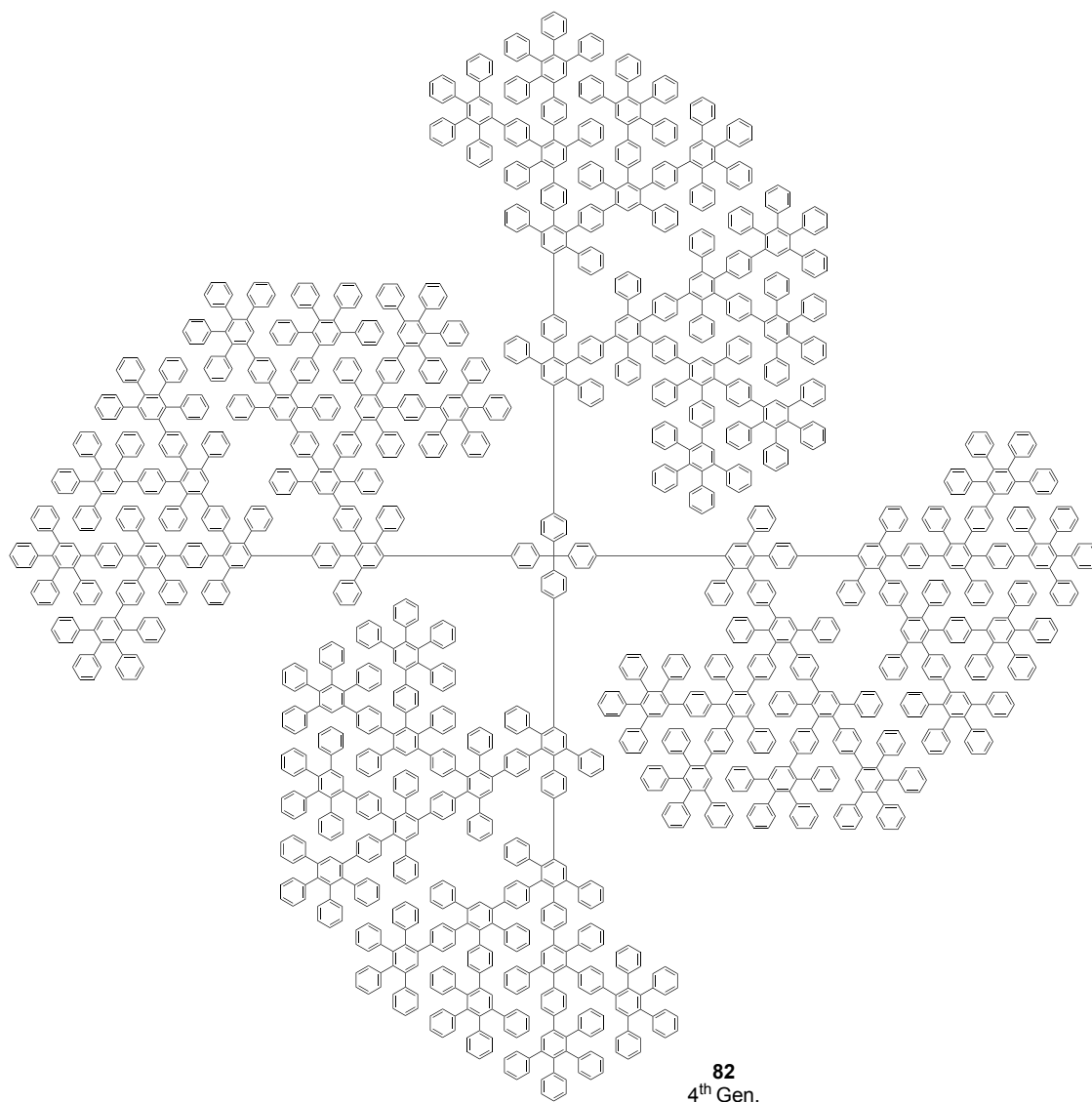
Scheme 30. Molecular structure of 4th generation PPh **82**.

As a result, stronger phenyl-phenyl interactions are generated, leading to a slight red-shift in the absorption spectra (Figure 12). Although composed by out-of-plane twisted phenyl units, branched polyphenylenes exhibit remarkable fluorescence (Φ_F= 17-46% in CH_2Cl_2, 18-45% in THF). The values of emission maxima and quantum yields (Φ_F) for the dendrimeric polyphenylenes, together with the emission spectra of the dendrimeric species and the excitation profile for **81** are reported in Figure 13.
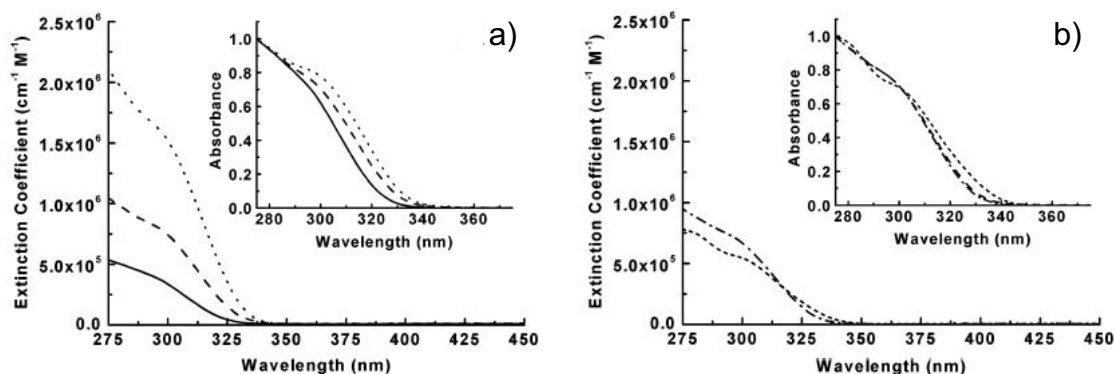
Figure 12. A) Extinction coefficients of dendrimers **80** (solid), **81** (dash), and **82** (dotted) in CH$_2$Cl$_2$. The inset shows the same spectra of **80**, **81**, and **82** normalized at 275 nm. B) Extinction coefficients of dendrimers **79** (dash dot) and **78** (short dash) in CH$_2$Cl$_2$. The inset shows the same spectra of **79**, and **78** normalized at 275 nm. Reprinted with permission from Liu, D.; De Feyter, S.; Cotlet, M.; Stefan, A.; Wiesler, U.-M.; Herrmann, A.; Grebel-Koehler, D.; Qu, J.; Müllen, K.; De Schryver, F. C. *Macromolecules* 2003, *36* (16), 5918-5925. Copyright (2003) American Chemical Society.

Dendrimer	λ_{max}, nm	Φ_F (%)	
		DCM	THF
80	362	17	18
81	363	28	30
82	366	25	27
79	365	24	26
78	368	46	45
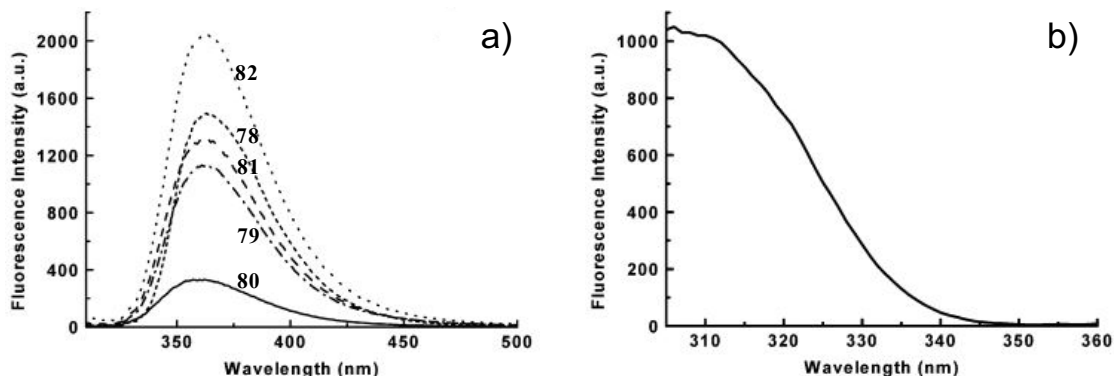
Figure 13. Table. Fluorescence maxima (λ_{max}) and quantum yields (Φ_F) of polyphenylenes **78-82** in CH$_2$Cl$_2$ and THF. A) Emission spectra of dendrimers **80** (solid), **81** (dash), and **82** (dotted), **79** (dash dot) and **78** (short dash) in THF (λ_{exc}= 310 nm). B) Excitation fluorescence spectrum of dendrimer **86** in THF (λ_{em}= 365 nm). Reprinted with permission from Liu, D.; De Feyter, S.; Cotlet, M.; Stefan, A.; Wiesler, U.-M.; Herrmann, A.; Grebel-Koehler, D.; Qu, J.; Müllen, K.; De Schryver, F. C. *Macromolecules* 2003, *36* (16), 5918-5925. Copyright (2003) American Chemical Society.

The studied dendrimers showed a strong emission in the near-UV region, and as a general tendency, an increase in fluorescence quantum yield is reported upon radial growth. Notably, the overcrowded molecule **78** showed a much higher fluorescence efficiency respect to species of same generation but with lower branching degree. This behaviour

can be related to the decrease of non-radiative decay pathways as a result of the higher rigidity of the system arising from steric congestion.

1.2.2.4 Phenylene-based energy harvesting systems

Since the discovery of the natural harvesting systems and the understanding of the sunlight energy gathering mechanism in plants and algae,[235–238] the prospect to mimic these highly efficient supramolecular natural architectures to produce clean energy has prompted a wave of research in the field.[239]
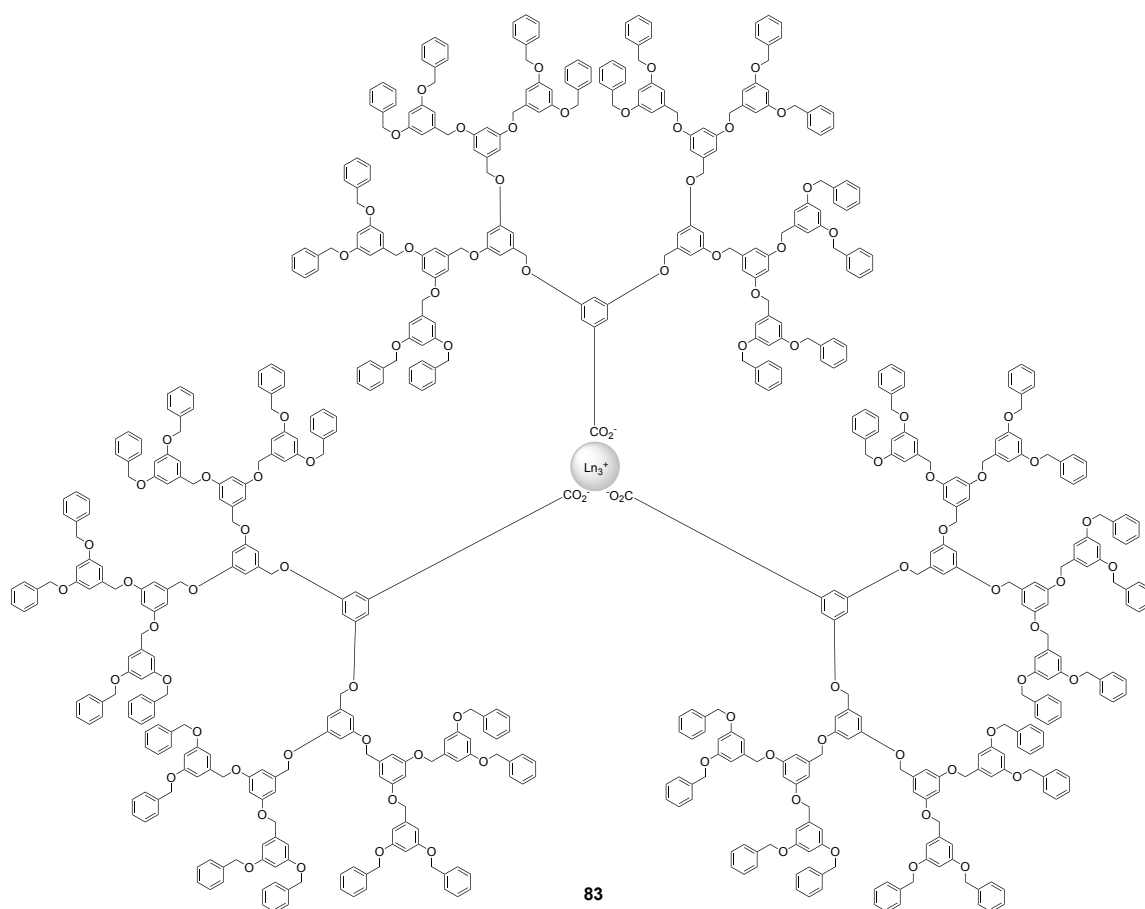
Scheme 31. Third generation lanthanide-cored polybenzyl ether dendrimer.

Similarly to natural antenna systems, artificial architectures are composed of donor molecules able to absorb high energy radiation, and acceptor moieties able to acquire energy from the donor fragments through energy transfer. These two counterparts can be connected at suitable distances by covalent scaffolds[239] or weak bonding interactions.[240] To have an efficient collection of radiative energy in form of visible light and a fast discharge to the acceptor functional centre, the systems must absorb light with great efficiency. Therefore, a great absorption cross section is required, resulting from a large

number of donor chromophores with high molar extinction coefficient (ε). When multiple chromophores compose the outside skirt of the system,[234,241,242] or the backbone as in the case of polyphenylene-based dyads,[243,244] hopping of the excitation energy must happen to favour an efficient and unidirectional energy transfer of the excitation towards the energy acceptor. Another important requirement for energy transfer to happen is the overlapping between the emission energies of the donor chromophore which absorbed light, and the absorption spectrum of the acceptor. To spread the chromophoric centres over space, maximizing the light absorbing area, the use of dendrimeric-type backbones has been revealed as a valuable option in many cases.[239,240] Surrounding luminescent molecules with dendritic structures can result in a double effect. If the dendrimeric backbone is capable of absorbing light at short wavelengths, it can discharge its high energy excitation to the central chromophore, acting as energy funnel. In addition, the steric protection provided by the branches attached to the central chromophore can hamper its aggregation, avoiding self-quenching phenomena thus boosting the emission output. *Fréchet* and co-workers encapsulated lanthanide cations (Er^{3+}, Tb^{3+}, and Eu^{3+}) into polyether dendrons (Scheme 31).[241,242] By increasing the interchromophoric distances, aggregation of these ions was drastically reduced. Ln^{3+} are indeed known to form clusters in the solid state leading to a weak fluorescence emission, a detrimental phenomena for their effectiveness as optical signal amplifiers for optical fibre communications.[245,246] Moreover, by selective excitation of the dendrimeric layer at 280-290 nm, a strong luminescence from the metallic core was observed (λ_{em}= 550 nm for Tb complex, 617 nm for Eu complex) together with enhancement of the emission intensity upon increase of the size of the organic periphery. This is possible thanks to an energy transfer process from the branches to the central ion. In particular, branch-to-core channelling of energy was more efficient for Tb^{3+} than for Er^{3+}, due to the better overlap between the dendrimer emission with the Tb^{3+} absorption. Singlet energy transfer could also be observed when the same branches were attached to organic molecules. Excitation at λ_{exc}= 280 nm of porphyrin-cored system **84** (Scheme 32) resulted in the emission of the sole central chromophore (λ_{em}= 656, 718 nm), which was responsible for the total quenching of the fluorescence coming from the branches.[247]
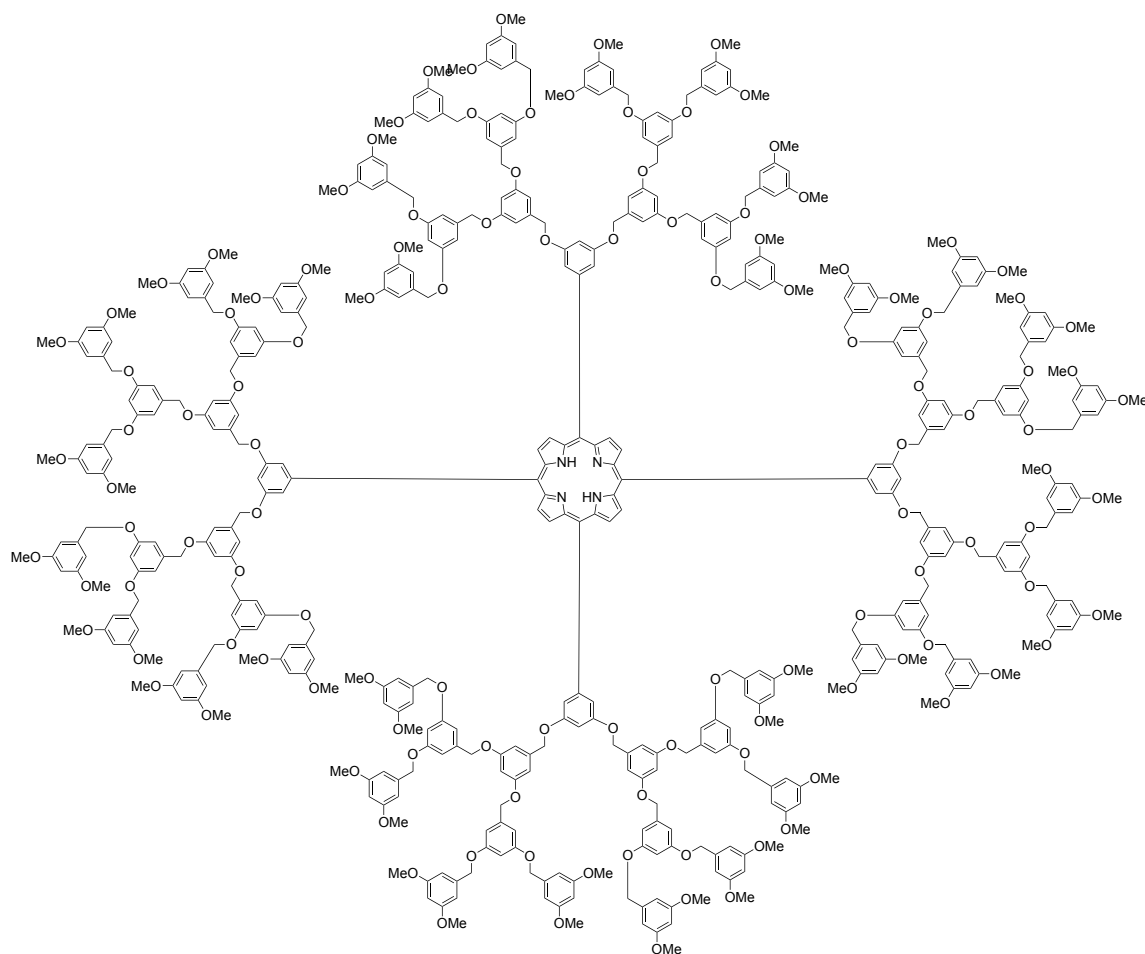
84

Scheme 32. Porphyrin-cored polybenzyl ether dendrimer **84**.

Notably, a dropping of energy transfer efficiency was detected when the porphyrin was only partially substituted with branched fragments. This indicates a relevant incidence of flexibility and conformational freedom on the energy hopping process, with the only sterically congested high-generation dendrimers being able to retain their properties at high temperatures.[247] Efficient energy transfer from a dendrimer-like network to a central full-organic chromophore was reported for the first time in 1993. *Moore* and co-workers covalently linked phenylacetylene dendrimers up to the 6th generation to a perylene core (Scheme 33, top).[248–250] Dendrimers similar to **85** showed absorption localized in the 250-470 nm range, with progressive enhancement of the molar extinction coefficient going from the first generation ($\varepsilon = 8.0 \times 10^4$) to the 6th ($3.5 \times 10^6$ cm^{-1}M^{-1}).[251] The luminescence displayed by the branched poly(phenylacetylene) systems at 350-450 nm could be totally quenched by connecting perylene to the structure. This was acting as energy sink, subtracting the excitation energy from the branches, and discharging it by emission of light at longer wavelengths (450-600 nm).
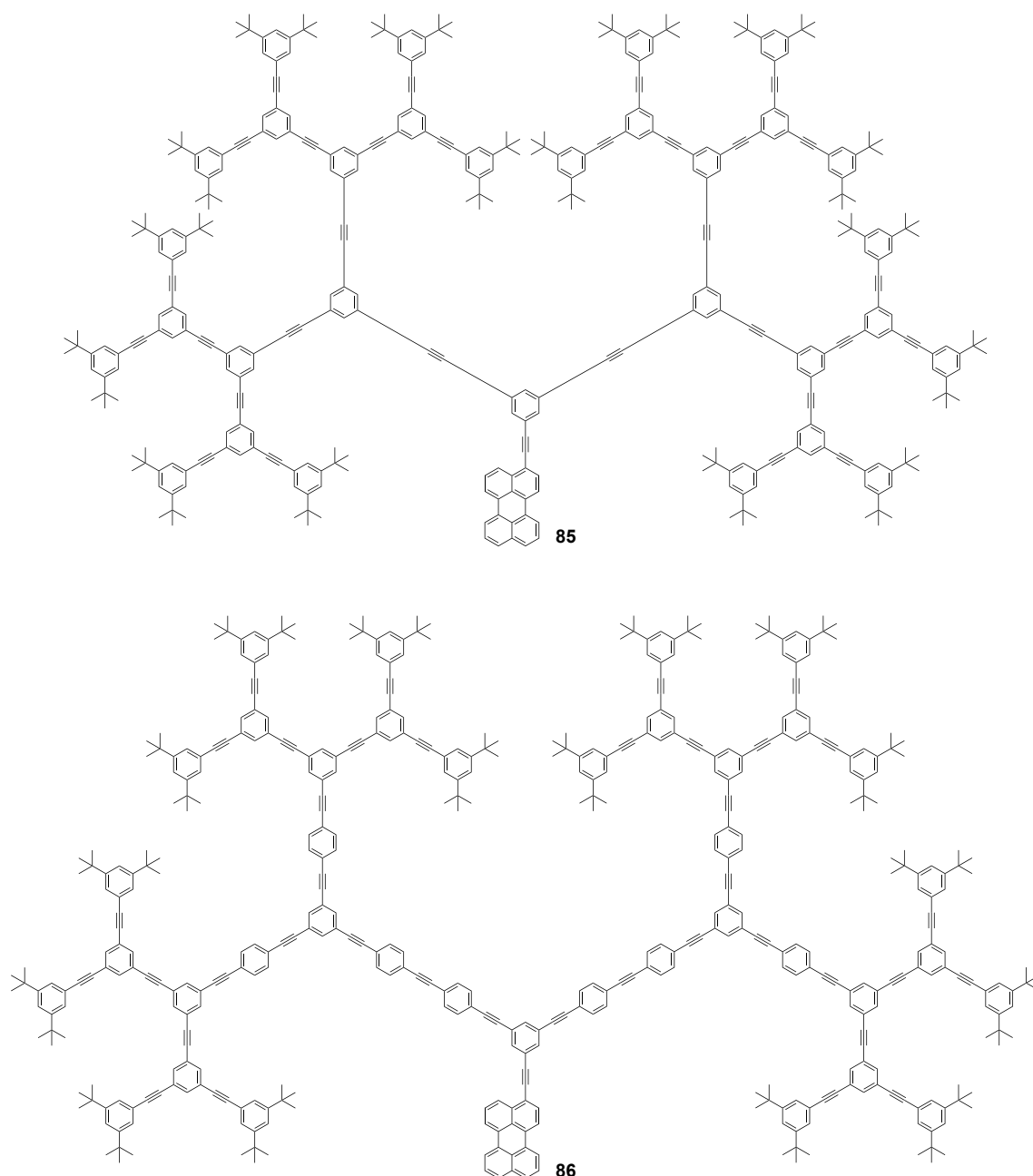
Scheme 33. Structure of the perylene-cored poly(phenylacetylene) dendrimers **85** and **86**.

In a further development, an energy gradient was created over similar dendritic nanoparticles by progressive elongation of the conjugated polyacetylene fragments when going from the outskirt to the core of the branched structure (Scheme 33, bottom).[252,253] As a result, a quantitative energy transfer could be obtained in **86**. Branched polyphenylenes have already been exploited as semi-rigid scaffolds for the covalent support of multichromophoric systems (see section 1.2.2.4).[254–256] In this respect, the structural rigidity of dendritic polyphenylenes provided steric shielding and optimal spacing between the chromophoric centres. For example, formation of aggregates could

be avoided for an NDI derivative by insertion of the dye into the core of a branched polyphenylene structure.[257] As result, fluorescence quenching due to formation of aggregates could be prevented in both solution and solid state. In addition, since these materials do not show absorption nor fluorescence at wavelengths above 400 nm, they cannot interfere with the absorption and emission activity of dye molecules.
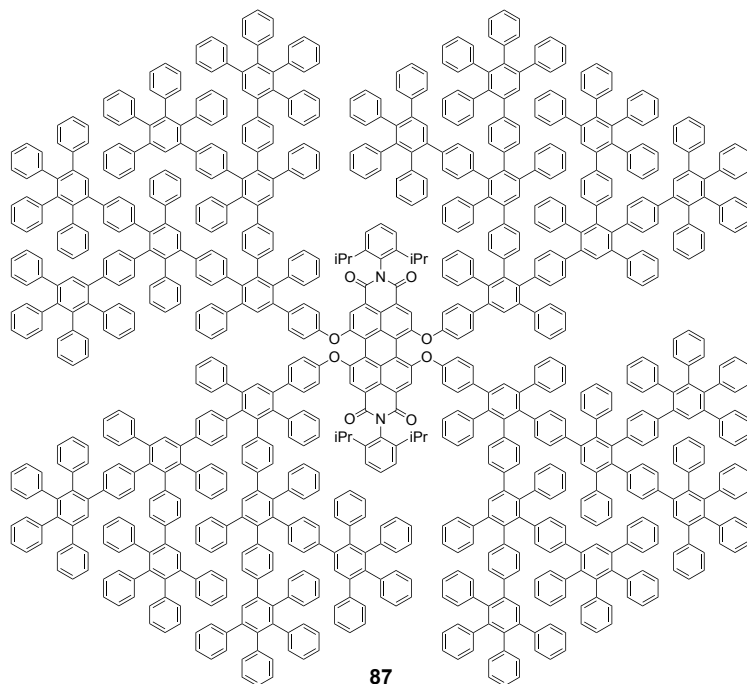
Scheme 34. Perylenediimide (PDI) **87**, functionalized with third generation polyphenylene dendrimeric branches.

When dendritic polyphenylene branches are grafted to perylenediimide (PDI) centres (molecule **87**, Scheme 34), efficient energy transfer towards the organic dye was observed.[234] Indeed, by shining light at 310 nm, emission in the visible region (λ_{em}= 610 nm) from the PDI core was predominantly observed. This clearly indicates a transfer of energy from the polyphenylene branches to the PDI core. Furthermore, when directly exciting the polycyclic diimide at 530 nm, a decrease in fluorescence quantum yield ($\mathbf{\Phi_F}$= 95 to 57%) could be observed upon growth of the branches, as the bulkiness of the substituents tends to favour nonradiative deactivation pathways. Notably, a negligible residual fluorescence centred at 365 nm could be observed for the PDI-polyphenylene dendrons of larger dimension. This phenomena indicates that there is a distance limit from the central chromophore at which energy transfer is occurring, and the excited states generated at the periphery of the dendron tend to deactivate through emission.[234] In other examples, pyrene[258] and PDI[257,259] cores were encapsulated into polyphenylene shells,

once again proving the strategy to be reliable and efficient in averting chromophore-chromophore interaction. Moreover, also in such systems the energy absorbed by the polyphenylene branches was transferred to the central chromophore, which displayed efficient emission upon selective excitation of the PPh structure at 310 nm.[257–259]
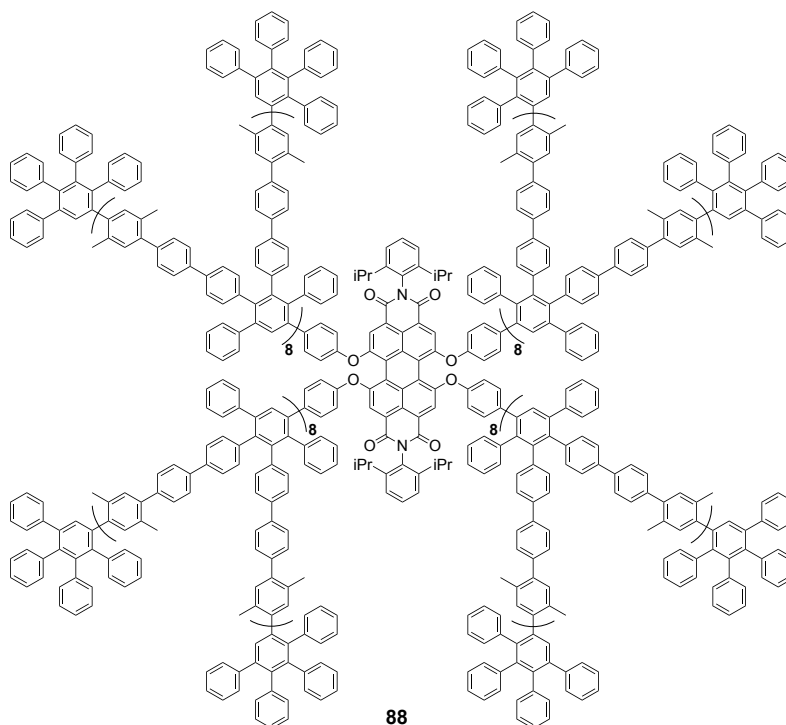
Scheme 35. Structure of 9th generation PDI-cored PPh dendrimer **88**.

The dendrimeric step growth was taken to the limit with the synthesis of a 9-generation perylenediimide (PDI) cored PPh **88** (Scheme 35). Transmission electronic microscopy (TEM) revealed a maximum diameter of 33 nm for the higher generation dendrimer.[260] In another set of reports, the synthesis of branched PPhs was undertaken in which chromophore molecules were grafted in different locations in the periphery.[261–269] Taking advantage of the same synthetic strategies and exploiting the structural rigidity of the branched polyphenylene, multi-chromophoric systems were developed in order to study and mimic the natural antennae systems. As the supramolecular interactions in natural energy-gathering systems,[270–272] in these artificial versions of antennae the PPh scaffolds were used to keep different chromophores at a given distance and in a given relative position. In this way, cascade energy transfers between the chromophoric units would be allowed and promoted. For this, chromophoric triad **89** was developed featuring a TDI (terrylenediimide) core, perylene imides in the inner shell and naphthalene imides in the

periphery (Scheme 36). The design of this light harvesting system, able to absorb over the whole visible spectrum, promoted a stepwise energy transfer from the high energy naphthalene absorbers (λ_{abs}= 370 nm) in the external part of the nanoparticle, to the internal perylene units and finally to the central TDI, which emits at λ_{em}= 701 nm.[254,273,274]
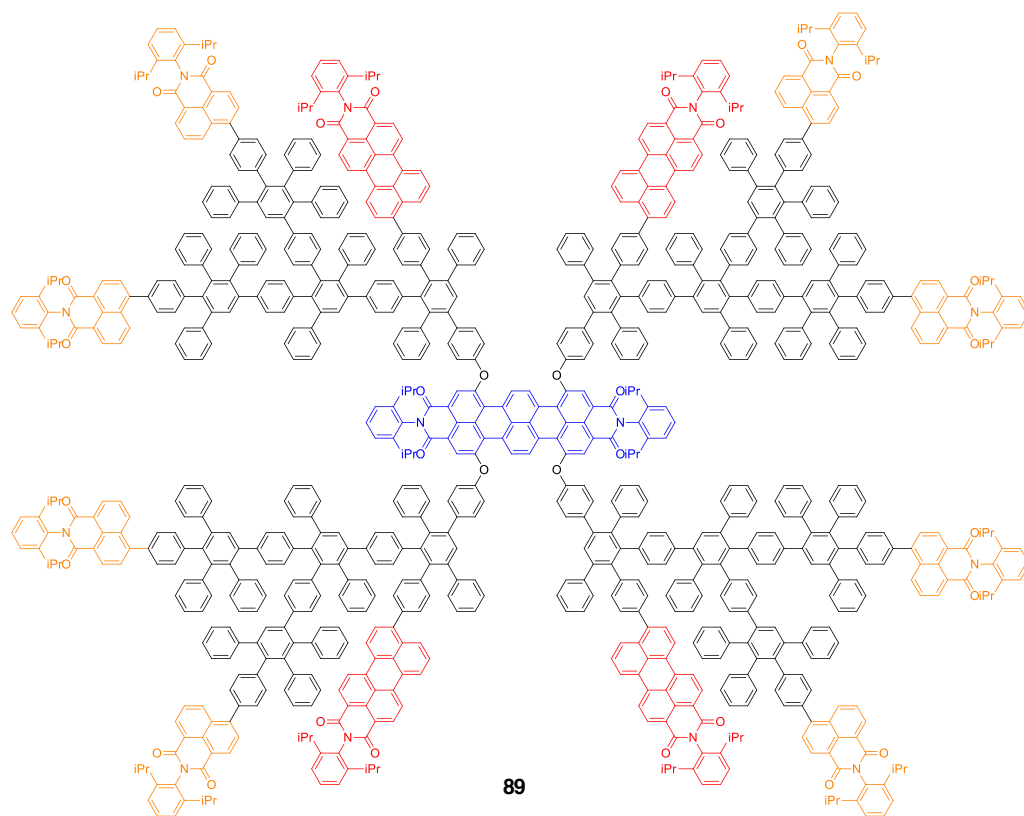
Scheme 36. Structure of TDI-cored multichromophoric PPh **89**.

Using essentially the same strategy and having a similar design, dendrimer **90** (Scheme 37) was made starting from pyrene at the core, triphenylene branches in the shell, and triphenylamine (TPA) at the surface of the particle.[275] The design produced a four-fold enhancement of the luminescence quantum yield in both solution and thin film with respect to the dendrimer without the core emitter. Moreover, when used as emissive material in a OLED device, this triad displayed efficient blue emission (λ_{em}= 463 nm) also thanks to the surface TPA groups that helped both hole capturing and injection ability.

90
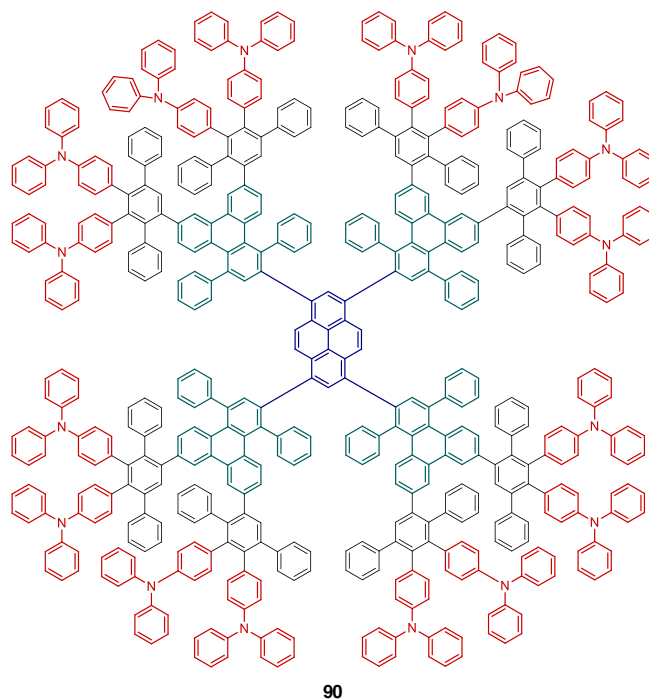
Scheme 37. Pyrene-cored blue-emitting triad **90**.

More recently, the role of the surface group was further reviewed studying different amino-groups and aza-heterocycles to optimize the performances of the multichromophoric blue emitter.[276]

1.2.2.5 Precursors for graphene substructures

In the specific case of optoelectronics, branched polyphenylenes were also used as starting materials for the bottom-up generation of fully-planarized graphene substructures.[167,209] Through the simple synthetic routes involving Diels-Alder cycloaddition[198–200] or transition-metal-catalyzed cyclotimerization,[191,194–197] 3D polyphenylene precursors could be synthesized with precise control over size and shape. Planarization of these systems could be achieved with high yields (>80%) thanks to a series of mild oxidative cyclodehydrogenation procedures involving $FeCl_3/CH_3NO_2$, $CuCl_2/AlCl_3/CS_2$, or $Cu(OTf)_2/AlCl_3/CS_2$,[212,277] to give large polycyclic aromatic hydrocarbons (PAHs) with a wide range of shapes and properties (Scheme 38). Thanks to this bottom-up approach, a fine tuning of the optoelectronic properties was obtained, and reduction of the HOMO-LUMO gap was observed upon enlargement of the planar structures.[278]
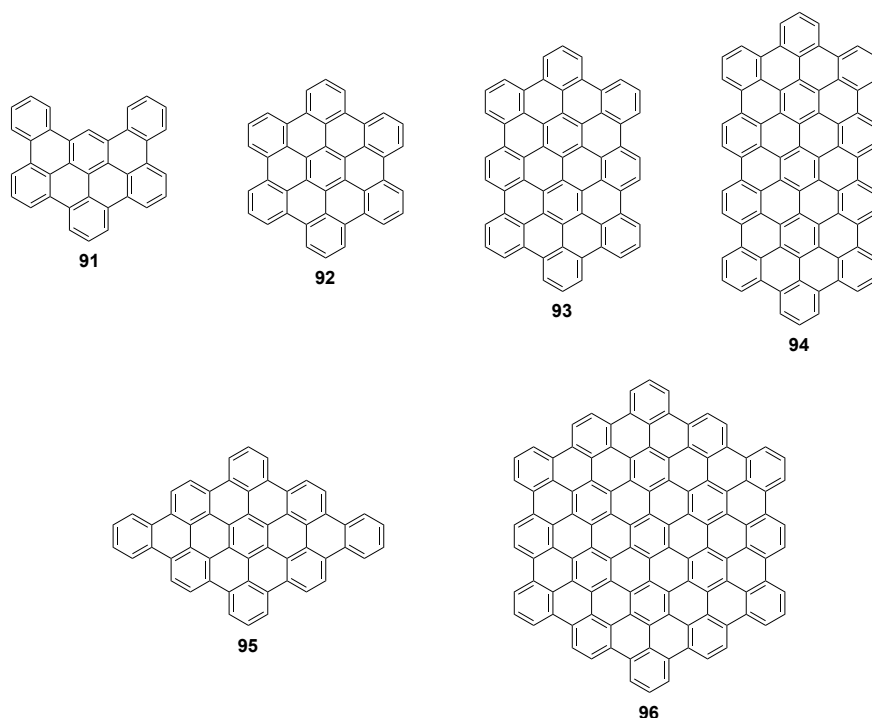
Scheme 38. Representative graphene sub-structures having different sizes.

For example, PAHs **98**, **100**, and **102** were obtained with 75, 87, and 89% yields, respectively, employing $Cu(OSO_2CF_3)_2$ and $AlCl_3$ in CS_2 at r.t. (Scheme 39).[278] UV/Vis spectra of these derivatives revealed a red shift of the absorption maxima upon size enlargement, with λ_{abs}= 387, 415, and 440 nm for **98**, **100**, and **101**, respectively.
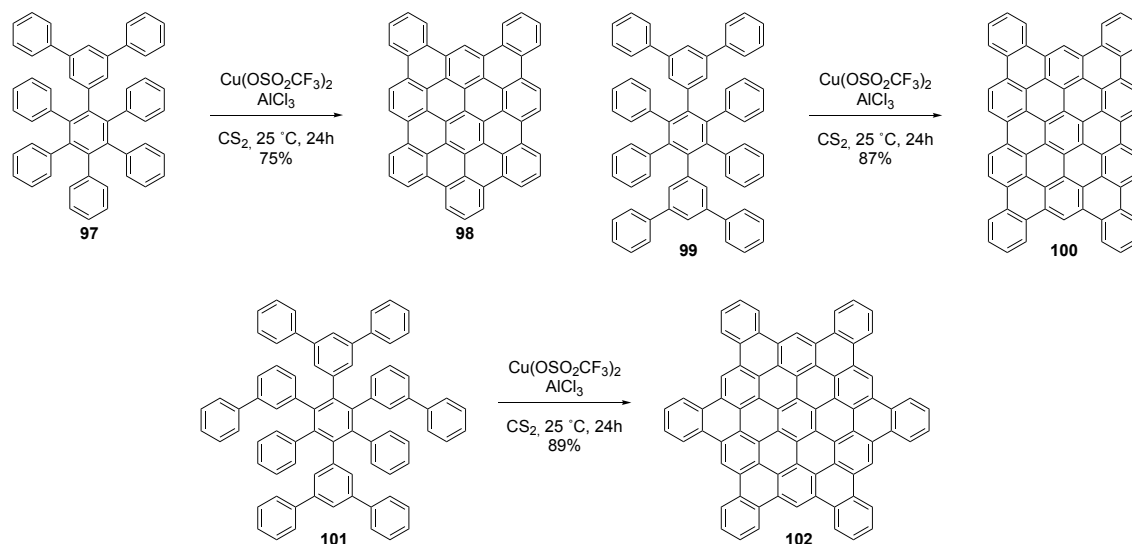
Scheme 39. Synthesis of PAHs **98**, **100**, and **102** by oxidative cyclodehydrogenation.

The use of polyphenylenes for the scalable and reproducible bottom-up synthesis of small-to-large PAH domains, has been regarded as a fundamental breakthrough providing

access to materials with similar chemical nature but different physico-chemical and optoelectronic features.

1.2.3 General considerations on branched polyphenylenes

Thanks to their structural features, stability, and photophysical properties, oligo- and poly-phenylenes have been continuously studied for the last five decades. During this introduction, examples regarding their use as functional molecules, and precursors for the bottom-up synthesis of large PAHs and graphene substructures, have been discussed. The results achieved in material science and the production of a large number of functional polyphenylene molecules must be attributed to the possibility to control size and shape of these species thanks to the use of the decarbonylative Diels-Alder cycloaddition. However, despite the extensive studies on these branched polyarene scaffolds, the possibility to modify the composition and electronic features through doping with borazine, has never been taken into consideration. Therefore, it is the intent of this thesis project to fill this gap by using B_3N_3 as a versatile building block, just like benzene, for the construction of large borazine-PPh structures. In the next chapter, the aims of this work, together with the envisaged strategies to accomplish them, will be disclosed.

Chapter 2: Aim of the work

2.1 Bottom-up synthesis of BN-doped polyphenylenes having different doping dosage and orientation

Given the chemical stability of polyphenylenes and yet, their ease of functionalization, these carbon-based structures have been used for a wide range of applications (see section 1.2.2). In spite of this, the photophysical properties of unsubstituted polyphenylenes have never been thoroughly exploited.[234] To the best of our knowledge, no study taking in account the modification of the photophysical properties of this UV-emitters is currently present in the literature. Fine tuning of the chemical and optoelectronic properties can be achieved in conjugated molecules exploiting different synthetic tools, for instance, by functionalization with electron-withdrawing or electron-donating groups.[279–281] However, the replacement of carbon atoms with iso-structural and iso-electronic elements is regarded as one of the most successful and effective ways to modify the electronic properties of π-conjugates.[35,47,151,152] In this context, the doping of small polycyclic aromatic hydrocarbons (PAHs) with boron and nitrogen leads to a perturbation of the electronic conjugated cloud conferring polarity to the system, and altering the HOMO-LUMO gap without affecting the geometry of the molecule. The interest in the field was prompted by the successes in the synthesis of scaffolds doped with a single[50,52,282] or double[283] BN pairs, or with NBN, BNN, BNB, NBNB, NBBN, or BNNB motifs,[284] which proved the effectiveness of boron and nitrogen doping in the modification of the electronic features,[47,284] and in the development of heteroaromatic species with catalytic properties.[285] The full replacement of a benzene ring with borazine and its effect on the electronic properties of small oligophenylenes have been already studied in our group (see section 1.1.5.3).[91] Hexaphenylbenzene displayed a fluorescence with maximum value at 330 nm and quantum yield ($\mathbf{\Phi_F}$) of 0.5% in CH_3CN, while for its borazine-doped analogue **43** (Scheme 16) a three-fold increase in the value of $\mathbf{\Phi_F}$ could be observed. Tri-*N*-phenyl-tri-*B*-mesitylborazine **45** (Scheme 17) showed the highest value of the series ($\mathbf{\Phi_F}$= 7.2%). In addition, the maximum of fluorescence for the latter was reached at 310 nm, highlighting a hipsochromic shift of ~20 nm with respect to the all-carbon counterpart.

Given the differences in electronic properties between hexaarylborazine derivatives and hexaphenylbenzene, one can anticipate that the partial replacement of benzene rings in

larger PPh structures with their inorganic BN analogues can lead to a modification of the optoelectronic properties. With this in mind, the first objective of this thesis work is the connection of hexarylbenzene and hexaarylborazine building blocks to form BNC hybrid PPh derivatives featuring different doping parameters (Scheme 40). Hence, these derivatives will be submitted to a detailed study on the absorption and emission properties in order to gather important insights on the effects of borazine doping on branched polyphenylene structures.

From a synthetic point of view, the preparation of these derivatives is inspired by the same approaches used for the bottom-up synthesis of functional semi-rigid polyphenylenes (see section 1.2). Indeed, one can think of connecting different reactive partners bearing ethynyl (**R1**, **R2**) functional groups and tetraphenylcyclopentadienyl (CPD) moieties (**R3**, **R4**), to form a PPh framework through Diels-Alder cycloaddition.
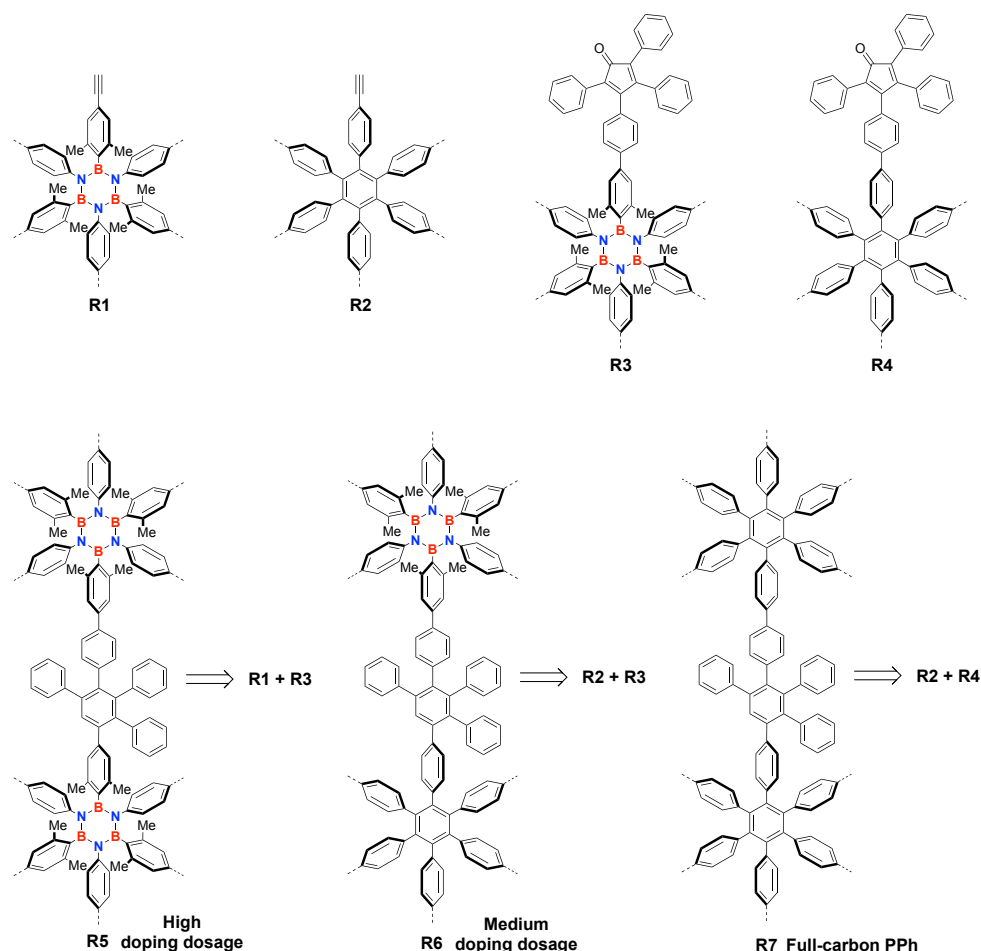
Scheme 40. General retrosynthetic analysis for the generation of portions of hybrid BNC polyphenylenes. By using borazine-doped (**R1**, **R3**) and full-carbon (**R2**, **R4**) units, sections of polyphenylenes having different doping dosage will be generated. The possible peripheral substituents of the arylborazine units are replaced by dashed bonds for simplicity.

In particular, by using borazine-doped building blocks (**R1, R3**), and full-carbon analogues (**R2**, **R4**), the interconnection of these moieties will generate different polyphenylenes-based species having different content of borazine units. Therefore, the resulting extended structures will be characterized by a different **doping dosage (ρ)**. This value consists of the percentage ratio between benzene and borazine rings composing the structures, and will be determined by the type of building blocks connected.
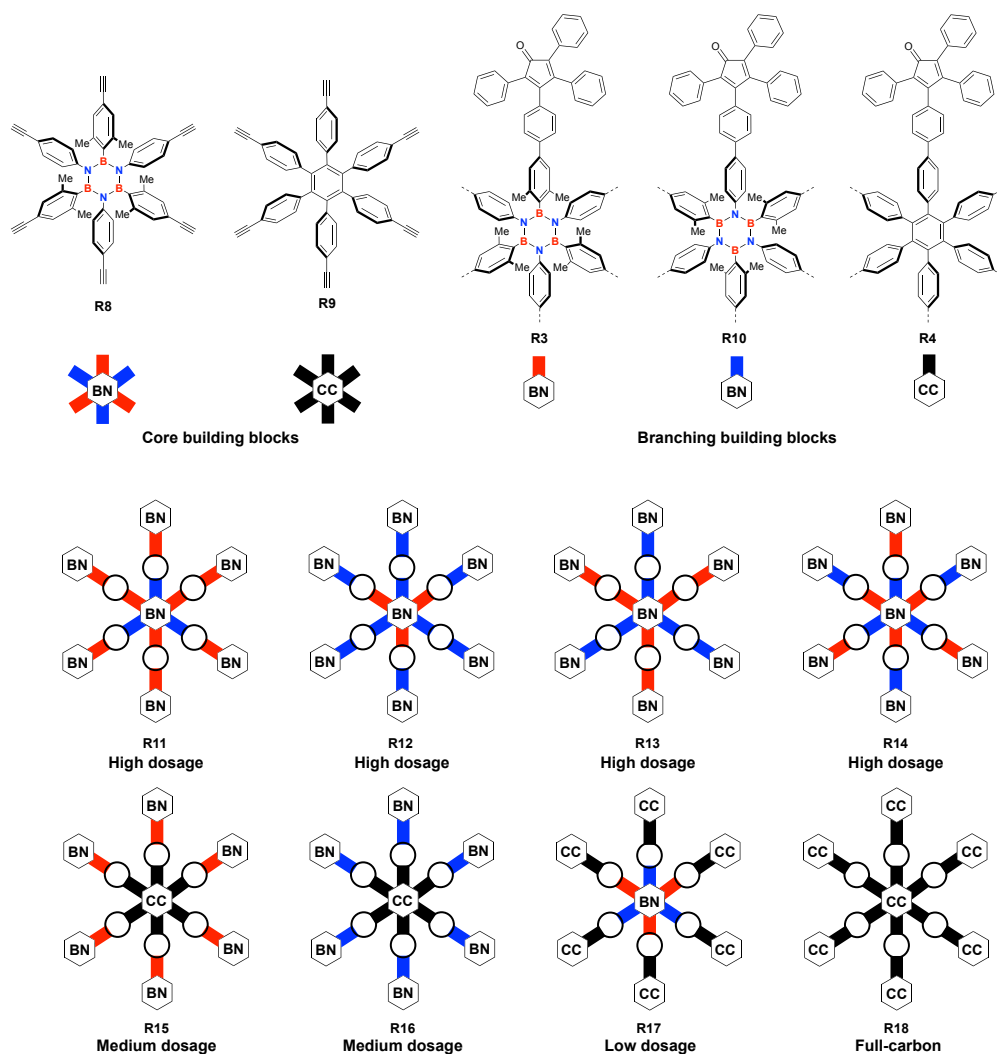
Scheme 41. Top: designed core (**R8**, **R9**) and branching (**R3**, **R10**, **R4**) building blocks. Bottom: designed hexa-branched polyphenylenes **R11-R17** featuring different doping dosage.

The use of the (1+1'+1+1'+1+1') hexamerization approach (see also section 1.1.1.2) was envisaged to prepare hexaarylborazine derivatives featuring different functional groups at the *B*- or at the *N*- sites.[106] Therefore, BN-doped building blocks having six ethynyl functional groups (**R8**) or a single CPD moiety grafted in different positions (**R3**, **R10**, Scheme 41), were designed. Instead, full-carbon hexaphenylbenzene derivatives bearing six ethynyl groups (**R9**) or a single CPD fragment (**R4**, Scheme 41) can be obtained by

using a metal-catalyzed cyclotrimerization reaction.[194] To each one of the building blocks presented in Scheme 41 (top), a schematic representation and a colour code is associated in order to help the reader to understand the type of molecule described. In this representation, the central six-membered ring is labelled to indicate the composition (BN= borazine, CC= full-carbon). The colour of the segments attached to this defines whether the reactive functional group (ethynyl or CPD) is attached at the *B*-site (red), the *N*-site (blue), or to a non-doped unit (black). The simplified schemes **R11**-**R18** (Scheme 41, bottom) are displayed in order to anticipate the synthetic result of the cycloaddition reactions between these building blocks. These represent the hexa-branched borazine-doped polyphenylenes that will be produced starting from the core units **R8** and **R9**, and the branching units **R3**, **R4**, and **R10**. In the next chapter, the strategy to obtain the building blocks and the final molecules will be outlined.

In addition to the doping dosage, it is important to note that depending on the combination of core and branching building blocks, the designed hexa-branched derivatives having medium and high doping dosage (**R11**-**R16**) differ also by the way the borazine-doped units are connected. Depending on the position of the reactive groups functionalized on the precursors used for the synthesis of the hexa-branched BN-polyphenylenes, one can have the different units connected through the *B*-sites or the *N*-sites. The designed derivatives featuring a medium doping dosage, (**R15**, **R16**, Scheme 41, bottom) are distinguished only by the way the peripheral doped units are connected to the full-carbon core: through the *B*-sites (**R15**) or the *N*-sites (**R16**). However, for those having high ρ (**R11**-**R14**), a more comprehensive descripton of the doping pattern must be introduced. In Scheme 42, the different connections expressed in the hexa-branched **R11** (top) and **R12** (bottom) are reported as an example. Defining the core units as the reference, it is clear that the branching units attached to it can have two different orientations. To better describe the **doping orientation** (*o*) of the high-dosage derivatives **R11**-**R14**, a notation is introduced. When the peripheral unit has the same orientation with respect to the reference, it has "α" orientation. Rather, when it is rotated by 60˚, it will assume a "β" orientation. To complete this simple notation, the atom of the reference unit to which the branching BN unit is attached will be added as a subscript to the appropriate Greek letter used (α_N, α_B, β_N, β_B).
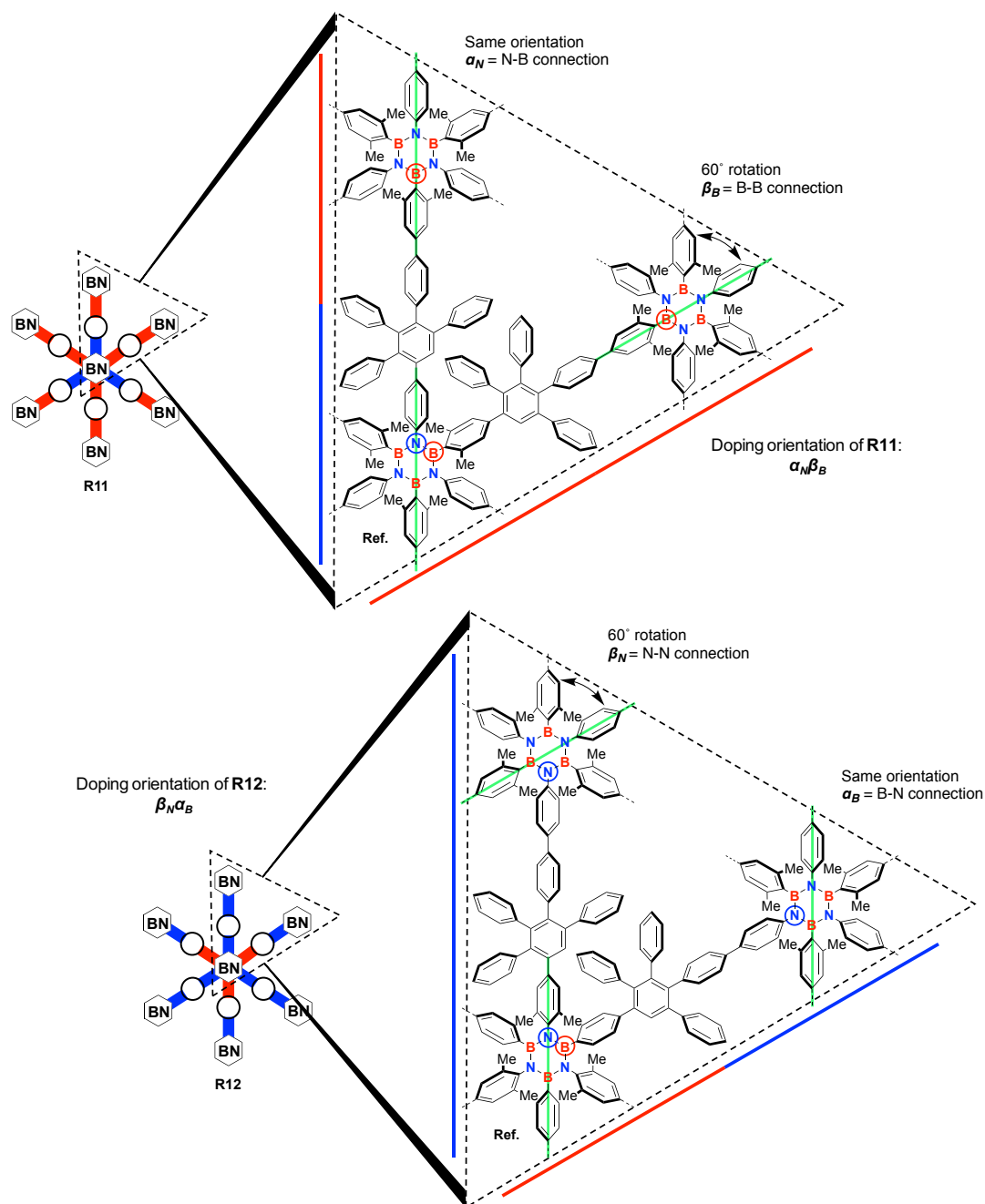
Scheme 42. Molecular sections of **R11** (top) and **R12** (bottom) showing the orientations (*o*) of the branching BN units (green bar) with respect to the reference BN unit. The connection type of **R11** ($\alpha_N\beta_B$) and **R12** ($\beta_N\alpha_B$) is highlighted using the colour code: red (B), blue (N).

For instance, the branched BNC hybrid **R11** (Scheme 42, top) is constituted by two types of different connections with respect to the reference core unit:

- one in which the peripheral unit has same orientation (α) and is connected to the *N*-site of the reference borazine (α_N, N-B connection),

- one in which the peripheral unit is rotated by 60˚ (β) and is connected to the *B*-site of the reference borazine (β_B, B-B connection).

For hybrid polyphenylene **R12** instead (Scheme 42, bottom), the two different connections with the reference borazine can be described as follows:

- one in which the peripheral unit is rotated by 60° (β) and is connected to the *N*-site of the reference borazine (β_N, N-N connection),

- one in which the peripheral unit has same orientation (α) and is connected to the *B*-site of the reference borazine (α_B, B-N connection).

In light of this notation, and considering the nature of the connections present, the doping orientation (*o*) of the two BNC hybrid frameworks taken as example, can be described as $\alpha_N\beta_B$ (**R11**), and $\beta_N\alpha_B$ (**R12**). Using the same principle, **R13** and **R14** (Scheme 41) will have $\beta_N\beta_B$ and $\alpha_N\alpha_B$ doping orientation, respectively.

Finally, to describe the topology of the borazine doping in the PPh frameworks a last notation must be introduced: the **doping vector** (*d_i*). Considering the projection of the borazine-PPh framework on a plane, a hexagonal honeycomb can be generated. In this 2D architecture, *d_i* describes the position of each doping unit following the *x* and *y* axes with respect to a reference borazine unit defined as the (0, 0) position (Figure 14). Each position is identified by the number of six-membered rings encountered along the two axes (*x*, *y*). Considering the nature of the hexabranched borazine-PPh **R11**-**R14** (Scheme 41) designed for this first objective, the six peripheral doping units connected to the reference borazine core will be described by the doping vectors: *d_1*= (-5, 10), *d_2*= (5, 5), *d_3*= (10, -5), *d_4*= (5, -10), *d_5*= (-5, -5), *d_6*= (-10, 5). As a general example, a section of BN-PPh **R11** is depicted in Figure 14. In this, the doping vectors *d_1* and *d_2* (green arrows) for the doping units numbered as '1' and '2' are shown.

For a more comprehensive description, the **doping descriptor** (**D**, Figure 14) can be used to depict every possible borazine-doped framework. All the different doping vectors are included in it, together with the orientation parameter *o*. More in detail, **D** is constituted by the sum of the *d* and *o* associated to each doping unit. For example, for **R11** the doping descriptor **D** will assume the form:

$$\mathbf{D} = (-5, 10)\alpha_N, (5, 5)\beta_B, (10, -5)\alpha_N, (5, -10)\beta_B, (-5, -5)\alpha_N, (-10, 5)\beta_B$$
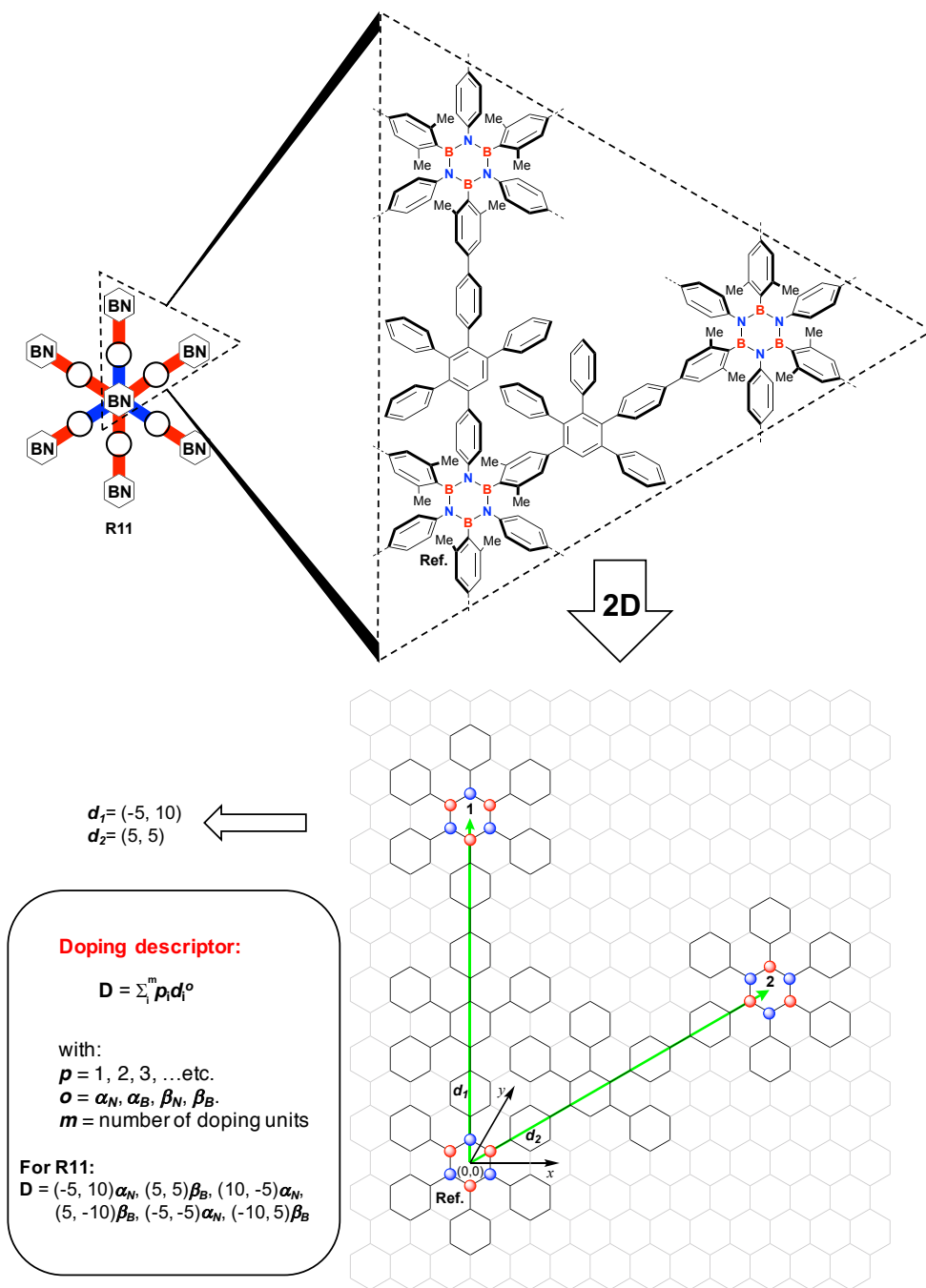
Figure 14. Representation of a section of hexabranched borazine-PPh **R11** in the 2D hexagonal lattice. The doping vectors d_1 and d_2 are represented by the green arrows.

To summarize, the first synthetic efforts described in this manuscript concerns the preparation of a series of hexabranched polyphenylene derivatives featuring different BN content (doping dosage, ρ), different connections between the doping units (doping orientation, o), and different topology (doping vector, d). Subsequently, the effects of this differentiation on the absorption and emission features will be evaluated by means of UV-Vis spectroscopy.

2.2 Synthesis of a BN-polyphenylene energy harvesting system

Prompted by the literature reports describing the use of dendritic networks as light harvesting systems (see section 1.2.2.4), the second objective of the work is related to the use of BNC hybrid branched polyphenylene networks as semi-rigid scaffolds for the construction of energy harvesting systems. To assess the ability of the borazine-doped frameworks to transfer excitation energy, a multichromophoric system constituted by an organic chromophore supported on a BN-doped polyphenylene scaffold, is designed (Scheme 43).
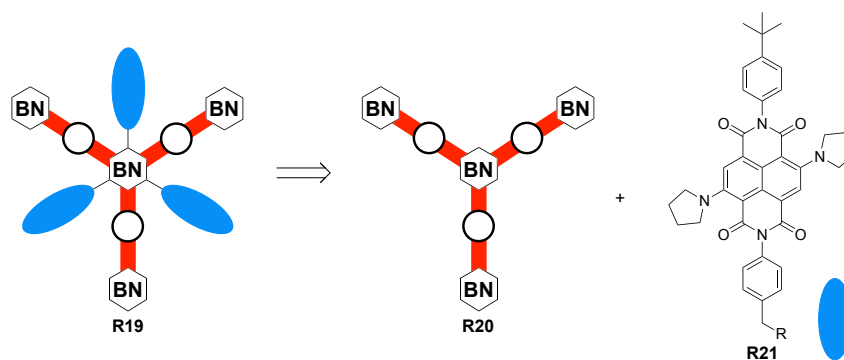
Scheme 43.Synthetic strategy for multichromophoric system **R19** requiring functionalization of three-branched borazine-doped polyphenylene **R20** with blue naphtalenediimide (NDI) **R21**.

To accomplish the synthesis of **R19**, a suitable organic chromophore will be chosen as energy acceptor and grafted to a three-branched borazine-doped polyphenylene. More specifically, a tri-branched BN-doped framework (**R20**) will be covalently functionalized with a blue naphtalenediimide (NDI, **R21**). Given the C_3-symmetry of borazine derivatives, it is possible to graft the organic acceptors in between the energy donating BNC-doped semi-rigid branches, to give a well-defined architecture. As a result, the energy transfer will be favoured by the reduced distance between the donor and acceptor chromophores. In this study, the effects of doping dosage and orientation of the BN-polyphenylene scaffold on the ability to perform energy transfer will not be considered. Therefore, the energy acceptor will be grafted only on one scaffold (**R20**), featuring β_B orientation. Instead, the choice of the dye (**R21**), is made in order to fulfil the requirements for energy transfer. Indeed, NDI derivatives present three absorption bands, two in the UV region (290-325 nm, 340-400 nm), and one in the visible part of the spectra (500-650 nm) (Figure 15).[279]
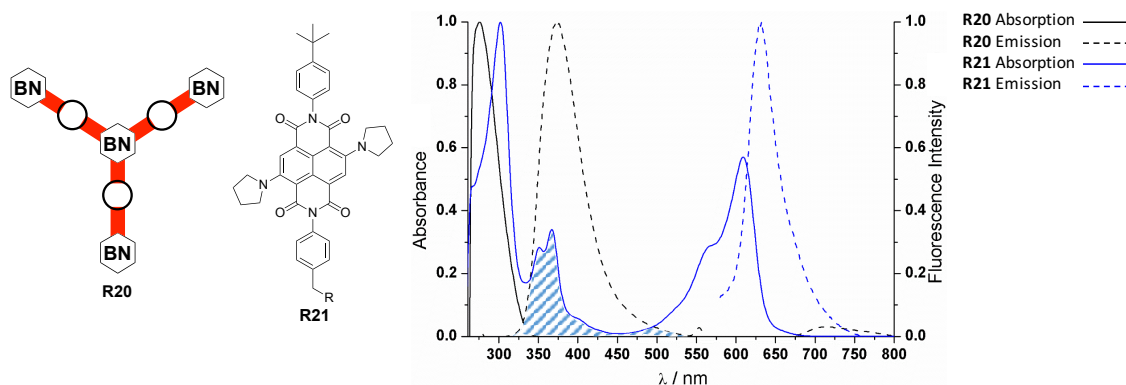
Figure 15. Absorption (solid) and emission (dashed) spectra of three-branched borazine-polyphenylene **R20** (black) and NDI **R21** (blue). The overlap between emission and absorption of **R20** and **R21** is highlighted.

By excitation of substituted NDI derivatives in any of the absorption bands, a visible radiation will be emitted at different wavelengths depending on the substituents on the naphthalene core. When NDI is core-substituted with two amino-groups (pyrrolidinyl-groups in this case), a red emission band (600-700 nm) is obtained.[279] In Figure 15, the matching between the second absorption band of bis-pyrrolydinyl-NDI derivative **R21** (340-400 nm) and the emission of borazine-doped PPh **R20**[117] is highlighted. Thanks to the overlap between the emission of the donor and the absorption of the acceptor, the most important condition is verified, enabling theoretically the energy transfer phenomena. In the following chapter, the nature of **R19**, **R20**, and the R group of **R21** will be disclosed. Hence, the synthetic strategy, preparation, and assessment of the ability of the designed multichromophore **R19** to perform energy transfer, will be investigated by means of UV-Vis absorption and emission measurements.

2.3 Synthesis of borazine-doped graphene substructures

The perspectives to create a bandgap on graphene and, therefore, the use of this material for optoelectronic applications, were boosted by the breakthrough studies on the formation of *h*-BN-graphene sheets (see also section 1.1.5.4).[41,42,45,162−165] However, the top-down synthetic procedures used did not allow the precise control over the BN content and the topology of *h*-BN regions embedded in the graphene framework. For this reason, the development of a bottom-up synthetic methodology for the formation of graphene-like structures featuring doping patterns with pre-determined topology is of high interest. The exact control of the quantity and position of the doping units is of key importance for the accurate tailoring of the bandgap of graphene. In this context, the use of arylborazine

precursors is regarded as one of the most promising strategies for the BN-doping of graphene-like structures. In particular, this has been the object of recent studies from the group of *Bettinger* (see also section 1.1.1.3, Scheme 8),[286] which attempted the synthesis of HBBNC **21** using the same chemistry developed for the oxidative dehydrogenation of polyarenes.[212,213,287–289] However, submitting hexaphenylborazine to the Scholl reaction using combinations of Lewis acids and oxidants including $FeCl_3$ in nitromethane, $CuCl_2$ and $AlCl_3$ in CS_2, $(CF_3COO)_2I^{III}C_6H_5$ (PIFA) with $BF_3 \cdot OEt_2$ in CH_2Cl_2, and $MoCl_5$ in CH_2Cl_2, failed to produce the desired product due to instability of the borazine core under oxidative conditions. Subsequently, formation of HBBNC was achieved by the same group through pyrolysis at 550 ˚C,[83] and surface assisted cyclodehydrogenation at 300 ˚C on a Ag(111) substrate.[139] Unfortunately, despite the formation of the product was confirmed by mass spectrometry, this could not be isolated due to its poor solubility. Subsequently, the formation of soluble tri-substituted HBBNC **57** was achieved by our group[114] using an in-solution Friedel-Crafts procedure (see also section 1.1.5.4).[166] In this case, the presence of *ortho*-fluoride groups conferred resistance to borazine **56**, shielding the boron atoms. However, in presence of a silyl-cation, these were transformed in good leaving groups, triggering the planarization reaction and causing the formation of the desired product **57** (Scheme 20). Given this, the third objective of this thesis work is the development of a scalable synthetic methodology for the preparation of BNC hybrid polyphenylene frameworks featuring *B*-aryl substituents functionalized with *ortho*-fluoride atoms (**R24**, **R27**, **R30**, Scheme 44). Then, these will be planarized to obtain graphene substructures with defined shape and embedded borazine doping with precise topology (**R22**, **R25**, **R28**). In the retrosynthetic analysis (Scheme 44) for the planarization process to give **R22**, **R25**, and **R28**, two steps are considered. Initially, a Friedel-Crafts-type reaction[166] will afford partially planarized derivatives **R23**, **R26**, and **R29** from **R24**, **R27**, and **R30**, respectively. Once the inner shell of each borazine core is cyclized, an increased resistance of the BN ring towards strong electrophiles is ensured given the enhanced delocalization of the lone pairs of the N atoms.[114] Therefore, a final cyclization process is envisaged through Scholl reaction on derivatives **R23**, **R26**, and **R29**. To confer solubility to fully planar derivatives **R22**, **R25**, and **R28**, the precursors must bear peripheral bulky groups, in order to prevent aggregation of the large π-systems. In Chapter 3, the strategy used for the synthesis of fluoride-functionalized borazine-

polyphenylenes **R24**, **R27**, and **R30**, and the synthetic efforts done for the fulfilment of this third objective, will be disclosed.
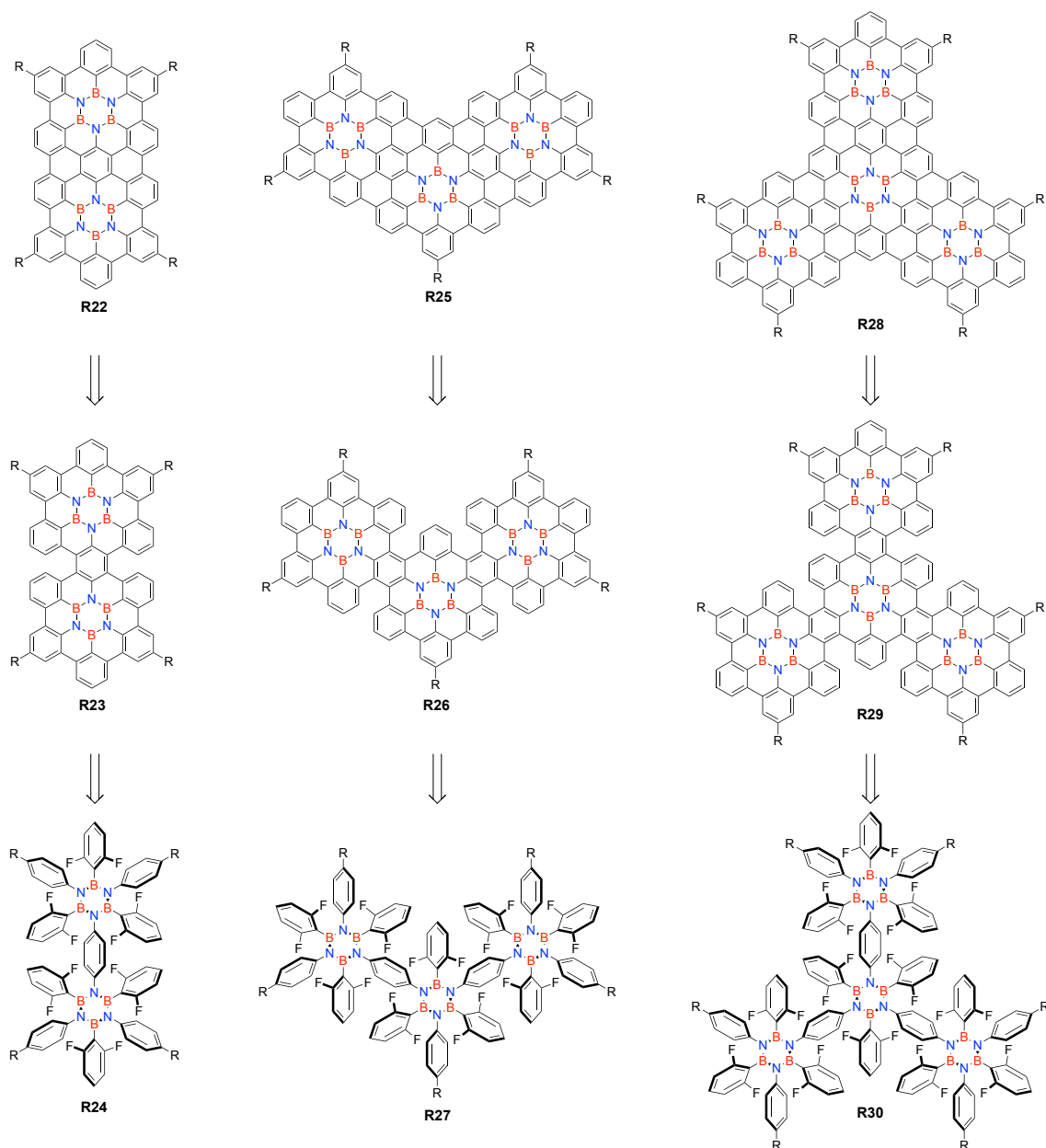
Scheme 44. Rethrosynthetic pathway for the synthesis of planar borazino-doped graphene substructures **R22**, **R25**, and **R28**.

Chapter 3: Results and discussion

In the initial section of this chapter (section 3.1), the synthesis of the borazine-doped, and full-carbon core- and branching-units will be addressed. Starting from these, the synthesis of hybrid BNC frameworks will be described. This will be followed by the absorption and emission investigation of the targeted hexa-branched hybrid BNC polyphenylenes. In section 3.2, the grafting of a blue chromophore on a borazine-doped polyphenylene scaffold will be regarded. In particular, the use of these BNC hybrid semi-rigid structures as support for the construction of functional molecules will be tested by covalent attachment of a naphthalene diimide (NDI) derivative on a three-branched BN-PPh framework. Hence, assessment of the presence of energy transfer from the borazine-doped PPh backbone to the blue dye will be detailed. Finally, section 3.3 features the study undertaken for the definition of a suitable synthetic methodology for the construction of borazine-doped graphene substructures. The synthesis and spectroscopic characterisation of the three-branched borazine-PPh **164**-**173** (section 3.1.4) were carried out by *Francesco Fasano*. All the measurements were done in collaboration with Dr. *Andrea Fermi* and *Francesco Fasano*, while the calculations on hexaphenylborazine **43** were performed by *Nicolas Biot*. All these collaborators are working in the research group of Prof. *Bonifazi* at Cardiff University (UK), where this thesis work has been carried out. Instead, the X-ray analyses presented in this chapter were performed by *Dr. Nicola Demitri* (Elettra Sincrotrone, Trieste).

3.1 Bottom-up synthesis and characterization of borazine-doped polyphenylenes

3.1.1 Synthesis of borazine-doped building blocks

Core units

For the synthesis of the arylborazine modules bearing ethynyl or CPD functional groups, that will be used as core- and branching-units in the final transformations to give the hybrid polyphenylenes, a modified version of the (1+1'+1+1'+1+1') hexamerization developed by *Groszos* and *Stafiej* was employed.[106] The procedure relies on the treatment of the substituted aniline of choice (**R31**) with BCl_3 in refluxing toluene (Scheme 45). The tri-*B*-chloroborazine derivative (**R32**) formed is then reacted with an aryllithium

derivative **R33** that, having methyl substituents in the *ortho*-positions, confers stability towards hydrolysis to the newly formed arylborazine **R34** (see also sections 1.1.2).
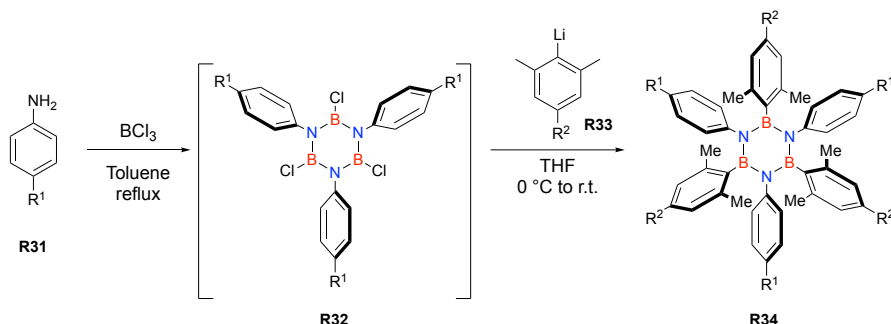
Scheme 45. General synthetic methodology for borazines bearing different aryl-substituents at the *N*- and *B*- sites.

Depending on the choice of the arylamine and the aryllithium derivatives, one can place useful functional groups either in the *N*- or the *B*-site, respectively. Following this strategy, the synthesis of a borazine derivative bearing six ethynyl functional groups was devised. In particular, an aryl-borazine derivative featuring TIPS-protected ethynyl functionalities at the *N*-sites, and TMS-protected groups at the *B*-sites, has been envisaged. The possibility to operate a selective removal of the TMS-groups, leaving reactive ethynyl moieties at only the *B*-sites, is of great interest for the purposes of this work. In fact, the Diels-Alder cycloaddition proceeds smoothly with unprotected acetylene groups, but becomes much slower when these are functionalized with bulky groups. As will be pointed out in the following sections of this manuscript, the selective deprotection of the ethynyl groups will be exploited to graft different branching modules at the B and N positions of a borazine-doped core unit. To synthesise the arylborazine module (Scheme 46), bearing TIPS-ethynyl groups at the *N*-sites, aniline derivative **104** was chosen as the N source. This was synthesised in 84% yield by Pd/Cu-catalysed Sonogashira cross-coupling from commercially available 4-iodoaniline **103** and TIPSA. After treatment of **104** with BCl$_3$, the formed tri-*B*-chloroborazine intermediate was reacted with the lithium derivative of 2,6-dimethyl-4-(ethynyltrimethylsilyl)bromobenzene **106**, affording borazine **107** with a modest 14% yield. Full deprotection of **107** was possible by treatment with TBAF in THF, affording borazine **108**, with free ethynyl functional groups grafted at both *B*- and *N*-sites. Treating **107** with potassium carbonate in a 1:1 MeOH/THF mixture, resulted instead in its partial deprotection. Only the less sterically demanding TMS-groups, grafted at the *B*-sites, were indeed removed to generate borazine **109** in 69% yield.
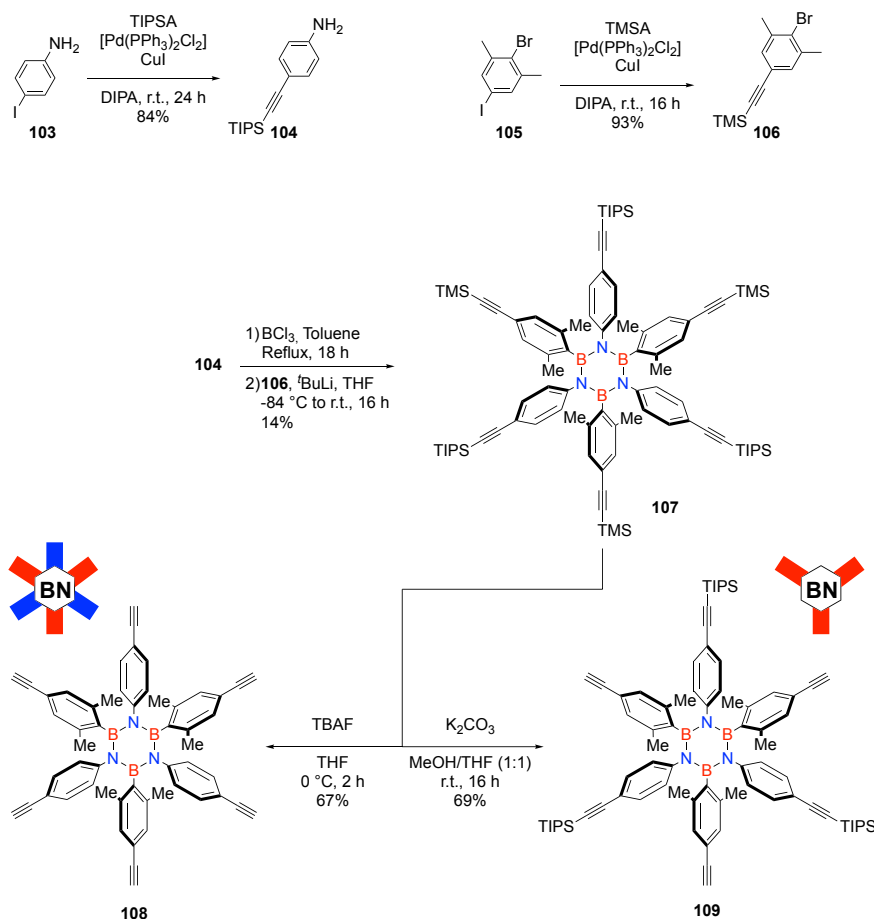
Scheme 46. Synthesis of borazine **107** and different de-protection strategies. Complete de-protection to give borazine **108**, featuring free ethynyl moieties at both *N*- and *B*-sites, and partial de-protection to obtain borazine **109** bearing free-ethynyl groups only at the *B*-sites. Insets: schematic representations of the doping pattern for the core building blocks prepared.

Branching units
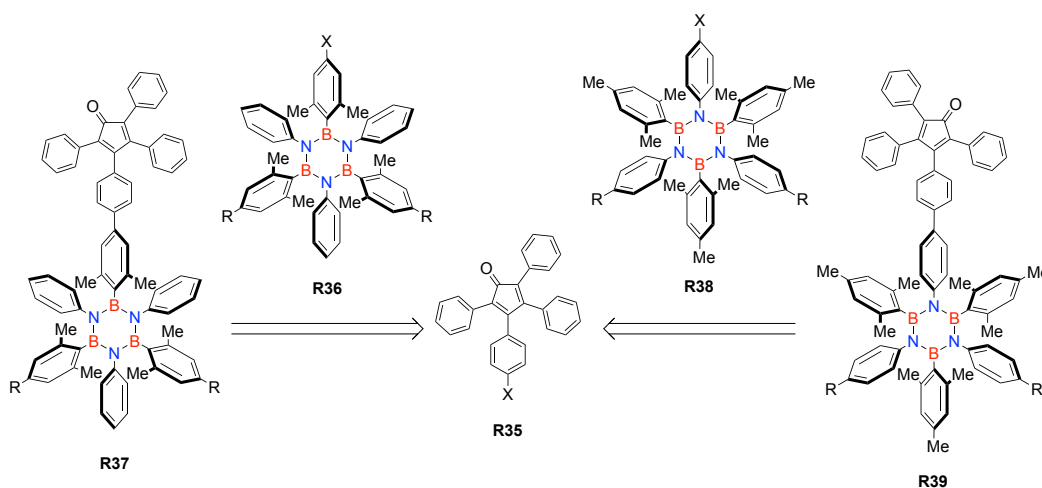
Scheme 47. Retrosynthetic analysis for the preparation of borazine-doped branching units featuring a CPD moiety grafted at the *B*-site (**R37**) or at the *N*-site (**R39**).

With the aim of connecting a single cyclopentadienyl moiety to a hexaarylborazine derivative, a novel synthetic methodology was designed. The strategy relies on a stepwise Suzuki cross-coupling reaction starting from a borazine unit bearing an appropriate functional group (halide, triflate) at either the *B*- (**R36**) or the *N*-sites (**R38**). This would afford suitable coupling partners which can be functionalized with the CPD synthon **R35**, providing the borazine-doped branching units to be used in the final D.A. cycloaddition reaction for the divergent bottom-up synthesis of BNC hybrid PPh (Scheme 47).
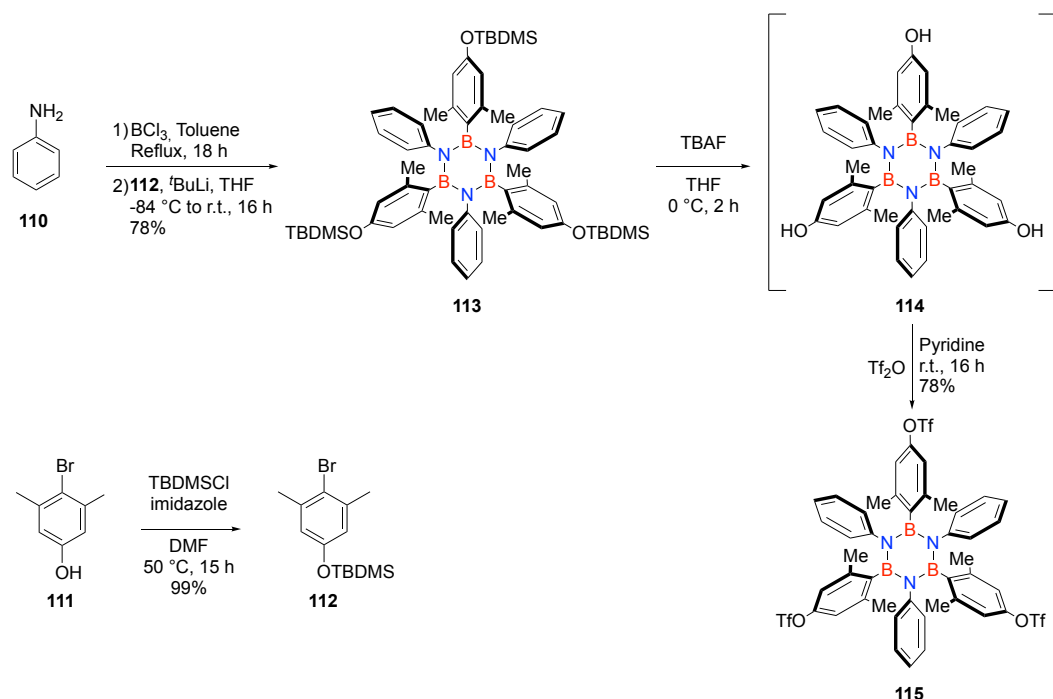
Scheme 48. Synthesis of borazine derivative **115**, bearing triflate functional groups at the *B*-sites.

For this purpose, following the same synthetic approach previously used (Scheme 45), borazine derivative **113**, featuring TBDMS-protected alcohol groups at the *B*-sites, was obtained starting from aniline (**110**) and bromobenzene derivative **112** (Scheme 48). More in detail, TBDMS-protected bromobenzene **112** was obtained in quantitative yield reacting 3,5-dimethyl-4-bromophenol **111** with *t*butyl-dimethylsilyl chloride (TBDMSCl) in the presence of imidazole (Scheme 48). Removal of TBDMS-groups in **113** in the presence of TBAF at 0 °C gave tri-hydroxyl borazine derivative **114**. The product precipitated upon addition of TBAF to the THF solution of **113**. The white solid was recovered by filtration and immediately treated with an excess of trfluoromethanesulphonic anhydride (Tf$_2$O) using pyridine as solvent.
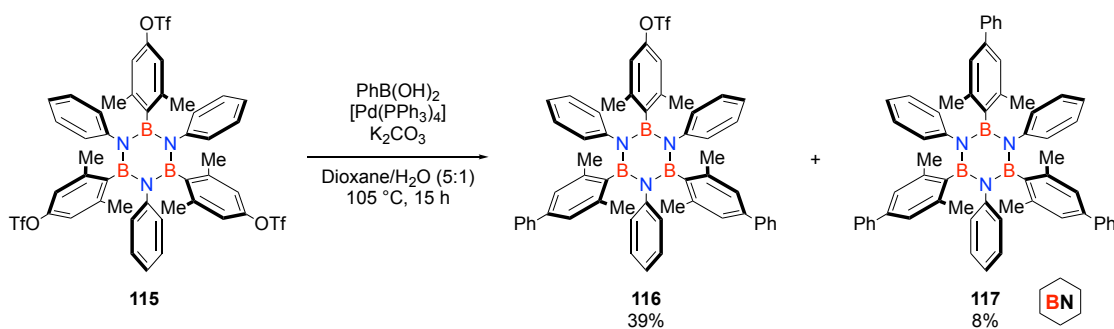
Scheme 49. Suzuki cross-coupling reaction to obtain mono-triflate borazine **116** and tri-phenyl borazine derivative **117**. Inset: schematic representation of the doping pattern for mono-doped hexaarylborazine **117**.

Borazine **115**, functionalized with triflate-groups at the *B*-sites, was obtained in 78% yield after silica gel column chromatography. In order to prepare mono-triflate derivative **116** suitable for further derivatisation, Pd-catalysed reaction was carried out treating **115** with 1.8 molar equivalents of phenylboronic acid as coupling partner in a dioxane/water mixture at 105 ˚C for 15 h, affording mono-triflate **116** and tri-phenyl derivative **117** in 39% and 8% yield, respectively (Scheme 49), after purification by silica gel column chromatography. This latter (**117**), will be used as mono-doped oligophenylene reference during the absorption and emission study of the borazine-doped PPh series. Notably, the suitability of the *ortho*-protected borazine core in such strong basic conditions at elevated temperatures highlights once again the great resistance of this molecular module to nucleophilic attack.
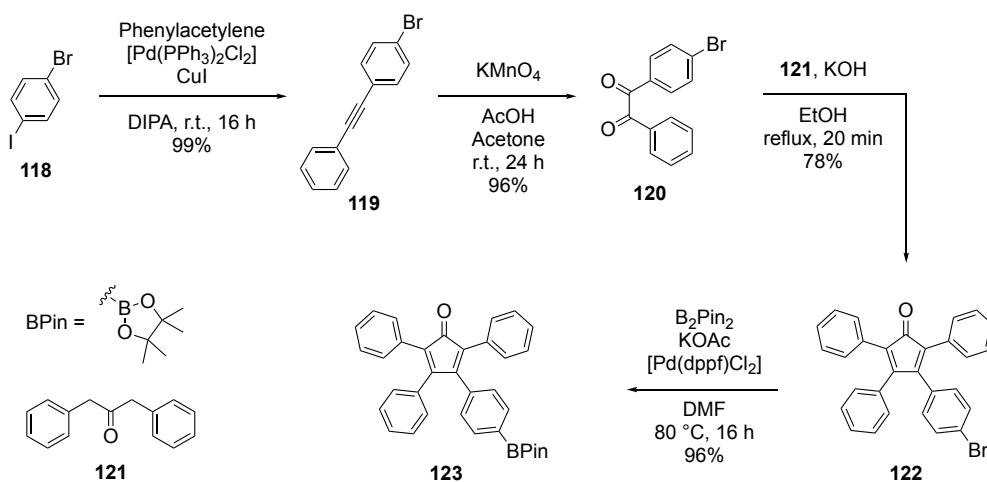
Scheme 50. Synthetic pathway to CPD derivative **123**.

To complete the envisaged synthesis for the borazine-based branching units (Scheme 47), the use of the boronic ester of CPD (**123**) is required. This is synthesised starting from 4-iodobromobenzene **118** which was coupled with phenylacetylene by Pd/Cu catalysed

Sonogashira reaction to give bromo-diphenylacetylene **119** in quantitative yield (Scheme 50). Compound **119** was oxidized with $KMnO_4$ in the presence of AcOH to give diketone **120** with 96% yield. Knoevenagel reaction of the latter with diphenylacetone (**121**) in refluxing EtOH gave Br-CPD **122** in good yield as a deep red solid. Finally, **122** was transformed into its boronic ester derivative **123** by Miyaura reaction using bis(pinacolato)diboron (B_2Pin_2), [Pd(dppf)Cl$_2$] as catalyst, and KOAc in DMF at 80 ˚C.
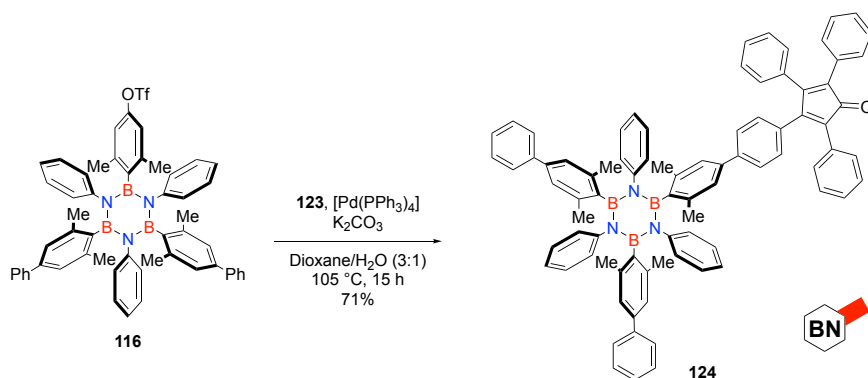
Scheme 51. Synthesis of borazine derivative **124**, bearing a CPD fragment at the *B*-site. Inset: c

Having prepared mono-triflate borazine **116** and CPD boronic ester **123**, borazine-doped branching core **124**, in which the CPD moiety is grafted to the *B*-site, was synthesised using Pd-catalysed Suzuki coupling (Scheme 51).
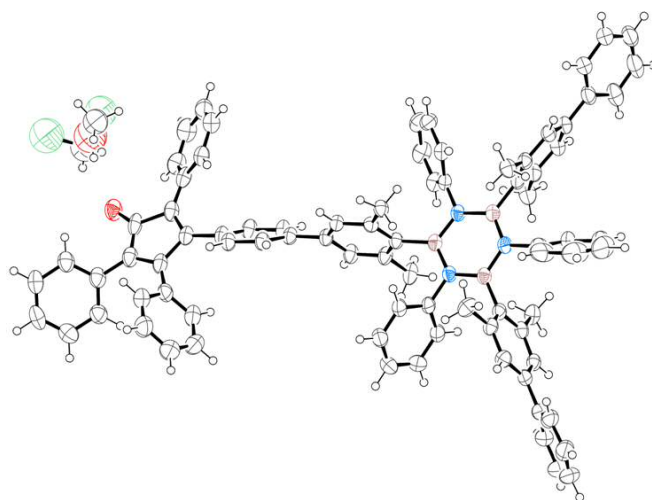
Figure 16. ORTEP representation of borazine-polyphenylene **124** as determined by X-ray diffraction (atom colours: green Cl, red O, blue N, pink B, white C; atomic displacement parameters, obtained at 223 K, are drawn at the 50% probability level). The ASU contain also a solvent site partially occupied by a MeOH or a CH_2Cl_2 molecule. Space group: P-1.

Specifically, compound **116** was reacted with boronic ester **123** in the presence of [Pd(PPh$_3$)$_4$] in a mixture of dioxane and water at 105 °C, to give desired **124** in 71 % yield as a deep-red solid after silica gel column chromatography. X-ray diffraction of a small deep-red crystal of **124**, obtained by slow diffusion of MeOH in a CH$_2$Cl$_2$ solution, confirmed the structure of the derivative (Figure 16).

Using the same synthetic procedure and starting from 4-chloroaniline **125**, borazine **127** was obtained in 62% yield (Scheme 52). This time, the functional group which will allow the grafting of the CPD moiety is positioned at the *N*-site. In particular, aniline **125** was chosen as the N source due to the resistance of aryl chlorides towards Li-halogen exchange. In fact, given the presence of the Li-derivative of **126** in the reaction mixture, possible side reactions can be avoided by choosing Cl as *p*-substituent for the aryl groups grafted at the *N*-sites. At the same time, Ar-Cl groups are capable of undergoing Pd-catalyzed cross-coupling reactions.[290]
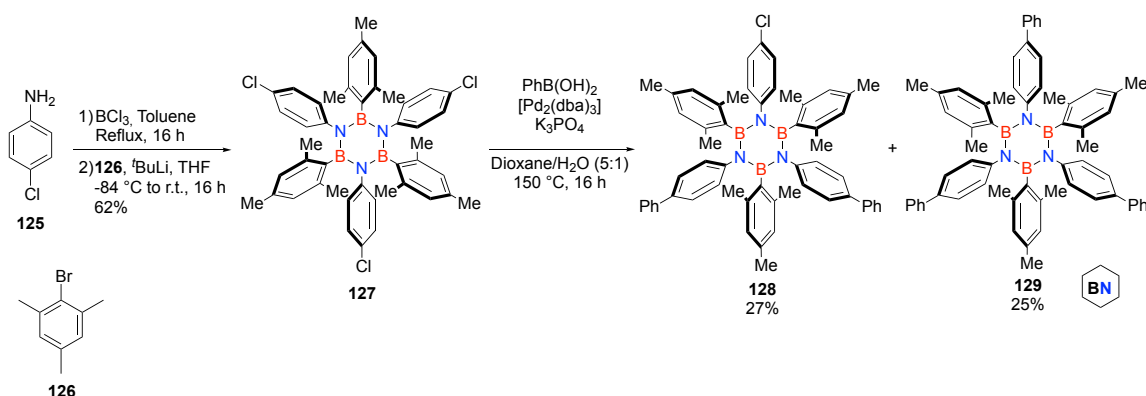
Scheme 52. Synthesis of mono-chloro borazine derivative **128** and triphenyl borazine derivative **129**. Inset: schematic representation of the doping pattern for mono-doped hexaarylborazine **129**.

Hence, tri-*B*-mesityl-*N*-(4-chlorophenyl)borazine **127** was submitted to Suzuki cross-coupling using 2.2 molar equivalents of phenylboronic acid obtaining a mixture of products. As for the synthesis of molecules **116** and **117** (Scheme 49), disubstituted borazine **128**, bearing a single chloride at the *N*-site, and trisubstituted borazine **129**, were separated by silica gel column chromatography in 27 and 25% yield, respectively. Derivative **128** was furtherly treated under Suzuki reaction conditions employing BPin-CPD **123** as coupling partner (Scheme 53). Borazine-doped branching unit **130**, in which the CPD fragment is grafted at the *N*-site, was obtained in 23% yield. Notably, the coupling reactions of borazine units functionalized with Cl functional groups gave

satisfactory results only at 150 °C in a pressurized vessel using [Pd$_2$(dba)$_3$] as catalyst and K$_3$PO$_4$ as base.
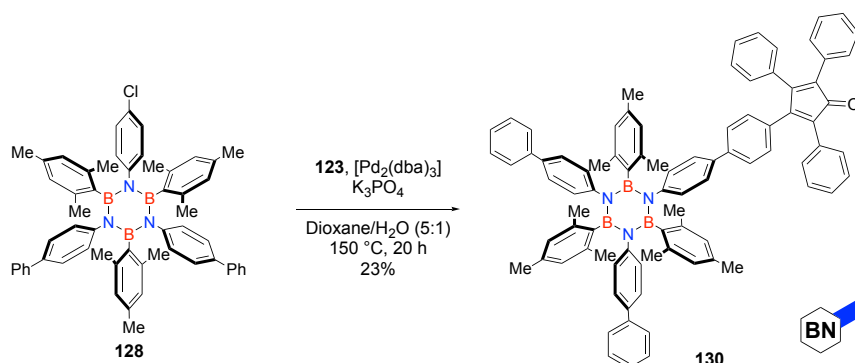
Scheme 53. Synthesis of borazine derivative **130**, bearing the CPD fragment at the nitrogen position. Inset: schematic representation of the doping pattern for the branching building block prepared.

3.1.2 Synthesis of full-carbon building blocks

Core units

In order to construct hybrid polyphenylenes varying the doping ratio ρ, the access to non-doped units is necessary. As briefly pointed out in section 1.2.1, thanks to the cyclotrimerization reaction it is possible to generate a new aromatic centre starting from acetylene derivatives.
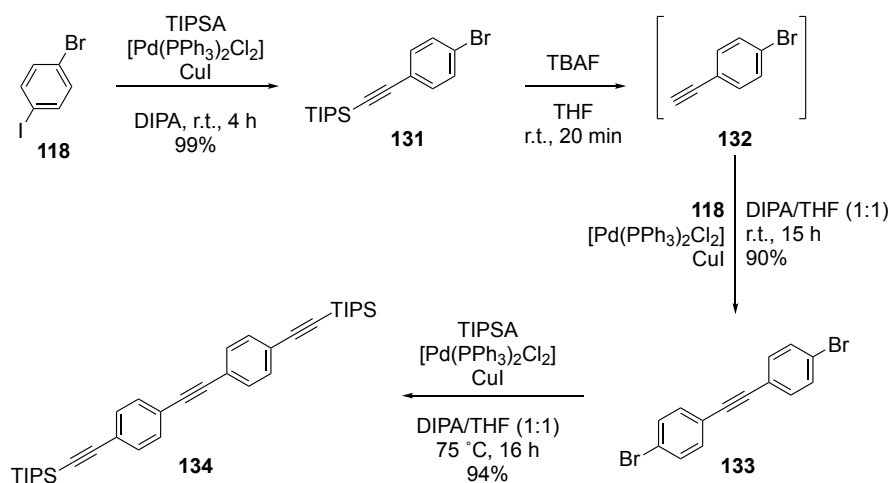
Scheme 54. Synthetic pathway for diphenylacetylene derivative **134**.

Thus, in order to prepare a hexaphenylbenzene derivative, bearing six TIPS-protected ethynyl moieties, diphenylacetylene derivative **134** was chosen as building block. The synthesis of **134** (Scheme 54) commenced by submitting 4-bromoiodobenzene **118** to Sonogashira coupling with TMSA in the presence of [Pd(PPh$_3$)$_2$Cl$_2$] and CuI to obtain

derivative **131** in quantitative yield. Subsequent removal of the protecting TMS group with TBAF in THF yielded **132**. The latter, bearing an unprotected ethynyl group, was not isolated and used in the following step without further purification. Using a similar Pd/Cu-catalysed protocol for the Sonogashira reaction, ethynyl derivative **132** was coupled again with 4-bromo-iodobenzene **118** to obtain di(4-bromophenyl)ethylene **133** in 90% yield.
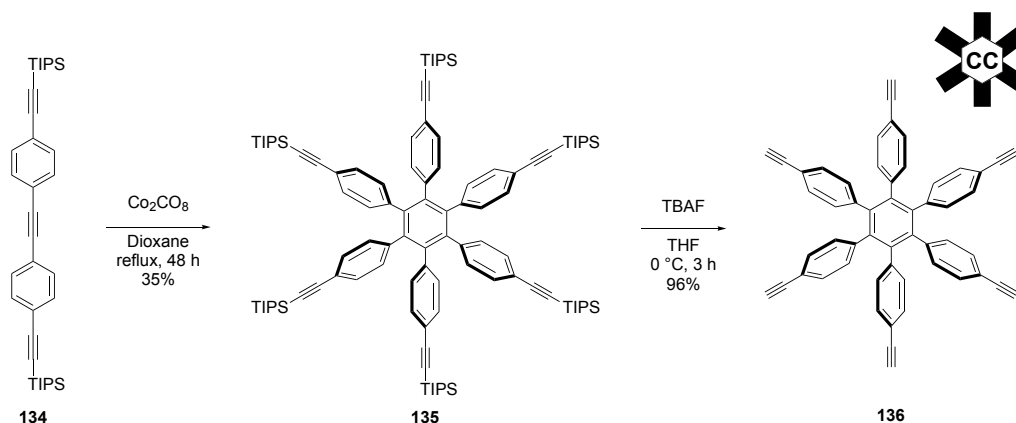
Scheme 55. Synthesis of full-carbon core unit **136** bearing six ethynyl moieties. Inset: schematic representation of the core building blocks prepared.

A last Sonogashira cross-coupling between **133** and TIPSA afforded derivative **134**, bearing three ethynyl moieties, in good yield. Subsequently, the latter was used as starting material for the Co-catalysed cyclotrimerization reaction that led to hexaphenylbenzene derivative **135** in 35% yield (Scheme 55).[194] Finally, full removal of the protective groups using TBAF, afforded full-carbon core unit **136** in nearly quantitatively yield.

Branching units

Analogously to the synthesis of all-carbon core unit **136** (Scheme 55), the synthesis of a hexaphenyl benzene derivative bearing three interchangeable functional groups began with the preparation of diphenylacetylene **138** by Sonogashira reaction starting from 4-iodoanisole **137** and phenylacetylene in the presence of [Pd(PPh$_3$)$_2$Cl$_2$] and CuI (Scheme 56). Subsequent Co-catalysed cyclotrimerization reaction of **138** in refluxing dioxane afforded an inseparable mixture of isomers (**139** and **140**). This mixture was treated with BBr$_3$, to give a mixture of isomers bearing unprotected hydroxyl groups. This time, the different isomers could be easily resolved by silica gel column chromatography taking advantage of the lower polarity of targeted isomer **142**, which was obtained with 14% yield.
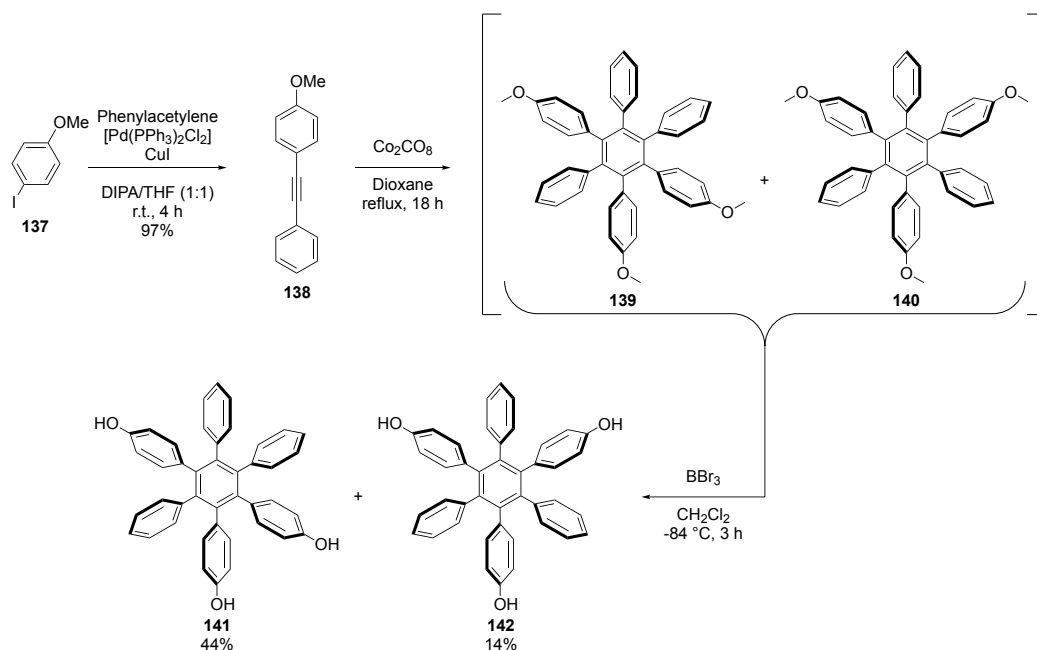
Scheme 56. Synthetic route adopted for the preparation of tri-hydroxy hexaphenylbenzene derivative **142**.

Using the same methodology for the synthesis of tri-triflate borazine **115** (Scheme 48), tri-hydroxy hexaphenylbenxene **142** could be converted to the corresponding tri-triflate derivative **143** in 90% yield (Scheme 57).
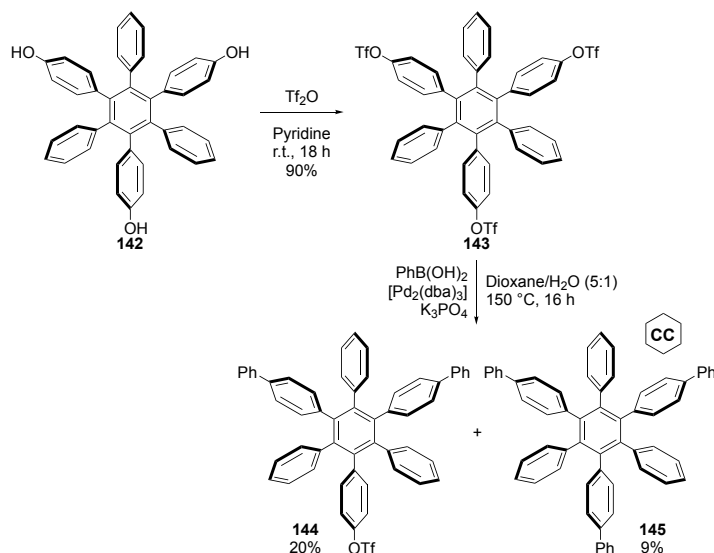
Scheme 57. Formation of tri-triflate derivative **143** and Suzuki cross coupling to give mono-triflate **144** and tri-phenyl derivative **145**. Inset: schematic representation of hexaarylbenzene **145**.

The Suzuki cross-coupling on **143** with phenylboronic acid afforded desired mono-triflate derivative **144** in 20% yield along with the product of tris-coupling **145** (9% yield). The final Pd-catalysed cross-coupling between mono-triflate derivative **144** and BPin-CPD **123** in a refluxing mixture of dioxane and water, gave all-carbon branching unit **146**,

bearing a CPD moiety, in 68% yield (Scheme 58). With all the borazine-based and full-carbon branching and core units in hand, the attention is now focused on the combination of these building blocks and to the construction of polyphenylene networks with different doping ratios and orientations.
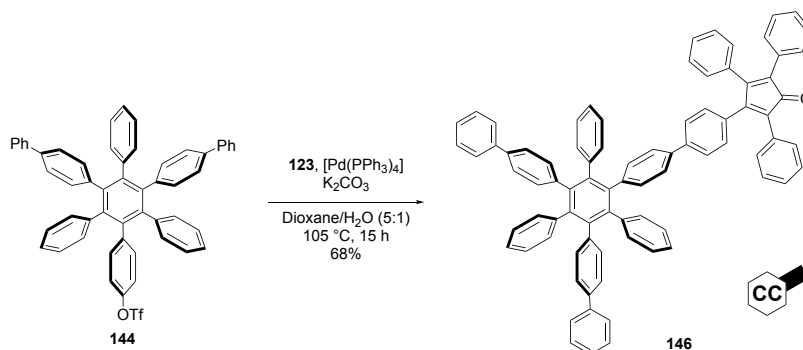
Scheme 58. Final Suzuki reaction for the synthesis of full-carbon branching unit **146**. Inset: schematic representation of the doping pattern of the hybrid-polyphenylene prepared.

These intermediates have been fully characterized by ^{1}H-NMR, ^{13}C-NMR, ^{11}B-NMR, ^{19}F-NMR spectroscopy, high-resolution and low-resolution mass spectrometry and IR spectroscopy. The spectral details are reported in the experimental section together with the synthetic procedures employed for their synthesis (Chapter 4).

3.1.3 Bottom-up synthesis of borazine-doped polyphenylenes

In the next sections, the synthesis of borazine-doped hexabranched PPh derivatives with different doping dosage (ρ) and orientations ($\alpha_N\beta_B$, $\beta_N\alpha_B$, $\beta_N\beta_B$, $\alpha_N\alpha_B$) will be disclosed. All the experimental procedures and characterization details for the molecules whose synthesis is described in this section (^{1}H-NMR, ^{13}C-NMR, ^{11}B-NMR spectroscopy, HR and LR mass spectrometry and IR spectroscopy), are reported in the experimental section (Chapter 4). Instead, only some representative ^{1}H-NMR spectra, Rec-GPC chromatograms, and mass spectrograms will be shown in this section. For a complete overview of the spectral details, the reader can consult the published literature.[117]

3.1.3.1 Synthesis of BN-polyphenylene with ρ= 2.8%

As mentioned previously (section 2.1), the fulfilment of the objectives of this thesis work and the synthesis of the hybrid BNC polyphenylenes takes into account the use of the Diels-Alder cycloaddition. Due to the nature and the great steric hindrance of the chosen coupling partners (aryl-acetylene and CPD derivative), the reaction requires elevated

activation temperatures.[198–200] In particular, the reaction conditions were chosen given the achievements of the group of *Müllen* in the synthesis of polyphenylene nanoparticles.[214,257,291,292]
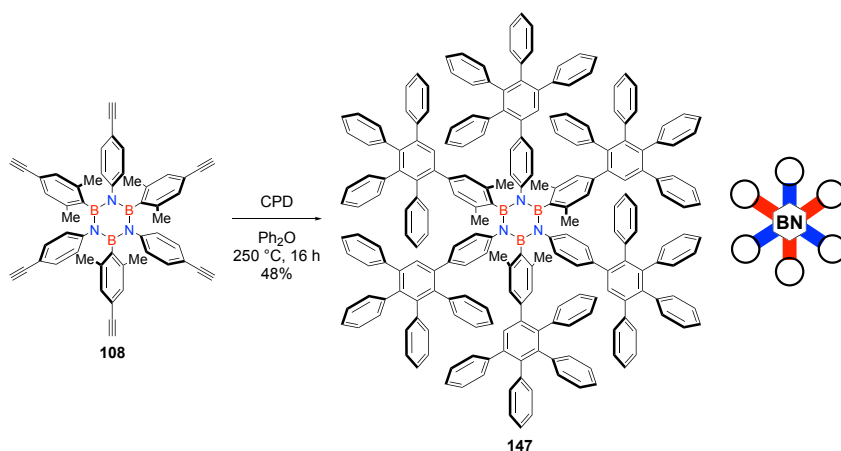
Scheme 59. Synthesis of borazine-polyphenylene **147**, featuring six pentaphenylbenzene moieties. Inset: schematic representation of the doping pattern of the hybrid-polyphenylene prepared.
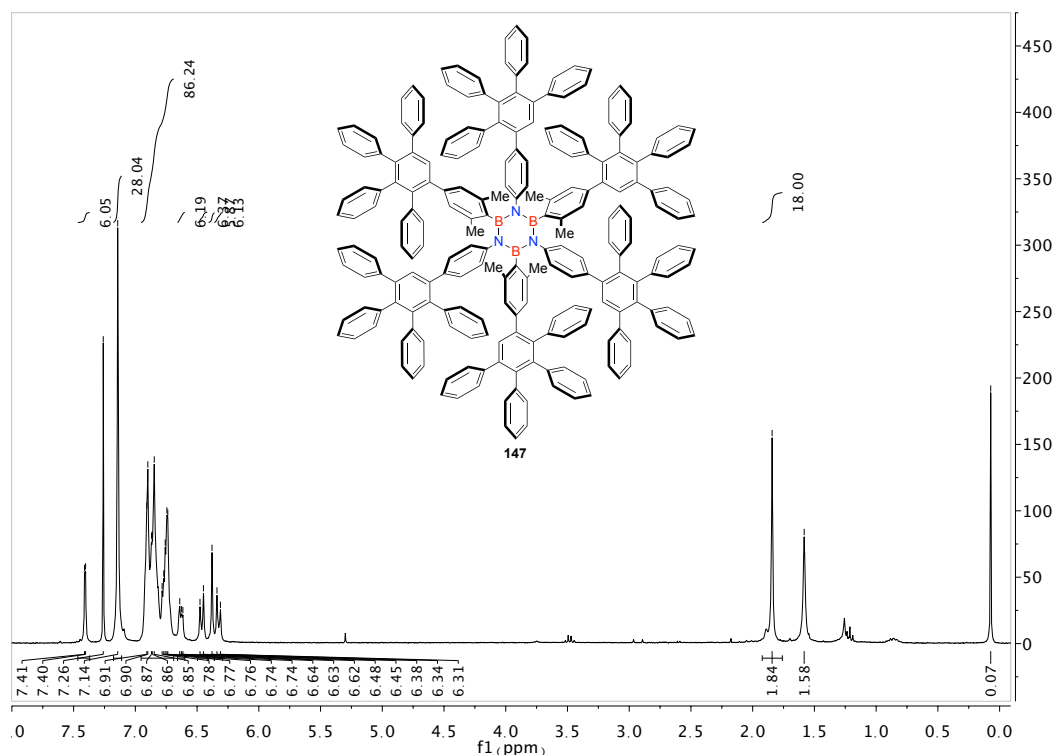
Figure 17 ^{1}H-NMR spectrum of **147** in CDCl$_3$ (400 MHz).

The first step before venturing into the preparation of the targeted hybrid polyphenylenes would be the investigation of the stability of the borazine core to such temperatures. For this reason, borazine core unit **108**, bearing six free ethynyl groups, was reacted with CPD in de-oxygenated diphenyl ether (Ph$_2$O) at 250 °C for 16 h (Scheme 59). Molecule **147**, featuring six pentaphenylbenzene branches and a doping dosage of $\rho = 2.8\%$, was

obtained in 48% yield. The ^{1}H-NMR spectrum (Figure 17) revealed the expected singlet in the aliphatic region (1.84 ppm) generated by the *o*-Me groups on the *B*-substituents. Instead, the aromatic region is constituted by complex multiplets, and only the signal of the protons attached to the central benzene of the pentaphenylbenzene branches stands out as a double singlet at 7.41 and 7.40 ppm. Furthermore, to confirm the nature of the BNC hybrid derivatives having high molecular weights, matrix-assisted laser desorption ionization (MALDI) mass spectrometry was used. Through this technique, detection of the high-resolution signal at *m/z* 2903.3126 (calc. for $[C_{222}H_{163}B_3N_3]^+$: 2903.3076), unambiguously confirmed the nature of molecule **147**. This structural confirmation proved the thermal resistance of borazine to such temperatures and, hence, the feasibility of the proposed strategy.

3.1.3.2 Synthesis of BN-polyphenylene with ρ= 8.3%
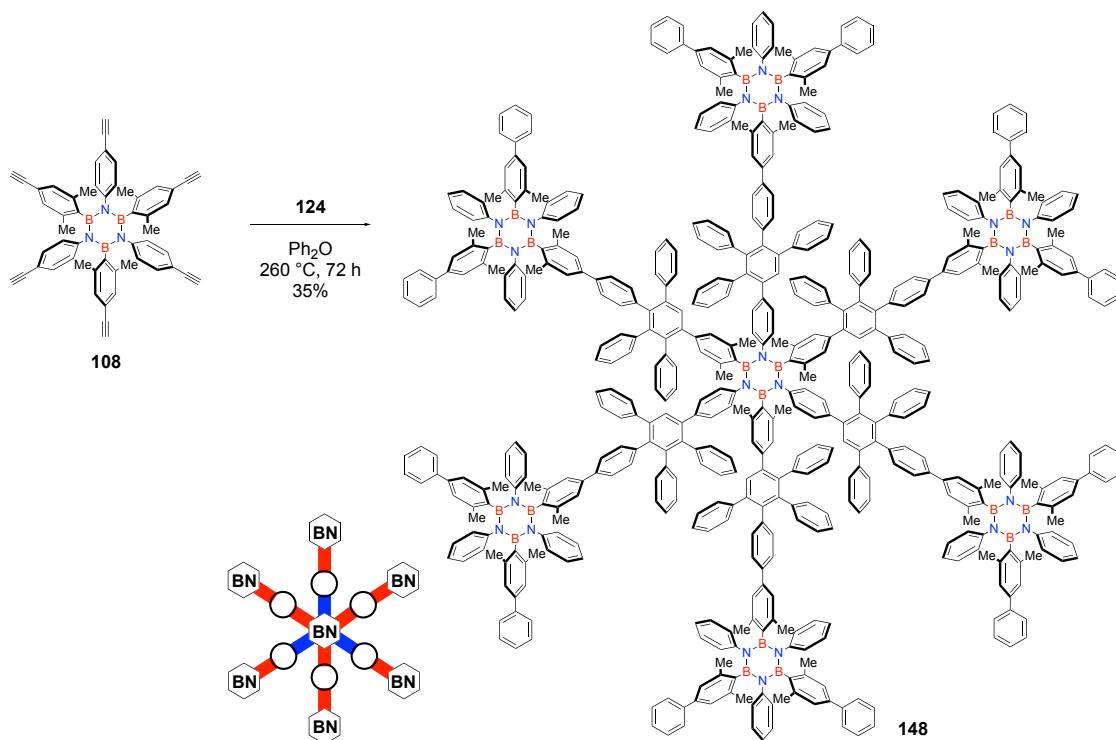
Scheme 60. Synthesis of borazine-doped hexa-branched polyphenylene **148** (ρ= 8.3%; $\alpha_N\beta_B$) Inset: schematic representation of the doping pattern of the hybrid-polyphenylene prepared.

Starting from borazine **108**, the six branches could be covalently linked pushing the temperatures up to the boiling point of Ph$_2$O (260 °C). When borazine-CPD **124** was used, molecule **148** (ρ= 8.3%) was obtained with 35% yield (Scheme 60) after 72 h.
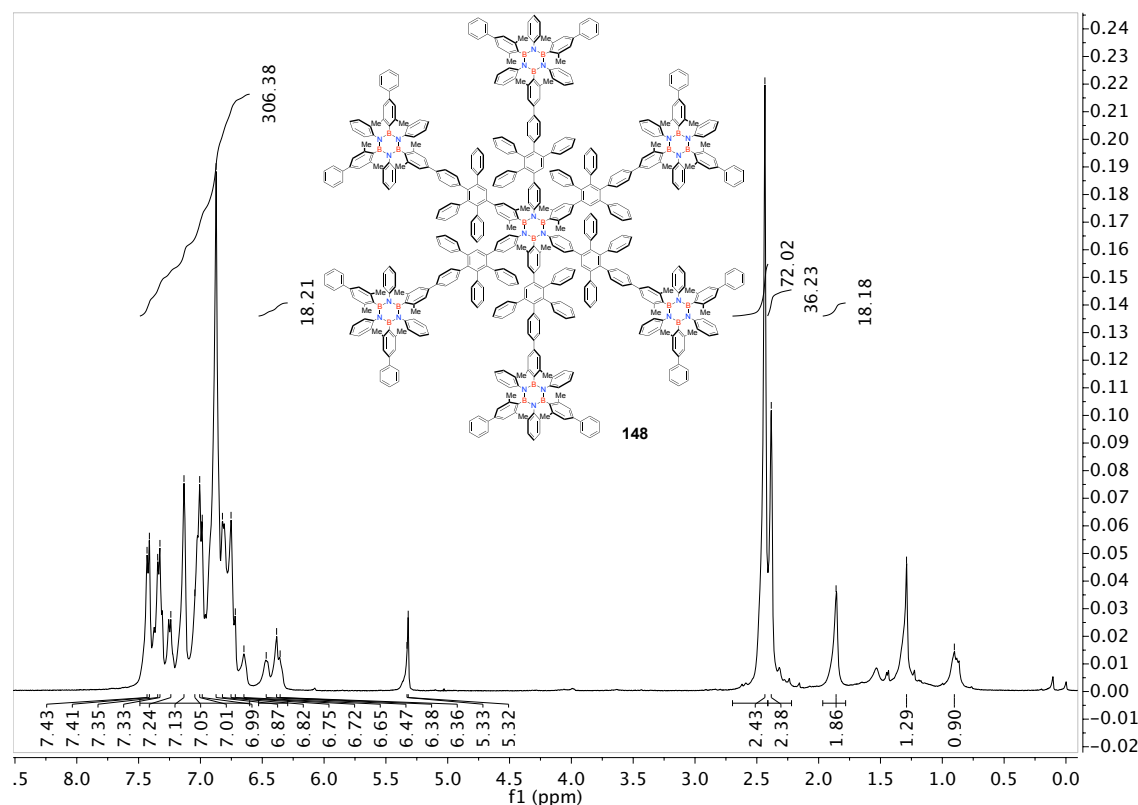
Figure 18. ^{1}H-NMR spectrum of **148** in CD$_2$Cl$_2$ (400 MHz).

The external doping units are connected through the boron sites at either the *B*- and *N*-sites of the central borazine core, therefore an $\alpha_N\beta_B$ connection has been generated. Once again, the structure was confirmed by ^{1}H-NMR spectroscopy (Figure 18). In molecule **148**, the *o*-Me groups resonate with singlets at 3 different frequencies: 1,85, 2.38, and 2.43 ppm. On the contrary, the large number of aromatic protons is reflected in the presence of a broad complex multiplet at 6.36-7.43 ppm. Further structural confirmation came from HR-MALDI mass analysis through detection of the signal at *m/z* 7532.8324 (calc. for [C$_{546}$H$_{450}$B$_{21}$N$_{21}$]$^+$: 7532.8144, see Chapter 4).

Using borazine-CPD **130** instead, led to formation of star-shaped molecule **149**, having the same doping dosage (ρ= 8.3%), in 36% yield (Scheme 61). In this case the external borazines are connected to the central one through the *N*-sites. The hybrid network is therefore characterized by $\beta_N\alpha_B$ connections.
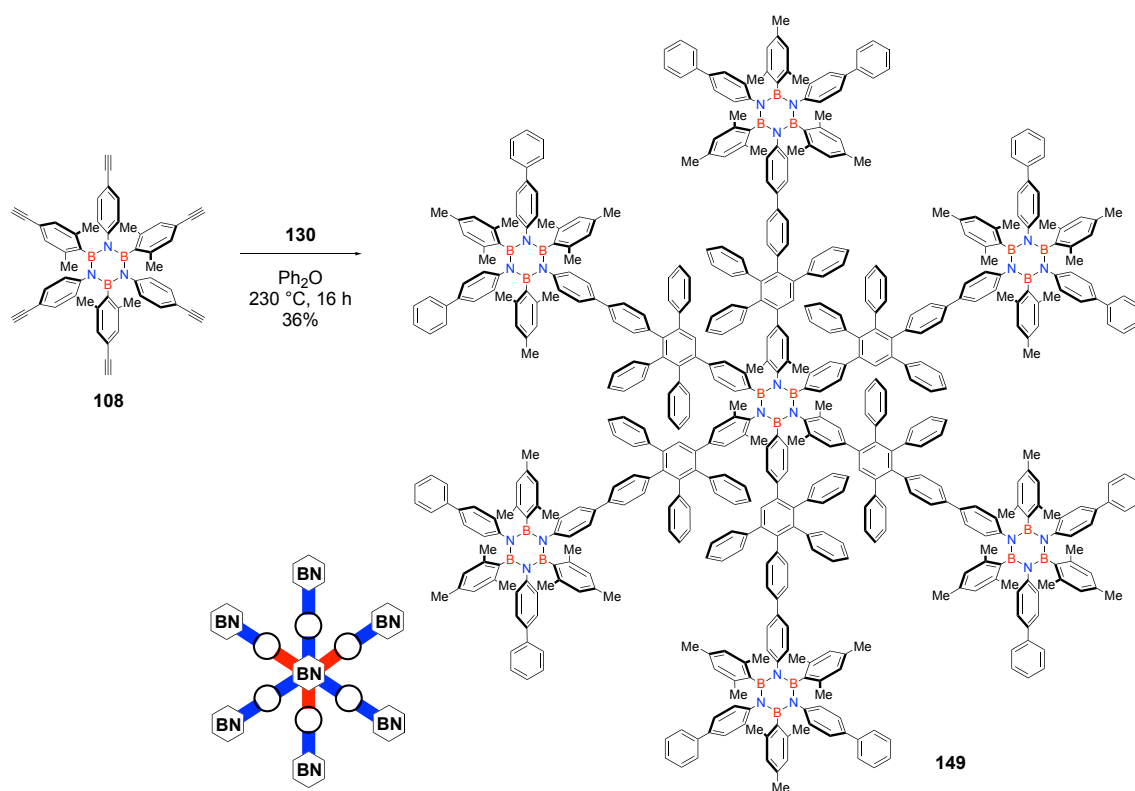
Scheme 61. Synthesis of borazine-doped hexa-branched polyphenylene **149** (ρ= 8.3%; $\beta_N\alpha_B$). Inset: schematic representation of the doping pattern of the hybrid-polyphenylene prepared.
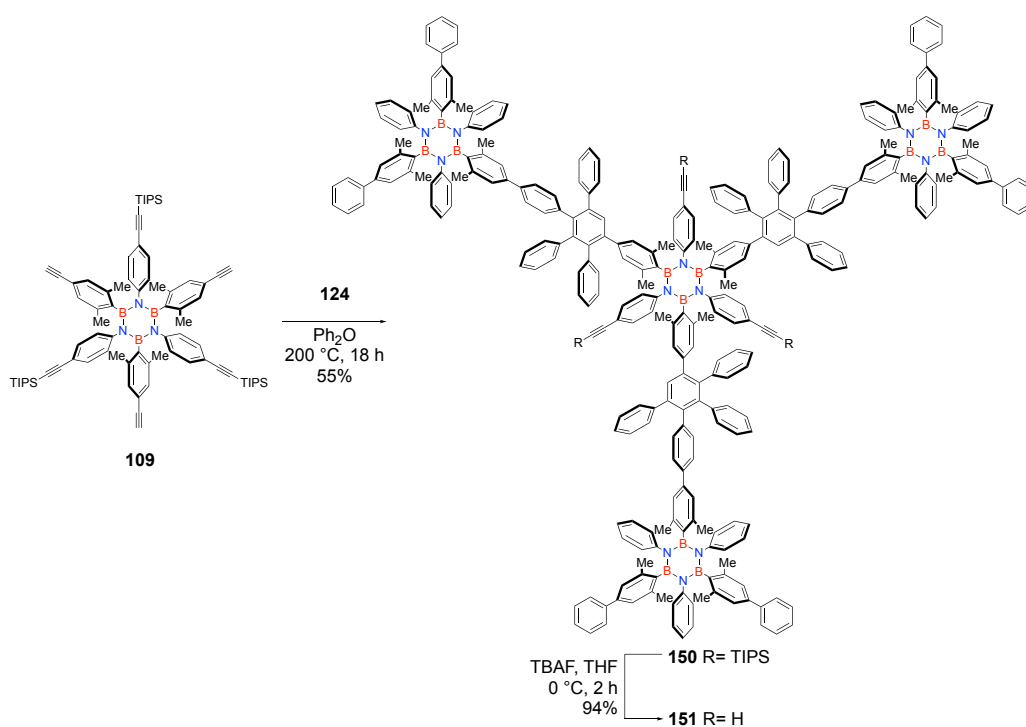
Scheme 62. Synthesis of three-branched borazine-doped PPh **151**, featuring β_B connections and three unprotected ethynyl groups at the *N*-sites.

As already pointed out in Scheme 46, taking advantage of the different steric hindrance of the TMS and of the TIPS groups, it is possible to obtain partially protected borazine core unit **109** by treatment of hexa-protected derivative **107** with K_2CO_3 in a MeOH/THF 1:1 mixture. Such intermediate was used as a building block to complete the library of borazino-doped hybrid networks and to generate the different combinations of doping orientations. Scheme 63 shows the synthesis of a star-shaped doped PPh where three B-B and three N-N connections are expressed. Borazine unit **109** was reacted with derivative **124** by cycloaddition reaction to form three-branched framework **150** in 55% yield. Total deprotection of the TIPS groups using TBAF afforded molecule **151** in almost quantitative yield after silica gel column chromatography (Scheme 62). Final Diels-Alder cycloaddition between **151** and **130** in refluxing Ph_2O afforded targeted molecule **152**, having doping dosage ρ of 8.3% and a $\beta_N\beta_B$ doping orientation, in 54% yield (Scheme 63).
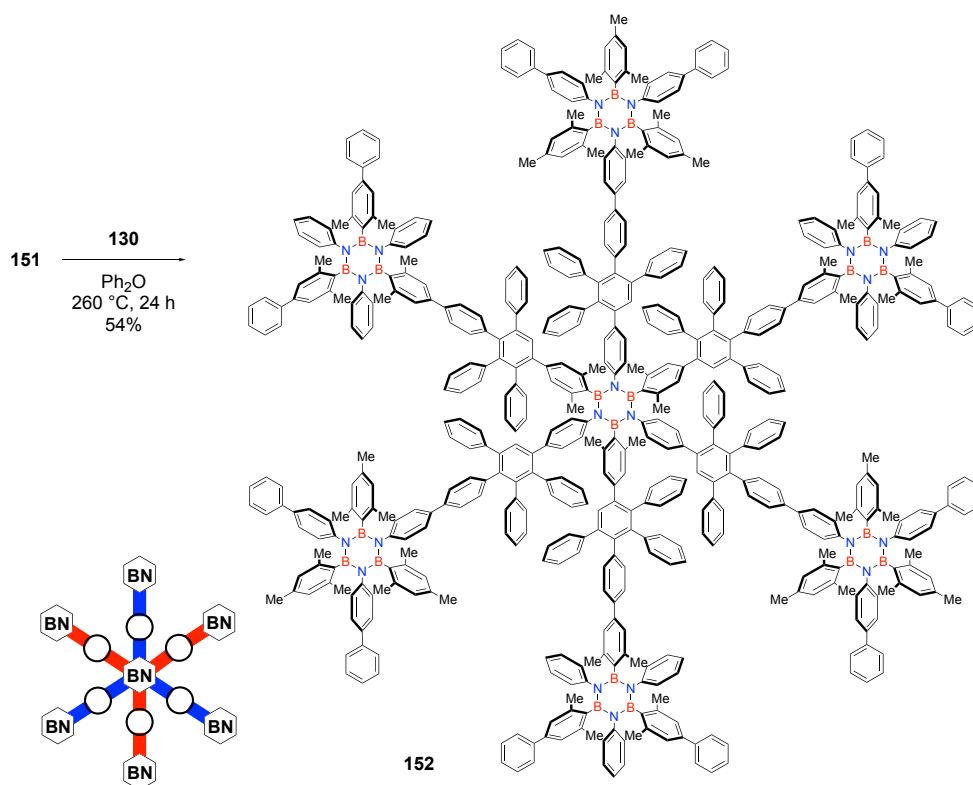
Scheme 63. Synthesis of borazine-doped polyphenylene **152** (ρ= 8.3%; $\beta_N\beta_B$). Inset: schematic representation of the doping pattern of the hybrid-polyphenylene prepared.

Analogously, borazine-doped polyphenylene **155**, with same doping dosage of **152** (ρ= 8.3%), but with a $\alpha_N\alpha_B$ doping pattern, could be synthesised in three steps starting from borazine **109** (Scheme 65).
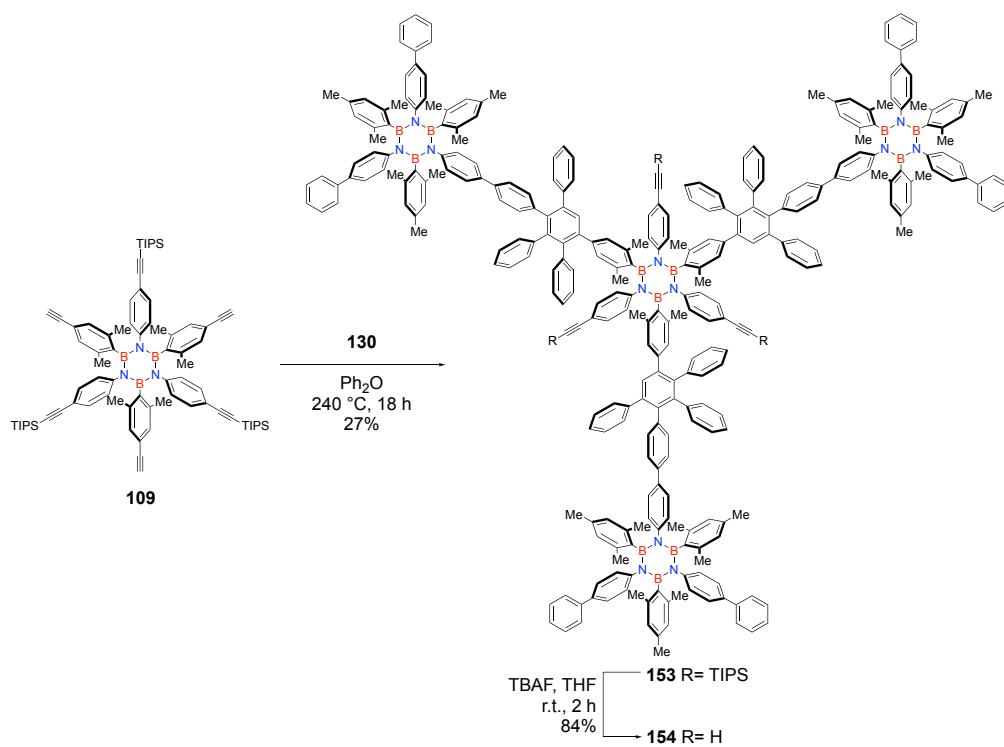
Scheme 64. Synthesis of three-branched borazine-doped PPh **154**, featuring α_B connections and three unprotected ethynyl groups at the *N*-sites.
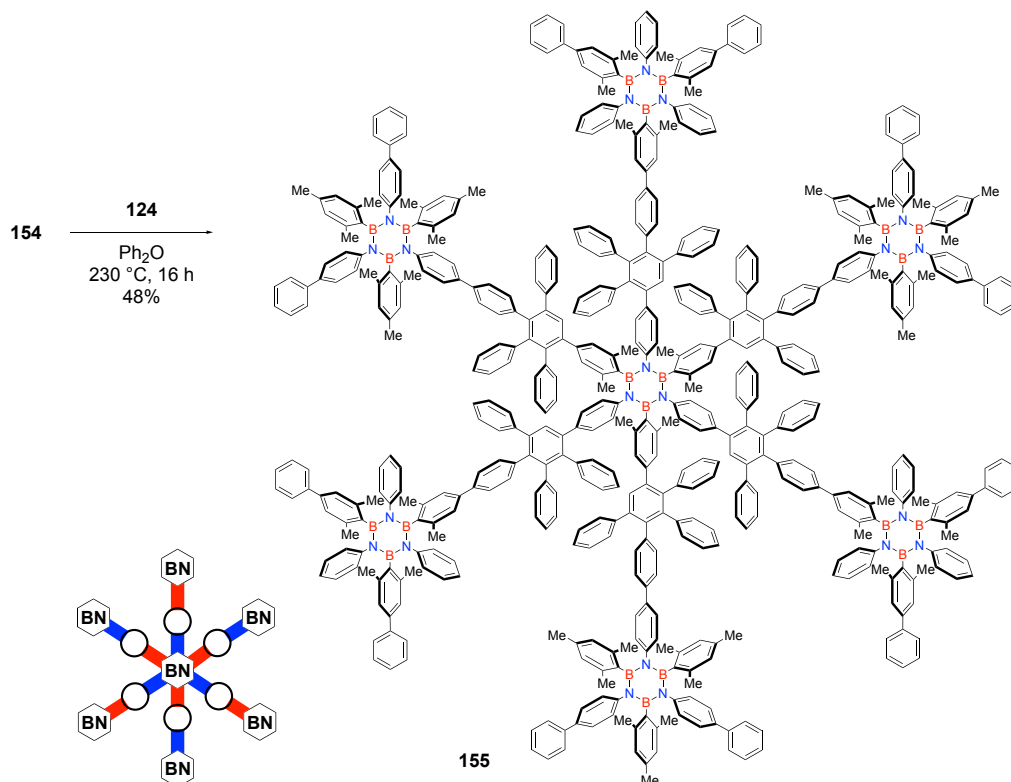
Scheme 65. Synthesis of borazine-doped polyphenylene **155** (ρ= 8.3%; $\alpha_N\alpha_B$). Inset: schematic representation of the doping pattern of the hybrid-polyphenylene prepared.

This was coupled with CPD intermediate **130** to give protected framework **153** in 27% yield. The TIPS-groups were removed by usual treatment with TBAF to afford molecule **154** that was submitted to the final cycloaddition with branching unit **124,** affording final product **155** in 48% yield (Scheme 65).

3.1.3.3 Synthesis of BN-polyphenylene with ρ= 7.1%
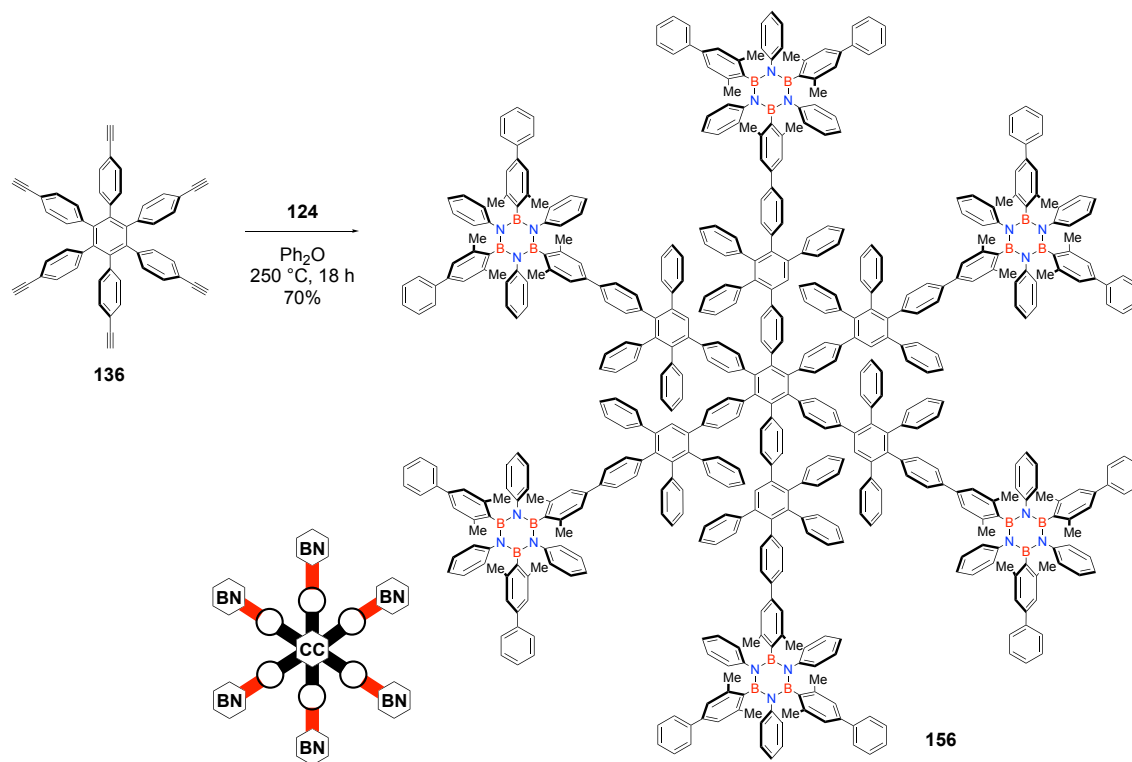
Scheme 66. Synthesis of borazine-doped network **156** (ρ= 7.1). Inset: schematic representation of the doping pattern of the hybrid-polyphenylene prepared.

Replacing the core unit with full-carbon derivative **136**, bearing six ethynyl groups, led to the formation of hybrid borazine frameworks **156** and **157**, after reaction with CPD-derivatives **124** (Scheme 66) and **130** (Scheme 67), respectively. While these two targeted molecules have the same doping dosage (ρ= 7.1%), they differ in the way the doped branching units are connected to the core. In molecule **156** the borazine units are connected to the central unit through the *B*-sites. In BN-PPh **157**, the peripheral units are instead attached by the *N*-sites. ^{1}H-NMR spectroscopy of **157** in CDCl₃ (Figure 19) shows the singlets from the *o*-Me groups at 2.26-2.24 and 1.98-1.96 ppm, which display similar δ values to those seen for borazine **45** (Scheme 17, section 1.1.4).[91] Instead, in the aromatic region most of the signals are mixed to form multiplets between 7.39 and 6.27 ppm.
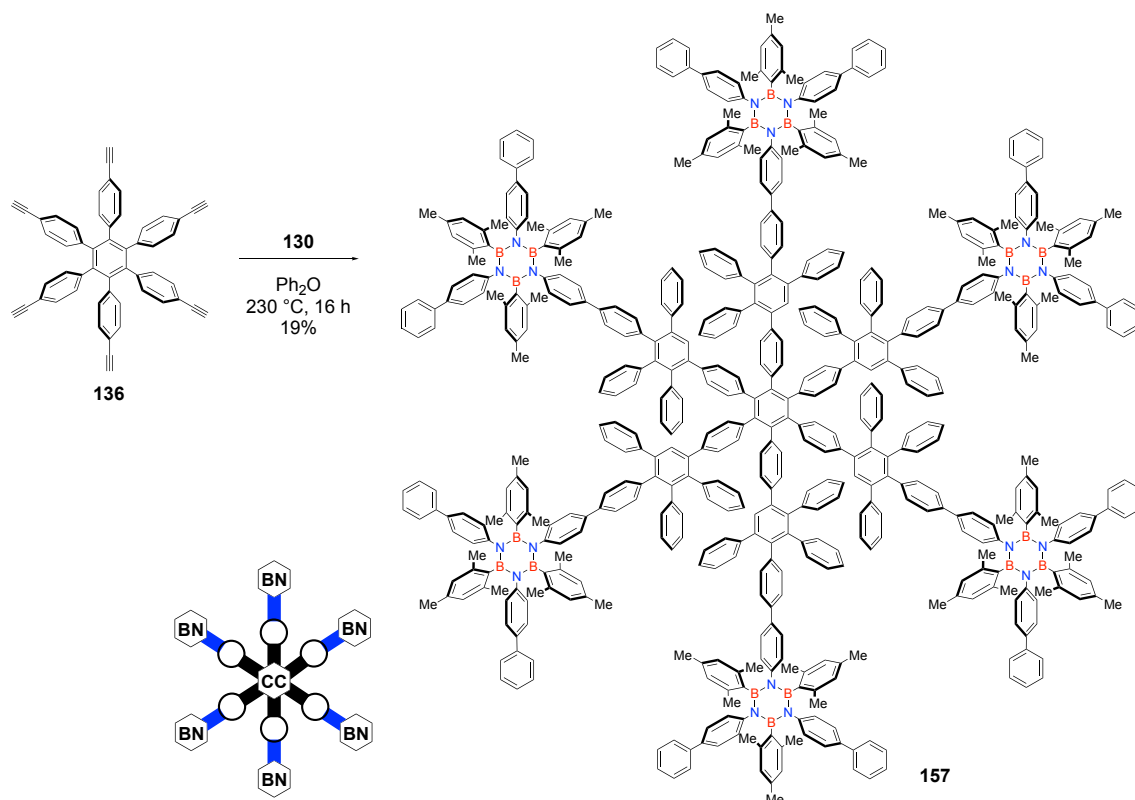
Scheme 67. Synthesis of borazine-doped network **157** (ρ= 7.1%). Insets: schematic representation of the doping pattern of the hybrid-polyphenylene prepared.
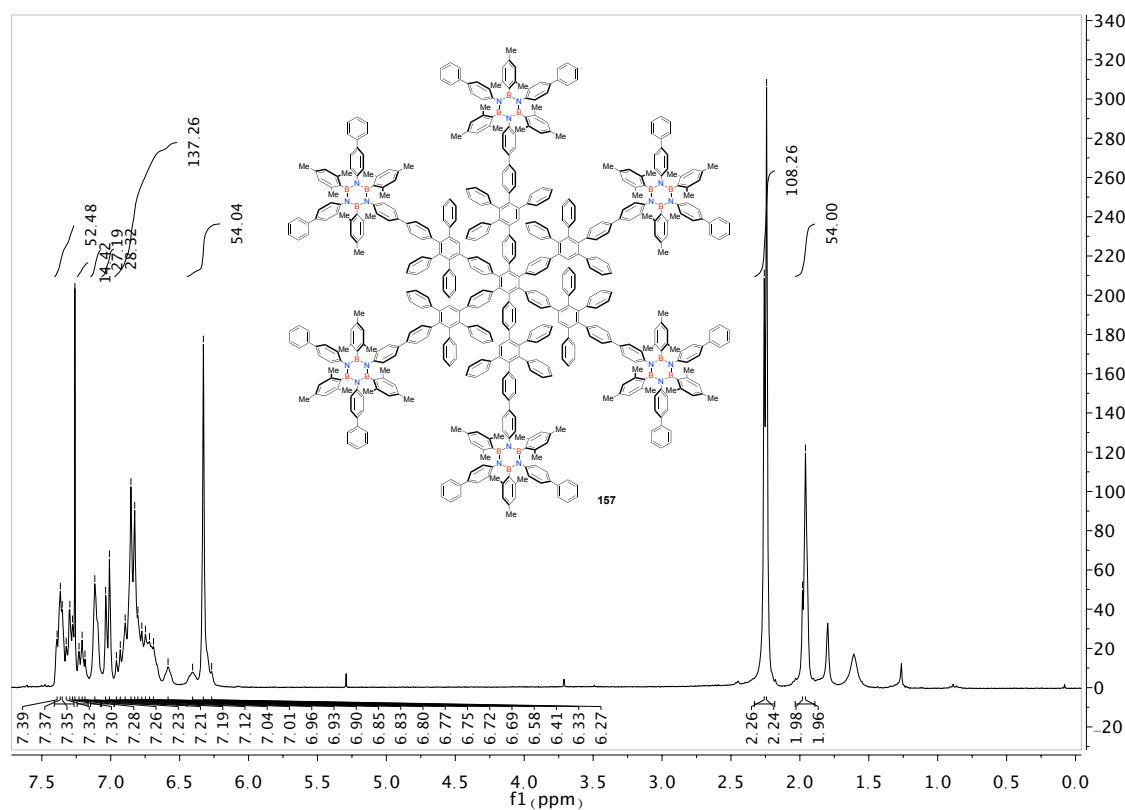
Figure 19. ^{1}H-NMR spectrum of **157** in CDCl$_3$ (300 MHz).

3.1.3.4 Synthesis of BN-polyphenylene with ρ= 1.1%

Mono-doped borazino-polyphenylene **158**, featuring a low doping dosage (ρ= 1.1%), was instead obtained in 46% yield after reaction between borazine **108** and CPD derivative **146** at 260 ˚C in Ph$_2$O for 30 h (Scheme 68).
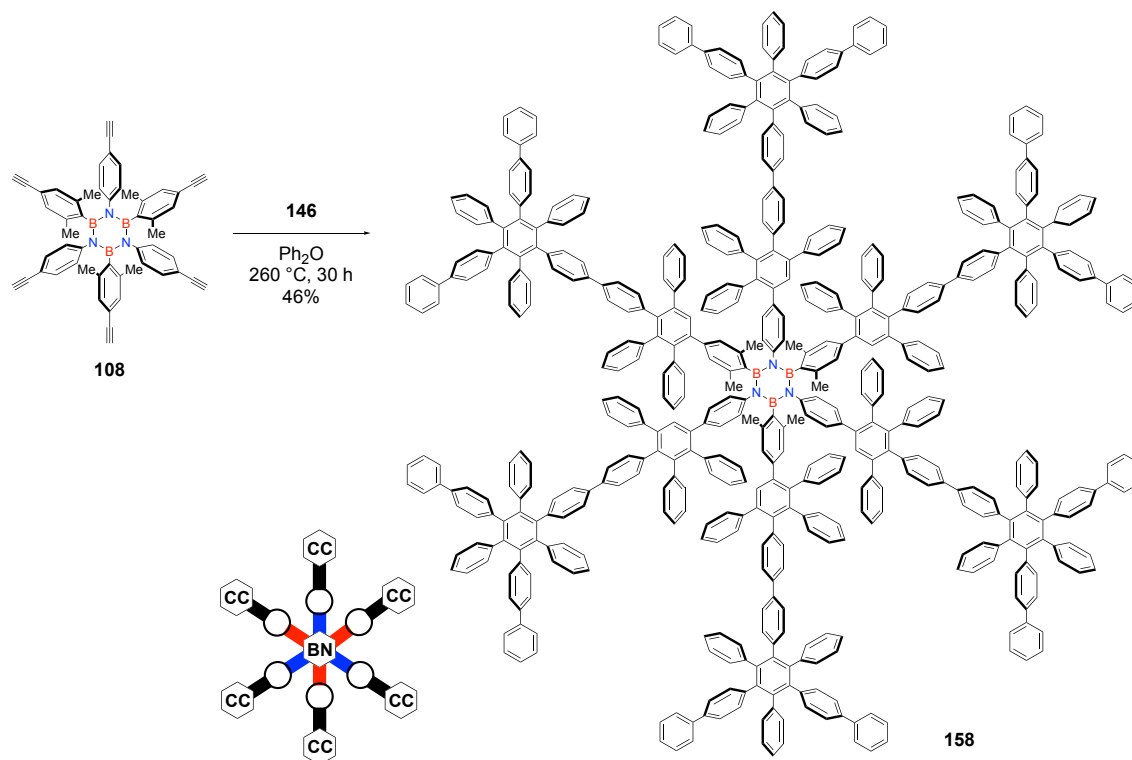
Scheme 68. Synthesis of hybrid hexa-branched borazine-polyphenylene **158** (ρ= 1.1%). Inset: schematic representation of the doping pattern of the hybrid-polyphenylene prepared.

3.1.3.5 Synthesis of full-carbon polyphenylene and reference molecules

Finally, full-carbon star-shaped polyphenylene **159** is obtained in 49% yield upon reaction of **136** and **146** (Scheme 69). While having completed the synthesis of the polyphenylene networks having different doping dosages and orientations, a last synthetic effort has been done in order to prepare molecules **161**, **162**, and **163** (Scheme 70). These molecules represent the references to probe the photophysical features of the single pentaphenylbenzene fragment, and the mono-branched borazine units. By reacting phenylacetylene (**160**) with CPD, and with borazines **124** and **130** under MW irradiation, it was possible to obtain unsubstituted pentaphenylbenzene **161** with 92% yield, and borazines **162** and **163**, bearing a single oligophenylene fragment at the *B*- and *N*-site, respectively, both having a doping dosage ρ of 7.1%. Between the reference molecules that will take part in the photophysical study, also hexaarylborazines **117** (ρ= 11%,

Scheme 49), **129** (ρ= 11%, Scheme 52), and hexaarylbenzene **145** (Scheme 57) will be included.
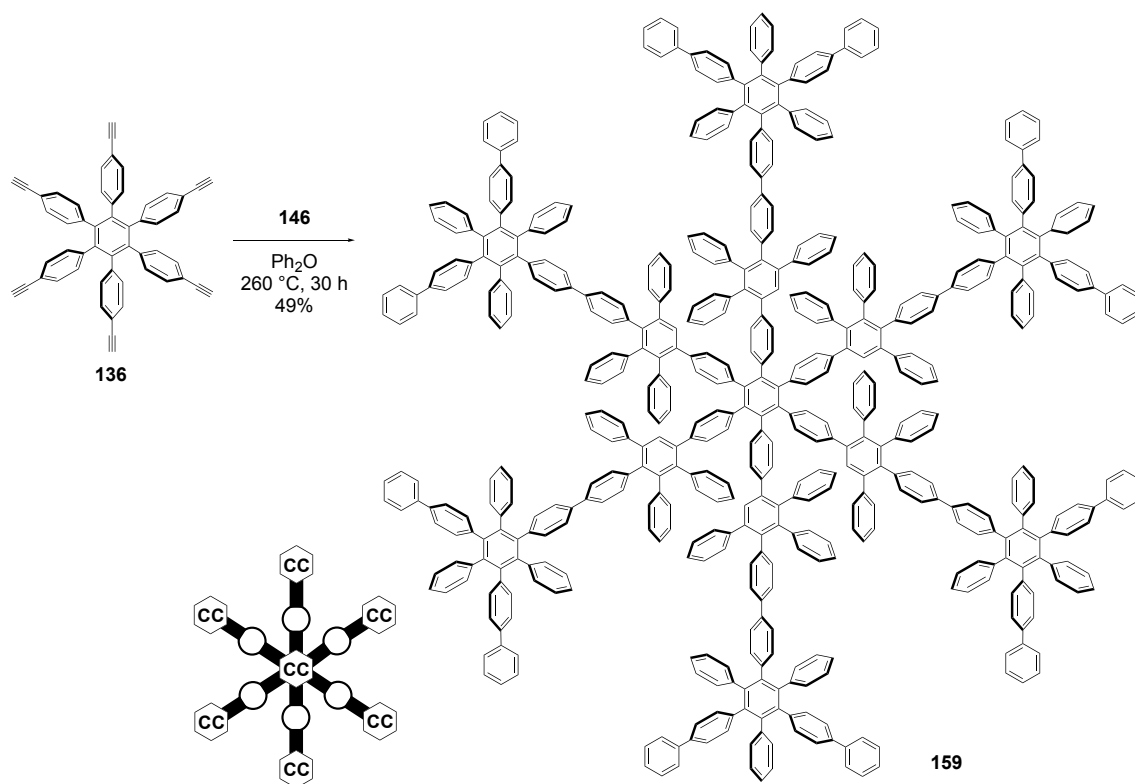
Scheme 69. Synthesis of full-carbon polyphenylene **159**. Inset: schematic representation of the doping pattern of the full-carbon PPh prepared.
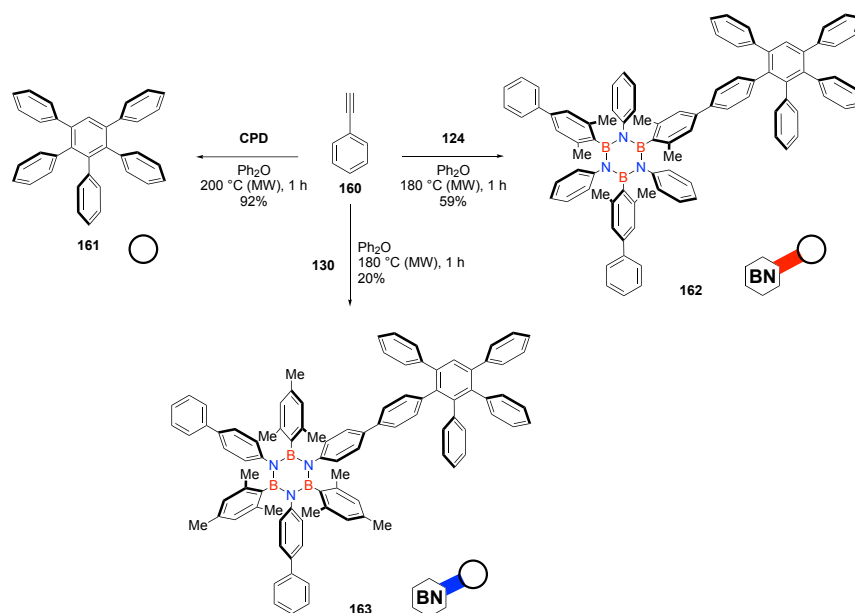
Scheme 70. Synthesis of reference full-carbon molecule **161**, and reference borazines **162** and **163** (ρ= 7.1%, both). Insets (bottom of molecules **161**, **162**, and **163**): schematic representations of the doping pattern of the hybrid-polyphenylenes prepared.

3.1.4 Spectroscopic studies of hybrid BNC polyphenylenes
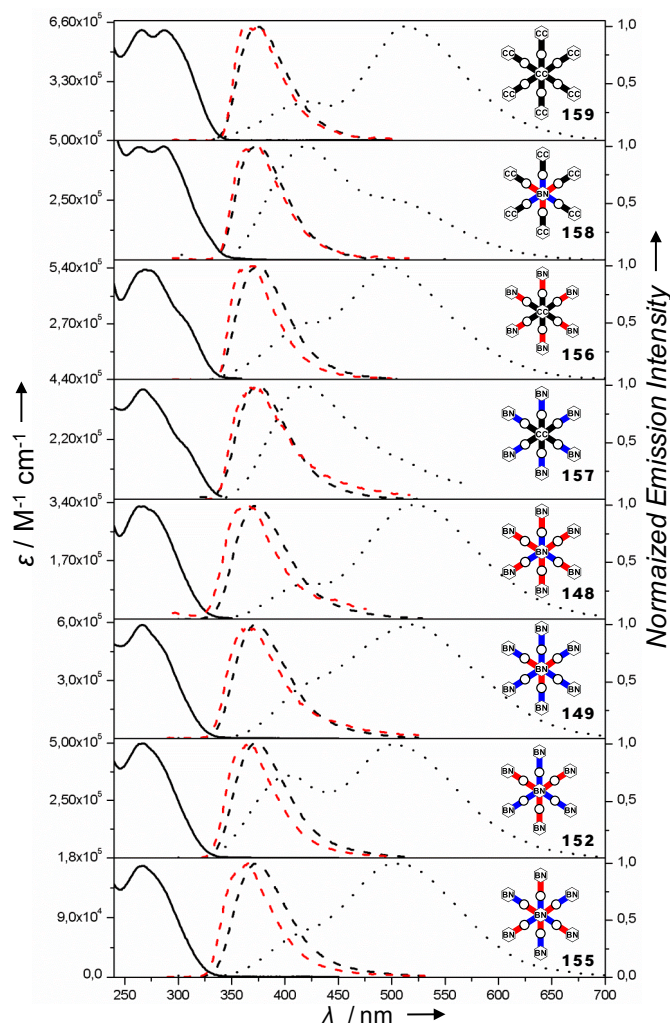
Figure 20. Normalized absorption at 298 K (solid), fluorescence at 298 K (dash, black), fluorescence at 77 K (dash, red), and phosphorescence at 77 K (dotted) spectra of BN-PPh **148**, **149**, **152**, and **155-159** in CH$_2$Cl$_2$.

In this section, the optical properties of the hexa-branched borazine-doped polyphenylene derivatives with different doping dosages (ρ) were studied in detail. Figure 20 shows the spectra of absorption and emission at room temperature in CH$_2$Cl$_2$ solutions, with the fluorescence and phosphorescence profiles obtained at 77 K for the borazine-doped PPh derivatives **148**, **149**, **152**, and **155-159**. Moreover, the results obtained for the reference molecules (linker **161**, full-carbon unit **145**, borazine units **117** and **129**, mono-branched borazines **162** and **163**, and hexa-branched borazine **147**) are shown in Figure 21, and the key measured data are summarized in Table 3. The absorption spectra for hexa-branched PPh lie in a narrow region between 250 and 325 nm in the deep UV. As demonstrated by *de Schryver* et al.,[234] increasing the size of the system and, thus, the number of phenyl

units composing the structure, leads to an enhancement of the molar extinction coefficient (ε) at the maximum of absorption and to a broadening of the band.
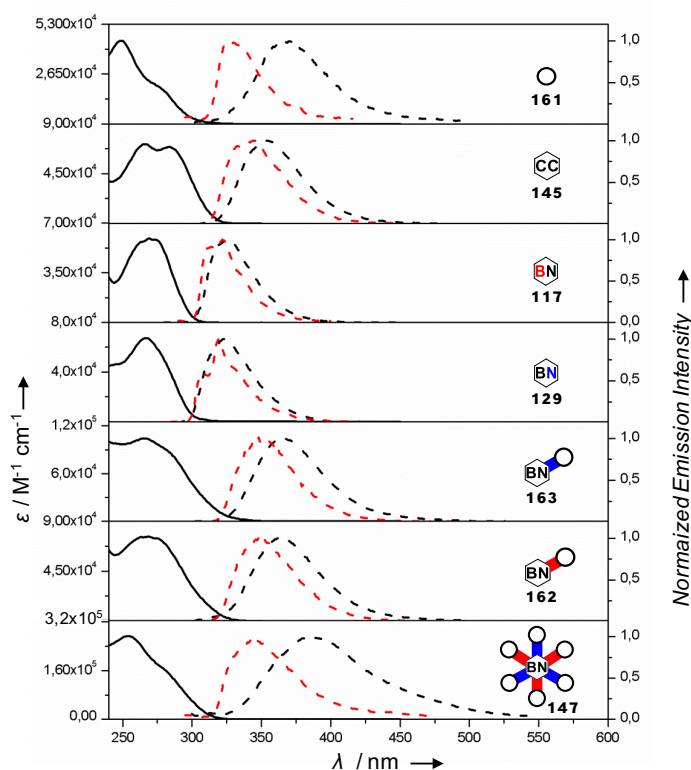
Figure 21. Absorption at 298 K (solid), emission at 298 K (dash, black), emission at 77 K (dash, red) of phenylenes **161** and **145**, and borazine-doped derivatives **117**, **129**, **147**, **162** and **163** in CH_2Cl_2.

Monomeric reference borazines **117** and **129** display ε values of ~6 x 10^4 M^{-1} cm^{-1} while the full-carbon unit **145** has a slightly higher value of 7.1 x 10^4 M^{-1} cm^{-1}. For the hexa-branched hybrid frameworks (**148**, **149**, **152**, and **155-159**), a very efficient absorption was observed with values of ε lying between 1.7 $\times$ 10^5 M^{-1} cm^{-1} and 6.1 $\times$ 10^5 M^{-1} cm^{-1}. Single band broad absorption profiles originate from molecules with high doping dosage ρ, while lower BN percentages generate two bands whose combination results in a two-peak profile with an interval of ~40 nm between the maxima. Luminescence measurement on air-equilibrated CH_2Cl_2 solutions showed a significant emission in the near-UV region, with no significant shift of the emission maxima throughout the hexa-branched hybrid frameworks series. Additionally, short fluorescence lifetimes (0.4-0.8 ns) were measured, indicating fast radiative deactivation from the singlet excited state. The excitation spectra of the derivatives mainly correspond to the absorption profiles, confirming the uniform contribution to the emission by all the components of the absorption bands. When the emission spectra were recorded at 77 K, only a slight hypsochromic shift of the

fluorescence maxima was observed. Fluorescence quantum yields range between 18% and 77%, and reveal a clear inverse dependence of the emission efficiencies on the doping dosage ρ.

Table 3. Steady-state absorption and emission properties of the BN-doped and all-carbon polyphenylene derivatives in CH_2Cl_2.

class	compd. (ρ)	Absorption λ_{max} [nm]	ε ($M^{-1}\,cm^{-1}$)	λ_{exc} [nm]	λ_{max} 298 K [nm] (Φ_F)[a]	τ_F[b] [ns]	Emission k_F[c] [ns^{-1}]	$k_v+k_{ISC}+k_{CS}$[d] [ns^{-1}]	λ_{max} 77 K [nm]	$\lambda_{max,PH}$ 77 K [nm]
hexa-branched	159 (0%)	266	6.1×10^5	280	376 (77%)	0.5	1.54	0.46	376	510, 423[e]
	158 (1.1%)	265	4.7×10^5	268	372 (71%)	0.6	1.18	0.42	372	420, 504[e]
	156 (7.1%)	269	5.3×10^5	263	370 (62%)	0.8	0.77	0.48	373	498, 423[e]
	157 (7.1%)	267	4.0×10^5	266	375 (57%)	0.8	0.71	0.54	373	419
	148 (8.3%)	263	3.3×10^5	275	374 (26%)	0.8	0.32	0.92	365	521, 414[e]
	149 (8.3%)	266	5.8×10^5	274	373 (25%)	0.5	0.5	1.5	366	519, 420[e]
	152 (8.3%)	267	4.9×10^5	271	377 (22%)	0.4	0.55	1.95	369	504, 402[e]
	155 (8.3%)	267	1.7×10^5	272	373 (18%)	0.4	0.45	2.05	365	504, 417[e]
reference	161 (0%)	248	4.4×10^4	259	369 (0.8%)	< 0.1	-	-	325	-
	145 (0%)	266	7.1×10^4	264	355 (9%)	0.3	0.30	3.03	344	-
mono	117 (11%)	269	5.9×10^4	263	327 (20%)	0.7	0.28	1.14	322	476, 451[e], 478[e], 505[e]
	129 (11%)	267	6.7×10^4	273	322 (34%)	2.7	0.12	0.25	319	478
	163 (7.1%)	266	7.6×10^5	273	362 (20%)	0.3	0.66	2.67	348	-
	162 (7.1%)	268	1.0×10^5	275	365 (16%)	0.3	0.53	2.8	350	-
	147 (2.8%)	254	2.7×10^5	264	385 (1%)	0.3	0.03	3.3	343	-

[a] Φ_{em}: emission quantum yield. [b] Lifetime at 295 nm. [c] Radiative rate constant, given by $k_F = \Phi_{em}/\tau_F$. [d] Total non-radiative rate constant, given by $(1/\tau_F) - k_F$; k_v: vibrational relaxation rate constant, k_{ISC}: inter-system crossing rate constant, k_{CS}: charge separation rate constant. [e] Shoulder phosphorescence peaks.

3.1.4.1 Monomeric and reference derivatives

Reference borazines **117** and **129** differ from the peripheral substitution with phenyl groups at the *B* and *N*-sites, respectively, and have the highest doping dosage (ρ= 11%) among the molecules taking part in this study. Grafting phenyl substituents in the outer shell lead to an enhancement of the quantum yields (Φ_F= 20% for **117**, Φ_F= 34% for **129**) and shortening of the lifetimes (τ_F= 0.7 ns for **117**, τ_F= 2.7 ns **129**) with respect to *B,B',B''*-trimesityl-*N,N',N''*-triphenylborazine **45** (Φ_F= 7.7%; τ_F= 7.1 ns).[91] The all-carbon relative **145** has similar lifetime (τ_f= 0.3 ns), but shows less efficient emission having a quantum yield of 9%. Mono-doped borazines **117** and **129** show the lowest Stoke-shift with emission maxima at 327 and 322 nm, while full-carbon congener **145** displayed a greater difference between its absorption (266 nm) and emission (355 nm) maxima. The enhancement in the emission intensities for borazine-doped relatives can be ascribed to the *o*-Me groups that hampers the rotation, rigidifying the hexaaryl-substituted BN-doped structures (**117**, **129**) compared to that of hexaphenyl benzene derivative **145**. As a consequence of rigidity, decay of the excited states through vibrational non-radiative pathway can indeed be prevented, thus increasing the quantum yields. Upon branching of the scaffold, the emission intensity decreases as more pentaphenylbenzene spokes are added (Φ_F= 20% and 16% for **163** and **162**, respectively), with hexakis-(pentaphenylbenzene)-substituted reference borazine **147** displaying one of the weakest emission intensities throughout the library (Φ_F= 1%) (Figure 21; Table 3). Given the low emission contribution from the pentaphenylbenzene moieties (Φ_F< 1% for **161**), the responsibility for the weakening of the intensities, observed for the reference molecules, can be assigned to the peripheral pentaphenylbenzene fragments that trigger vibrational non-radiative deactivation pathways. Notably, molecules **129** and **163,** in which the branching functionalities are grafted exclusively at the *N*-sites show a slightly higher emission efficiency in comparison to **117** and **162**, the corresponding derivatives with functionalization at the *B*-sites. The differences between these similar derivatives suggest that the functionalization pattern plays a relevant role in the electronic properties of the system and it is not as innocent as one could think in the first place given the structural similarities. Since the double bond character for the BN bonds is lower than 20% (the double bond character for *h*-BN is ~22%),[293] one can consider the boron and nitrogen atoms to be neutral.[294] This allows the assumption that the electronic richness is essentially retained by the N atoms, while the B atoms keep their electronic deficiency.
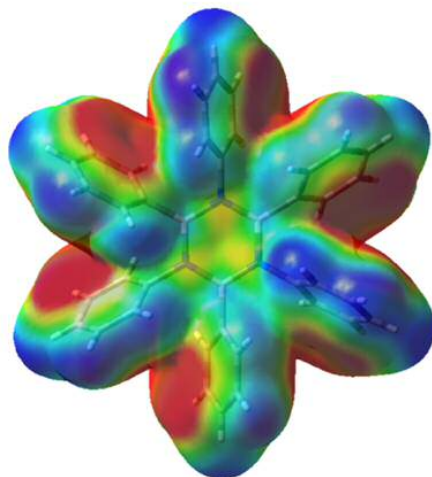
Figure 22. Electrostatic surface potential were generated at B3LYP/6-31G(d,p) level of theory and mapped on the van Der Waals surface of molecules up to an electron density of 0.001 electron/bohr³ (calculated using Gaussian 09 at B3LYP/6-31G(d,p) level of theory) for hexaphenylborazine **43**. The red and blue indicate negative and positive charge densities.

To confirm the hypothesis, further clues are provided by the calculated electrostatic surface potential (ESP) plot (Figure 22). This shows a charge polarization of the sp^2-hybridized B_3N_3 surface, where negatively charged N atoms and positively charged B atoms can be clearly seen. As demonstrated in previous studies on BN-doped donor-acceptor conjugated derivatives,[295–298] the emissive excited states could be deactivated by the presence of dynamic processes involving photo-induced short-living CS (charge separated) states that can take place between the electron donating and electron withdrawing moieties.

3.1.4.2 Hexa-branched polyphenylenes

Moving away from the reference molecules and mono-doped small oligophenylene derivatives, in this section the attention will be focused on the derivatives possessing six branches. Contrarily to what one can predict taking into account previous studies[91] and the results obtained with monomeric and reference derivative series, for these BNC hybrids, a neat decrease in emission efficiency is observed when increasing the doping dosage (Figure 23, and Table 3). All-carbon framework **159** shows the strongest emission (Φ_F= 77%). When the central benzene ring is replaced with the inorganic borazine analogue, generating molecule **158** with ρ= 1.1%, a modest quenching of the fluorescence was obtained (Φ_F= 71%). Consequently, when the six peripheral units were doped generating derivatives **157** and **156**, increasing the doping dosage to a value of 7.1%, a more consistent decrease in the quantum yield values could be observed (57% and 62%,

respectively). Again, as observed for the three-branched hybrid derivatives, the simultaneous presence of the central and the peripheral borazine units causes an even more significant lowering of emission intensities. For hepta-borazine derivatives **149**, **148**, **152**, and **155** the quantum yields dropped to values between 18% and 26%. Notably, the Φ_F seems to be very lightly affected by the doping pattern, and in particular by the relative orientation between the borazine doping units ($\beta_N\alpha_B$ for **149**, $\alpha_N\beta_B$ for **148**, and $\beta_N\beta_B$ for **152**, $\alpha_N\alpha_B$ for **155**). Taking into account the calculated radiative and total non-radiative deactivation rate constants (k_F and k_{NR}) shown in Table 3, one can further observe the progressive suppression of the radiative deactivation of the singlet excited states operated by the presence of the borazine dopant units.
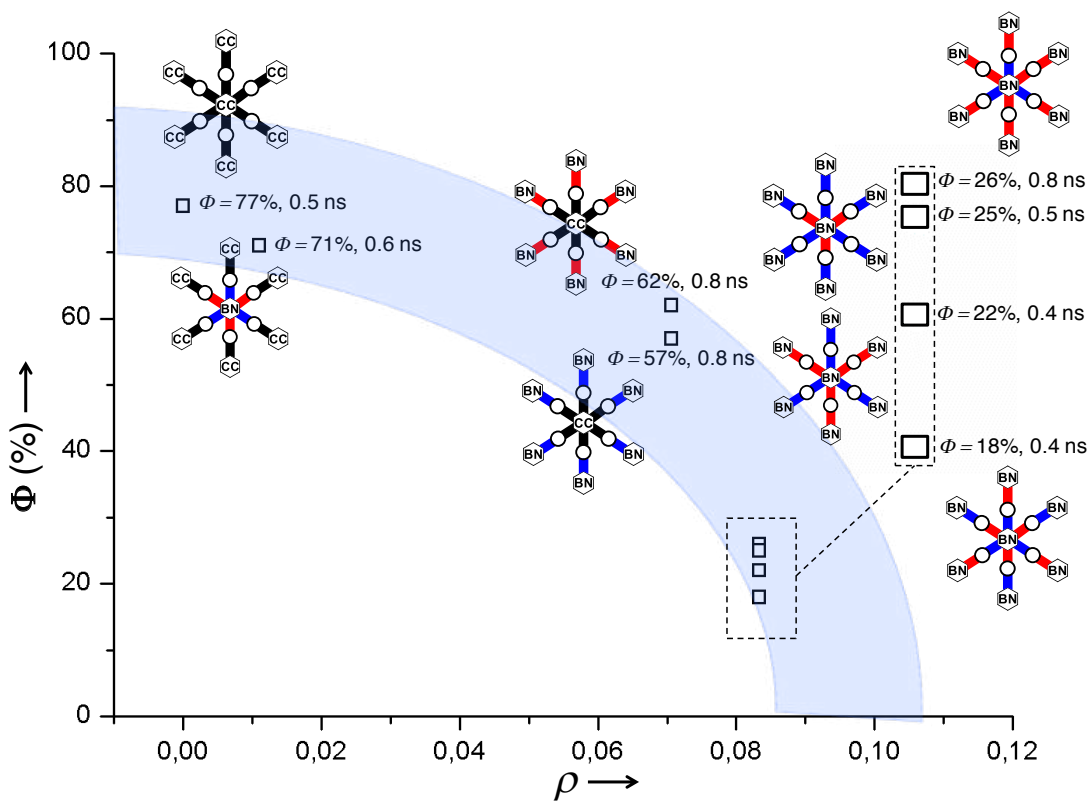
Figure 23. Emission quantum yield as a function of the dosage and orientational doping for the hexa-branched polyphenylenes series.

However, having high doping dosage and mixing of the different possible connections between borazine units (B-N, B-B, or N-N) within single derivatives, just a negligible effect of doping orientation was observed on the quantum yield of hepta-borazines **149**, **148**, **152**, and **155**. Thus, it is possible that at high ρ the emission intensities of these

BNC hybrid frameworks are averaged due to the presence of multiple intramolecular electronic interaction.

3.1.4.3 Three-branched borazine-doped polyphenylenes

During the course of this thesis work, a parallel project was undertaken in the same research group by *Francesco Fasano*. His synthetic effort consisted in the bottom-up synthesis of three-branched borazine-doped polyphenylenes.
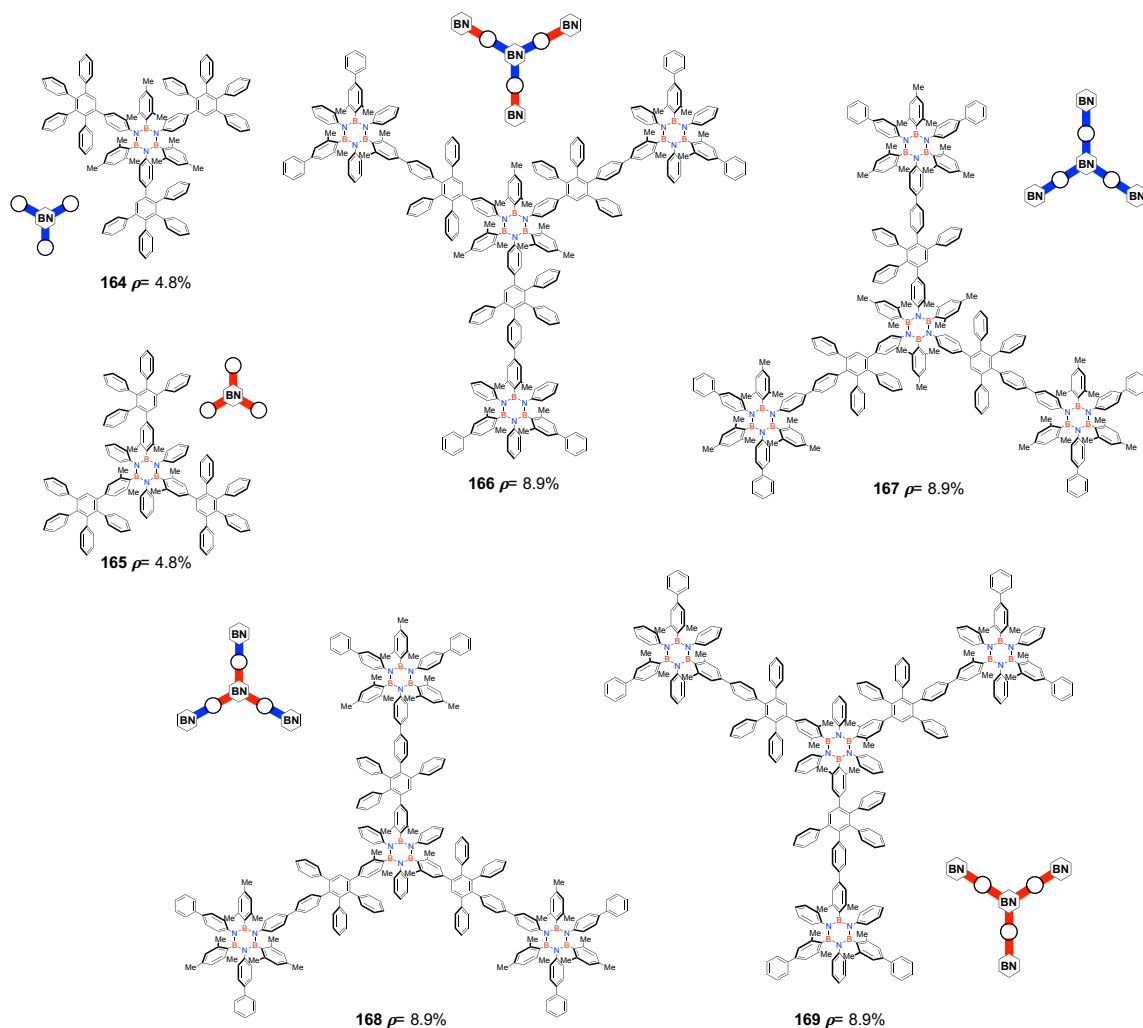
Scheme 71. Structure of the three-branched borazine-doped PPh **164-169**, synthesised in a parallel work. Insets: schematic representations of the doping pattern of the hybrid-polyphenylenes prepared.

These derivatives were prepared following a similar strategy to that used in this work for the synthesis of hexa-branched borazine-doped polyphenylenes. In Scheme 71 and Scheme 72, the structures of the three-branched BNC hybrid polyphenylenes are disclosed. The synthesis, characterization, and the absorption and emission study of these hybrid-BNC derivatives have been published together with the other borazine-doped

polyphenylenes reported in this thesis manuscript.[117] The results obtained from this series helped to disclose the effects of size and doping orientation and dosage on the photochemical features of BNC hybrid polyphenylenes.
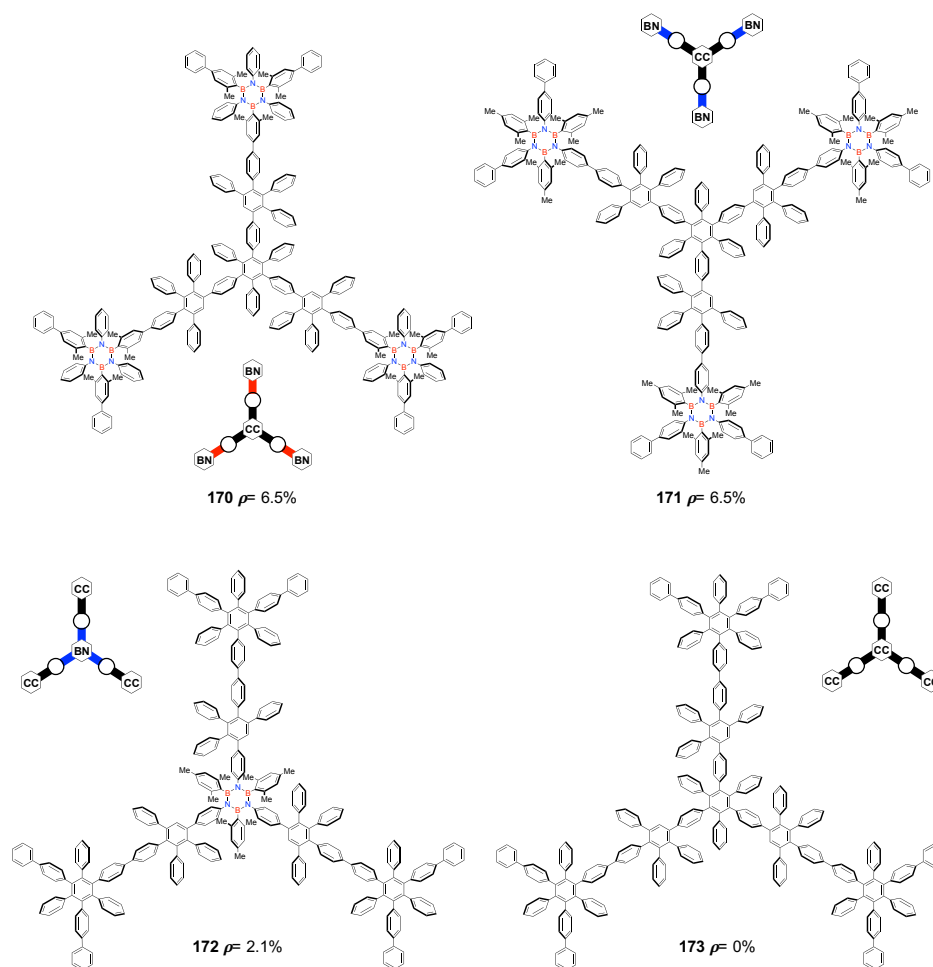
Scheme 72. Structure of the three-branched borazine-doped and full-carbon PPh **170-173**, synthesised in a parallel work. Insets: schematic representations of the doping pattern of the hybrid-polyphenylenes prepared.

Analogously to the series of hexa-branched BNC hybrid frameworks, also for the series composed of smaller three-branched derivatives, a decrease in emission efficiency is observed upon increase of the doping ratio ρ. Throughout the series, the values of fluorescence quantum yield (Φ_F) range between 7% and 76%, with the full carbon derivative showing again the best emission. As a general consideration regarding the effect of doping orientation in the derivatives with high doping dosage (ρ= 8.9%), the major fluorescence quenching is observed for molecules **169** (Φ_F= 7%) and **168** (Φ_F= 11%) where the peripheral borazine-doped units branch from the core of one through the *B*-sites of the latter. Rather, molecules **166** and **167**, where the branches are attached to

the *N*-sites of the core borazine unit, show values of Φ_F of 33% and 29%, respectively. Instead, no considerable effect of the doping orientation was observed with molecules **170** and **171**, featuring a full-carbon core and borazine-doped branches, displaying essentially the same Φ_F value (45% and 44%, respectively).

3.2 Synthesis of a multichromophoric BNC hybrid polyphenylene

3.2.1 Synthesis of blue-labelled borazine-doped polyphenylene

Starting from β_B three-branched PPh **151**, bearing three ethynyl groups (Scheme 63), covalent attachment of the blue NDI acceptor to the BNC framework will be provided by Cu-catalyzed azide-alkyne cycloaddition through formation of an aromatic five-membered 1,2,3-triazole ring.[299] The synthesis of the naphtalenediimide (NDI) chromophore **174** was achieved taking advantage of the methodology developed by *Berezin* and *Bonifazi* for the preparation of AB-type N-substituted NDIs (Scheme 73).[300]
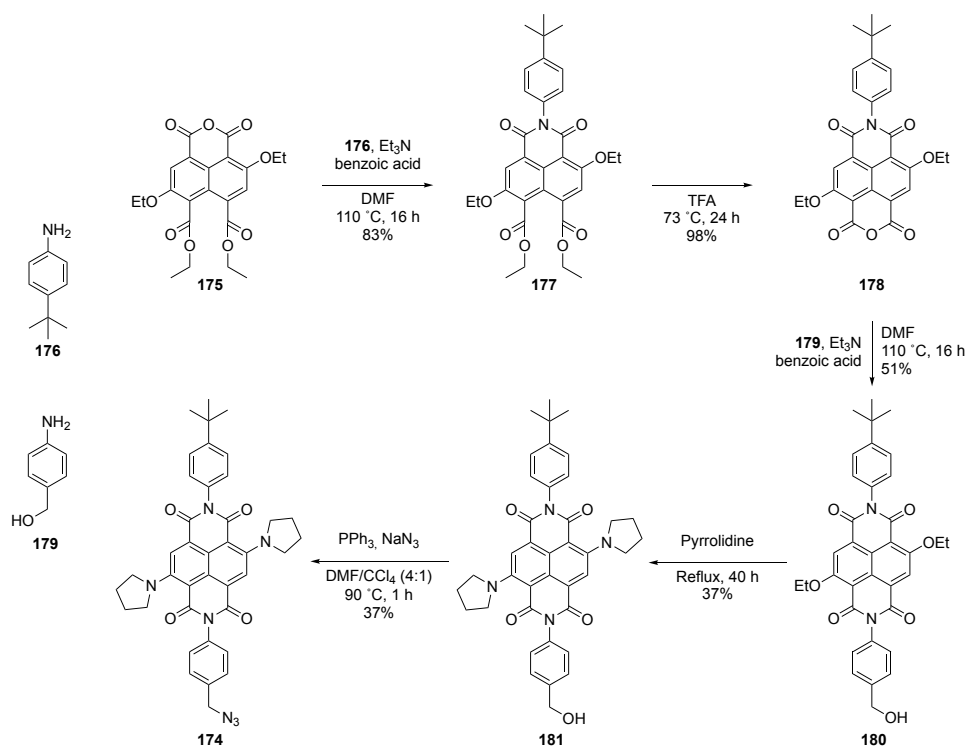
Scheme 73. Rational synthesis of the AB-type *N*-azide NDI **174**.

By reaction of naphtalene monoanhydride **175** with 4-*t*butylaniline (**176**) in the presence of Et$_3$N and benzoic acid, monoimide **177** was obtained in high yield. This was quantitatively converted into anhydride **178** in TFA under refluxing conditions. Similarly to intermediate **177**, diimide **180** was obtained in moderate yield by reaction of anhydride

178 with 4-amino-benzylalcohol (**179**) in DMF at 110 ˚C. Core substitution of the ethoxy groups with pyrrolidinyl groups was achieved by refluxing diimide **180** in pyrrolidine for 40 h. Finally, the azide group was introduced using a modified Appel reaction protocol, reacting **181** with PPh$_3$ and CCl$_4$ in the presence of NaN$_3$.[301] Having in hand azide-NDI derivative **174** and tri-ethynyl borazine-doped PPh **151** (Scheme 63, section 3.1.3.2) targeted molecule **182** was obtained by the methodology developed by *Sharpless*.[299] Thus, molecules **151** and **174** were reacted in the presence of CuI, DIPEA, and AcOH in CH$_2$Cl$_2$ (Scheme 74) for 96 h at r.t., giving **182** with a 58% yield.
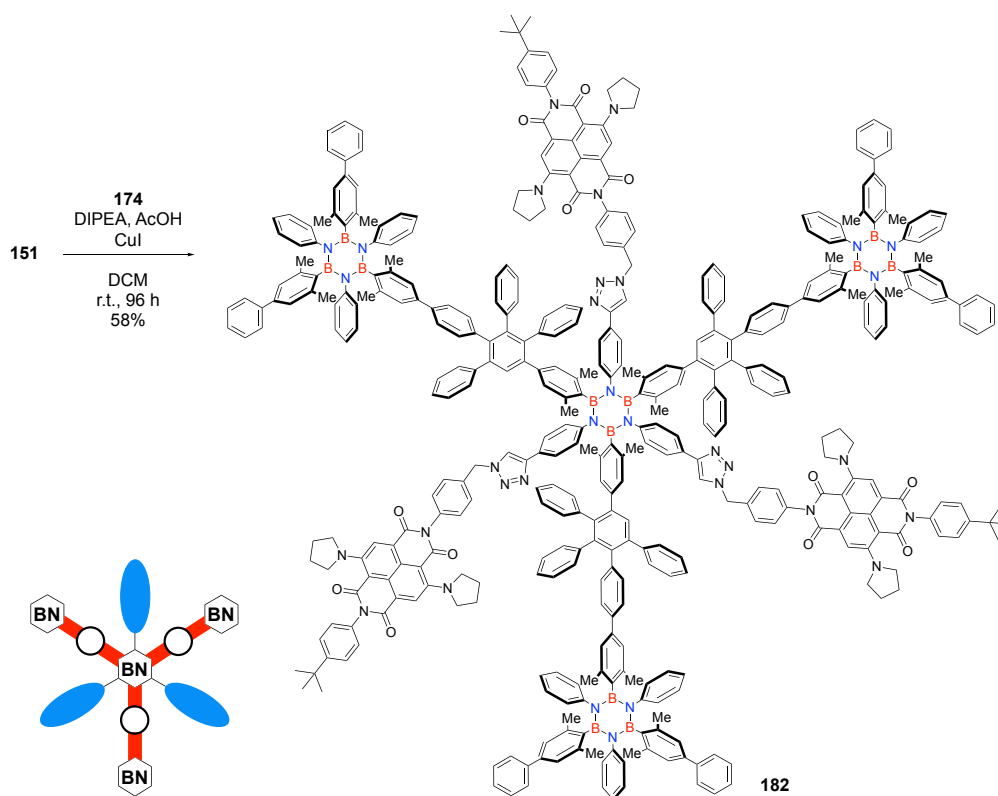
Scheme 74. Synthesis of multichromophoric borazine **182**.

Due to the steric hindrance generated by the PPh branches, the accessibility of the ethynyl groups is clearly reduced, and the formation of 1,2,3-triazole linkers appeared, in fact, to be very slow (4 days of reaction at r.t.). The blue product, featuring three NDI fragments, was separated by silica gel column chromatography and further purified by Rec-GPC to remove the by-products of mono- and bis-addition. Besides ^{1}H-NMR (Figure 25), the nature of molecule **182** was undoubtedly confirmed by MALDI-mass spectrometry through the detection of the low resolution peak corresponding to the molecular ion (M$^+$) at *m/z* 6152.02 (calc. for [C$_{417}$H$_{357}$B$_{12}$N$_{33}$]$^+$: 6151.97).
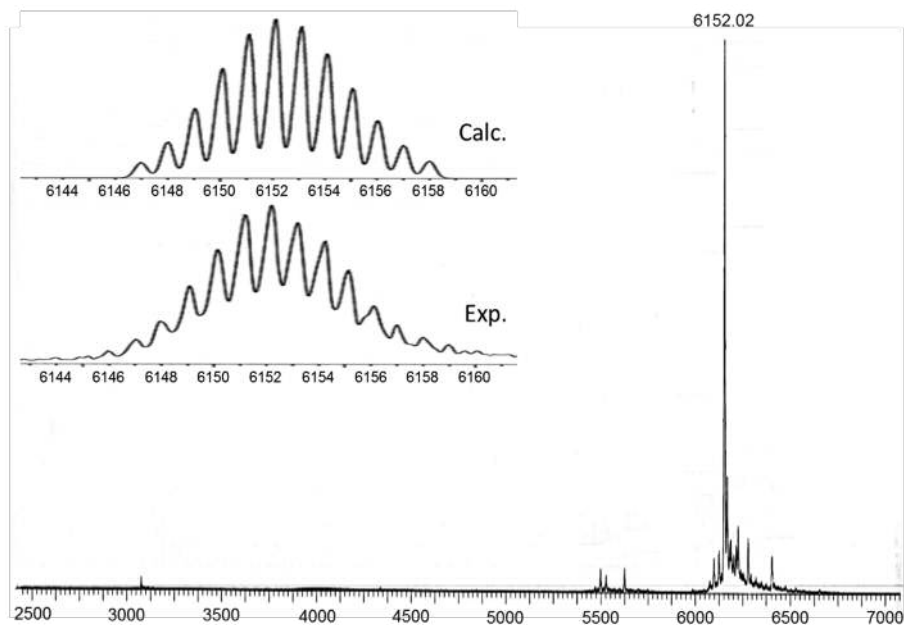
Figure 24. MALDI-Mass spectrometry of molecule **182**. Inset: calculated (top) and experimental (bottom) isotopic pattern.
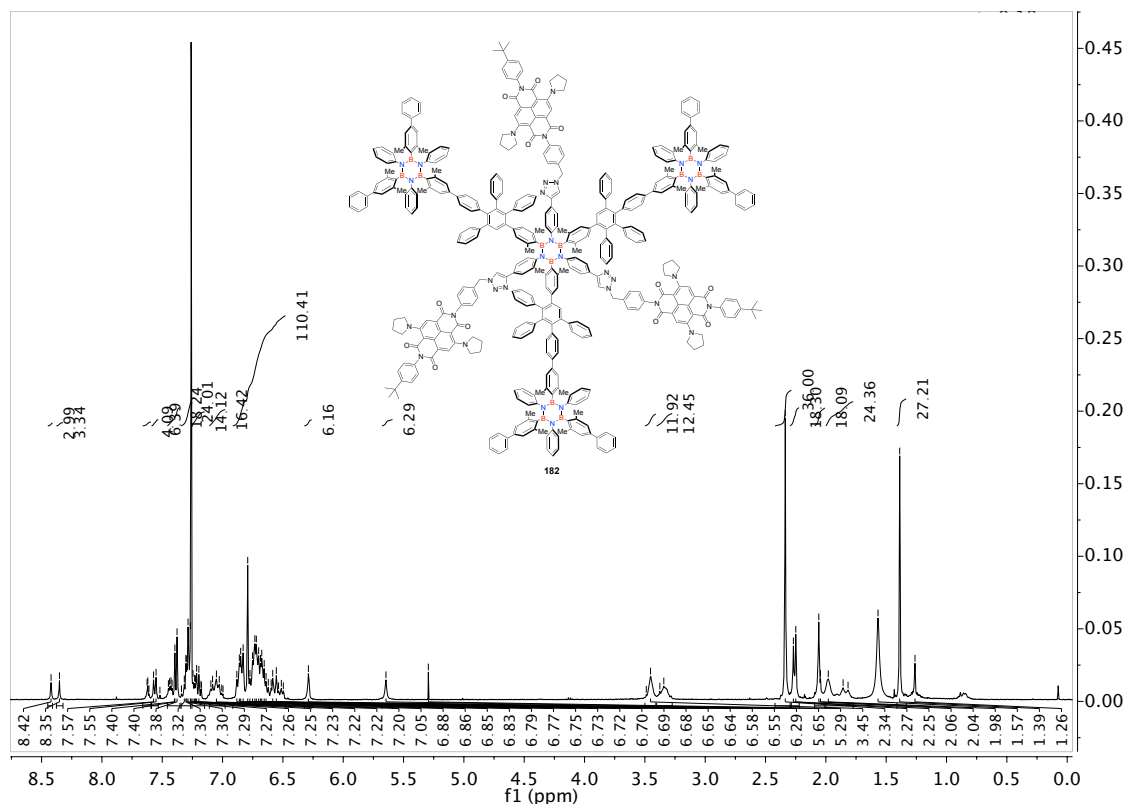
Figure 25. ¹H-NMR spectrum of blue-labelled polyphenylene **182** in CDCl₃ (300 MHz).

In Figure 24, the mass spectrogram, showing the matching calculated and experimental isotopic patterns, is reported. The ¹H-NMR spectrum of **182** in CDCl₃ (Figure 25) shows broad multiplets in the aromatic region (7.45-6.50 ppm), while at 8.42 ppm and 8.35 ppm

two de-shielded singlets are distinguishable, belonging to the proton bonded to the central benzene ring of the pentaphenylbenzene fragments, and to those in the triazole rings. At lower chemical shifts, the broad singlets belonging to the pyrrolydine substituents generate broad singlets at 3.45 and 3.34 and a multiplet at 1.98-1.82 ppm. Finally, the singlets at 2.34, 2.26, and 2.06 ppm indicate the signals of the *o*-Me groups of the borazine units, while the singlet at 1.39 ppm can be assigned to the protons of the ^{t}Bu groups.

3.2.2 Photophysical characterization and estimation of the energy transfer

The photophysical features of blue coloured borazine-doped PPh **182**, bearing three NDI centres, were investigated by absorption and emission studies in solution of CH_2Cl_2.
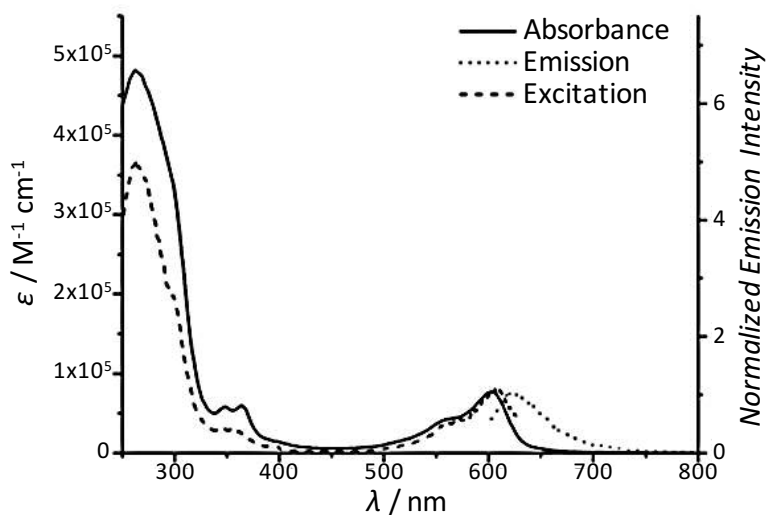
Figure 26. Extinction coefficient (solid, $\varepsilon_{max} = 4.8 \times 10^5$ L mol^{-1} cm^{-1} at $\lambda = 262$ nm), emission (pointed, λ_{exc} = 263 nm) and excitation profiles (dashed, $\lambda_{em} = 640$ nm) of blue-labelled **182** in CH_2Cl_2 at 25 °C.

In the absorption spectrum of **182** (Figure 26, solid), it is possible to recognize the characteristic signals at 347, 364, and 603 nm, identifying the NDI units, and at 262 nm, typical of the borazine doped framework. At this wavelength though, the molar extinction coefficient was found to be slightly higher than that of three-branched borazine-polyphenylene **169** itself ($\varepsilon_{max} = 2.3 \times 10^5$ M^{-1}cm^{-1}),[117] revealing a contribution to the absorption from the NDI fragments. By excitation at 262 nm it was possible to record the emission profile of **182**, having a maximum at 627 nm (Figure 26, dotted).

Table 4. Φ_{em} of borazine derivative **182** in CH_2Cl_2 at 25 °C. The Φ_{em} of blue-coloured tetraborazylene **182** was determined using N,N'-di(2,6-diisopropylphenyl)-1,6,7,12-tetraphenoxyperylene-3,4:9,10-tetracarboxylic acid bisimide as reference (Φ_{em} = 0.96 in CHCl$_3$).[302]

Compounds	λ_{exc}	Excitation unit	Φ_{em} (%)
182	272 nm	BN-PPh	0.5
182	560 nm	NDI	0.17

Irradiating **182** at λ_{exc}= 273 nm, where the borazine-doped scaffold mostly absorbs, emission from the NDI chromophores having Φ_{em}= 0.5% was measured observing the emission at λ_{em}= 627 nm and using a tetraphenoxy-sybstituted PDI derivative as fluorescence standard.[303] By selective excitation of the NDI fragments at λ_{exc}= 560 nm, the Φ_{em} value dropped to 0.17% (Table 4). The excitation profile (Figure 26, dashed), recorded by observing the emission at 640 nm, revealed a strong contribution in the region at 270-300 nm, where the absorption maxima of the BNC hybrid backbone is located.
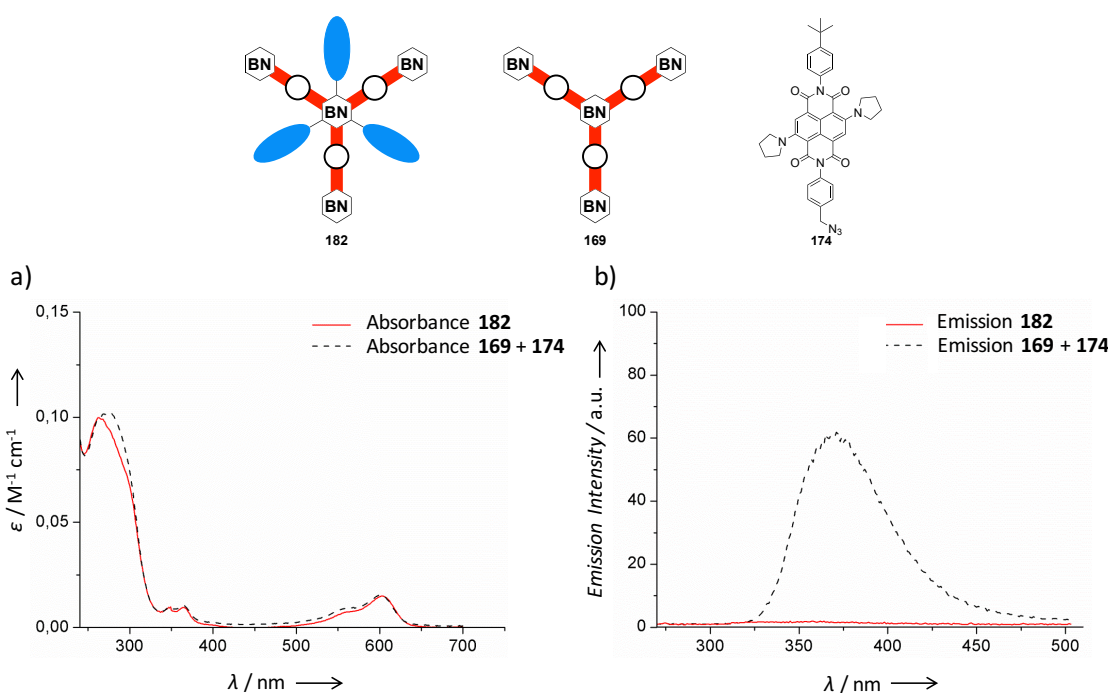
Figure 27. a) Absorption spectra of **182** (—, 2.27×10^{-6} molL^{-1} in CH_2Cl_2) and of a 1:3 mixture of **169** (2.27×10^{-6} molL^{-1}) and **174** (6.81×10^{-6} molL^{-1}) (---, in CH_2Cl_2 at 25 °C. b) Emission spectrum of **182** (—, λ_{exc} = 272 nm) and of a 1:3 mixture of **169** and **174** (---, λ_{exc} = 272 nm) in the emission region of the borazine-doped framework in CH_2Cl_2 at 25 °C.

Figure 27a shows the comparison between the absorption spectra of **182** and that of a 1:3 mixture of **169** and **174**. The good overlap between the two spectra indicates that the covalent linkage between the NDI fragments and the BNC framework has no particular

effect on the electronic properties at the ground state of the chromophore. In addition, by excitation of the 1:3 mixture of **169** (2.27×10^{-6} molL^{-1}) and **174** (6.81×10^{-6} molL^{-1}) at λ_{exc}= 272 nm, a fluorescence emission in the near-UV region (λ_{exc}= 372 nm), typical of the polyphenylene, is observed (Figure 27b, dashed black). Instead, using the same excitation energy with blue molecule **182**, just a scarce emission was observed from the borazine-PPh backbone (Figure 27b, solid red). Notably, a 98% reduction of the emission from the BN-PPh is calculated as the ratio between the fluorescence intensities at 372 nm. This suggests a nearly quantitative quenching of the fluorescence operated by the NDI acceptors. In order to rule out the presence of dynamic (collisional) quenching, the fluorescence of three-branched borazine-doped PPh **169** was measured in the presence of increasing concentrations of NDI **174** (Figure 28a).
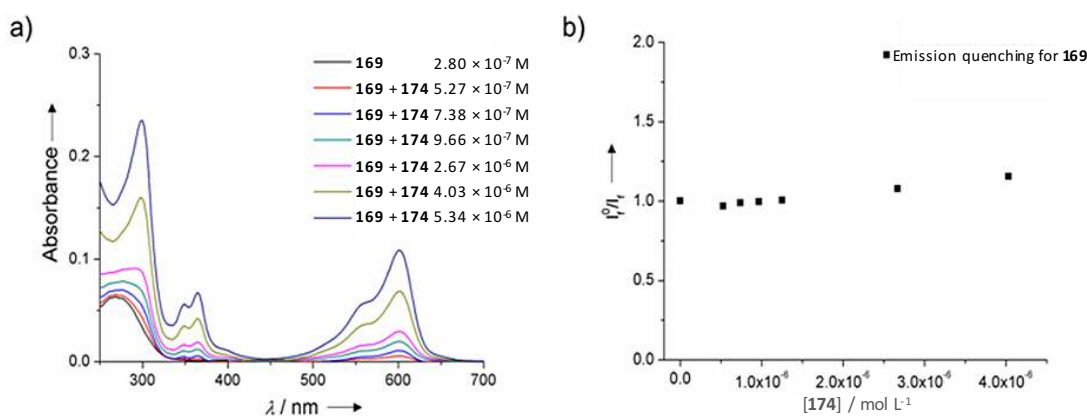
Figure 28. a) Effect of concentration of **174** on the absorption spectrum of **169** in CH$_2$Cl$_2$ at 25 °C, [**169**] = 2.8×10^{-7} M; [**174**] = 5.27×10^{-7} M, 7.38×10^{-7} M, 9.66×10^{-7} M, 2.67×10^{-6} M, 4.03×10^{-6} M, 5.34×10^{-6} M. b) Stern–Volmer plot: ratio between I_F^0 and I_F for molecule **169** at different concentration of NDI acceptor **174** in CH$_2$Cl$_2$ at 25 °C.

The variation of fluorescence intensity of **169** with the concentration of the quencher **174** have been plotted (Figure 28b) according to the Stern-Volmer equation:

(*Eq. 1*)
$$\frac{I_F^0}{I_F} = 1 + k_q \tau_0 [Q]$$

where I_F^0 and I_F are the fluorescence intensities in the absence and in the presence of a quencher (respectively), k_q is the quencher rate coefficient, τ_0 is the lifetime of the emissive excited state of the molecule in the absence of the quencher, and [Q] is the concentration of the quencher, **174** in this case. Using comparable concentrations of quencher with respect to those used for the fluorescence quenching analysis showed in

Figure 28b, the negligible variation of the I_F^0/I_F ratio upon increasing [Q] indicates no incidence of collisional mechanism on the energy decay process of the borazine-doped framework. Furthermore, this suggests the occurrence of energy transfer from the BNC scaffold to the red-emitting chromophore. This conclusion is also assisted by the great contribution from the polyphenylene backbone noticeable in the UV region of the excitation spectrum in Figure 26 (dashed). The efficiency of this process (Φ_{ET}) can be quantified following the method of *Mellinger*,[304] considering the ratio between excitation and absorption intensities of **182** at a given wavelength, both normalized and corrected for the absorption of the NDI fragments. More in detail, the residual absorption of the diimide has been calculated considering the value of ε for **169** at 262 nm, where an absorption minimum can be found for **174** (Figure 29). Considering the value of ε_{174} (19542 M^{-1} cm^{-1}, at λ= 262 nm), and of ε_{169} (164945 M^{-1} cm^{-1}, at λ= 262 nm), the percentage of absorbed radiation by the borazine-PPh (AR_{169}) at that wavelength can be calculated by Equation 2, as follows:

(*Eq. 2*)
$$AR_{169} = \frac{\varepsilon_{169}}{\varepsilon_{169} + (\varepsilon_{174} \times 3)} \times 100 = 74\%$$
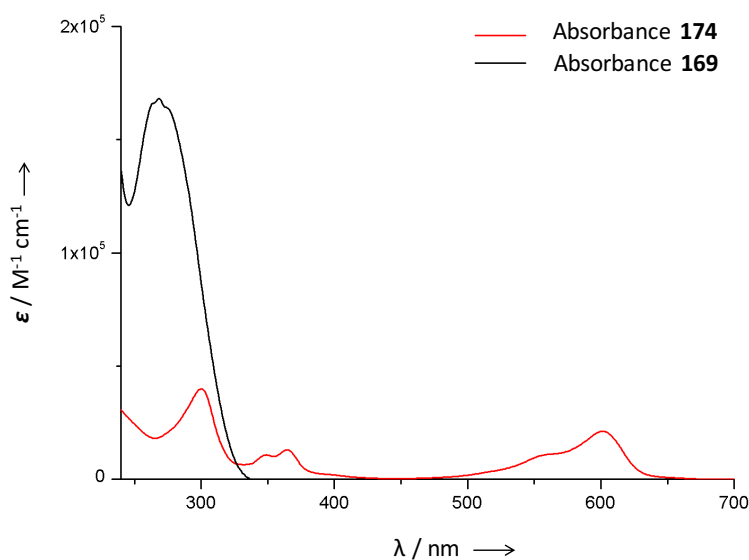
Figure 29. Absorption spectra of borazine **169** (black) and **174** (red) in CH_2Cl_2 at 25 °C.

The value calculated above (Equation 2) shows that the absorption of NDI is not negligible, and that the absorption of the diimide moieties must be considered in the determination of the energy transfer quantum yield (Φ_{ET}). Knowing the value of ε_{174} at a

chosen λ, Φ_{ET} can be determined by Equation 3, comparing the excitation and absorption spectra, both normalized at λ= 603 nm. The correction is applied by subtracting a triple value of extinction coefficient of **174** to the normalized excitation and absorption, giving a remarkable value of energy transfer (Φ_{ET}= 83%).

$$(Eq.\ 3) \qquad\qquad \Phi_{ET} = \frac{E_{182} - (A_{174} \times 3)}{A_{182} - (A_{174} \times 3)} \times 100 = 83\%$$

Where E_{183} and A_{183} are fluorescence intensity and absorption, respectively, of dyad **182**, taken at λ= 262 nm in the normalized excitation and absorption spectra in Figure 26.
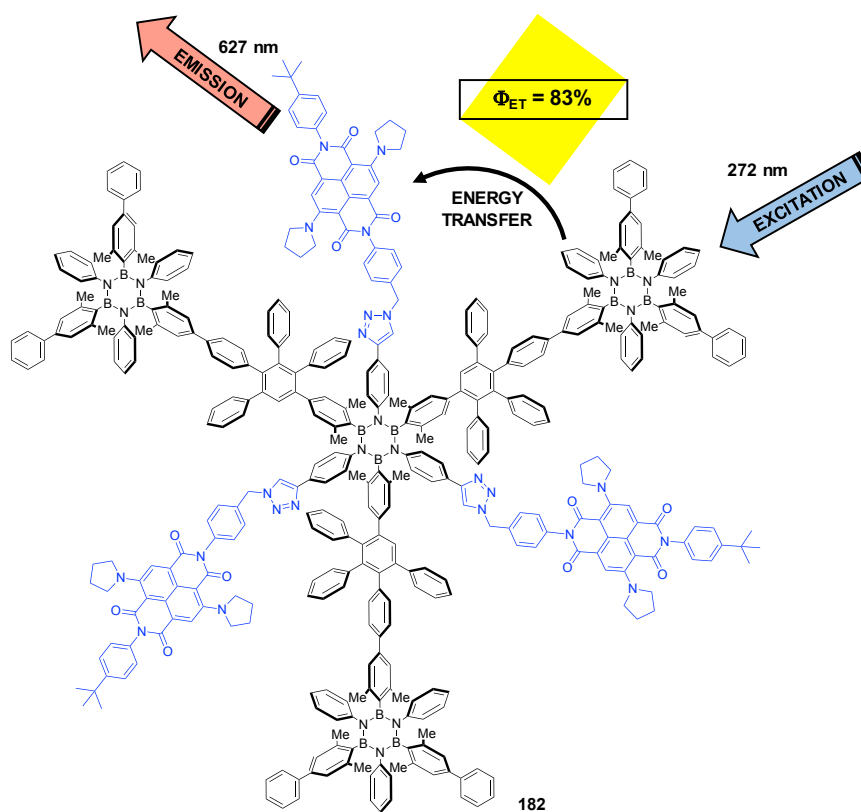
Figure 30. Schematic representation of the energy transfer phenomena detected for molecule **182**.

As previously reported for full-carbon polyphenylene derivative,[254,259,305] these results suggest that BNC hybrid materials can also behave as energy harvesters, and their rigidity, shape persistence, chemical and thermal resistance, can be of great utility for the construction of antenna systems.

3.3 Synthesis of borazine-doped PAHs and graphene-like structures

3.3.1 Synthesis of borazine-polyphenylene precursors

To accomplish the synthesis of the designed graphene-like structures **R22**, **R25**, and **R28** featuring embedded borazine units (Scheme 43, section 2.3), a synthetic route comprising the planarization of borazine-PPh precursors **R24**, **R27**, and **R30**, is envisaged. In particular, cyclization of these BNC hybrid frameworks, bearing *o*-fluoride-functionalized substituents, is expected through the same Friedel-Craft procedure used for the synthesis of HBBNC **57** (see section 1.1.5.4).[114] Therefore, the first synthetic challenge for the fulfilment of this objective, regards the synthesis of the BN-PPh precursors.
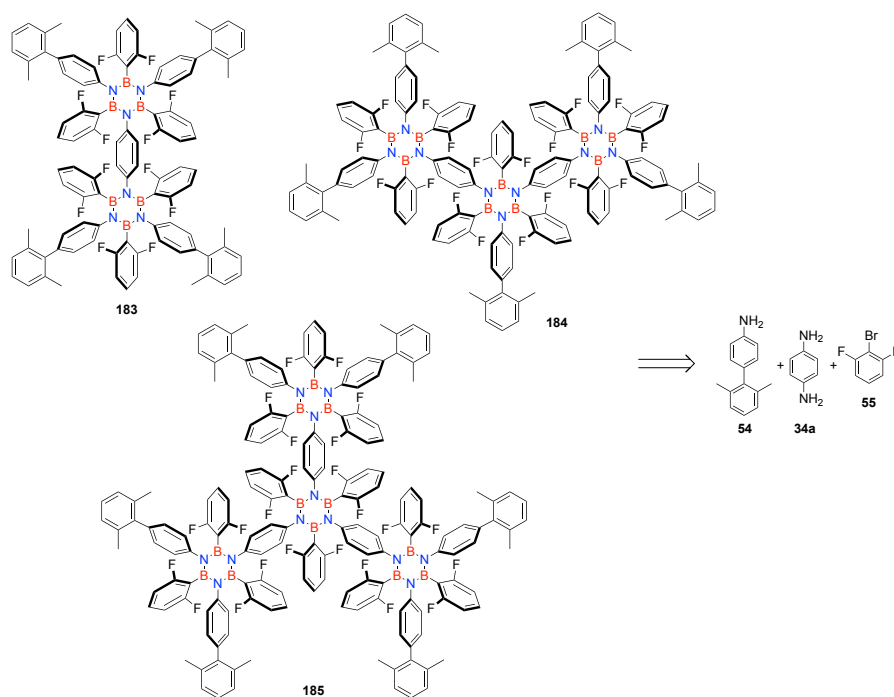
Scheme 75. Rethrosynthetic analysis for the generation of fluoride-functionalized bis- (**183**), tris- (**184**), and tetra- (**185**) borazine-doped precursors for graphene sub-structures.

Inspired by the report by *El-Kaderi* et al.,[75] describing the preparation of an arylborazine polymer by reaction of *p*-phenylenediamine (**34a**) with BCl_3 or BBr_3 (see sections 1.1.1.1 and 1.1.1.2), we envisaged that by reacting a mixture of *p*-xylylaniline **54** and *p*-phenylenediamine **34a**, a statistical mixture of bis-, tris-, and tetra-borazine derivatives (**183**, **184**, and **185**, respectively) will be produced (Scheme 75). In particular, *p*-xylylaniline **54** was chosen as starting material due to the need of a bulky and inert peripheral group, that would ensure solubility of the final planar products.
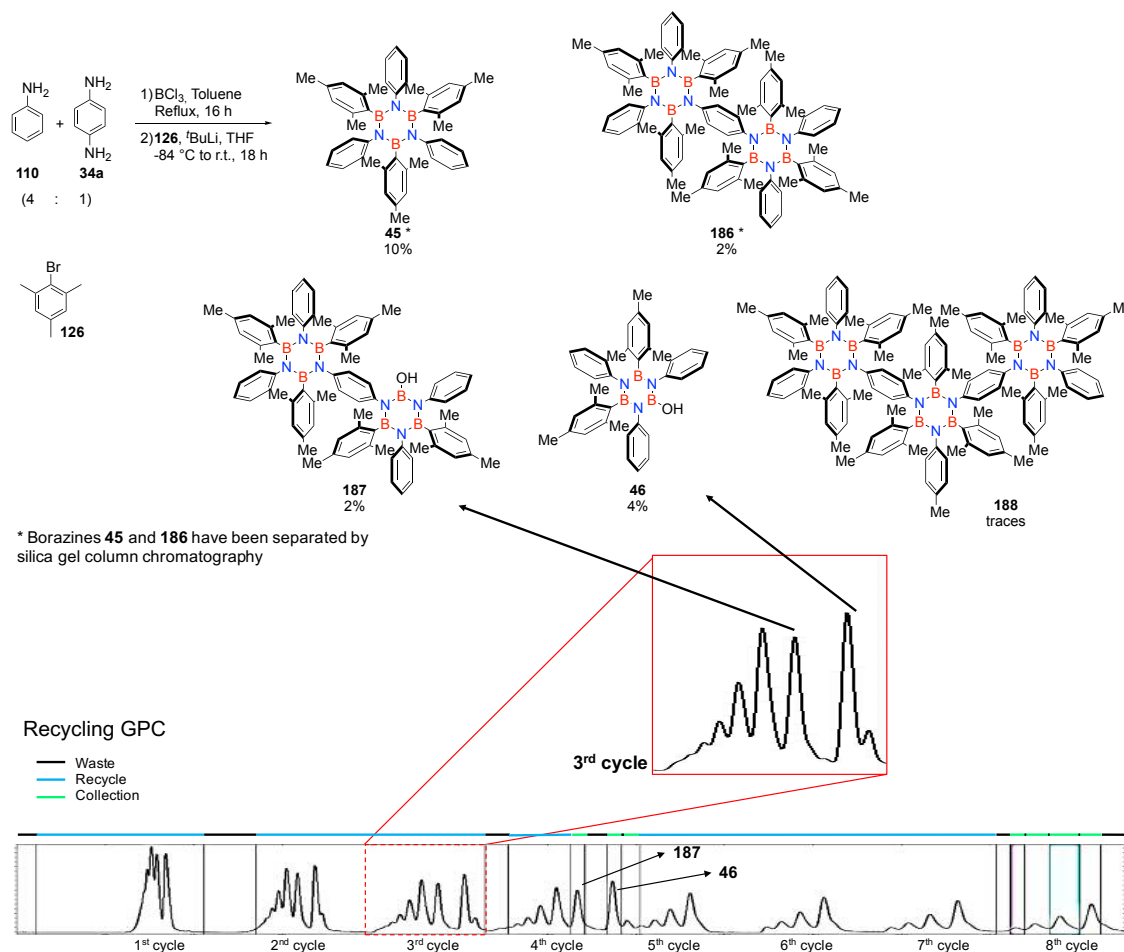
Scheme 76. Top: synthesis of mesityl-protected multiborazine derivatives using a 4:1 **110** to **34a** ratio. Bottom: Rec-GPC trace of the crude mixture after silica gel column chromatography, showing the waste (black), recycle (blue), and collection (green) sequence. Inset: zoom of the chromatogram at the 3rd cycle.

In order to test the effectiveness of this one-pot procedure, a first synthetic attempt was carried-out using unsubstituted aniline (**110**) and *p*-phenylenediamine (**34a**), and inserting mesityl groups at the *B*-sites, instead of 2,6-difluorobenzene. Therefore, reaction of a 4:1 mixture of **110** and **34a**, respectively, and subsequent treatment with MesLi, afforded a complex mixture of products (Scheme 76, top; Table 5, entry 1). Notably, addition of BCl$_3$ to the mixture of **110** and **34a** in toluene, was done at 80 ˚C, to overcome the poor solubility of **34a**. A first purification of the crude mixture through silica gel column chromatography afforded tri-*N*-phenyl-tri-*B*-mesitylborazine **45** and bis-borazine derivative **186** in 10% and 2% yield, respectively. In particular, the latter could be identified through ^{1}H-NMR in CDCl$_3$ (Figure 31), which is composed by four singlets from the *o*-Me groups at 2.15, 2.10, 1.95, and 1.89 ppm, and further four well-resolved signals from the aromatic hydrogens at 6.69, 6.39, 6.29, and 6.12 ppm.
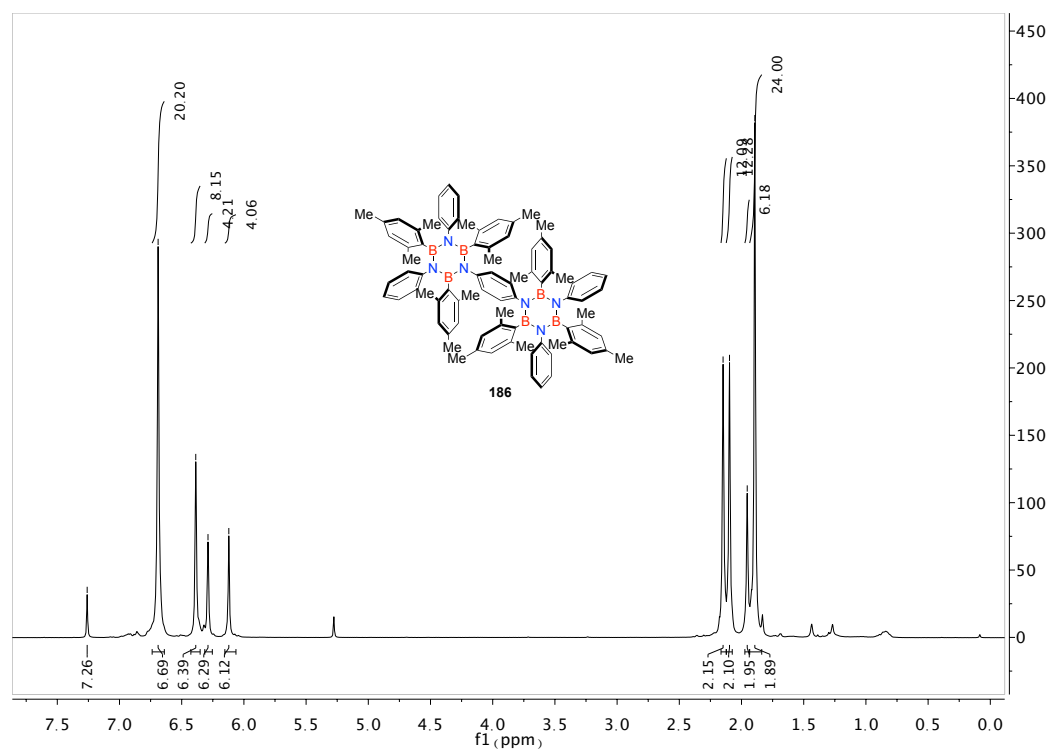
Figure 31. ^{1}H-NMR spectrum of bis-borazine derivative **186** in CDCl$_3$ (300 MHz).
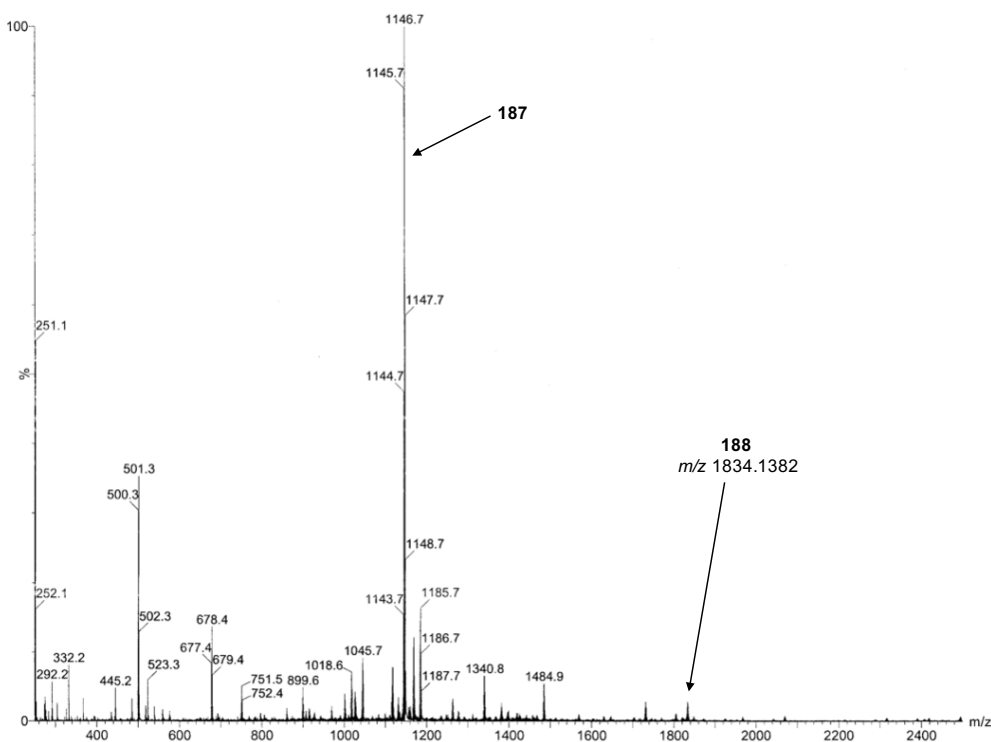
Figure 32. MALDI mass spectrogram of **187**, together with a trace amount of tris-borazine derivative **188** in the positive ion mode (matrix used: DCTB; N$_2$ laser at 337 nm).

Moreover, HR-MALDI mass spectrometry (calc. for $[C_{84}H_{91}N_6B_6]^+$: 1248.7932, found: 1248.7616) confirmed the presence of the product. The remaining components of the

mixture could be separated using Rec-GPC (Scheme 76, bottom). Between the fractions collected during the 4th cycle of the Rec-GPC analysis, hydroxyl-borazine **46** (4% yield) could be identified by ^{1}H-NMR and compared to known data from literature,[137] while hydroxyl-bis-borazine **187** (2% yield) could be identified by LR MALDI-mass spectrometry through the detection of the molecular peak at *m/z* 1146.7 (calc. for $[C_{75}H_{80}N_6B_6O]^+$: 1146.7, Figure 32). Notably, together with **187**, a trace amount of tris-borazine derivative **188** (Scheme 77) was present, and could be identified by the HR-MALDI peak at *m/z* 1834.1382 (calc. for $[C_{123}H_{132}N_9B_9]^+$: 1834.1443).
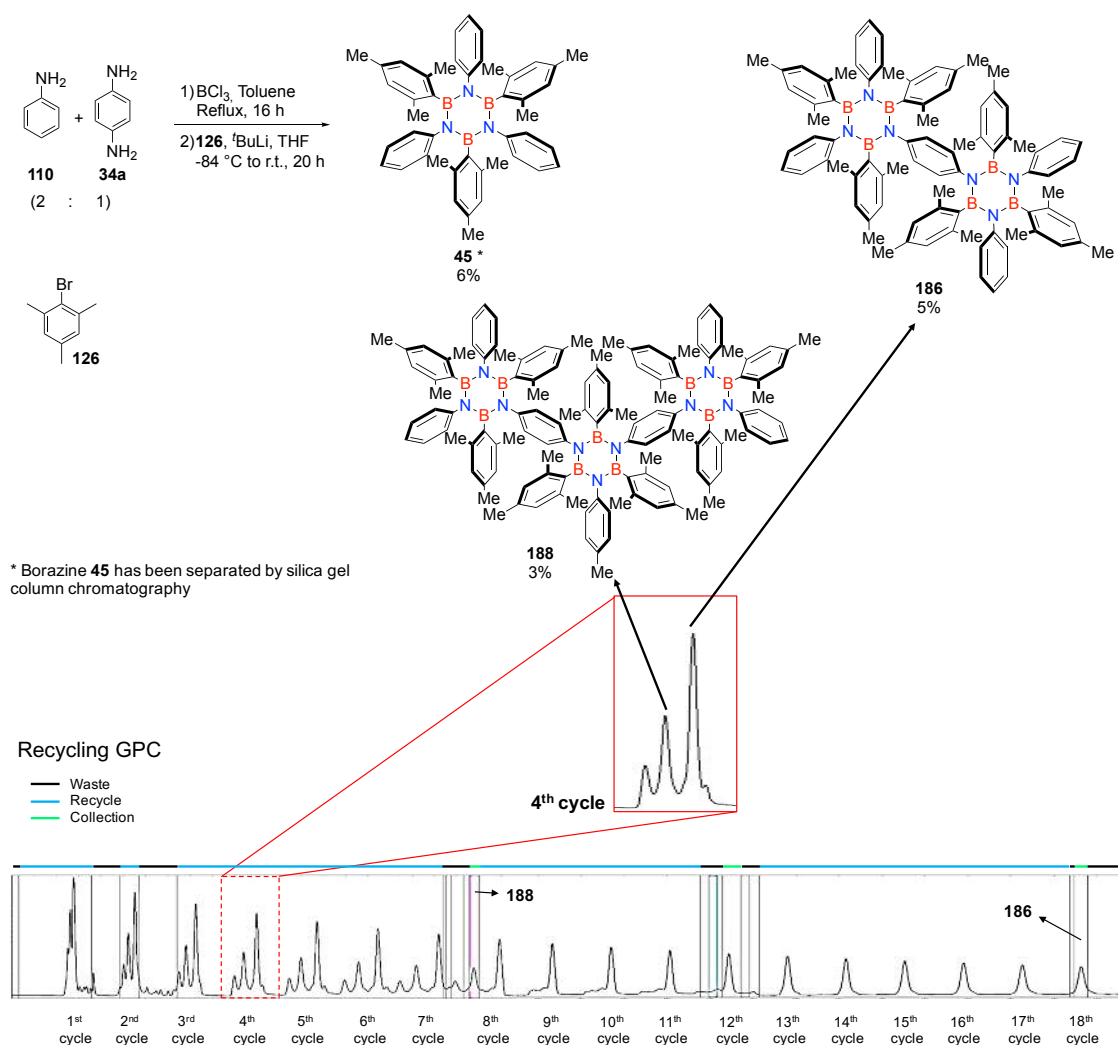
Scheme 77. Top: synthesis of mesityl-protected multiborazine derivatives using a 2:1 **110** to **34a** ratio. Bottom: Rec-GPC trace of the crude mixture after silica gel column chromatography, showing the waste (black), recycle (blue), and collection (green) sequence. Inset: zoom of the chromatogram at the 4th cycle.

To force the formation of reasonable amounts of tris-, and tetra-borazine derivatives, a second reaction was carried out increasing the ratio between **110** and **34a** at 2:1 (Scheme 77, top; Table 5, entry 2), respectively. In this case, formation of a white insoluble

product, probably composed of a polymeric form, was noticed after refluxing the mixture in toluene overnight. However, the nature of this was not investigated further. Similarly to the previous attempt, tri-*N*-phenyl-tri-*B*-mesitylborazine **44** (6% yield) was separated by silica gel column chromatography. However, submitting the rest of the reaction mixture to Rec-GPC analysis, tris-borazine **188** (3%, collected at the 8th cycle) and bis-borazine **186** (5%, collected at the 18th cycle), were obtained. Notably, when using the mesityl group as *B*-substituent, degradation of bis-borazine derivative **186** and tris-borazine **188** was noticed upon storage of the sample in the presence of moisture.
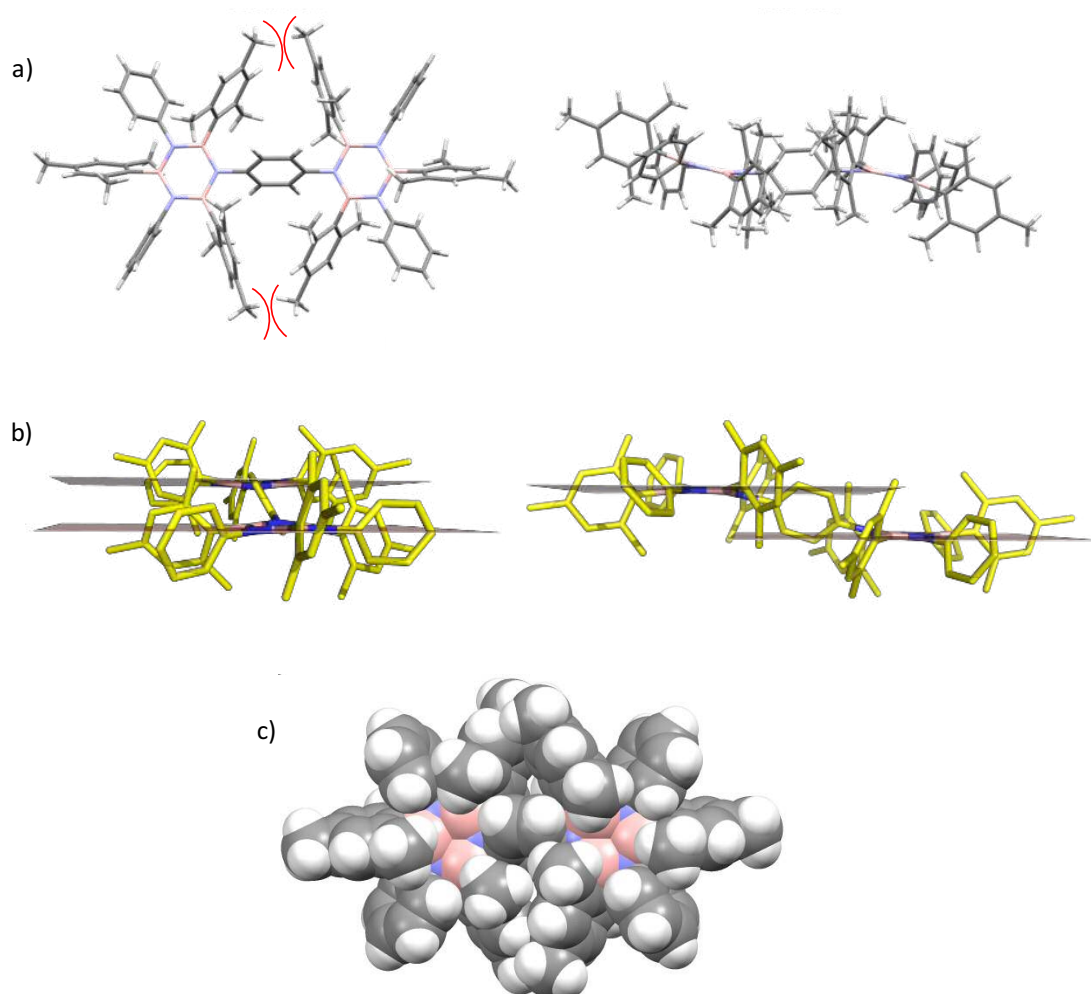
Figure 33. Crystalline structure of molecule **186**. a) Front and side view (stick representation) with highlight on the clashing between the *p*-Me substituents. b) Borazine planes are highlighted and show how steric hindrance between neighbour BN cores is minimized with shifting. Hydrogens and disorder are omitted for clarity. c) Spacefill representation showing inhomogeneous shielding of the B atoms. Crystals obtained by slow evaporation from CHCl$_3$, space group: P bca.

Crystals of **186** suitable for X-ray diffraction were obtained by slow evaporation of a solution of CHCl$_3$. Looking at the crystal structure of **186** (Figure 33), one can explain the reactivity of the system in terms of steric hindrance between the methyl groups in

para-position of aryl-substituents belonging to different borazine units, which causes a peculiar distortion of the molecule in which the two borazine rings are forced in shifted parallel planes with no rotation (dihedral angle= 0˚, Figure 33b). As a consequence, the steric shielding of the B atoms operated by the *o*-Me groups is partially disrupted and not homogeneous anymore (Figure 33c), affecting the inertness of the borazine ring in the presence of nucleophiles like water. Absorption and emission spectra of **186** were recorded in CH_2Cl_2 solution at room temperature (Figure 33). The absorption profile reveals two close maxima at 263 nm and 268 nm, in addition to a shoulder localized at 278 nm. The fluorescence spectrum presents a maximum at 302 nm, and using a solution of naphtalene in CHX as fluorescence standard, a modest quantum yield ($\mathbf{\Phi_{em}}$= 5%) was measured.
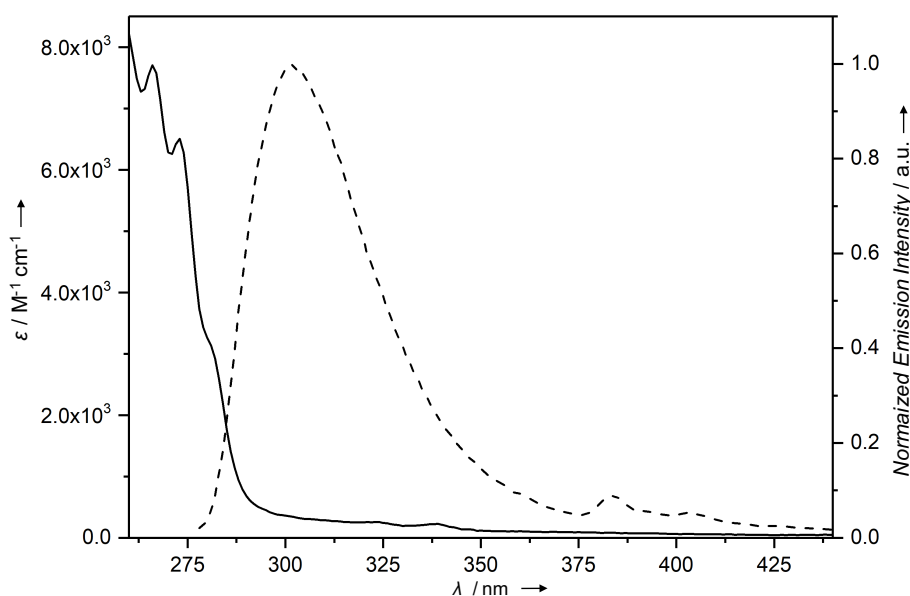
Figure 34. Absorption (solid) and emission (dashed) of bis-borazine derivative **186** in CH_2Cl_2.

Notably, the maximum energy of emission is hypsochromically shifted of about 70 nm in respect to the borazine-doped polyphenylene derivatives studied in this work (see section 3.14), probably caused by a conjugation breaking due to the structural distortion. In additional attempts, **110** to **34a** ratio was increased to 1:1 and 1:2 (Table 5, entries 3 and 4), affording a white insoluble solid, in which no soluble borazine derivatives were identified, probably due to complete conversion of the starting materials to the polymeric form.
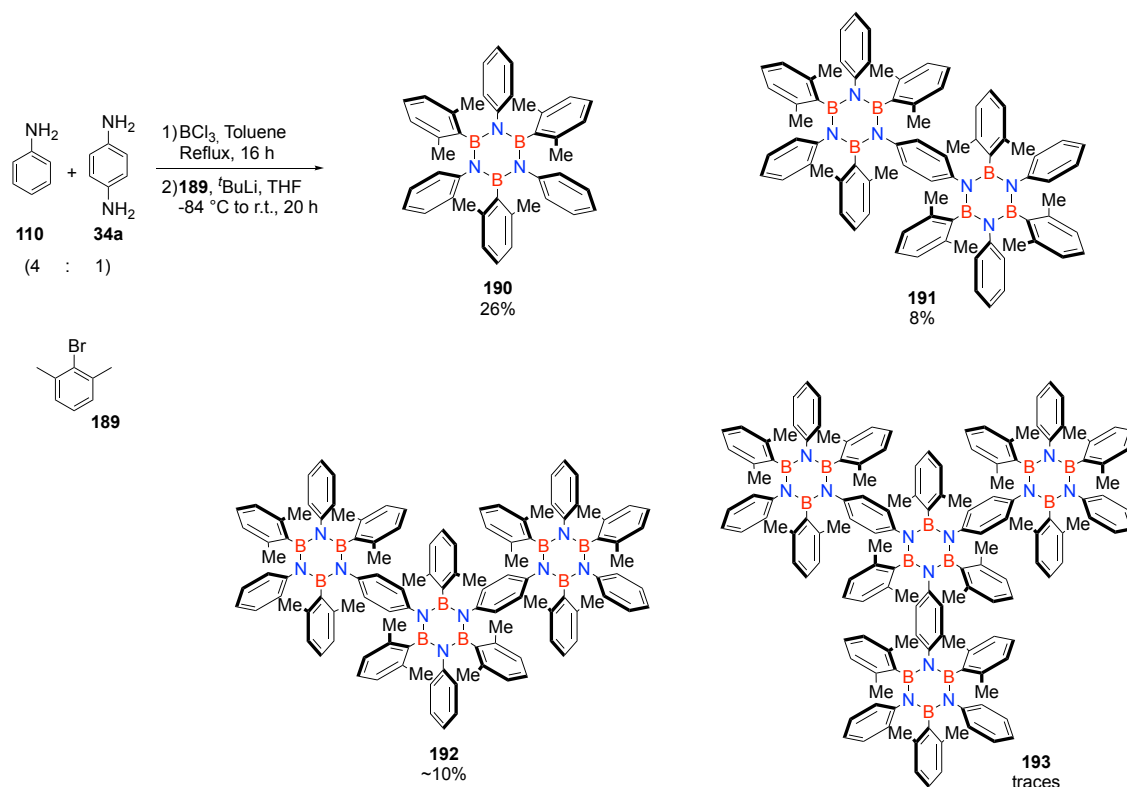
Scheme 78. Synthesis of *B*-xylyl derivatives of mono- (**190**), bis- (**191**), tris- (**192**), and tetra-borazine (**193**).

To suppress the structural strain, and therefore, the reactivity of multi-borazine derivatives towards moisture, the *B*-mesityl groups were replaced by *B*-xylyl groups (Scheme 78). Using the same strategy depicted in Scheme 76, but using the lithium derivative of 2,6-dimethylbromobenzene **189** in the second step of the reaction of formation of the borazine derivatives, tri-*N*-phenyl-tri-*B*-xylylborazine **190** and bis-borazine **191**, bearing xylyl groups on the B atoms, were separated by silica gel column chromatography with 26% and 8% yields, respectively (Table 5, entry 5). Structural analysis of **191** through XRD (Figure 35) revealed a relevant suppression of the distortion on the system and an increased flexibility with respect to molecule **186**. Predictably, reactivity of the intermediate was suppressed as no signs of degradation were observed on the sample when stored without particular precautions (in the presence of moisture). Indeed, by looking at the spacefill representation (Figure 35c) one can certainly notice a better coverage of the BN ring by the *o*-Me groups. On the other hand, this is not perfect as the different B atoms display slightly different degrees of exposure, probably due to a residual distortion of the system due to the vicinity of multiple aryl-substituents.
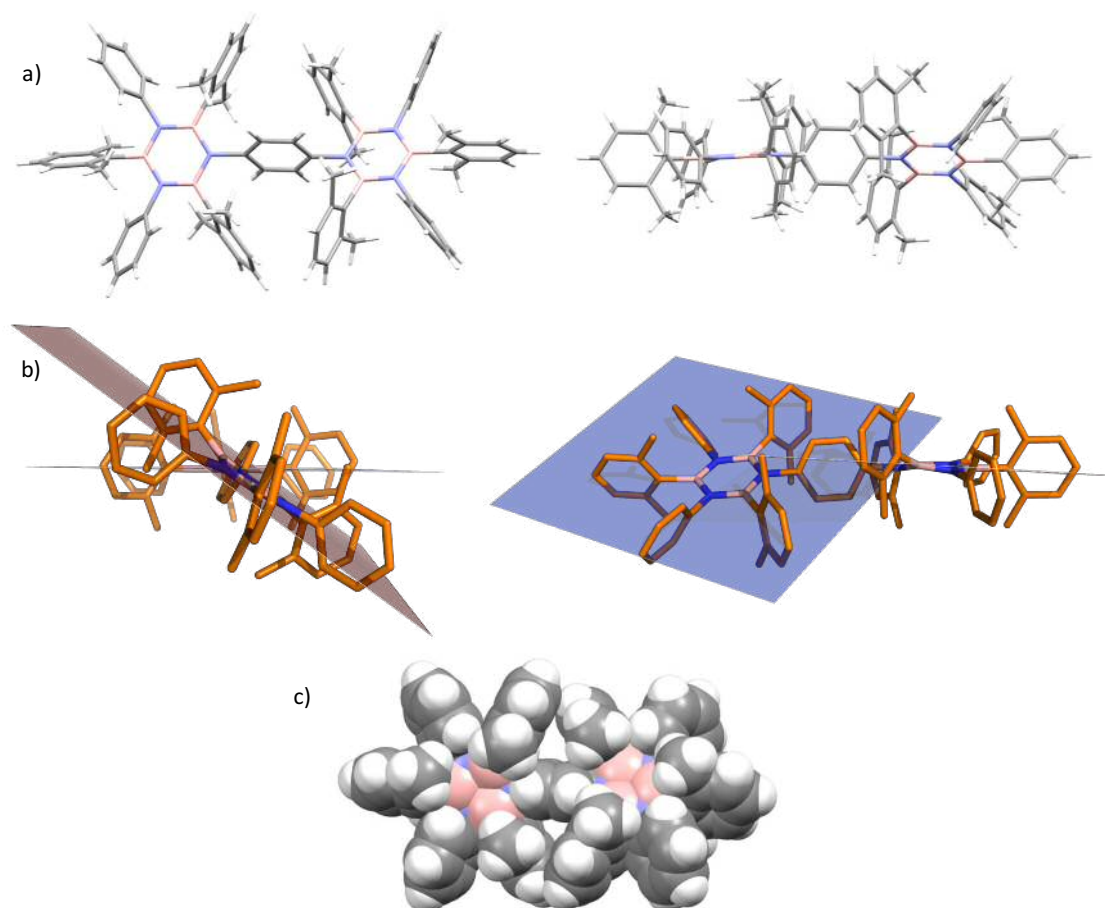
Figure 35. Crystalline structure of molecule **191**. a) Front and side view (stick representation). b) Borazine planes are highlighted and show how steric hindrance between neighbour BN cores is minimized with tilting. Hydrogens and disorder are omitted for clarity. c) Spacefill representation showing inhomogeneous shielding of the B atoms. Crystals obtained by slow diffusion of pentane into a $CHCl_3$ solution, space group: P -1.

Additionally, identification of tris-borazine derivative **192** (~10% yield) was possible through LR-MALDI-mass analysis on a third fraction through the identification of the molecular peak at *m/z* 1707.1 (calc. for $[C_{114}H_{114}B_9N_9]^+$: 1707.5). However, precise calculation of the yield of this product was impossible due to the presence of a minor quantity of tetra-borazine derivative **193** (<1% yield) in the sample, that wasn't purified further. This latter was identified by detection of the HR signal at *m/z* 2250.3357 (calc. for $[C_{150}H_{150}B_{12}N_{12}]^+$: 2250.3259). Although not pure, a small transparent crystal of **192** could be obtained by slow diffusion of pentane into a $CHCl_3$ solution. The crystal structure obtained from this is reported in Figure 36. Also in this case, one can notice that the suppression of the steric hindrance between the different connected borazine units results in the tilting of the BN planes (Figure 36b), demonstrating an intrinsic flexibility of the system. To summarize the information gathered by XRD measurements, the presence of colliding mesityl groups in **186** results in the shifting of the borazine planes,

with no rotation (dihedral angle= 0°, Figure 33). Rather, multi-doped borazine-PPh systems **191** and **192** demonstrate an intrinsic flexibility. As shown by the presence of alternative conformations resulting from the tilting of the borazine planes, no relevant steric hindrance between the aryl-substituents, belonging to different borazine units, is present (Figure 35).
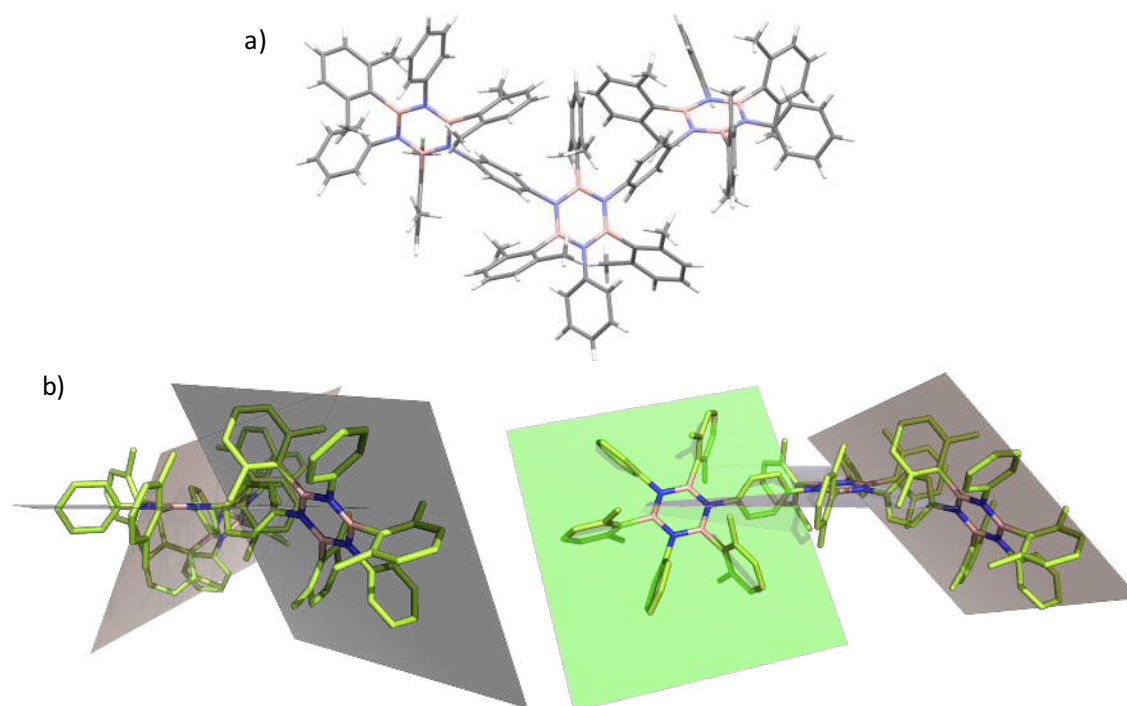
Figure 36. Crystal structure of tris-borazine **192**. a) Stick representation. b) Borazine planes are highlighted and show how steric hindrance between neighbour BN cores is minimized with tilting. Hydrogens and disorder are omitted for clarity. Crystals obtained by slow diffusion of pentane into a CHCl₃ solution, space group: P-3.

Table 5. Summary of the reaction conditions used for the synthesis of mono-, bis-, tris-, and tetra-doped borazine-polyphenylene derivatives.

Entry	110 : 34a ratio	B-Ar substituent	Yield (%)				Yield Other products
			Mono-BN	Bis-BN	Tris-BN	Tetra-BN	
1	4:1	Mesityl	10	2	-	-	**187** (2%); **46** (4%)
2	2:1	Mesityl	6	5	3	-	-
3	1:1	Mesityl	-	-	-	-	-[a]
4	2:1	Mesityl	-	-	-	-	-[a]
5	4:1	Xylyl	26	8	~10[b]	<1[b]	-

[a]Formation of an unidentified white insoluble solid. [b]Rough estimation of the yield done on the mixture containing tris-BN **192** and tetra-BN **193**.

In Table 5, the results obtained by reacting aniline (**110**) and *p*-phenylenediamine (**34a**) are summarized. As expected, by increasing the amount of **34a**, formation of the products with higher degree of branching (bis-, tris-, and tetra-borazine derivatives) is favoured. However, by using one or more equivalents of diamine **34a** with respect to **110** (entries 3 and 4), an insoluble polymeric form was produced. Finally, the use of xylyl-groups as *B*-aryl substituents (entry 5) resulted in the improvement of the overall yield.

Having developed a suitable strategy to obtain polyphenylene derivatives with well-defined shape, and bearing multiple borazine rings in determined positions, the next step consisted in the synthesis of the designed precursors bearing fluoride-groups (**183**, **184**, and **185**, Scheme 75).
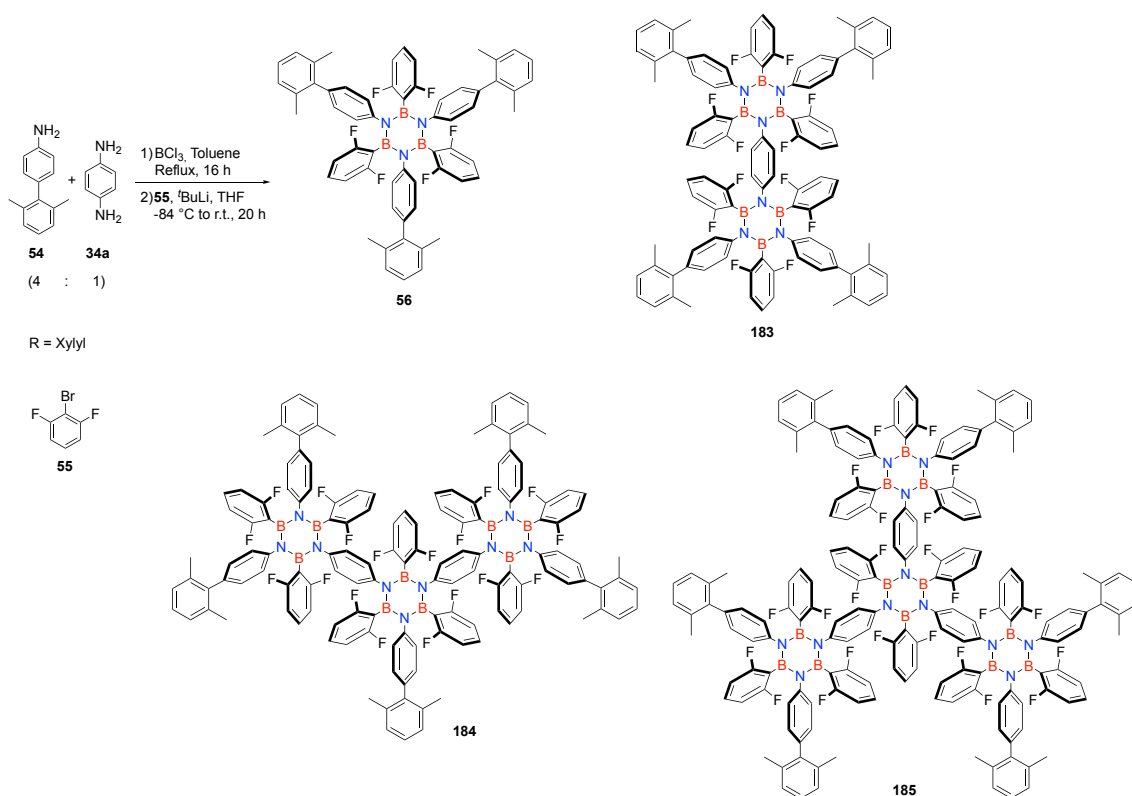
Scheme 79. Synthesis of multi-borazine series bearing *ortho*-fluoride *B*-substituents.

Then, these will be used to produce the planar borazine-doped graphene substructures. For this reason, 4-xylylaniline **54** and **34a** (4:1 ratio) were reacted with BCl₃. The reaction mixture was then treated with 2,6-difluorophenyllithium **184**, obtained by reaction between 2,6-difluorobromobenzene **55** and *t*BuLi at -84 ˚C. Similarly to the test reactions mentioned before (Scheme 76, Scheme 77, and Scheme 78), TLC analysis of the reaction crude revealed a complex mixture. Despite this, only mono-borazine derivative **56** could

be isolated with 18% yield, as unfortunately, the remaining of the products seemed to be slowly degrading. In fact, after silica gel column chromatography a white insoluble precipitate formed from the collected fractions. TLC analysis of these revealed once again a complex mixture, clearly indicating degradation, probably due to instability of the derivatives in the conditions in which the separation was carried out. Additionally, direct purification through Rec-GPC couldn't be done, as the formation of insoluble by-products would compromise the polymeric stationary phase. Even though borazine derivative **56** is known to be very resistant towards hydrolysis,[114] the degradation of the fluoride-functionalized multi-doped derivatives **183**-**185** must not surprise in light of the crystal structures of derivative **191** (Figure 35). Indeed, we have seen that due to the presence of crowded neighbouring arylborazine units, the B atoms are not homogeneously covered as they are in the mono-borazine derivative.[91] Despite this, the size of the *o*-Me groups seems to be sufficient to protect the BN ring from nucleophilic attacks, as derivative **191** happens to be stable in presence of moisture. However, switching the *o*-Me groups with the smaller *o*-F groups results in the uncovering of the B atoms, resulting in the susceptibility of derivatives **183**-**185** (Scheme 79) towards hydrolysis.

3.3.2 Synthesis of a borazine-doped PAH with extended conjugated area

Given the susceptibility of molecules **183**-**185** (Scheme 79) towards hydrolysis, we decided to focus our attention on the synthesis of a mono-doped unit, and to use it for the synthesis of HBBNC derivative **194** (Scheme 80), featuring an extended conjugated area. To do so, the classical procedure is envisaged to synthesise borazine-PPh **196** by employing aromatic amine **197** and the lithium derivative of **55** (Scheme 82). The inner core of borazine **196** would then be cyclized through the same procedure used for the synthesis of HBBNC **57**,[114] followed by Scholl reaction[178,289,306] to planarize the outskirt of the structure in **195**, giving final borazine-PAH **194**. The synthesis of aniline derivative **197** (Scheme 81), started from molecule **134**, which was quantitatively functionalized with xylyl groups by Suzuki cross-coupling with boronic acid **198**. Oxidation to diketone **200** was achieved in 70% yield using $KMnO_4$ at r.t. in a mixture of acetone and AcOH.
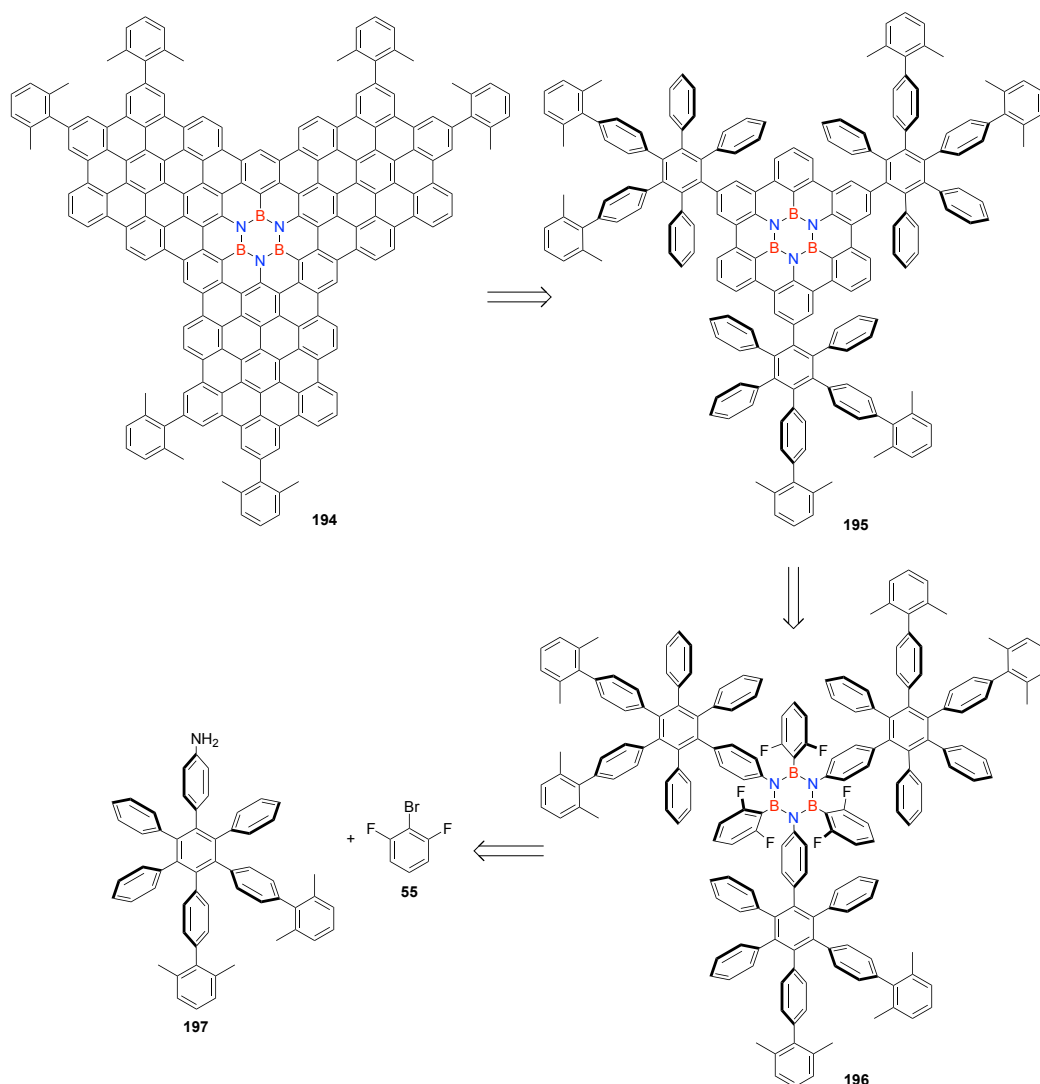
Scheme 80. Retrosynthetic pathway towards borazine-doped PAH **194**.

Derivative **200** was then submitted to Knoevenagel condensation with diphenylacetone (**121**), affording CPD derivative **201** with 60% yield. In parallel, aniline **202** was obtained with high yield by Pd/Cu-catalyzed Sonogashira cross coupling between *p*-iodoaniline (**103**) and phenylacetylene (**160**). The decarbonylative D.A. cycloaddition between **201** and **202** (Scheme 81) afforded aniline **197** with 40% yield. Having in hands the latter, we proceeded with the synthesis of the mono-doped fluoride-functionalized borazine precursor **196**. Therefore, **197** was reacted with BCl₃ in refluxing toluene, followed by treatment with the lithium derivative of **55** (Scheme 82). However, this attempt to generate borazine **196** failed. Notably, 60% of starting amine **197** was recovered by silica gel column chromatography after the reaction, and no trace of the product could be observed.
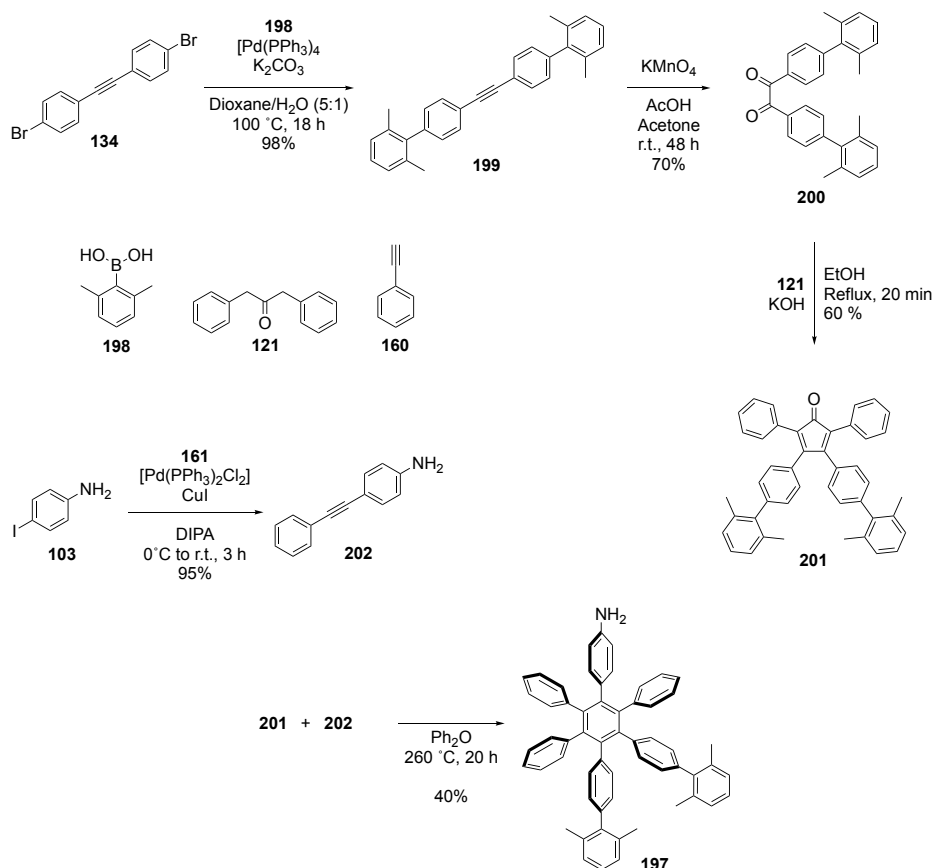
Scheme 81. Synthetic pathways towards CPD **201**, aniline derivative **202**, followed by synthesis of aniline-PPh derivative **197** through D.A. cycloaddition.

This is probably due to the presence of steric hindrance caused by the hexaphenylbenzene substituents, which disfavour the attack of the 2,6-difluorophenyllithium nucleophile on the *B*-chloroborazine intermediate.
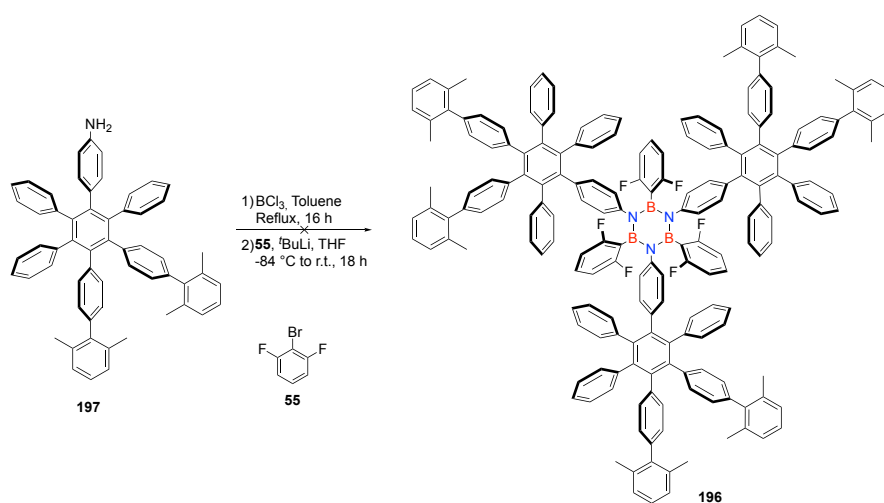
Scheme 82 Attempted synthesis of extended mono-borazine-doped PPh precursor **196**.

As a second hypothesis, isolation of **196** was not possible due to instability of it during the aqueous workup of the reaction. In fact, the steric hindrance of the PPh branches connected at the *N*-sites can generate a distortion of the aryl substituents directly attached to the BN core in **196**. As seen for molecule **186**, this can lead to a disruption of the shielding effect operated by the *o*-substituents on the B atoms (Figure 33), and therefore to a reduced resistance of the borazine ring towards nucleophilic attack. In particular, the protection of the BN core can be disrupted more effectively when fluoride atoms are present as *o*-substituents.

3.3.3 Perspectives towards the planarization of borazine-doped polyphenylenes

Given the impossibility to use the planned route for the formation of borazine-doped graphene substructures, the development of new and alternative methodologies for the planarization of aryl-borazine systems was taken in consideration. In particular, the careful choice of the *o*-groups functionalized at the *B*-substituents of the borazine core is of key importance as it should provide protection against hydrolysis. However, when submitted to certain conditions, should behave as leaving group, triggering planarization of the aryl system and formation of the 2D BN-PAH structure. Recently in our group, the synthesis of the moisture resistant tri-*N*-phenyl-tri-*B*-2,6-dimethoxyphenylborazine **203** (Scheme 83) was accomplished by Dr. *María Mercedes Lorenzo Garcia*. The inertness of derivative **203** towards hydrolysis demonstrates the suitability of the methoxy-group as a *o*-protective group for the B_3N_3 ring.

203
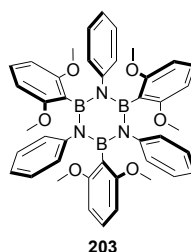
Scheme 83. Structure of *o*-methoxy-functionalized borazine **203**.

However, the -OMe group is notoriously a bad leaving group, especially when bound to aryl systems. To take advantage of this *o*-group, its transformation into a good leaving-group is therefore necessary. To the best of our knowledge, the methodologies currently known for the activation of the C-OMe bond, refer only to those groups bound to sp^3 carbon centres.[307–309] Ideally, in the case of molecule **203**, transformation of the o-

substituents into good leaving groups could trigger the intramolecular electrophilic attack of the neighbouring Ph groups attached at the *N*-sites (Scheme 84), leading to planarization of the system.
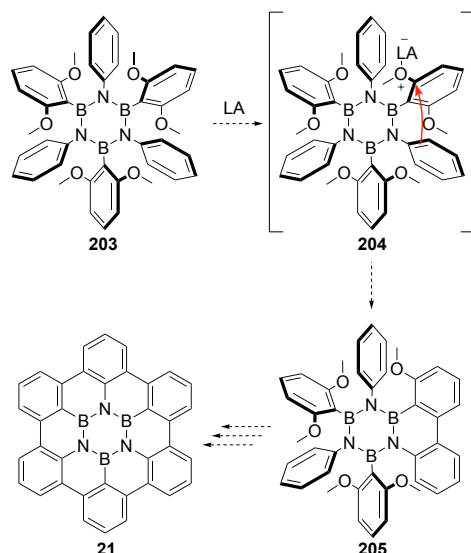
Scheme 84. Hypothetical route towards HBBNC **21** through Lewis acid activation of –OMe groups.

In particular, we envisaged that this would be favoured by strong Lewis acids, that would create a positive charge in the oxygen atom, favouring its exit. In the quest for a species with strong electrophilicity, we came across the report from *Müller*, describing the synthesis of hydrogen-bridged 1,8-naphtalenedisilyl cation **206** (Scheme 85) and its use in the catalytic C-F activation.[310]
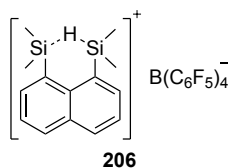
Scheme 85. Structure of the H-bridged silylium salt **206**.

We hypothesised that in the presence of a generic OMe-functionalized arene systems (**R42**, Scheme 86), a stoichiometric amount of molecule **206** would form an adduct in which a new Si-O bond is formed. Reduction of the methyl group would then take place, and the formation of a second Si-O bond would be accomplished after elimination of a molecule of CH_4. At this point, a new C-C bond would be formed by intramolecular attack of the neighbouring phenyl group. The aromaticity of the system would then be restored by first elimination of 1,8-disilylnaphtalene derivative **207**, then by deprotonation of the Wheland intermediate **R46**.
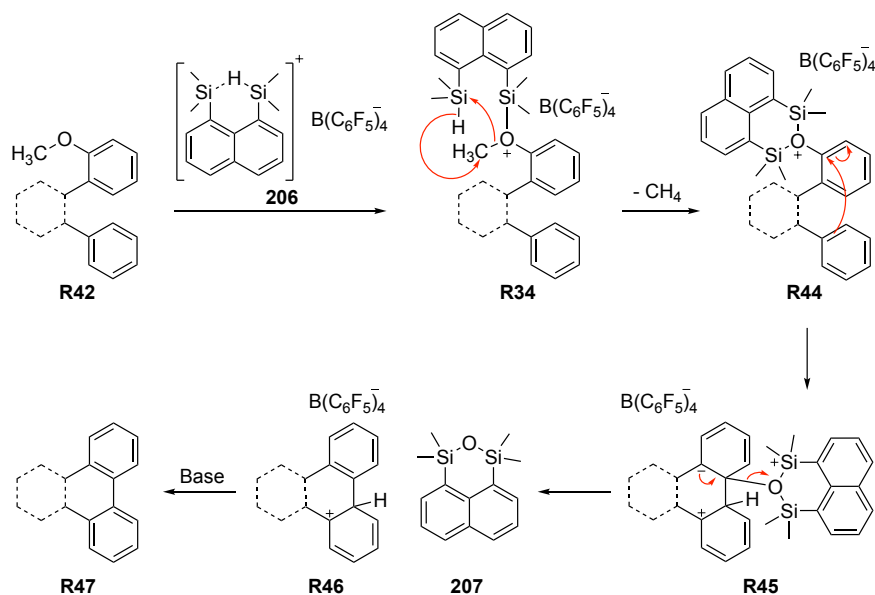
Scheme 86. Hypothetical methanism for cyclization of arene-OMe system using a stoichiometric amount of **206**.

In order to confirm our hypothesis regarding the reactivity of aryl-OMe systems in the presence of salt **206**, we decided to attempt this cyclization reaction choosing molecule **210** (Scheme 87) as test substrate due to its similarity with the aryl-OMe system present in borazine **203**. Therefore, synthesis of silylium salt **206** was accomplished by hydride abstraction on **209** using trityl tetra(pentafluorophenyl)borane (TrPFPhB). In turn, 1,8-bis(dimethylsilyl)naphtalene **209** was accessible by reaction of 1,8-dibromonaphtalene **208** with 2 equivalents of ^{n}BuLi and an excess amount of Me_2SiHCl.[310] The test reaction between silylium salt **206** and substrate **210** was carried out in the presence of the sterically hindered base P(*o*-tol)$_3$ and using chlorobenzene as solvent (Scheme 87). Notably, no reaction happened at r.t., while very poor conversion accompanied by formation of a new product, was observed when the temperature was raised at 50 ˚C. However, the reaction did not proceed any further, not even by increasing the temperature at 100 ˚C. Although the very poor overall conversion, mass spectrometry on the reaction crude revealed a complex mixture of products. However, a trace of triphenylene (**211**) was detected (calc. for $[C_{18}H_{13}]^+$: 229.1017, found: 229.0997), indicating formation of an aryl-aryl linkage and providing an initial positive insight on the effectiveness of the reaction. However, further studies will be necessary to make the reaction usable for the purpose.
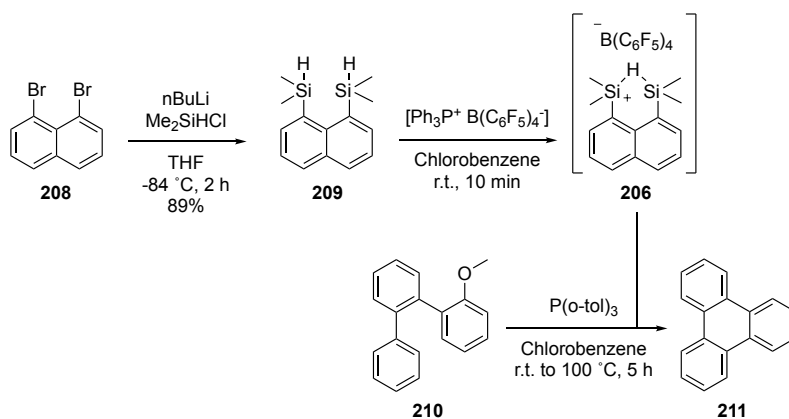
Scheme 87 Intramolecular cyclization test reaction using silylium derivative **206** on 2-(2'-phenyl)-phenylanisole **210** to produce triphenylene **211**.

Opportunistically, the removal of Me-groups from **203** was also envisaged, for example, by deprotection with BBr$_3$. Therefore, given the possibility to obtain borazine derivative **212**, featuring *o*-OH groups, we also investigated the possibility to transform the OH groups into good leaving groups in order to trigger the planarization of aryl-OH systems.
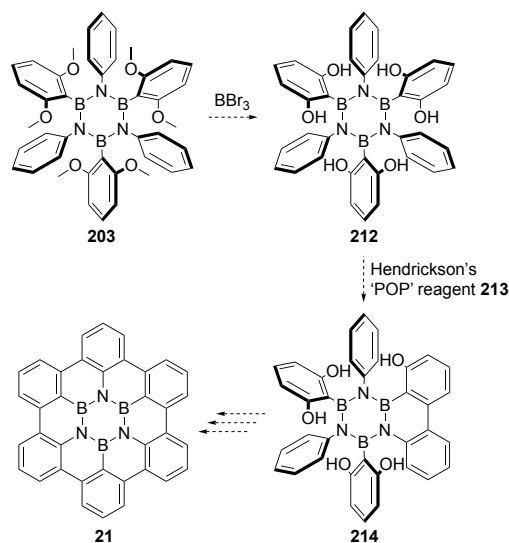
Scheme 88. Hypothetical route towards HBBNC **21** through activation of C(sp^2)-OH bonds using the Hendrickson's 'POP' reagent **213**.

Following the same approach for the planarization of aryl-OMe systems (Scheme 87), the activation of the C(sp^2)-OH was investigated by using bis(triphenyl)oxodiphosphonium trifluoromethane-sulfonate **213** (Scheme 89), known also as Hendrickson's 'POP' reagent,[311] in the test reaction choosing phenol derivative **215** as substrate. This electrophile, was used in particular for the dehydration of aldoximes,[312] carboxylic acids,[312,313] ketones,[314] diols and epoxides.[315] In particular, its use in conjunction with a strong Lewis acid (BF$_3$) and *o*-dichlorobenzene (*o*DCB) as solvent (Scheme 89). The POP

reagent **213**, is prepared by reaction Tf$_2$O with 2 eq. of Ph$_3$PO, and then united with a solution of **215** in *o*DCB.
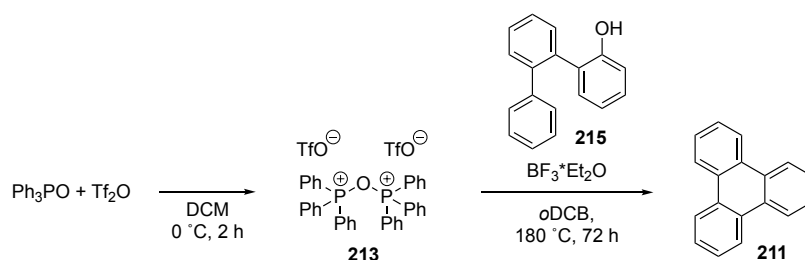
Scheme 89. Test reaction for the activation of the C(sp^2)-O bond and cyclization on test substrate.

After refluxing the mixture for 3 h no conversion of the starting material could be observed by TLC. Therefore, an excess amount of BF$_3$·Et$_2$O was added and the mixture was refluxed for further 24 h. In this case, the conversion of the starting material was still very poor, but the cyclized product **211** was observed by both TLC and mass analysis by detection of the peak at *m/z* 228.09 (calc. for [C$_{18}$H$_{12}$]$^+$: 228.09). Taken altogether, these two preliminary reactions on test substrates, constitute a clear indication about the possibility to use methoxy- or hydroxy-groups as leaving groups and activate the C(sp^2)-O bond, facilitating an intramolecular attack from a neighbouring aryl ring, and thus, planarization of the system.
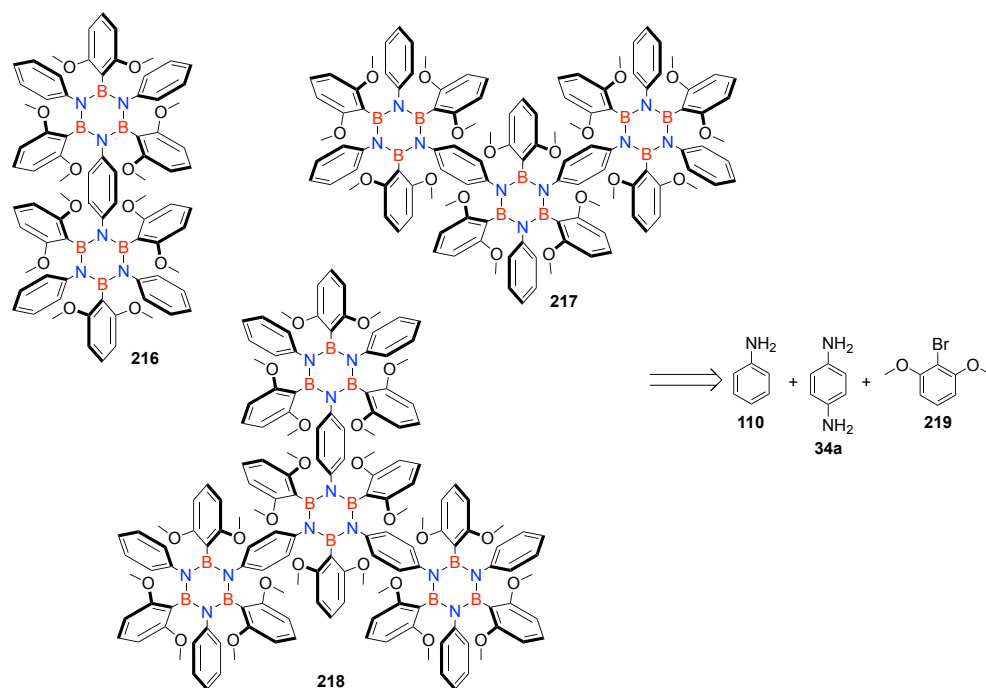
Scheme 90. Rethrosynthetic analysis for the preparation of bis- (**216**) tris- (**217**), and tetra- (**218**) OMe-functionalized borazine-doped precursors for graphene substructures.

Before optimizing the aforementioned procedures for the planarization of aryl-OMe and aryl-OH systems, we also commenced an investigation about the synthesis of OMe-functionalized borazine-PPh.
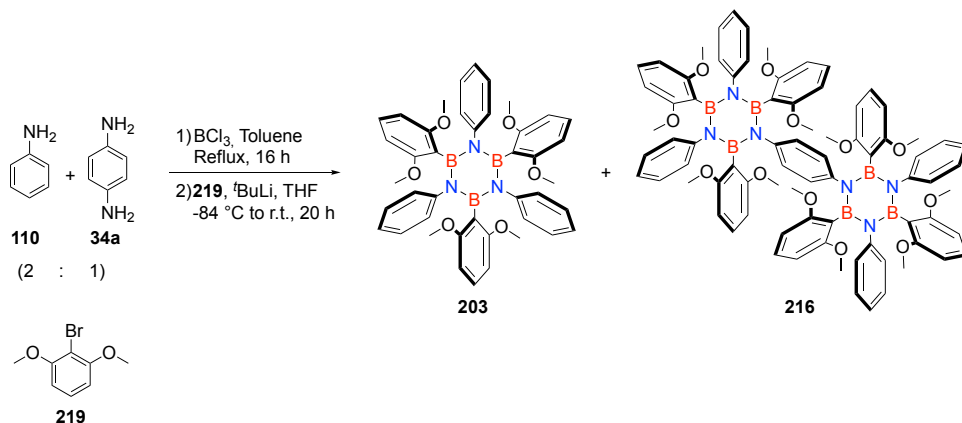
Scheme 91. Synthesis of OMe-protected borazine-doped PPh derivatives.

In a future perspective, in case the optimization of the new methodologies for the planarization of arene systems will be successful, PPhs **216-218** will be used as precursors for the synthesis of borazine-doped graphene substructures. In particular, these intermediates will be prepared again using a mixture of aniline (**110**) and *p*-phenylenediamine (**34a**, Scheme 90), in the same conditions that led to the synthesis of borazine-PPh **186** and **188** (Scheme 77, see section 3.3.1).
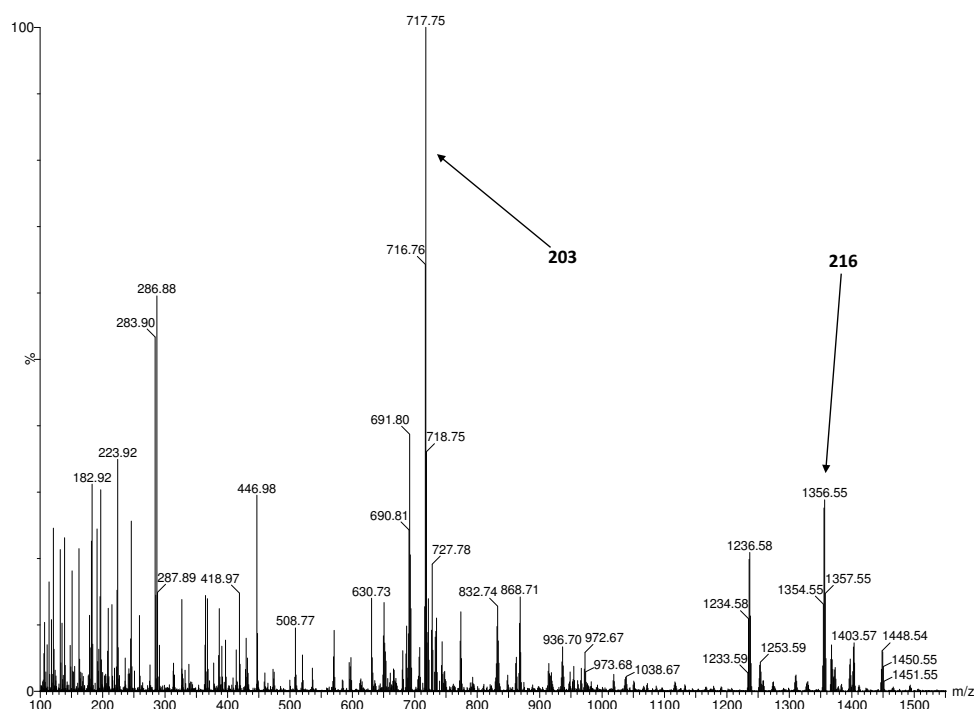
Figure 37. LR-ESI mass spectrogram of a mixture containing **203** and **216**.

Therefore, a first attempt was carried out reacting a 2:1 mixture of **110** and **34a** with BCl$_3$ in refluxing toluene, followed by treatment with the Li-derivative of 2,6-dimethoxybromobenzene **219**. Resolution of the complex mixture obtained after the reaction, was attempted by silica gel column chromatography. However, due to the poor solubility of the mixture of products, the separation was not successful. Albeit not pure, the collected fractions were analysed by ESI-mass analysis. In one of these, presence of mono-borazine **203** and bis-borazine **216** could be observed by detection of the low-resolution molecular peaks at *m/z* 717.7 (calc. for [C$_{42}$H$_{42}$N$_3$B$_3$O$_6$]$^+$: 717.3) and *m/z* 1356.5 (calc. for [C$_{78}$H$_{78}$N$_6$B$_6$O$_{12}$]$^+$: 1356.6), respectively (Figure 37).
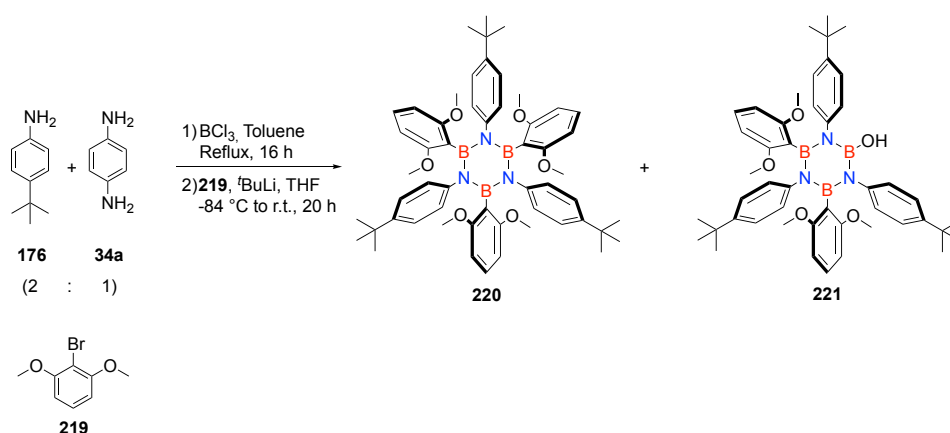
Scheme 92. Synthesis of OMe-protected borazine-doped PPh bearing ^{t}butyl solubilizing groups.
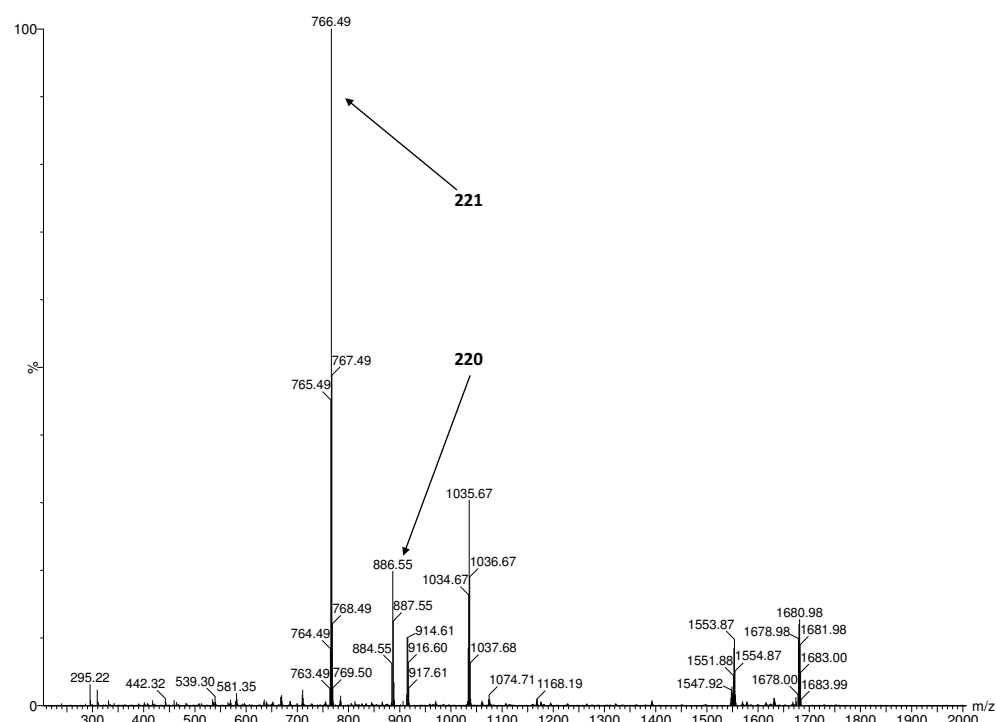
Figure 38. LR-ESI mass spectrogram of a mixture containing **220** and **221**.

Trying to improve the solubility of the products, unsubstituted aniline **110** was replaced by 4-*t*butylaniline (**176**, Scheme 92). However, results were disappointing as solubility, and thus separation of the products through silica gel column chromatography, did not improve. In this case, mass analysis of the impure fractions revealed presence, amongst other unidentified species, of mono-borazine **220** (calc. for $[C_{54}H_{67}N_3B_3O_6]^+$: 885.53, found: 886.55), and hydroxyl-mono-borazine **221** (calc. for $[C_{46}H_{58}N_3B_3O_5]^+$: 766.47, found: 766.49, Figure 38).

In this last section, the investigation of a novel methodology for the planarization of OMe-aryl systems, is presented. Aiming to the definition of a suitable procedure to transform OMe-borazine **203** in a planar BN-doped structure, a reaction on test substrate OMe-arene **211** in the presence of silylium salt **206** (Scheme 87), was carried out. Following the same approach, another reaction for the planarization of arene-OH **215** was tested. Notably, in both attempts the formation of the targeted product was observed, albeit with poor yield. In the near future, further studies on the reactivity of such systems will be done, and optimization of this new methodology will hopefully pave the way for the development of a scalable rational synthesis of borazine-doped PAHs and graphene substructures. Regarding the synthesis of OMe-functionalized borazine-doped PPh precursors, a first attempt gave encouraging results, since formation of one of the desired products was observed. However, its isolation was prevented by a poor solubility. Surprisingly, an attempt to increase the solubility by functionalization with *t*Bu groups, did not lead to the expected results. Therefore, to solve the solubility issue related to these BNC hybrid derivatives, the use of a different solubilizing group (like a long alkyl chain) must be investigated in the future.

3.4 Conclusions

During the last five decades, the synthesis and applications of polyphenylenes have been thoroughly reviewed and deepened. Thanks to a step-growth approach, these molecules composed by the repeating 1,2,3,4,5-pentaphenylbenzene motif, could be shaped in a wide range of designs and sizes. Moreover, these structures demonstrated a great chemical stability and yet, the possibility for structural diversification and post-functionalization allow for the expansion of the application scope and for the generation of systems which could be used in nanoscience, optoelectronics, catalysis, host-guest and coordination chemistry. In the research group where this thesis work has been carried out,

the determination of the diversity originating upon doping of polyphenylenes with the inorganic analogue of benzene, borazine, has been an ever-present topic. The investigation of the synthesis, reactivity, chemical and optical properties of these systems started with the doping of small oligophenylene units,[91,137,138,149] providing important insights on the supramolecular and physical chemistry of aryl-borazines. As a natural extension of those efforts, the work presented here concerns the structural expansion of hexa-aryl borazines and for the first time introduces the cycloaddition methodology, extensively used for the growth of PPh dendrimers, to borazine-containing oligophenylene building blocks. The development of synthetic strategies for the selective functionalization of the borazine core with different groups grafted at the aryl-substituents either at the *N*- or *B*-sites, gave access to borazine derivatives bearing donor groups (ethynyl), or acceptor groups (CPD). In turn, this was possible by using aryl substituents, whose *ortho*-methyl groups provided steric protection of the electrophilic boron atoms, making borazines stable towards hydrolysis and nucleophilic attacks. The use of these aryl-borazine derivatives as molecular synthons, resulted in the generation of a library composed of hybrid BNC polyphenylenes having specific sizes, doping ratios, different position and relative orientation of the doping borazine rings. Therefore, a series of hexa-branched borazine-doped PPhs were synthesised. A detailed investigation about the photophysical properties revealed that luminescence is progressively reduced upon increasing the doping dosage (Φ_{em}= 76% to 7%), suggesting a major role of BN-doping on favouring non-radiative deactivation pathways. To further expand the chemical toolbox for the functionalization of these derivatives and to prove the energy harvesting properties of BNC hybrids, a multichromophoric derivative was synthesised grafting a blue NDI derivative to a three-branched borazine-doped PPh through Cu-catalysed 1,3-dipolar cycloaddition. Photophysical investigations on the BNC hybrid dye revealed an efficient energy transfer from the borazine-doped PPh beckbone to the chosen covalently grafted chromophore.

Altogether, the results presented here constitute a proof of the synthetic versatility of borazine derivatives that can be used like benzene for the construction of functional molecules. Also, the possibility to achieve precise doping patterns makes these BNC hybrid architectures interesting precursors for the synthesis of planar graphitic nanostructures featuring controlled doping. Aiming to prepare graphene-like conjugated structures featuring one or multiple borazine units embedded in the planar molecules, in

a further development of this thesis work the synthesis of borazine-doped PPh derivatives bearing suitable protective/leaving groups was attempted. To assess the possibility to synthesise the precursors for the designed BN-doped PAH species, the classic procedure for the production of aryl-borazines was used starting from a mixture of mono- and bis-amines and grafting *ortho*-substituted aryl-groups at the *B*-sites. This study provided important insights about the stability and reactivity of the designed multi-borazine derivatives, and confirmed the applicability of the devised synthesis. However, the attempts to obtain the multi-doped derivatives, where the *ortho*-protective groups at the *B*-sites are replaced by fluoride atoms or OMe groups, failed due to stability issue or lack of solubility of the products. The use of suitable purification techniques under inert conditions to prevent degradation of the fluoro-substituted borazine derivatives, and the employment of a better solubilizing group for the OMe-functionalized borazine-doped PPh, will be object of future studies and developments of this work. Moreover, parallel investigations regarding the reactivity of OMe- and OH-substituted aryl-systems showed promising results that need, however, further investigation and optimization prior to the use of this functional group as *ortho*-protective group and as suitable trigger for the planarization of multi-borazine-doped polyphenylenes.

Chapter 4: Experimental section

4.1 General remarks

Instrumentation: ***Thin layer chromatography*** (TLC) was conducted on pre-coated aluminium sheets with 0.20 mm *Machevery-Nagel Alugram SIL G/UV254* with fluorescent indicator UV254. ***Column chromatography*** was carried out using *Merck Gerduran* silica gel 60 (particle size 63-200 µm). ***Melting points*** (mp) were measured on a *Büchi Melting Point B-545* in open capillary tubes and have not been corrected. ***Nuclear magnetic resonance*** (NMR) ^{1}H, ^{13}C, ^{11}B and ^{19}F spectra were obtained on a *Jeol JNM EX-400* 400 MHz spectrometer, on a *Bruker Fourier* 300 MHz spectrometer equipped with a dual (^{13}C, ^{1}H) probe, or a *Bruker AVANCE III HD* 400 MHz spectrometer equipped with a Broadband multinuclear (BBFO) *SmartProbeTM*. ^{1}H spectra were obtained at 400 or 300 MHz, ^{13}C spectra were obtained at 75 or 100 MHz NMR, ^{19}F spectra were obtained at 276 MHz and ^{11}B were obtained at 128 MHz all spectra were obtained at room temperature (r.t.) unless otherwise stated. Chemical shifts were reported in ppm according to tetramethylsilane using the solvent residual signal as an internal reference (CDCl$_3$: δ_H = 7.26 ppm, δ_C = 77.16 ppm; CD$_2$Cl$_2$: δ_H = 5.32 ppm, δ_C = 53.84 ppm; MeOD: δ_H = 3.31 ppm, δ_C = 49 ppm, DMSO-d$_6$: δ_H = 2.50 ppm, δ_C = 39.52 ppm). Coupling constants (J) were given in Hz. Resonance multiplicity was described as s (singlet), d (doublet), t (triplet), dd (doublet of doublets), dt (doublet of triplets), td (triplet of doublets), q (quartet), m (multiplet). Carbon, boron, and fluoride spectra were acquired with a complete decoupling for the proton. ***Infrared spectra*** (IR) were recorded on a *Perkin-Elmer Spectrum II FTIR System* with *Specac* Silver Gate Evolution single-reflection ATR mounted with a diamond mono-crystal, or on a *Shimadzu IR Affinity 1S FTIR* spectrometer in ATR mode with a diamond mono-crystal. ***GPC analysis and purifications*** on a preparative scale (maximum 20 mg) were performed on a *JAI LC-9160NEXT* using GPC columns *JAIGEL-2.5HH* and *3HH* in recycling mode and CHCl$_3$ (HPLC grade) as eluent. ***Mass spectrometry*** was generally performed by the *Centre de spectrométrie de masse* at the *Université de Mons in Belgium* where they performed MALDI-MS, on using the following instrumentation. MALDI-MS were recorded using a *Waters QtoF Premier mass spectrometer* equipped with, operating at 337 nm with a maximum output of 500 mW delivered to the sample in 4 ns pulses at 20 Hz repeating rate. Time-of-flight (TOF) analyses were performed in the reflectron mode at a resolution

of about 10,000. The matrix, trans-2-[3-(4-tert-butyl-phenyl)-2-methyl-2-propenylidene]malonitrile (DCTB), was prepared as a 40 mg/mL solution in $CHCl_3$. The matrix solution (1 μL) was applied to a stainless-steel target and air-dried. Analytic samples were dissolved in a suitable solvent to obtain 1 mg/mL solutions. 1 μL aliquots of those solutions were applied onto the target area already bearing the matrix crystals, and air-dried. For the recording of the single-stage MS spectra, the quadrupole (rf-only mode) was set to pass ions from 100 to 1000 Th, and all ions were transmitted into the pusher region of the time-of-flight analyser mass. ***UV-Vis absorptions*** were recorded on a *Varian Cary 5000 Bio* UV-Vis spectrophotometer using quartz cells (1 cm path length). ***Fluorescence*** was measured on a *Cary Eclipse Fluorescence spectrophotometer* using quartz cell (1 cm path length). ***Photophysical*** data were obtained on a *JobinYvon-Horiba Fluorolog* spectrometer fitted with a *JY TBX* picoseconds photodetection module as chloroform solutions. Emission spectra were uncorrected and excitation spectra were instrument corrected. The pulsed source was a *NanoLED* configured for 295 nm output operating at 1 MHz. Luminescence lifetime profiles were obtained using the *JobinYvon-Horiba FluoroHub* single photon couting module and the data fits yielded the lifetime values using the provided DAS6 deconvolution software.

Materials and methods: Chemicals were purchased from *Sigma Aldrich*, *Acros Organics*, *TCI*, *Alfa Aesar*, *Apollo Scientific*, and *Fluorochem*, and were used as received. Solvents were purchased from *Sigma Aldrich*, while deuterated solvents from *Eurisotop* and *Fluorochem*. Et_2O, THF, and toluene, were distilled from calcium hydride. Anhydrous DMF and pyridine were purchased from *Acros Organics*. MeOH, $CHCl_3$ and acetone were purchased from *Sigma-Aldrich* as reagent-grade and used without further purification. Low temperature baths were prepared using different solvent mixtures depending on the desired temperature: -84°C with liquid N_2/EtOAc, and 0 °C with ice/H_2O. Anhydrous conditions were achieved by drying Schlenk tubes or 2-neck flasks by flaming with a heat gun under vacuum and then purging with Argon. The inert atmosphere was maintained using Argon-filled balloons equipped with a syringe and needle that was used to penetrate the silicon stoppers used to close the flasks necks. Additions of liquid reagents were performed using disposable plastic syringes.

4.2 Experimental details for section 3.1

Synthesis of 4-(trisisopropylsilylethynyl)aniline 104
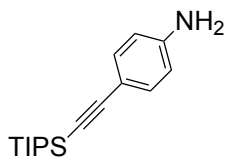
In a 250 mL Schlenk-type flask DIPA (70 mL) was degassed by 4 FPT cycles. 4-iodoaniline **103** (5.00 g, 22.8 mmol), TMSA (5.60 mL, 25.0 mmol), [Pd(PPh$_3$)$_2$Cl$_2$] (0.323 g, 0.46 mmol) and CuI (0.089 g, 0.46 mmol) were added and the mixture was furtherly degassed by 3 FPT cycles. The suspension was stirred at r.t. for 24 h, then diluted with EtOAc (200 mL) and washed with water (3 × 200 mL) and brine (100 mL). The organic layer was dried over MgSO$_4$ and evaporated under reduced pressure. The product was purified by silica gel column chromatography (eluent: CHX/EtOAc, 8:2) to afford **104** as a yellow oil (5.25 g, 84%); ^{1}H-NMR (400 MHz, CDCl$_3$) δ: 7.28 (d, J= 8.7 Hz, 2 H); 6.58 (d, J= 8.7 Hz, 2 H); 1.11 (s, 21 H). ^{13}C-NMR (100 MHz, CDCl$_3$) δ: 146.76, 133.49, 114.62, 113.10, 108.02, 87.55, 18.81, 11.50. ESI-HRMS calc. for [C$_{17}$H$_{28}$NSi]$^+$: 274.4950; found: 274.2390. IR (neat film) v$_{max}$ (cm^{-1}): 3382.91, 2491.33, 2890.59, 2863.78, 2147.07, 1620.08, 1605.35, 1510.79, 1462.12,1382.66, 1365.66, 1289.36, 1230.36, 1174.86, 1126.06, 1072.00, 1014.96, 995.31, 918.73, 881.43, 848.07, 827.12, 787.85, 728.54, 673.85, 657.44, 612.17, 596.42, 534.57, 488.51.

Synthesis of ((4-bromo-3,5-dimethylphenyl)ethynyl)trimethylsilane 106
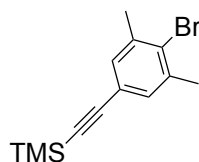
In a 250 mL Schlenk-type flask 2-bromo-5-iodo-m-xylene **105** (0.50 g, 1.6 mmol), [PdCl$_2$(PPh$_3$)$_2$] (0.034 g, 0.048 mmol), CuI (0.018 g, 0.096 mmol), and DIPA (10 mL), were added. The mixture was degassed by 3 FPT cycles and then TMSA (0.272 mL, 1.92 mmol) was added. The suspension was stirred for 16 h at r.t., then diluted with EtOAc (30 mL) and washed with water (3 × 100 mL), and brine (30 mL). The organic layer was dried over MgSO$_4$ and evaporated under reduced pressure. The product was purified by silica gel column chromatography (eluent: CHX), affording **106** as yellow oil (0.42 g, 93%). ^{1}H-NMR (400 MHz, CDCl$_3$) δ: 7.18 (s, 2 H); 2.36 (s, 6 H); 0.23 (s, 9 H). ^{13}C-NMR (100 MHz, CDCl$_3$) δ: 138.39, 131.44, 131.43, 128.27, 121.99, 104.55, 94.54. ESI-MS:

calc. for $[C_{13}H_{17}BrSi]^+$: 281.3, found: 282.2. IR (film in CH_2Cl_2) v_{max} (cm^{-1}): 2956.29, 2925.06, 2898.22, 2154.27, 2132.28, 1941.86, 1740.73, 1561.42, 1462.99, 1433.13, 1406.04, 1380.12, 1305.8, 1248.01, 1173.09, 1136.11, 1022.54, 962.52, 871.01, 835.25, 757.05, 689.02, 615.13, 598.54, 580.61, 565.84.

Synthesis of N,N',N''-tri(4-triisopropylsilylethynyl)phenyl-B,B',B''-tri(4-trimethylsilyl ethynyl)phenylborazine 107
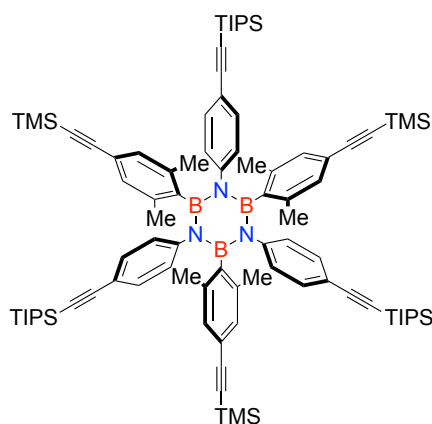
In a 50 mL Schlenk-type flask, **104** (2.75 g, 10.06 mmol), and dry toluene (20 mL) were added. To the solution under Ar, BCl_3 (1 M in heptane, 13.08 mL, 13.08 mmol) was added dropwise at 0 °C. The resulting scarlet-red solution was stirred under refluxing conditions for 18 h, then it was cooled down to r.t. and subjected to 5 FPT cycles to remove the excess of HCl. In parallel, to a solution of **106** (3.4 g, 12.078 mmol) in dry THF (30 mL), ^{t}BuLi (1.7 M in hexane, 15.0 mL, 25.36 mmol) was added dropwise at -84 °C under Ar. The mixture was allowed to warm up at 0 °C and stirred for 10 min. The degassed toluene mixture was thus transferred to the organometallic-containing solution in THF at 0 °C and allowed to react for 16 h at r.t.. The final mixture was diluted with EtOAc (50 mL), washed with water (3 × 50 mL) and brine (50 mL). The organic layer was dried over $MgSO_4$ and evaporated under reduced pressure. The product was purified by silica gel column chromatography (eluent: CHX/CH_2Cl_2, 9:1) to afford **107** as a white solid (0.70 g, 14%); mp 183-185 °C. ^{1}H NMR (400 MHz, $CDCl_3$) δ: 6.89-6.66 (m, 18 H); 2.21 (s, 18 H); 1.07 (s, 63 H); 0.18 (s, 27 H). ^{13}C NMR (100 MHz, $CDCl_3$) δ: 145.04, 137.48, 131.41, 129.53, 121.63, 120.44, 106.78, 105.85, 93.48, 90.37, 22.98, 18.85, 11.48, 0.07. ^{11}B NMR (128 MHz, $CDCl_3$) δ: 36.04. ESI-HRMS calc. for $[C_{90}H_{126}B_3N_3Si_6]^+$: 1450.8984, found: 1450.8956. IR (film in CH_2Cl_2) v_{max} (cm^{-1}): 3042.03, 2943.2, 2893.92, 2864.93, 2153.18, 1602.46, 1539.08, 1505.14, 1462.87, 1435.12, 1407.18, 1355.11, 1301.33, 1291.58, 1248.77, 1220.62, 1159.02, 1103.67, 1072.66, 1017.73, 995.98, 957.55, 911.27, 881.39,

854.28, 797.23, 759.5, 730.99, 703.44, 676.39, 654.99, 616.75, 595.36, 557.88, 509.68, 462.54.

Synthesis of N,N',N''-tri(4-ethynyl)phenyl-B,B',B''-tri(4-ethynyl-2,6-dimethyl)phenyl borazine 108
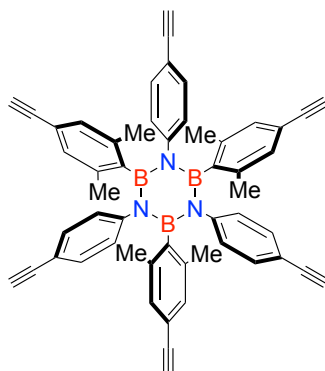
In a 25 mL round flask, to a solution of molecule **107** (0.710 g, 0.489 mmol) in THF (7 mL), TBAF (1 M solution in THF, 4.0 mL, 4.0 mmol) was added dropwise at 0 °C. The reaction mixture was stirred at r.t. for 2 h, then diluted with EtOAc (30 mL) and washed with water (3 × 30 mL) and brine (30 mL). The organic layer was dried over MgSO$_4$ and evaporated under reduced pressure. The product was purified by silica gel column chromatography (eluent: CHX/CH$_2$Cl$_2$, 7:3) affording **108** as a white solid (0.25 g, 67%); mp 270-272 °C (decomp.). ^{1}H NMR (400 MHz, CDCl$_3$) δ: 6.94 (d, J= 8.32 Hz, 6 H); 6.73 (s, 6 H); 6.71 (d, J= 8.36 Hz, 6 H); 2.92-2.91 (2s, 6 H); 2.21 (s, 18 H). ^{13}C NMR (100 MHz, CDCl$_3$) δ: 145.80, 137.53, 131.42, 129.57, 126.69, 121.12, 118.88, 84.09, 83.28, 77.33, 76.69, 22.92. ^{11}B NMR (128 MHz, CDCl$_3$) δ: 36.44. MALDI-HRMS calc. for [C$_{54}$H$_{42}$B$_3$N$_3$]$^+$: 765.3682, found: 765.3658. IR (film in CH$_2$Cl$_2$) ν$_{max}$ (cm^{-1}): 3290.74, 3042.92, 2955.8, 2921.68, 2861.77, 2108.41, 1601.29, 1542.22, 1506.48, 1434.41, 1408.53, 1357.92, 1303.27, 1284.39, 1262.28, 1235.31, 1149.26, 1104.42, 1019.04, 943.66, 868.16, 841.64, 764.42, 748.83, 732.09, 672.21, 617.65, 553.35, 515.85, 459.3.

Synthesis of N,N',N''-tri(4-triisopropylsilylethynyl)phenyl-B,B',B''-tri-4-ethynylphenyl borazine 109
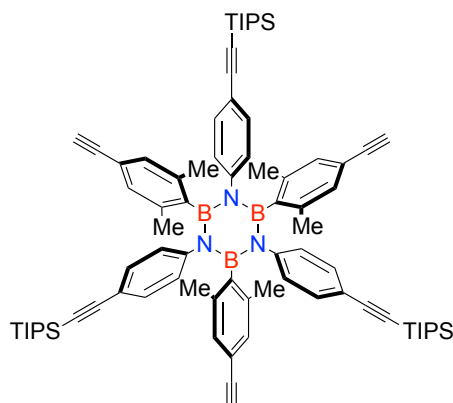
In a 25 mL round flask, to a solution of **107** (0.150 g, 0.1034 mmol) in THF/MeOH (1:1, 6 mL), K_2CO_3 (0.085 g, 0.620 mmol) was added. The mixture was stirred at r.t. for 16 h, then diluted with CH_2Cl_2 (30 mL) and washed with water (3 × 30 mL), and brine (30 mL). The organic phase was dried over $MgSO_4$ and evaporated under reduced pressure. The product was purified by silica gel column chromatography (eluent: CHX/CH_2Cl_2, 9:1) affording **109** as a white solid (0.088 g, 69%); mp 285-287 °C (decomp.). ^{1}H NMR (400 MHz, $CDCl_3$) δ: 6.90 (d, J= 8.49 Hz, 6 H); 6.76 (s, 6 H); 6.76 (d, J= 8.46 Hz, 6 H); 2.93 (s, 3 H); 2.22 (s, 18 H); 1.07 (s, 63 H). ^{13}C NMR (100 MHz, $CDCl_3$) δ: 145.41, 137.62, 131.40, 129.66, 126.46, 120.86, 120.43, 106.77, 90.38, 84.30, 76.58, 22.99, 18.83, 11.49. ^{11}B NMR (128 MHz, $CDCl_3$) δ: 36.07. ESI-HRMS calc. for $[C_{81}H_{102}B_3N_3Si_3]^+$: 1234.7761, found: 1234.7767. IR (film in CH_2Cl_2) ν_{max} (cm^{-1}): 3300.38, 3041.76, 2942.48, 2864.68, 2155.65, 1601.67, 1541.75, 1505.51, 1462.31, 1435.89, 1407.41, 1359.55, 1301.96, 1221.32, 1104.01, 1073.58, 996.24, 919.35, 882.22, 836.82, 795.32, 768.94, 731.19, 677, 646.39, 606.43, 559.31, 500.43, 466.49.

Synthesis of 2,6-dimethyl-4-(tertbuthyldimethylsilyloxy)bromo benzene 112

In a 250 mL round flask, 3,5-dimethil-4-bromophenol **111** (10 g, 49.8 mmol), TBDMSCl (10.5 g, 69.7 mmol), imidazole (10.2 g, 150 mmol), and DMF (60 mL), were added. The reaction mixture was stirred at 50 °C for 15 h, then diluted with EtOAc (200 mL) and washed with water (3 × 200 mL) and brine (100 mL). The organic layer was dried over $MgSO_4$ and evaporated under reduced pressure. The excess of TBDMSCl was removed

by evaporation under reduced pressure (6 mbar) at 75 °C for 2 h, affording **112** as pale-yellow oil (15.6 g, 99%) without need of further purification. ^{1}H NMR (400 MHz, CDCl$_3$) δ: 6.57 (s, 2 H); 2.34 (s, 6 H); 0.97 (s, 9 H); 0.18 (s, 6 H). ^{13}C NMR (100 MHz, CDCl$_3$) δ: 154.39, 139.27, 120.20, 119.27, 25.94, 24.19, 18.43, 4.15. ESI-HRMS calc. for [C$_{14}$H$_{24}$BrOSi]$^+$: 316.3293; found: 315.0774. IR (neat film) ν$_{max}$ (cm^{-1}): 2954.99, 2929.33, 2896.32, 2857.62, 1581.86, 1464.27, 1409.75, 1390.06, 1361.9, 1321.15, 1252.45, 1166.6, 1052.62, 1031.36, 1019.95, 1005.73, 977.96, 939.08, 864.97, 834.13, 778.72, 695.61, 673.42, 569.33, 524.01, 496.95, 469.72, 460.87.

Synthesis of N,N',N''-triphenyl-B,B',B''-tri(2,6-dimethyl-4-(tertbuthyl dimethylsilyloxy) phenyl) borazine 113
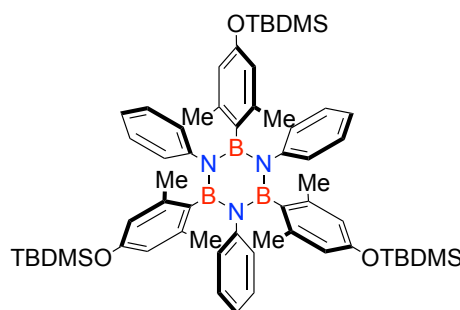
In a 50 mL Schlenk-type flask, **110** (1.0 mL, 10.95 mmol), and dry toluene (20 mL), were added. To the solution under Ar, BCl$_3$ (1 M in heptane, 12.0 mL, 12.0 mmol) was added dropwise at 0 °C. The resulting suspension was stirred under refluxing conditions for 18 h, then it was cooled down to r.t. and subjected to 5 FPT cycles to remove the excess of HCl. In parallel, to a solution of **112** (3.78 g, 12.0 mmol) in dry THF (20 mL), ^{t}BuLi (1.7 M in hexane, 14.7 mL, 25.0 mmol) was added dropwise at -84 °C under Ar. The solution was allowed to warm up at 0 °C and stirred for 10 min. The degassed toluene mixture was thus transferred to the organometallic-containing solution in THF at 0°C and allowed to react for 16 h at r.t.. The final mixture was diluted with EtOAc (100 mL) and washed with water (3 × 100 mL) and brine (100 mL). The organic layer was dried over MgSO$_4$ and evaporated under reduced pressure. The yellow deliquescent solid was re-dissolved in EtOAc (10 mL) and to the solution MeOH was added until formation of a precipitate. This was recovered by filtration to afford **113** as a white solid (2.89 g, 78%); mp 205-207 °C. ^{1}H-NMR (400 MHz, CDCl$_3$) δ: 6.78-6.67 (m, 15 H); 6.05 (s, 6 H); 2.18 (s, 18 H); 0.84 (s, 27 H); -0.04 (18 H). ^{13}C NMR (100 MHz, CDCl$_3$) δ: 154.60, 146.24, 138.98, 127.15, 126.72, 124.15, 117.64, 25.84, 23.11, 18.30, 4.47. ^{11}B-NMR (128 MHz, CDCl$_3$) δ: 36.05. MALDI-HRMS calc. for [C$_{60}$H$_{85}$B$_3$N$_3$O$_3$Si$_3$]$^+$: 1011.6100, found: 1011.6081.

IR (film in CH$_2$Cl$_2$) ν_{max} (cm^{-1}) 3039.83, 2955.44, 2929.15, 2857.3, 1597.15, 1562.22, 1491.27, 1471.67, 1462.76, 1452.53, 1356.81, 1303.38, 1251.38, 1191.84, 1150.76, 1087.19, 1074.67, 1037.98, 1005.57, 967.82, 938.92, 904.69, 866.51, 848.51, 848.2, 835.76, 814.05, 778.53, 758.26, 736.54, 698.43, 683.96, 666.53, 617.95, 579.02, 565.09, 518.75, 470.11.

Synthesis of N,N',N''-triphenyl-B,B',B''-tri(2,6-dimethyl-4-(trifluoromethane sulphonate)phenyl)borazine 115
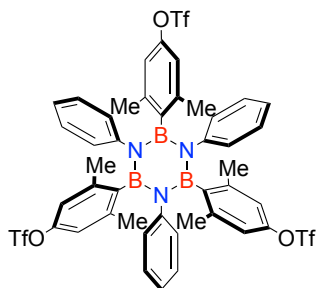
In a 100 mL round flask a solution of **113** (1.60 g, 1.58 mmol) in THF (30 mL) was stirred at 0 °C while TBAF (1 M in THF, 5.22 mL, 5.22 mmol) was dropwise added whereupon a white precipitate formed. The white suspension was stirred for 2 h, then the solid was recovered by filtration and dried under high vacuum for 3 h. Dry pyridine (24 mL) was directly added to the solid and the resulting suspension cooled down at 0 °C. To this, Tf$_2$O (2.28 mL, 17.0 mmol) was added dropwise. The orange solution was stirred for 16 h at r.t., then diluted with EtOAc (100 mL) and washed with a HCl 0.5 M aqueous solution (3 × 300 mL), water (100 mL), and brine (100 mL). The organic layer was dried over MgSO$_4$ and evaporated under reduced pressure. The product was purified by silica gel column chromatography (eluent: CHX/EtOAc 8:2) affording **115** as white solid (1.30 g, 78%); mp 236-238 °C. ^{1}H NMR (400 MHz, CDCl$_3$) δ: 6.82-6.75 (m, 15 H); 6.49 (s, 6 H); 2.31 (s, 18 H). ^{13}C NMR (100 MHz, CDCl$_3$) δ: 149.18, 144.80, 140.32, 127.47, 126.37, 125.44, 120.22, 118.03, 117.06, 23.19. ^{11}B NMR (128 MHz, CDCl$_3$) δ: 35.68. ^{19}F NMR (376 MHz, CDCl$_3$) δ: -72.77. MALDI-HRMS calc. for [C$_{45}$H$_{39}$B$_3$F$_9$N$_3$O$_9$S$_3$]$^+$: 1065.4195, found: 1066.2067. IR (film in CH$_2$Cl$_2$) ν_{max} (cm^{-1}): 2924.08, 1590.18, 1492.23, 1418.87, 1364.41, 1310.89, 1239.85, 1207.06, 1141.01, 1120.98, 1075.81, 1012.81, 945.78, 908.64, 870.17, 844.82, 813.16, 769.42, 748.68, 701.64, 648.01, 610.15, 582.87, 568.27, 531.51.

Synthesis of N,N',N''-triphenyl-B,B'-di(2,6-dimethyl-4-phenyl)-B''-2,6-dimethyl-4-(trifluoromethanesulphonate)phenyl)borazine 116 and N,N',N''-triphenyl-B,B',B''-tri((2,6-dimethyl-4-phenyl)phenyl)borazine 117

116   **117**
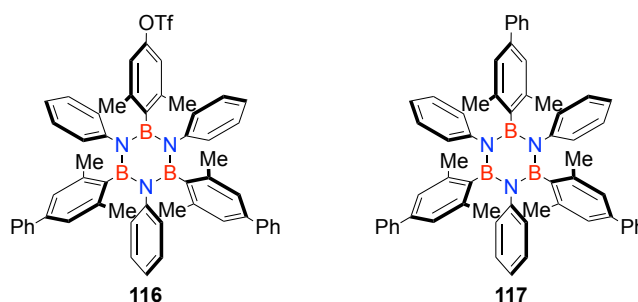
In a 10 mL Schlenk-type flask **115** (0.65 g, 0.61 mmol), K_2CO_3, and dioxane/H_2O 3:1 (3 mL) were added (0.73 g, 5.25 mmol). The mixture was degassed by bubbling Ar (40 min). [Pd(PPh$_3$)$_4$] (0.028 g, 0.025 mmol) and phenylboronic acid (0.13 g, 1.10 mmol) were added and the mixture was stirred at 105 °C for 16 h, then diluted with EtOAc (100 mL), washed with water (3 × 100 mL) and brine (100 mL). The organic layer was dried over $MgSO_4$ and evaporated under reduced pressure. The products were purified by silica gel column chromatography (eluent: CHX/EtOAc 9:1) to afford **116** (0.219 g, 39%) and **117** (0.042 g, 8%) as white solids.

116: mp 188-190 °C. ^{1}H NMR (400 MHz, CDCl$_3$) δ: 7.41-7.38 (m, 4 H); 7.31-7.27 (m, 4 H); 7.22-7.20 (m, 2 H); 6.90-6.70 (m, 19 H); 6.48 (s, 2 H); 2.36 (s, 6 H); 2.35(s, 12 H). ^{13}C NMR (100 MHz, CDCl$_3$) δ: 149.15, 149.09, 146.01, 145.77, 145.54, 141.35, 141.24, 140.45, 139.56, 139.37, 138.05, 137.98, 128.50, 127.20, 126.73, 126.72, 117.94, 117.84, 23.34, 23.22. ^{11}B NMR (128 MHz, CDCl$_3$) δ: 36.66. ^{19}F NMR (376 MHz, CDCl$_3$) δ: -72.72. MALDI-HRMS calc. for [C$_{55}$H$_{49}$B$_3$F$_3$N$_3$O$_3$S]$^+$: 921.3726, found: 921.3757. IR (film in CH_2Cl_2) ν_{max} (cm^{-1}): 3061.3, 3029.92, 2947.79, 2916.28, 2856.71, 1942.07, 1597.11, 1554.8, 1491.65, 1452.73, 1418.37, 1355.99, 1309.01, 1239, 1206.85, 1141.43, 1119.56, 1103.82, 1074.87, 1025.56, 1013.33, 944.26, 908.35, 870.56, 836.53, 813.79, 793.79, 761.82, 748.98, 732.28, 697.97, 666.8, 649.13, 610.6, 581.4, 565.72, 531.27.

117: mp 259-261 °C. ^{1}H NMR (400 MHz, CDCl$_3$) δ: 7.44-7.41 (m, 5 H); 7.33-7.20 (m, 10 H); 6.93-6.70 (m, 21 H); 2.40 (s, 18 H). ^{13}C NMR (100 MHz, CDCl$_3$) δ: 146.01, 141.34, 139.36, 138.06, 128.50, 127.03, 127.00, 126.76, 126.74, 124.62, 124.19, 23.39. ^{11}B NMR (128 MHz, CDCl$_3$) δ: 35.96. MALDI-HRMS calc. for [C$_{60}$H$_{54}$B$_3$N$_3$]$^+$: 849.4597, found: 849.4607. IR (film in CH_2Cl_2) ν_{max} (cm^{-1}): 3060.55, 3029.40, 2915.14,

1598.20, 1554.71, 1491.98, 1452.90, 1433.82, 1361.00, 1309.10, 1103.42, 1074.64, 1027.08, 908.56, 869.85, 815.10, 761.67, 749.65, 726.47, 698.50, 565.18, 531.19.

Synthesis of 1-bromo-4-(phenylacetynyl)benzene 119
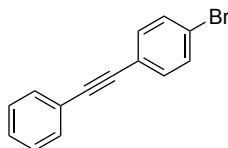
In a 250 mL Schlenk-type flask 4-bromoiodobenzene **118** (5.00 g, 17.67 mmol), [Pd(PPh$_3$)$_2$Cl$_2$] (0.12 g, 0.17 mmol), CuI (0.033 g, 0.17 mmol), and DIPA (40 mL), were added. The mixture was degassed by 3 FPT cycles, then TIPSA (1.95 mL, 17.76 mmol) was added and 3 further FPT cycles were done. The suspension was stirred at r.t. for 16 h, then diluted with EtOAc (100 mL), and washed with water (3 × 100 mL) and brine (100 mL). The organic layer was dried over MgSO$_4$ and evaporated under reduced pressure. The product was purified by silica gel column chromatography (eluent: PE) affording **119** as a white solid (4.50 g, 99%); mp 77-78 °C. ^{1}H NMR (400 MHz, CDCl$_3$) δ: 7.54-7.48 (m, 4 H); 7.40-7.35 (m, 5 H). ^{13}C NMR (100 MHz, CDCl$_3$) δ: 133.17, 131.75, 128.67, 128.56, 123.04, 122.64, 122.36, 90.68, 88.50. ESI-HRMS calc. for [C$_{14}$H$_{10}$Br]$^+$: 256.996039, found: 256.996075. IR (film in CH$_2$Cl$_2$) ν$_{max}$ (cm^{-1}): 3049.69, 1908.84, 1651.23, 1598.83, 1580.76, 1503.66, 1490.89, 1478.57, 1441.20, 1393.45, 1309.20, 1268.69, 1178.94, 1112.27, 1096.30, 1068.50, 1028.25, 1007.52, 909.60, 828.51, 821.55, 755.37, 717.23, 686.93, 510.55, 469.71.

Synthesis of 1-(4-bromophenyl)-2-phenylethane-1,2-dione 120
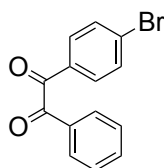
In a 500 mL round flask 1-bromo-4-(phenylacetynyl)benzene **119** (1.77 g, 6.88 mmol, acetone (260 mL), AcOH (2.60 mL), and KMnO$_4$ (2.78 g, 17.20 mmol), were added. The purple mixture was stirred at r.t. for 24 h and then filtered through celite. The volatiles were removed under reduced pressure and the crude mixture re-dissolved in EtOAc (100 mL) and washed with water (3 × 100 mL) and brine (50 mL). The yellow organic layer was dried over MgSO$_4$ and evaporated under reduced pressure to afford **120** as a yellow solid. (1.91 g, 96%); mp 74-75 °C. ^{1}H NMR (400 MHz, DMSO-d$_6$) δ: 7.94 (d, J= 8.3 Hz, 2 H); 7.86 (s, 4 H); 7.81 (t, J= 7.8 Hz, 1 H) 7.63 (t, J= 7.4 Hz, 2 H). ^{13}C NMR (100 MHz,

DMSO-d$_6$) δ: 194.59, 194.12, 136.11, 133.13, 132.61, 131.97, 131.75, 130.51, 130.26, 129.97. ESI-HRMS calc. for [C$_{14}$H$_{10}$O$_2$Br]$^+$: 288.9858, found: 288.9862. IR (film in CH$_2$Cl$_2$) v_{max} (cm^{-1}): 3088.76, 3064.22, 2923.41, 2853.38, 1919.41, 1703.49, 1665.42, 1579.13, 1483.26, 1449.95, 1398.99, 1321.53, 1205.15, 1172.87, 1112.37, 1069.64, 1023.89, 1010.07, 1000.63, 967.03, 933.33, 872.05, 830.15, 796.19, 751.34, 725.41, 708.06, 681.22, 656.96, 623.19, 614.73, 508.25, 479.31, 453.33.

Synthesis of 3-(4-bromophenyl)-2,4,5-triphenylcyclopenta-2,4-dien-1-one 122
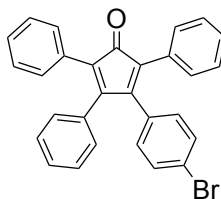
In a 25 mL round flask equipped with a condenser, 1-(4-bromophenyl)-2-phenylethane-1,2-dione **120** (2.00 g, 6.92 mmol), 1,3-diphenylacetone **121** (1.45 g, 6.92 mmol) and EtOH (10 mL) were added and stirred under refluxing conditions. A solution of KOH (0.20 g, 3.46 mmol) in EtOH (0.5 mL) was added through the condenser in two portions. The yellow solution immediately turned dark red and after 20 min it was cooled down to 0 ˚C, whereupon a precipitate formed. The product was recovered by filtration and washed with cold EtOH affording **122** as a dark red solid (2.50 g, 78%); mp 206-207 ˚C. ^{1}H NMR (400 MHz, CDCl$_3$) δ: 7.31-7.19 (m, 15 H); 6.94-6.91 (m, 2 H); 6.80-6.78 (m, 2 H). ^{13}C NMR (100 MHz, CDCl$_3$) δ: 200.06, 154.12, 153.14, 132.93, 132.02, 131.41, 131.15, 130.64, 130.52, 130.23, 129.37, 128.82, 128.32, 128.18, 127.85, 127.69, 125.83, 125.56, 123.05. MALDI-HRMS calc. for [C$_{29}$H$_{19}$OBr]$^+$: 462.0619, found: 462.0615. IR (film in CH$_2$Cl$_2$) v_{max} (cm^{-1}): 3052.91, 1709.41, 1588.49, 1483.11, 1442.54, 1392.48, 1355.47, 1305.94, 1264.09, 1180.18, 1109.73, 1086.29, 1071.79, 1027.14, 1008.81, 966.31, 918.52, 895.31, 841.91, 829.42, 802.41, 787.81, 730.50, 709.03, 693.43, 638.56, 617.31, 565.62, 546.51, 523.12, 500.97, 487.49.

Synthesis of 2,3,5-triphenyl-4-(4-(4,4,5,5-tetramethyl-1,3,2-dioxa borolan-2-yl)phenyl) cyclopenta-2,4-dienone 123
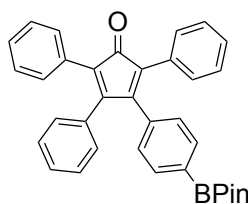
In a 10 mL Schlenk flask, 2,3,5-triphenyl-4-(4-bromophenyl) cyclopenta-2,4-dienone **122** (0.104 g, 0.224 mmol), KOAc (0.068 g, 0.672 mmol), and in dry DMF (5 mL) were added. The mixture was degassed by 3 FPT cycles and then [Pd(dppf)Cl$_2$] (0.010 g, 0.011 mmol) and B$_2$Pin$_2$ (0.061 g, 0.235 mmol) were added. The solution was stirred at 80 °C for 16 h, then diluted with EtOAc (30 mL) and washed with water (3 × 50 mL). The organic layer was dried over MgSO$_4$ and evaporated under reduced pressure. The brownish solid was purified by silica gel column chromatography (eluent: CHX/EtOAc 7:3) to give **123** as a deep purple solid (0.110 g, 96 %); mp 250-252 °C. ^{1}H NMR (400 MHz, CDCl$_3$) δ: 7.60-7.58 (m, 2 H); 7.25-7.15 (m, 13 H); 6.93-6.90 (m, 4 H); 1.33 (s, 12 H). ^{13}C NMR (100 MHz, CDCl$_3$) δ: 200.38, 154.868, 154.35, 135.97, 134.32, 133.07, 130.84, 130.73, 130.25, 129.37, 128.72, 128.64, 128.19, 128.13, 127.61, 127.56, 125.76, 125.41, 84.08, 25.03. ^{11}B NMR (128 MHz, CDCl$_3$) δ: 30.70. MALDI-HRMS calc. for [C$_{35}$H$_{31}$BO$_3$]$^+$: 510.4400, found: 511.2439. IR (film in CH$_2$Cl$_2$) ν$_{max}$ (cm^{-1}): 3053.87, 2978.06, 1710.20, 1607.58, 1513.05, 1490.55, 1443.42, 1397.45, 1353.03, 1323.16, 1299.97, 1265.52, 1213.00, 1142.49, 1092.84, 1019.42, 962.68, 918.36, 857.72, 803.91, 789.40, 739.09, 710.31, 694.82, 671.76, 656.23, 639.05, 568.93, 548.27, 523.65, 488.32.

Synthesis of N,N',N''-triphenyl-B,B'-di(2,6-dimethyl-4-phenyl)-B''-2,6-dimethyl-4-(2,3,5-triphenyl-4-(phenyl-4'-yl))cyclopenta-2,4-dienone borazine) 124
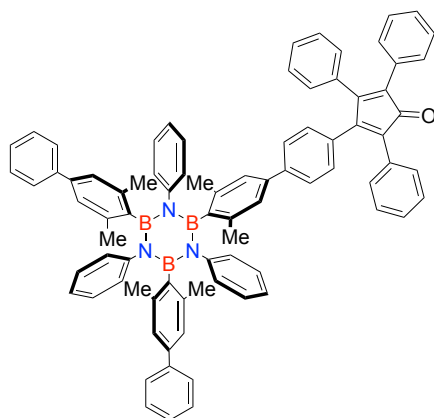
In a 20 mL Schlenk-type flask, **116** (0.07 g, 0.075 mmol), K$_2$CO$_3$ (0.042 g, 0.304 mmol), and a dioxane/water 3:1 mixture (8 mL) was added. The suspension was degassed by 3 FPT cycles, then [Pd(PPh$_3$)$_4$] (0.005 g; 0.005 mmol) and **123** (0.077 g, 0.152 mmol) were added. The mixture was stirred at 105 °C for 16 h, then diluted with EtOAc (20 mL), and washed with water (3 × 20 mL) and brine (30 mL). The organic layer was dried over MgSO$_4$ and evaporated under reduced pressure. The product was purified by silica gel column chromatography (eluent: CHX/EtOAc 9:1) to afford **124** as a red solid (0.061 g,

71%); mp 284-286 °C. ^{1}H NMR (400 MHz, CD$_2$Cl$_2$) δ: 7.41-7.7.40 (m, 4 H); 7.33-7.16 (m, 24 H); 7.01-6.93 (m, 8 H); 6.89-6.77 (m, 16 H); 2.42 (s, 12 H); 2.41 (s, 6 H). ^{13}C NMR (100 MHz, CDCl$_3$) δ: 200.39, 154.50, 154.28, 138.04, 130.28, 128.53, 128.21, 128.17, 128.12, 127.10, 127.08, 126.99, 126.75, 124.20, 115.14, 23.41, 23.40. ^{11}B NMR (128 MHz, CDCl$_3$) δ: 35.79. MALDI-HRMS calc. for [C$_{83}$H$_{68}$B$_3$N$_3$O]$^+$: 1155.5642, found: 1155.5642. IR (film in CH$_2$Cl$_2$) ν$_{max}$ (cm^{-1}): 3059.44, 3029.61, 2915.9, 2856.24, 1711.56, 1598.07, 1554.16, 1491.68, 1452.63, 1441.93, 1359.79, 1308.53, 1181.91, 1156.13, 1104.08, 1074.19, 1026.78, 966.11, 915.98, 870.19, 843.98, 815.03, 803.59, 791.55, 762.03, 748.11, 698.11, 639.22, 610.28, 594.1,565.92, 531.06, 489.81.

Synthesis of N,N',N''-tri(4-chlorophenyl)-B,B',B''-trimesityl borazine 127
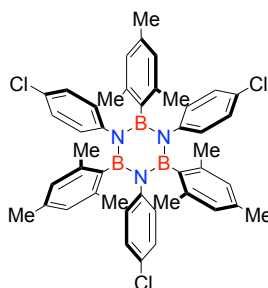
In a 50 mL Schlenk-type flask, 4-chloroaniline **125** (1.50 g, 11.80 mmol), and dry toluene (20 mL), were added. To the solution under Ar, BCl$_3$ (1 M in heptane, 14.20 mL, 14.20 mmol) was added dropwise at 0 °C. The resulting suspension was stirred under refluxing conditions for 16 h, then it was cooled down to r.t. and subjected to 5 FPT cycles to remove the excess of HCl. In parallel, to a solution of mesityl bromide **126** (2.59 g, 13.00 mmol) in dry THF (40 mL), ^{t}BuLi (1.7 M in hexane, 15.60 mL, 26.65 mmol) was added dropwise at -84 °C under Ar. The solution was allowed to warm at 0 °C and stirred for 10 min. The degassed toluene mixture was thus transferred to the organometallic-containing THF solution at 0 °C and allowed to react for 16 h at r.t.. The final mixture was diluted with EtOAc (100 mL) and washed with water (3 × 100 mL) and brine (100 mL). The organic layer was dried over MgSO$_4$ and evaporated under reduced pressure. The product was purified by silica gel column chromatography (eluent: PE/CH$_2$Cl$_2$, 9:1) to afford **127** as a white solid (1.86 g, 62%); mp 236-237 °C. ^{1}H NMR (400 MHz, CDCl$_3$) δ: 6.75-6.67 (m, 12 H); 6.37 (s, 6 H); 2.16 (s, 18 H); 2.03 (s, 9 H). ^{13}C NMR (100 MHz, CDCl$_3$) δ: 144.72, 136.94, 136.79, 129.83, 128.11, 127.01, 126.65, 22.95, 21.11. ^{11}B NMR (128 MHz, CDCl$_3$) δ: 34.01. MALDI-HRMS calc. for [C$_{45}$H$_{45}$B$_3$N$_3$Cl$_3$]$^+$: 765.2983, found: 765.2958. IR (film in CH$_2$Cl$_2$) ν$_{max}$ (cm^{-1}): 3223.05, 2978.09, 2702.27, 2177.63,

2027.19, 1689.64, 1658.78, 1435.04, 1408.04, 1043.49, 867.97, 810.10, 794.67, 748.38, 734.88, 713.66, 677.01, 624.94.

Synthesis of N,N'-tri(4-phenyl)phenyl- N''-4-chlorophenyl- B,B',B''-tri mesitylborazine 122 and N,N',N''-tri(4-phenyl)phenyl-B,B',B''-trimesityl borazine 123
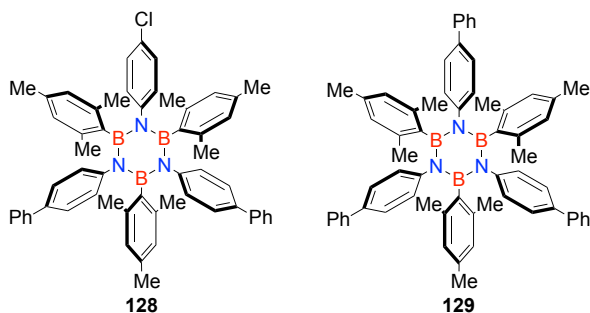
In a 50 mL Schlenk-type high pressure vessel, **127** (1.32 g, 1.72 mmol), phenylboronic acid (0.46 g, 3.79 mmol), K_3PO_4 (1.47 g, 6.91 mmol), $[Pd_2(dba)_3]$ (0.079 g, 0.086 mmol), and XPhos (0.083 g, 0.174 mmol) were added and placed under inert N_2 atmosphere. Separately, a dioxane/H_2O 5:1 mixture (20 mL) was degassed by N_2 bubbling under sonication at 50 °C for 1.5 h, then added to the reaction vessel containing the reagents. The flask was sealed and the red mixture was stirred for 16 h at 150 ˚C, then diluted with EtOAc (100 mL), and washed with water (3 × 100 mL) and brine (100 mL). The organic layer was dried over $MgSO_4$ and evaporated under reduced pressure. The products were purified by silica gel column chromatography (eluent: PE/CH_2Cl_2 8:2) to afford **128** (0.39 g, 27%) and **129** (0.33 g, 25%) as white solids.

128: mp 215-217 °C. ^{1}H NMR (400 MHz, CDCl$_3$) δ: 7.41-7.28 (m, 8 H); 7.23-7.18 (m, 2 H); 7.09-6.74 (m, 12 H), 6.36-6.33 (m, 6 H); 2.28-2.23 (m, 18 H); 2.00-1.96 (m, 9 H). ^{13}C NMR (100 MHz, CDCl$_3$) δ: 145.61, 140.47, 137.39, 137.24, 137.17, 136.55, 136.40, 136.01, 129.72, 128.50, 128.33, 127.75, 127.47, 127.37, 127.31, 126.96, 126.74, 126.59, 126.52, 126.31, 125.31, 125.26, 23.21, 23.13, 23.08, 21.11, 21.08, 20.96, 20.01. ^{11}B NMR (128 MHz, CDCl$_3$) δ: 36.21. MALDI-HRMS calc. for $[C_{57}H_{55}B_3N_3]^+$ (de-chlorination during analysis): 814.4670, found: 814.4672. IR (film in CH_2Cl_2) v_{max} (cm^{-1}): 3221.12, 3035.96, 2970.38, 2704.20, 2152.56, 2015.61, 1676.14, 1527.62, 1452.40, 1384.89, 1348.24, 1174.65, 1103.28, 1014.56, 885.33, 796.60, 783.10, 736.81, 715.59, 700.16, 690.52, 675.09, 636.51, 623.01, 613.36.

129: mp 249-252 °C. ^{1}H NMR (400 MHz, CDCl$_3$) δ: 7.41-7.38 (m, 6 H); 7.32-7.27 (m, 6 H); 7.23-7.18 (m, 3 H); 7.05-7.03 (m, 6 H); 6.88-6.85 (m, 6 H); 6.34 (s, 6 H); 2.27 (s, 18 H); 1.97 (s, 9 H). ^{13}C NMR (100 MHz, CDCl$_3$) δ: 145.76, 140.50, 137.29, 136.29, 136.24, 128.50, 127.38, 126.69, 126.57, 126.48, 125.20, 23.15, 21.10. ^{11}B NMR (128 MHz, CDCl$_3$) δ: 36.02. MALDI-HRMS calc. for [C$_{63}$H$_{60}$B$_3$N$_3$]$^+$: 891.5093, found: 891.5066. IR (film in CH$_2$Cl$_2$) v_{max} (cm^{-1}): 3035.96, 2970.38, 2706.13, 2015.61, 1815.02, 1678.07, 1527.62, 1452.40, 1386.82, 1103.28, 1014.56, 858.32, 792.74, 746.45, 734.88, 717.52, 636.51, 624.94.

N,N'-tri(4-phenyl)phenyl-N''-4-(2,3,5-triphenyl-4-(phenyl-4'-yl))cyclo penta-2,4-dienone borazine)-B,B',B''-trimesityl borazine 130
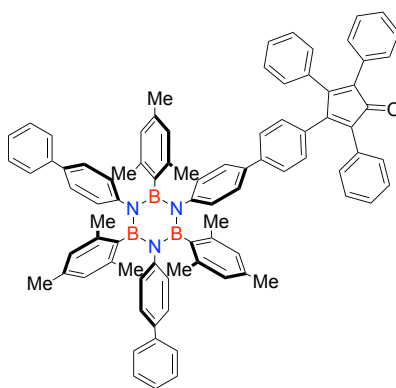
In a 50 mL Schlenk-type high pressure vessel, **128** (0.52 g, 0.61 mmol), boronic ester **123** (0.63 g, 1.23 mmol), K$_3$PO$_4$ (0.39 g, 1.85 mmol), [Pd$_2$(dba)$_3$] (0.036 g, 0.039 mmol), and XPhos (0.039 g, 0.081 mmol) were added and placed under inert N$_2$ atmosphere. Separately, a dioxane/H$_2$O 5:1 mixture (20 mL) was degassed by N$_2$ bubbling under sonication at 50 °C for 1.5 h, then added to the reaction vessel containing the reagents. The flask was sealed and the red mixture was stirred for 20 h at 150 ˚C, then diluted with EtOAc (100 mL) and washed with water (3 × 100 mL) and brine (100 mL). The organic layer was dried over MgSO$_4$ and evaporated under reduced pressure. The products were purified by silica gel column chromatography (eluent: PE/CH$_2$Cl$_2$ 7:3) to afford **130** as a red solid (0.17 g, 23%); mp 265-267 °C. ^{1}H NMR (400 MHz, CDCl$_3$) δ: 7.40-76.85 (m, 41 H); 6.38-6.36 (m, 6 H); 2.30 (s, 18 H); 2.00-1.98 (m, 9 H). ^{13}C NMR (100 MHz, CDCl$_3$) δ: 200.23, 154.35, 154.04, 146.29, 145.66, 140.56, 137.27, 137.21, 136.27, 135.35, 133.27, 131.10, 130.98, 130.77, 130.18, 129.82, 129.36, 128.52, 128.13, 127.33, 126.72, 126.57, 126.44, 125.90, 125.64, 125.30, 125.15, 23.07, 21.09. ^{11}B NMR (128 MHz, CDCl$_3$) δ: 33.96. MALDI-HRMS calc. for [C$_{86}$H$_{74}$B$_3$N$_3$O]$^+$: 1197.6111, found: 1197.6112. IR (film in CH$_2$Cl$_2$) v_{max} (cm^{-1}): 3194.12, 2981.95, 2706.13, 2600.04,

2052.26, 1616.35, 1585.49, 1500.62, 1435.04, 1132.21, 1087.85, 979.84, 856.39, 825.53, 810.10, 792.74, 777.31, 750.31, 734.88, 713.66, 700.16, 686.66, 667.37, 640.37, 626.87.

Synthesis of ((4-bromophenyl)ethynyl)triisopropylsilane 131
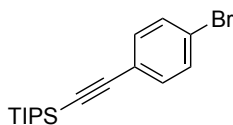
In a 50 mL Schlenk-type flask, 4-bromoiodobenzene **118** (6.00 g, 21.2 mmol), [Pd(PPh$_3$)$_2$Cl$_2$] (0.30 g, 0.42 mmol), CuI (0.081 g, 0.42 mmol), DIPA (25 mL), and THF (25 mL) were added. The mixture was degassed by 3 FPT cycles, then TIPSA (4.76 mL, 21.2 mmol) was added and further 2 FPT cycles were done. The suspension was stirred at r.t. for 4 h, then diluted with EtOAc (200 mL) and washed with water (3 × 200 mL) and brine (100 mL). The organic layer was dried over MgSO$_4$ and evaporated under reduced pressure. The product was purified by silica gel column chromatography (eluent: PE) to afford **131** as a colourless oil (7.14 g, 99%). ^{1}H NMR (300 MHz, CDCl$_3$) δ: 7.44-7.31 (m, 4 H), 1.11 (s, 21 H). ^{13}C NMR (100 MHz, CDCl$_3$) δ: 133.47, 131.43, 122.47, 105.84, 92.06, 18.66, 11.26. ESI-HRMS calc. for [C$_{17}$H$_{25}$BrSi]$^+$: 336.0909, found: 335.9758. IR (film in CH$_2$Cl$_2$) v_{max} (cm^{-1}): 2956.87, 2941.44, 2891.30, 2864.29, 2156.42, 1483.26, 1463.97, 1392.61, 1238.30, 1213.23, 1095.57, 1070.49, 1010.70, 995.27, 918.12, 881.47, 821.68, 798.53, 669.30, 642.30, 570.93, 528.50, 507.28, 470.63, 449.41, 401.19.

Synthesis of 1,2-bis(4-bromophenyl)ethyne 133
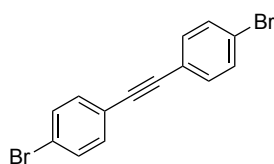
In a 100 mL round flask, ((4-bromophenyl)ethynyl)triisopropylsilane **131** (6.12 g, 18.1 mmol) was dissolved in THF (25 mL). To the stirring mixture at r.t., a 1 M TBAF solution in THF (20.0 mL, 20.0 mmol) was slowly added. After 20 min the solution was diluted with EtOAc (100 mL) and washed with water (3 × 200 mL) and brine (100 mL). The organic layer was dried over MgSO$_4$ and evaporated under reduced pressure. The orange deliquescent solid obtained was added in a 250 mL Schenk-type flask together with [Pd(PPh$_3$)$_2$Cl$_2$] (0.13 g, 0.18 mmol), CuI (0.036 g, 0.18 mmol), 4-bromoiodobenzene **118** (5.13 g, 18.1 mmol). Separately, a mixture of DIPA (30 mL) and THF (30 mL) was degassed by 4 FPT cycles, then added to the Schlenk-type flask. The final suspension was

stirred at r.t. for 15 h, then it was diluted with EtOAc (200 mL) and washed with water (3 × 200 mL) and brine (100 mL). The organic layer was dried over $MgSO_4$ and evaporated under reduced pressure. The product was purified by silica gel column chromatography (eluent: PE) to afford **133** as a white solid (5.48 g, 90%); mp 168-170 °C. ^{1}H NMR (300 MHz, $CDCl_3$) δ: 7.49 (d, J = 7.8 Hz, 4 H); 7.38 (d, J = 7.9 Hz, 4 H). ESI-HRMS calc. for $[C_{14}H_8Br_2]^+$: 333.8993, found: 333.8988. IR (film in CH_2Cl_2) v_{max} (cm^{-1}): 2943.37, 2891.30, 2866.22, 1463.97, 1386.82, 1263.37, 1080.14, 1072.42, 1045.42, 1004.91, 918.12, 883.40, 827.46, 819.75, 734.88, 704.02, 673.16, 650.01, 613.36, 565.14, 524.64, 509.21, 462.92, 445.56, 426.27, 412.77.

Synthesis of 1,2-bis(4-((triisopropylsilyl)ethynyl)phenyl)ethyne 134
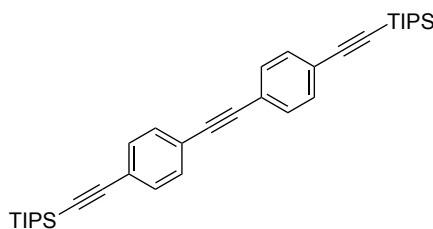
In a 250 mL Schlenk-type flask, 1,2-bis(4-bromophenyl)ethyne **133** (1.00 g, 2.98 mmol), $[Pd(PPh_3)_2Cl_2]$ (0.041 g, 0.06 mmol), CuI (0.011 g, 0.06 mmol), DIPA (20 mL), and THF (20 mL) were added. The mixture was degassed by 3 FPT cycles, then TIPSA (1.14 mL, 6.25 mmol) was added and 2 FPT cycles were done. The suspension was stirred at r.t. for 4 h, then diluted with EtOAc (150 mL) and washed with water (3 × 200 mL) and brine (100 mL). The organic layer was dried over $MgSO_4$ and evaporated under reduced pressure. The product was purified by silica gel column chromatography (eluent: PE) to afford **134** as a colourless oil (1.51 g, 94%). ^{1}H NMR (300 MHz, $CDCl_3$) δ: 7.45 (s, 8 H); 1.13 (s, 42 H). ^{13}C NMR (100 MHz, $CDCl_3$) δ: 132.00, 131.38, 123.52, 122.86, 106.60, 92.94, 90.90, 18.68, 18.31. ESI-HRMS calc. for $[C_{36}H_{50}Si_2]^+$: 539.3529, found: 539.3503. IR (film in CH_2Cl_2) v_{max} (cm^{-1}): 2943.37, 2891.30, 2864.29, 2154.49, 1512.19, 1462.04, 1382.96, 1232.51, 1219.01, 1101.35, 1072.42, 1049.28, 1016.49, 995.27, 906.54, 881.47, 856.39, 837.11, 798.53, 731.02, 673.16, 650.01, 607.58, 545.85, 499.56, 455.20, 443.63, 412.77.

Synthesis of hexa(4-(triisopropylsilylacetynyl)phenyl)benzene 135
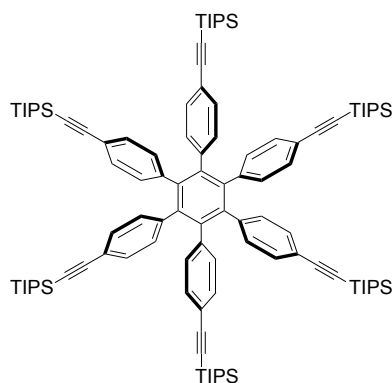
In a 20 mL Schenk-type flask, **134** (0.54 g, 1.00 mmol), $Co_2(CO)_8$ (0.007 g, 0.02 mmol), and dioxane (10 mL) were added. The solution was degassed by 5 FPT cycles. A condenser was applied to the flask and the mixture was stirred and refluxed under N_2 atmosphere for 48 h. The volatiles were removed under reduced pressure, then the crude mixture was re-dissolved in a PE/CH_2Cl_2 (8:2) mixture to which MeOH was added. The precipitate formed was recovered by filtration and subjected to further precipitations with the same method. After five precipitation-filtration cycles, **135** was obtained as a white solid (0.185 g, 35%); mp >300 °C. ^{1}H NMR (300 MHz, CD_2Cl_2) δ: 7.05-6.77 (m, 24 H); 1.07 (s, 126 H). ^{13}C NMR (100 MHz, CD_2Cl_2) δ: 142.07, 141.64, 132.90, 132.42, 122.63, 108.61, 92.47, 20.21, 13.13. ESI-MS calc. for $[C_{108}H_{151}Si_6]^+$: 1617.05, found: 1617.04. IR (film in CH_2Cl_2) v_{max} (cm^{-1}): 2941.44, 2889.37, 2864.29, 2360.87, 2331.94, 2154.49, 1508.33, 1462.04, 1382.96, 1220.94, 1072.42, 1018.41, 995.27, 918.12, 881.47, 829.39, 775.38, 719.45, 677.01, 599.86, 455.20.

Synthesis of hexa(4-acetynylphenyl)benzene 136
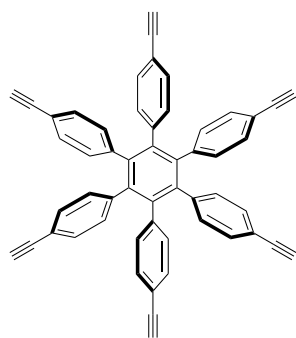
In a 25 mL round flask, **135** (0.16 g, 0.099 mmol) was dissolved in THF (10 mL). To the solution stirring at r.t., a 1 M TBAF solution (0.694 mL, 0.694 mmol) was slowly added. The final mixture was stirred for 3 h, then diluted with EtOAc (50 mL) and washed with water (3 × 100 mL) and brine (50 mL). The organic layer was dried over $MgSO_4$ and

evaporated under reduced pressure. The product was purified by silica gel column chromatography (eluent: PE/CH$_2$Cl$_2$ 6:4) to afford **136** as a white solid (0.064 g, 96%); mp > 300 °C (decomp.). ^{1}H NMR (300 MHz, CD$_2$Cl$_2$) δ: 7.05-6.77 (m, 24 H); 3.03 (s, 6 H). ^{13}C NMR (100 MHz, CD$_2$Cl$_2$) δ: 140.51, 139.71, 131.13, 130.73, 119.43, 83.26, 77.14. ESI-HRMS calc. for [C$_{54}$H$_{31}$]$^+$: 679.2426, found: 679.2427. IR (film in CH$_2$Cl$_2$) ν_{max} (cm^{-1}): 3290.56, 2954.95, 2922.16, 2852.72, 2360.87, 2343.51, 1508.33, 1458.18, 1396.46, 1305.81, 1267.23, 1246.02, 1099.43, 1018.41, 842.89, 792.74, 734.88, 702.09, 651.94, 644.22, 623.01, 605.65, 545.85, 518.85, 460.99, 420.48.

Synthesis of 1-methoxy-4-(phenylethynyl)benzene 138
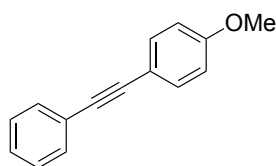
In a 250 mL Schlenk-type flask, 4-iodoanisole **137** (5.00 g, 21.4 mmol), [Pd(PPh$_3$)$_2$Cl$_2$] (0.155 g, 0.214 mmol), CuI (0.042 g, 0.214 mmol), DIPA (25 mL), and THF (25 mL) were added. The mixture was degassed by 3 FPT cycles, then phenylacetylene (2.35 mL, 21.41 mmol) was added and 2 FPT cycles were done. The suspension was stirred at r.t. for 4 h, then diluted with EtOAc (300 mL) and washed with water (3 × 200 mL) and brine (100 mL). The organic layer was dried over MgSO$_4$ and evaporated under reduced pressure. The product was purified by silica gel column chromatography (eluent: PE/CH$_2$Cl$_2$ 8:2) to afford **138** as a colourless oil (4.30 g, 97%). ^{1}H NMR (300 MHz, CDCl$_3$) δ: 7.53-7.45 (m, 4 H); 7.38-7.30 (m, 3 H); 6.91-6.86 (m, 2 H). ^{13}C NMR (100 MHz, CDCl$_3$) δ: 159.64, 133.08, 131.48, 128.35, 127.97, 123.61, 115.38, 114.02, 89.41, 88.10, 55.32. ESI-HRMS calc. for [C$_{15}$H$_{12}$O]$^+$: 208.0888, found: 208.0880. IR (film in CH$_2$Cl$_2$) ν_{max} (cm^{-1}): 403.12, 418.55, 472.56, 518.85, 640.37, 653.87, 756.10, 779.24, 819.75, 835.18, 914.26, 989.48, 1024.20, 1107.14, 1136.07, 1174.65, 1246.02, 1284.59, 1438.90, 1458.18, 1508.33, 1604.77, 2214.28, 2345.44, 2837.29, 2895.15, 3010.88, 3051.39.

Synthesis of 1,3,5-(4'-hydroxyphenyl)-2,4,6-phenylbenzene 142
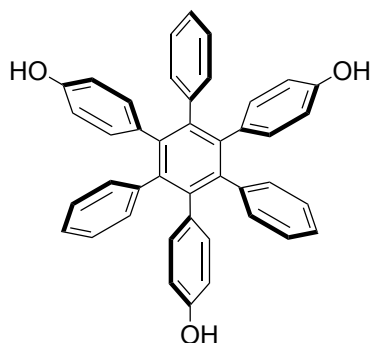
In a 20 mL Schenk-type flask, **138** (3.99 g, 19.2 mmol), $Co_2(CO)_8$ (0.329 g, 1.92 mmol), and dioxane (10 mL), were added. The solution was degassed by 5 FPT cycles, then a condenser was applied to the flask and the mixture was stirred and refluxed under N_2 atmosphere for 18 h. Then the solvent was removed under reduced pressure. The crude mixture was filtered through silica gel (eluent: PE/CH_2Cl_2 7:3) to afford a red solid (3.24 g). This was added to a flame-dried 250 mL Shlenk-type flask and dissolved in dry CH_2Cl_2 (50 mL). The red solution was stirred at -84 °C while a BBr_3 (1 M solution in CH_2Cl_2, 31 mL, 31.0 mmol) was slowly added. The solution was allowed to react at r.t. for 3 h, then water (10 mL) was slowly added. The mixture was diluted with EtOAc (200 mL) and washed with water (3 × 200 mL) and brine (100 mL). The organic layer was dried over $MgSO_4$ and evaporated under vacuum. The product was purified by silica gel column chromatography (eluent: PE/CH_2Cl_2 9:1) to afford **142** as a white solid (0.513 g, 14%); mp >300 °C. ^{1}H NMR (300 MHz, CD_3OD) δ: 6.87-6.80 (m, 15 H); 6.61-6.58 (m, 6 H); 6.25-6.22 (m, 6 H). ^{13}C NMR (100 MHz, CD_3OD) δ: 154.21, 141.30, 140.69, 141.07, 132.21, 131.31, 126.19, 124.57, 113.07. ESI-HRMS calc. for $[C_{42}H_{30}O_3]^+$: 582.2195, found: 582.2194. IR (film in CH_2Cl_2) ν_{max} (cm^{-1}): 405.05, 408.91, 416.62, 547.78, 702.09, 769.60, 796.60, 817.82, 831.32, 950.91, 1166.93, 1242.16, 1261.45, 1516.05, 1610.56, 2972.31, 3554.81.

Synthesis of 1,3,5-(4'-trifluoromethansulphonylphenyl)-2,4,6-phenyl benzene 143
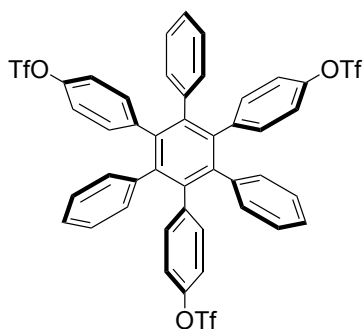
In a 25 mL round flask, **142** (0.143 g, 0.245 mmol) and dry pyridine (5 mL) were added. The suspension was stirred at 0 °C while Tf_2O (0.494 mL, 2.94 mmol) was slowly added. The mixture was stirred for 18 h, then the volatiles were removed under reduced pressure. The product was purified by silica gel column chromatography (eluent: PE/EtOAc 8:2) to afford **143** as white solid (0.216 g, 90%); mp 235-237 °C. ^{1}H NMR (300 MHz, CD_2Cl_2) δ: 6.95-6.90 (m, 14 H); 6.83-6.79 (m, 12 H). ^{13}C NMR (100 MHz, CD_2Cl_2) δ: 147.49, 140.96, 140.80, 139.34, 138.82, 132.95, 131.07, 127.09, 125.90, 120.71, 119.52. ESI-MS calc. for $[C_{45}H_{28}F_9O_9S_3]^+$: 979.08, found: 978.06. IR (film in CH_2Cl_2) ν_{max} (cm^{-1}): 405.05, 455.20, 507.28, 524.64, 551.64, 559.36, 576.72, 601.79, 634.58, 665.44, 700.16, 736.81, 754.17, 771.53, 788.89, 840.96, 858.32, 881.47, 1018.41, 1074.35, 1103.28, 1132.21, 1178.51, 1205.51, 1247.94, 1267.23, 1421.54, 1502.55, 1980.02.

Synthesis of 1,3-bis-(4-(phenyl)phenyl)-5-(4'-trifluoromethanesulphonylphenyl)-2,4,6-phenylbenzene 144 and 1,3,5-tris-(4-(phenyl)phenyl)-2,4,6-phenylbenzene 145

144   **145**
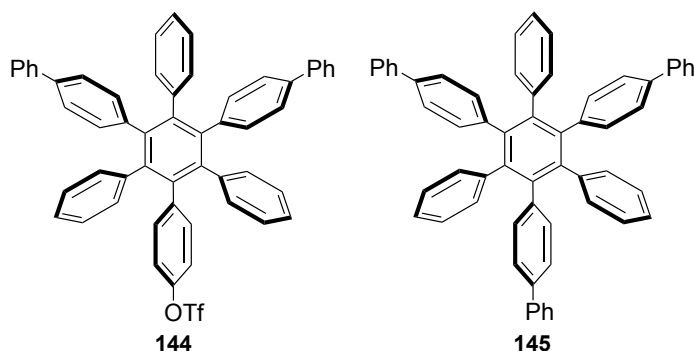
In a 100 mL Schlenk-type vessel **143** (0.547 g, 0.56 mmol), phenylboronic acid (0.109 g, 0.896 mmol), $Pd(PPh_3)_4$ (0.045 g, 0.038 mmol), K_2CO_3 (0.621 g, 4.49 mmol) were added and placed under N_2 atmosphere. Separately, a mixture of dioxane (20 mL) and water (4 mL) was degassed by N_2 bubbling under sonication for 3 h, then added to the flask containing the reagents. The suspension was stirred for 15 h at 105 ˚C, then it was diluted with EtOAc (50 mL) and washed with water (3 × 100 mL) and brine (100 mL). The organic layer was dried over $MgSO_4$ and evaporated under reduced pressure. The product was purified by silica gel column chromatography (eluent: CHX/CH_2Cl_2 8:2) to afford compounds **144** (0.093 g, 20%) and **145** (0.0386 g, 9%) as white solids.

144: mp 282-285 °C. ^{1}H NMR (300 MHz, CD_2Cl_2) δ: 7.46-7.42 (m, 4 H); 7.37-7.31 (m, 4 H); 7.28-7.22 (m, 2 H); 7.18-7.15 (m, 4 H); 6.96-6.79 (m, 22 H). ^{13}C NMR (100 MHz, CD_2Cl_2) δ: 147.34, 141.60, 141.10, 140.42, 140.37, 140.25, 140.13, 139.64, 138.72, 137.54, 133.06, 131.82, 131.32, 131.29, 128.63, 127.09, 126.87, 126.73, 126.48, 125.58,

125.48, 124.99, 119.35. ESI-MS calc. for $[C_{55}H_{37}F_3O_3S]^+$: 834.2416, found: 834.2425. IR (film in CH_2Cl_2) ν_{max} (cm^{-1}): 509.21, 569.00, 578.64, 605.65, 632.65, 669.30, 696.30, 734.88, 752.24, 765.74, 788.89, 839.03, 856.39, 885.33, 1008.77, 1018.41, 1074.35, 1103.28, 1136.07, 1176.58, 1209.37, 1249.87, 1423.47, 1442.75, 1485.19, 1500.62, 1598.99, 2980.02, 3028.24, 3055.24.

145: mp >300 °C. ^{1}H NMR (300 MHz, CD_2Cl_2) δ: 7.46-7.42 (m, 6 H); 7.37-7.31 (m, 6 H); 7.28-7.25 (m, 3 H); 7.18-7.14 (m, 6 H); 6.97-6.86 (m, 21 H). ^{13}C NMR (100 MHz, CD_2Cl_2) δ: 140.65, 140.54, 140.31, 140.07, 139.96, 137.38, 131.90, 131.41, 128.62, 127.05, 126.69, 126.48, 125.37, 124.92. ESI-MS calc. for $[C_{60}H_{42}]^+$: 762.3287, found: 762.3287. IR (film in CH_2Cl_2) ν_{max} (cm^{-1}): 403.12, 410.84, 430.13,513.07, 543.93, 557.43, 570.93, 615.29, 638.44, 669.30, 696.30, 738.74, 750.31, 767.67, 786.96, 800.46, 823.60, 833.25, 839.03, 856.39, 910.40, 995.27, 1008.77, 1028.06, 1072.42, 1112.93, 1141.86, 1159.22, 1442.75, 1485.19, 1598.99, 3028.24, 3051.39, 3080.32.

Synthesis of 1,3-bis-(biphenyl)-5-(4'-(2,3,5-triphenyl-4-(phenyl-4'-yl))cyclopenta-2,4-dienone)-2,4,6-phenylbenzene 146
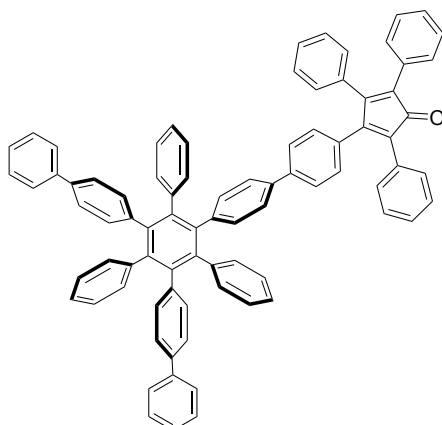
In a 25 mL Schlenk-type vessel, **144** (0.208 g, 0.25 mmol), **123** (0.32 g, 0.63 mmol), [Pd(PPh$_3$)$_4$] (0.018 g, 0.016 mmol), and K$_2$CO$_3$ (0.138 g, 0.99 mmol) were added and placed under N$_2$ atmosphere. Separately, a mixture of dioxane (5 mL) and water (1 mL) was degassed by N$_2$ bubbling under sonication for 3 h, then added to the flask containing the reagents. The mixture was stirred for 15 h at 105 ˚C, then it was diluted with EtOAc (50 mL) and washed with water (3 × 100 mL) and brine (100 mL). The organic layer was dried over MgSO$_4$ and evaporated under reduced pressure. The product was purified by silica gel column chromatography (eluent: CHX/CH$_2$Cl$_2$ 7:3) to afford **146** as a red solid (0.18 g, 68%); mp 294-296 °C. ^{1}H NMR (300 MHz, CD$_2$Cl$_2$) δ: 7.47-7.15 (m, 31 H); 6.99-6.88 (m, 25 H). ^{13}C NMR (100 MHz, CDCl$_3$) δ: 200.24, 154.37, 154.03, 140.73,

140.66, 140.59, 140.50, 140.29, 140.25, 139.80, 139.74, 137.42, 136.50, 133.19, 132.02, 131.86, 131.49, 131.38, 130.93, 130.77, 130.20, 129.86, 129.39, 128.60, 128.14, 128.10, 128.05, 127.48, 126.95, 126.85, 126.73, 126.08, 125.59, 125.37, 125.28, 125.19, 125.04. ESI-HRMS calc. for $[C_{83}H_{57}O]^+$: 1069.4409, found: 1069.4395. IR (film in CH_2Cl_2) ν_{max} (cm^{-1}): 401.19, 511.14, 524.64, 540.07, 569.00, 574.79, 638.44, 648.08, 669.30, 694.37, 731.02, 752.24, 765.74, 788.89, 804.32, 829.39, 839.03, 850.61, 906.54, 1006.84, 1026.13, 1072.42, 1087.85, 1111.00, 1139.93, 1211.30, 1260.45, 1394.53, 1442.75, 1487.12, 1598.99, 1710.86, 2980.02, 3028.24, 3055.24.

Synthesis of N,N',N''-(4-(1',2',3',4'-tetraphenyl)phenyl-B,B',B''-tri-(4-(1',2',3',4'-tetraphenyl)phenylborazine 147
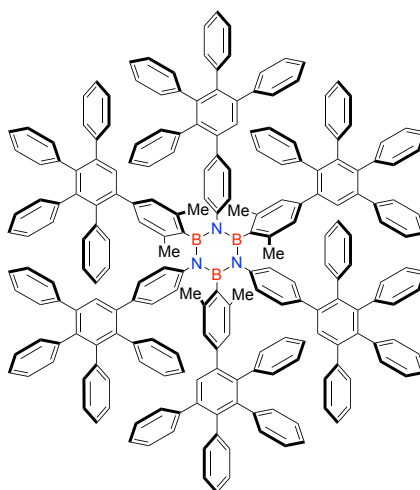
In a 10 mL Schlenk-type vessel, **108** (0.013 g, 0.018 mmol), CPD (0.061 mg, 0.16 mmol), and Ph$_2$O (1.0 mL) were added. The dark red solution was degassed by Ar bubbling for 30 min at 40 ˚C, then stirred for 16 h at 250 ˚C. The reaction mixture was purified by silica gel column chromatography (eluent: pentane/CH_2Cl_2 6:4) affording a white solid. A final purification was performed by Rec-HPLC (eluent: hexane/$CHCl_3$ 3:7) affording **147** as a white solid (0.024 g, 48 %); mp >300 °C. ^{1}H NMR (300 MHz, CDCl$_3$) δ: 7.41 (d, J = 2.6 Hz, 6 H); 7.14 (s, 28 H); 6.91-6.74 (m, 86 H); 6.64-6.62 (m, 6 H); 6.46 (d, J = 8.4 Hz, 6 H); 6.38 (s, 6 H); 6.33 (d, J = 8.4 Hz, 6 H); 1.84 (s, 18 H). ^{11}B NMR (128 MHz, CDCl$_3$) δ: 35.47. MALDI-HRMS calc. for $[C_{222}H_{163}B_3N_3]^+$: 2903.3076, found: 2903.3126. IR (film in CH_2Cl_2) ν_{max} (cm^{-1}): 3012.12, 2946.23, 2903.17, 1846.57, 1644.72, 1543.20, 1510.38, 1426.59, 1299.76, 1286.24, 1222.44, 1150.60, 1104.71, 956.33, 911.57, 846.57, 823.03, 725.39, 701.46, 652.32, 629.86, 581.26, 512.22.

Synthesis of borazine-polyphenylene 148
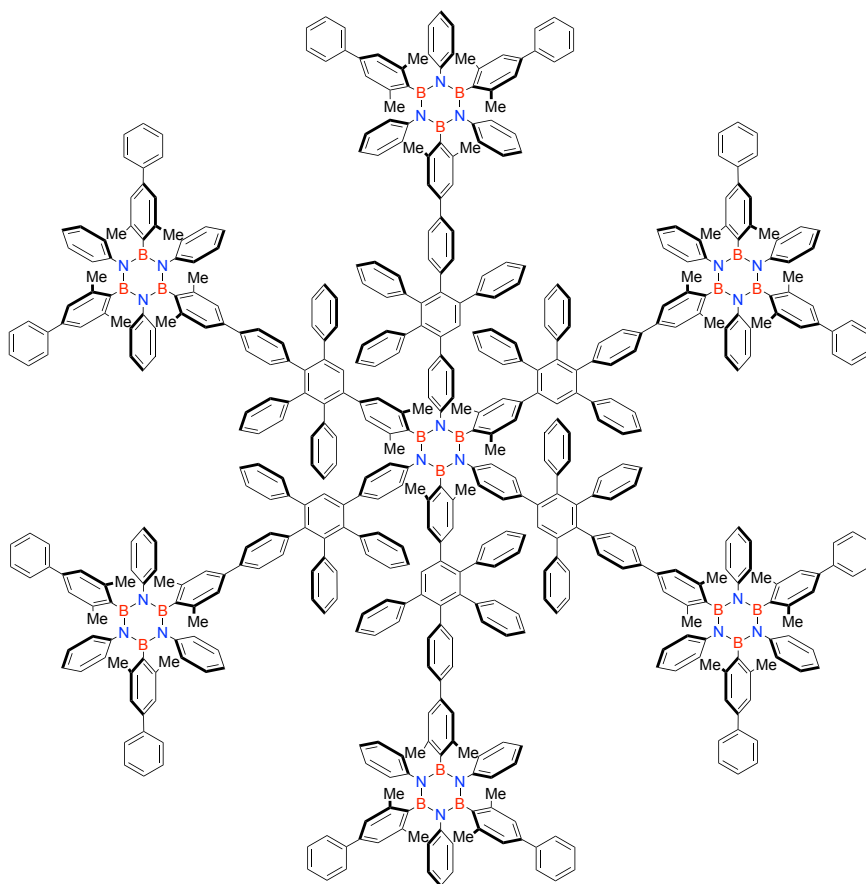
In a 10 mL Schlenk-type vessel **108** (0.009 g, 0.0124 mmol), **124** (0.106 mg, 0.091 mmol), and Ph$_2$O (1 mL), were added. The dark red solution was degassed by Ar bubbling for 45 min at 40 °C, then stirred for 72 h at 260 °C. The reaction mixture was purified by silica gel column chromatography (eluent: CHX/CH$_2$Cl$_2$ 7:3) to afford **148** as a white solid (0.033 g, 35%); mp >300 °C (decomp.). ^{1}H NMR (400 MHz, CD$_2$Cl$_2$) δ: 7.43-6.65 (m, 306 H); 6.47-6.36 (m, 18 H); 2.43 (s, 72 H); 2.38 (s, 36 H); 1.86 (s, 18 H). ^{13}C NMR (100 MHz, CD$_2$Cl$_2$) δ: 146.86, 146.81, 144.54, 142.55, 142.15, 141.75, 141.52, 141.31, 141.04, 140.79, 140.42, 139.69, 139.33, 138.83, 138.73, 138.59, 137.62, 137.35, 132.42, 132.02, 131.90, 130.41, 129.08, 128.07, 127.99, 127.65, 127.41, 127.31, 126.92, 125.84, 125.84, 125.29, 124.93, 124.39, 123.82, 30.82, 23.76, 23.71, 23.07. ^{11}B NMR (128 MHz, CD$_2$Cl$_2$) δ: 33.06. MALDI-HRMS calc. for [C$_{546}$H$_{450}$B$_{21}$N$_{21}$]$^+$: 7532.8144, found: 7532.8324. IR (film in CH$_2$Cl$_2$) ν$_{max}$ (cm^{-1}): 3026.63, 2921.86, 2853.13, 1598.25, 1554.27, 1491.8, 1452.42, 1434.51, 1356.35, 1307.13, 1276.03, 1262.3, 1155.92, 1103.9, 1073.85, 1025.31, 899.1, 870.04, 838.59, 792.41, 762.98, 749.59, 697.31, 655.75, 594.7, 565.14, 531.05.

Synthesis of borazine-polyphenylene 149
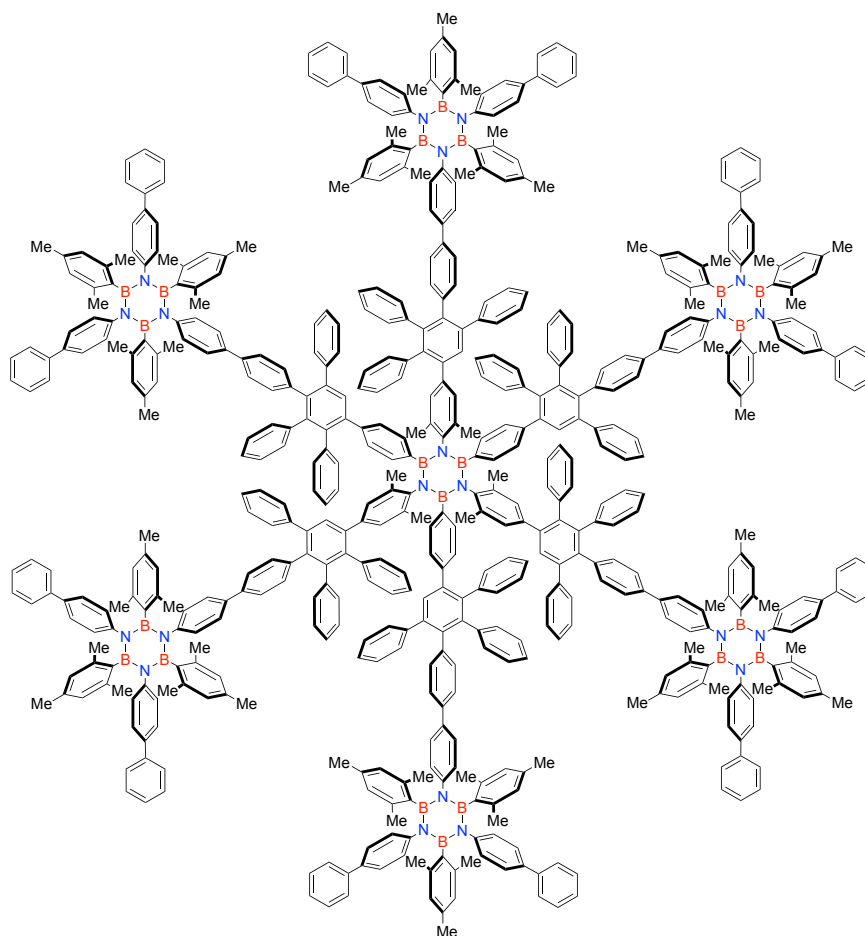
In a 10 mL Schlenk-type vessel **108** (0.0067 g, 0.0087 mmol), **130** (0.084 g, 0.070 mmol), and Ph$_2$O (1 mL) were added. The dark red solution was degassed by Ar bubbling for 30 min at 40 °C, then stirred for 16 h at 230 °C. The reaction mixture was purified by silica gel column chromatography (eluent: PE/CH$_2$Cl$_2$ 1:1) to obtain a white solid. This was re-dissolved in EtOAc (1 mL) and to this solution MeOH was added until formation of a precipitate. This was recovered by filtration and furtherly purified by Rec-GPC (eluent: CHCl$_3$) to afford **149** as a white solid (0.024 g, 36%); mp >300 °C. ^{1}H NMR (400 MHz, CDCl$_3$) δ: 7.37-6.57 (m, 268 H); 6.33 (s, 38 H); 2.25-2.24 (m, 126 H); 1.96 (s, 54 H). ^{13}C NMR (100 MHz, CDCl$_3$) δ: 145.73, 140.58, 140.20, 137.23, 136.31, 136.17, 131.71, 131.52, 131.38, 129.97, 128.52, 127.66, 127.35, 127.07, 126.70, 126.57, 126.43, 125.11, 112.12, 23.08, 23.06, 22.72, 21.08. ^{11}B NMR (128 MHz, CDCl$_3$) δ: 36.03. MALDI-LRMS calc. for [C$_{564}$H$_{486}$B$_{21}$N$_{21}$]$^{+}$: 7785.1, found: 7785.1. IR (film in CH$_2$Cl$_2$) ν$_{max}$ (cm^{-1}): 3033.26, 2987.91, 2863.39, 1658.49, 1591.54, 1564.58, 1481.43, 1449.02, 1425.28, 1355.81, 1297.80, 1254.30, 1208.29, 1146.83, 1086.08, 1010.97, 948.56, 895.98, 866.35, 841.76, 750.28, 688.70, 652.38, 584.59, 562.21.

Synthesis of borazine-polyphenylene 150
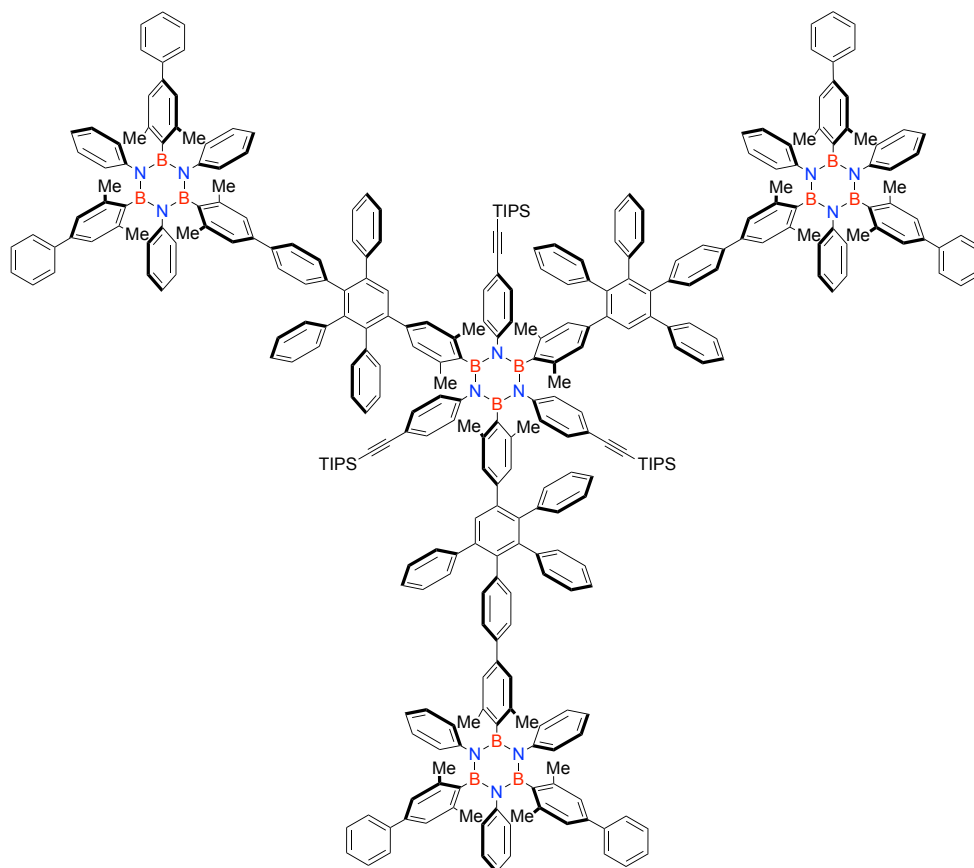
In a 10 mL Schlenk flask, **109** (0.040 g, 0.0324 mmol), **124** (0.150 mg, 0.129 mmol), and Ph$_2$O (1 mL), were added. The dark red solution was degassed by Ar bubbling for 45 min at 40 °C, then stirred for 18 h at 200 °C. The reaction mixture was purified by silica gel column chromatography (eluent: CHX/CH$_2$Cl$_2$ 8:2) to afford **150** as a white solid (0.083 g, 55%); mp >300 °C. ^{1}H NMR (400 MHz, CD$_2$Cl$_2$) δ: 7.41-7.39 (m, 11 H); 7.33-7.29 (m, 14 H); 7.24-7.20 (m, 6 H); 7.15-6.60 (m, 154 H); 6.34 (s, 6 H); 2.41 (s, 36 H); 2.35 (s, 18 H); 2.04 (s, 18 H); 1.10 (s, 61 H). ^{13}C NMR (100 MHz, CDCl$_3$) δ: 146.27, 146.07, 141.40, 140.84, 140.67, 140.25, 139.99, 139.39, 139.07, 138.93, 138.52, 138.05, 137.82, 137.79, 137.74, 136.50, 131.72, 131.35, 131.17, 130.05, 129.95, 128.52, 127.72, 127.07, 127.05, 127.00, 126.76, 126.65, 125.09, 124.78, 124.64, 124.20, 123.94, 89.93, 77.36, 27.07, 23.40, 23.34, 18.88, 11.51. ^{11}B NMR (128 MHz, CD$_2$Cl$_2$) δ: 33.47. MALDI-HRMS calc. for [C$_{327}$H$_{306}$B$_{12}$N$_{12}$Si$_3$]$^+$: 4617.4980, found: 4617.4816. IR (film in CH$_2$Cl$_2$) ν_{max} (cm^{-1}): 3029.98, 2923.78, 2854.27, 2152.17, 1599.26, 1491.99, 1454.12, 1363.32, 1308.34, 1074.03, 1026.49, 879.7, 1026.49, 879.7, 837.21, 762.08, 699.61, 565.04, 531.35, 470.64.

Synthesis of borazine-polyphenylene 151
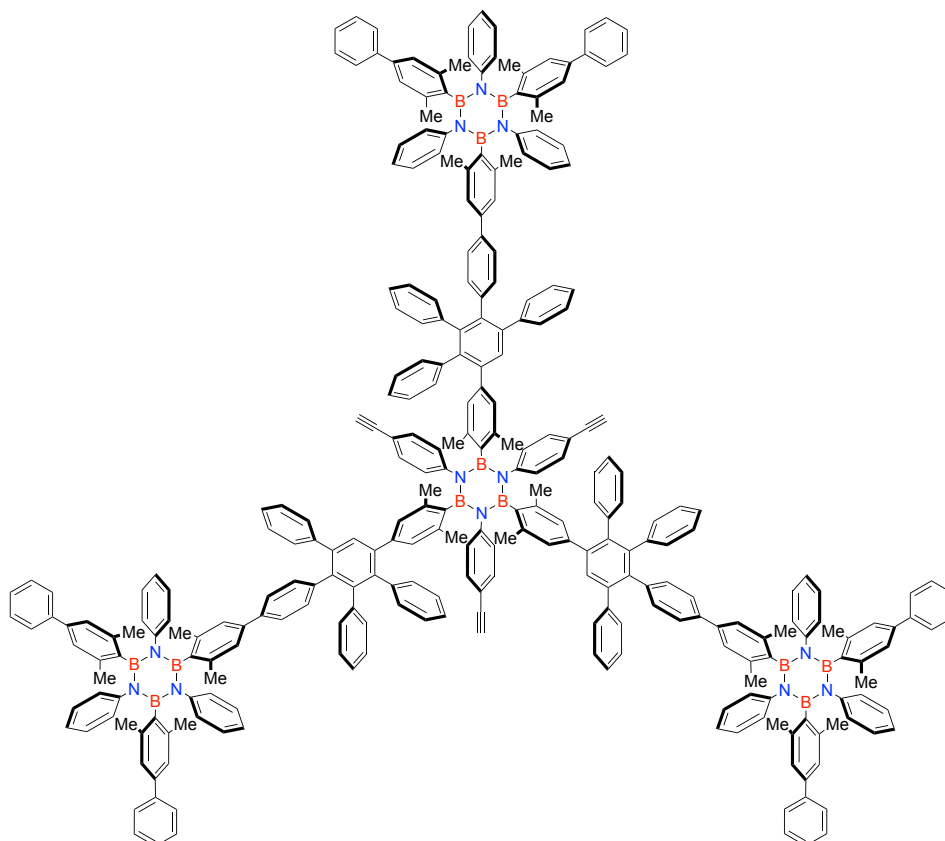
In a 25 mL round flask, **150** (0.069 g, 0.015 mmol) was dissolved in THF (4 mL), then TBAF (1M solution in THF, 0.06 mL, 0.06 mmol) was added dropwise at 0 °C. The reaction mixture was stirred for 2 h at r.t., then diluted with EtOAc (30 mL) and washed with water (3 x 30 mL) and brine (30 mL). The organic layer was dried over MgSO$_4$ and evaporated under reduced pressure. The product was purified by silica gel column chromatography (eluent: CHX/CH$_2$Cl$_2$ 6:4) to afford **151** as a white solid (0.058 g, 94%); mp: >300 °C. ^{1}H NMR (400 MHz, CDCl$_3$) δ: 7.42-7.40 (m, 12 H); 7.33-7.29 (m, 14 H); 7.22-7.14 (m, 21 H); 6.96-6.64 (m, 120 H); 6.35-6.33 (m, 4 H); 3.02 (s, 3 H); 2.37 (s, 36 H); 2.33 (s, 18 H); 2.01 (s, 18 H). ^{13}C NMR (100 MHz, CDCl$_3$) δ: 146.46, 146.03, 142.15, 141.61, 141.33, 140.67, 140.58, 140.49, 140.21, 140.00, 139.30, 138.96, 138.83, 138.47, 138.44, 138.02, 137.5, 137.69, 136.54, 131.62, 131.37, 131.09, 130.04, 128.50, 127.73, 127.57, 127.04, 127.02, 126.96, 126.75, 126.15, 125.06, 124.60, 124.14, 123.89, 83.81, 77.34, 23.38, 23.32, 22.90. ^{11}B NMR (128 MHz, CDCl$_3$) δ: 34.01. MALDI-LRMS calc. for [C$_{300}$H$_{246}$B$_{12}$N$_{12}$]$^+$: 4149.1 found: 4149.3. IR (film in CH$_2$Cl$_2$) ν$_{max}$ (cm^{-1}): 3290.96, 3028.34, 2916.69, 1599.05, 1553.31, 1492.05, 1452.65, 1436.8, 1362.7, 1308.42, 1210.07, 1103.6, 1074.24, 1026.32, 871.13, 838.07, 762.13, 699.28, 565.32, 552.64, 530.7.

Synthesis of borazine-polyphenylene 152
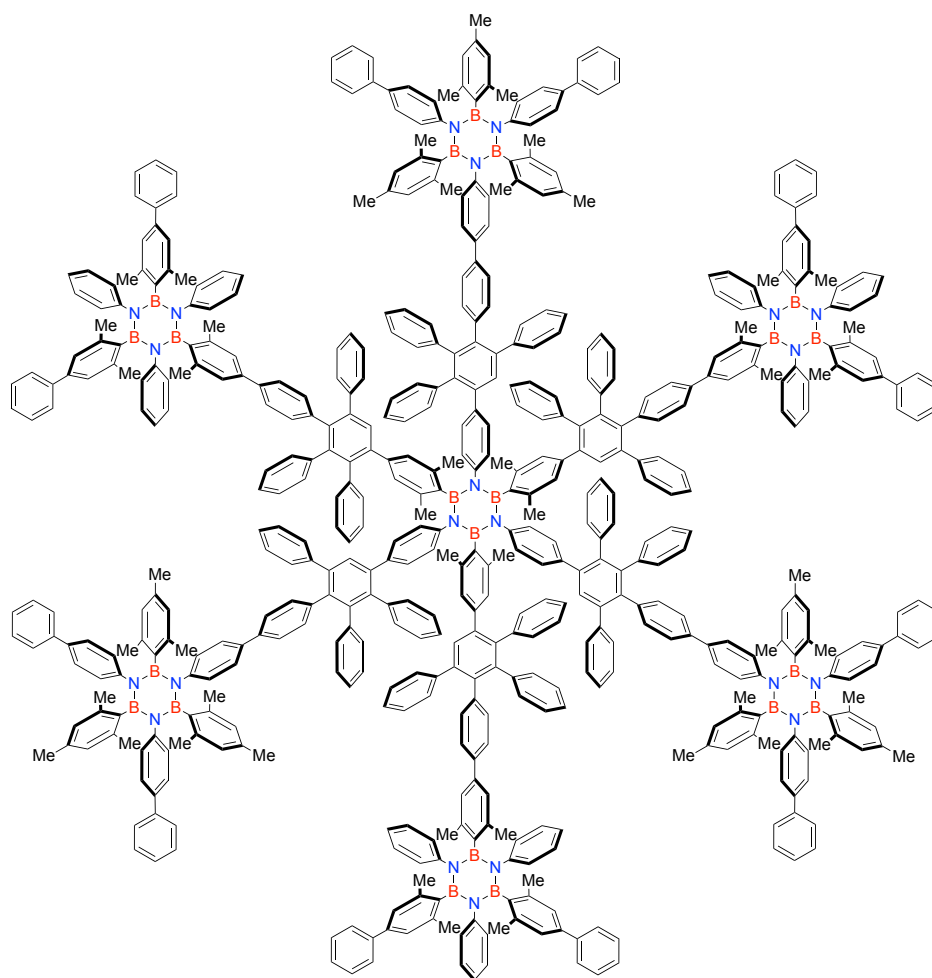
In a 10 mL Schlenk-type flask **151** (0.007 g, 0.017 mmol), **130** (0.0.16 g, 0.014 mmol), and Ph$_2$O (1 mL), were added. The dark red solution was degassed by Ar bubbling for 30 min at 40 °C, then stirred for 24 h at 260 °C. The reaction mixture was purified by silica gel column chromatography (eluent: PE/CH$_2$Cl$_2$ 7:3) to obtain a white solid. This was re-dissolved in EtOAc (1 mL) and to this solution MeOH was added until formation of a precipitate. This was recovered by filtration and furtherly purified by Rec-GPC (eluent: CHCl$_3$) to afford **152** as a white solid (0.007 g, 54%); mp >300 °C. ^{1}H NMR (300 MHz, CDCl$_3$) δ: 7.40-7.29 (m, 53 H); 7.22-6.67 (m, 232 H); 6.32 (s, 31 H); 2.34-2.23 (m, 115 H); 1.97-1.95 (m, 38 H). ^{11}B NMR (128 MHz, CDCl$_3$) δ: 35.18. MALDI-LRMS calc. for [C$_{555}$H$_{468}$B$_{21}$N$_{21}$]$^+$: 7659.0, found: 7659.1. IR (film in CH$_2$Cl$_2$) v_{max} (cm^{-1}):. 3024.36, 2956.27, 2845.86, 1625.76, 1546.56, 1485.63, 1449.89, 1420.29, 1326.03, 1299.48, 1254.26, 1205.09, 1155.02, 1113.94, 1056.88, 1005.25, 963.82, 899.58, 876.69, 840.49, 777.66, 750.86, 698.56, 648.02, 591.30, 562.68, 517.10.

Synthesis of borazine-polyphenylene 153
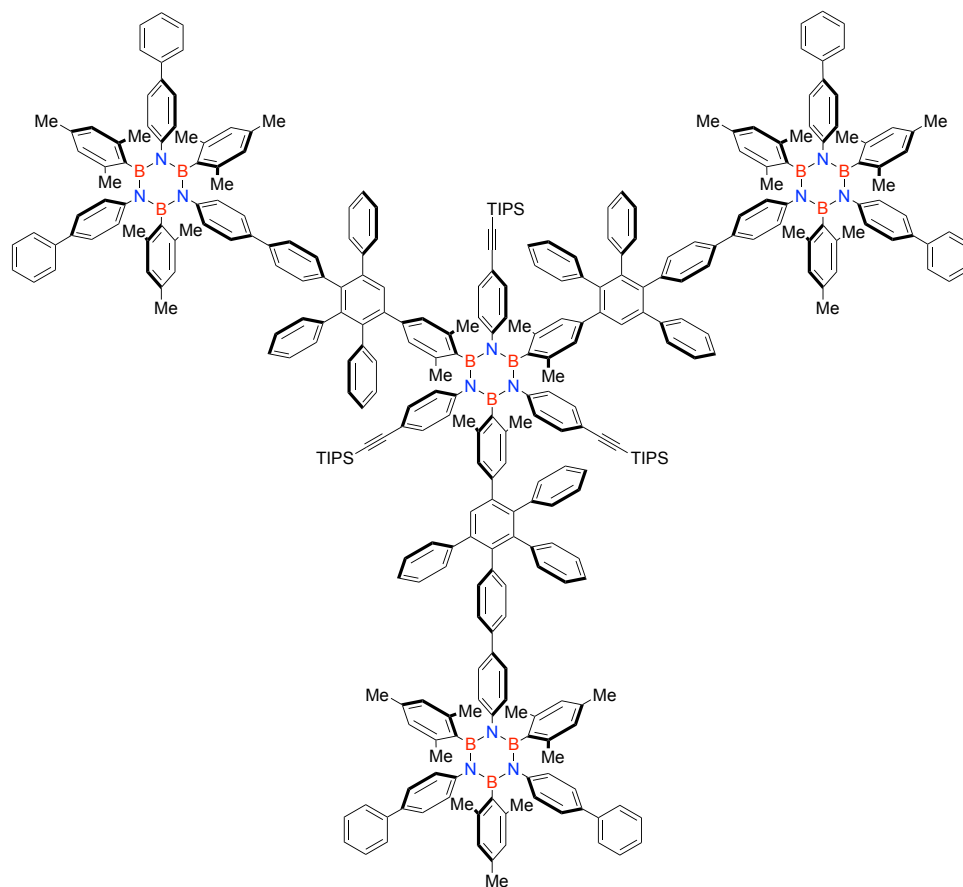
In a 10 mL Schlenk-type vessel **109** (0.025 g, 0.021 mmol), **130** (0.100 mg, 0.084 mmol), and Ph$_2$O (1 mL), were added. The dark red solution was degassed by Ar bubbling for 45 min at 40 °C, then stirred for 18 h at 240 °C. The reaction mixture was purified by silica gel column chromatography (eluent: CHX/CH$_2$Cl$_2$ 7:3) to obtain a white solid This was re-dissolved in EtOAc (1 mL) and to this solution MeOH was added until formation of a precipitate. This was recovered by filtration and furtherly purified by Rec-GPC (eluent: CHCl$_3$) to afford **153** as a white solid (0.026 g, 27%); mp >300 °C. ^{1}H NMR (300 MHz, CDCl$_3$) δ: 7.39-7.27 (m, 26 H); 7.23-7.13 (m, 21 H); 7.03-6.56 (m, 94 H); 6.34 (s, 24 H); 2.26-2.24 (m, 54 H); 2.01-1.96 (m, 45 H); 1.13 (s, 63 H). ^{13}C NMR (100 MHz, CDCl$_3$) δ: 145.73, 140.58, 139.83, 139.34, 137.22, 136.40, 136.17, 131.17, 131.57, 131.23, 129.95, 128.52, 127.35, 127.07, 126.70, 126.57, 126.43, 125.12, 119.31, 107.27, 89.84, 23.07, 21.09, 18.80, 11.40. MALDI-HRMS calc. for [C$_{336}$H$_{324}$B$_{12}$N$_{12}$Si$_3$]$^+$: 4743.7164, found: 4743.6943. IR (film in CH$_2$Cl$_2$) ν$_{max}$ (cm^{-1}): 3029.57, 2958.56, 2847.89, 2151.84, 1605.28, 1587.45, 1499.75, 1444.52, 1359.19, 1315.66, 1074.58, 1043.86, 966.11, 877.99, 833.47, 752.60, 685.54, 547.26, 520.10, 502.30, 471.65.

Synthesis of borazine-polyphenylene 154
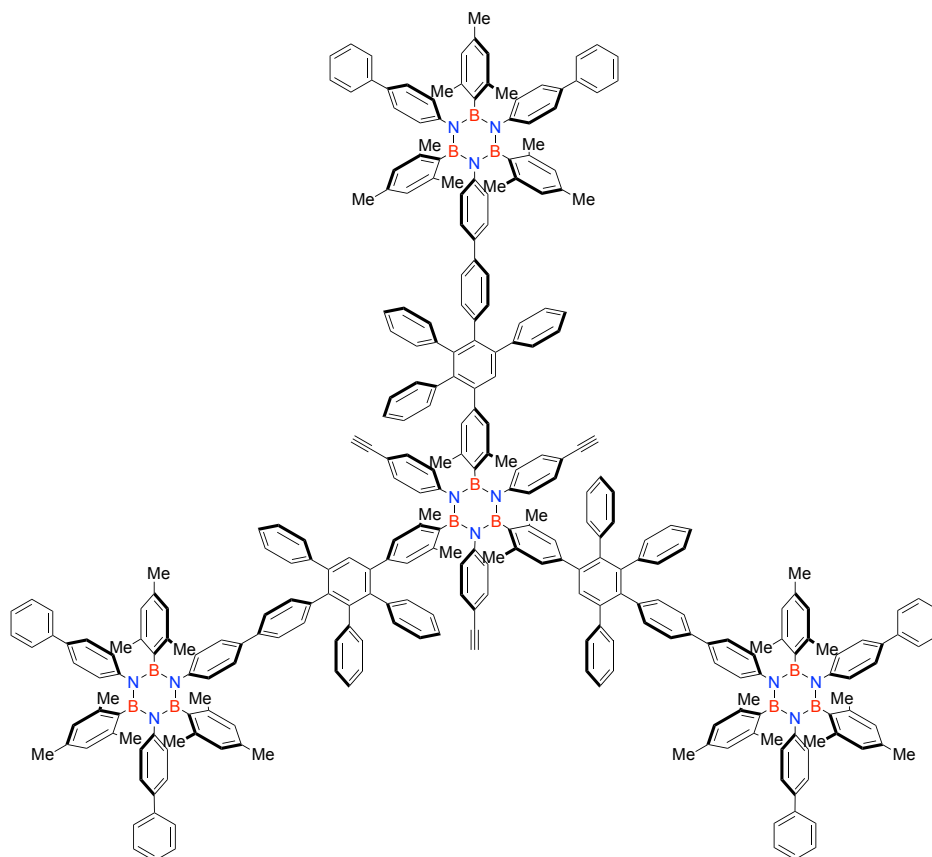
In a 25 mL round flask, **153** (0.028 g, 0.006 mmol) was dissolved in THF (3 mL), then TBAF (1M solution in THF, 0.024 mL, 0.024 mmol) was added dropwise at 0 °C. The reaction mixture was stirred for 2 h at r.t., then diluted with EtOAc (30 mL) and washed with water (3 x 30 mL) and brine (30 mL). The organic phase was dried over MgSO$_4$ and evaporated under reduced pressure. The product was purified by silica gel column chromatography (eluent: PE/CH$_2$Cl$_2$, 6:4) affording **154** as a white solid (0.021 g, 84%); mp >300 °C (decomp.). ^{1}H NMR (300 MHz, CDCl$_3$) δ: 7.40-7.30 (m, 28 H); 7.23-6.60 (m, 114 H); 6.32 (s, 22 H); 3.01 (s, 3 H); 2.24-2.22 (m, 53 H); 1.97-1.95 (m, 46 H). IR (film in CH$_2$Cl$_2$) ν$_{max}$ (cm^{-1}): 3320.69, 3035.84, 3002.36, 2985.58, 1668.69, 1605.73, 1582.46, 1469.58, 1418.57, 1356.49, 1328.71, 1258.33, 1148.47, 1107.30, 986.57, 915.38, 846.29, 758.44, 658.48, 652.38, 601.37, 548.58, 520.14.

Synthesis of borazine-polyphenylene 155
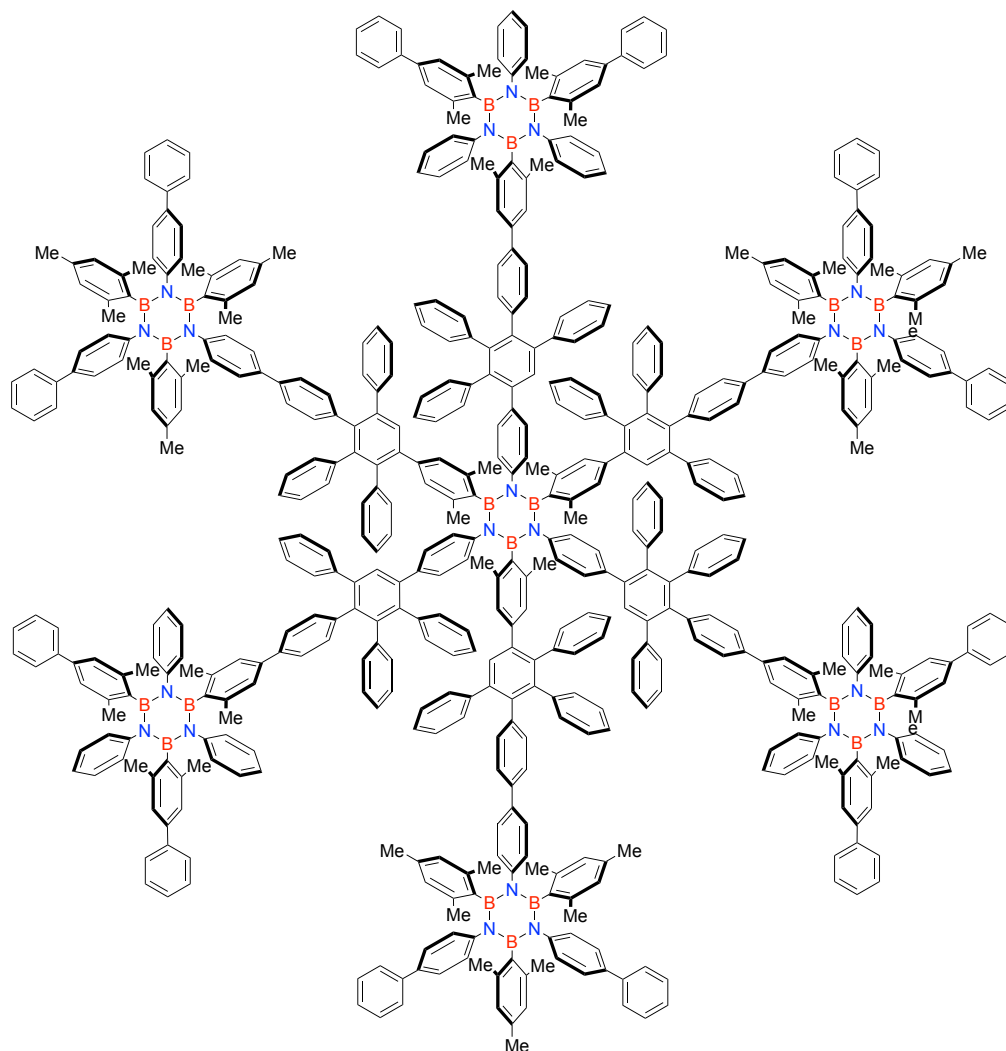
In a 10 mL Schlenk-type flask, **154** (0.021 g, 0.005 mmol), **124** (0.024 g, 0.020 mmol), and Ph$_2$O (3 mL), were added. The dark red solution was degassed by Ar bubbling for 30 min at 40 °C, then stirred for 16 h at 230 °C. The reaction mixture was purified by silica gel column chromatography (eluent: PE/CH$_2$Cl$_2$ 1:1) to obtain a white solid. This was re-dissolved in EtOAc (1 mL) and to this solution MeOH was added until formation of a precipitate. This was recovered by filtration and furtherly purified by Rec-GPC (eluent: CHCl$_3$) to afford **155** as a white solid (0.018 g, 48%); mp >300 °C. ^{1}H NMR (300 MHz, CDCl$_3$) δ: 7.38-7.29 (m, 57 H); 7.23-7.11 (m, 47 H); 7.02-6.65 (m, 181 H); 6.32 (s, 34 H); 2.35-1.95 (m, 153 H). ^{11}B NMR (128 MHz, CDCl$_3$) δ: 36.72. MALDI-LRMS calc. for [C$_{555}$H$_{468}$B$_{21}$N$_{21}$]$^+$: 7659.0, found: 7659.0. IR (film in CH$_2$Cl$_2$) ν_{max} (cm^{-1}): 3033.36, 3016.27, 2981.82, 1620.03, 1566.46, 1527.89, 1425.36, 1359.48, 1248.47, 1146.50, 1119.49, 1010.93, 992.37, 863.25, 764.56, 721.37, 642.37, 608.39, 586.39, 520.47, 486.88.

Synthesis of borazine-polyphenylene 156
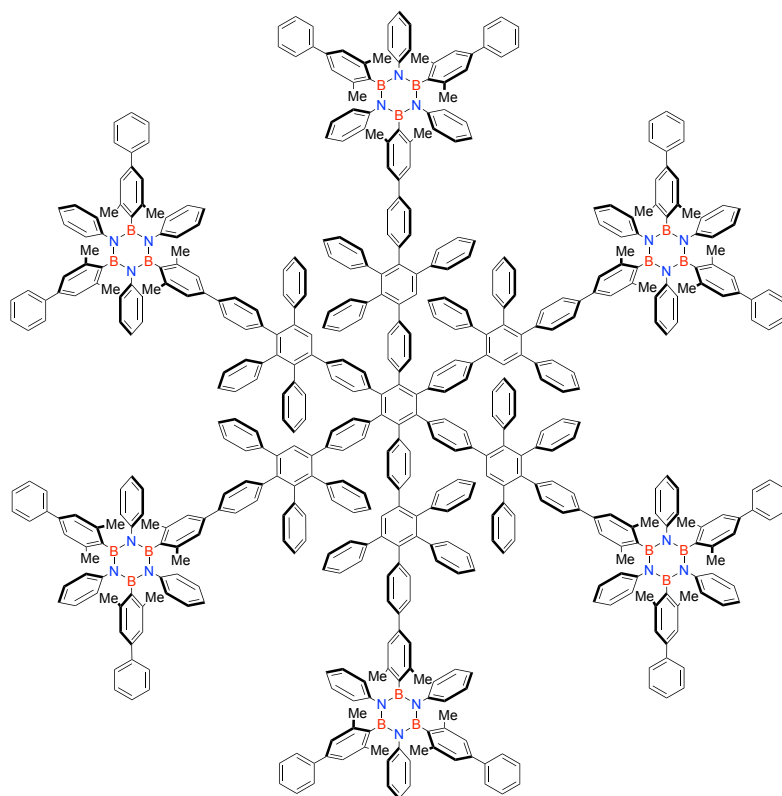
In a 10 mL Schenk-type flask, **136** (0.023 g, 0.034 mmol), **124** (0.31 g, 0.27 mmol) and Ph$_2$O (1.00 mL), were added. The dark red solution was degassed by Ar bubbling for 1 h at 40 °C, then stirred for 18 h at 250 °C. The mixture was cooled down and diluted with CH$_2$Cl$_2$ (2.00 mL), then PE was slowly added until formation of a precipitate. This was recovered by filtration and purified by silica gel column chromatography (eluent: PE/CH$_2$Cl$_2$ 7:3) to afford a white solid. This was furtherly purified by Rec-GPC (eluent: CHCl$_3$) to afford **156** (0.178 g, 70%); mp >300 °C (decomp.). ^{1}H NMR (300 MHz, CD$_2$Cl$_2$) δ: 7.42 (t, J = 7.0 Hz, 30 H); 7.36-7.30 (m, 26 H); 7.24 (t, J = 7.2 Hz, 12 H); 7.14 (s, 28 H); 7.08-6.71 (m, 210 H); 6.63 (d, J = 6.8 Hz, 12 H); 6.37 (d, J = 8.0 Hz, 12 H); 2.44 (s, 72 H); 2.39 (s, 36 H). ^{13}C NMR (100 MHz, CD$_2$Cl$_2$) δ: 146.25, 140.75, 140.55, 139.12, 138.27, 138.18, 131.86, 131.46, 131.11, 129.86, 128.53, 127.56, 127.10, 126.87, 126.76, 126.36, 124.73, 124.42, 123.83, 123.26, 23.21. ^{11}B NMR (128 MHz, CD$_2$Cl$_2$) δ: 34.91. MALDI-LRMS calc. for [C$_{546}$H$_{438}$B$_{18}$N$_{18}$]$^+$: 7445.7, found: 7445.7. IR (film in CH$_2$Cl$_2$) v_{max} (cm^{-1}): 3057.17, 3026.31, 2916.37, 2856.58, 2364.73, 2335.80, 1597.06, 1490.97, 1452.40, 1433.11, 1355.96, 1307.74, 1265.30, 1103.28, 1072.42, 1022.27, 869.90, 839.03, 761.88, 734.88, 717.52, 696.30, 653.87, 565.14, 530.42.

Synthesis of borazine-polyphenylene 157
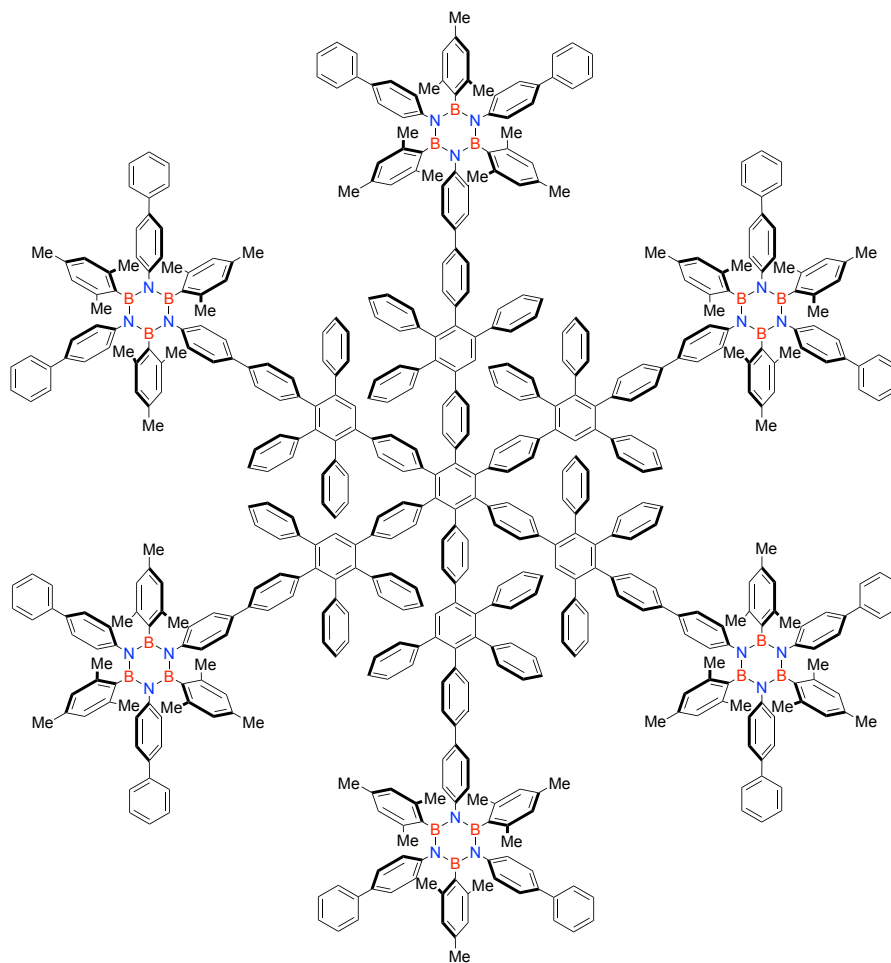
In a 10 mL Schenk-type flask, **136** (0.0088 g, 0.013 mmol), **130** (0.11 g, 0.092 mmol) and Ph_2O (3.00 mL) were added. The dark red solution was degassed by Ar bubbling for 1 h at 40 °C, then stirred for 16 h at 230 °C. The mixture was cooled down and diluted with CH_2Cl_2 (2.00 mL), then PE was slowly added until formation of a precipitate. This was recovered by filtration and purified by silica gel column chromatography (eluent: PE/CH_2Cl_2 7:3) to afford a white solid. This was furtherly purified by Rec-GPC (eluent: $CHCl_3$) to afford **157** (0.019 g, 19%); mp >300 °C (decomp.). ^{1}H NMR (300 MHz, $CDCl_3$) δ: 7.39-7.28 (m, 52 H); 7.23-7.19 (m, 14 H); 7.12 (m, 27 H); 7.02 (d, J = 8.3 Hz, 28 H); 6.96-6.58 (m, 137 H); 6.41-6.27 (m, 54 H); 2.26-2.24 (m, 108 H), 1.98-1.96 (m, 54 H). ^{13}C NMR (100 MHz, $CDCl_3$) δ: 145.71, 140.57, 140.46, 137.22, 137.19, 136.29, 136.15, 133.71, 131.72, 130.20, 129.93, 128.53, 128.50, 128.31, 127.65, 127.50, 127.32, .127.07, 127.02, 126.67, 126.55, 126.41, 126.35, 125.08, 29.73, 23.05, 23.02, 21.05. ^{11}B NMR (128 MHz, $CDCl_3$) δ: 33.99. MALDI-MS calc. for $[C_{564}H_{474}B_{18}N_{18}]^+$: 7699.0, found: 7698.1. IR (film in CH_2Cl_2) v_{max} (cm^{-1}): 3030.80, 3001.29, 2958.68, 1654.57, 1601.25, 1523.36, 1496.57, 1423.82, 1367.86, 1345.62, 129.67, 1233.37, 1150.30, 1116.81, 1047.96, 963.27, 910.26, 763.51, 742.32, 659.86, 635.24, 542.26, 520.23.

Synthesis of borazine-polyphenylene 158
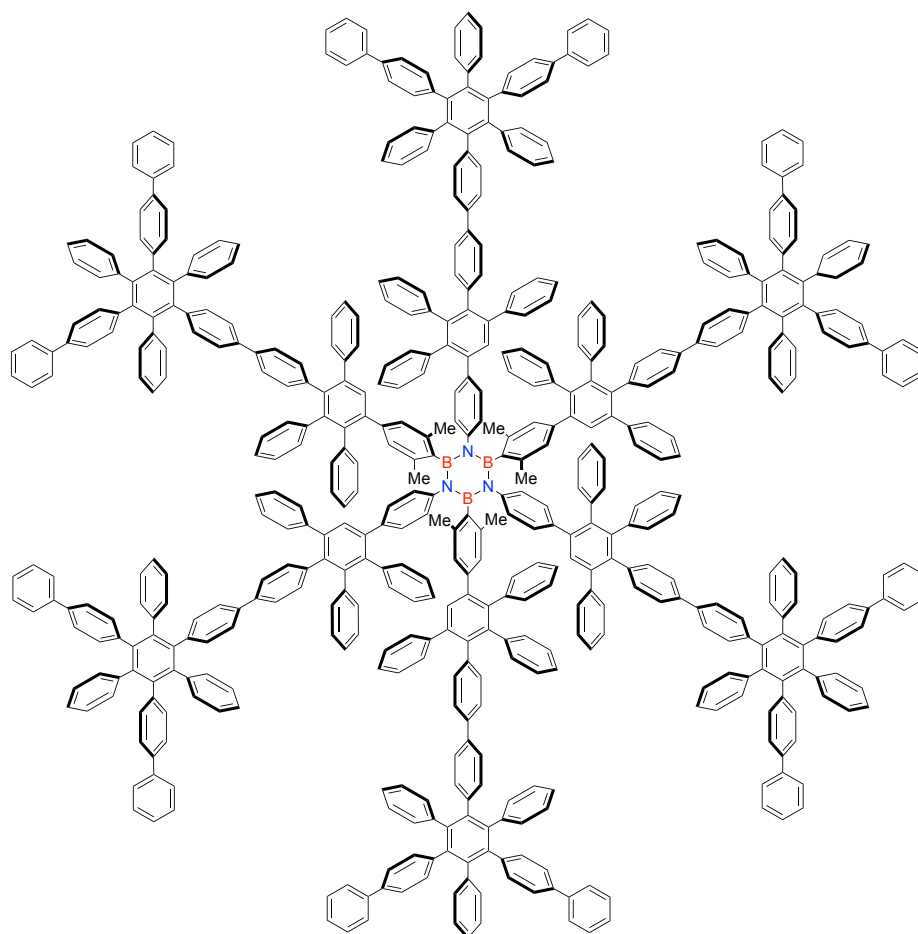
In a 10 mL Schlenk-type flask, **108** (5.03 mg, 0.0066 mmol), **146** (56.8 mg, 0.053 mmol), and Ph_2O (1 mL), were added. The dark red solution was degassed by Ar bubbling for 40 min at 40 °C, then stirred for 30 h at 260 °C. The mixture was cooled down and diluted with CH_2Cl_2 (2.00 mL), then this solution was poured into PE. The precipitate formed was recovered by filtration and purified by Rec-GPC (eluent: $CHCl_3$) to afford **158** as a white solid (0.022 g, 46%); mp >300 °C. ^{1}H NMR (300 MHz, CD_2Cl_2) δ: 7.44 (d, J = 7.7 Hz, 24 H); 7.37-7.23 (m, 46 H); 7.17-6.63 (m, 276 H); 6.48-6.33 (m, 16 H); 1.85 (s, 18 H). ^{13}C NMR (100 MHz, CD_2Cl_2) δ: 144.00, 142.05, 142.02, 141.96, 141.62, 141.03, 140.82, 140.65, 140.60, 140.52, 140.33, 140.09, 139.94, 139.89, 139.41, 139.33, 139.10, 139.00, 138.79, 138.52, 138.21, 137.38, 137.07, 136.79, 136.72, 136.47, 136.35, 131.95, 131.87, 131.83, 131.40, 131.34, 129.86, 128.62, 128.42, 127.56, 127.43, 127.17, 127.05, 126.78, 126.68, 126.48, 125.46, 125.36, 124.90, 124.56, 124.39, 124.34, 22.51. ^{11}B NMR (128 MHz, CD_2Cl_2) δ: 35.64. MALDI-LRMS calc. for $[C_{546}H_{380}B_3N_3]^+$: 7013.0, found: 7013.1. IR (film in CH_2Cl_2) ν_{max} (cm^{-1}): 3025.60, 2980.02, 2889.45, 2365.32, 1598.87, 1498.69, 1414.58, 1378.56, 1263.35, 1155.35, 1108.69, 1072.54, 1029.98, 1004.58,

952.96, 912.38, 826.32, 763.56, 754.26, 734.25, 695.32, 652.65, 617.47, 590.25, 572.23, 540.07, 520.21, 418.60, 413.50, 403.20.

Synthesis of polyphenylene 159
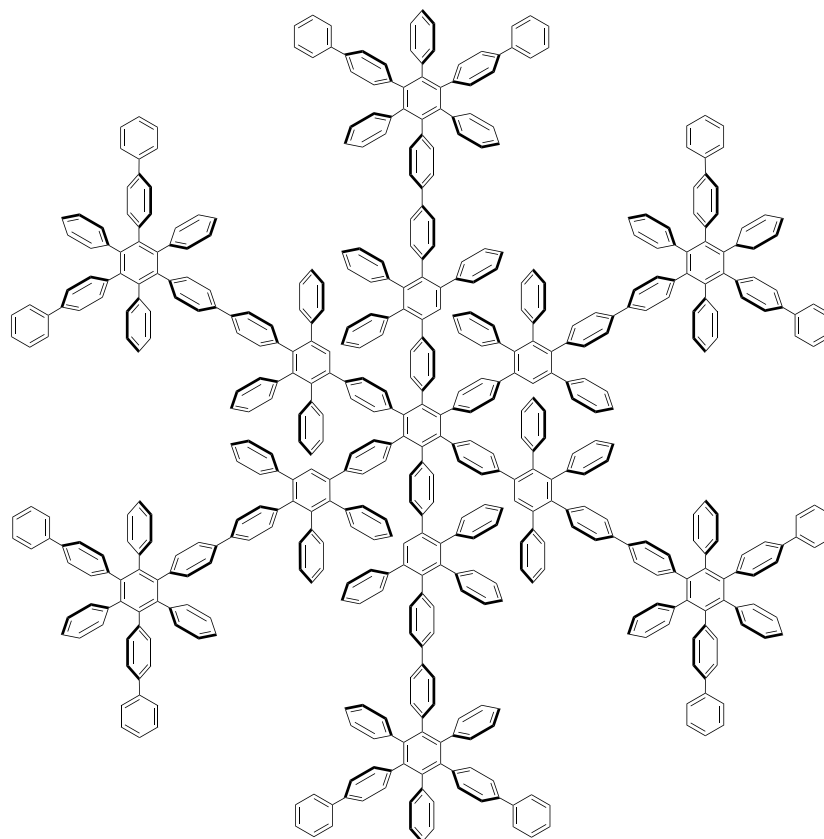
In a 10 mL Schlenk-type flask, **136** (5.18 mg, 0.0076 mmol), **146** (65.4 mg, 0.0612 mmol), and Ph_2O (1 mL), were added. The dark red solution was degassed by Ar bubbling for 40 min at 40 °C, then stirred for 30 h at 260 °C. The mixture was cooled down and diluted with CH_2Cl_2 (2.00 mL), then this solution was poured into PE. The precipitate formed was recovered by filtration and purified by Rec-GPC (eluent: $CHCl_3$) to afford **159** as a white solid (26 mg, 49%); mp >300 °C. ^1H NMR (300 MHz, CD_2Cl_2) δ: 7.44 (d, J = 7.6 Hz, 24 H); 7.38-7.32 (m, 28 H); 7.28-7.23 (m, 12 H); 7.17-6.71 (m, 280 H); 6.62 (d, J = 7.4 Hz, 12 H); 6.35 (d, J = 8.1 Hz, 12 H). ^{13}C NMR (100 MHz, CD_2Cl_2) δ: 141.88, 141.84, 141.72, 141.13, 140.72, 140.65, 140.61, 140.53, 140.34, 140.10, 139.95, 139.91, 139.77, 139.32, 139.20, 139.10, 138.61, 138.54, 138.25, 137.39, 136.82, 136.47, 131.88, 131.85, 131.56, 131.46, 131.41, 131.35, 131.11, 129.87, 128.62, 128.27, 127.61, 127.48, 127.06, 126.85, 126.69, 126.49, 126.31, 125.72, 125.48, 125.38, 124.91, 124.61, 124.42, 124.38, 124.30. MALDI-LRMS calc. for $[C_{546}H_{368}]^+$: 6926.9, found: 6926.8. IR (film in CH_2Cl_2) v_{max} (cm^{-1}): 3026.31, 2980.02, 2889.37, 2360.87, 1598.88, 1496.76, 1442.75,

1442.75, 1386.82, 1263.37, 1155.36, 1141.86, 1109.07, 1072.42, 1006.84, 952.84, 831.32, 734.88, 698.23, 574.79

Synthesis of 1,2,3,4,5-pentaphenylbenzene 161
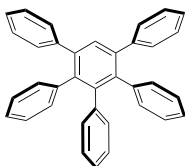
In a MW-type vessel CPD (0.70 gr, 1.82 mmol), phenylacetylene (0.22 mL, 2.00 mmol), and Ph_2O (1.5 mL), were added. The mixture was heated at 200 °C in a MW reactor for 1 h, then it was diluted with CH_2Cl_2 (2.00 mL) and poured into PE. The precipitate formed was recovered by filtration and purified by silica gel column chromatography (eluent: PE/CH_2Cl_2 8:2) to afford **161** as a white solid (0.85 g, 92%); mp: 225-227 °C. ^{1}H NMR (400 MHz, $CDCl_3$) δ: 7.59 (s, 1 H); 7.17 (s, 10 H); 6.95-6.78 (m, 15 H). ^{13}C NMR (100 MHz, $CDCl_3$) δ: 141.80, 141.75, 140.82, 140.39, 140.01, 139.33, 131.60, 131.54, 131.03, 127.69, 127.02, 126.72, 126.34, 125.69, 125.42. ESI-HRMS calc. for $[C_{36}H_{26}]^+$: 458.2035, found: 458.2042. IR (film in CH_2Cl_2) v_{max} (cm^{-1}): 3197.98, 2980.02, 2883.58, 2727.35, 2146.77, 2050.33, 0197.66, 1598.99, 1543.05, 1519.91, 1454.33, 1390.68, 1298.09, 1087.85, 869.90, 856.39, 833.25, 792.74, 783.10, 754.17, 715.59, 688.59, 626.87.

Synthesis of N,N',N''-triphenyl-B,B'-di(2,6-dimethyl-4-phenyl)-B''-2,6-dimethyl-4-(2,3,4,6-tetraphenyl-(phenyl-4'-yl))borazine 162
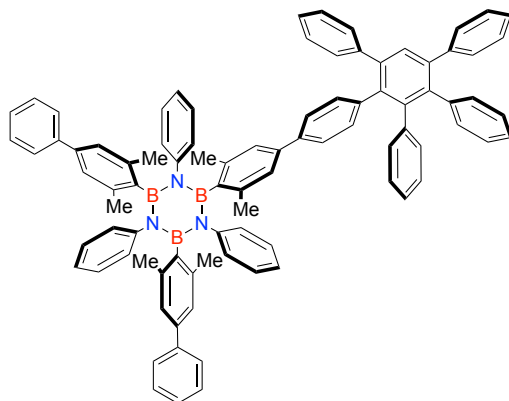
In a MW-type vial, **124** (0.016 gr, 0.014 mmol), phenylacetylene (0.004 gr, 0.04 mmol), and Ph_2O (0.4 mL), were added. The mixture was degassed by N_2 bubbling for 30 min, then heated at 180 °C for 1 h in a MW reactor. The deep-orange solution was diluted with CH_2Cl_2 (1 mL) and poured into MeOH. The precipitate formed was recovered by filtration and purified by silica gel column chromatography (eluent: PE/CH_2Cl_2 6:4). The

white solid obtained was furtherly purified by Rec-HPLC (eluent: hexane/CHCl$_3$ 2:8) to afford **162** (0.010 gr, 59 %); mp 258-260 °C. ^{1}H NMR (400 MHz, CDCl$_3$) δ: 7.54 (s, 1 H); 7.41-7.39 (m, 4 H); 7.32-7.27 (m, 4 H); 7.23-7.14 (m, 11 H); 7.01-6.64 (m, 34 H); 2.35-2.30 (m, 18 H). ^{13}C NMR (100 MHz, CDCl$_3$) δ: 146.33, 141.63, 141.26, 139.59, 138.32, 132.01, 131.93, 131.86, 130.34, 128.81, 128.12, 127.97, 127.43, 127.35, 127.27, 127.14, 127.03, 126.60, 125.47, 124.90, 124.44, 124.20, 23.69. MALDI-HRMS calc. for [C$_{90}$H$_{74}$B$_3$N$_3$]$^+$: 1228.6198, found: 1228.6228. IR (film in CH$_2$Cl$_2$) ν_{max} (cm^{-1}): 3218.25, 2958.64, 1658.47, 1620.54, 1554.23, 1502.16, 1448.80, 1398.46, 1345.78, 1310.27, 1256.84, 1153.49, 1053.63, 956.34, 896.34, 852.08, 741.10, 620.49, 590.32, 562.16, 530.54.

Synthesis of N,N'-tri(4-phenyl)phenyl-N''-4-(2,3,4,6-tetraphenyl-(phenyl-4'-yl))-B,B',B''-trimesitylborazine 163
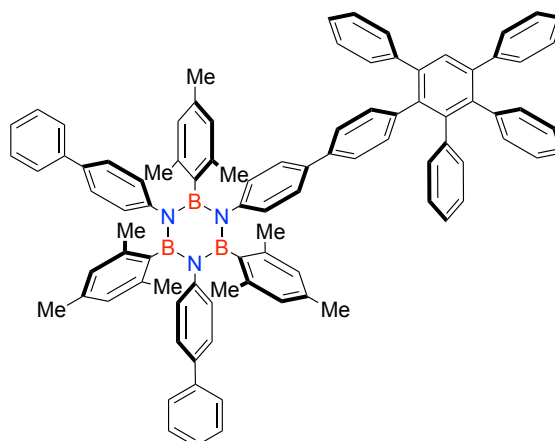
In a MW-type vial **130** (0.022 gr, 0.018 mmol), phenylacetylene (0.009 gr, 0.091 mmol), and Ph$_2$O (0.4 mL), were added. The mixture was degassed by N$_2$ bubbling for 30 min, then heated at 180 °C for 1 h in a MW reactor. The deep-orange solution was diluted with CH$_2$Cl$_2$ (1 mL) and poured into MeOH (10 mL). The precipitate formed was recovered by filtration and purified by silica gel column chromatography (eluent: PE/CH$_2$Cl$_2$ 6:4). The white solid obtained was furtherly purified by Rec-HPLC (eluent: hexane/CHCl$_3$ 3:7) to afford **163** (0.0045 gr, 20 %); mp 249-253 °C. ^{1}H NMR (400 MHz, CDCl$_3$) δ: 7.54 (s, 1 H); 7.40-7.27 (m, 8 H); 7.23-7.18 (m, 2 H); 7.15-7.13 (m, 8 H); 7.03-6.71 (m, 28 H), 6.33 (s, 6 H); 2.25-2.23 (m, 18 H); 1.98-1.96 (m, 9 H). ^{13}C NMR (100 MHz, CDCl$_3$) δ: 145.27, 145.31, 141.78, 140.60, 140.06, 137.25, 136.16, 131.56, 129.96, 127.59, 127.34, 127.05, 126.70, 126.57,16.41, 125.10. MALDI-MS calc. for [C$_{93}$H$_{80}$B$_3$N$_3$]$^+$: 1272.1, found: 1271.8. IR (film in CH$_2$Cl$_2$) ν_{max} (cm^{-1}): 3021.56, 2992.34, 2984.46, 1658.47,

1603.23, 1548.75, 1487.46, 1412.33, 1344.66, 1300.69, 1205.88, 1087.65, 1002.36, 960.44, 866.74, 824.36, 789.96, 752.26, 691.34, 588.78, 563.42, 526.27, 496.37.

4.3 Experimental details for section 3.2

Synthesis of diethyl2-(4-tert-butylphenyl)-4,8-diethoxy-1,3-dioxo-2,3-dihydro-1H-benzo[de]isoquinoline-6,7-dicarboxylate 177
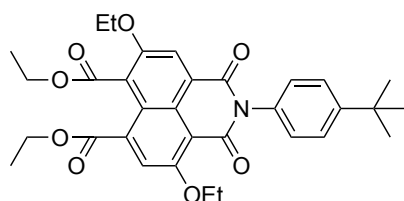
In a 25 mL round flask, diethyl 4,8-diethoxy-1,3-dioxo-1,3-dihydrobenzo[de]isochromene-6,7-dicarboxylate **175** (1.13 g, 2.62 mmol), *p*-*t*butylaniline **176** (0.43 g, 2.90 mmol), benzoic acid (0.20 g, 1.60 mmol), Et$_3$N (0.22 mL, 1.60 mmol), and DMF (4 mL) were added and stirred for 18 h at 110 ˚C. The mixture was then diluted with EtOAc (50 mL) and washed with water (3 × 50 mL) and brine (50 mL). The organic layer was dried over MgSO$_4$ and evaporated under reduced pressure. The product was purified by silica gel column chromatography (eluent: CHX/EtOAc 8:2) to afford **177** as a yellow solid (1.22 g, 83%); mp 167-168 ˚C. ^{1}H NMR (400 MHz, CDCl$_3$) δ: 8.43 (s, 1 H); 7.74 (s, 1 H); 7.53 (d, J= 8.5 Hz, 2 H); 7.20 (d, J= 8.5 Hz, 2 H); 4.46-4.35 (m, 6 H); 4.28 (q, J= 6.9 Hz, 2 H); 1.55 (t, J= 6.9 Hz, 3 H); 1.49-1.41 (m, 9 H). ^{13}C NMR (68 MHz, CDCl$_3$) δ: 167.3, 166.7, 163.3, 161.7, 159.9, 154.3, 151.3, 136.6, 132.5, 127.9, 126.5, 128.4, 126.4, 124.7, 123.3, 122.1, 119.8, 119.0, 109.2, 66.0, 65.9, 62.3, 61.7, 43.6, 34.7, 31.3, 14.8, 14.7, 14.1, 14.0. ESI-HRMS calc. for [C$_{32}$H$_{36}$NO$_8$]$^+$: 562.2435, found: 562.2433. IR (film in CH$_2$Cl$_2$) ν$_{max}$ (cm^{-1}): 2979.23, 2964.67, 2925.20, 2849.89, 1705.30, 1665.54, 1609.62, 1579.36, 1502.83, 1502.73, 1450.62, 1428.44, 1405.70, 1388.24, 1371.98, 1347.45, 1295.62, 1242.56, 1216.37, 1154.73, 1141.41, 1108.70, 1094.60, 1075.37, 1041.69, 1028.50, 054.78, 880.56, 880.32, 861.72, 827.75, 812.91, 784.80, 763.02, 731.66, 681.40, 663.38, 637.21, 594.89, 564.88, 531.70, 468.58.[300]

Synthesis of 7-(4-Tert-butylphenyl)-4,9-diethoxy-1H-isochromeno-[6,5,4-def]-isoquinoline-1,3,6,8(7H)-tetraone 178
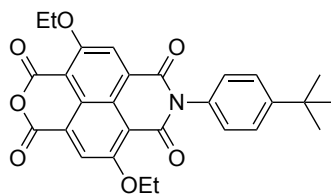
In a 100 mL round flask equipped with a condenser, diethyl 2-(4-tert-butylphenyl)-4,8-diethoxy-1,3-dioxo-2,3-dihydro-1H-benzo[de]isoquinoline-6,7-dicarboxylate **177** (1.22 g, 2.17 mmol), and TFA (20 mL) were added. The solution was stirred under refluxing conditions at 73 °C. After 45 h the volatiles were removed under reduced pressure and **178** was obtained as a yellow solid without further purification (1.04 g, 98%); mp 292-294 °C. ^{1}H NMR (270 MHz, CDCl$_3$) δ: 8.50 (s, 1 H); 8.46 (s, 1 H); 7.56 (d, J= 8.3 Hz, 2 H); 7.20 (d, J=8.3 Hz, 2 H); 4.58-4.40 (m, 4 H); 1.70-1.58 (m, 6 H); 1.37 (s, 9 H). ^{13}C NMR (68 MHz, CDCl$_3$) δ: 162.2, 161.1, 160.8, 160.1, 159.6, 155.0, 151.8, 131.9, 128.7, 127.8, 126.5, 125.6, 123.7, 123.2, 121.4, 119.7, 112.1, 106.7, 66.7, 66.6, 34.7, 31.3, 14.6, 14.5. ESI-HRMS calc. for [C$_{28}$H$_{26}$NO$_7$]$^+$: 488.1704, found: 488.1705. IR (film in CH$_2$Cl$_2$) ν_{max} (cm^{-1}): 2957.74, 2870.91, 1775.46, 1738.88, 1726.47, 1672.55, 1576.12, 1516.42, 1506.09, 1495.83, 1461.78, 1441.50, 1405.32, 1378.80, 1361.43, 1349.52, 1304.66, 1268.89, 1255.36, 1238.97, 1211.19, 1162.30, 1142.60, 1107.59, 1038.61, 1017.16, 985.33, 961.63, 896.41, 885.82, 873.19, 856.45, 826.01, 783.92, 777.37, 759.50, 745.16, 732.18, 710.74, 702.16, 684.85, 658.46, 692.51, 621.81, 563.98, 516.67, 486.45, 468.33.[300]

Synthesis of 2-(4-hydroxymethylphenyl)-7-(4-tert-butylphenyl)-4,9-diethoxybenzo-[lmn][3,8]-phenanthroline-1,3,6,8(2H,7H)-tetraone 180
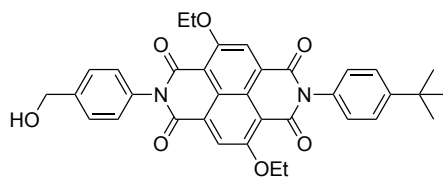
In a 25 mL round flask, 7-(4-Tert-butylphenyl)-4,9-diethoxy-1H-isochromeno-[6,5,4-def]-isoquinoline-1,3,6,8(7H)-tetraone **178** (0.21 g, 0.43 mmol), p-aminobenzylalcohol **179** (0.06 g, 0.48 mmol), benzoic acid (0.033 g, 0.26 mmol), Et$_3$N (0.037 mL, 0.26 mmol), and DMF (2 mL) were added. The mixture was stirred for 21 h at 110 °C, then diluted by EtOAc (50 mL) and washed with water (3 × 50 mL) and brine (50 mL). The organic layer was dried over MgSO$_4$ and evaporated under reduced pressure. The product was purified by silica gel column chromatography (eluent: CHX/EtOAc 8:2) to afford **180** as an orange

solid (0.20 g, 51%); mp >300 ˚C. ^{1}H NMR (400 MHz, DMSO-d$_6$) δ: 8.21 (d, J = 2.3 Hz, 2 H); 7.56 (d, J = 8.5 Hz, 2 H); 7.46 (d, J = 8.3 Hz, 2 H); 7.39-7.33 (m, 4 H); 5.32 (t, J = 5.8 Hz, 1 H); 4.60 (d, J = 5.7 Hz, 2 H); 4.36 (q, J = 6.8 Hz, 4 H); 1.41 (m, 6 H); 1.37 (s, 9 H). ^{13}C NMR (68 MHz, CDCl$_3$) δ: 162.39, 160.82, 160.77, 159.63, 151.14, 143.25, 134.73, 133.67, 129.33, 129.18, 127.41, 126.22, 123.41, 119.34, 110.40, 66.23, 63.15, 40.70, 40.49, 40.28, 40.07, 39.86, 39.65, 39.44, 35.02, 31.74, 30.15, 26.84, 15.02, 15.00. MALDI-HRMS calc. for [C$_{35}$H$_{32}$N$_2$O$_7$]$^+$: 592.2210, found: 592.2210. IR (film in CH$_2$Cl$_2$) ν_{max} (cm^{-1}): 2957.80, 1711.59, 1663.02, 1577.99, 1512.89, 1443.01, 1379.78, 1357.34, 1297.22, 1227.09, 1209.24, 1147.37, 1120.85, 1107.59, 1032.93, 968.14, 886.45, 832.28, 791.69, 763.02, 750.86, 729.54, 682.40, 577.40, 563.90, 519.93.

Synthesis of 2-(4-hydroxymethylphenyl)-7-(4-tert-butylphenyl)-4,9-di-N-pyrrolidino-[lmn][3,8]-phenanthroline-1,3,6,8(2H,7H)-tetraone 181
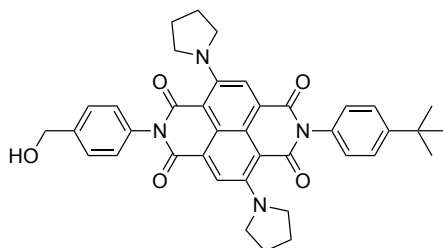
In a 100 mL round flask, 2-(4-hydroxymethylphenyl)-7-(4-tert-butylphenyl)-4,9-diethoxybenzo-[lmn][3,8]-phenanthroline-1,3,6,8(2H,7H)-tetraone **180** (0.51 g, 0.86 mmol), and pyrrolidine (25 mL), were added. The mixture was stirred under refluxing conditions at 87 ˚C. After 40 h the volatiles were removed under reduced pressure. The product was purified by silica gel column chromatography (eluent: CHX/EtOAc 8:2) to afford **181** as a blue solid (0.17 g, 37%); mp >300 ˚C. ^{1}H NMR (400 MHz, DMSO-d$_6$) δ: 8.21 (s, 2 H); 7.54 (d, J = 8.5 Hz, 2 H); 7.46 (d, J = 8.3 Hz, 2 H); 7.31-7.26 (m, 4 H); 5.32 (t, J = 5.8 Hz, 1 H); 4.59 (d, J = 5.7 Hz, 2 H); 3.38 (s, 8 H); 1.94 (s, 8 H); 1.37 (s, 9 H). ^{13}C NMR (100 MHz, CDCl$_3$) δ: 163.65, 162.38, 161.78, 159.21, 150.82, 149.21, 147.13, 144.88, 142.97, 136.80, 134.49, 133.45, 129.34, 129.16, 128.51, 127.49, 127.04, 126.29, 125.51, 125.27, 124.26, 122.49, 121.55, 121.33, 117.24, 105.48, 96.32, 63.17, 58.63, 52.67, 44.13, 40.66, 40.46, 40.25, 40.04, 39.83, 39.62, 39.41, 35.54, 35.00, 33.11, 31.74, 29.82, 26.00, 11.74. MALDI-HRMS calc. for [C$_{39}$H$_{38}$N$_4$O$_5$]$^+$: 642.2842, found: 642.2836. IR (film in CH$_2$Cl$_2$) ν_{max} (cm^{-1}): 2967.53, 2936.30, 1720.46, 1635.45, 1592.40, 1511.98, 1443.23, 1383.76, 1346.85, 1262.67, 1230.10, 1199.51, 1137.79, 1100.30,

1051.56, 1023.79, 998.78, 956.89, 901.27, 856.24, 837.80, 735.34, 712.56, 677.80, 653.22, 612.13, 589.71, 564.22, 532.30.

Synthesis of 2-(4-azidomethylphenyl)-7-(4-tert-butylphenyl)-4,9-di-N-pyrrolidino-[lmn][3,8]-phenanthroline-1,3,6,8(2H,7H)-tetraone 174
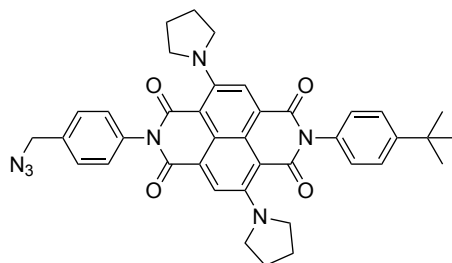
In a 10 mL round flask, 2-(4-tert-butylphenyl)-4,9-di-N-pyrrolidyl-7-(4-hydroxymethylphenyl) benzo[lmn][3,8] phenanthroline-1,3,6,8(2H,7H)-tetraone **181** (0.15 g, 0.23 mmol), PPh$_3$ (0.064 g, 0.23 mmol), NaN$_3$ (0.019 g, 0.28 mmol), DMF (1 mL), and CCl$_4$ (0.25 mL), were added. The solution was stirred for 1 h at 90 °C, then diluted with EtOAc (20 mL) and washed with water (3 × 30 mL). The organic layer was dried over MgSO$_4$ and evaporated under reduced pressure. The product was purified by silica gel column chromatography (eluent CHX/EtOAc 7:3) to afford **174** as a blue solid (0.057 g, 37%); mp 136-138 °C. ^{1}H NMR (400 MHz, DMSO-d$_6$) δ: 8.24 (s, 2 H); 7.54 (t, J = 7.9 Hz, 4 H); 7.40 (d, J = 7.6 Hz, 2 H); 7.27 (d, J = 7.7 Hz, 2 H); 4.58 (s, 2 H); 3.41 (s, 8 H); 1.95 (s, 8 H); 1.37 (s, 9 H). MALDI-HRMS calc. for [C$_{39}$H$_{37}$N$_7$O$_4$Na]$^+$: 690.2805; found: 690.2802. IR (film in CH$_2$Cl$_2$) ν$_{max}$ (cm^{-1}): 2961.89, 2095.85, 1689.30, 1651.47, 1565.22, 1513.06, 1476.26, 1446.31, 1416.88, 1353.81, 1330.36, 1314.80, 1260.06, 1209.37, 1160.39, 1134.75, 1106.41, 1057.41, 1023.86, 978.10, 937.69, 900.46, 866.94, 800.93, 780.34, 753.34, 727.88, 693.81, 658.02, 564.81, 550.15, 524.81.

Synthesis of NDI-functionalized borazine-polyphenylene 182
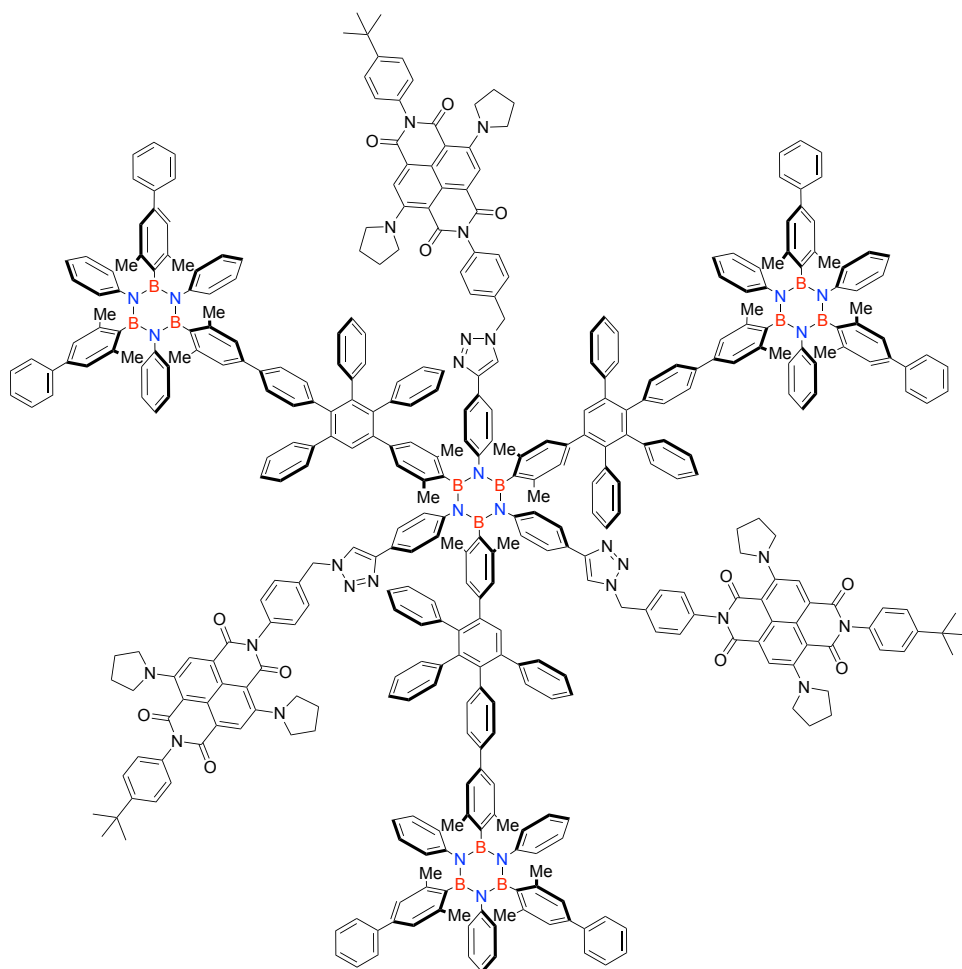
In a 10 mL Schlenk-type flask, **151** (0.052 g, 0.012 mmol), **174** (0.034 mg, 0.52 mmol), CuI (0.0004 g, 0.002 mmol), and CH_2Cl_2 (1 mL), were added. The mixture was degassed by 3 FPT cycles. In parallel, a solution of DIPEA (0.014 mL), CH_2Cl_2 (4 mL), and AcOH (0.0046 mL), was degassed by bubbling Ar for 40 min. 0.2 mL of the resulting solution were added to the reaction mixture and allowed to react for 96 h at r.t.. After filtration through Celite, the deep blue solution was evaporated. The crude mixture was diluted with water (50 mL) and extracted with EtOAc (3 × 50 mL). The combined organic layers were dried over $MgSO_4$ and evaporated under reduced pressure. The product was purified by silica gel column chromatography (eluent: CHX/EtOAc 7:3), followed by Rec-GPC (eluent: $CHCl_3$) to afford **182** as a blue solid (0.042 g, 58%); mp: 310-312. ^{1}H NMR (400 MHz, $CDCl_3$) δ: 8.42 (s, 3 H); 8.35 (s, 3 H); 7.63-7.61 (m, 4 H); 7.56 (d, J = 8.3 Hz, 6 H); 7.45-7.38 (m, 18 H); 7.34-7.27 (m, 24 H); 7.25-7.18 (m, 14 H); 7.10-7.00 (m, 16 H); 6.88-6.50 (m, 110 H); 6.29 (s, 6 H); 5.65 (s, 6 H); 3.45 (s, 12 H); 3.34 (s, 12 H); 2.34 (s, 36 H); 2.26 (d, J = 7.9 Hz, 18 H); 2.06 (s, 18 H); 1.98-1.82 (m, 24 H); 1.39 (s, 27 H). ^{13}C NMR

(100 MHz, CDCl$_3$) δ: 164.02, 163.82, 161.86, 161.69, 151.38, 148.41, 147.55, 147.45, 147.37, 146.14, 146.03, 141.42, 141.36, 140.97, 140.73, 140.55, 140.31, 139.99, 139.36, 139.26, 139.18, 139.04, 138.83, 138.79, 138.61, 138.23, 138.16, 137.99, 137.74, 137.69, 136.70, 136.62, 135.12, 135.10, 133.29, 131.70, 131.61, 131.56, 131.39, 131.36, 131.13, 130.01, 129.82, 128.88, 128.84, 128.46, 128.18, 127.65, 127.54, 127.49, 127.00, 126.92, 126.71, 126.55, 126.44, 126.34, 126.03, 125.55, 124.86, 124.58, 124.42, 124.13, 123.85, 123.72, 123.19, 123.03, 122.15, 122.08, 119.21, 105.42, 53.84, 52.78, 34.84, 31.48, 30.75, 27.01, 25.94, 25.85, 23.34, 23.26, 22.98, 14.18. ^{11}B NMR (128 MHz, CDCl$_3$) δ: 33.93. MALDI-LRMS calc. for [C$_{417}$H$_{357}$B$_{12}$N$_{33}$O$_{12}$]$^+$: 6151.97, found: 6152.02. IR (film in CH$_2$Cl$_2$) ν$_{max}$ (cm^{-1}): 3027.38, 2962.59, 2869.01, 1694.99, 1658.65, 1598.28, 1567.4, 1514.77, 1491.62, 1450.53, 1360.01, 1310.38, 1275.62, 1260.87, 1212.54, 1157.25, 1136, 1106.62, 1073.75, 1023.84, 976.65, 900.85, 870.76, 839.6, 798.4, 763.88, 749.71, 699.71, 613.96, 564.99, 531.02.

4.4 Experimental details for section 3.3

Synthesis of molecules 45, 186, 187, and 46
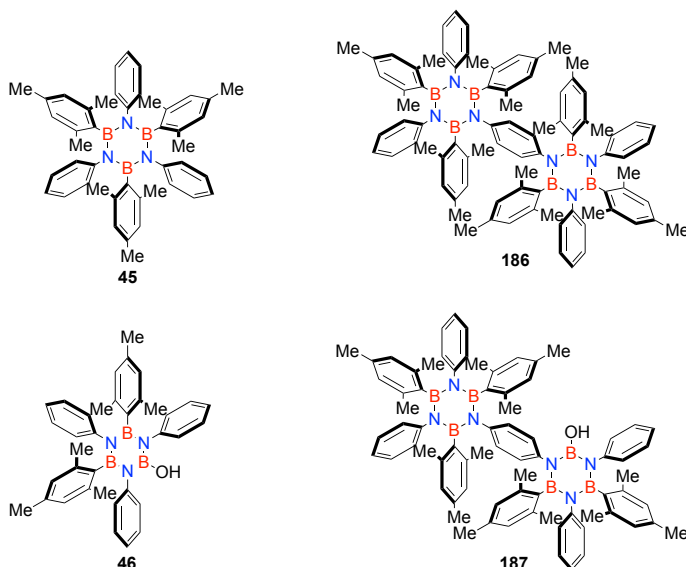
In a 20 mL Schlenk-type flask, **110** (0.24 mL, 2.61 mmol), **34a** (0.071 g, 0.65 mmol), and dry toluene (8 mL), were added. The mixture was stirred at 80 ˚C under Ar and BCl$_3$ (1 M in heptane, 5.00 mL, 5.00 mmol) was added dropwise. The resulting suspension was stirred under refluxing conditions for 18 h, then it was cooled down to r.t. and subjected to 5 FPT cycles to remove the excess of HCl. In parallel, to a solution of **126** (0.71 mL, 4.70 mmol) in dry THF (15 mL), ^{t}BuLi (1.7 M in hexane, 5.80 mL, 9.90 mmol) was added dropwise at -84 °C under Ar. The solution was allowed to warm at 0 °C and stirred for

10 min. The degassed toluene mixture was thus transferred to the organometallic-containing THF solution at 0°C and allowed to react for 16 h at r.t.. The final mixture was diluted with EtOAc (70 mL) and washed with water (3 × 100 mL) and brine (50 mL). The organic layer was dried over MgSO$_4$ and evaporated under reduced pressure. The products were purified by silica gel column chromatography (eluent: PE/CH$_2$Cl$_2$ 8:2) to afford **45** (61 mg, 10%) and **186** (18 mg, 2%) as white solids. Additionally, a mixture of other products was obtained. These were separated by Rec-GPC using CHCl$_3$ as eluent, to afford **187** (12 mg, 2%) and **46** (17 mg, 4%) as white solids.

186; mp: >300 ˚C. ^{1}H-NMR (Figure 31, section 3.3.1; 400 MHz, CDCl$_3$) δ: 6.69 (s, 20 H); 6.39 (s, 8 H); 6.29 (s, 4 H); 6.12 (s, 4 H); 2.15 (s, 12 H); 2.10 (s, 12 H); 1.95 (s, 6 H); 1.89 (s, 24 H). ^{13}C NMR (100 MHz, CDCl$_3$) δ: 146.18, 141.90, 137.38, 137.25, 136.53, 136.02, 135.45, 127.17, 126.47, 126.31, 126.12, 125.75, 123.98, 22.80, 22.50, 21.22, 21.07. IR (film in CH$_2$Cl$_2$) ν$_{max}$ (cm^{-1}): 3030.17, 2916.37, 2854.65, 2358.94, 2331.94, 1734.01, 1683.86, 1608.63, 1558.48, 1541.12, 1508.33, 1490.97, 1456.26, 1350.17, 1305.81, 1286.52, 1263.37, 1078.21, 1020.34, 846.75, 732.95, 698.23, 615.29, 578.64, 532.35, 418.55. MALDI-HRMS calc. for [C$_{84}$H$_{91}$N$_6$B$_6$]$^+$: 1248.7932; found: 1248.7616.

Synthesis of molecules 45, 186, and 188
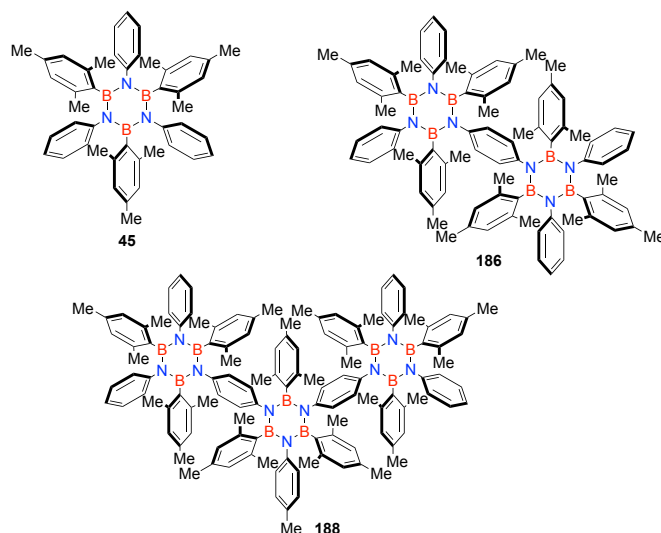
In a 20 mL Schlenk-type flask, **110** (0.26 mL, 2.80 mmol), **34a** (0.15 g, 1.40 mmol), and dry toluene (6 mL), were added. The mixture was stirred at 80 ˚C under Ar and BCl$_3$ (1 M in heptane, 6.00 mL, 6.00 mmol) was added dropwise. The resulting suspension was stirred under refluxing conditions for 18 h, then it was cooled down to r.t. and subjected to 5 FPT cycles to remove the excess of HCl. In parallel, to a solution of **126** (0.71 mL,

4.70 mmol) in dry THF (15 mL), ^{t}BuLi (1.7 M in hexane, 5.80 mL, 9.90 mmol) was added dropwise at -84 °C. The solution was allowed to warm at 0 °C and stirred for 10 min. The degassed toluene mixture was thus transferred to the organometallic-containing THF solution at 0 °C and allowed to react for 18 h at r.t.. The final mixture was diluted with EtOAc (90 mL) and washed with water (3 × 100 mL) and brine (50 mL). The organic layer was dried over MgSO$_4$ and evaporated under reduced pressure. The products were purified by silica gel column chromatography (eluent: PE/CH$_2$Cl$_2$ 8:2) to afford **45** (36 mg, 6%) as a white solid. Additionally, a mixture of other products was obtained. These were separated by Rec-GPC using CHCl$_3$ as eluent, to afford **186** (40 mg, 5%) and **188** (32 mg, 3%) as white solids.

Synthesis of molecules 190-193
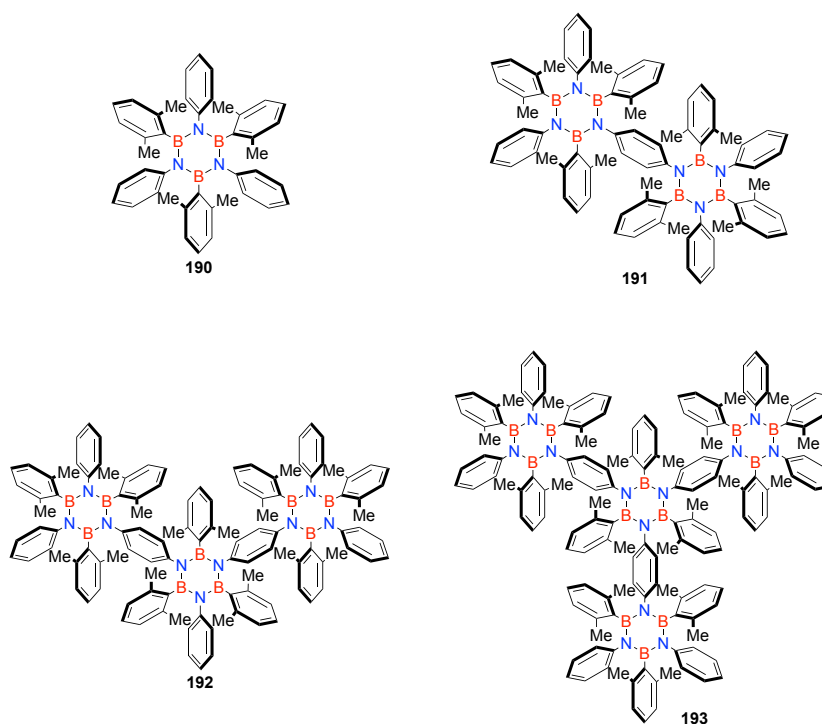
In a 20 mL Schlenk-type flask, **110** (0.32 mL, 3.48 mmol), **34a** (0.094 g, 0.87 mmol), and dry toluene (7 mL mL), were added. The mixture was stirred at 80 °C under Ar and BCl$_3$ (1 M in heptane, 5.80 mL, 5.80 mmol) was added dropwise. The resulting suspension was stirred under refluxing conditions for 18 h, then it was cooled down to r.t. and subjected to 5 FPT cycles to remove the excess of HCl. In parallel, to a solution of **189** (1.85 mL, 13.9 mmol) in dry THF (25 mL), ^{t}BuLi (1.7 M in hexane, 17.20 mL, 29.20 mmol) was added dropwise at -84 °C under Ar. The solution was allowed to warm up at 0 °C and stirred for 10 min. The degassed toluene mixture was thus transferred to the

organometallic-containing THF solution at 0°C and allowed to react for 18 h at r.t.. The final mixture was diluted with EtOAc (100 mL) and washed with water (3 × 100 mL) and brine (50 mL). The organic layer was dried over $MgSO_4$ and evaporated under reduced pressure. The products were purified by silica gel column chromatography (eluent: PE/CH_2Cl_2 7:3) to afford **190** (186 mg, 26%), **191** (80 mg, 8%), **192** (~10%) and **193** (<1%) as white solids.

190; mp: >300 ˚C. ^{1}H NMR (400 MHz, CDCl$_3$) δ: 6.87-6.84 (m, 6 H); 6.79-6.70 (m, 12 H); 6.54 (s, 3 H); 6.52 (s, 3 H); 2.30 (s, 18 H). ^{13}C NMR (100 MHz, CDCl$_3$) δ: 145.99, 137.39, 127.04, 126.86, 126.80, 125.29, 124.51, 23.17. IR (film in CH_2Cl_2) ν_{max} (cm^{-1}): 2916.37, 2358.94, 1734.01, 1683.86, 1610.56, 1558.48, 1541.12, 1508.33, 1490.97, 1456.26, 1074.35, 1018.41, 844.82, 750.31, 721.38, 698.23, 615.29, 578.64, 418.55.

191; mp: >300 ˚C. ^{1}H NMR (400 MHz, CDCl$_3$) δ: 6.84-6.79 (m, 6 H); 6.69 (s, 20 H); 6.56-6.47 (m, 12 H); 6.19 (4 H); 2.15 (s, 12 H); 1.94 (s, 24 H). ^{13}C NMR (100 MHz, CDCl$_3$) δ: 145.86, 142.00, 137.51, 137.44, 127.03, 126.72, 126.59, 125.80, 125.56, 125.27, 124.35, 23.02, 22.90. MALDI-HRMS calc. for [C$_{78}$H$_{78}$N$_6$B$_6$]$^+$: 1164.6846; found: 1164.6876. IR (film in CH_2Cl_2) ν_{max} (cm^{-1}): 2914.44, 2358.94, 1683.86, 1610.56, 1558.48, 1541.12, 1508.33, 1490.97, 1456.26, 1435.04, 1350.17, 1300.02, 1286.52, 1018.41, 844.82, 744.52, 698.23, 576.72.

Synthesis of 1,2-bis(2',6'-dimethyl-[1,1'-biphenyl]-4-yl)ethyne 199
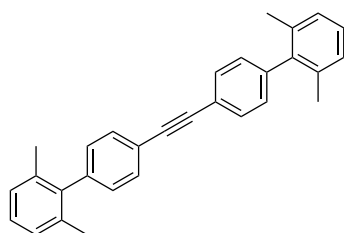
In a 20 mL Schlenk-type vessel, **134** (0.10 g, 0.30 mmol), **198** (0.095 g, 0.63 mmol), [Pd(PPh$_3$)$_4$] (0.020 g, 0.018 mmol), and K$_2$CO$_3$ (0.25 g, 1.80 mmol), were added and placed under N$_2$ atmosphere. Separately, a mixture of dioxane (7.5 mL) and water (1.5 mL) was degassed by N$_2$ bubbling under sonication for 1 h at 40 ˚C, then added to the flask containing the reagents. The mixture was stirred for 18 h at 100 °C, then it was diluted with EtOAc (20 mL) and washed with water (3 × 70 mL) and brine (70 mL). The organic layer was dried over MgSO$_4$ and evaporated under reduced pressure. The product crude was purified by silica gel column chromatography (eluent: PE/CH_2Cl_2 8:2) to afford

199 as a yellow solid (0.11 g, 98%); mp 201-203 °C. ^{1}H NMR (300 MHz, CDCl$_3$) δ: 7.63 (d, J = 8.0 Hz, 4 H); 7.15 (dd, J = 8.3, 3.4 Hz, 10 H); 2.06 (s, 12 H). EI-HRMS calc. for [C$_{30}$H$_{26}$]$^+$: 386.2035, found: 386.2039.

Synthesis of 1,2-bis(2',6'-dimethyl-[1,1'-biphenyl]-4-yl)ethane-1,2-dione 200
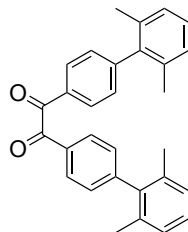
In a 250 mL round flask, 1,2-bis(2',6'-dimethyl-[1,1'-biphenyl]-4-yl)ethyne **199** (1.40 g, 3.64 mmol), acetone (70 mL), AcOH (3 mL), and KMnO$_4$ (1.27 g, 8.00 mmol), were added. The purple solution was stirred for 48 h at r.t. and then filtered through celite. The volatiles were removed under reduced pressure and the crude mixture re-dissolved in EtOAc (100 mL) and washed with water (3 × 100 mL) and brine (50 mL). The organic layer was dried over MgSO$_4$ and evaporated under reduced pressure to afford **200** as a yellow solid. (1.08 g, 70%); mp 145-148 °C. ^{1}H NMR (400 MHz, CDCl$_3$) δ: 8.11 (d, J = 8.1 Hz, 4 H); 7.35 (d, J = 8.1 Hz, 4 H); 7.21 (dd, J = 8.6, 6.2 Hz, 2 H); 7.13 (d, J = 7.3 Hz, 4 H); 2.04 (s, 12 H). ^{13}C NMR (100 MHz, CDCl$_3$) δ: 193.88, 148.31, 140.08, 135.19, 131.25, 130.04, 129.73, 127.49, 127.27, 20.56. API-HRMS calc. for [C$_{30}$H$_{27}$O$_2$]$^+$: 419.2011, found: 419.2007.

Synthesis of 3,4-bis(2',6'-dimethyl-[1,1'-biphenyl]-4-yl)-2,5-diphenylcyclopenta-2,4-dien-1-one 201
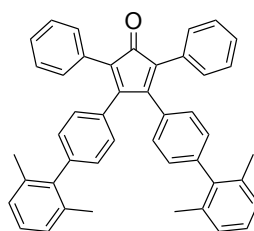
In a 10 mL round flask equipped with a condenser, 1,2-bis(2',6'-dimethyl-[1,1'-biphenyl]-4-yl)ethane-1,2-dione **200** (0.11 g, 0.27 mmol), 1,3-diphenylacetone **121** (0.057 g, 0.27 mmol) and EtOH (5 mL), were added and stirred under refluxing conditions. A solution of KOH (0.009 g, 0.136 mmol) in EtOH (0.2 mL) was added through the condenser in two portions. The yellow solution immediately turned dark red and after 20 min it was

cooled down to 0 ˚C, whereupon a precipitate formed. This was recovered by filtration and washed with cold EtOH to afford **201** as a dark red solid (0.096 g, 60%); mp 263-264 ˚C. ^{1}H NMR (400 MHz, CDCl$_3$) δ: 7.35-7.28 (m, 10 H); 7.21-6.92 (m, 14 H); 1.99 (s, 12 H). ^{13}C NMR (100 MHz, CDCl$_3$) δ: 154.68, 141.34, 141.21, 135.78, 131.78, 130.77, 130.15, 129.45, 128.73, 128.05, 127.55, 127.33, 124.91, 20.60. MALDI-HRMS calc. for [C$_{45}$H$_{37}$O]$^+$: 593.2844, found: 593.2865.

Synthesis of 4-(phenylethynyl)aniline 202
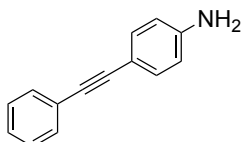
In a 50 mL Schlenk-type flask, DIPA (25 mL) was degassed by 4 FPT cycles. 4-iodoaniline **103** (2.00 g, 9.14 mmol), phenylacetylene (1.05 mL, 9.60 mmol), [Pd(PPh$_3$)$_2$Cl$_2$] (0.066 g, 0.098 mmol), and CuI (0.019 g, 0.098 mmol), were added and the mixture was furtherly degassed by 3 FPT cycles. The reaction mixture was stirred for 3 h at r.t., than it was diluted with EtOAc (50 mL) and washed with water (3 × 70 mL) and brine (70 mL). The organic layer was dried over MgSO$_4$ and evaporated under reduced pressure. The product was purified by recrystallization from hot hexane, to afford **202** as colourless crystalline solid (1.69 g, 95%); mp 168-170 ˚C. ^{1}H-NMR (400 MHz, CDCl$_3$) δ: 7.50 (dd, J = 7.8, 1.7 Hz, 2 H); 7.36-7.29 (m, 5 H); 6.64 (d, J = 8.5 Hz, 2 H); 3.82 (s, 2 H). ^{13}C-NMR (100 MHz, CDCl$_3$) δ: 146.76, 133.05, 131.44, 128.39, 127.78, 123.94, 114.84, 112.59, 90.24, 87.43. EI-HRMS calc. for [C$_{14}$H$_{11}$N]$^+$: 194.0970; found: 194.0985.

Synthesis of aniline-PPh 197
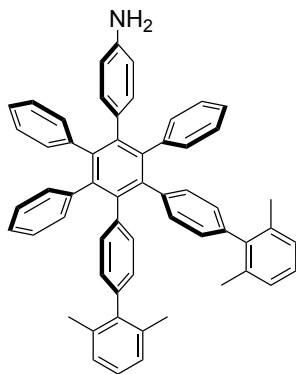
In a 10 mL Schlenk-type flask, 4-(phenylethynyl)aniline **202** (0.029 g, 0.15 mmol), 3,4-bis(2',6'-dimethyl-[1,1'-biphenyl]-4-yl)-2,5-diphenylcyclopenta-2,4-dien-1-one **201** (0.090 g, 0.15 mmol), and Ph$_2$O (0.5 mL), were added. The solution was degassed by N$_2$ bubbling for 30 min at 40 °C, then stirred for 4 h at 200 °C. The orange solution was diluted with CH$_2$Cl$_2$ (2 mL), then PE was slowly added until formation of a precipitate. This was recovered by filtration and washed with further PE (5 mL) to afford **197** as a white solid (0.095 g, 84%); mp >300 °C (degrad.). ^{1}H-NMR (400 MHz, CDCl$_3$) δ: 7.17-6.97 (m, 7 H); 6.96-6.82 (m, 18 H); 6.69-6.60 (m, 6 H); 6.25 (d, J = 6.9 Hz, 2 H); 3.36 (s, 2 H); 1.81 (s, 6 H); 1.78 (d, J = 3.3 Hz, 6 H). ^{13}C-NMR (100 MHz, CDCl$_3$) δ: 143.45, 141.90, 141.05, 140.99, 140.82, 140.51, 140.36, 140.20, 140.00, 139.44, 139.38, 137.72, 136.29, 135.80, 132.42, 131.66, 131.04, 127.18, 127.01, 126.93, 126.70, 126.64, 126.57, 125.10, 125.01, 124.92, 113.86, 20.51, 20.47. ESI-HRMS calc. for [C$_{58}$H$_{48}$N]$^+$: 758.3787; found: 758.3793.

Synthesis of 1,8-bis(dimethylsilyl)naphtalene 209
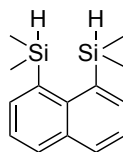
209

In a 10 mL Schlenk flask, 1,8-dibromonaphtalene **208** (0.21 g, 0.70 mmol), and dry THF (2 mL) were stirred at -84 °C while ^{n}BuLi (1.6 M in hexane, 1.10 mL, 1.76 mmol) was slowly added. The yellow solution was allowed to react at this temperature for 10 min, then at -15 °C for 5 min, then it was cooled down at -84 °C, whereupon DMSCl (0.31 mL, 2.82 mmol) was added dropwise and the reaction mixture allowed to slowly reach r.t.. After 15 h the colourless solution was diluted with PE (30 mL) and washed with water (2 × 40 mL) and brine (30 mL). The product was purified by silica gel column chromatography (eluent: PE) to afford **209** as a colourless oil (0.15 g, 89%). ^{1}H NMR (400 MHz, CDCl$_3$) δ: 7.84 (dd, J= 8.2, 1.3 Hz, 2 H); 7.80 (dd, J= 6.7, 1.1 Hz, 2 H); 7.45 (dd, J= 8.0, 6.9 Hz, 2 H); 5.05-4.97 (m, 2 H); 0.41 (d, J= 3.4 Hz, 12 H). ^{13}C NMR (100 MHz, CDCl$_3$) δ: 142.00, 138.84, 136.32, 134.25, 131.75, 125.04, 0.02, 0.00. ESI-HRMS calc. for [C$_{14}$H$_{20}$Si$_2$]$^+$: 244.1104, found: 244.1091.

Synthesis of triphenylene 211 through planarization reaction: silylium salt 206
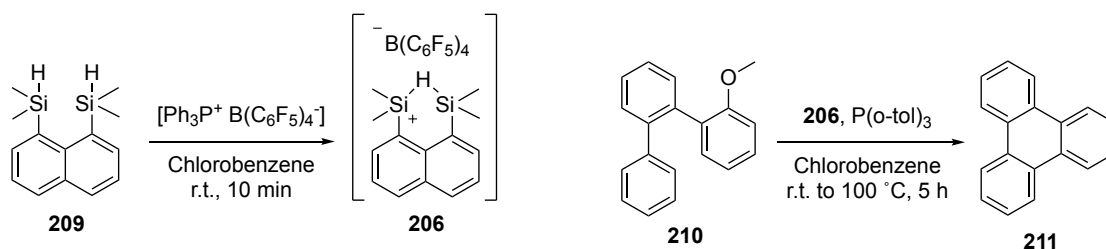
In a 10 mL Schlenk-type flask, **209** (0.026 g, 0.11 mmol) was added and placed under N_2. In a second 10 mL Schlenk-type flask, trityl TPFPB (0.10 g, 0.11 mmol) was dissolved in dry chlorobenzene (1.5 mL). The orange-yellow solution was slowly added to the vessel containing **209** under stirring at r.t., until colour persistence. To the pale-yellow solution containing salt **206** dry hexane was added until formation of an off-white precipitate. This was decanted and the solution removed with a syringe. The precipitate was then dissolved in dry chlorobenzene (1 mL) and added to a solution of 2-(2'-phenyl)-phenylanisole **210** (0.026 g, 0.10 mmol) and P(*o*-tol)₃ (0.034 g, 0.11 mmol) in dry chlorobenzene (2 mL). The final pale-yellow solution was stirred at r.t. for 1 h whereupon TLC analysis showed no substantial conversion. The reaction mixture was thus heated at 50 °C for 1 h. TLC analysis showed the formation of a new product. However, conversion remained poor even by increasing the temperature at 100 °C for 2 h. The mixture was diluted with EtOAc (30 mL) and washed with water (2 × 30 mL) and brine (30 mL). The organic layer was dried over MgSO₄ and evaporated under reduced pressure to a viscous pale-yellow oil (0.11 g). EI-HRMS analysis of the crude mixture revealed the mass of the desired product **211** (calc. for $[C_{18}H_{12}]^+$: 229.1017, found: 229.0997; Figure 131, section 4.7).

Attempted synthesis of triphenylene 211 through planarization reaction: use of the Hendrickson's 'POP' reagent 215
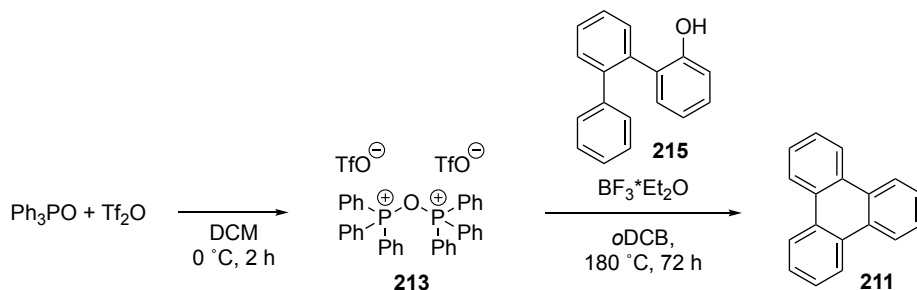
In a 10 mL Schlenk flask, Ph₃PO (0.34 g, 1.22 mmol), and dry CH₂Cl₂ (5 mL) were stirred at 0 °C while Tf₂O (0.10 mL, 0.60 mmol) was added. The pale-yellow solution was stirred at 0 °C for 1 h, then at r.t. for 30 min. A white precipitate formed. The volatiles were

removed under reduced pressure and to the pale-yellow solid a solution of 2-(2'-phenyl)-phenylphenol **215** (0.030 g, 0.12 mmol) in dry *o*DCB (3 mL), was added. The suspension was stirred under refluxing conditions and after 3 h it turned into a colourless solution. TLC analysis of the reaction mixture showed no conversion of the starting material. $BF_3 \cdot Et_2O$ (0.15 mL, 1.22 mmol) was added and the solution was refluxed for further 24 h. TLC showed poor conversion together with formation of a new product. The reaction mixture was diluted with EtOAc (30 mL) and washed with water (2 × 30 mL) and brine (30 mL). The organic layer was dried over $MgSO_4$ and evaporated to a brownish solid. EI-LRMS of the crude mixture confirmed the presence of a trace of the desired product **211** through detection of the signal at 228.09 g/mol (Figure 132, section 4.7).

4.5 Crystallographic data

Complete crystallographic structural characterization for molecules **124**, **186**, **196**, **197**, **198** were performed by *Nicola Demitri* at the X-ray diffraction beamLine (XRD1) of the Elettra Synchrotron, Trieste (Italy), with a Pilatus 2M Pilatus 2M hybrid-pixel area detector (DECTRIS Ltd., Baden-Daettwil, Switzerland). Complete datasets were collected at 100 K (nitrogen stream supplied through an Oxford Cryostream 700) with a monochromatic wavelength of 0.700 Å through the rotating crystal method. All the crystals were dipped in N-paratone or NHV oil (Jena Bioscience, Jena, Germany) and mounted on the goniometer head with kapton loops (MiTeGen, Ithaca, USA). Complete dataset for the triclinic crystal **124** form has been obtained merging two different data collections done on the same crystal, mounted with different orientations. For triclinic **191** crystal form, two different datasets collected from two different random orientations, have been merged using CCP4-AimLess code.[316,317] The diffraction data were indexed, integrated and scaled using XDS.[318] The structures were solved by direct methods using SIR2014,[319] Fourier analyzed and refined by the full-matrix least-squares based on F^2 implemented in SHELXL-2014.[320] The Coot program was used for modeling.[321] Anisotropic thermal motion was then applied to all atoms excluding disordered solvent molecules. Hydrogen atoms were included at calculated positions with isotropic $U_{factors}$ = 1.2 U_{eq} or $U_{factors}$ = 1.5 U_{eq} for methyl and hydroxyl groups. Restrain on bond lengths, angles and thermal motion (DFIX, DANG, SIMU and DELU) for disordered fragments and solvent molecules have been applied. One crystallographically independent moiety is present in compound **124** asymmetric unit (ASU) where also a solvent site is partially occupied by dichloromethane (60% of crystal cells) and methanol (40% of crystal cells) (Figure 39). For both structures crystal packing shows weak hydrophobic interactions with limited π-π and CH-π interactions; oxygen atom present in **124** coordinates a solvent methanol molecule, through hydrogen bond. Essential crystal and refinement data (Table 6) are reported below. None of the **192** crystals tested diffracted better than ~1.0 Å: this is consistent with the presence of huge voids in the crystal packing, filled with disordered solvent molecules. Electron content of cavities have been estimated with the SQUEEZE routine of PLATON. One ordered pentane molecule (with 50% occupancy) has been modeled in the asymmetric unit (ASU) of **192**, while not construable residual density has been squeezed (3098 electrons in 46%, 12399 Å^3, of the unit cell volume). The disordered solvent has been estimated as additional 11.5 pentane molecules in the ASU;

contributions of these molecules have been included in the properties reported in Table 6 and Table 7. Anisotropic thermal motion refinement has been used for all atoms, while disordered fragments of **192** have been treated isotropically. Hydrogen atoms were included at calculated positions with isotropic $U_{factors} = 1.2\ U_{eq}$ or $U_{factors} = 1.5\ U_{eq}$ for methyl groups (U_{eq} being the equivalent isotropic thermal factor of the bonded non-hydrogen atom). Restrains on bond lengths, angles and thermal motion parameters (DFIX, DANG, SIMU and DELU) have been applied on disordered borazine fragments (in **191** and **192**) and for pentane molecule (in **192**). Pictures were prepared using Ortep3[322] and Pymol[323] software. Essential crystal and refinement data are reported below (Table 7). Crystal forms of **190**, **191** and **192** are described by one complete molecule in the asymmetric unit (ASU; Figure 40). 186 structure has half molecule in the asymmetric unit and the full model is generated through an inversion center lying in the barycenter of the phenyl ring, that links borazine moieties. Crystal packing views (Figure 41, Figure 42, Figure 43, and Figure 44) show compact arrangements of molecules connected through hydrophobic interactions, with limited π-π and CH-π interactions. **192** packing show large channels (with a diameter of ~32 Å) aligned with crystallographic axis.
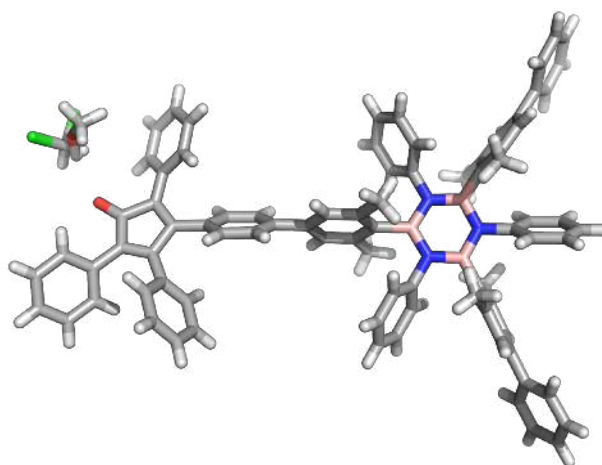
Figure 39. X-ray structure of **124** ($C_{83}H_{68}B_3N_3O$; stick representation). The ASU contain also a solvent site partially occupied by a methanol or a dichloromethane molecule.

Table 6. Crystallographic data and refinement details for compound **124** ($C_{83}H_{68}B_3N_3O$).

CCDC Number	1418729 (**124**)
Sum Formula	$C_{84}H_{70.80}B_3Cl_{1.20}N_3O_{1.40}$
Formula weight (Da)	1219.61
Temperature (K)	100(2)
Wavelength (Å)	0.700
Crystal system	Triclinic
Space Group	P -1
a (Å)	14.339(3)
b (Å)	14.788(3)
c (Å)	17.315(4)
α (°)	77.56(3)
β (°)	72.01(3)
γ (°)	70.78(3)
V ($Å^3$)	3271.0(14)
Z	2
ρ ($g \cdot cm^{-3}$)	1.238
F(000)	1285
μ (mm^{-1})	0.115
θ min,max (°)	1.2, 24.3
Resolution (Å)	0.85
Total refl. collctd	19281
Independent refl.	10976 [R(int) = 0.0340]
Obs. Refl. [Fo>4σ(Fo)]	8854
I/σ(I) (all data)	28.90
I/σ(I) (max resltn)	7.90
Completeness (all data)	0.99
Completeness (max resltn)	0.98
Rmerge (all data)	0.051
Rmerge (max resltn,)	0.224
Multiplicity (all data)	4.6
Multiplicity (max resltn)	4.6
Data/restraint/parameters	10976/12/839
Goof	1.030
$R_1{}^a$ [I>2.0σ(I)], wR$_2{}^a$	0.0935, 0.2576
$R_1{}^a$ (all data), wR$_2{}^a$ (all	0.1090, 0.2743

$^a R_1 = \Sigma \, |Fo| - |Fc| \, / \, \Sigma |Fo|$, $wR_2 = [\Sigma \, w \, (Fo^2 - Fc^2)^2 \, / \, \Sigma w \, (Fo^2)^2]^{1/2}$.

Table 7. Crystallographic data and refinement details for 191, 196, 197 and 198.

	186	**190**	**191**	**192·12C$_5$H$_{12}$**
Chemical Formula	C$_{84}$H$_{90}$B$_6$N$_6$	C$_{42}$H$_{42}$B$_3$N$_3$	C$_{78}$H$_{78}$B$_6$N$_6$	C$_{174}$H$_{258}$B$_9$N$_9$
Formula weight	1248.47	621.21	1164.32	2573.17
Temperature (K)	100(2)	100(2)	100(2)	100(2)
Wavelength (Å)	0.700	0.700	0.700	0.700
Crystal system	Orthorhombic	Monoclinic	Triclinic	Trigonal
Space Group	*P bca*	*C c*	*P* -1	*P* -3
Unit cell dimensions	a = 21.268(4)	a =	a =	a = 50.994(7) Å
	b = 14.952(3)	b =	b =	b = 50.994(7) Å
	c = 22.475(5)	c =	c =	c = 12.034(2) Å
	α = 90°	α = 90°	α =	α = 90°
	β = 90°	β =	β =	β = 90°
	γ = 90°	γ = 90°	γ = 68.48(3)°	γ = 120°
Volume (Å^3)	7147(2)	3532.8(13)	3331.8(14)	27101(9)
Z	4	4	2	6
Density (calculated)	1.160	1.168	1.161	0.946
Absorption coefficient	0.037	0.064	0.064	0.051
F(000)	2664	1320	1236	8460
Crystal size (mm^3)	0.50 x 0.12 x	0.10 x 0.10 x	0.05 x 0.03 x	0.05 x 0.05 x 0.03
Crystal habit	Colorless	Colorless	Colorless	Colorless thin rods
Theta range for data collection	1.78° to 30.96°	1.85° to 30.00°	1.06° to 30.00°	0.91° to 20.07°
Resolution (Å)	0.68	0.70	0.70	1.02
Index ranges	-31 ≤ h ≤ 31	-17 ≤ h ≤ 17	-17 ≤ h ≤ 17	-49 ≤ h ≤ 49
	-21 ≤ k ≤ 21	-28 ≤ k ≤ 28	-21 ≤ k ≤ 21	-49 ≤ k ≤ 49
	-31 ≤ l ≤ 31	-19 ≤ l ≤ 19	-28 ≤ l ≤ 28	-11 ≤ l ≤ 11
Reflections collected	78255	33042	96765	100789
Independent reflections	11797	10445	19920	17798 (9777)
Data multiplicity (max	6.36 (5.59)	5.53 (4.80)	4.76 (4.21)	5.66 (5.75)
I/σ(I) (max resltn)	29.85 (18.18)	38.86	20.50 (9.47)	8.73 (1.93)
R$_{merge}$ (max resltn)	0.0331	0.0350	0.0357	0.0822 (0.5901)
Data completeness	99.3%	97.1%	97.9%	99.9% (99.8%)
Refinement method	Full-matrix	Full-matrix	Full-matrix	Full-matrix
Data / restraints / parameters	11797 / 0 / 443	10445 / 2 / 440	19920 / 256 / 1079	17798 / 141 / 894
Goodness-of-fit on F^2	1.030	1.039	1.067	1.047
Δ/σ$_{max}$	0.001	0.001	0.005	0.009
Final R indices	R$_1$ = 0.0496,	R$_1$ = 0.0325,	R$_1$ = 0.0615,	R$_1$ = 0.1352,
R indices (all data)^a	R$_1$ = 0.0539,	R$_1$ = 0.0325,	R$_1$ = 0.0729,	R$_1$ = 0.1810,
Largest diff. peak and hole (e·Å^{-3})	0.482 and -0.245	0.323 and -0.225	0.452 and -0.374	0.463 and -0.595
R.M.S.	0.057	0.047	0.040	0.051

a)

b)

c)

d)
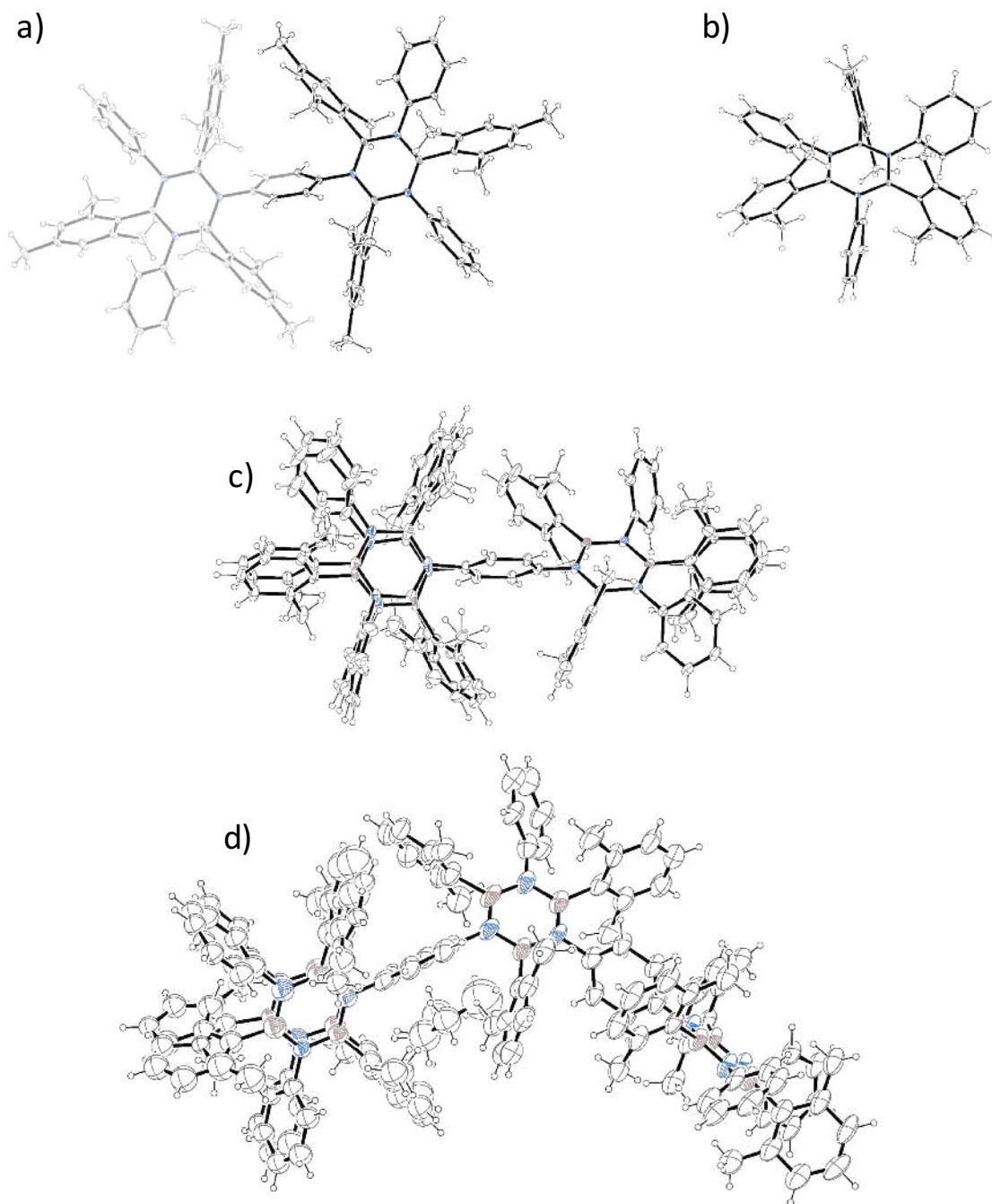
Figure 40. Ellipsoids representation of ASU contents (50% probability) for: a) **186**, b) **190**, c) **191** and d) **192**.
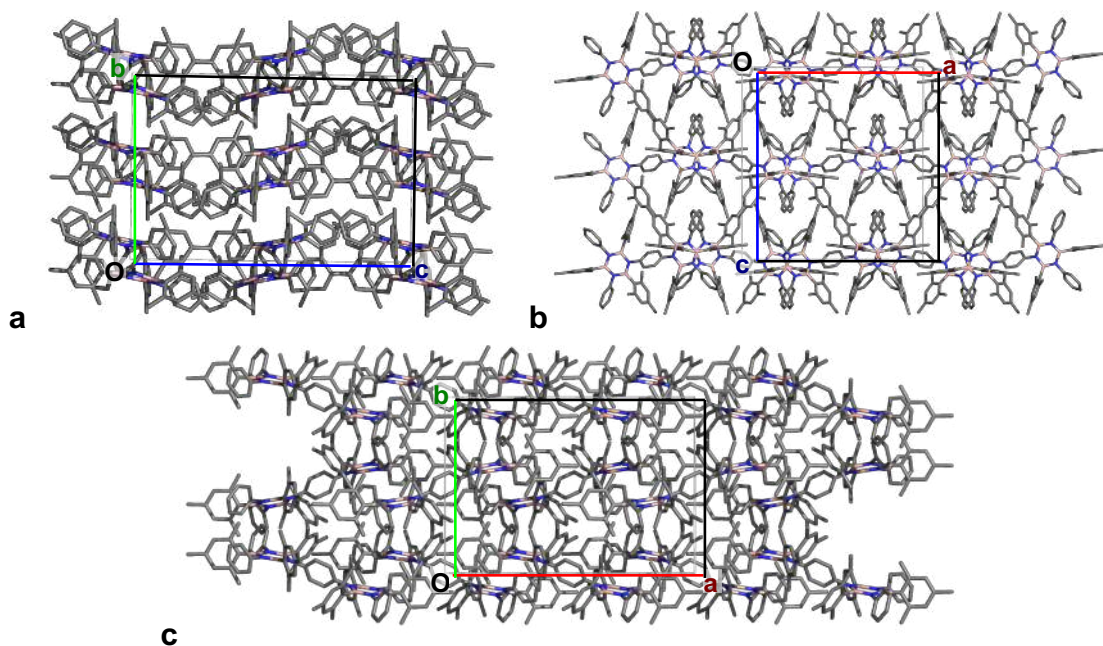
Figure 41. Crystal packing views of **186** along crystallographic a, b and c directions (hydrogens and disorder omitted for clarity).
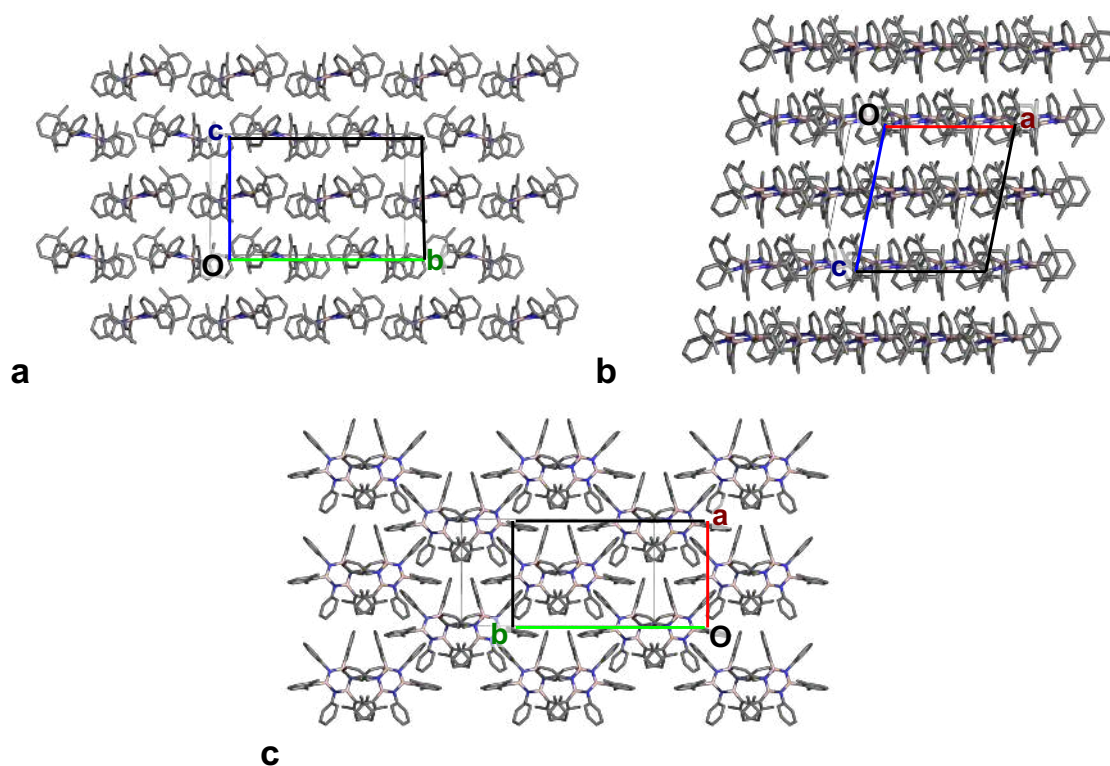
Figure 42. Crystal packing views of **190** along crystallographic a, b and c directions (hydrogens and disorder omitted for clarity).
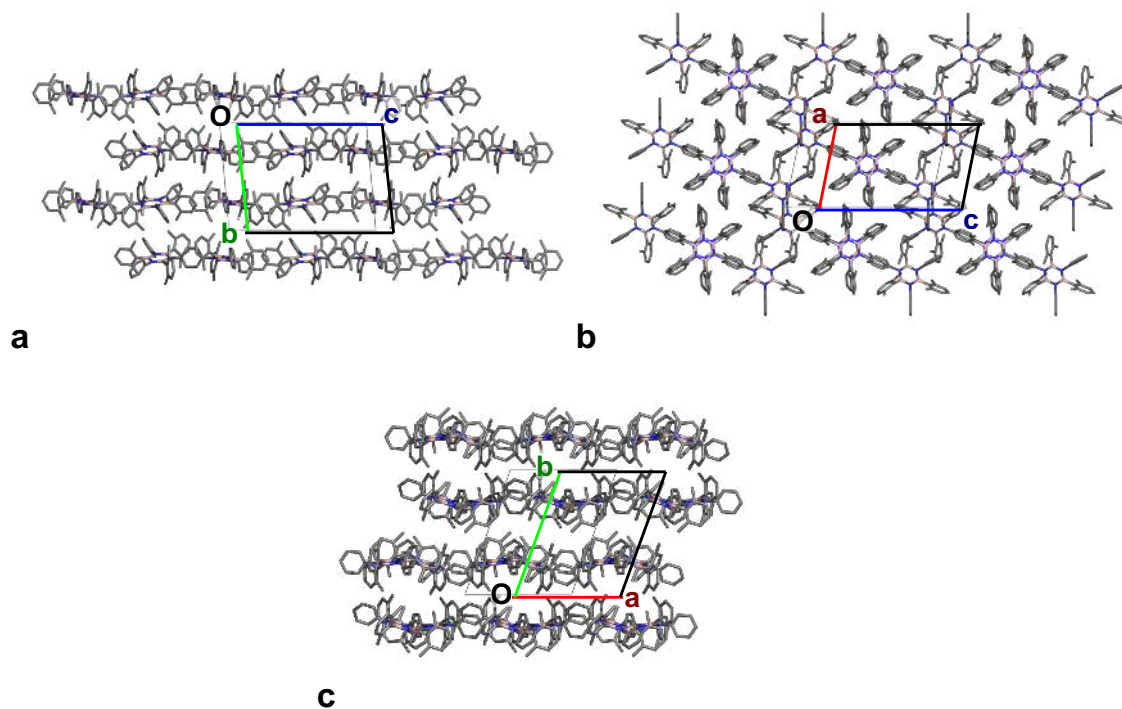
Figure 43. Crystal packing views of **191** along crystallographic a, b and c directions (hydrogens and disorder omitted for clarity).
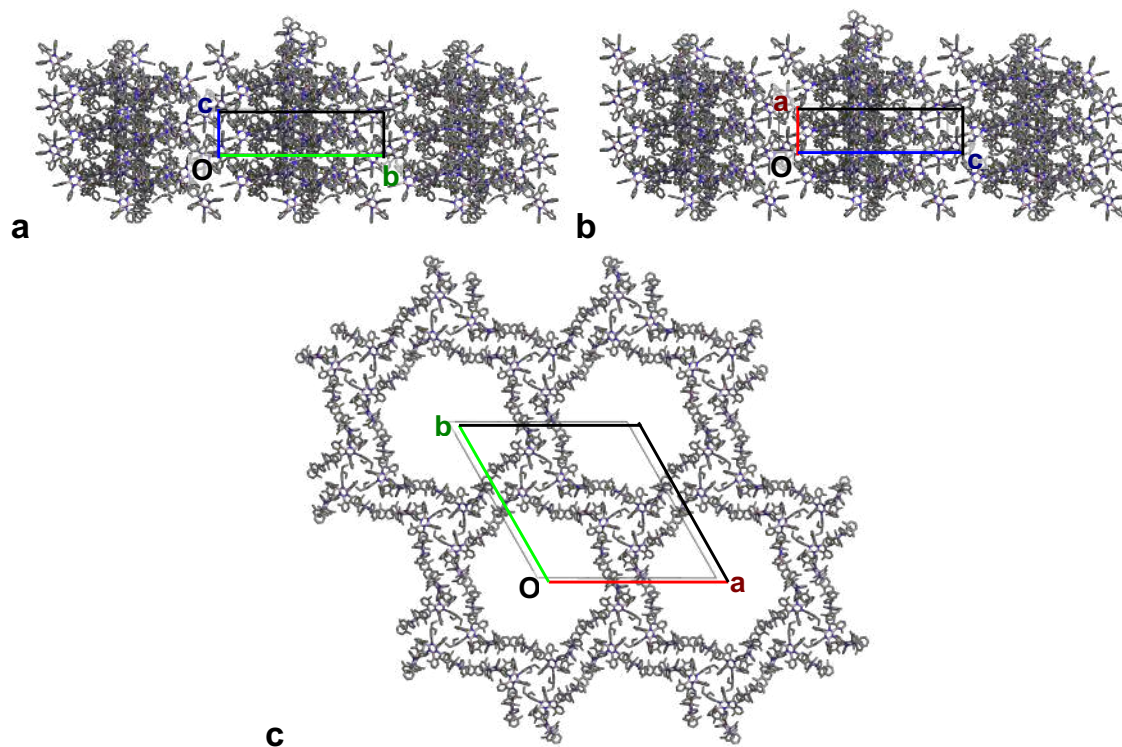
Figure 44. Crystal packing views of **192** along crystallographic a, b and c directions (hydrogens and disorder omitted for clarity).

4.6 Appendix

The structural characterization and spectral details (MALDI-mass spectrometry, ^{1}H-NMR, ^{13}C-NMR, ^{11}B-NMR, and Rec-GPC traces) referred to the molecules presented in this manuscript were recently published.[117] In this section, the characterization of the hexa-branched polyphenylene derivatives **147-159,** is presented. Furthermore, the characterization details for molecules **119**, **120**, **122**, **131**, **133**, **134**, **174**, **180**, **181**, **182**, **190**, **191**, **197**, **199**, **200**, **201**, **202**, are included.

Characterization of 119
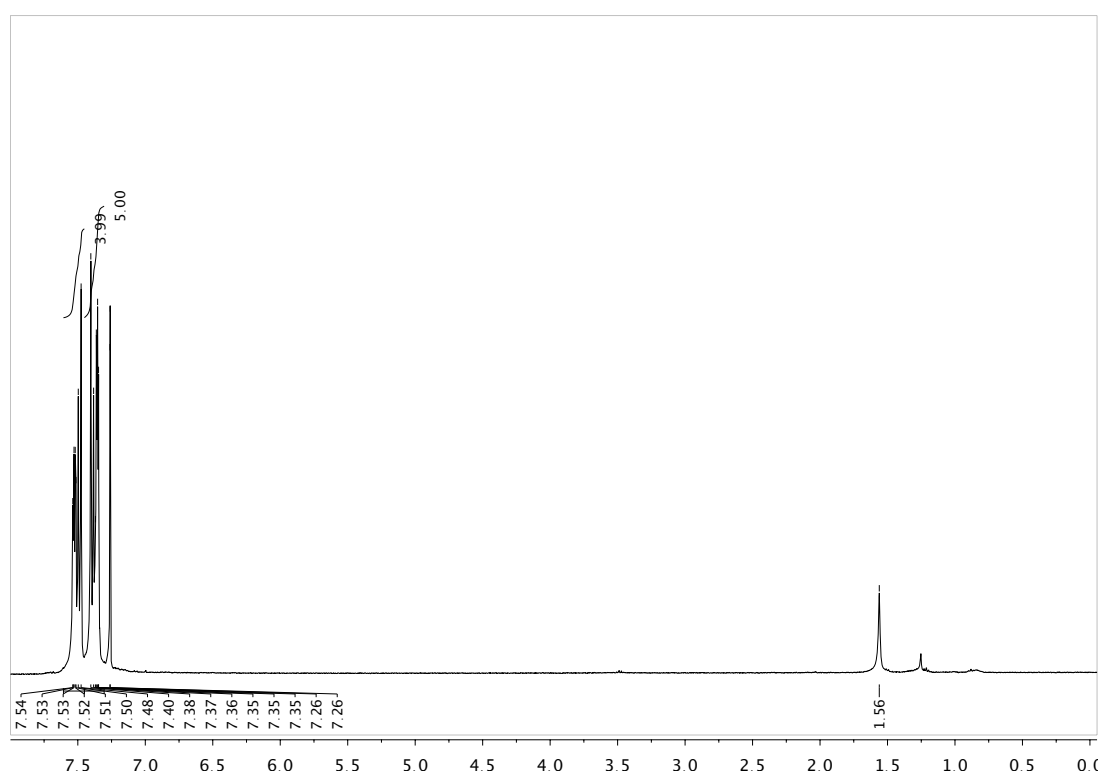
Figure 45. ^{1}H NMR spectrum of **119** in CDCl$_3$ (400 MHz).
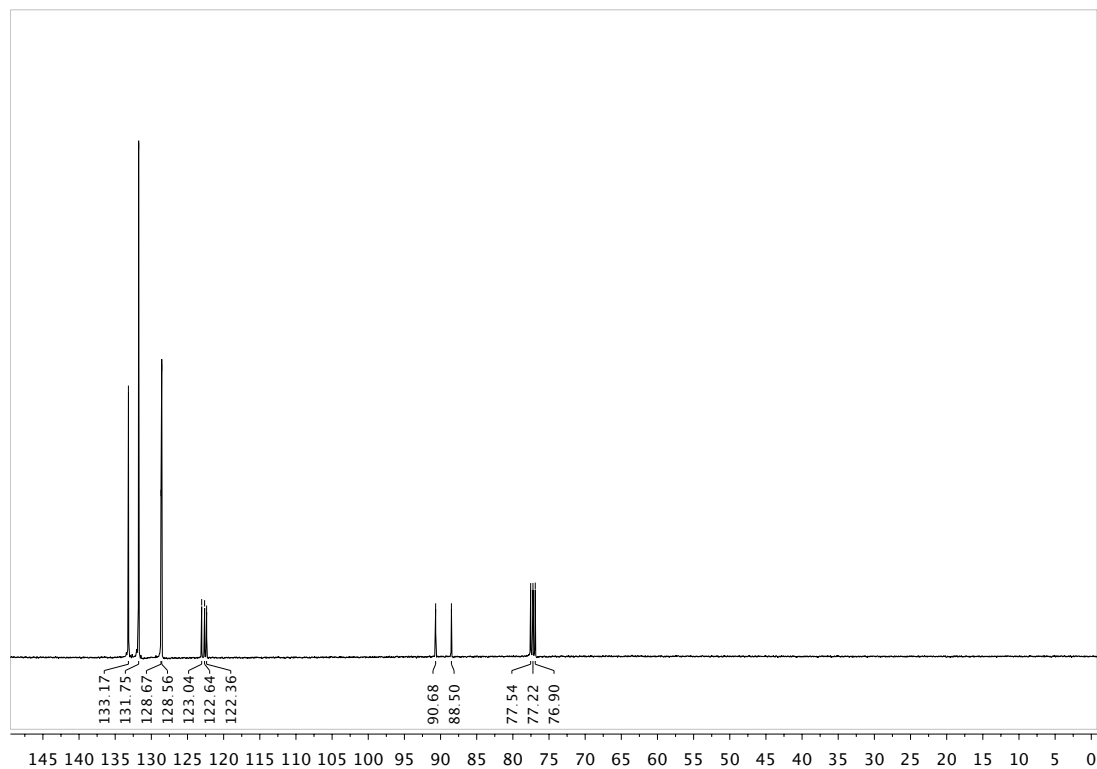
Figure 46. ^{3}C NMR spectrum of **119** in CDCl$_3$ (100 MHz).

Characterization of 120
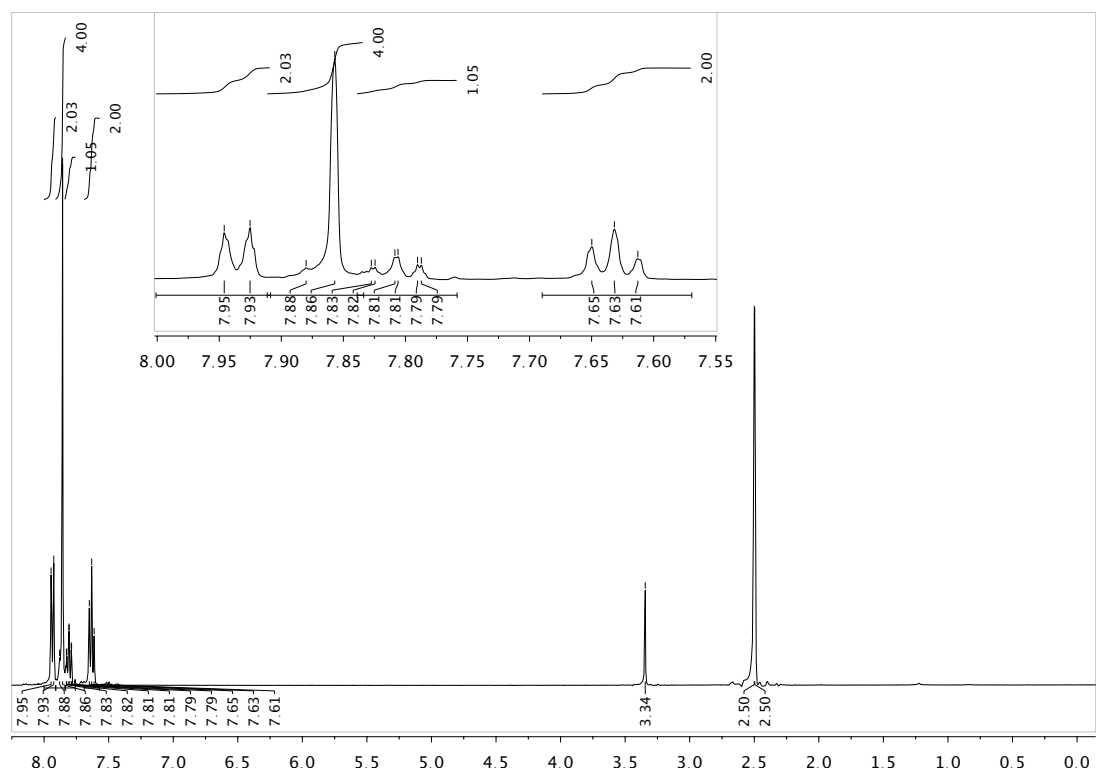
Figure 47. ^{1}H NMR spectrum of **120** in DMSO-d$_6$ (400 MHz).
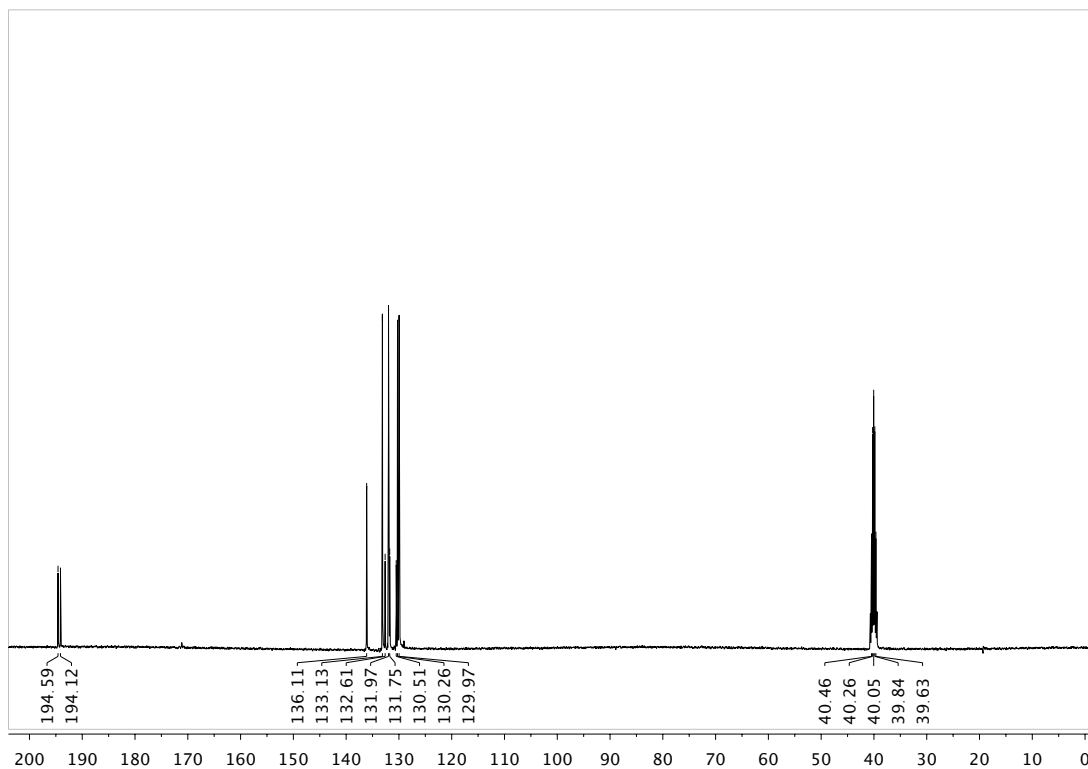
Figure 48. ^{13}C NMR spectrum of **120** in DMSO-d$_6$ (100 MHz).

Characterization of 122
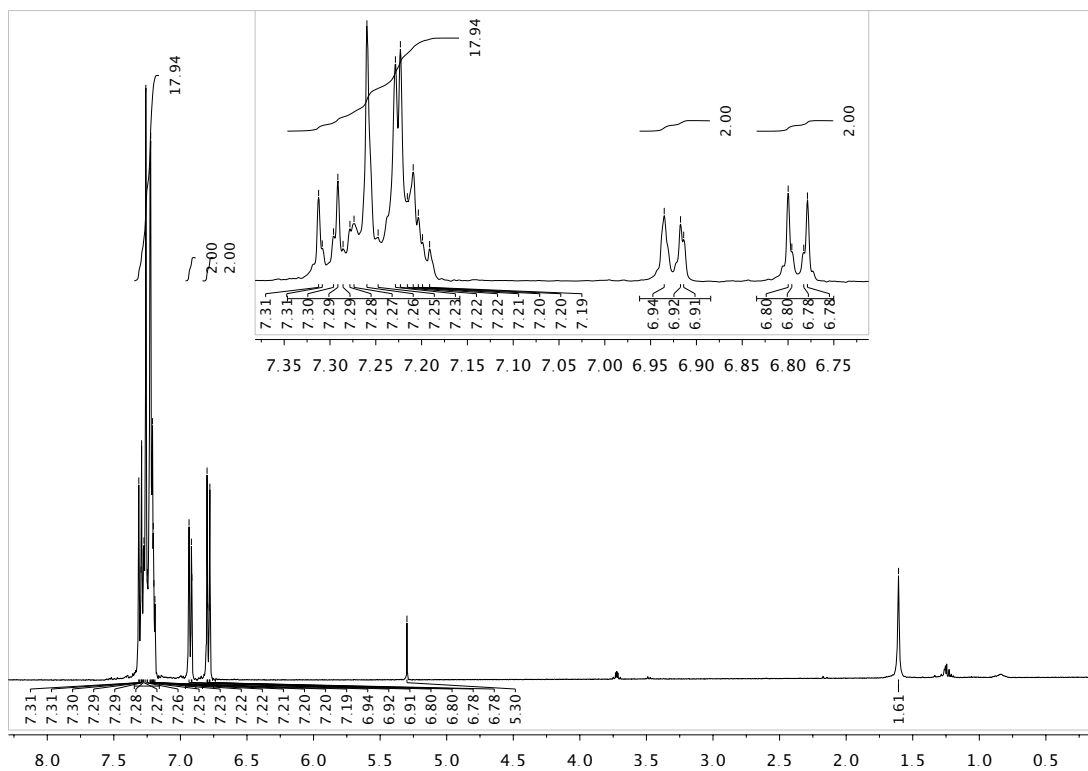
Figure 49. ^{1}H NMR spectrum of **122** in CDCl$_3$ (400 MHz).
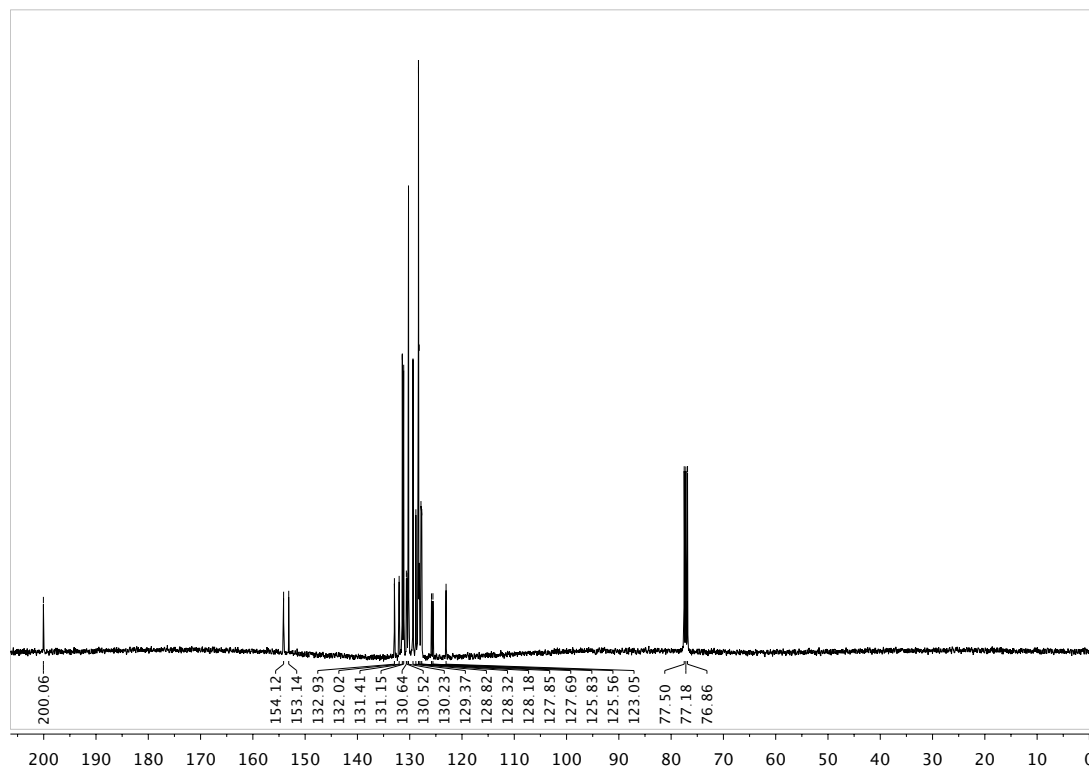
Figure 50. ^{13}C NMR spectrum of **122** in CDCl$_3$ (100 MHz).

Characterization of 131
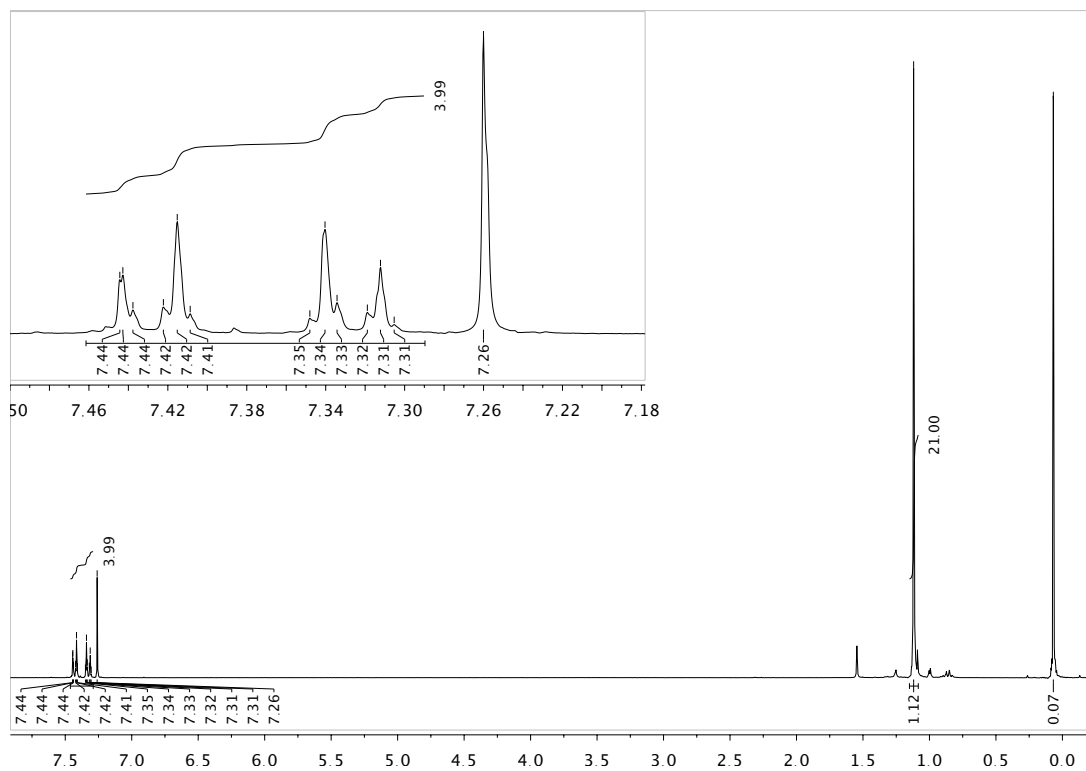
Figure 51. ^{1}H NMR spectrum of **131** in CDCl$_3$ (400 MHz).
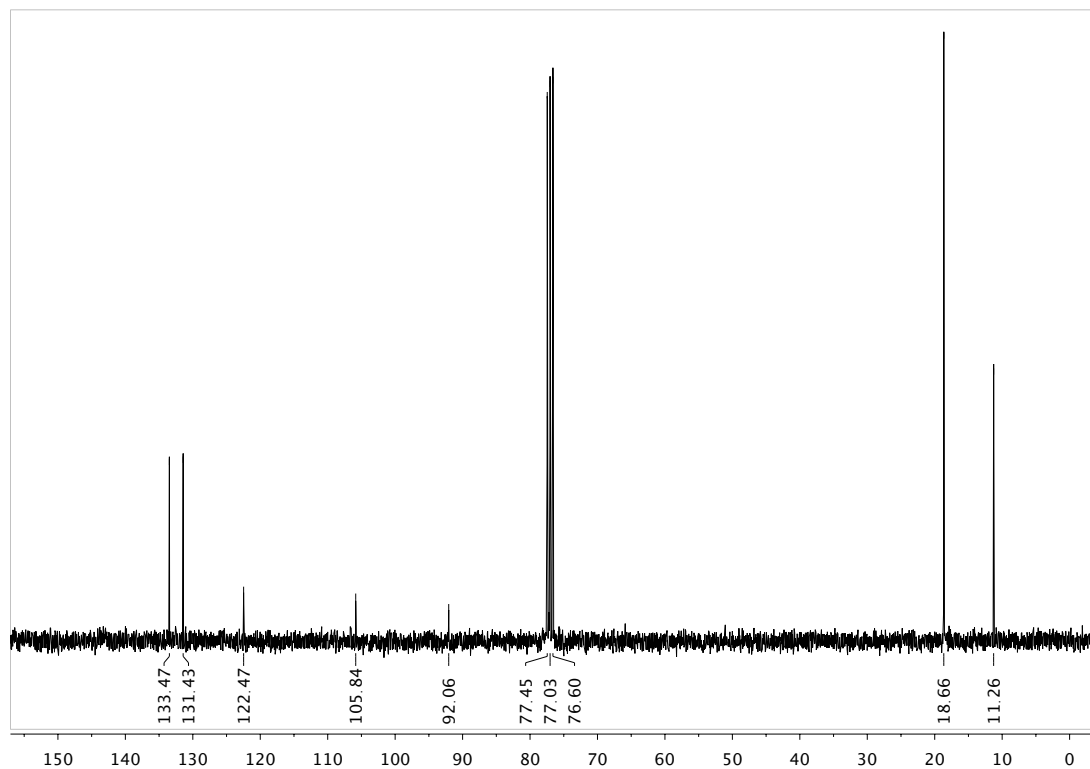
Figure 52. ^{13}C NMR spectrum of **131** in CDCl$_3$ (100 MHz).

Characterization of 133
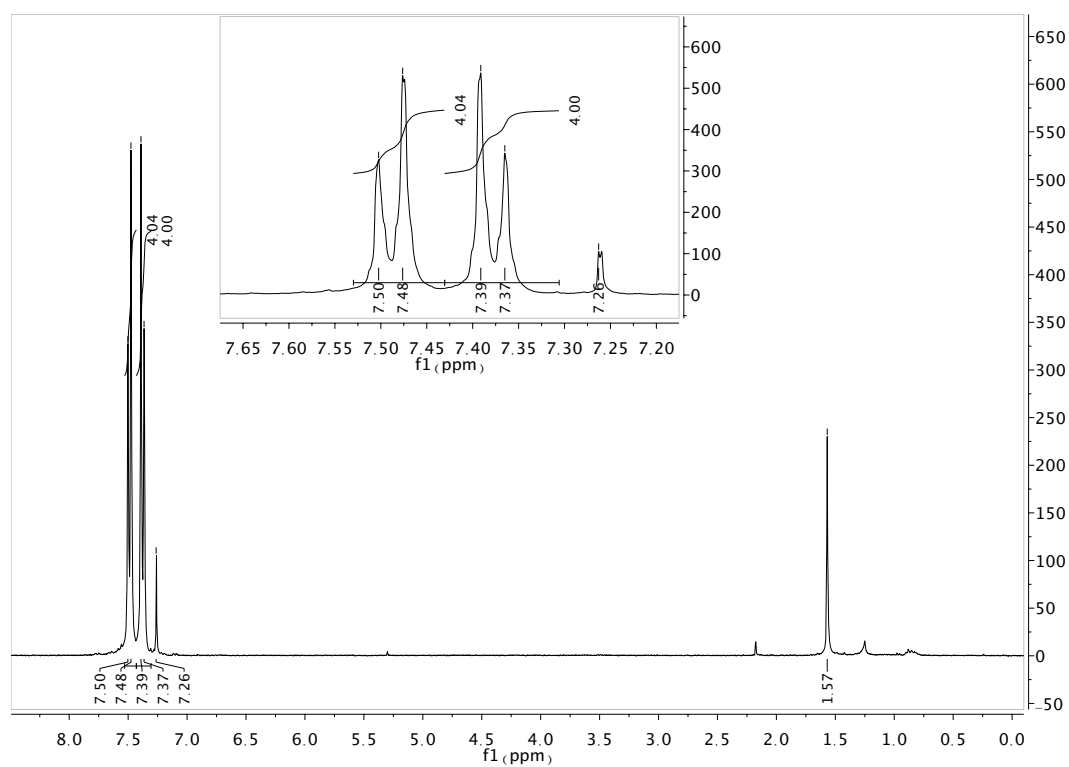
Figure 53. ^1H NMR spectrum of **133** in CDCl$_3$ (400 MHz).

Characterization of 134
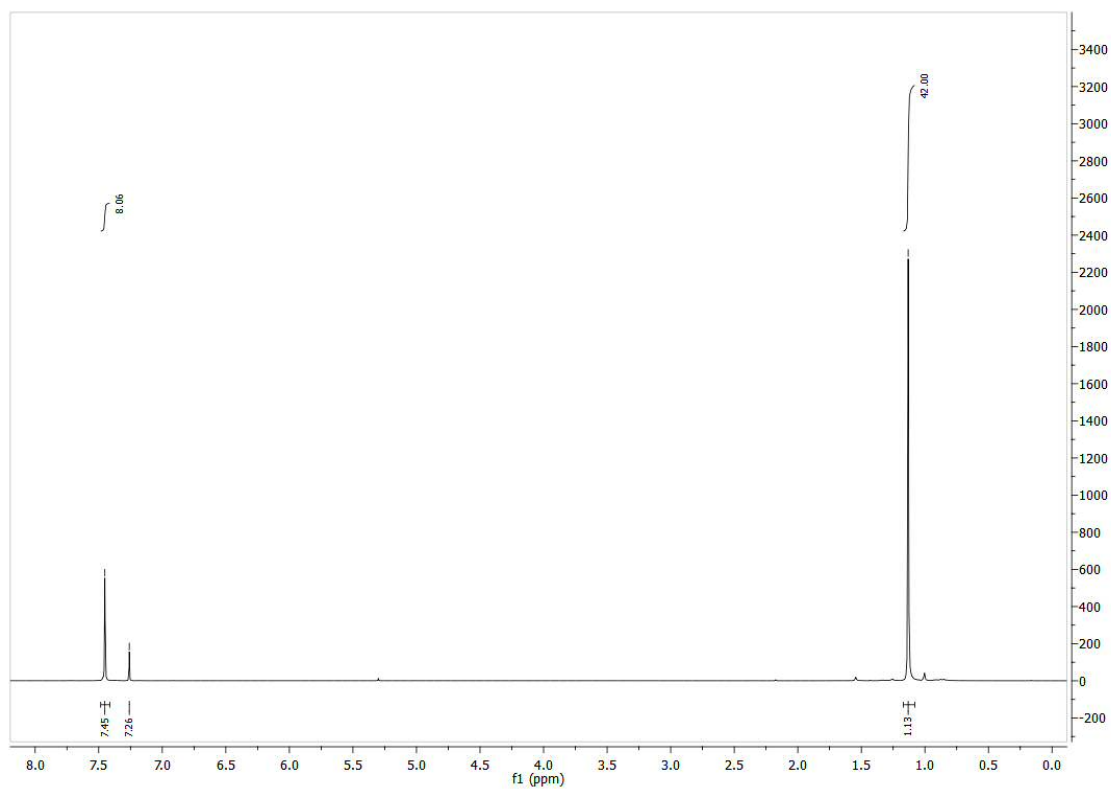
Figure 54. ^{1}H NMR spectrum of **134** in CDCl$_3$ (400 MHz).
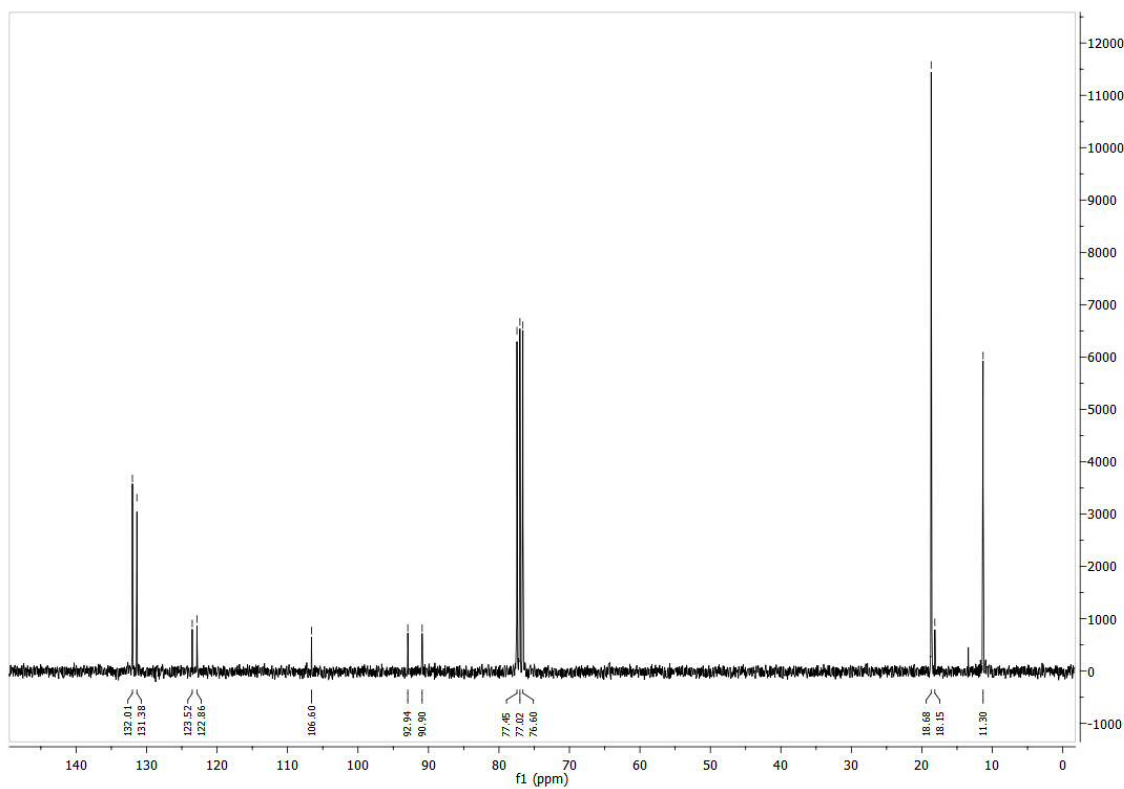
Figure 55. ^{13}C NMR spectrum of **134** in CDCl$_3$ (100 MHz).

Characterization of 147
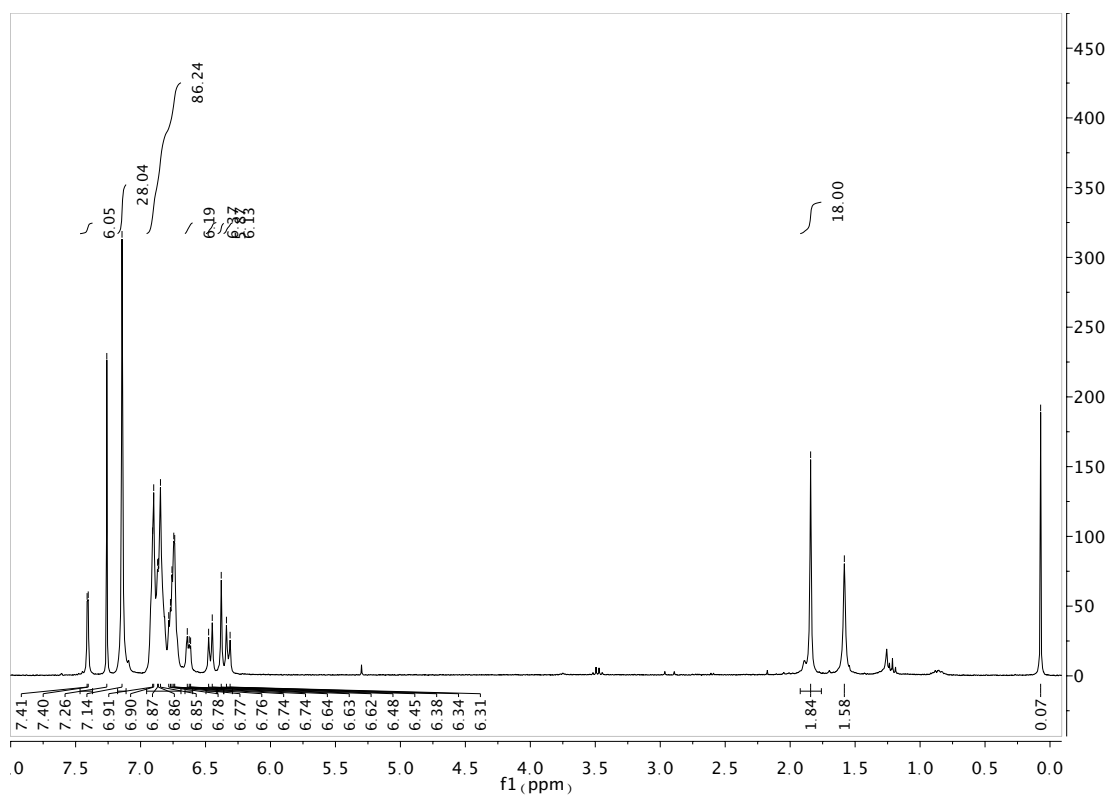
Figure 56. ^{1}H NMR spectrum of **147** in CDCl$_3$ (300 MHz).
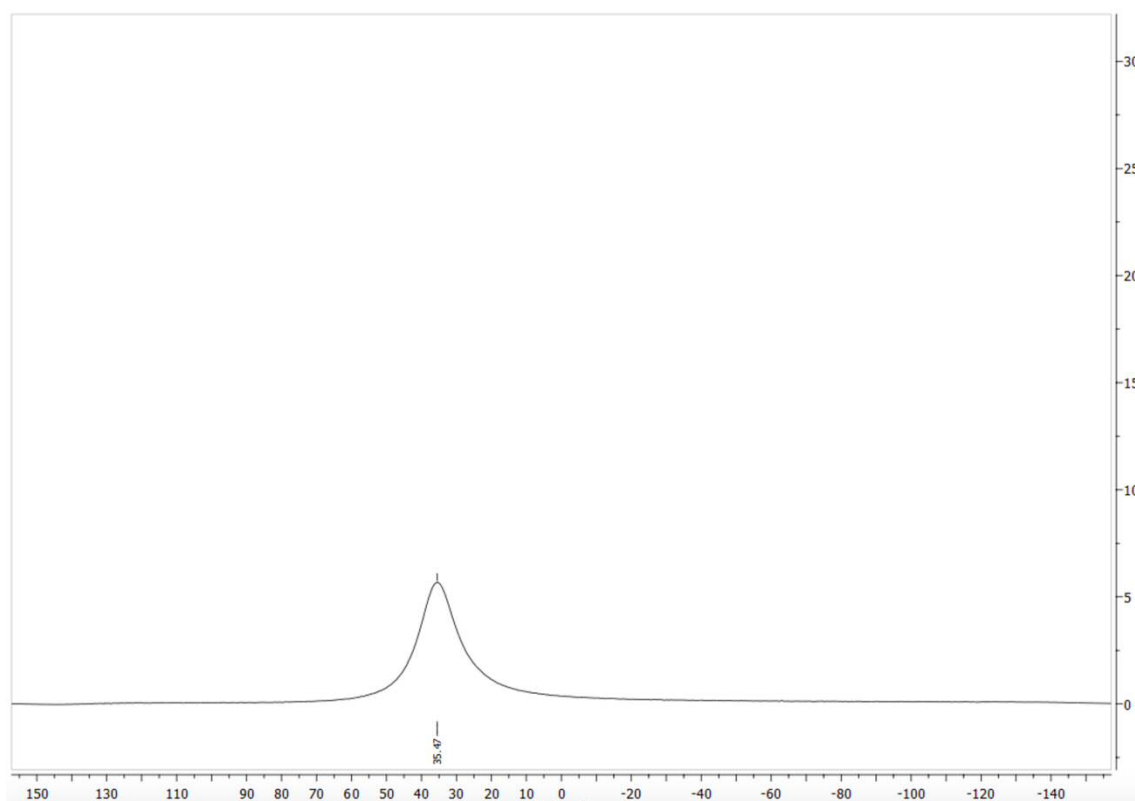
Figure 57. ^{11}B NMR spectrum of **147** in CDCl$_3$ (128 MHz).

Characterization of 148
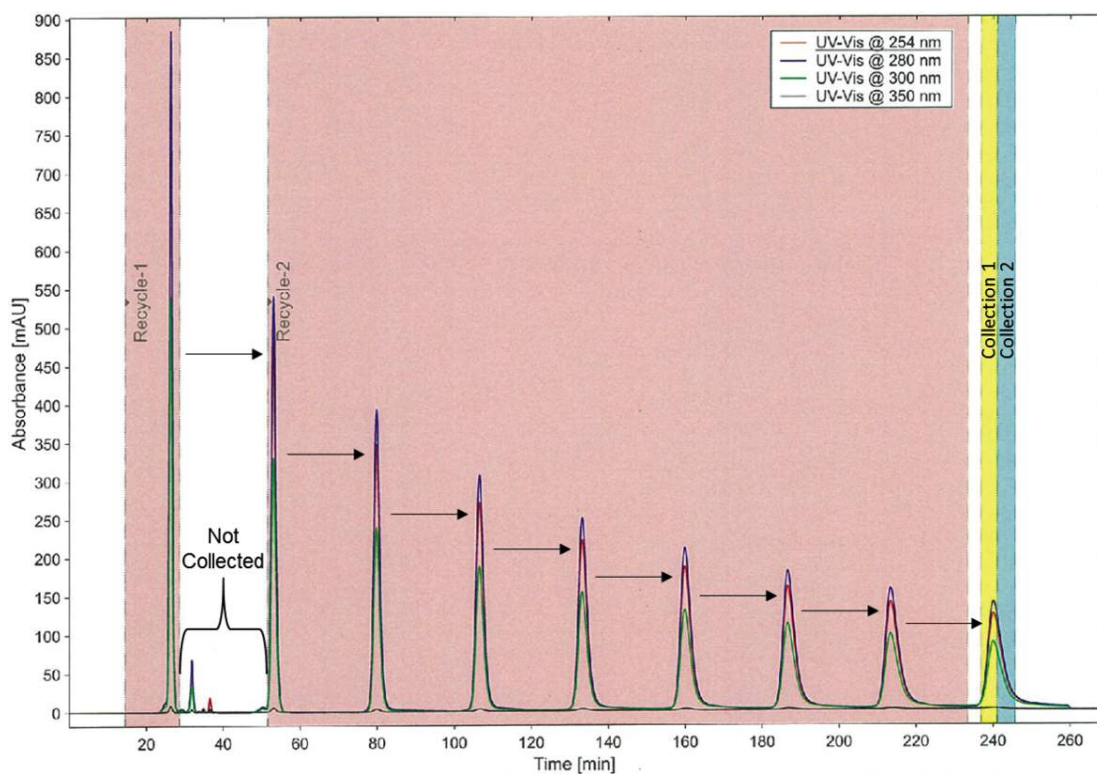
Figure 58. Gel permeation chromatography (GPC) for **148**, Recycling mode. Eluent: CHCl₃.
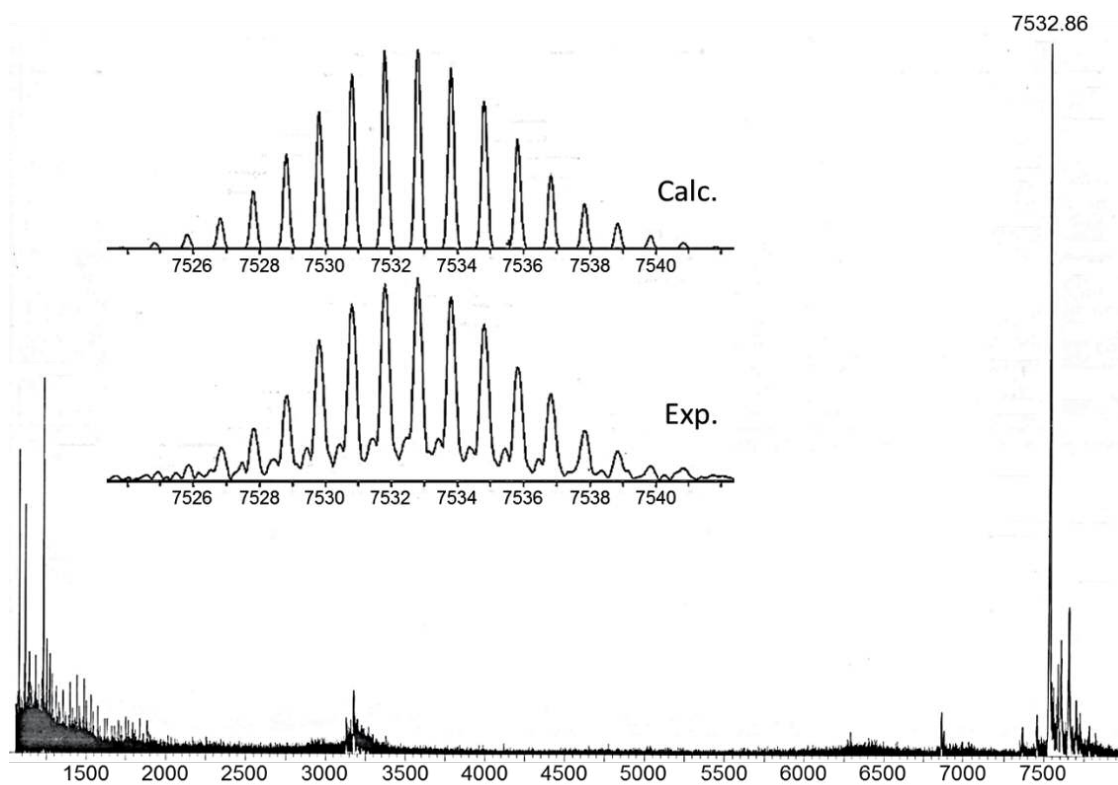
Figure 59. MALDI-TOF mass spectrometry of **148** (collection 1, from GPC run, above), matrix: trans-2-[3-(4-tert-butyl-phenyl)-2-methyl-2-propenylidene]malonitrile (DCTB).
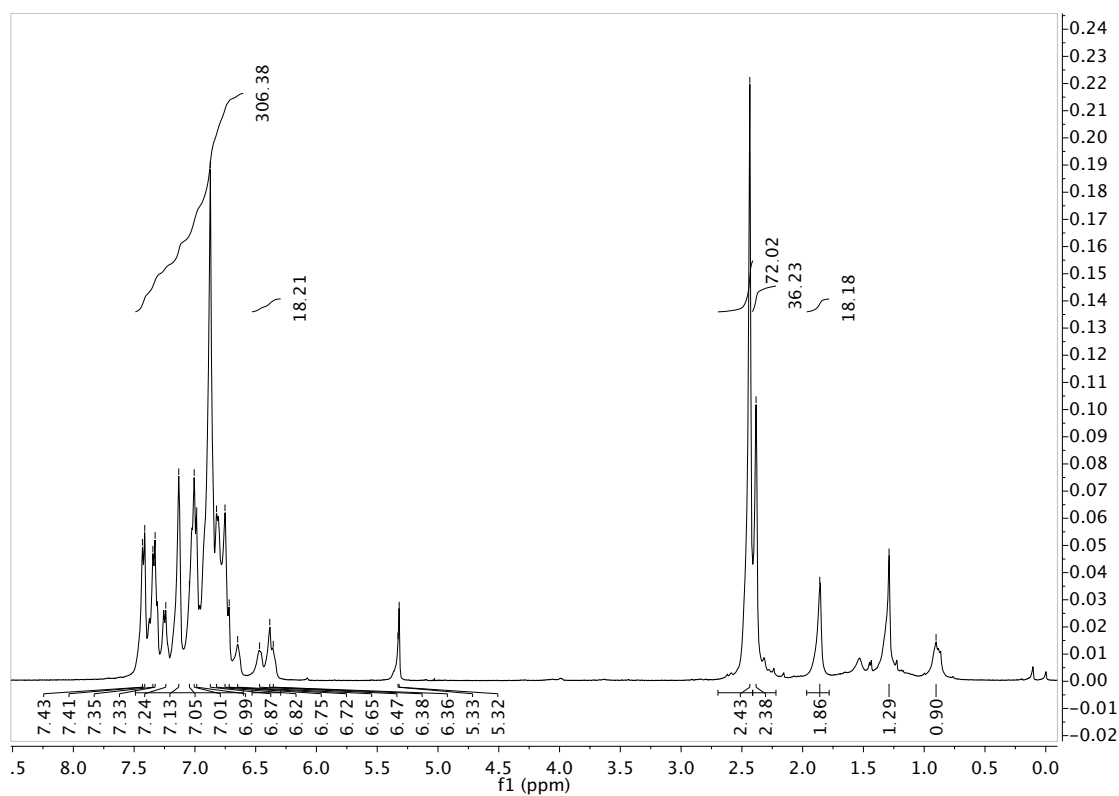
Figure 60. ^{1}H NMR spectrum of **148** in CD$_2$Cl$_2$ (400 MHz).
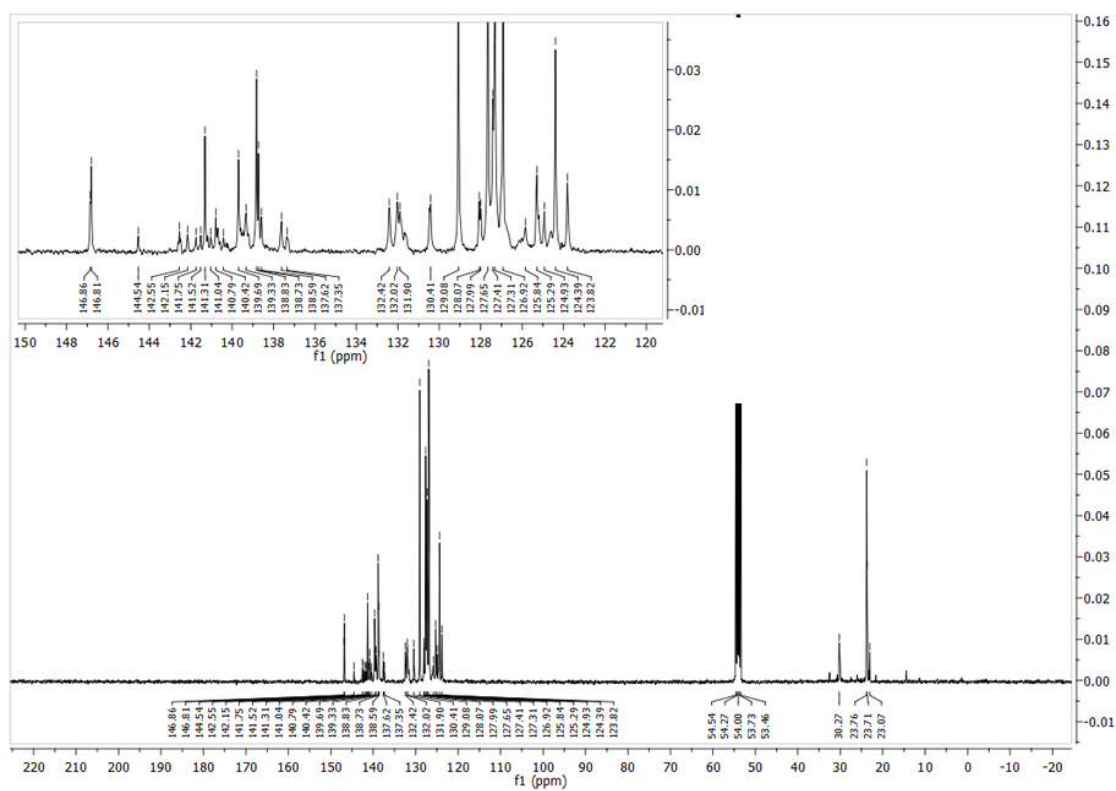
Figure 61. ^{13}C NMR spectrum of **148** in CD$_2$Cl$_2$ (100 MHz). Inset: zoom of the aromatic region (120-150 ppm)
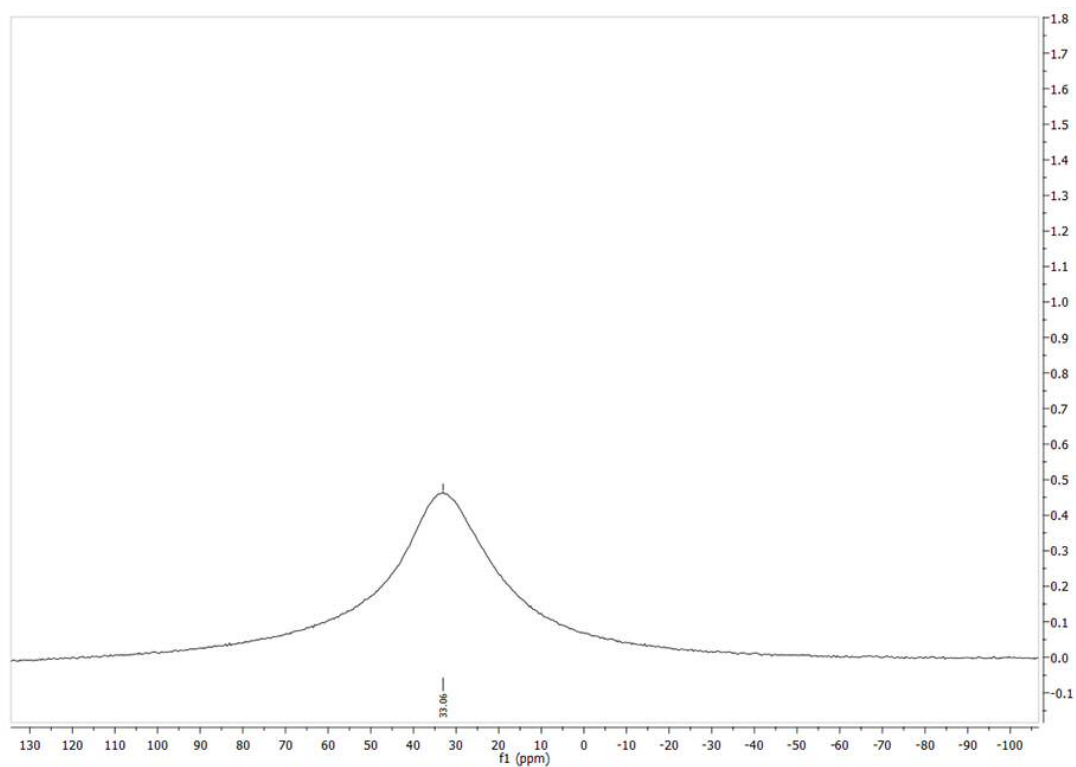
Figure 62. ^{11}B NMR spectrum of **148** in CD_2Cl_2 (128 MHz).

Characterization of 149
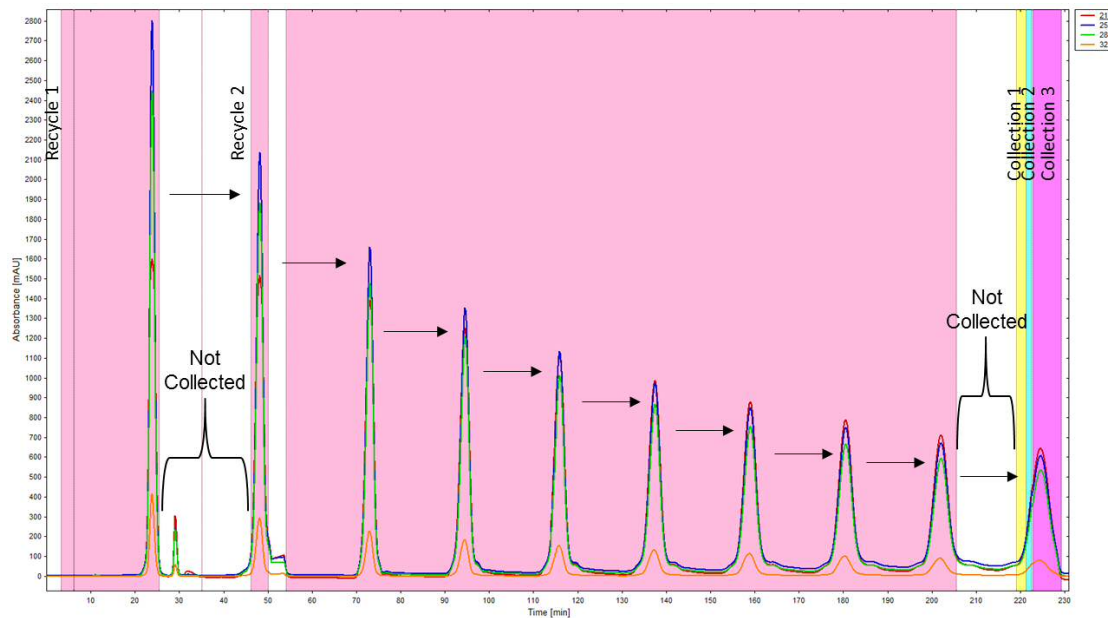
Figure 63. Gel permeation chromatography (GPC) for **149**, Recycling mode. Eluent: $CHCl_3$.
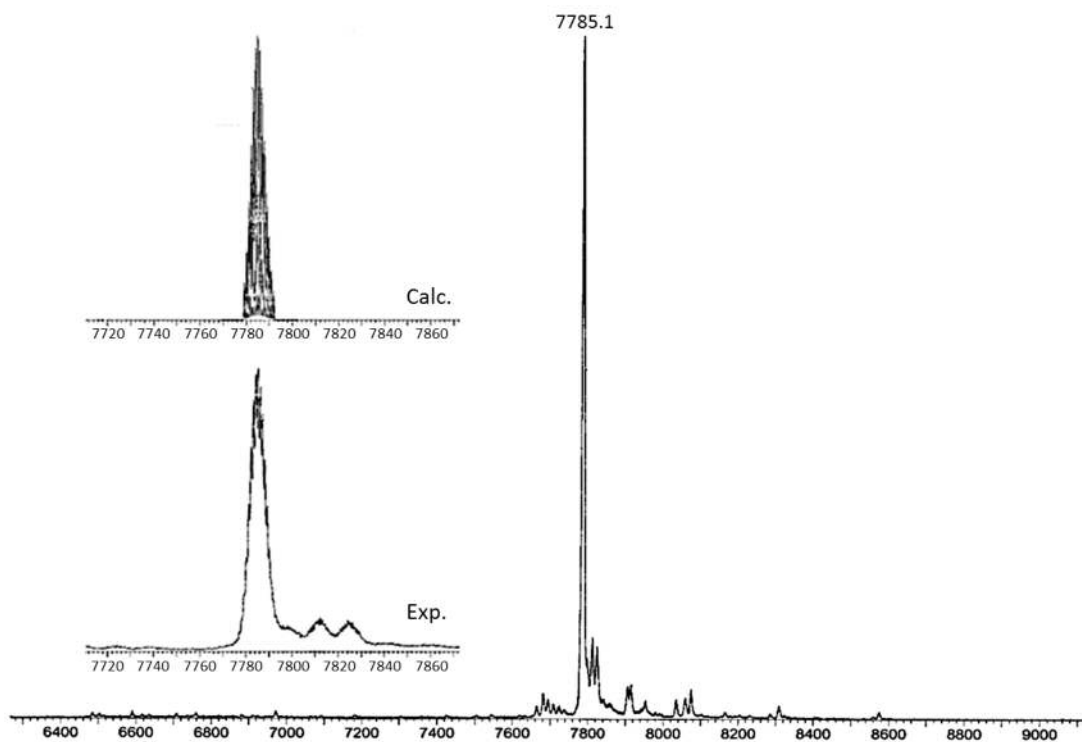
Figure 64. MALDI-TOF mass spectrometry of **149** (collection 3, from GPC run, above), matrix: trans-2-[3-(4-tert-butyl-phenyl)-2-methyl-2-propenylidene]malonitrile (DCTB).
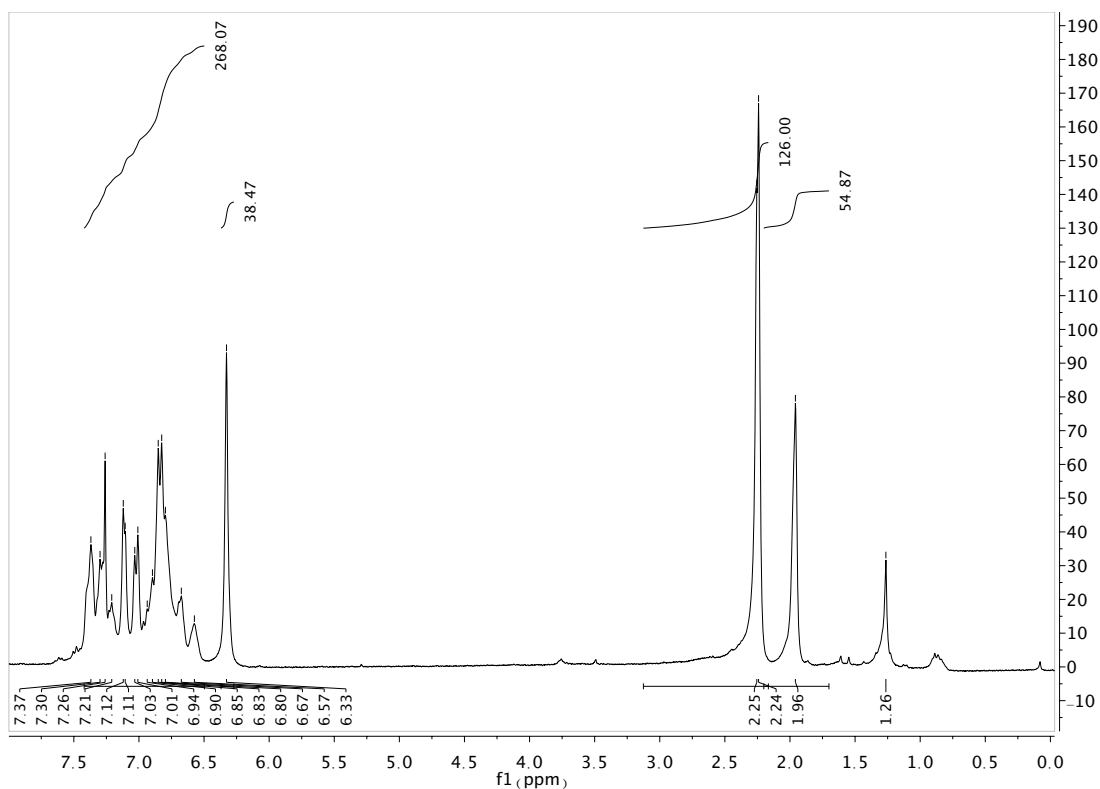
Figure 65. ^{1}H NMR spectrum of **149** in CDCl$_3$ (400 MHz).
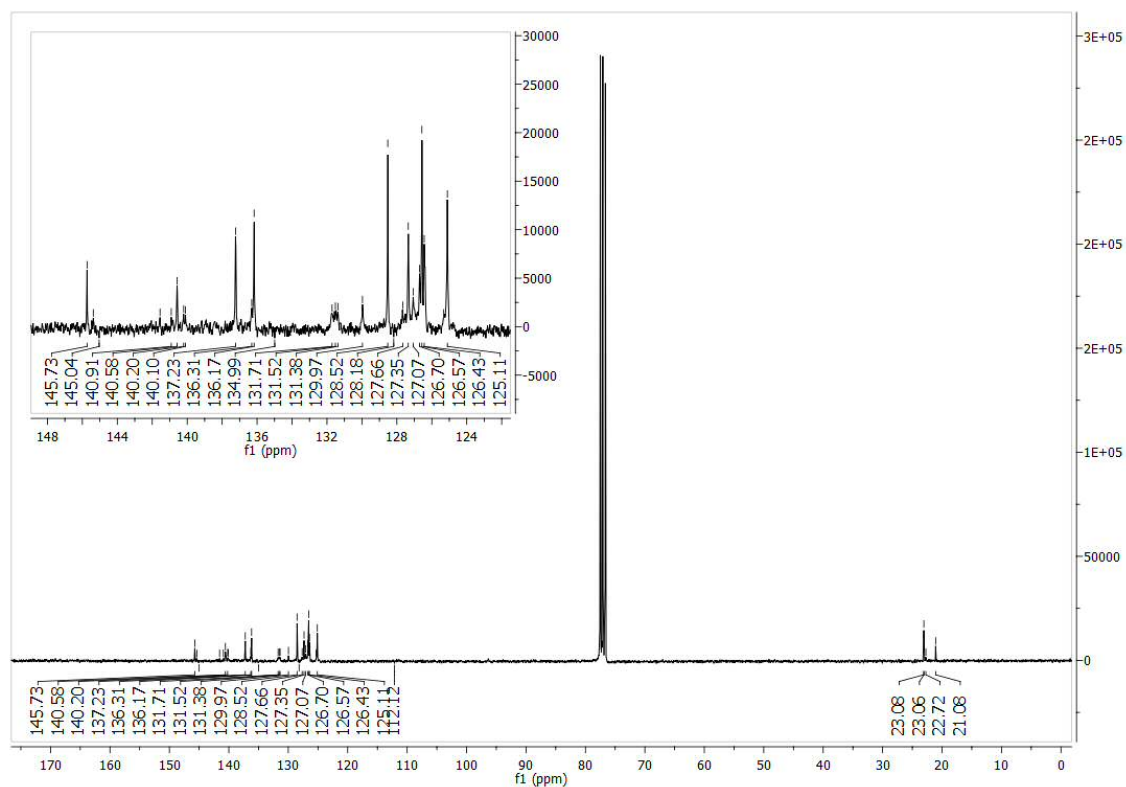
Figure 66. ^{13}C NMR spectrum of **149** in CDCl$_3$ (100 MHz).
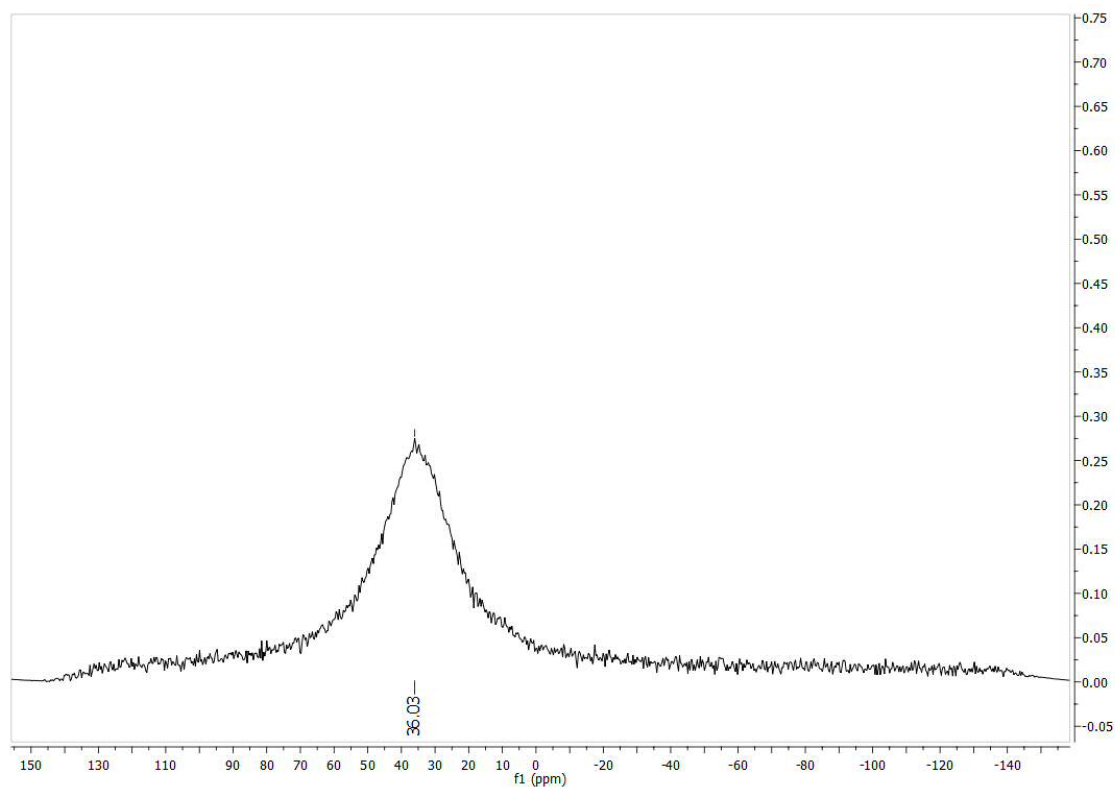
Figure 67. ^{11}B-NMR spectrum of **149** in CDCl$_3$ (128 MHz).

Characterization of 150
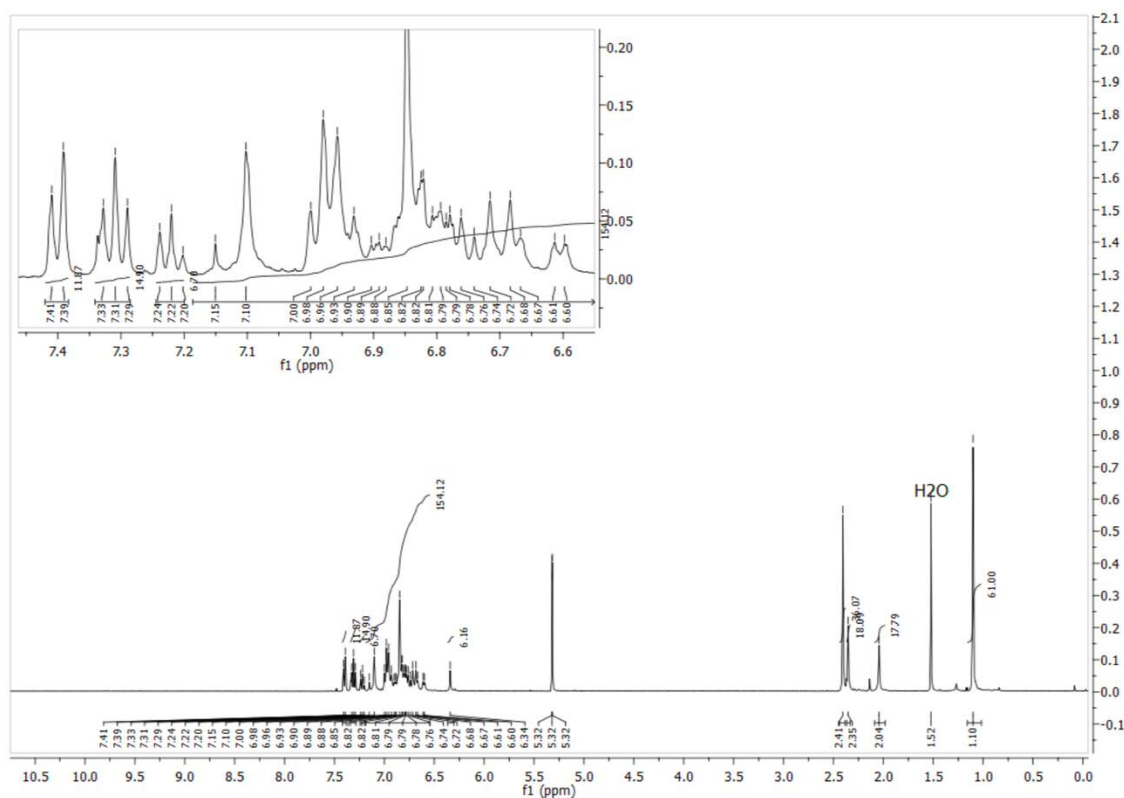
Figure 68. ^{1}H NMR spectrum of **150** in CD$_2$Cl$_2$ (400 MHz).
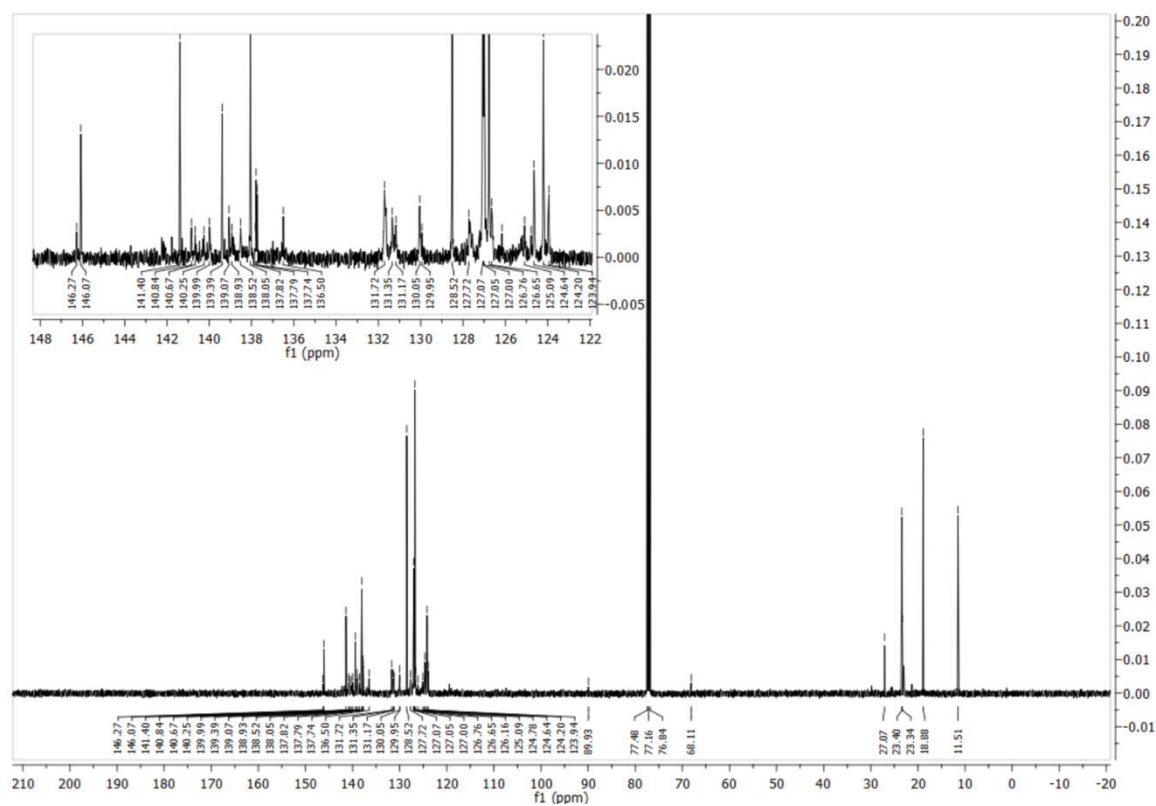
Figure 69. ^{13}C NMR spectrum of **150** in CDCl$_3$ (100 MHz).
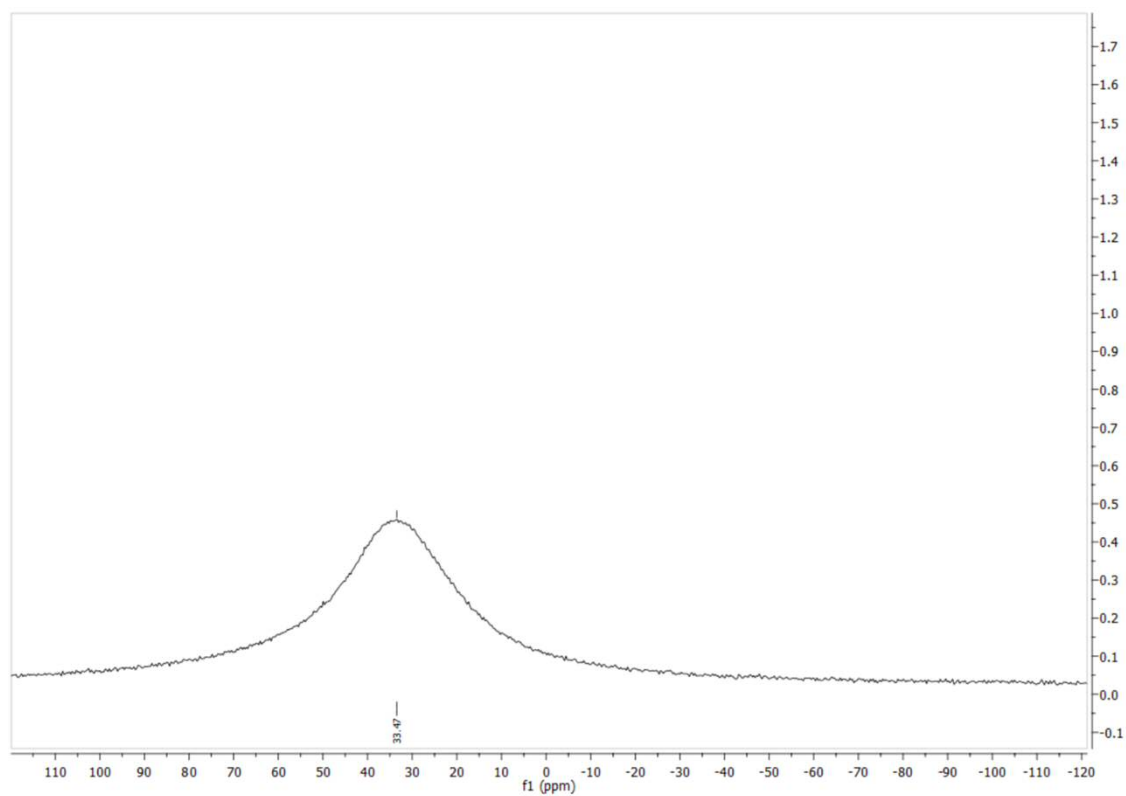
Figure 70. ^{1}B-NMR spectrum of **150** in CD_2Cl_2 (128 MHz).

Characterization of 151
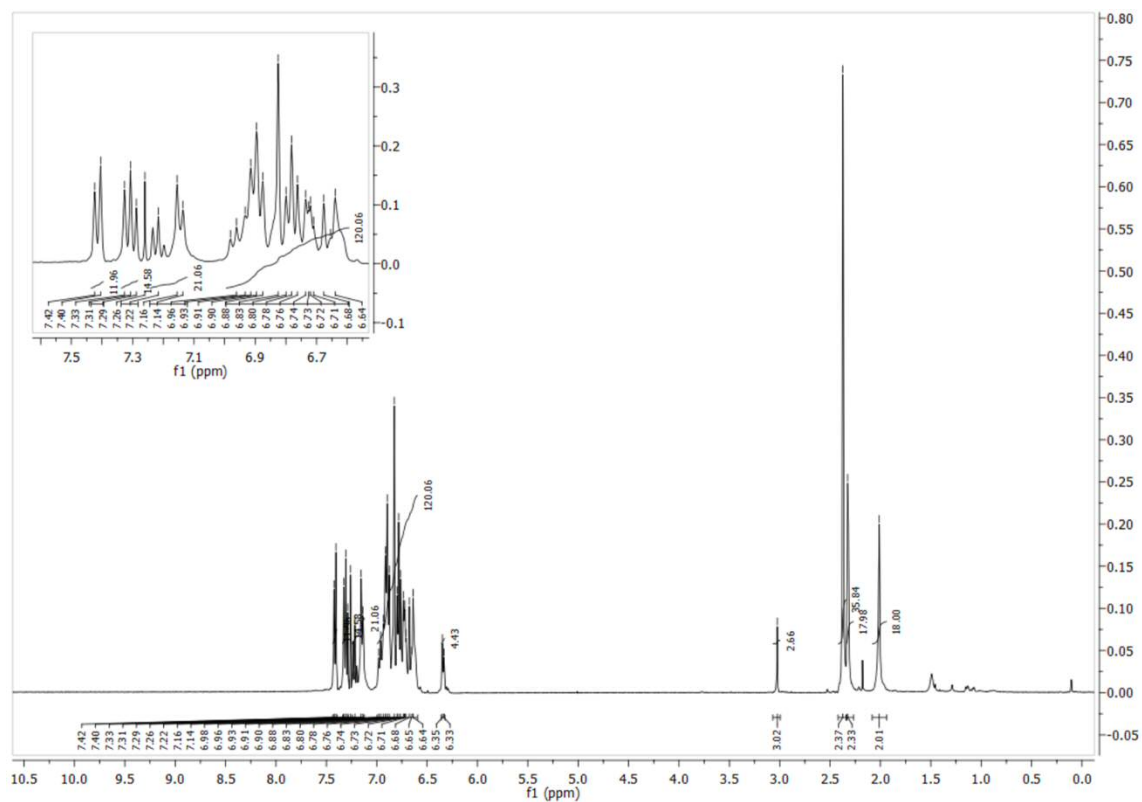
Figure 71. ^{1}H NMR spectrum of **151** in $CDCl_3$ (400 MHz).
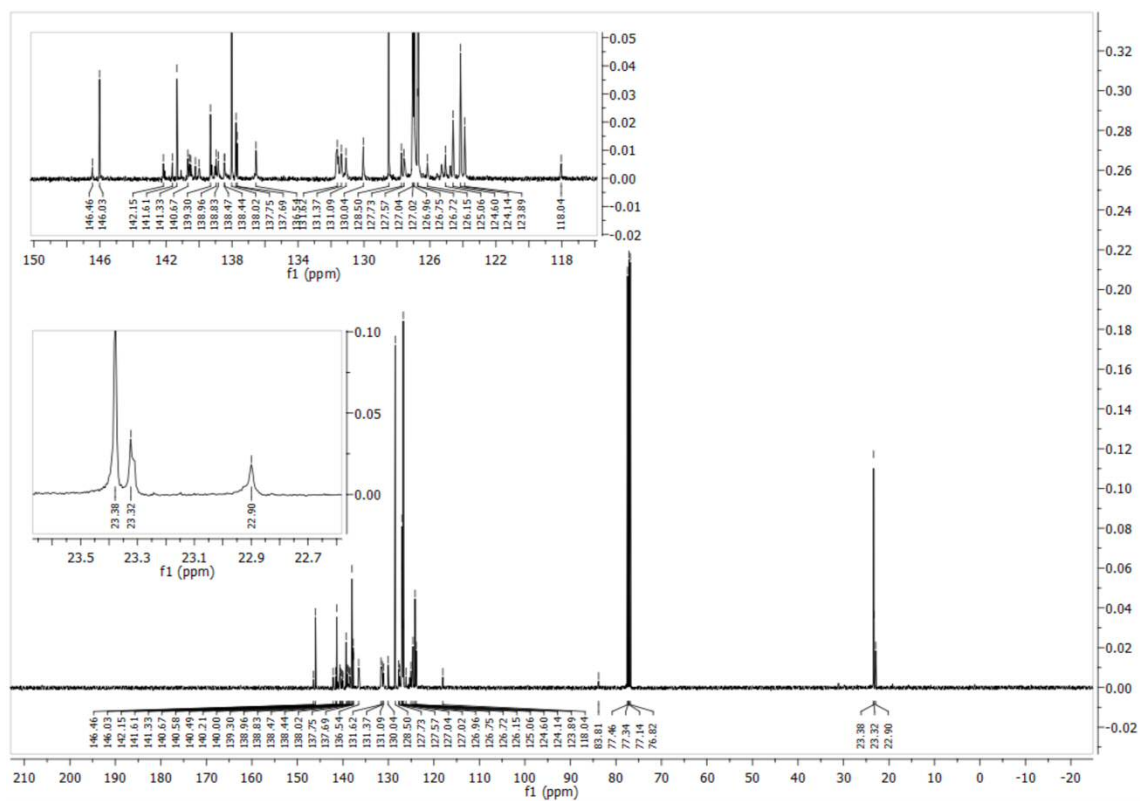
Figure 72. ^{13}C NMR spectrum of **151** in CDCl$_3$ (100 MHz).
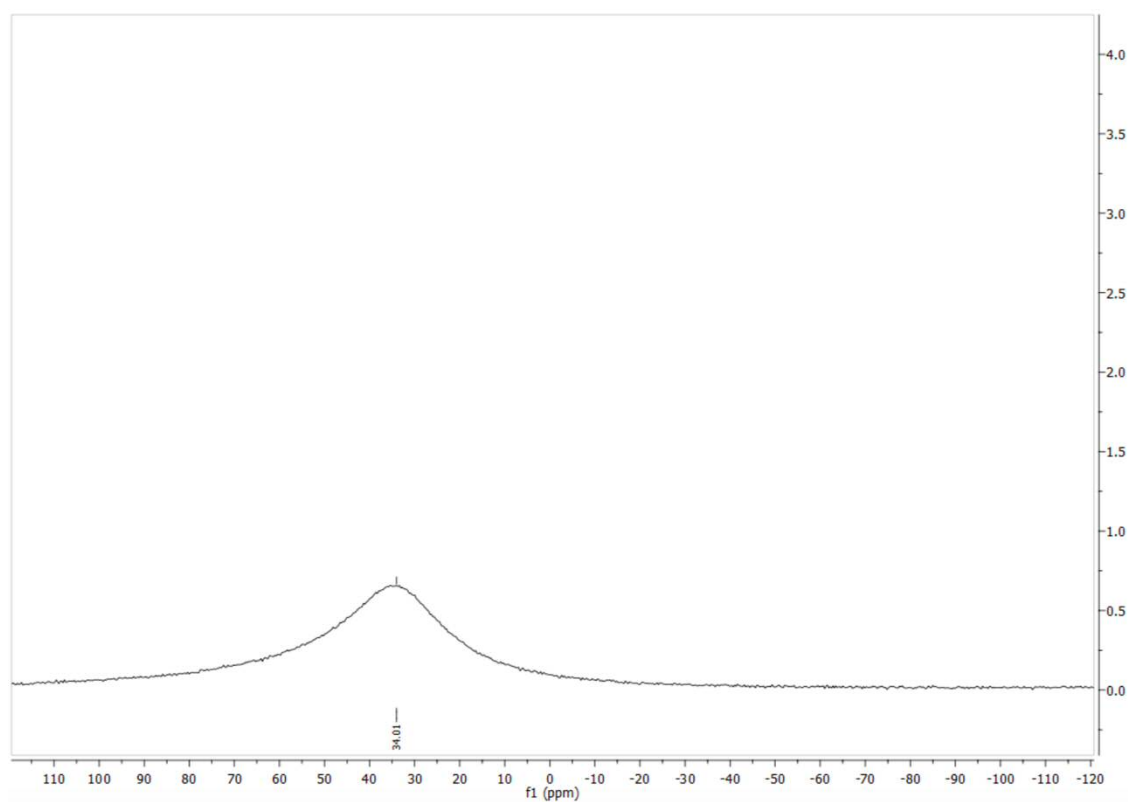
Figure 73. ^{1}B-NMR spectrum of **151** in CDCl$_3$ (128 MHz).

Characterization of 152
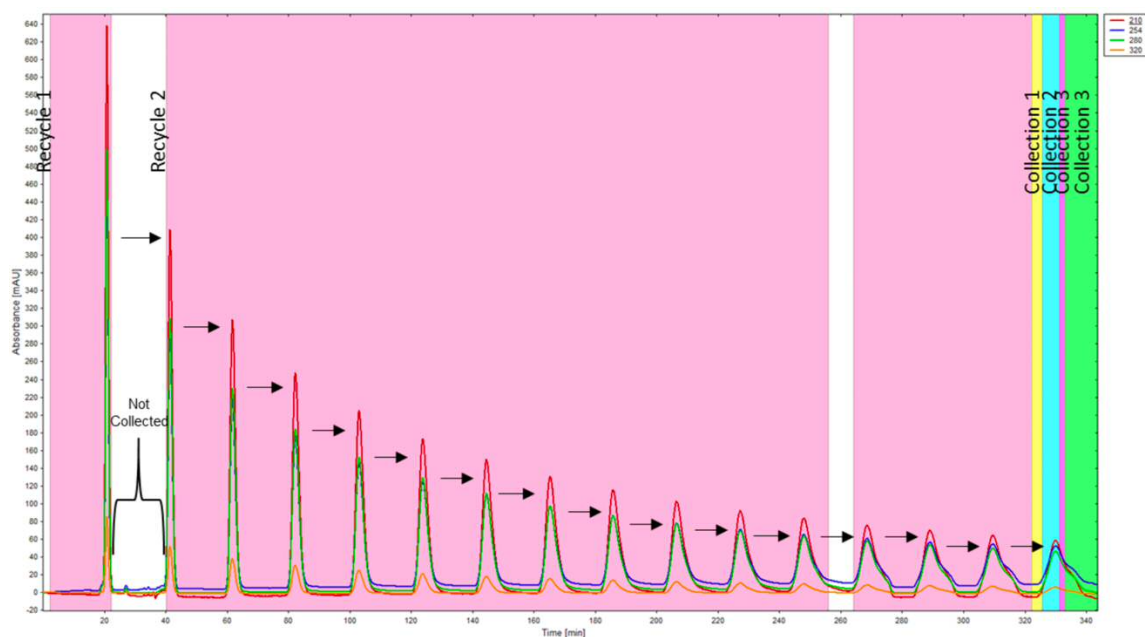
Figure 74. Gel permeation chromatography (GPC) for **152**, Recycling mode. Eluent: CHCl$_3$.
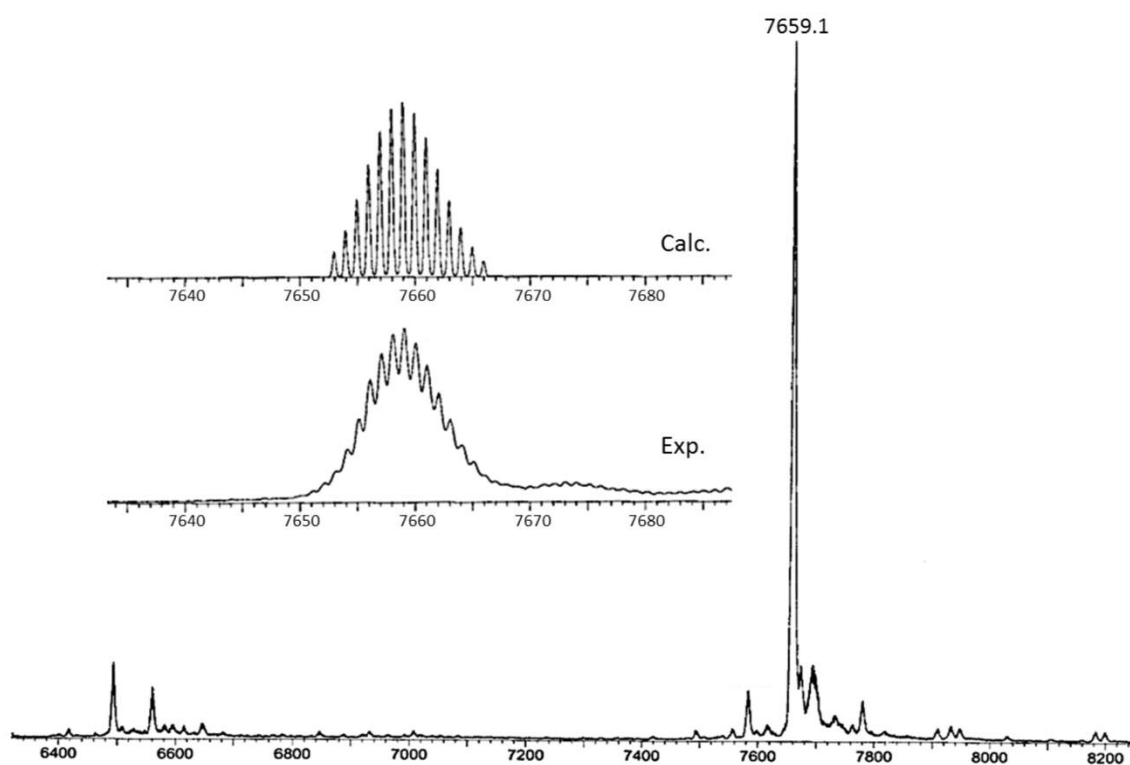
Figure 75. MALDI-TOF mass spectrometry of **152** (collection 2, from GPC run, above), matrix: trans-2-[3-(4-tert-butyl-phenyl)-2-methyl-2-propenylidene]malonitrile (DCTB).
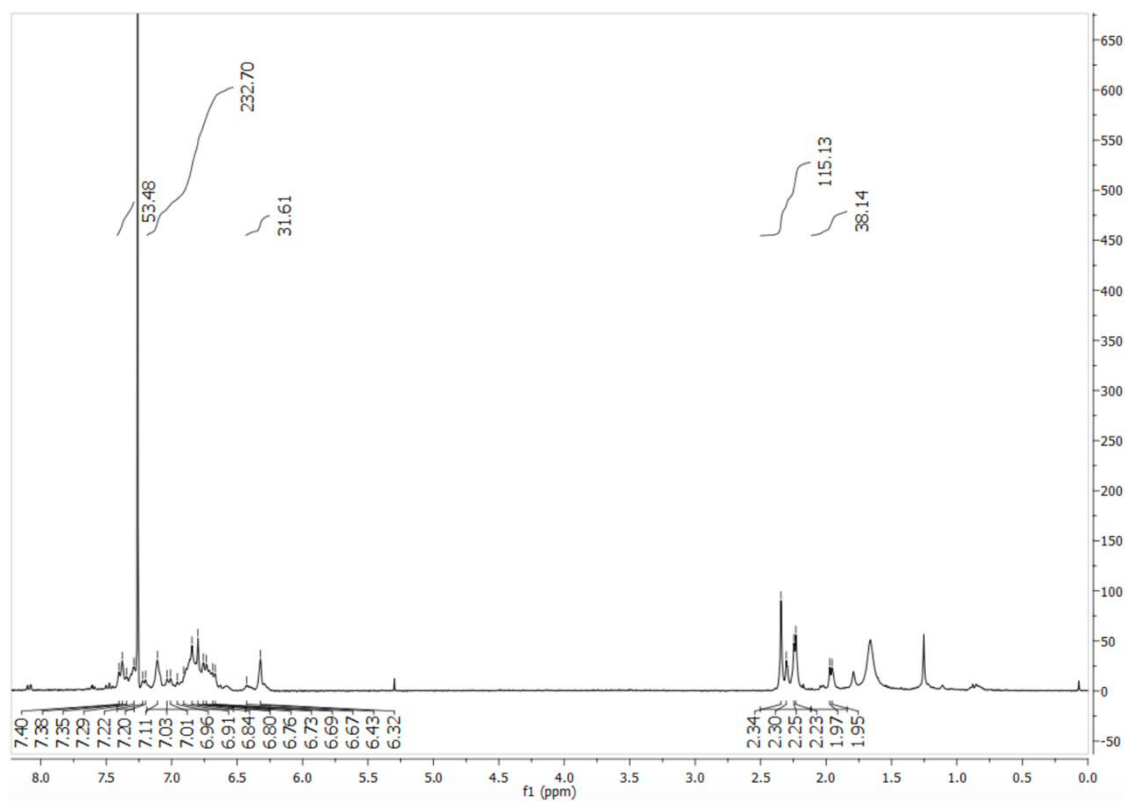
Figure 76. ^{1}H NMR spectrum of **152** in CDCl$_3$ (300 MHz).
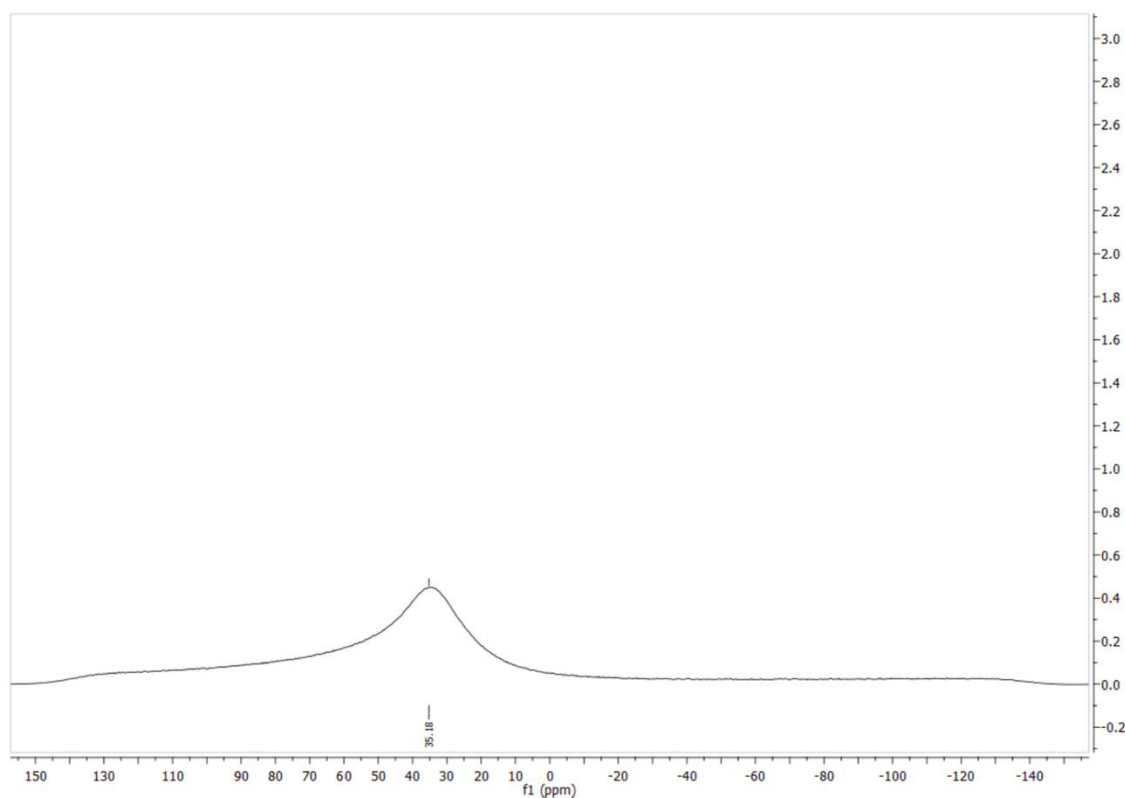
Figure 77. ^{11}B-NMR spectrum of **152** in CDCl$_3$ (128 MHz).

Characterization of 153
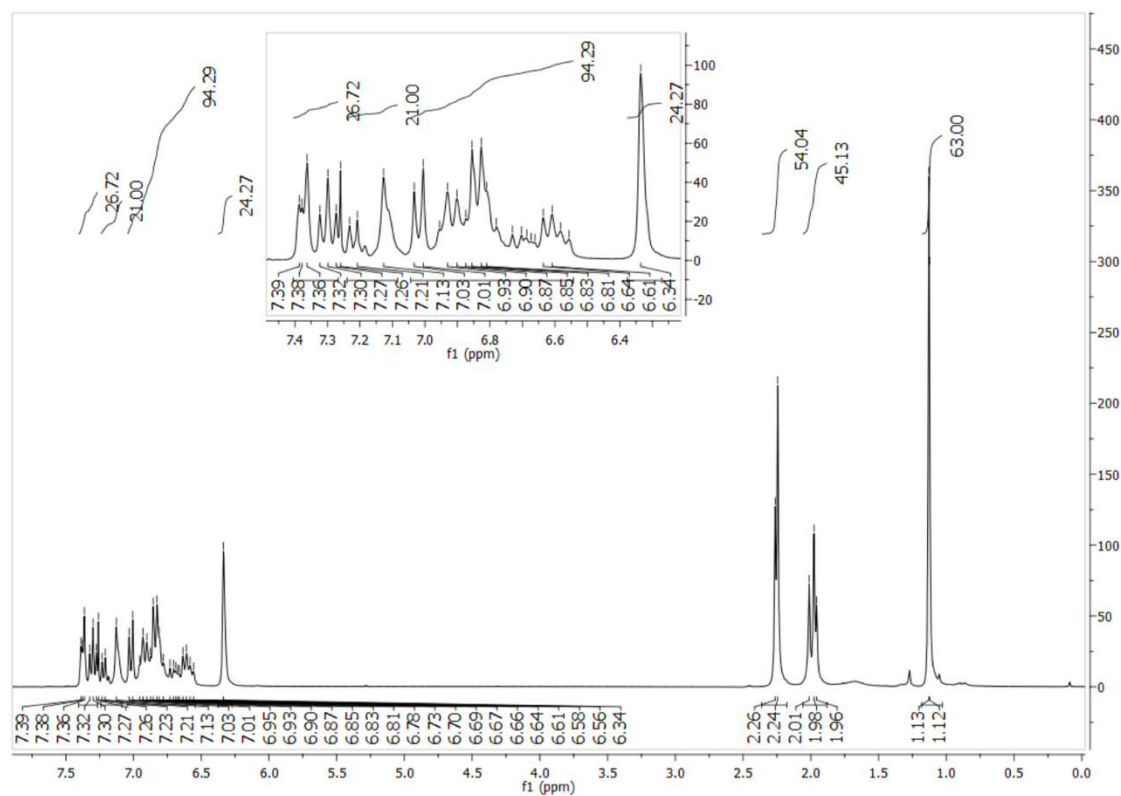
Figure 78. ¹H NMR spectrum of **153** in CDCl₃ (300 MHz).
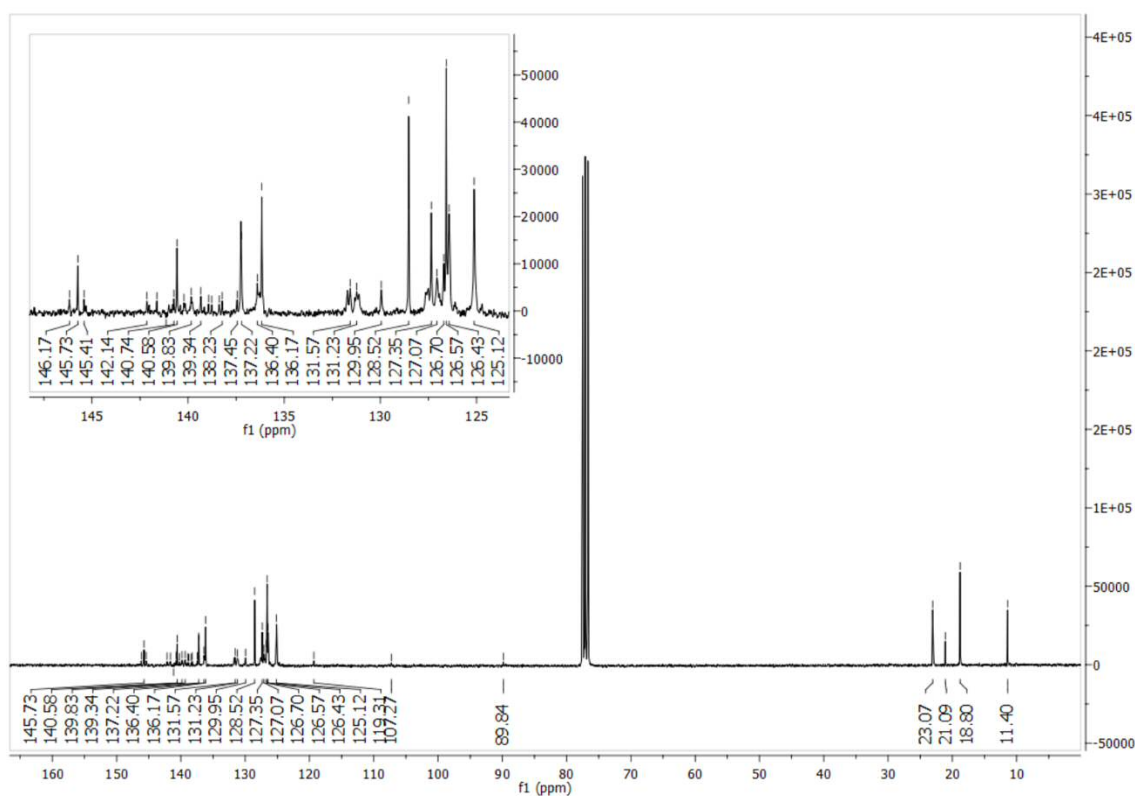
Figure 79. ¹³C NMR spectrum of **153** in CDCl₃ (100 MHz).

Characterization of 154
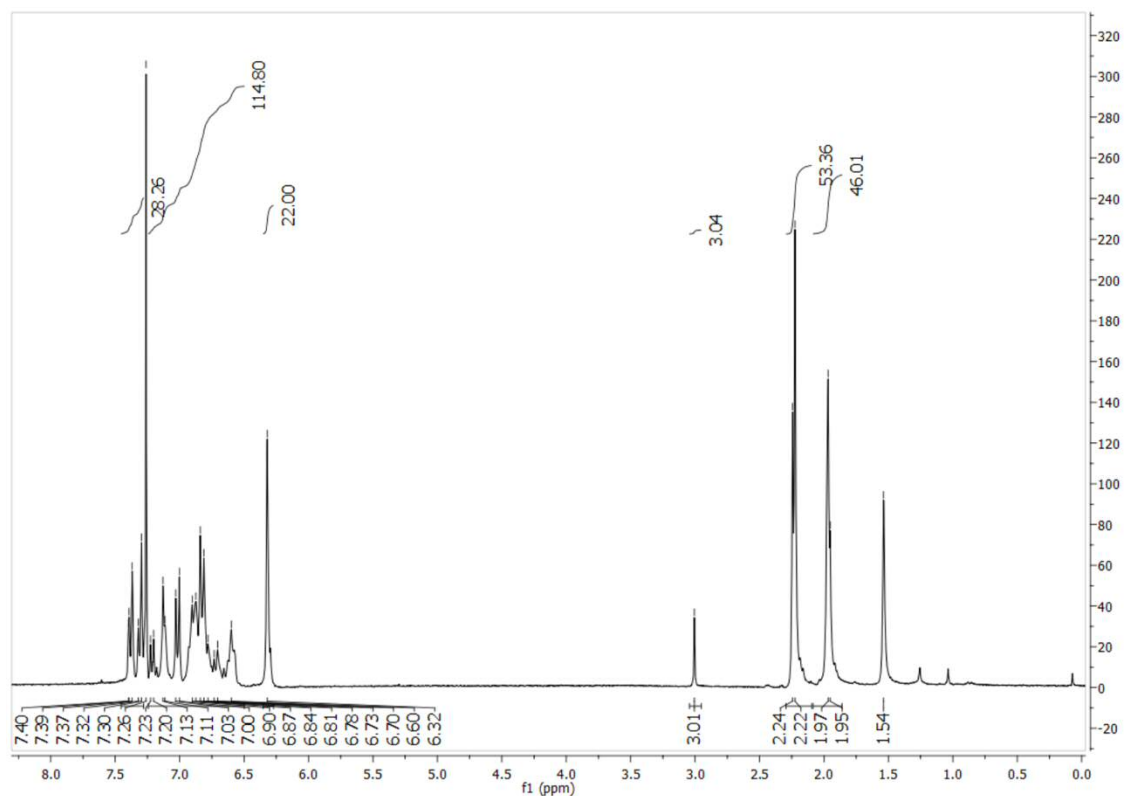
Figure 80. ^{1}H NMR spectrum of **154** in CDCl$_3$ (300 MHz).

Characterization of 155
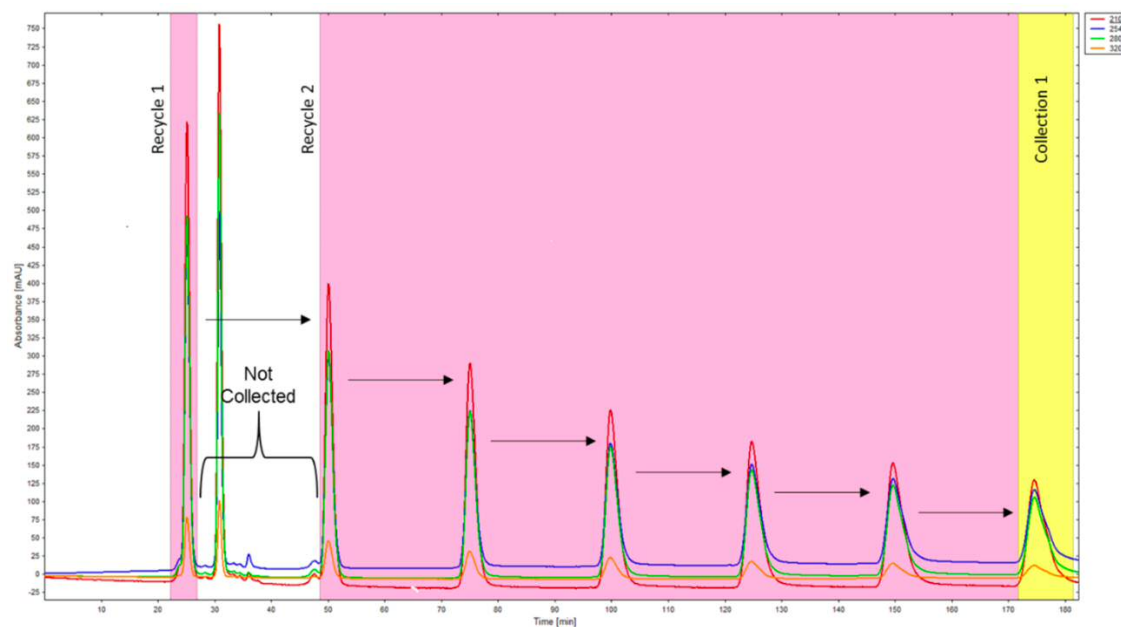
Figure 81. Gel permeation chromatography (GPC) for **155**, Recycling mode. Eluent: CHCl$_3$.
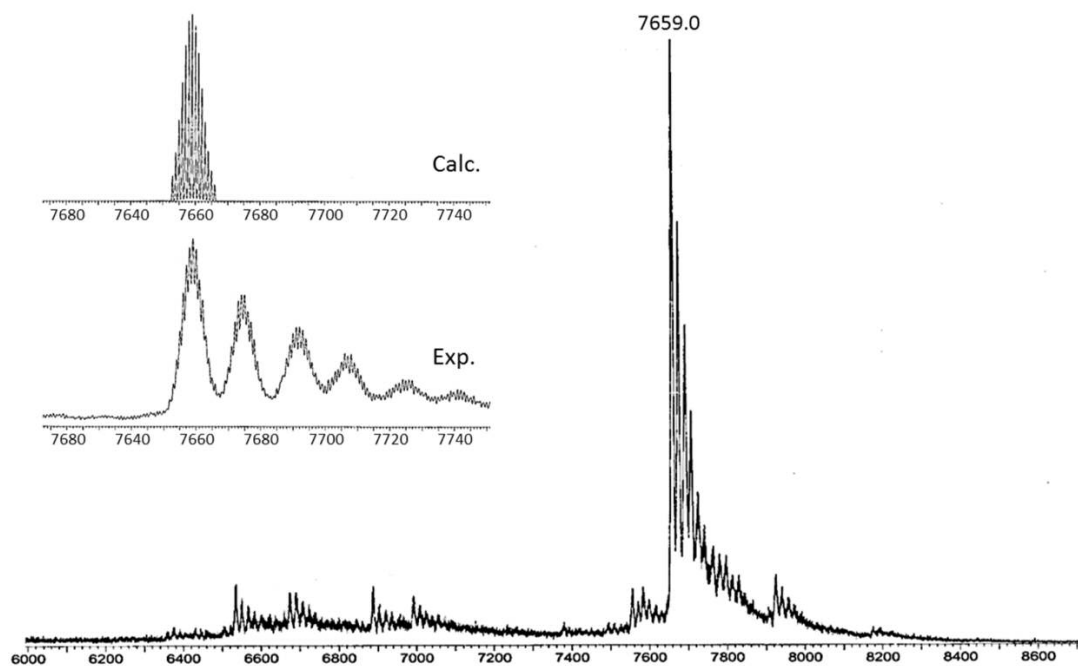
Figure 82. MALDI-TOF mass spectrometry of **155** (collection 2, from GPC run, above), matrix: trans-2-[3-(4-tert-butyl-phenyl)-2-methyl-2-propenylidene]malonitrile (DCTB).
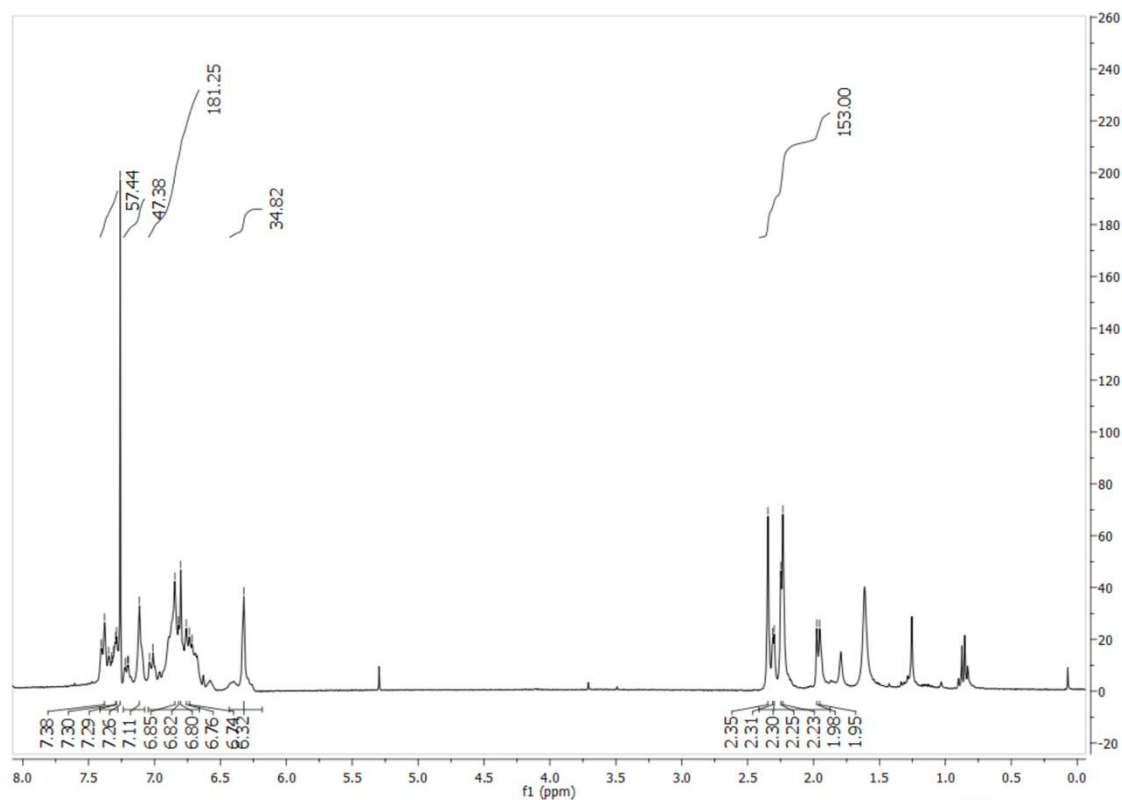
Figure 83. ^{1}H NMR spectrum of **155** in CDCl$_3$ (300 MHz).
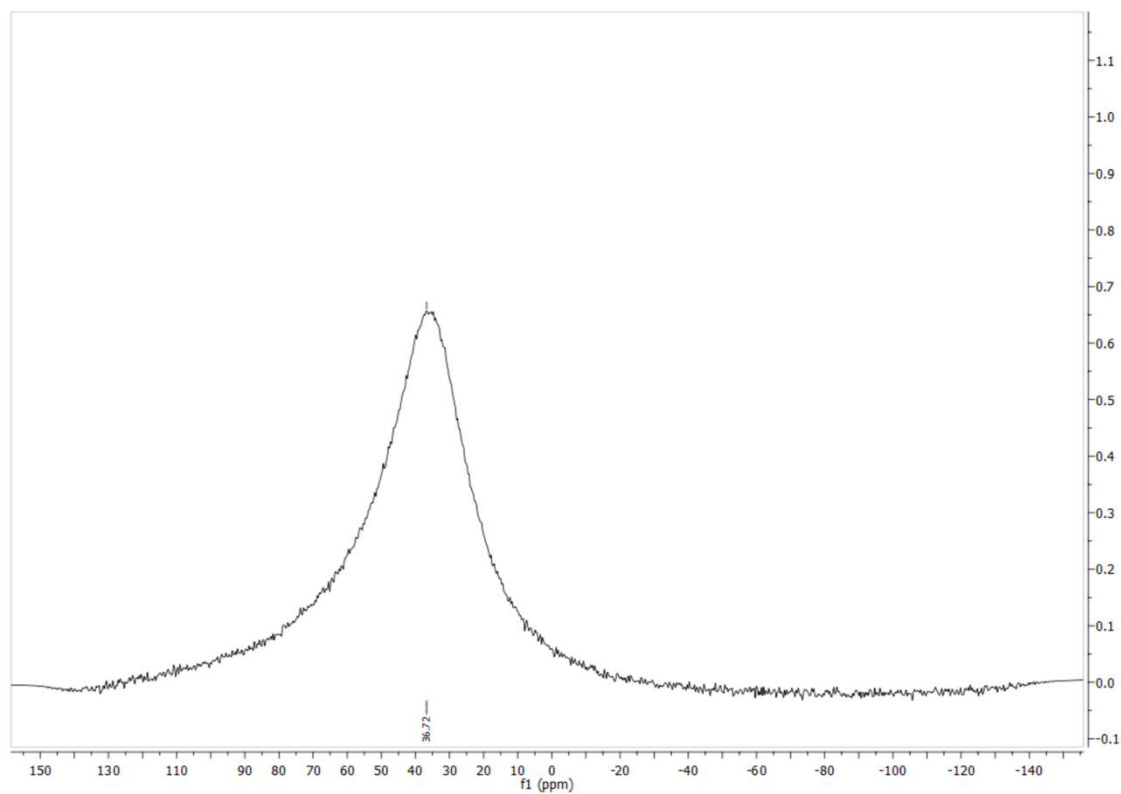
Figure 84. ^{11}B-NMR spectrum of **155** in CDCl$_3$ (128 MHz).

Characterization of 156
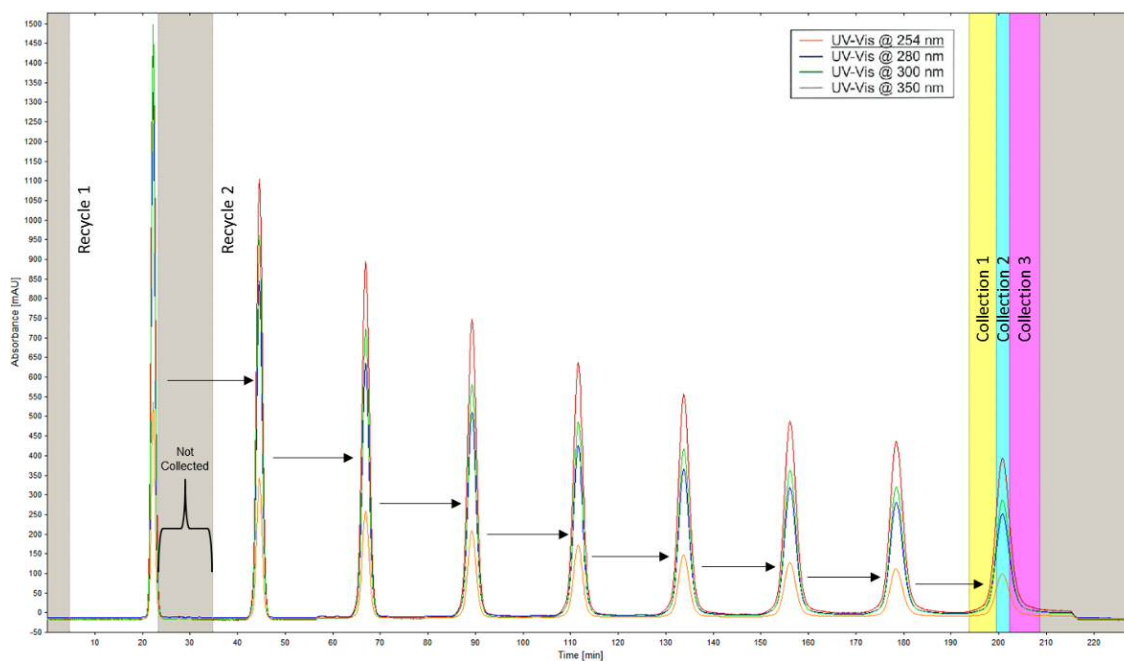
Figure 85. Gel permeation chromatography (GPC) for **156**, Recycling mode. Eluent: CHCl$_3$.
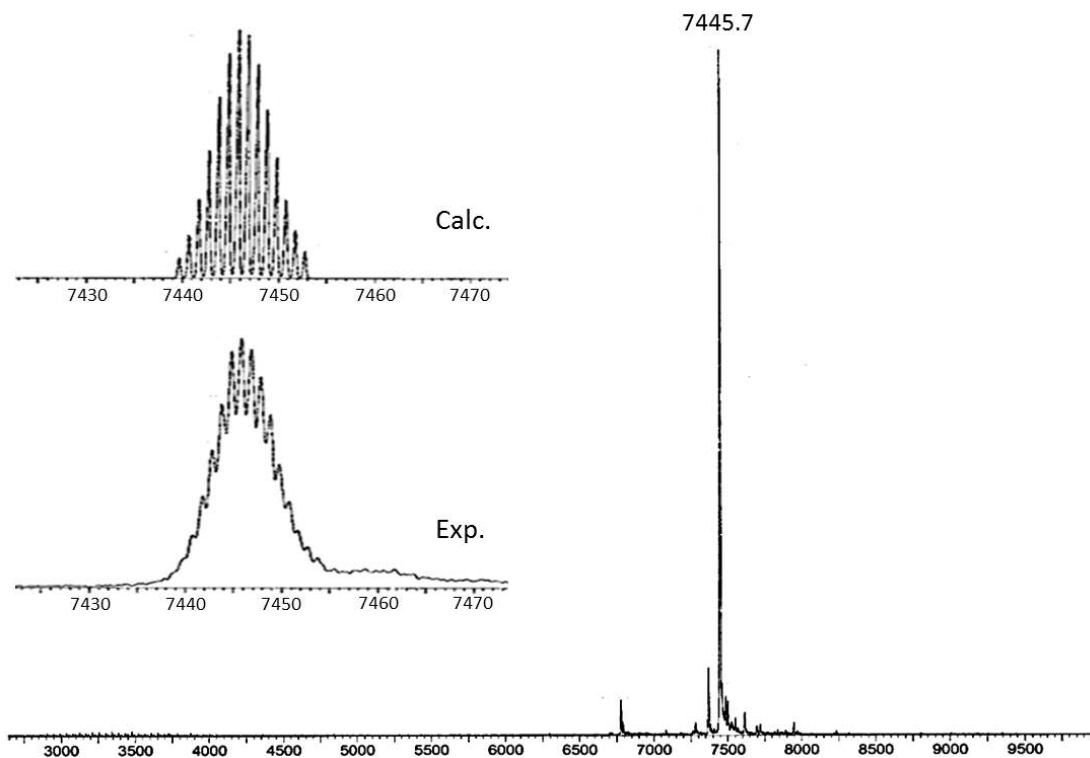
Figure 86. MALDI-TOF mass spectrometry of **156** (collection 2, from GPC run, above), matrix: trans-2-[3-(4-tert-butyl-phenyl)-2-methyl-2-propenylidene]malonitrile (DCTB).
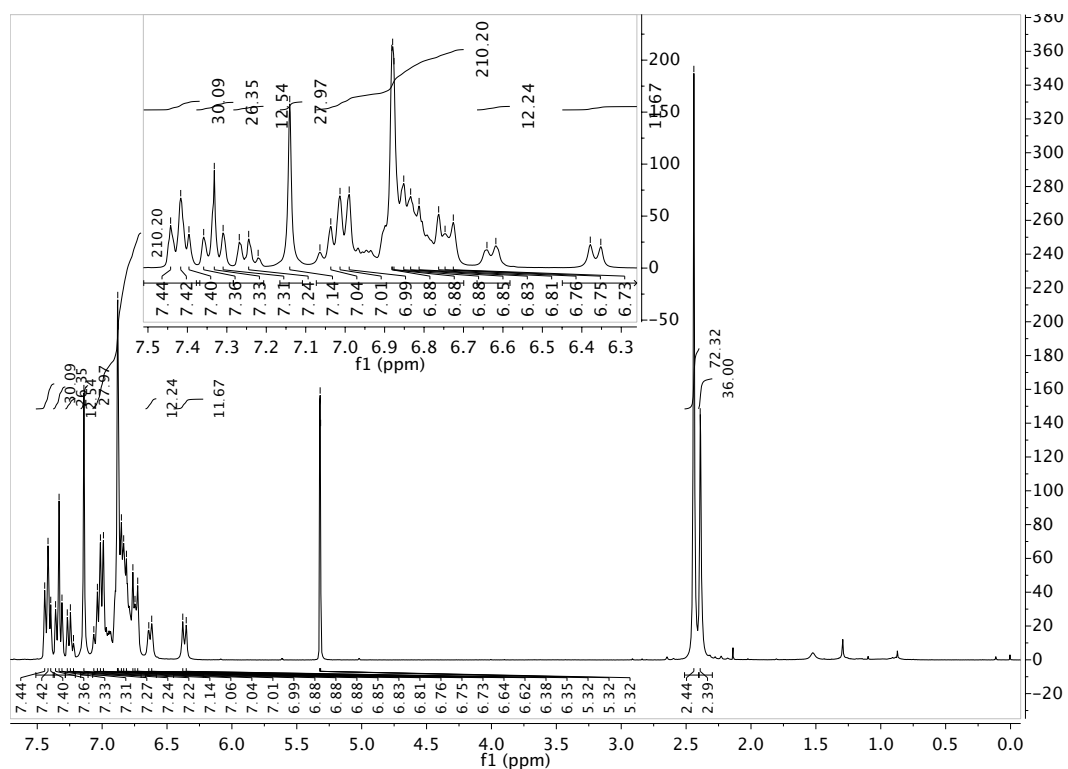
Figure 87. ^{1}H NMR spectrum of **156** in CD_2Cl_2 (300 MHz).
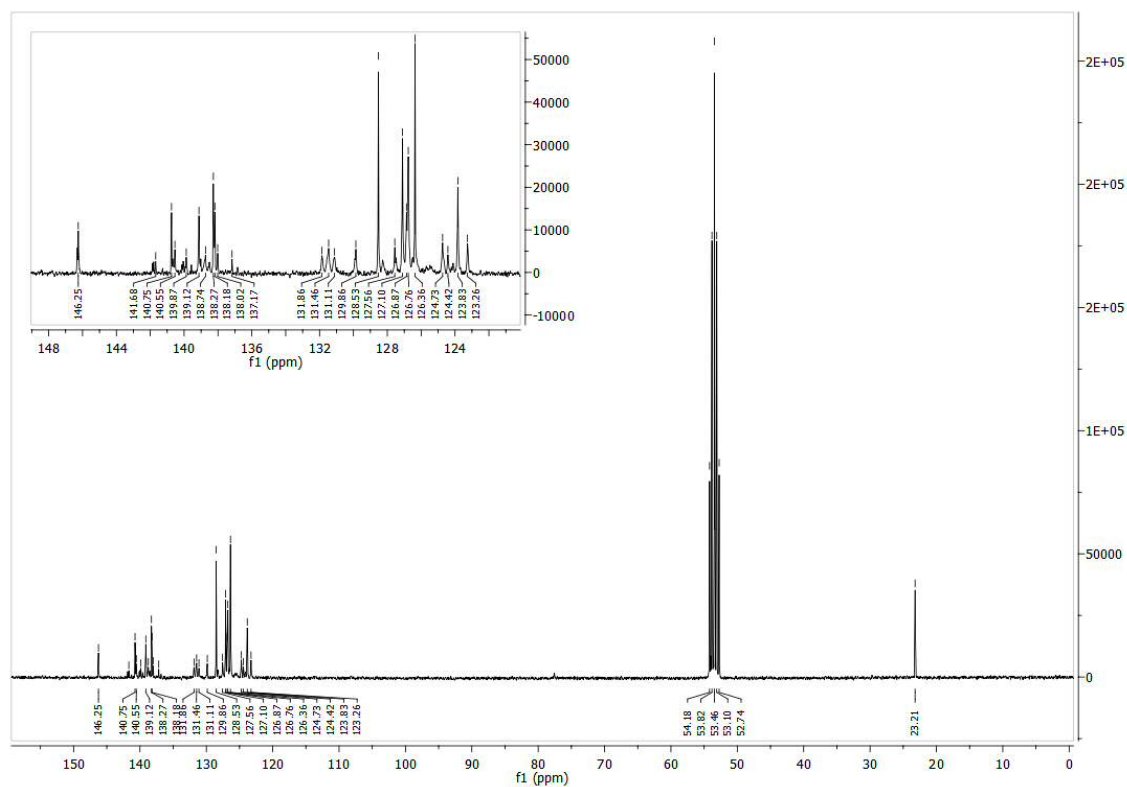
Figure 88. ^{13}C NMR spectrum of **156** in CD$_2$Cl$_2$ (100 MHz).
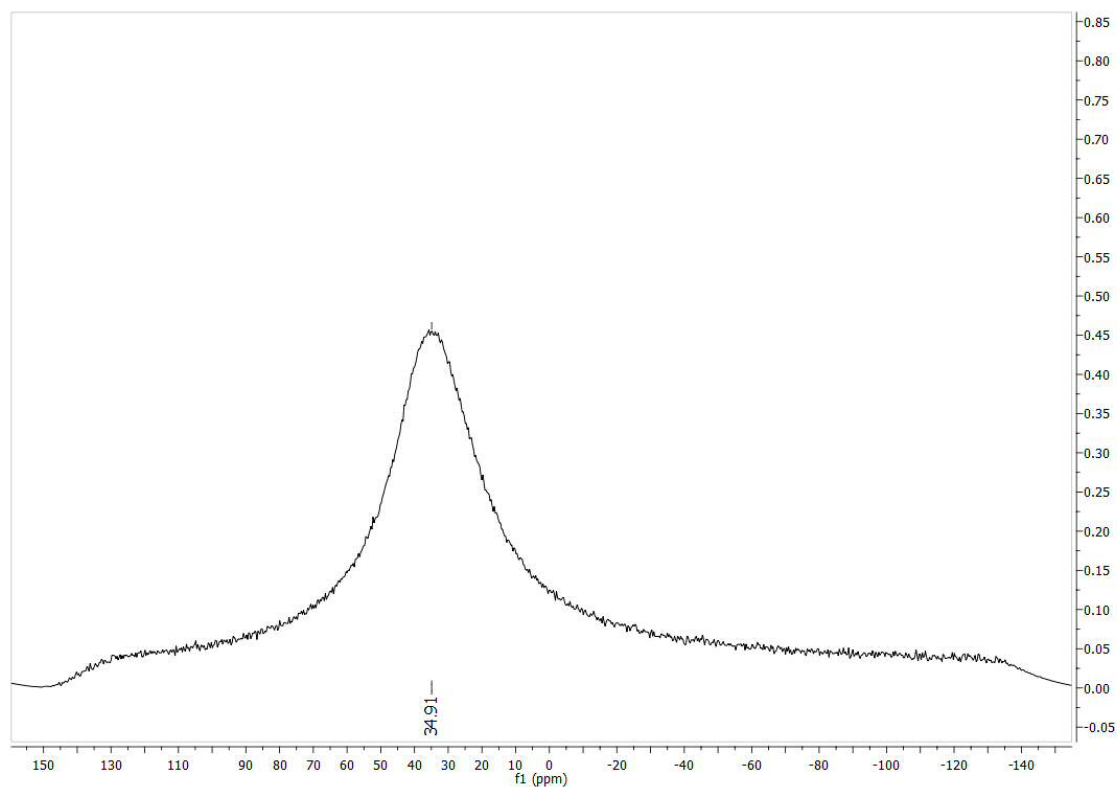
Figure 89. ^{11}B-NMR spectrum of **156** in CD$_2$Cl$_2$ (128 MHz).

Characterization of 157
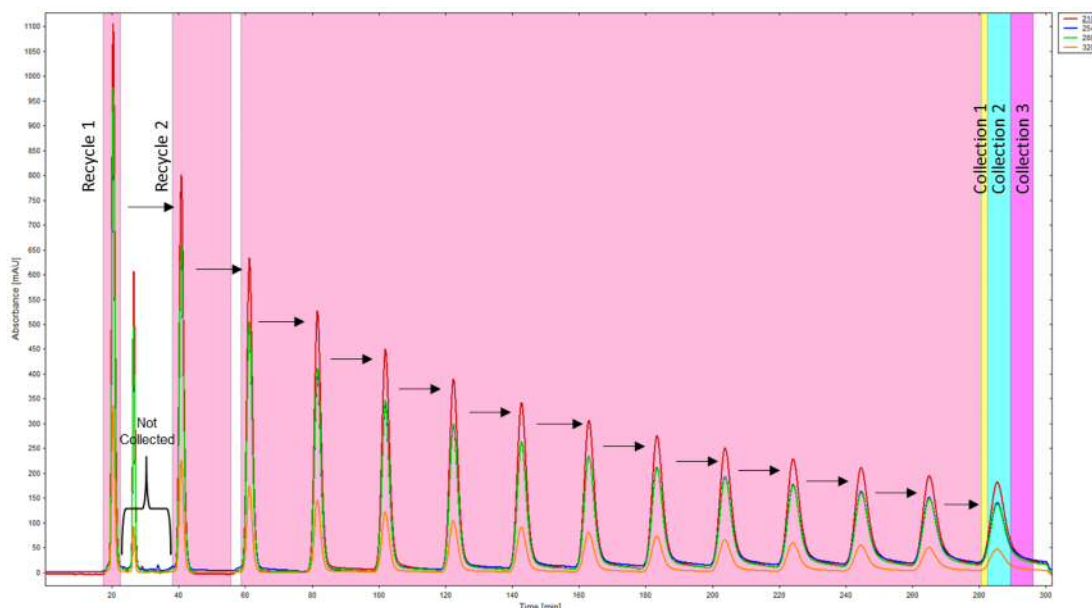
Figure 90. Gel permeation chromatography (GPC) for **157**, Recycling mode. Eluent: $CHCl_3$.
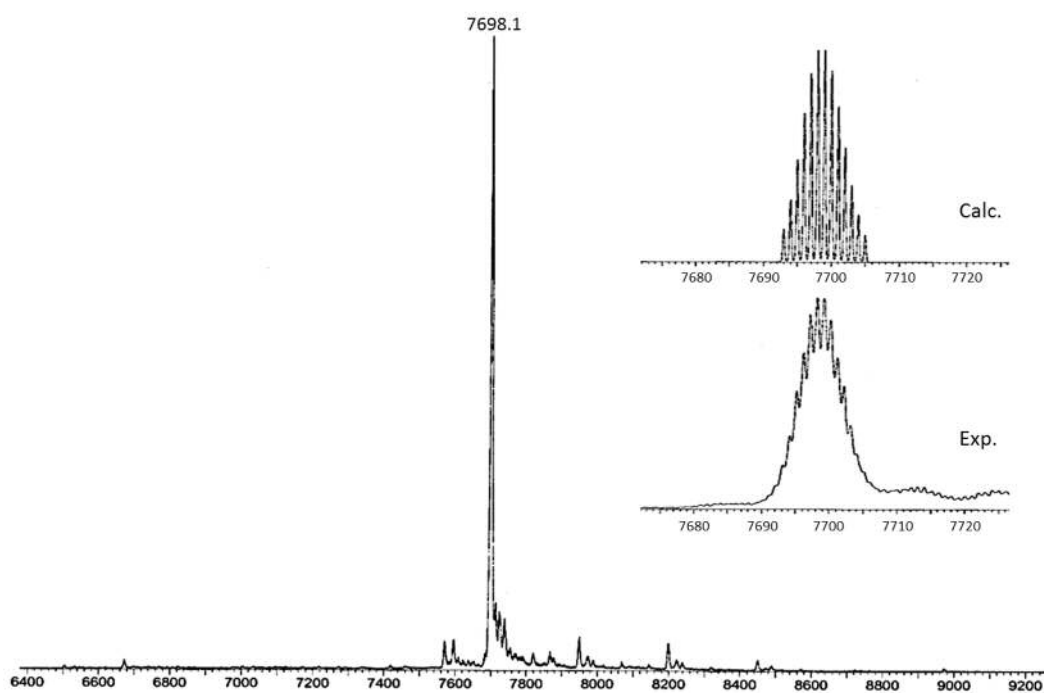
Figure 91. MALDI-TOF mass spectrometry of **157** (Collection 2, from GPC run, above), matrix: trans-2-[3-(4-tert-butyl-phenyl)-2-methyl-2-propenylidene]malonitrile (DCTB).
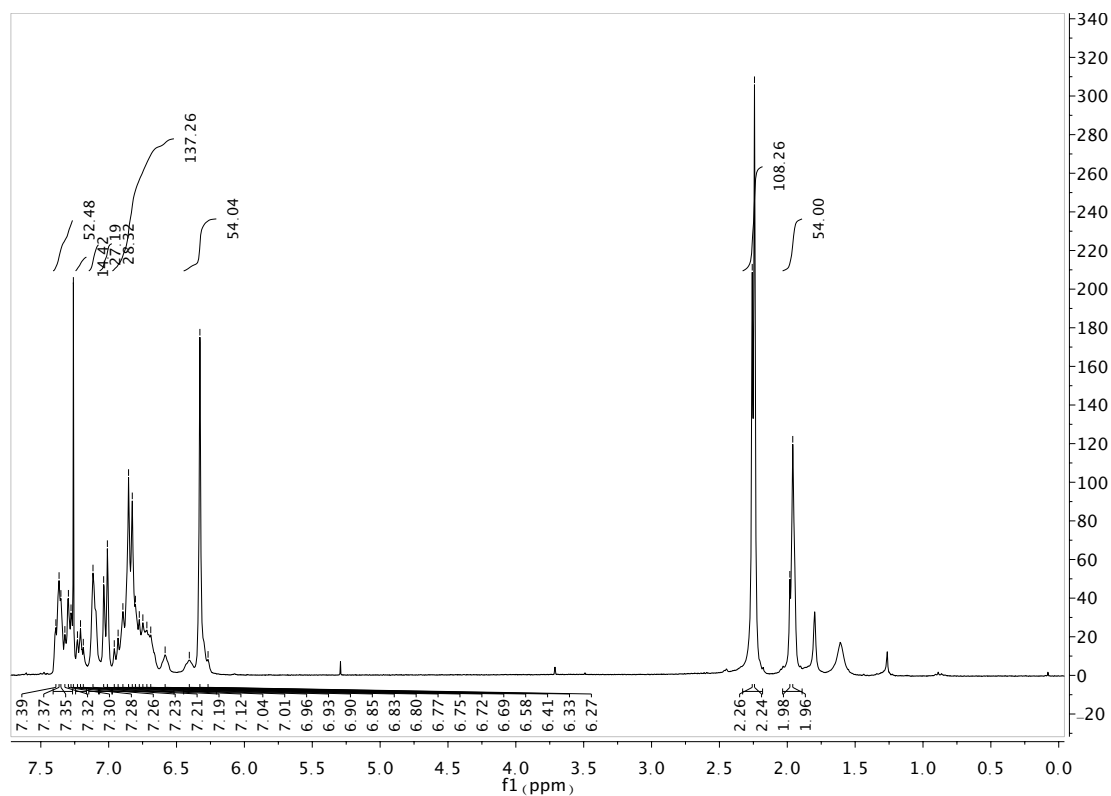
Figure 92. ^{1}H NMR spectrum of **157** in CDCl$_3$ (300 MHz).
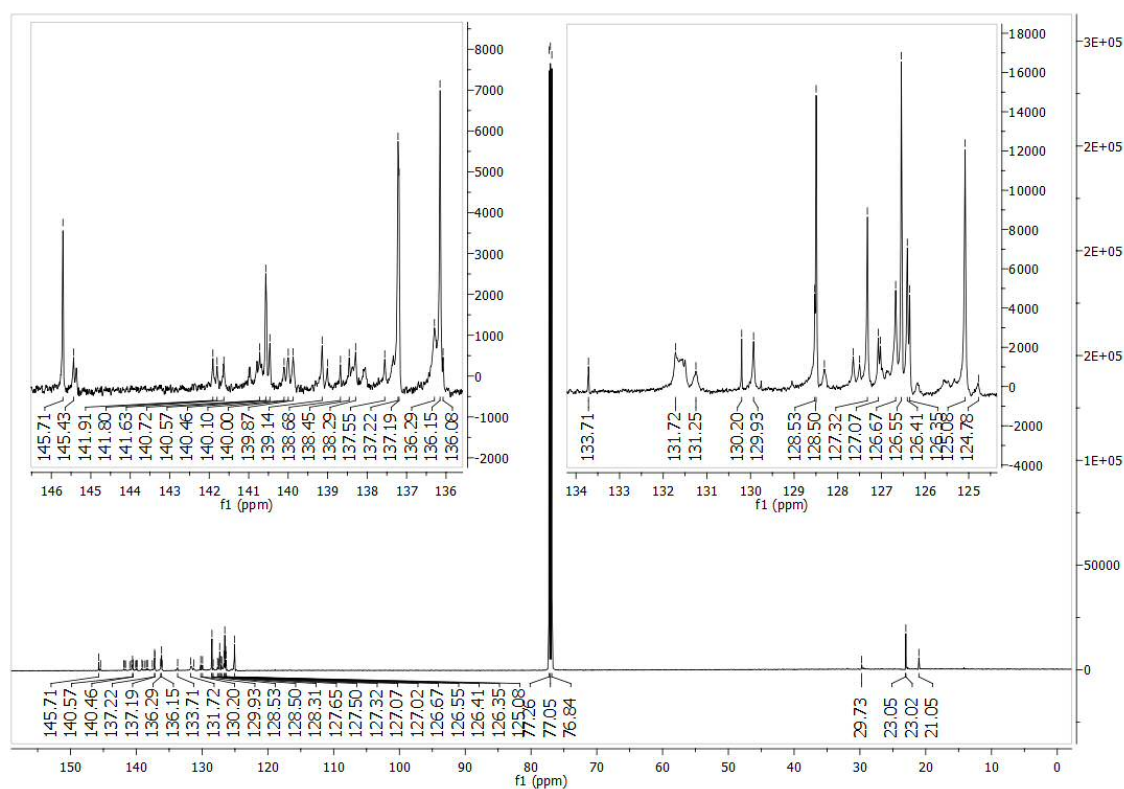
Figure 93. ^{13}C NMR spectrum of **157** in CDCl$_3$ (100 MHz).
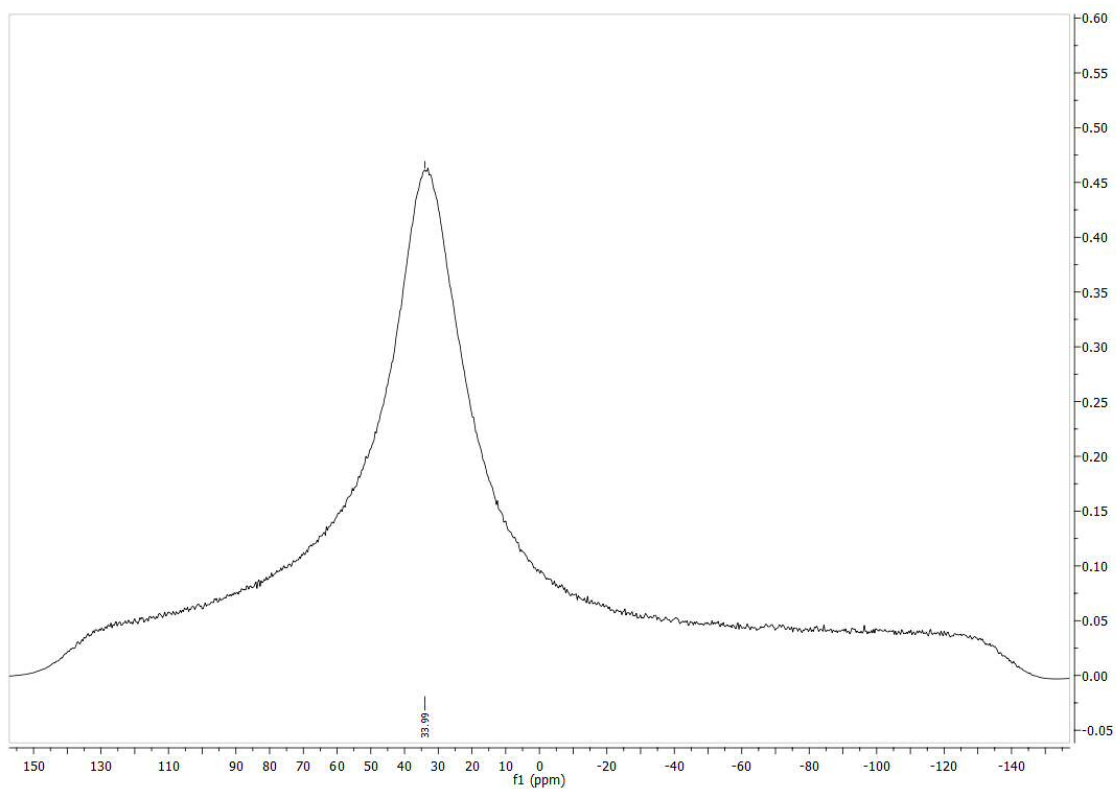
Figure 94. ^{11}B-NMR spectrum of **157** in CDCl$_3$ (128 MHz).

Characterization of 158
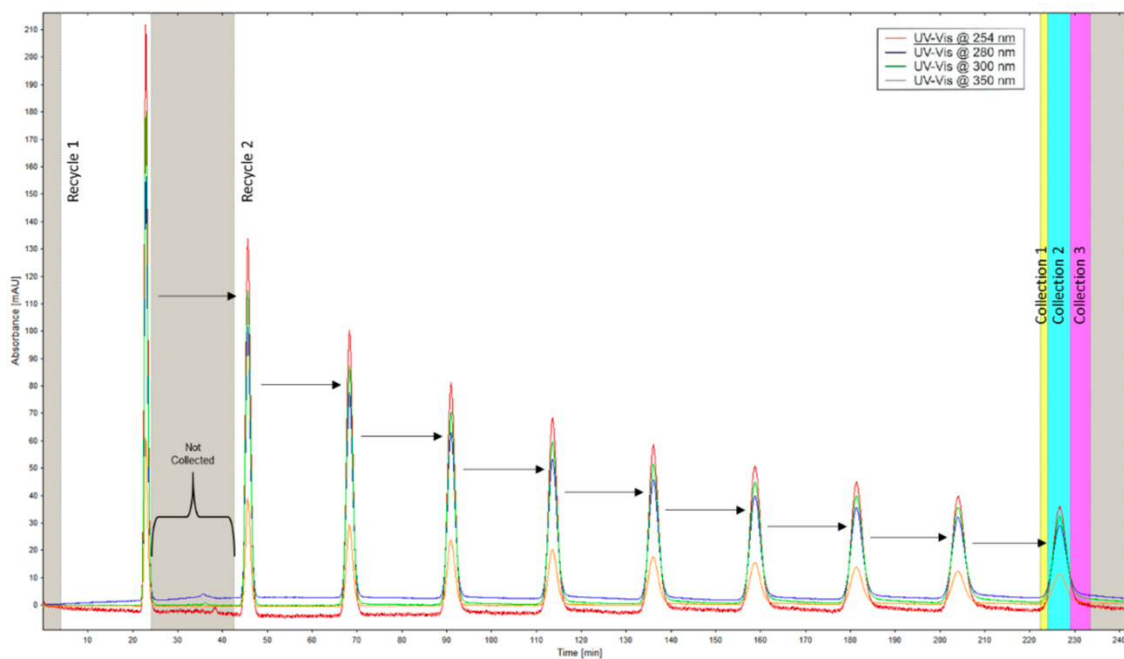
Figure 95. Gel permeation chromatography (GPC) for **158**, Recycling mode. Eluent: CHCl$_3$.
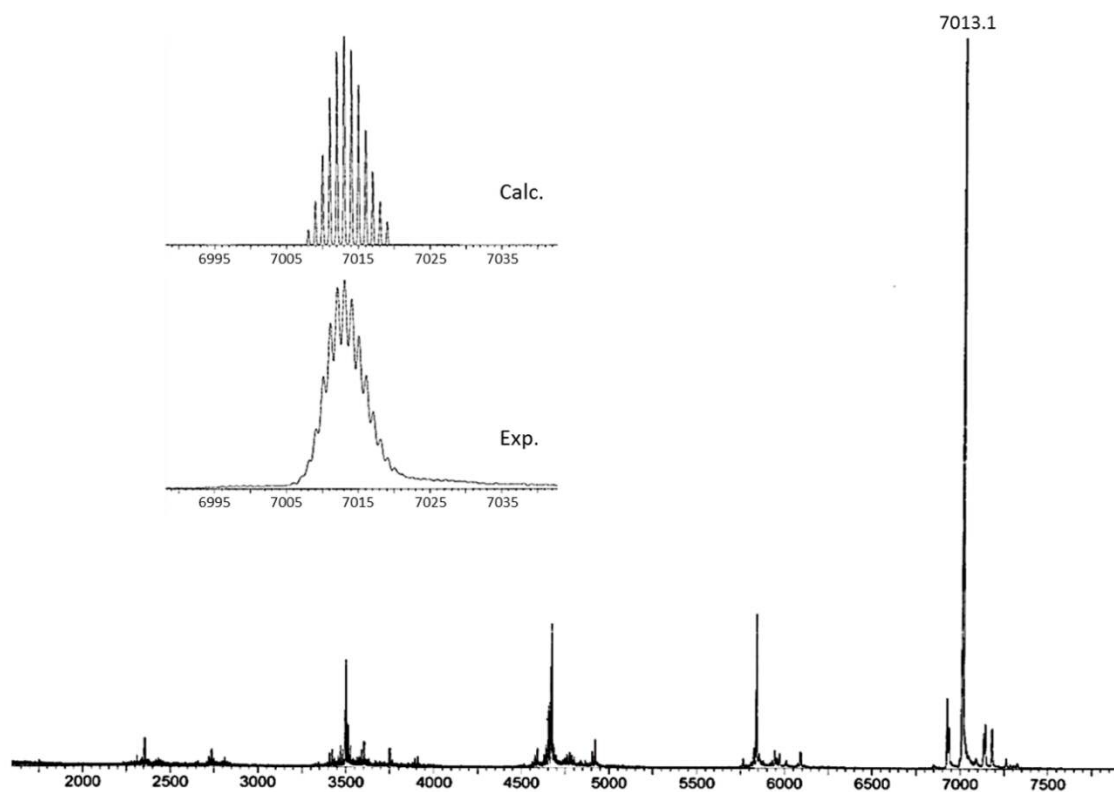
Figure 96. MALDI-TOF mass spectrometry of **158** (Collection 2, from GPC run, above), matrix: trans-2-[3-(4-tert-butyl-phenyl)-2-methyl-2-propenylidene]malonitrile (DCTB).
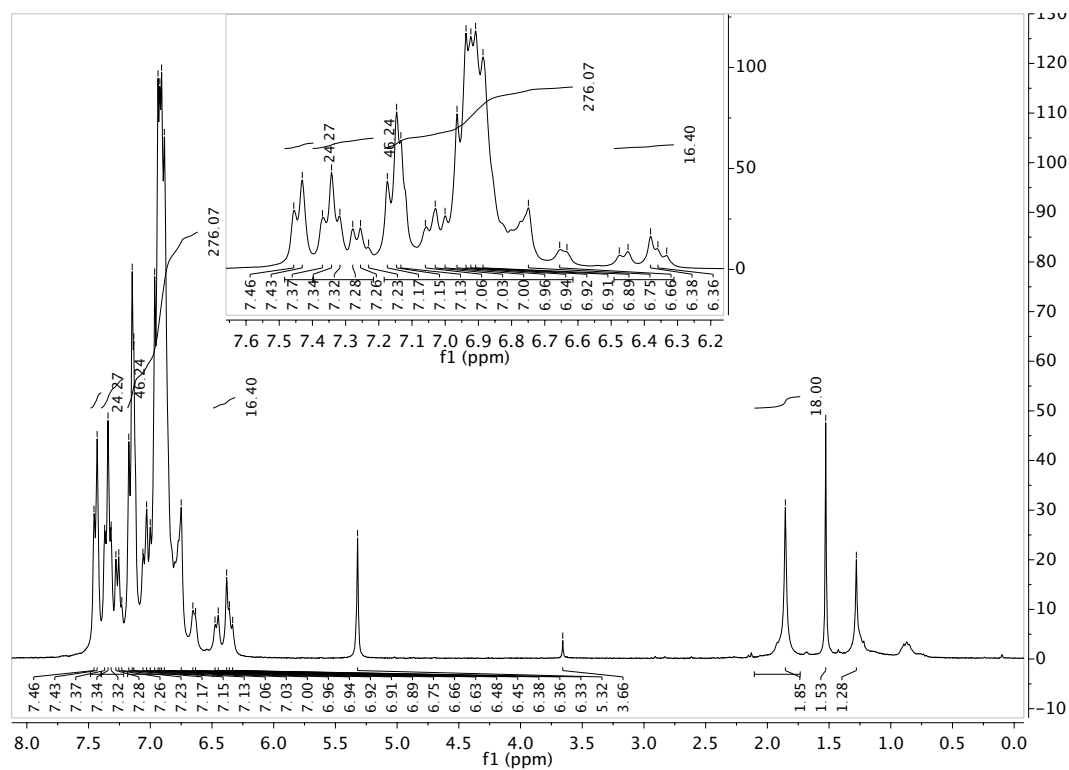
Figure 97. ^{1}H NMR spectrum of **158** in CD_2Cl_2 (300 MHz).
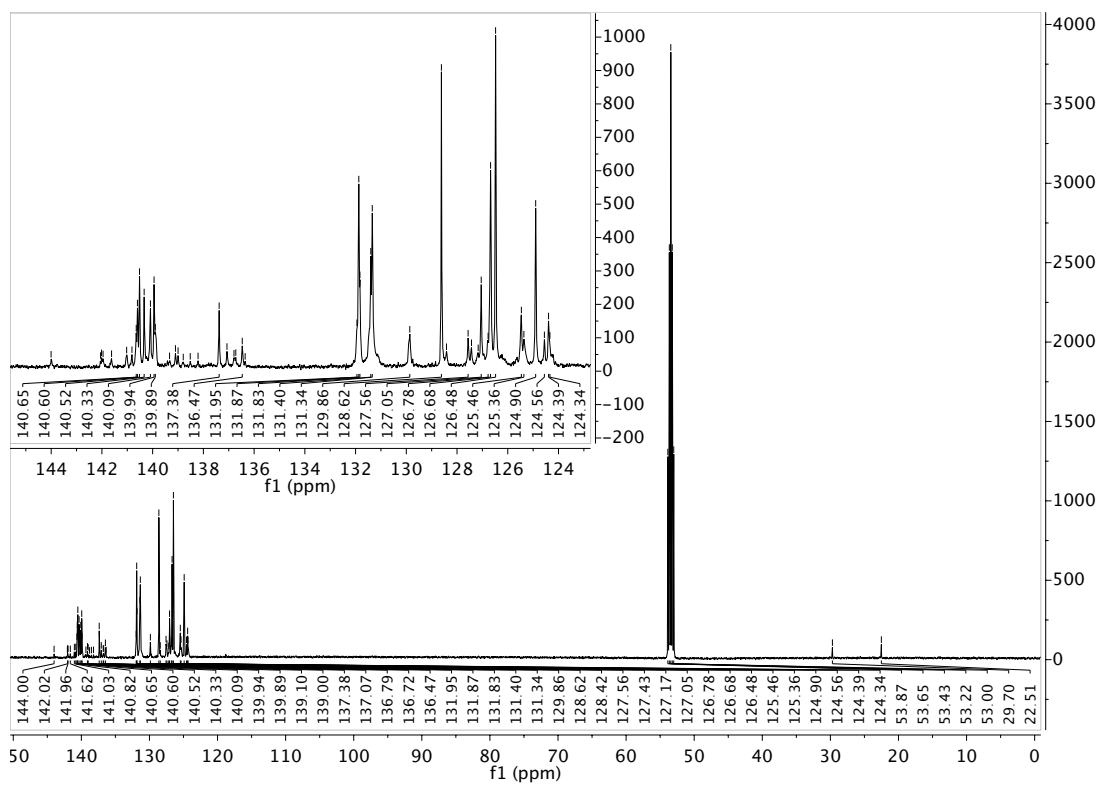
Figure 98. ^{13}C NMR spectrum of **158** in CD_2Cl_2 (100 MHz).
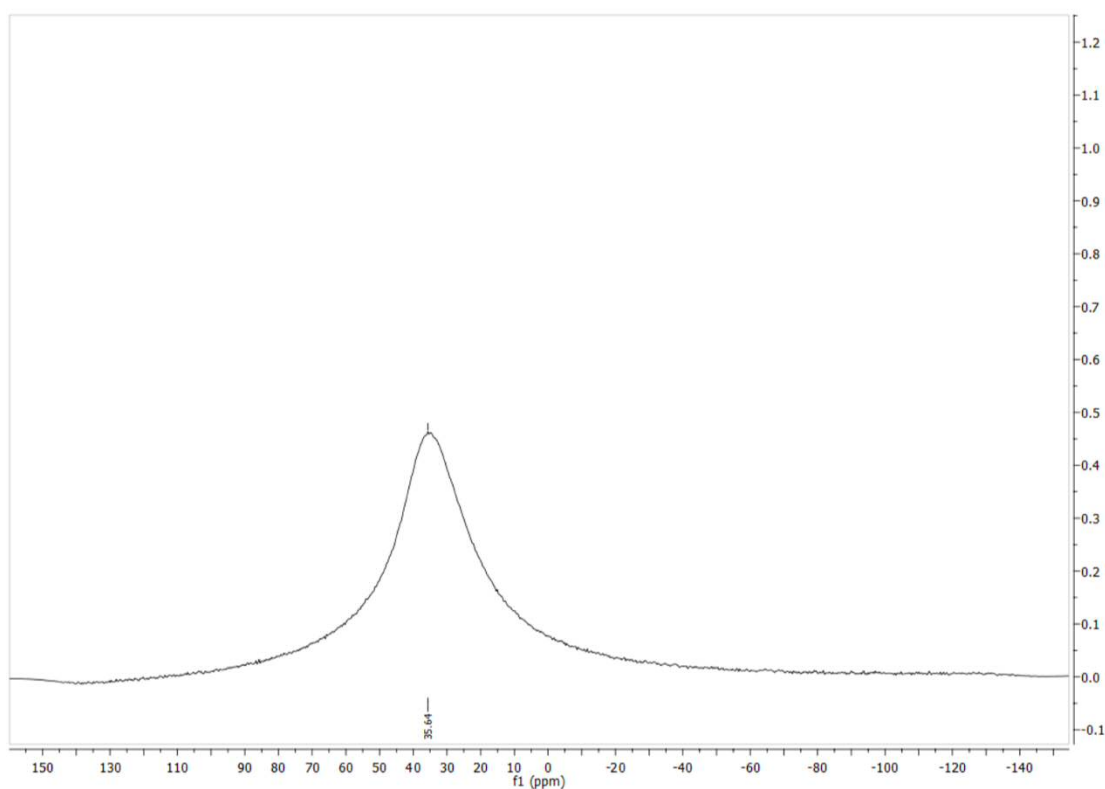
Figure 99. ^{11}B-NMR spectrum of **158** in CD_2Cl_2 (128 MHz).

Characterization of 159
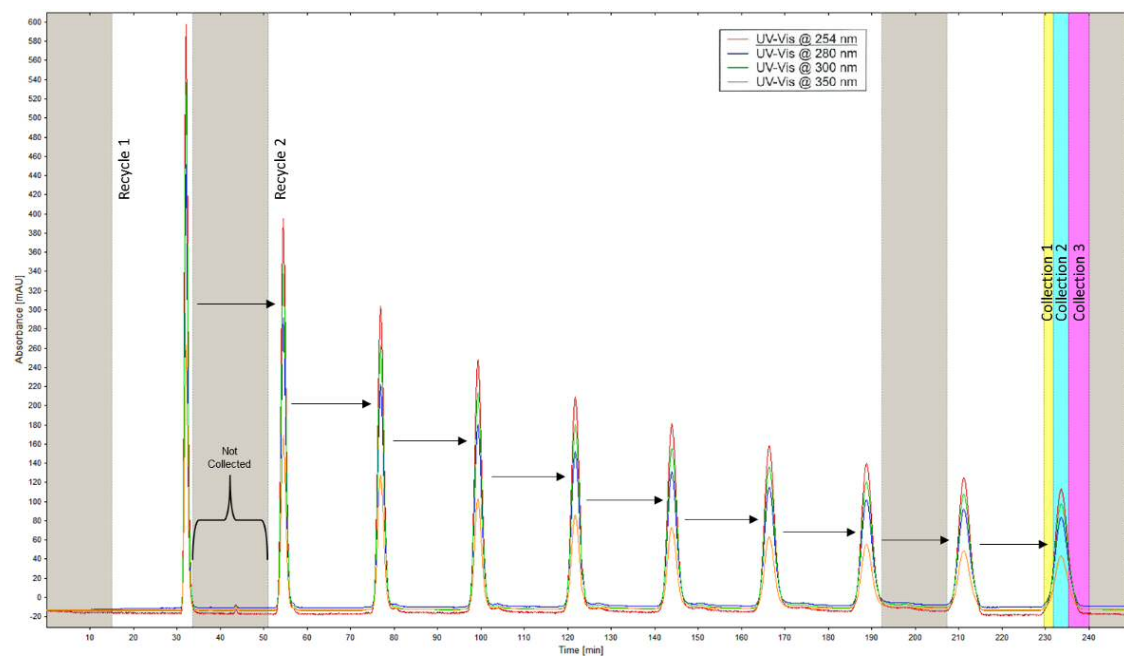
Figure 100. Gel permeation chromatography (GPC) for **159**, Recycling mode. Eluent: CHCl$_3$.
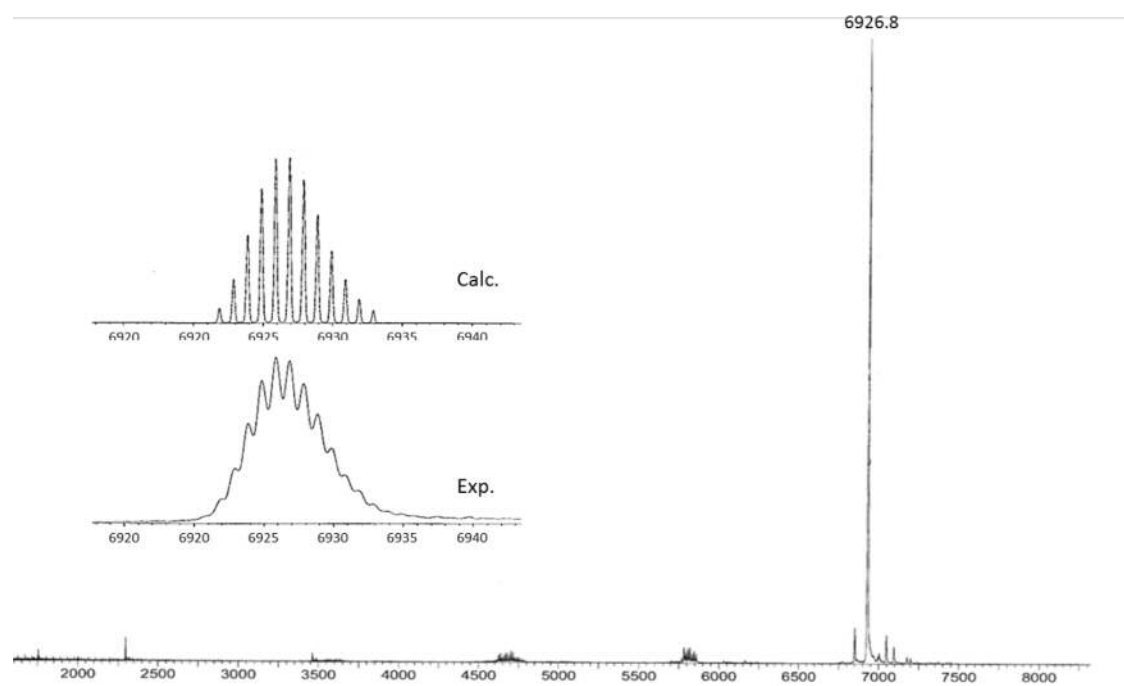
Figure 101. MALDI-TOF mass spectrometry of **159** (collection 2, from GPC run, above), matrix: trans-2-[3-(4-tert-butyl-phenyl)-2-methyl-2-propenylidene]malonitrile (DCTB).
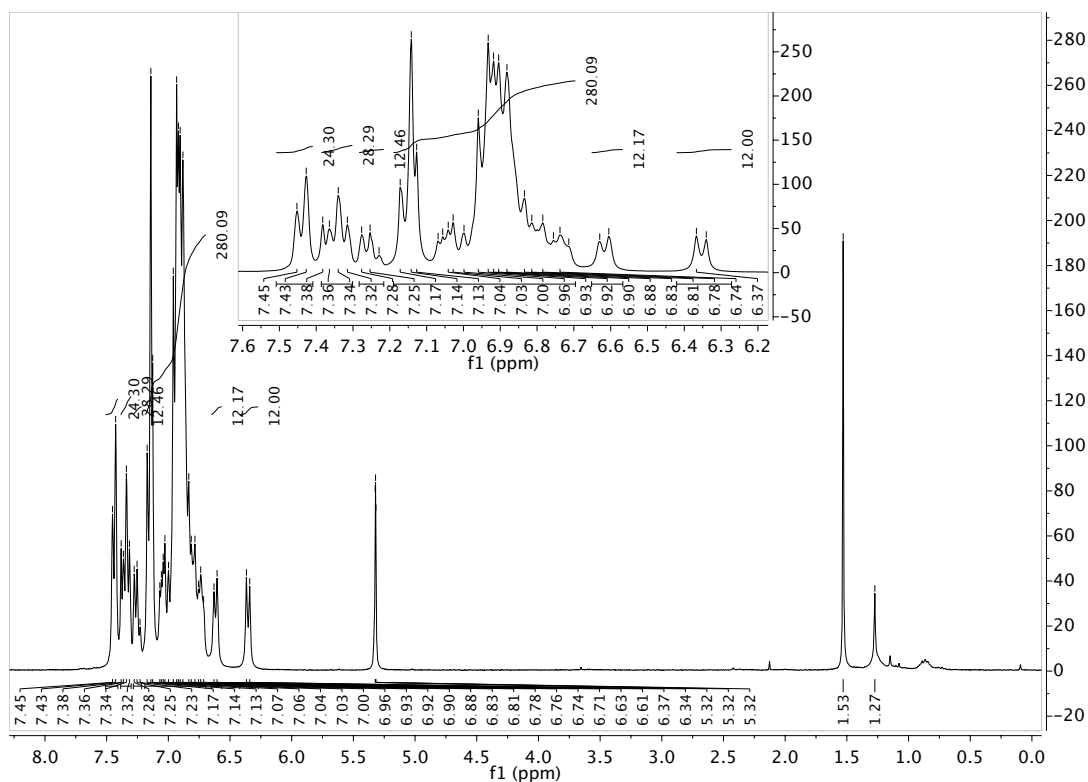
Figure 102. ^{1}H NMR spectrum of **159** in CD$_2$Cl$_2$ (300 MHz).
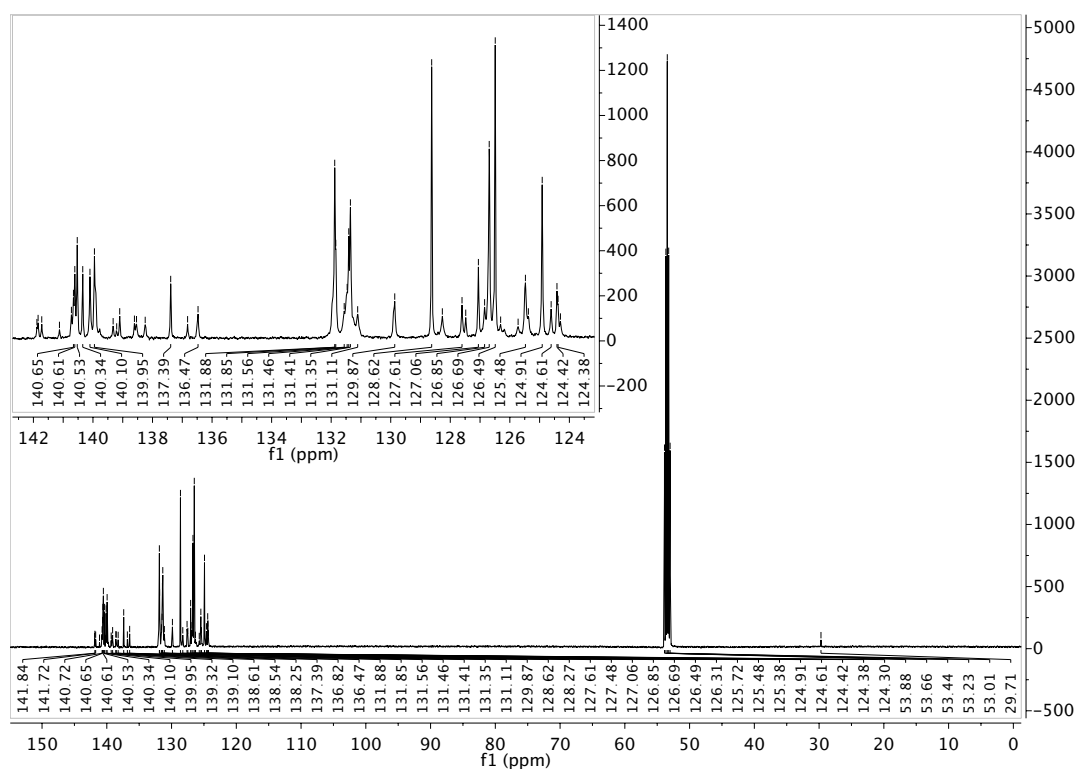
Figure 103. ^{13}C NMR spectrum of **159** in CD$_2$Cl$_2$ (100 MHz).

Characterization of 180
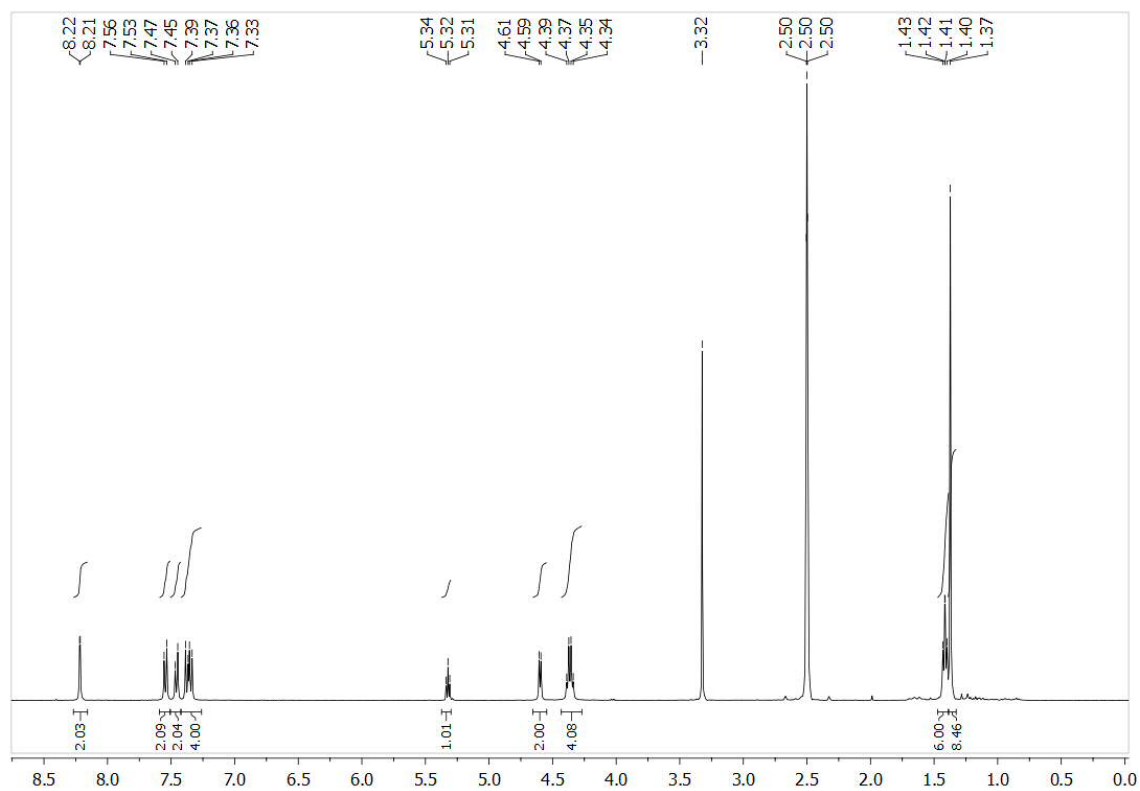
Figure 104. ^{1}H NMR spectrum of **180** in DMSO-d$_6$ (400 MHz).
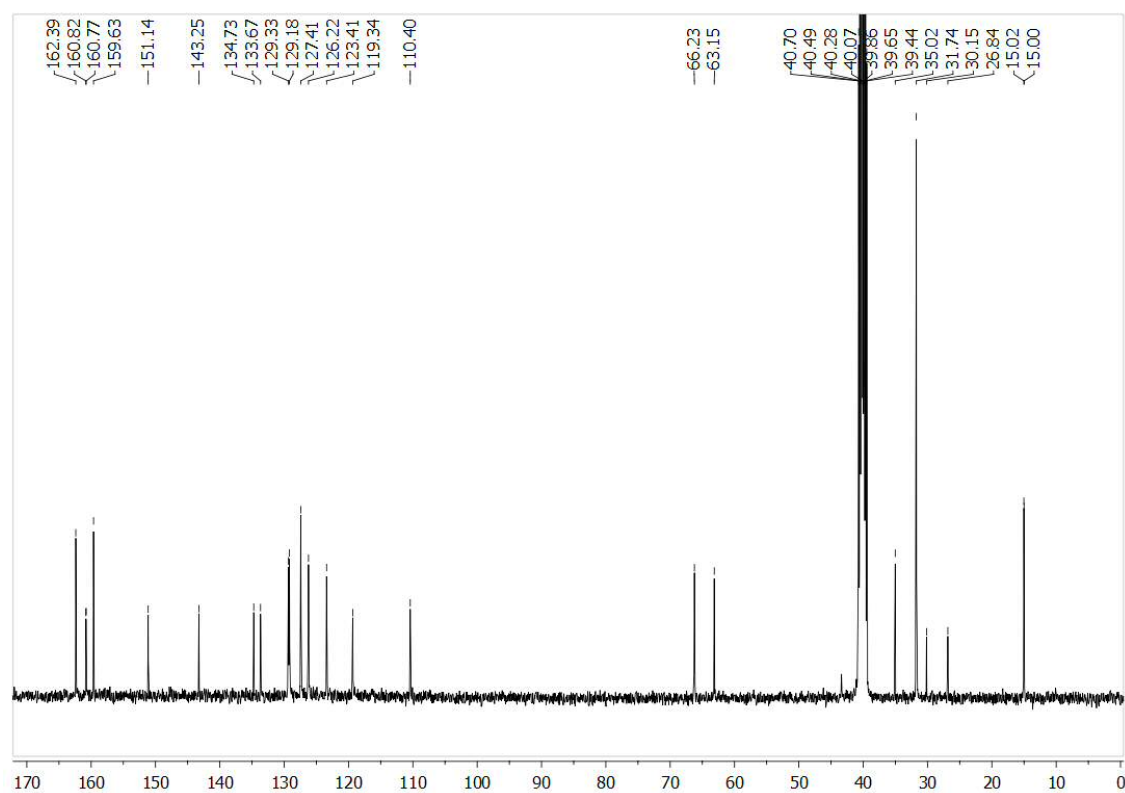
Figure 105. ^{13}C NMR spectrum of **180** in DMSO-d$_6$ (100 MHz).

Characterization of 181
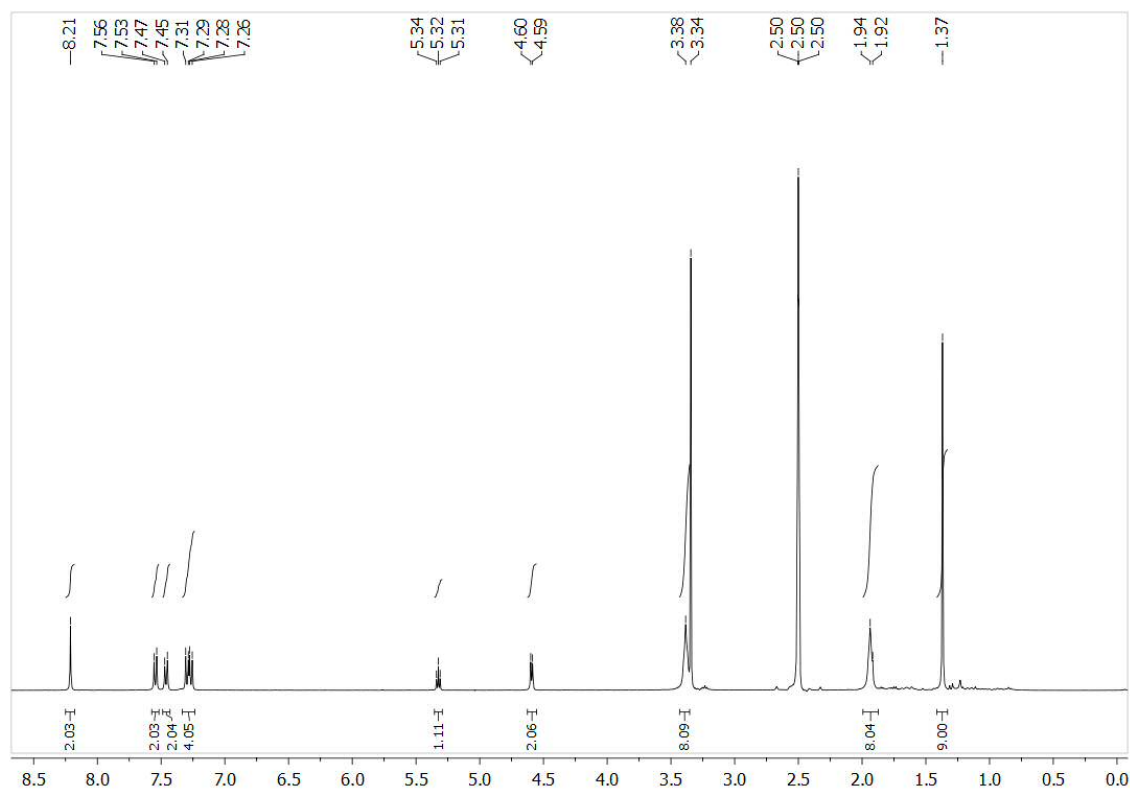
Figure 106. ^{1}H NMR spectrum of **181** in DMSO-d$_6$ (400 MHz).
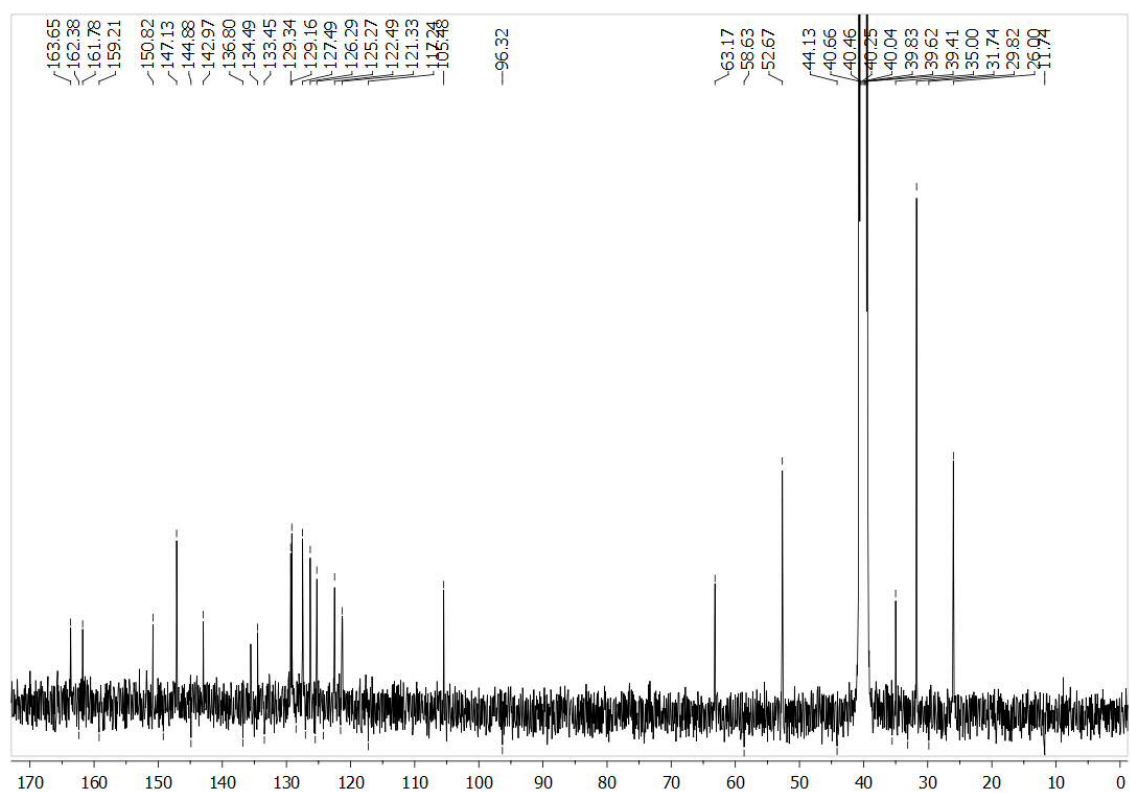
Figure 107. ^{13}C NMR spectrum of **181** in DMSO-d$_6$ (100 MHz).

Characterization of 174
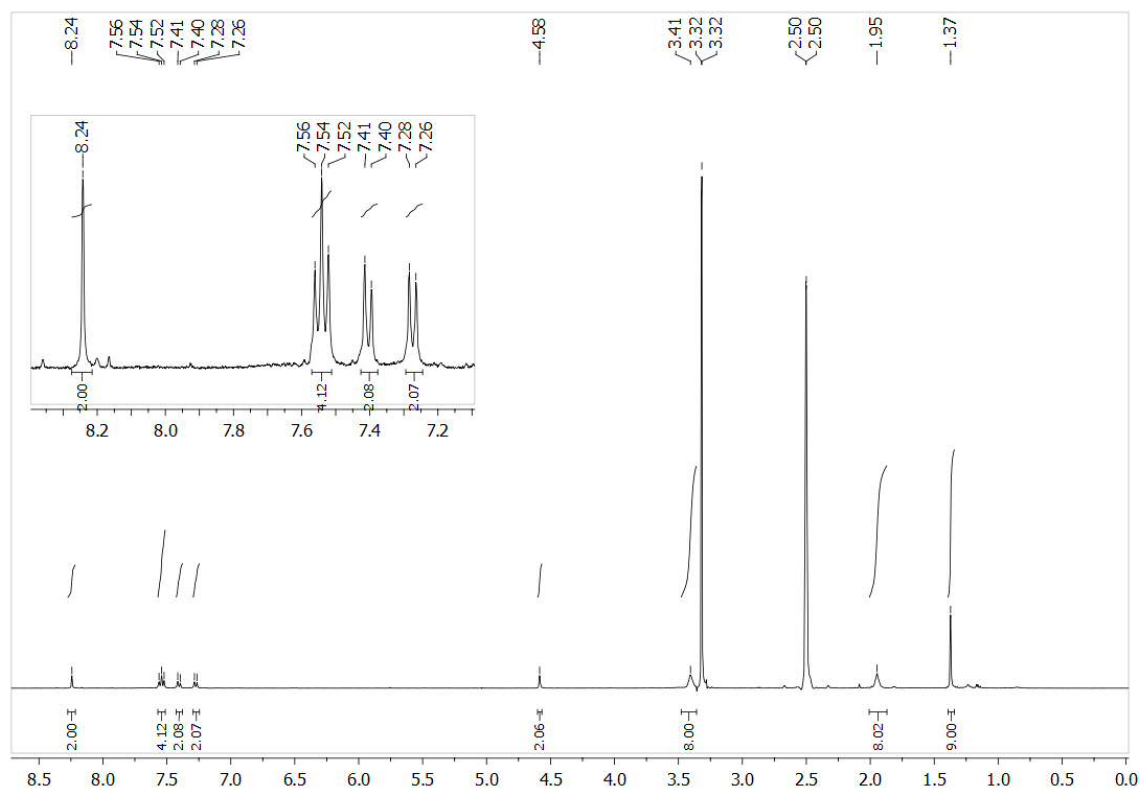
Figure 108. ^{1}H NMR spectrum of **174** in DMSO-d$_6$ (400 MHz).

Characterization of 182
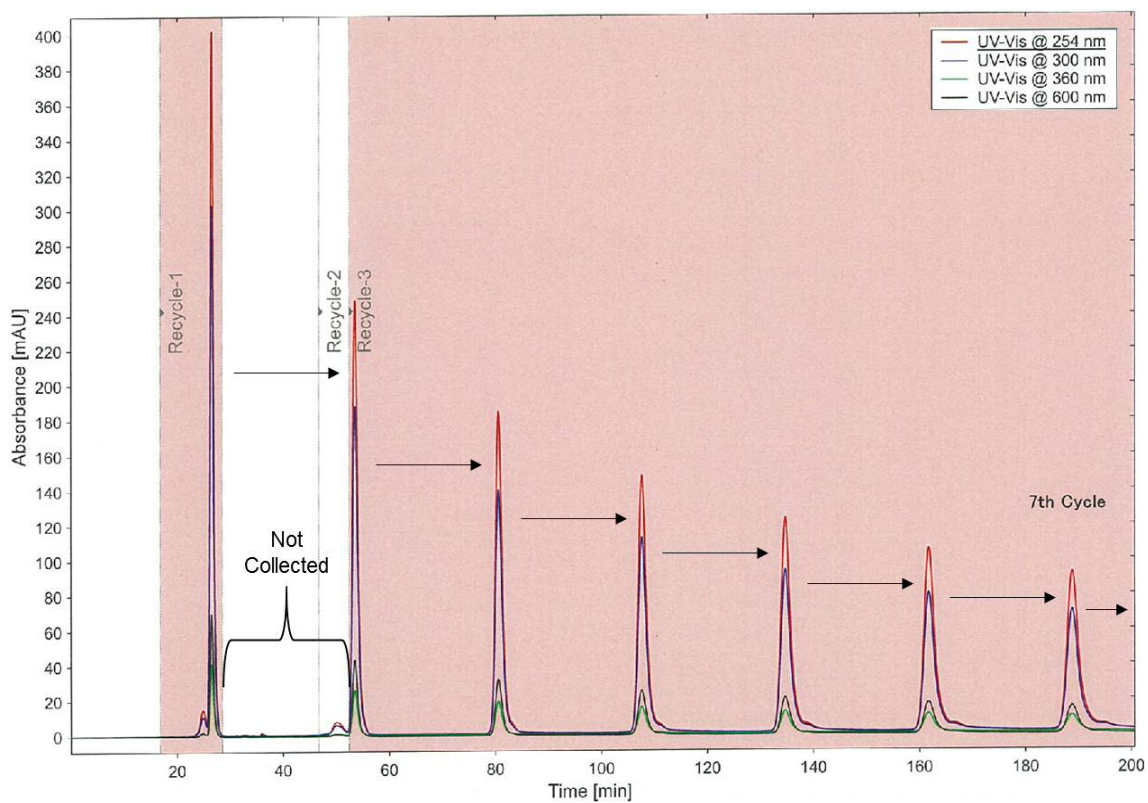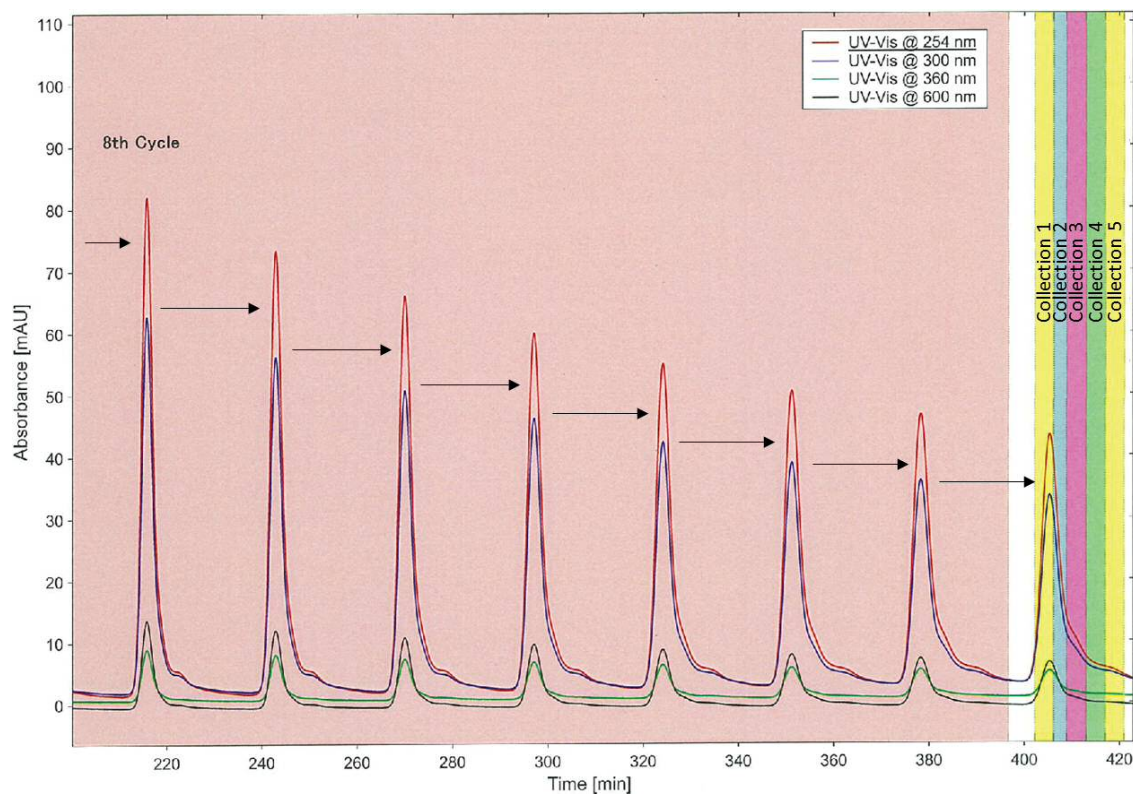
Figure 109. Gel permeation chromatography (GPC) for **182**, Recycling mode. Eluent: $CHCl_3$.
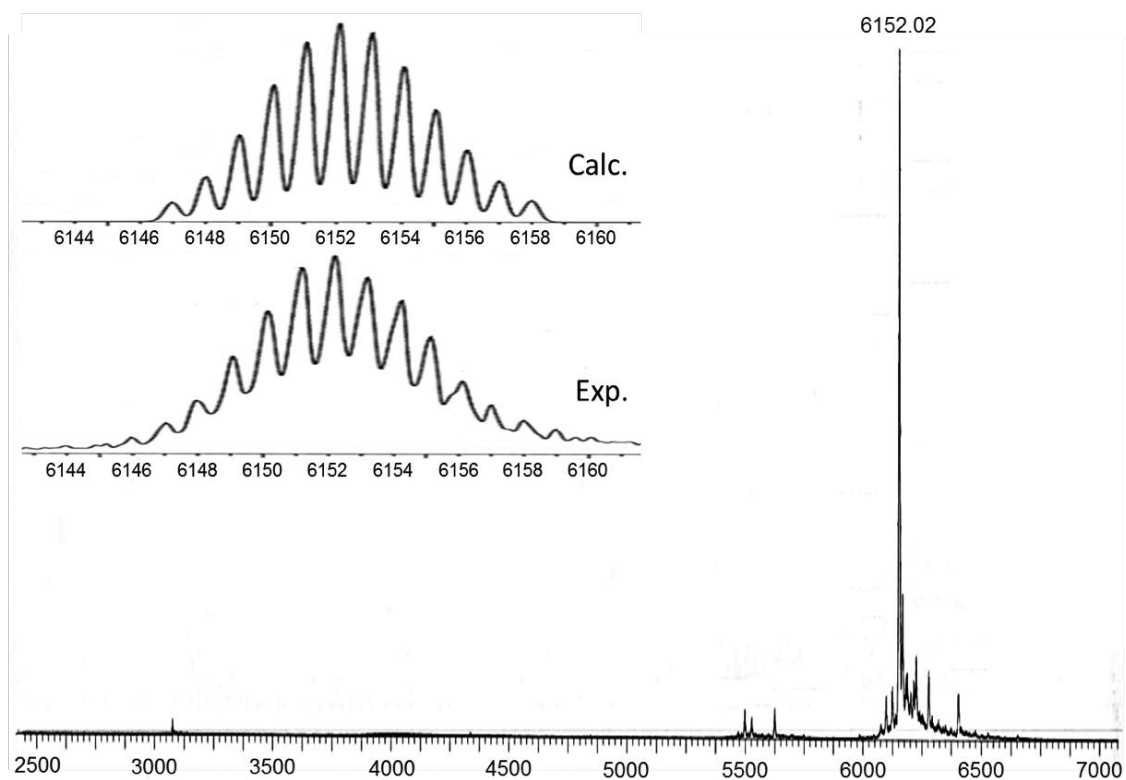
Figure 110. MALDI-TOF mass spectrometry of **182** (collection 1, from GPC run, above), matrix: trans-2-[3-(4-tert-butyl-phenyl)-2-methyl-2-propenylidene]malonitrile (DCTB).
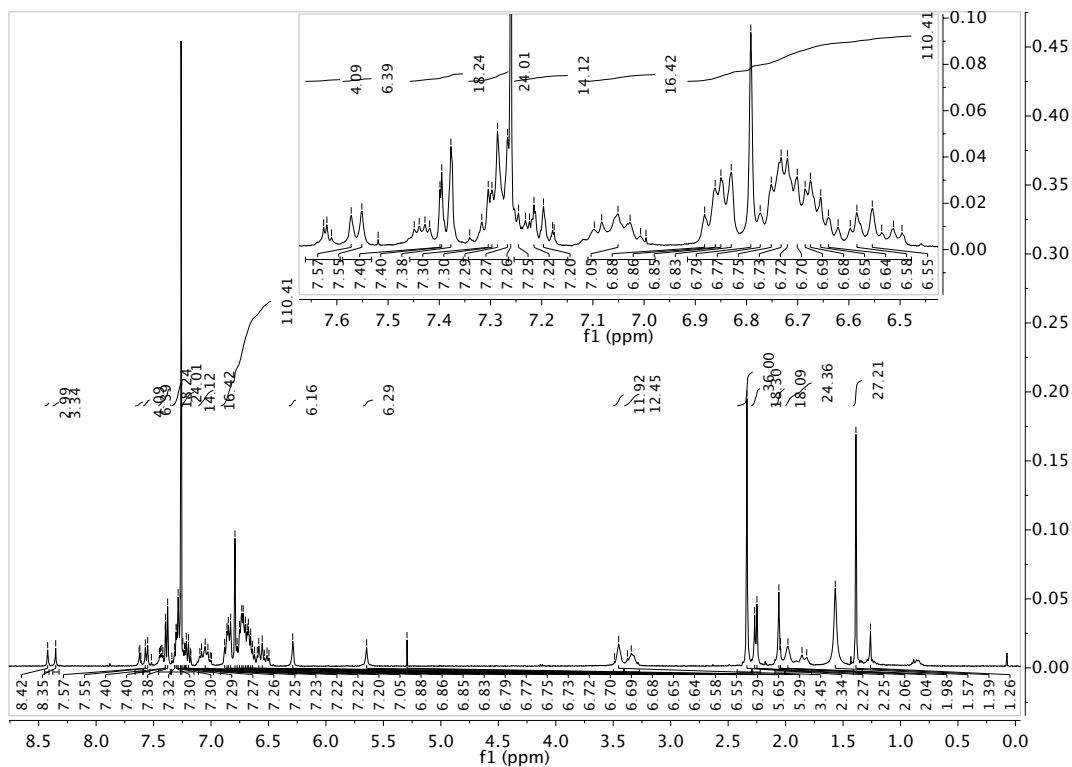
Figure 111. ^{1}H NMR spectrum of **182** in CDCl$_3$ (400 MHz)
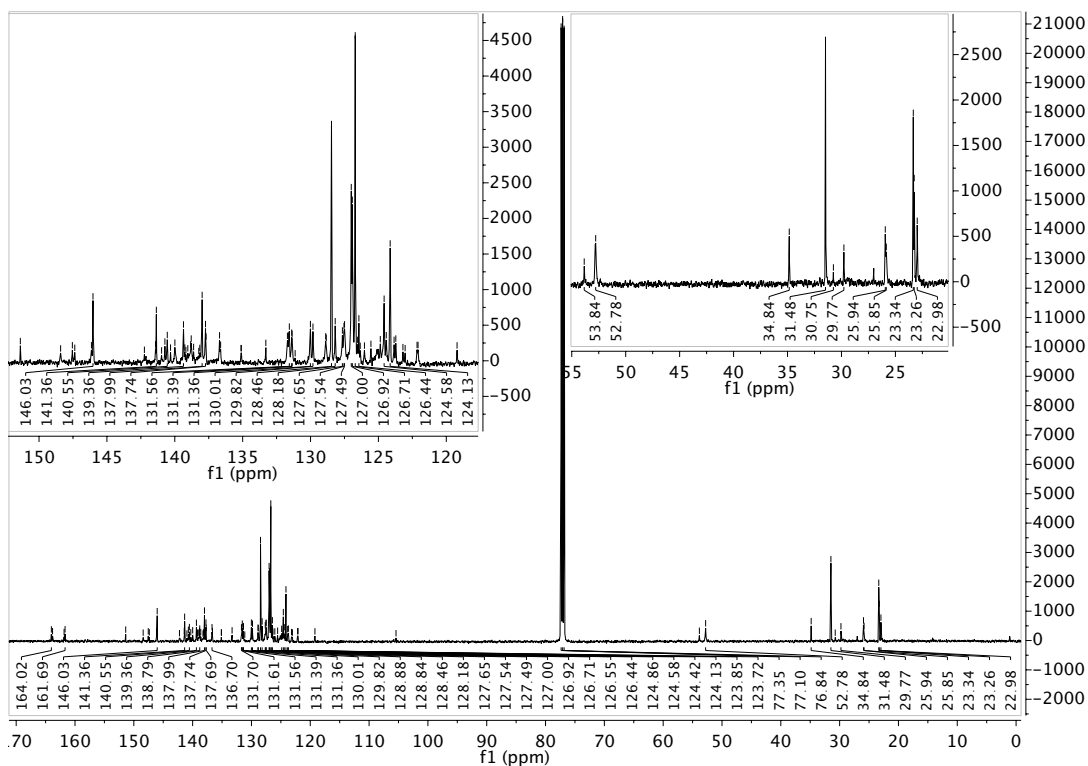
Figure 112. ^{13}C NMR spectrum of **182** in CDCl$_3$ (100 MHz)
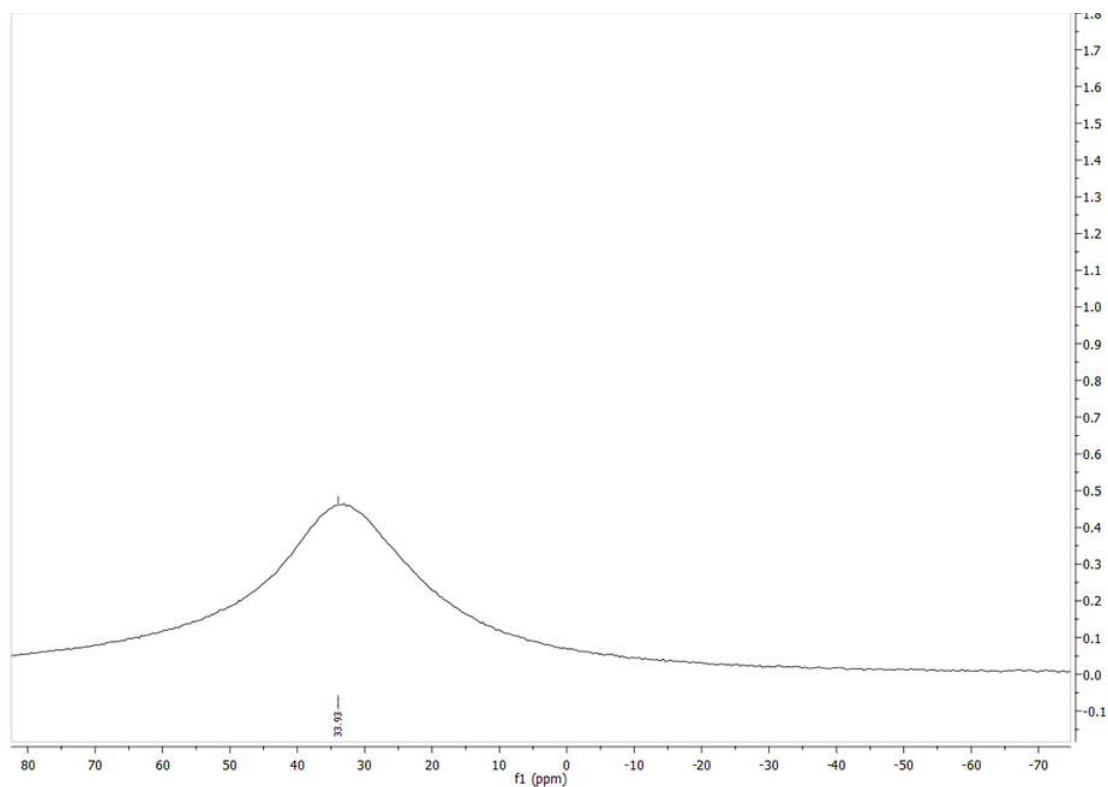
Figure 113. ^{11}B NMR spectrum of **182** in CDCl$_3$ (128 MHz).

Characterization of 186
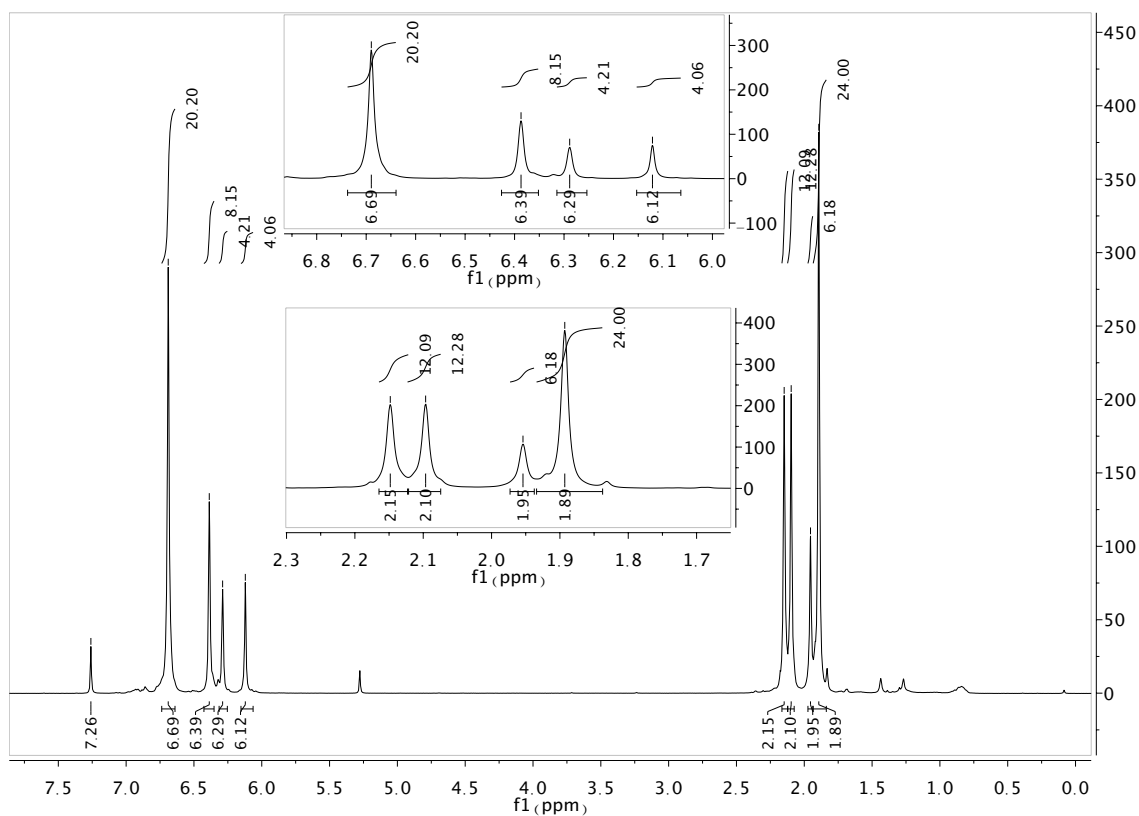
Figure 114. ^{1}H NMR spectrum of **186** in CDCl$_3$ (400 MHz).
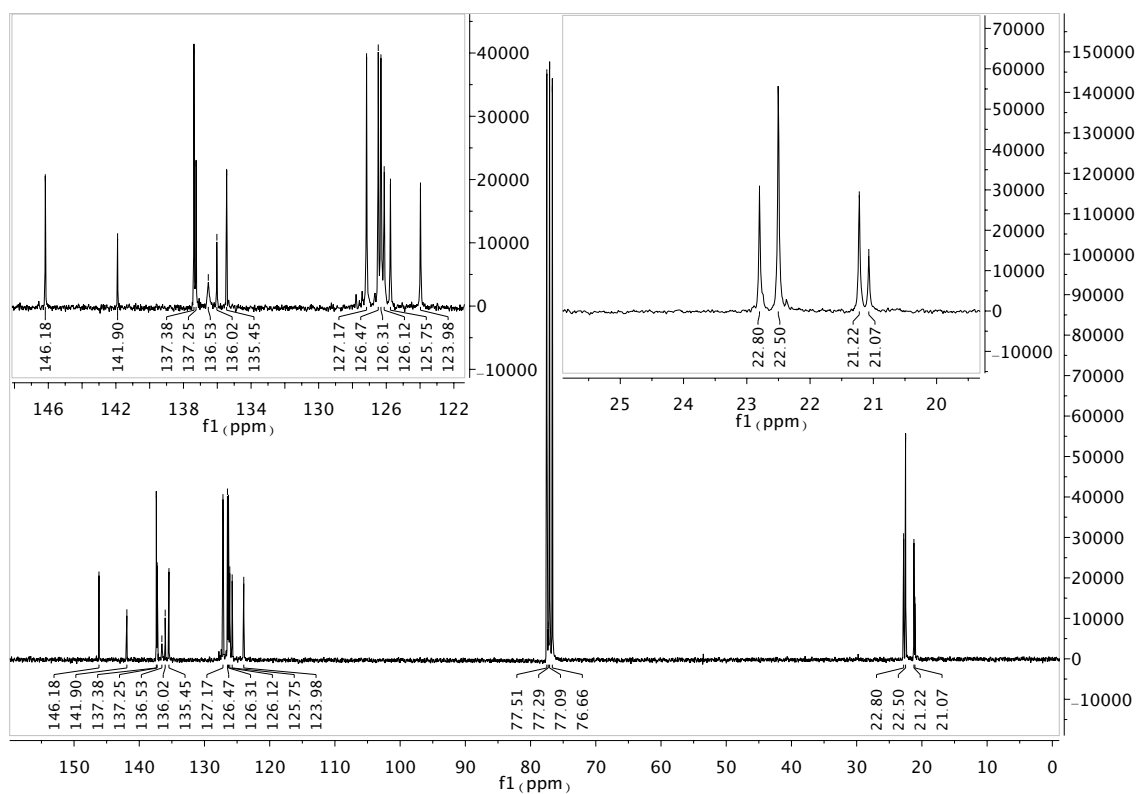
Figure 115. ^{13}C NMR spectrum of **186** in CDCl$_3$ (100 MHz).

Characterization of 190
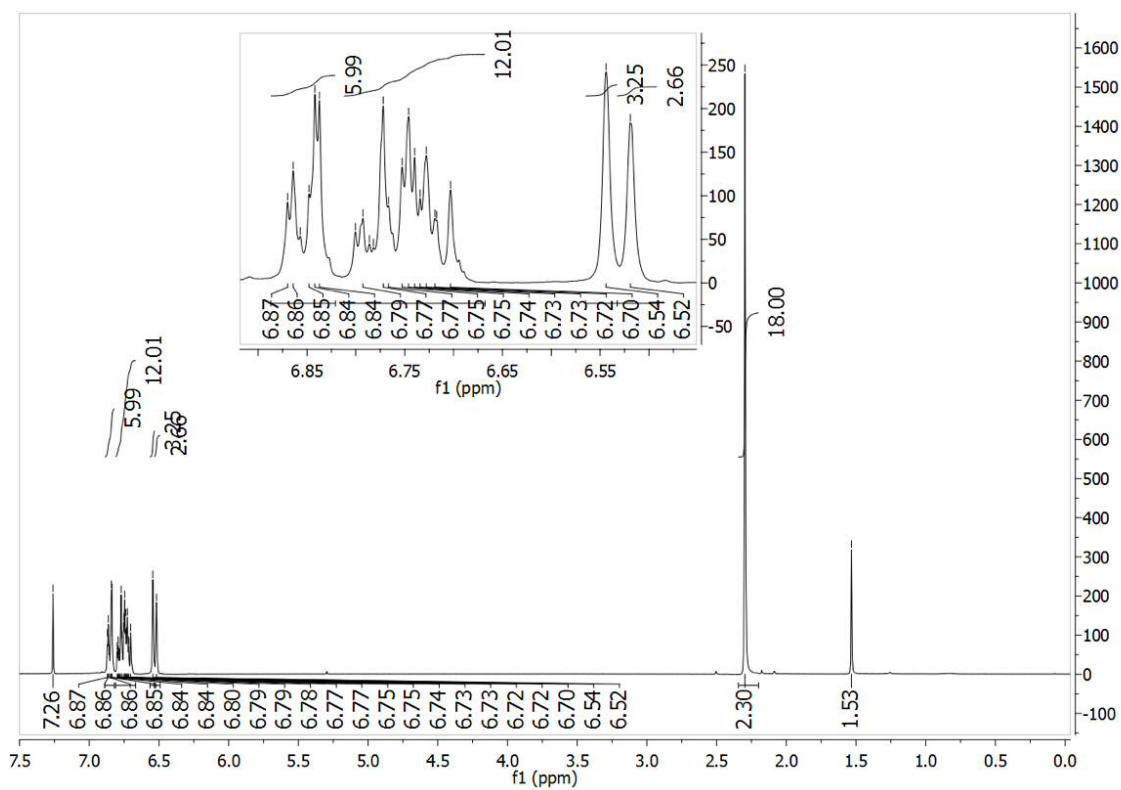
Figure 116. ^1H NMR spectrum of **190** in CDCl$_3$ (400 MHz).

Figure 117. ^{13}C NMR spectrum of **190** in CDCl$_3$ (100 MHz).
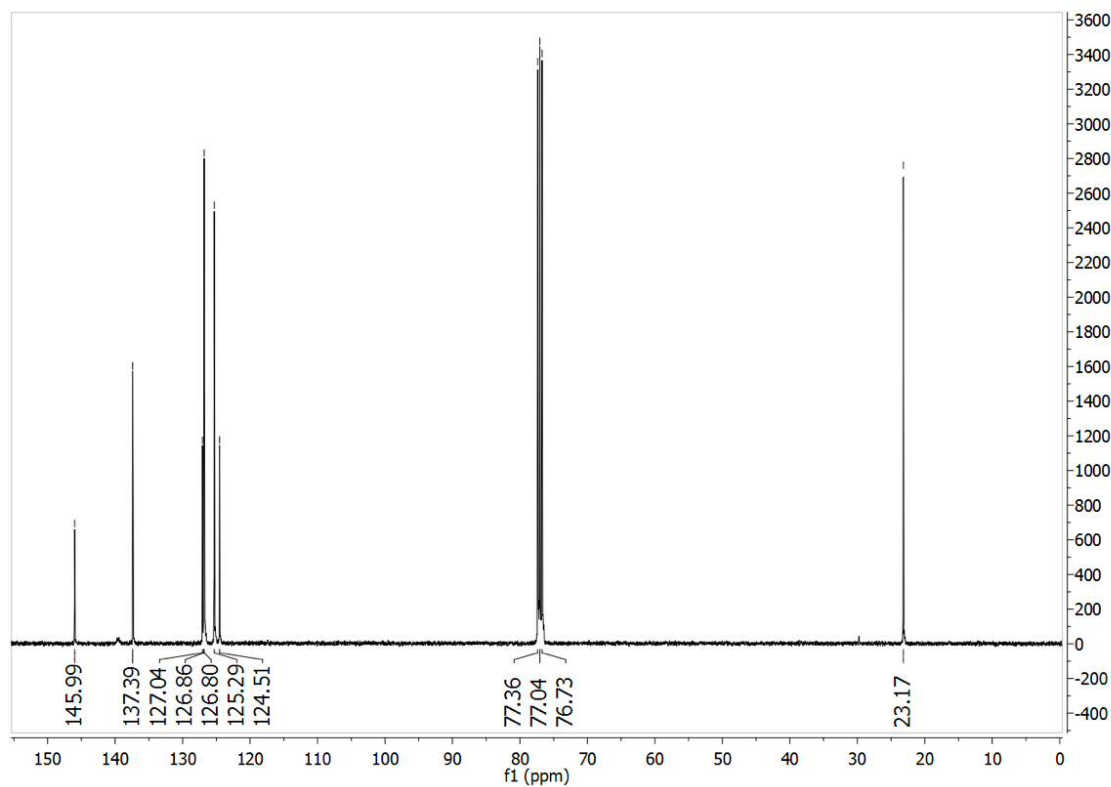
Characterization of 191

Figure 118. ^{1}H NMR spectrum of **191** in CDCl$_3$ (400 MHz).
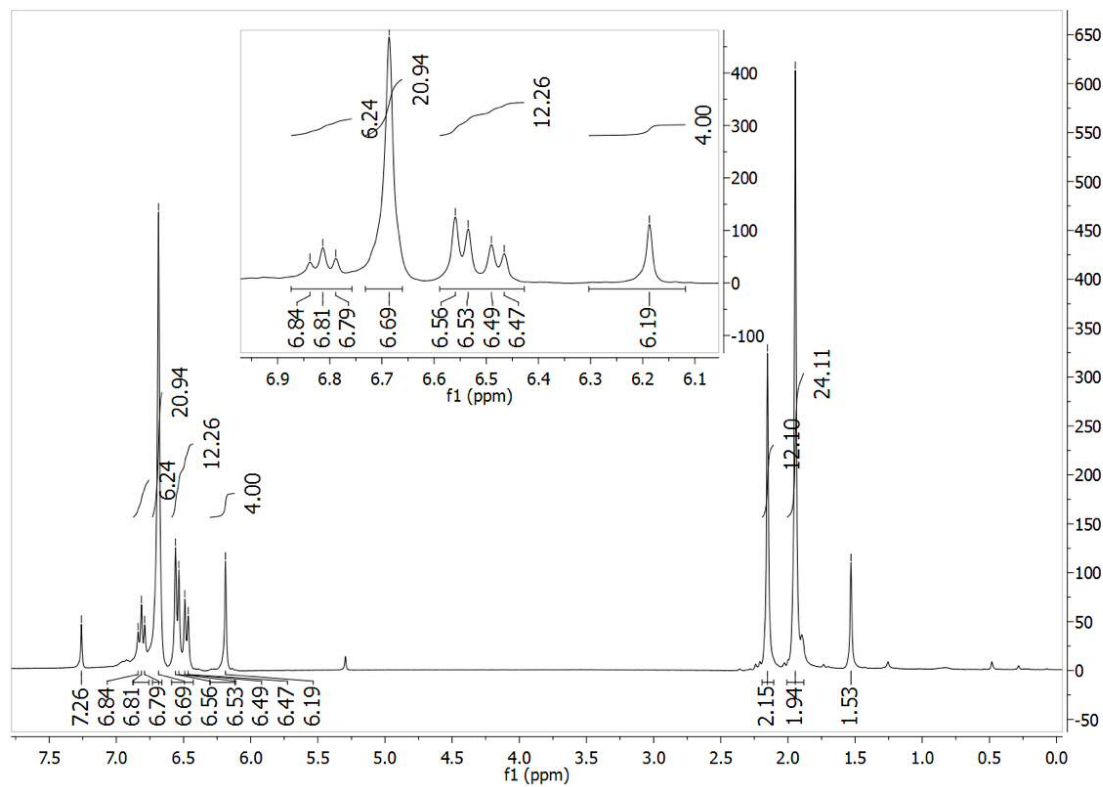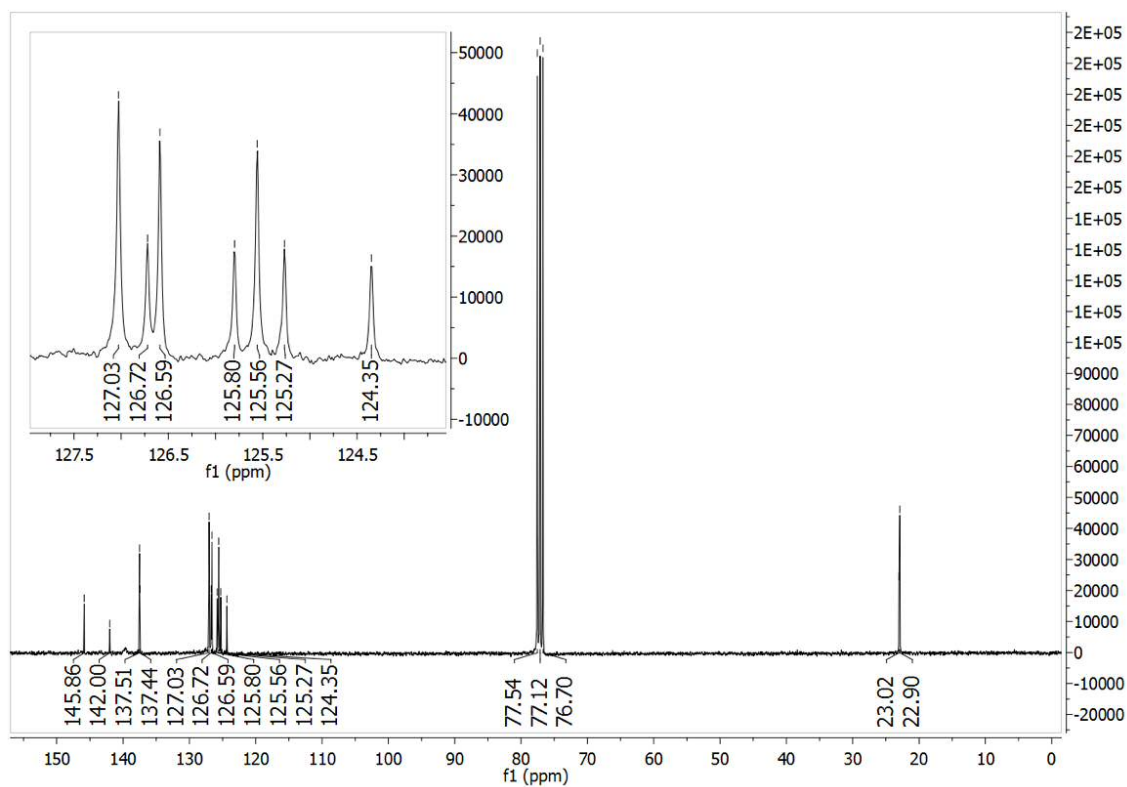
Figure 119. ^{13}C NMR spectrum of **191** in CDCl$_3$ (100 MHz).

Characterization of 192 (in the presence of 193 as impurity)
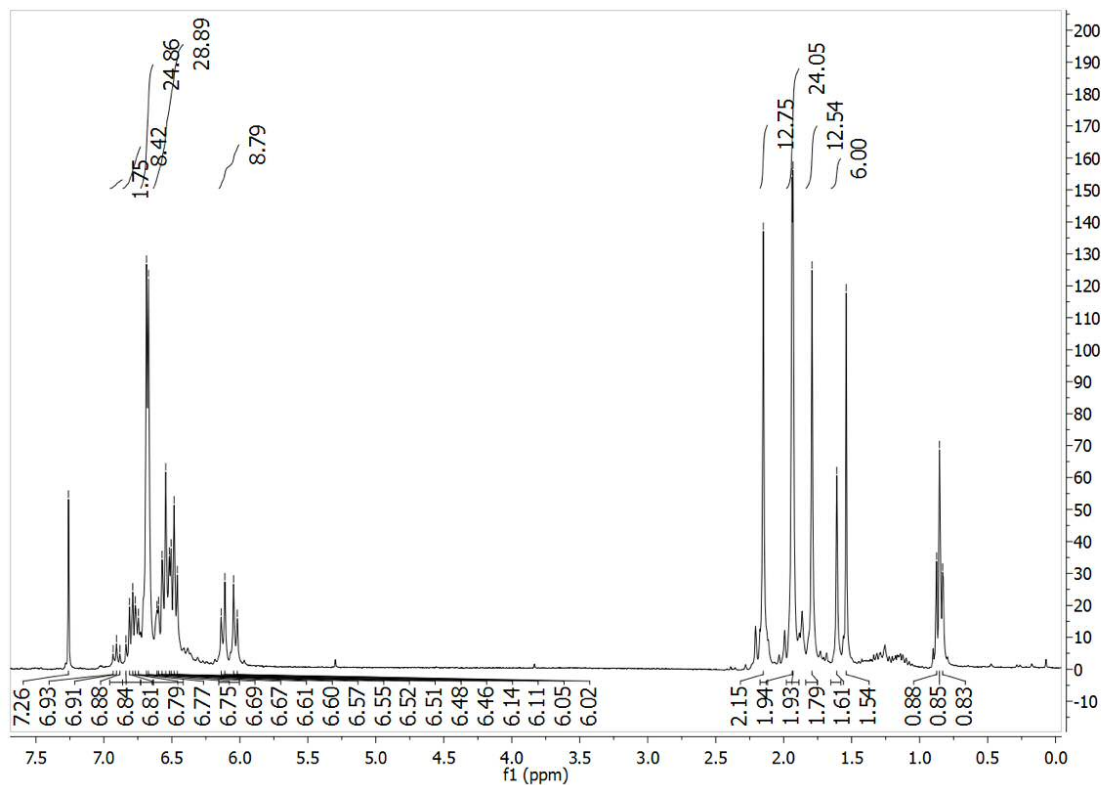
Figure 120. ^{1}H NMR spectrum of **192** in CDCl$_3$ (400 MHz).
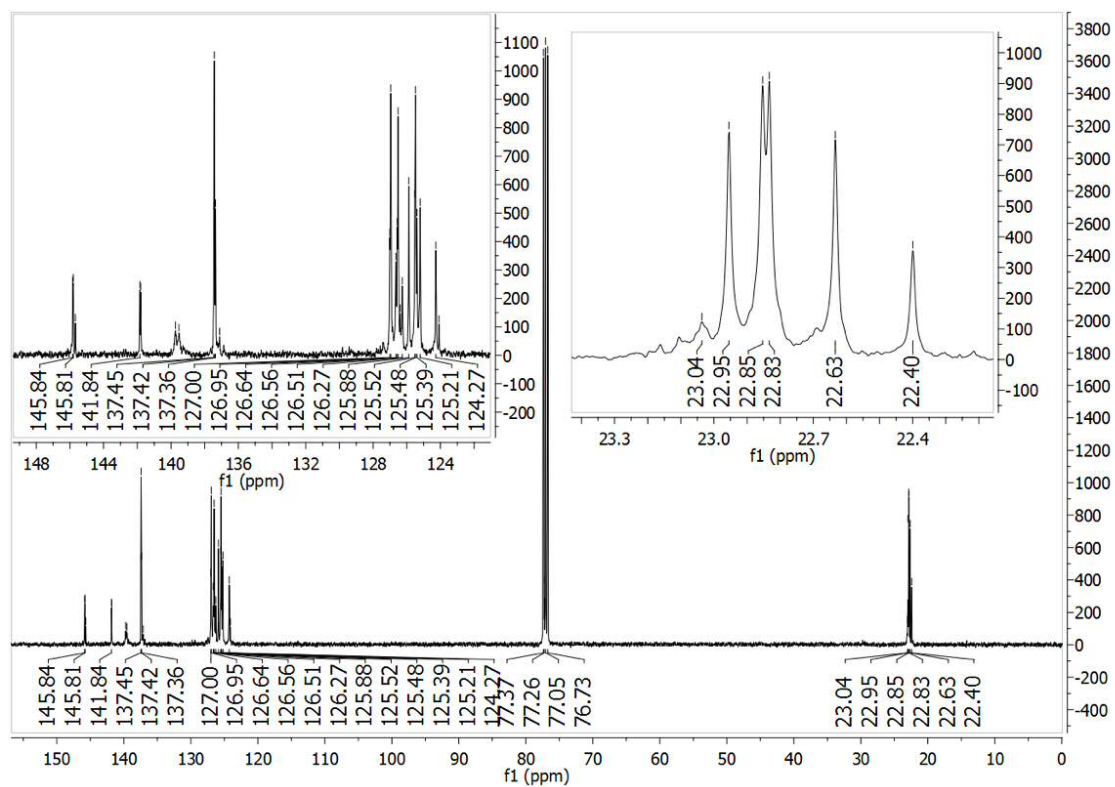
Figure 121. ^{13}C NMR spectrum of **198** in CDCl$_3$ (100 MHz).

Characterization of 199
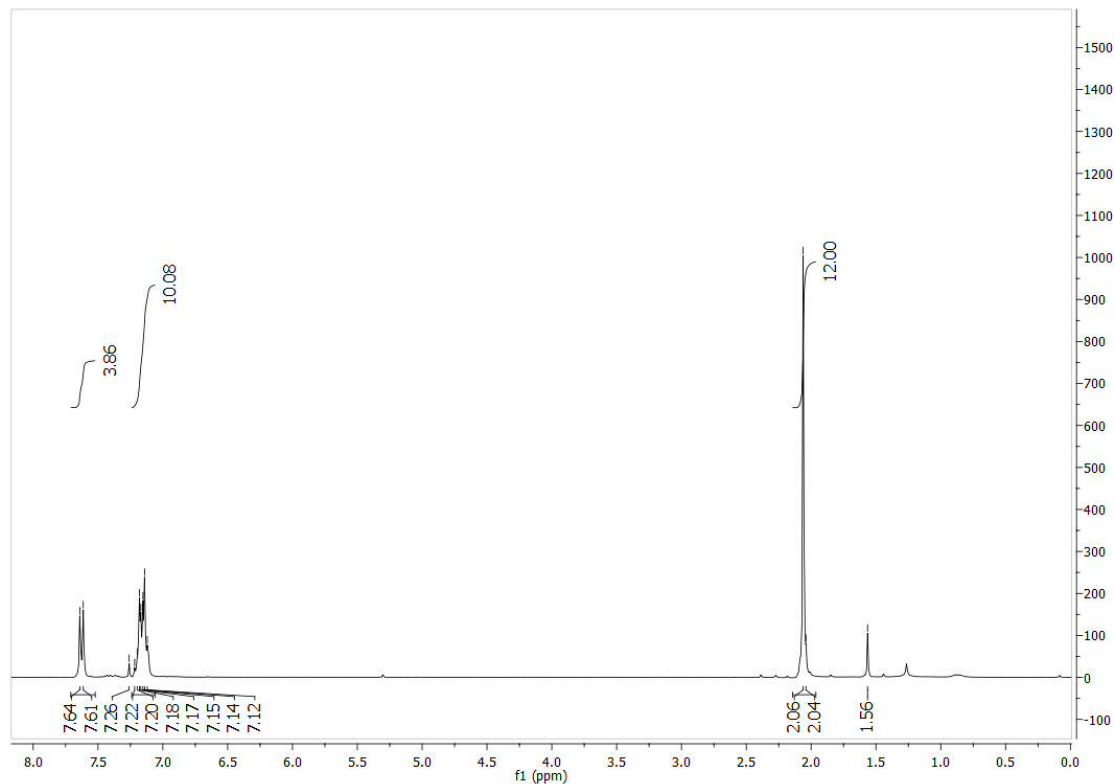
Figure 122. ^{1}H NMR spectrum of **199** in CDCl$_3$ (400 MHz).

Characterization of 200
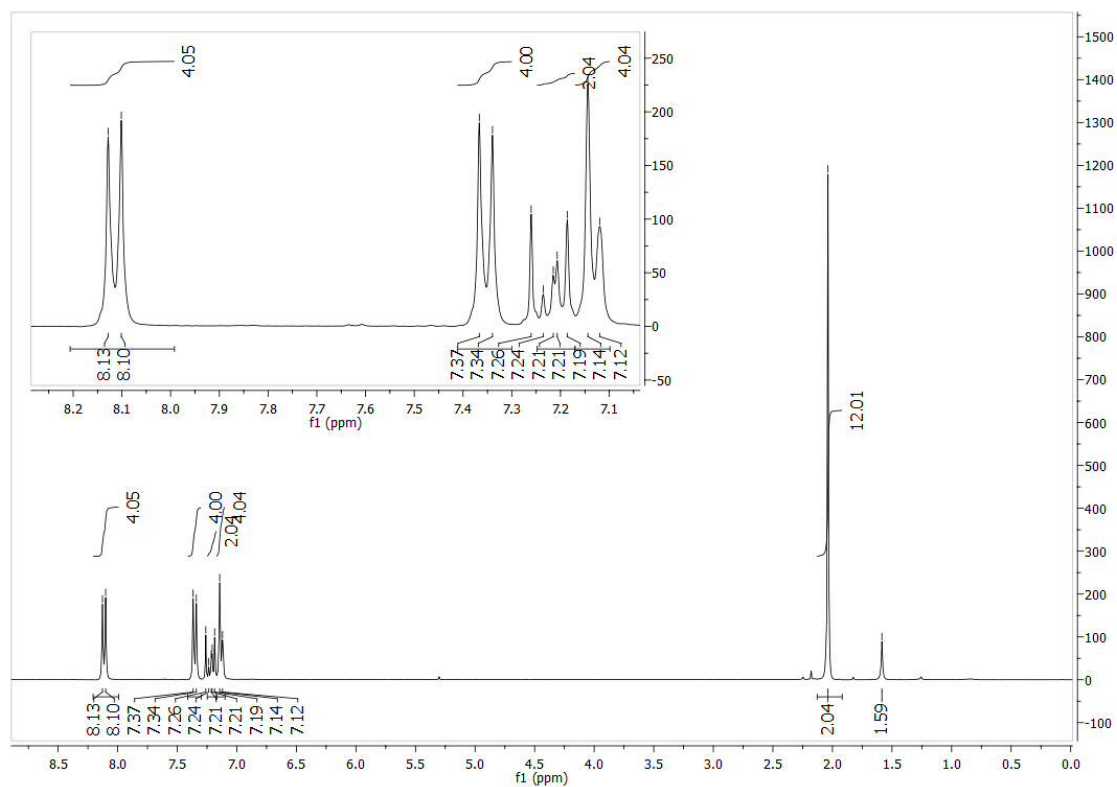
Figure 123. ^{1}H NMR spectrum of **200** in CDCl$_3$ (400 MHz).
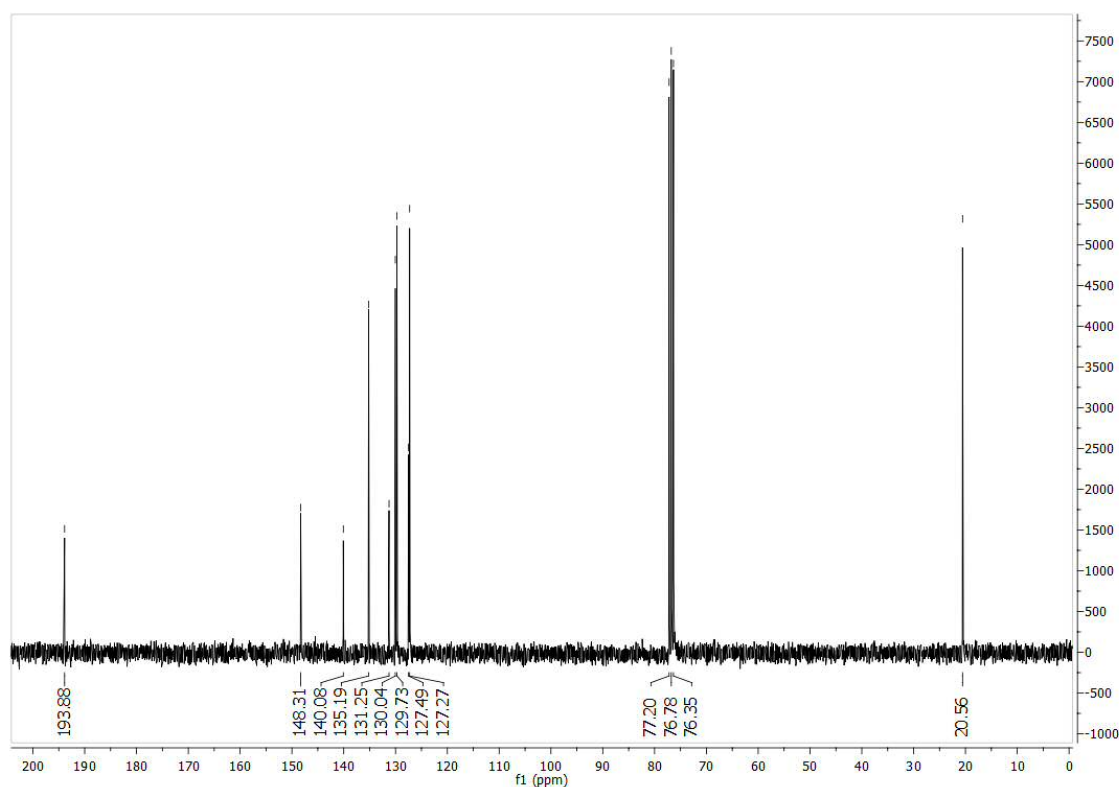
Figure 124. ^{13}C NMR spectrum of **200** in CDCl$_3$ (100 MHz).

Characterization of 201

219
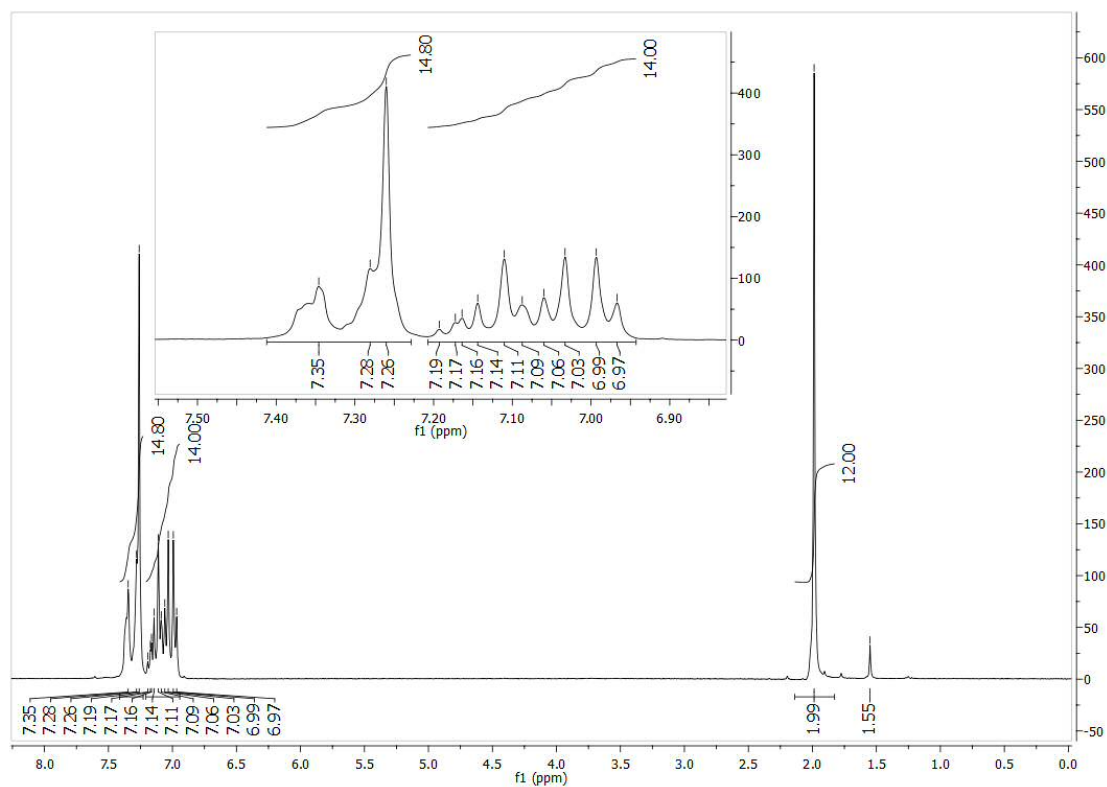
Figure 125. ^{1}H NMR spectrum of **201** in CDCl$_3$ (400 MHz).
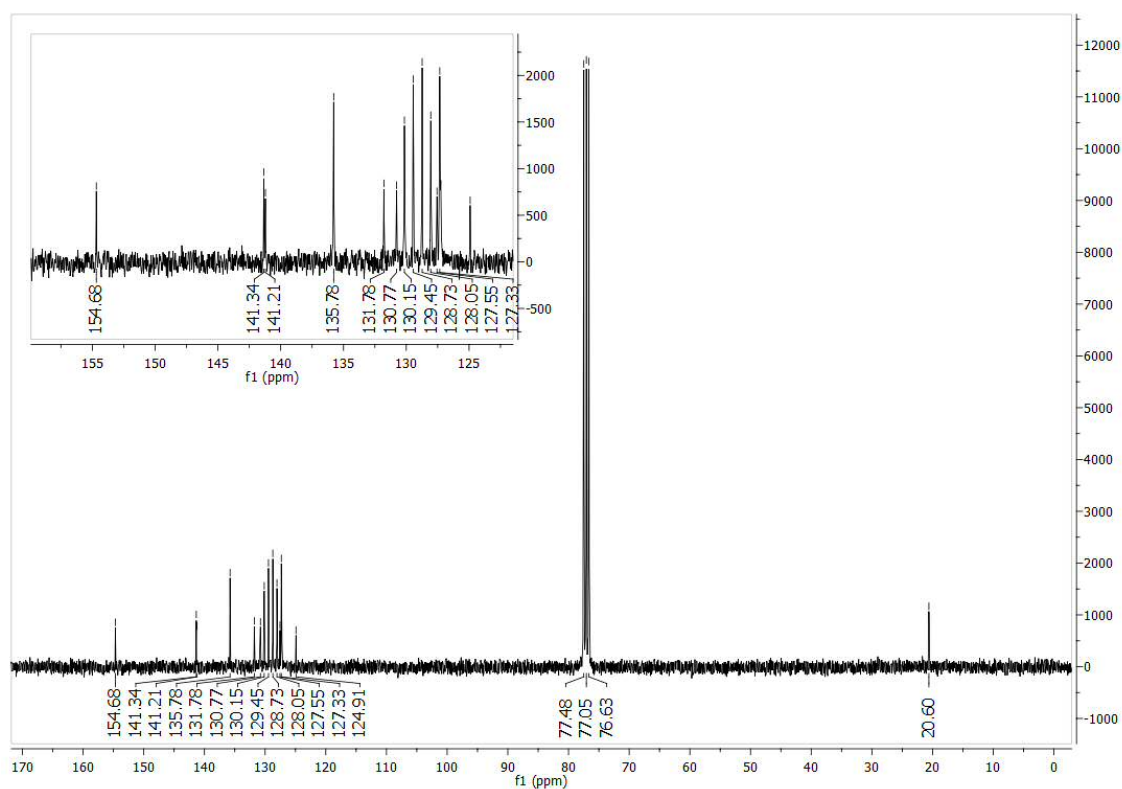
Figure 126. ^{13}C NMR spectrum of **201** in CDCl$_3$ (100 MHz).

Characterization of 202
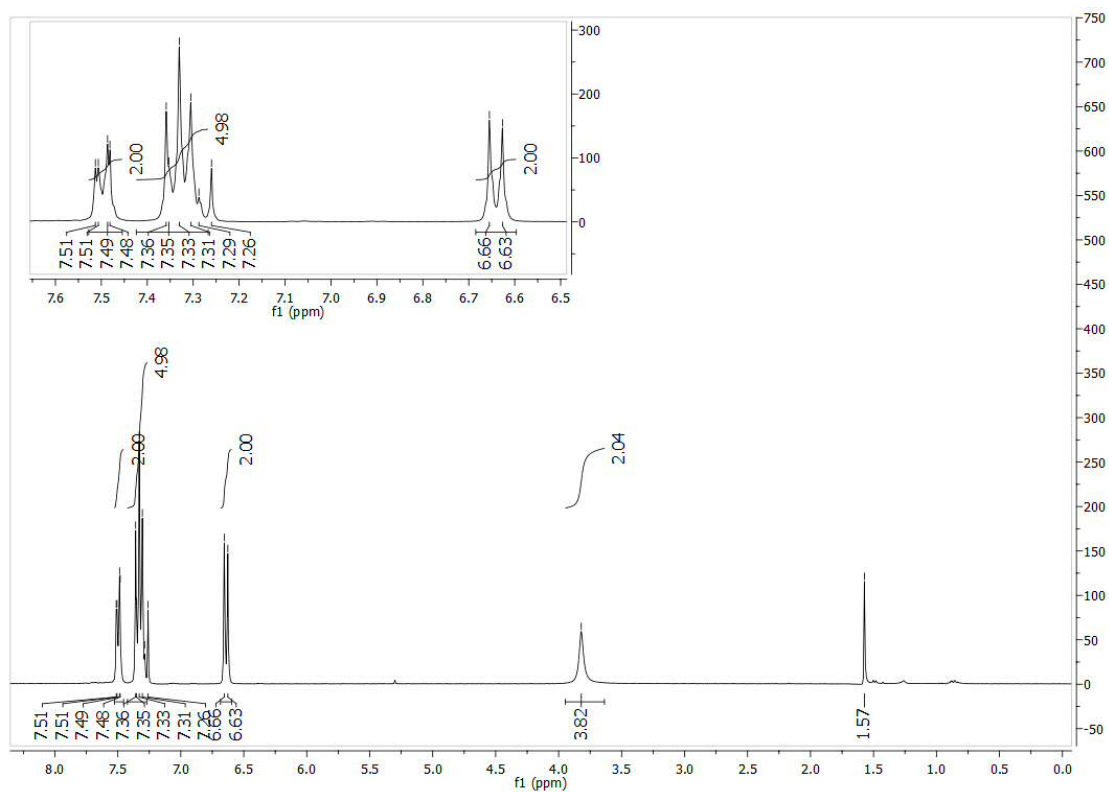
Figure 127. ^{1}H NMR spectrum of **202** in CDCl$_3$ (400 MHz).
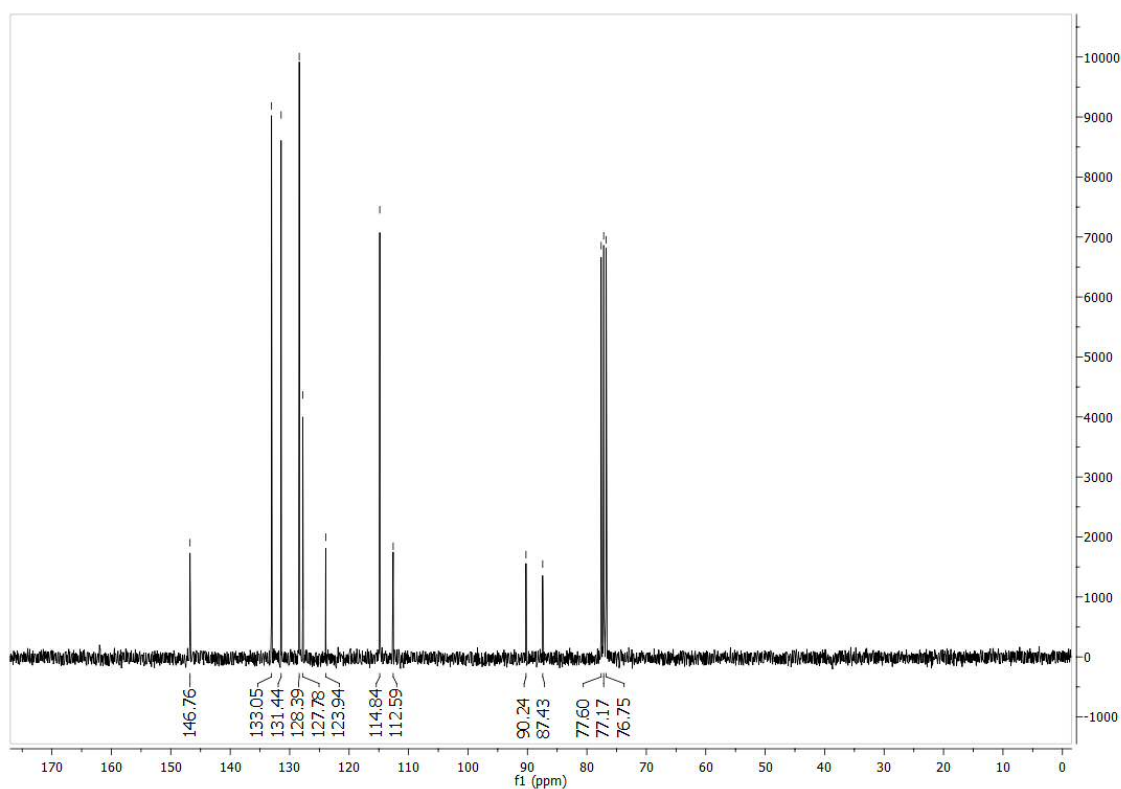
Figure 128. ^{13}C NMR spectrum of **202** in CDCl$_3$ (100 MHz).

Characterization of 197
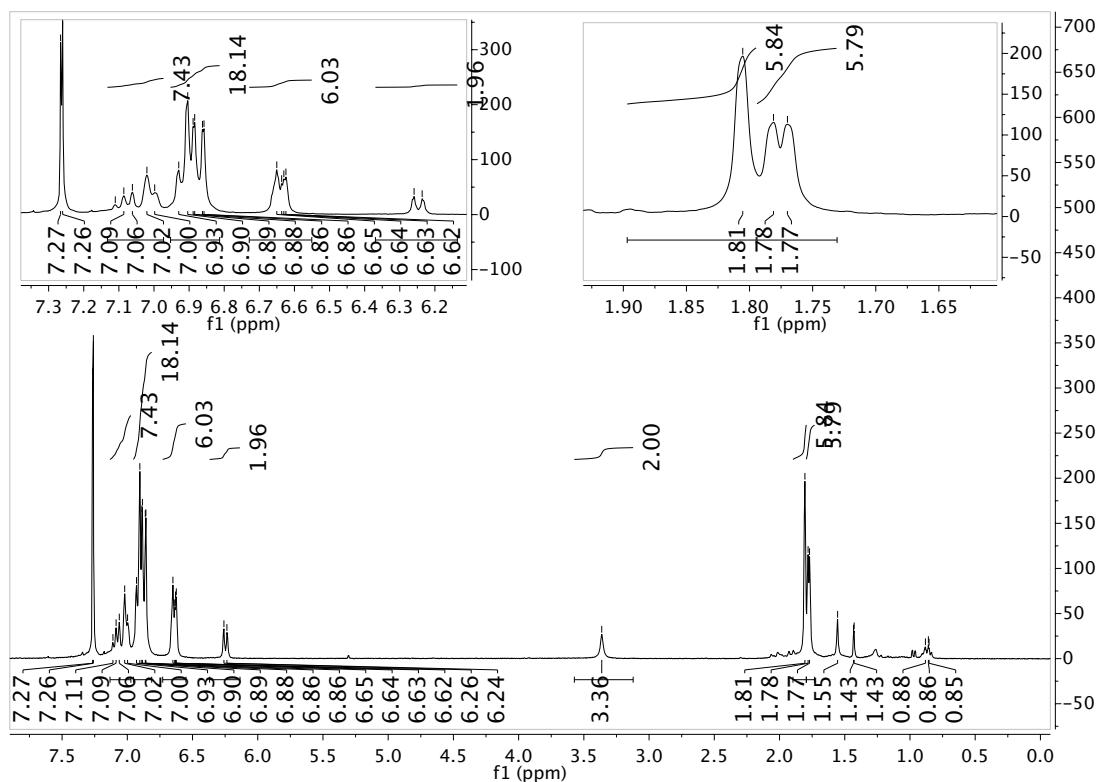
Figure 129. ^{1}H NMR spectrum of **197** in CDCl$_3$ (400 MHz).
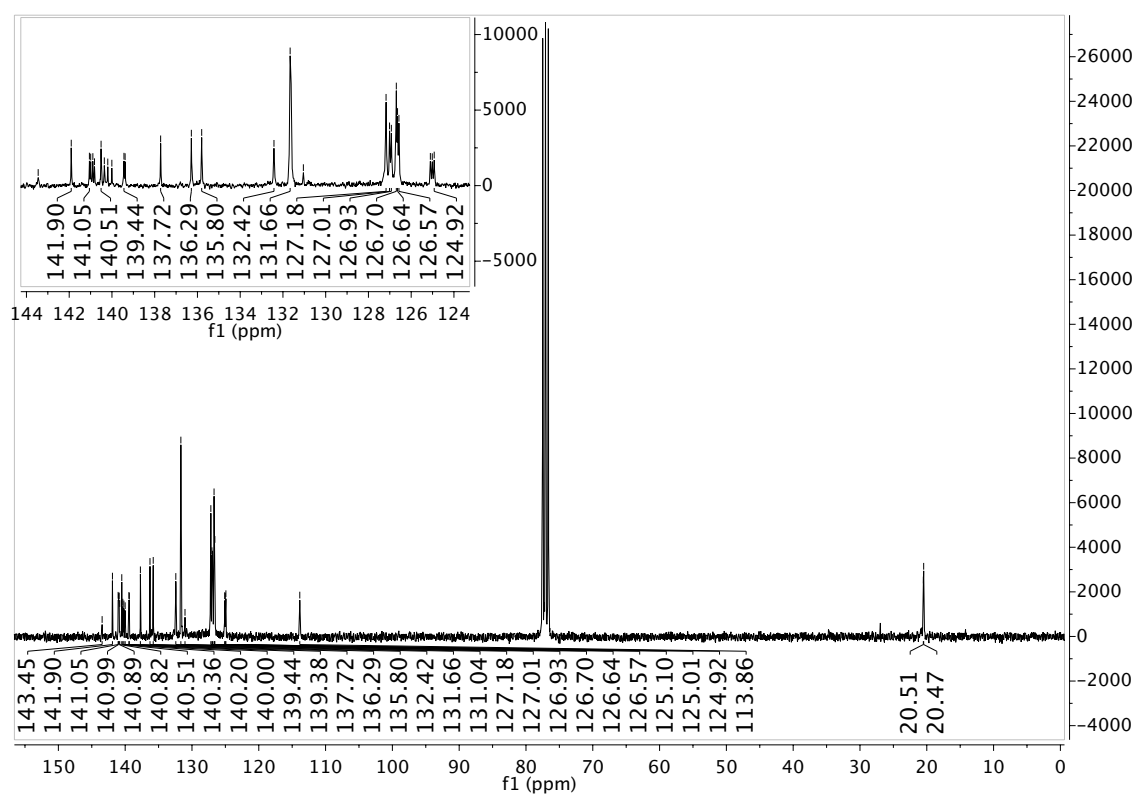
Figure 130. ^{13}C NMR spectrum of **197** in CDCl$_3$ (100 MHz).

Characterization of 211
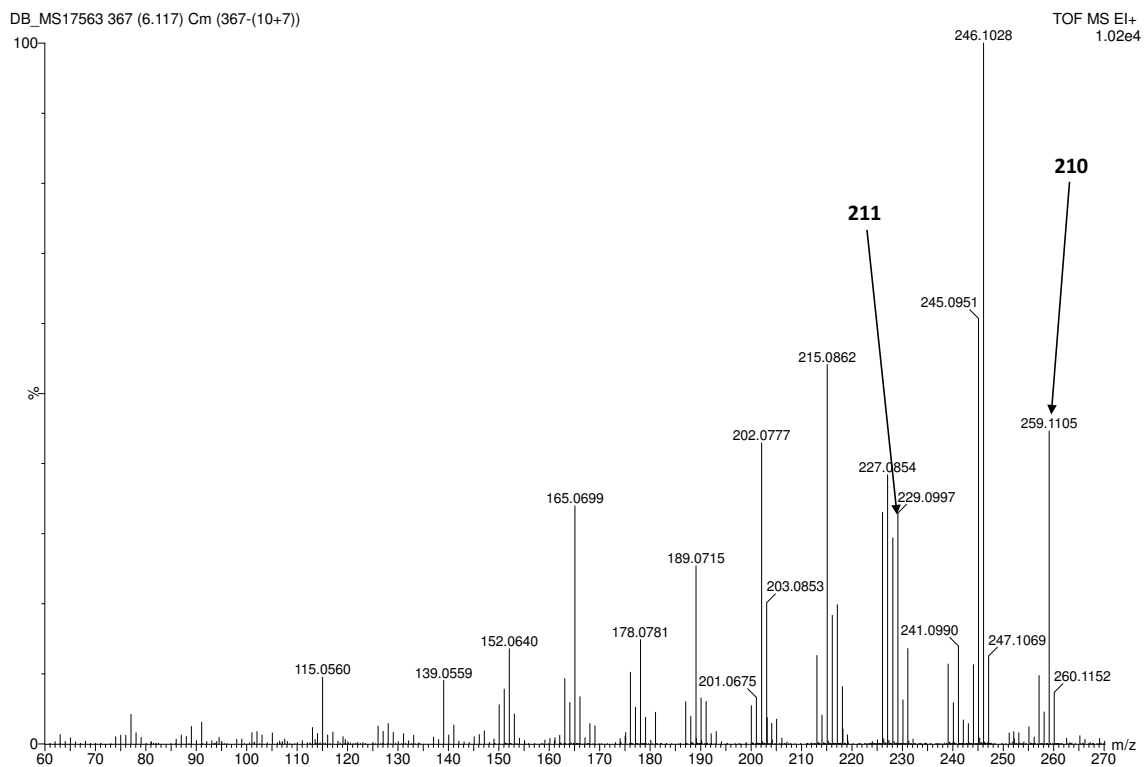
Figure 131. EI-MS analysis of the crude mixture from Scheme 85, containing the desired molecule **211** and starting material **210**.
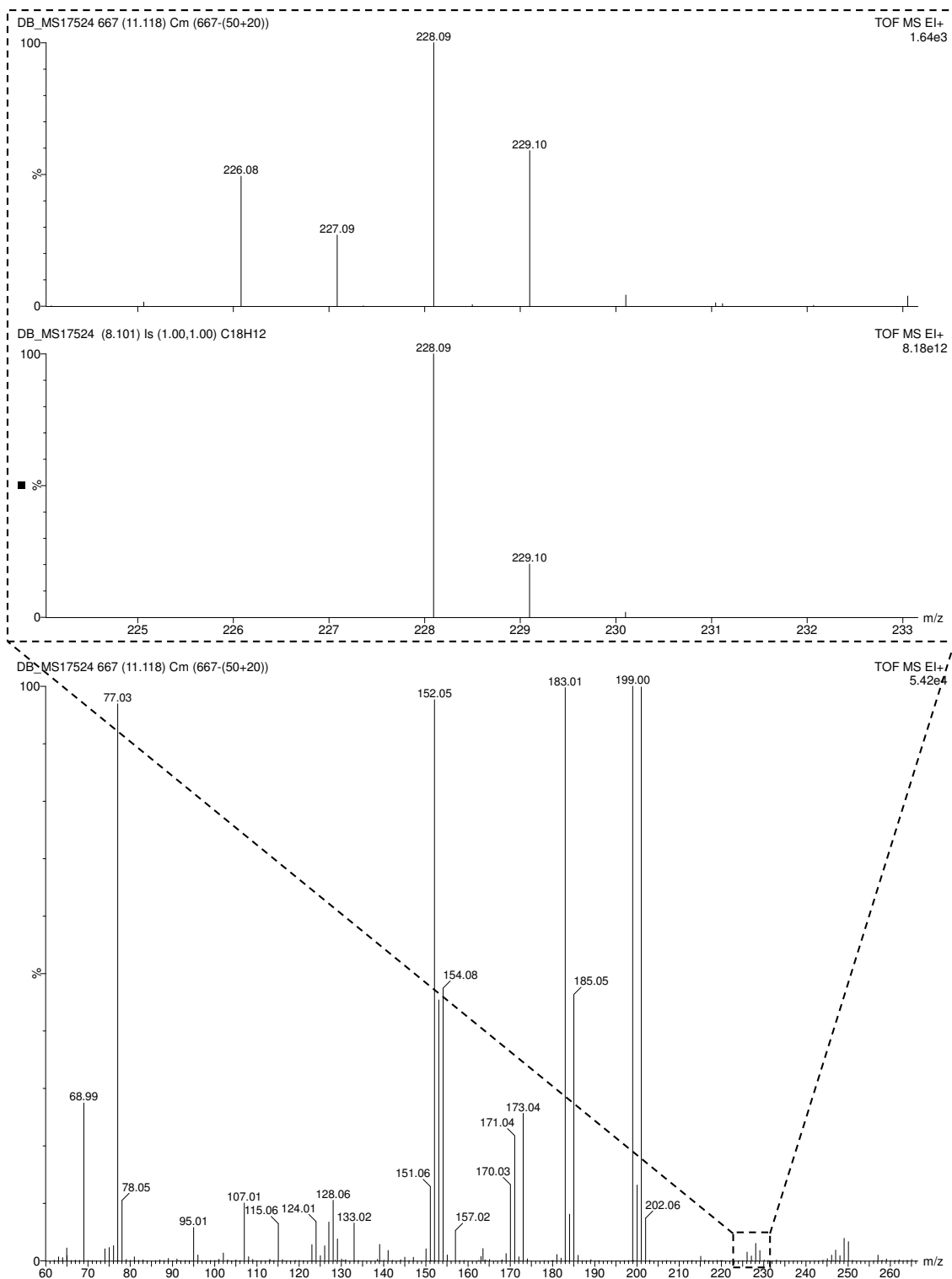
Figure 132. EI-MS analysis of crude mixture from Scheme 87, containing the desired molecule **211**. Dashed inset: zoom of the 224-233 m/z region showing the experimental (top) and calculated (bottom) isotopic pattern for **211**.

Chapter 5: Bibliography

(1)   Stock, A.; Pohland, E. *Ber. Dtsch. Chem. Ges. B* **1926**, *59* (9), 2215–2223.

(2)   Jeffrey, G. A.; Ruble, J. R.; McMullan, R. K.; Pople, J. A. *Proc. R. Soc. A Math. Phys. Eng. Sci.* **1987**, *414* (1846), 47–57.

(3)   Harshbarger, W.; Lee, G. H.; Porter, R. F.; Bauer, S. H. *Inorg. Chem.* **1969**, *8* (8), 1683–1689.

(4)   Kiran, B.; Phukan, A. K.; Jemmis, E. D. *Inorg. Chem.* **2001**, *40* (14), 3615–3618.

(5)   Islas, R.; Chamorro, E.; Robles, J.; Heine, T.; Santos, J. C.; Merino, G. *Struct. Chem.* **2007**, *18* (6), 833–839.

(6)   Boese, R.; Maulitz, A. H.; Stellberg, P. *Chem. Ber.* **1994**, *127* (10), 1887–1889.

(7)   Harismah, K.; Mirzaei, M.; Samadizadeh, M.; Rad, A. S. *Superlattices Microstruct.* **2017**, *109*, 360–365.

(8)   Kaldor, A. *J. Chem. Phys.* **1971**, *55* (9), 4641–4643.

(9)   Frost, D. C.; Herring, F. G.; McDowell, C. A.; Stenhouse, I. A. *Chem. Phys. Lett.* **1970**, *5* (5), 291–292.

(10)   Al-Joboury, M. I.; Turner, D. W. *J. Chem. Soc.* **1964**, 4434–4441.

(11)   Platt, J. R. J.; Klevens, H. B.; Schaeffer, G. W. *J. Chem. Phys.* **1947**, *15* (8), 598–601.

(12)   Tossell, J. A.; Moore, J. H.; McMillan, K.; Subramaniam, C. K.; Coplan, M. A. *J. Am. Chem. Soc.* **1992**, *114* (3), 1114–1115.

(13)   Wagner, R. I.; Bradford, J. L.; Ross, I. *Inorg. Chem.* **1962**, *1* (1), 93–97.

(14)   Nagasawa, K. *Inorg. Chem.* **1966**, *5* (3), 442–445.

(15)   Leffler, A. J. *Inorg. Chem.* **1964**, *3* (1), 145–146.

(16)   Narula, C. K.; Schaeffer, R.; Datye, A.; Paine, R. T. *Inorg. Chem.* **1989**, *28* (21), 4053–4055.

(17)   Maya, L. *Appl. Organomet. Chem.* **1996**, *10* (3–4), 175–182.

(18)   Moon, K. T.; Min, D. S.; Kim, D. P. *J. Ind. Eng. Chem.* **1997**, *3* (4), 288–292.

(19)   Sham, I. H. T.; Kwok, C.-C.; Che, C.-M.; Zhu, N. *Chem. Commun.* **2005**, *2* (28), 3547–3549.

(20)   Bronner, C.; Stremlau, S.; Gille, M.; Brauße, F.; Haase, A.; Hecht, S.; Tegeder, P. *Angew. Chem., Int. Ed.* **2013**, *52* (16), 4422–4425.

(21)   Liang, H.-W.; Zhuang, X.; Brüller, S.; Feng, X.; Müllen, K. *Nat. Commun.* **2014**, *5*, 4973–4980.

(22)   Makarov, N. S.; Mukhopadhyay, S.; Yesudas, K.; Brédas, J.-L.; Perry, J. W.; Pron, A.; Kivala, M.; Müllen, K. *J. Phys. Chem. A* **2012**, *116* (15), 3781–3793.

(23)   Cloke, R. R.; Marangoni, T.; Nguyen, G. D.; Joshi, T.; Rizzo, D. J.; Bronner, C.; Cao, T.; Louie, S. G.; Crommie, M. F.; Fischer, F. R. *J. Am. Chem. Soc.* **2015**, *137* (28), 8872–8875.

(24) Wu, J.; Pisula, W.; Müllen, K. *Chem. Rev.* **2007**, *107* (3), 718–747.

(25) Novoselov, K. S.; Geim, A. K.; Morozov, S. V.; Jiang, D.; Zhang, Y.; Dubonos, S. V.; Grigorieva, I. V.; Firsov, A. A. *Science* **2004**, *306* (5696), 666–669.

(26) Schwierz, F. *Nat. Nanotechnol.* **2010**, *5* (7), 487–496.

(27) Park, S.; Ruoff, R. S. *Nat. Nanotechnol.* **2009**, *4* (4), 217–224.

(28) Fujita, M.; Wakabayashi, K.; Nakada, K.; Kusakabe, K. *J. Phys. Soc. Japan* **1996**, *65* (7), 1920–1923.

(29) Liu, J.; Li, B.-W.; Tan, Y.-Z.; Giannakopoulos, A.; Sanchez-Sanchez, C.; Beljonne, D.; Ruffieux, P.; Fasel, R.; Feng, X.; Müllen, K. *J. Am. Chem. Soc.* **2015**, *137* (18), 6097–6103.

(30) Narita, A.; Feng, X.; Müllen, K. *Chem. Rec.* **2015**, *15* (1), 295–309.

(31) Cai, J.; Ruffieux, P.; Jaafar, R.; Bieri, M.; Braun, T.; Blankenburg, S.; Muoth, M.; Seitsonen, A. P.; Saleh, M.; Feng, X.; Müllen, K.; Fasel, R. *Nature* **2010**, *466* (7305), 470–473.

(32) Chen, C.; Wu, J. Z.; Lam, K. T.; Hong, G.; Gong, M.; Zhang, B.; Lu, Y.; Antaris, A. L.; Diao, S.; Guo, J.; Dai, H. *Adv. Mater.* **2015**, *27* (2), 303–309.

(33) Vo, T. H.; Shekhirev, M.; Kunkel, D. A.; Morton, M. D.; Berglund, E.; Kong, L.; Wilson, P. M.; Dowben, P. A.; Enders, A.; Sinitskii, A. *Nat. Commun.* **2014**, *5*, 3189–3196.

(34) Kosynkin, D. V.; Higginbotham, A. L.; Sinitskii, A.; Lomeda, J. R.; Dimiev, A.; Price, B. K.; Tour, J. M. *Nature* **2009**, *458* (7240), 872–876.

(35) Liu, Z.; Marder, T. B. B. *Angew. Chem., Int. Ed.* **2008**, *47* (2), 242–244.

(36) Watanabe, K.; Taniguchi, T.; Niiyama, T.; Miya, K.; Taniguchi, M. *Nat. Photonics* **2009**, *3* (10), 591–594.

(37) Watanabe, K.; Taniguchi, T.; Kanda, H. *Nat. Mater.* **2004**, *3* (6), 404–409.

(38) Golberg, D.; Bando, Y.; Huang, Y.; Terao, T.; Mitome, M.; Tang, C.; Zhi, C. *ACS Nano* **2010**, *4* (6), 2979–2993.

(39) Côté, M.; Haynes, P. D.; Molteni, C. *Phys. Rev. B* **2001**, *63* (12), 125207.

(40) Zhi, C.; Bando, Y.; Terao, T.; Tang, C.; Kuwahara, H.; Golberg, D. *Adv. Funct. Mater.* **2009**, *19* (12), 1857–1862.

(41) Ci, L.; Song, L.; Jin, C.; Jariwala, D.; Wu, D.; Li, Y.; Srivastava, A.; Wang, Z. F.; Storr, K.; Balicas, L.; Liu, F.; Ajayan, P. M. *Nat. Mater.* **2010**, *9* (5), 430–435.

(42) Huang, C.; Chen, C.; Zhang, M.; Lin, L.; Ye, X.; Lin, S.; Antonietti, M.; Wang, X. *Nat. Commun.* **2015**, *6*, 7698.

(43) Kazemi, A.; He, X.; Alaie, S.; Ghasemi, J.; Dawson, N. M.; Cavallo, F.; Habteyes, T. G.; Brueck, S. R. J.; Krishna, S. *Sci. Rep.* **2015**, *5* (1), 11463–11462.

(44) Kawaguchi, M.; Kawashima, T.; Nakajima, T. *Chem. Mater.* **1996**, *8* (6), 1197–1201.

(45) Guo, F.; Yang, P.; Pan, Z.; Cao, X.-N.; Xie, Z.; Wang, X. *Angew. Chem., Int. Ed.*

2017, *56* (28), 8231–8235.

(46) Dewar, M. J. S.; Marr, P. A. *J. Am. Chem. Soc.* **1962**, *84* (19), 3782–3782.

(47) Campbell, P. G.; Marwitz, A. J. V.; Liu, S.-Y. *Angew. Chem., Int. Ed.* **2012**, *51* (25), 6074–6092.

(48) Chissick, S. S.; Dewar, M. J. S.; Maitlis, P. M. *Tetrahedron Lett.* **1960**, *1* (44), 8–10.

(49) Bosdet, M. J. D.; Piers, W. E.; Sorensen, T. S.; Parvez, M. *Angew. Chem., Int. Ed.* **2007**, *46* (26), 4940–4943.

(50) Dewar, M. J. S.; Kubba, V. P.; Pettit, R. *J. Chem. Soc.* **1958**, 3073–3076.

(51) Bosdet, M. J. D.; Jaska, C. A.; Piers, W. E.; Sorensen, T. S.; Parvez, M. *Org. Lett.* **2007**, *9* (7), 1395–1398.

(52) Dewar, M. J. S.; Dietz, R. *J. Chem. Soc.* **1959**, 2728–2730.

(53) Paetzold, P.; Stanescu, C.; Stubenrauch, J. R.; Bienmüller, M.; Englert, U. *Z. Anorg. Allg. Chem.* **2004**, *630* (15), 2632–2640.

(54) Fang, X.; Yang, H.; Kampf, J. W.; Banaszak Holl, M. M.; Ashe, A. J. *Organometallics* **2006**, *25* (2), 513–518.

(55) Molander, G. A.; Wisniewski, S. R. *J. Org. Chem.* **2014**, *79* (14), 6663–6678.

(56) Wisniewski, S. R.; Guenther, C. L.; Argintaru, O. A.; Molander, G. A. *J. Org. Chem.* **2014**, *79* (1), 365–378.

(57) Schaeffer, G. W.; Schaeffer, R.; Schlesinger, H. I. *J. Am. Chem. Soc.* **1951**, *73* (4), 1612–1614.

(58) Framery, E.; Vaultier, M. *Heteroat. Chem.* **2000**, *11* (3), 218–225.

(59) Schlesinger, H. I.; Ritter, D. M.; Burg, A. B. *J. Am. Chem. Soc.* **1938**, *60* (6), 1296–1300.

(60) Wideman, T.; Sneddon, L. G. *Inorg. Chem.* **1995**, *34* (4), 1002–1003.

(61) Meller, A.; Schaschel, E. *Inorg. Nucl. Chem. Lett.* **1966**, *2* (2), 41–43.

(62) Jackson, K. T.; Reich, T. E.; El-Kaderi, H. M. *Chem. Commun.* **2012**, *48* (70), 8823–8825.

(63) G.W. Schaeffer; E.R. Anderson. *J. Amer. Chem. Soc.* **1949**, *71* (6), 2143–2145.

(64) Hough, W. V.; Schaeffer, G. W.; Dzurus, M.; Stewart, A. C. *J. Am. Chem. Soc.* **1955**, *77* (4), 864–865.

(65) Eméleus, H. J.; Wade, K. *J. Chem. Soc.* **1960**, 2614–2617.

(66) Yamamoto, Y.; Miyamoto, K.; Umeda, J.; Nakatani, Y.; Yamamoto, T.; Miyaura, N. *J. Organomet. Chem.* **2006**, *691* (23), 4909–4917.

(67) Jackson, K. T.; Rabbani, M. G.; Reich, T. E.; El-Kaderi, H. M. *Polym. Chem.* **2011**, *2* (12), 2775–2777.

(68) Jaska, C. a.; Temple, K.; Lough, A. J.; Manners, I. *J. Am. Chem. Soc.* **2003**, *125* (31), 9424–9434.

(69) García-Vivó, D.; Huergo, E.; Ruiz, M. a.; Travieso-Puente, R. *Eur. J. Inorg.*

Chem. **2013**, *28*, 4998–5008.

(70) Kawano, Y.; Uruichi, M.; Shimoi, M.; Taki, S.; Kawaguchi, T.; Kakizawa, T.; Ogino, H. *J. Am. Chem. Soc.* **2009**, *131* (41), 14946–14957.

(71) Kim, S.-K.; Cho, H.; Kim, M. J.; Lee, H.-J.; Park, J.; Lee, Y.-B.; Kim, H. C.; Yoon, C. W.; Nam, S. W.; Kang, S. O. *J. Mater. Chem. A* **2013**, *1* (6), 1976–1981.

(72) Li, J. S.; Zhang, C. R.; Li, B.; Cao, F.; Wang, S. Q. *Eur. J. Inorg. Chem.* **2010**, *5* (12), 1763–1766.

(73) Brown, C. A.; Laubengayer, A. W. *J. Am. Chem. Soc.* **1955**, *77* (14), 3699–3700.

(74) Smalley, J. H.; Stafiej, S. F. *J. Am. Chem. Soc.* **1959**, *81* (3), 582–586.

(75) Reich, T. E.; Jackson, K. T.; Li, S.; Jena, P.; El-Kaderi, H. M. *J. Mater. Chem.* **2011**, *21* (29), 10629–10632.

(76) Reich, T. E.; Behera, S.; Jackson, K. T.; Jena, P.; El-Kaderi, H. M. *J. Mater. Chem.* **2012**, *22* (27), 13524–13528.

(77) Luo, W.; Zakharov, L. N.; Liu, S.-Y. *J. Am. Chem. Soc.* **2011**, *133* (33), 13006–13009.

(78) Luo, W.; Campbell, P. G.; Zakharov, L. N.; Liu, S. *J. Am. Chem. Soc.* **2011**, *133* (48), 19326–19329.

(79) Biswas, S.; Müller, M.; Tönshoff, C.; Eichele, K.; Maichle-Mössmer, C.; Ruff, A.; Speiser, B.; Bettinger, H. F. *Eur. J. Org. Chem.* **2012**, *24*, 4634–4639.

(80) Müller, M.; Behnle, S.; Maichle-Mössmer, C.; Bettinger, H. F. *Chem. Commun.* **2014**, *50* (58), 7821–7823.

(81) Snyder, J. A.; Grüninger, P.; Bettinger, H. F.; Bragg, A. E. *J. Phys. Chem. A* **2017**, *121* (44), 8359–8367.

(82) Snyder, J. A.; Grüninger, P.; Bettinger, H. F.; Bragg, A. E. *J. Phys. Chem. A* **2017**, *121* (27), 5136–5146.

(83) Krieg, M.; Reicherter, F.; Haiss, P.; Ströbele, M.; Eichele, K.; Treanor, M.-J.; Schaub, R.; Bettinger, H. F. *Angew. Chem., Int. Ed.* **2015**, *54* (28), 8284–8286.

(84) Köster, R.; Bellut, H.; Hattori, S. *Justus Liebigs Ann. Chem.* **1968**, *720* (1), 1–22.

(85) Bielawski, J.; Das, M. K.; Hanecker, E.; Niedenzu, K.; Noeth, H. *Inorg. Chem.* **1986**, *25* (26), 4623.

(86) Das, M. K.; DeGraffenreid, A. L.; Edwards, K. D.; Komorowski, L.; Mariategui, J. F.; Miller, B. W.; Mojesky, M. T.; Niedenzu, K. *Inorg. Chem.* **1988**, *27* (18), 3085–3089.

(87) Atkinson, I. B.; Blundell, D. C.; Clapp, D. B. *J. Inorg. Nucl. Chem.* **1972**, *34* (10), 3037–3041.

(88) Massey, A. G.; Park, A. J. *J. Organomet. Chem.* **1964**, *2* (6), 461–465.

(89) Newsom, H. C.; English, W. D.; McCloskey, A. L.; Woods, W. G. *J. Am. Chem. Soc.* **1961**, *83* (20), 4134–4138.

(90) Watanabe, H.; Totani, T.; Yoshizaki, T. *Inorg. Chem.* **1965**, *4* (5), 657–660.

(91) Kervyn, S.; Fenwick, O.; Di Stasio, F.; Shin, Y. S.; Wouters, J.; Accorsi, G.; Osella, S.; Beljonne, D.; Cacialli, F.; Bonifazi, D. *Chem. Eur. J.* **2013**, *19* (24), 7771–7779.

(92) Wakamiya, A.; Ide, T.; Yamaguchi, S. *J. Am. Chem. Soc.* **2005**, *127* (42), 14859–14866.

(93) Werner, H.; Prinz, R.; Deckelmann, E. *Chem. Ber.* **1969**, *102* (1), 95–103.

(94) Fischer, E. O.; Öfele, K. *Chem. Ber.* **1957**, *90* (11), 2532–2535.

(95) Beckett, M. A.; Gilmore, R. J.; Idrees, K. *J. Organomet. Chem.* **1993**, *455* (1–2), 47–49.

(96) Nöth, H.; Troll, A. *Eur. J. Inorg. Chem.* **2005**, *2005* (17), 3524–3535.

(97) Stock, A.; Wiberg, E.; Martini, H. *Ber. Deut. Chem. Gesell.* **1930**, *63* (10), 2927–2937.

(98) Wiberg, E.; Bolz, A. *Ber. Deut. Chem. Gesell.* **1940**, *73* (3), 209–232.

(99) Laubengayer, A. W.; Beachley, O. T.; Porter, R. F. *Inorg. Chem.* **1965**, *4* (4), 578–582.

(100) Anton, K.; Fußstetter, H.; Nöth, H. *Chem. Ber.* **1981**, *114* (8), 2723–2730.

(101) Gemünda, B.; Günthera, B.; Nöth, H. *Arkivoc* **2008**, *2008* (5), 136–152.

(102) Carion, R.; Liégeois, V.; Champagne, B.; Bonifazi, D.; Pelloni, S.; Lazzeretti, P. *J. Phys. Chem. Lett.* **2010**, *1* (10), 1563–1568.

(103) Geri, J. B.; Szymczak, N. K. *J. Am. Chem. Soc.* **2017**, *139* (29), 9811–9814.

(104) Bai, J.; Niedenzu, K.; Serwatowska, J.; Serwatowski, J. *Inorg. Chem.* **1991**, *30* (24), 4631–4635.

(105) Riley, R. F.; Schack, C. J. *Inorg. Chem.* **1964**, *3* (11), 1651–1653.

(106) Groszos, S. J.; Stafiej, S. F. *J. Am. Chem. Soc.* **1958**, *80* (6), 1357–1360.

(107) Ryschkewitsch, G. E.; Harris, J. J.; Sisler, H. H. *J. Am. Chem. Soc.* **1958**, *80* (17), 4515–4517.

(108) Jackson, L. a.; Allen, C. W. *J. Chem. Soc. Dalt. Trans.* **1989**, *12*, 2423–2427.

(109) Haworth, D. T.; Hohnstedt, L. F. *J. Am. Chem. Soc.* **1960**, *82* (15), 3860–3862.

(110) Melcher, L. A.; Adcock, J. L.; Lagowski, J. J. *Inorg. Chem.* **1972**, *11* (6), 1247–1252.

(111) Riensch, N. A.; Deniz, A.; Kühl, S.; Müller, L.; Adams, A.; Pich, A.; Helten, H. *Polym. Chem.* **2017**, *8* (35), 5264–5268.

(112) Haberecht, J.; Krummland, A.; Breher, F.; Gebhardt, B.; Rüegger, H.; Nesper, R.; Grützmacher, H. *Dalt. Trans.* **2003**, *39* (11), 2126–2132.

(113) Müller, M.; Maichle-Mössmer, C.; Sirsch, P.; Bettinger, H. F. *Chempluschem* **2013**, *78* (9), 988–994.

(114) Dosso, J.; Tasseroul, J.; Fasano, F.; Marinelli, D.; Biot, N.; Fermi, A.; Bonifazi, D. *Angew. Chem., Int. Ed.* **2017**, *56* (16), 4483–4487.

(115) Wakamiya, A.; Ide, T.; Yamaguchi, S. *J. Am. Chem. Soc.* **2005**, *127* (42), 14859–

14866.

(116) Su, K.; Remsen, E. E.; Zank, G. A.; Sneddon, L. G. *Chem. Mater.* **1993**, *5* (4), 547–556.

(117) Marinelli, D.; Fasano, F.; Najjari, B.; Demitri, N.; Bonifazi, D. *J. Am. Chem. Soc.* **2017**, *139* (15), 5503–5519.

(118) Nghiem, Q. D.; Jeon, J.-K.; Hong, L.-Y.; Kim, D.-P. *J. Organomet. Chem.* **2003**, *688* (1), 27–35.

(119) Cornu, D.; Miele, P.; Toury, B.; Bonnetot, B.; Mongeot, H.; Bouix, J.; Bonnetot, B. *J. Mater. Chem.* **1999**, *9* (10), 2605–2610.

(120) Kho, J.-G.; Moon, K.-T.; Kim, J.-H.; Kim, D.-P. *J. Am. Ceram. Soc.* **2004**, *83* (11), 2681–2683.

(121) Meziani, M. J.; Song, W.-L.; Wang, P.; Lu, F.; Hou, Z.; Anderson, A.; Maimaiti, H.; Sun, Y.-P. *ChemPhysChem* **2015**, *16* (7), 1339–1346.

(122) Corso, M. *Science* **2004**, *303* (5655), 217–220.

(123) Urgel, J. I.; Schwarz, M.; Garnica, M.; Stassen, D.; Bonifazi, D.; Ecija, D.; Barth, J. V.; Auwärter, W. *J. Am. Chem. Soc.* **2015**, *137* (7), 2420–2423.

(124) Xie, S.; Istrate, O. M.; May, P.; Barwich, S.; Bell, A. P.; Khan, U.; Coleman, J. N. *Nanoscale* **2015**, *7* (10), 4443–4450.

(125) Dibandjo, P.; Chassagneux, F.; Bois, L.; Sigala, C.; Miele, P.; Pierotti, R. A.; Rouquerol, J.; Siemieniewska, T.; Tu, B.; Yu, C.; Terasaki, O.; Zhao, D. *J. Mater. Chem.* **2005**, *15* (19), 1917–1923.

(126) Dibandjo, P.; Chassagneux, F.; Bois, L.; Sigala, C.; Miele, P. *Microporous Mesoporous Mater.* **2006**, *92* (1), 286–291.

(127) Jaschke, B.; Klingebiel, U.; Riedel, R.; Doslik, N.; Gadow, R. *Appl. Organomet. Chem.* **2000**, *14* (11), 671–685.

(128) Paine, R. T.; Sneddon, L. G. *ACS Symp. Ser.* **1994**, *572*, 358–374.

(129) Forrest, S. R. *Nature* **2004**, *428* (6986), 911–918.

(130) Murphy, A. R.; Fréchet, J. M. J. *Chem. Rev.* **2007**, *107* (4), 1066–1096.

(131) Facchetti, A. *Chem. Mater.* **2011**, *23* (3), 733–758.

(132) Della Pia, A.; Riello, M.; Floris, A.; Stassen, D.; Jones, T. S.; Bonifazi, D.; De Vita, A.; Costantini, G. *ACS Nano* **2014**, *8* (12), 12356–12364.

(133) Bonifazi, D.; Mohnani, S.; Llanes-Pallas, A. *Chem. Eur. J.* **2009**, *15* (29), 7004–7025.

(134) Barth, J. V.; Costantini, G.; Kern, K. *Nature* **2005**, *437* (7059), 671–679.

(135) Elemans, J. A. A. W.; Lei, S.; De Feyter, S. *Angew. Chem., Int. Ed.* **2009**, *48* (40), 7298–7332.

(136) Otero, R.; Gallego, J. M.; de Parga, A. L. V.; Martín, N.; Miranda, R. *Adv. Mater.* **2011**, *23* (44), 5148–5176.

(137) Kervyn, S.; Kalashnyk, N.; Riello, M.; Moreton, B.; Tasseroul, J.; Wouters, J.; Jones, T. S.; De Vita, A.; Costantini, G.; Bonifazi, D. *Angew. Chem., Int. Ed.*

2013, *52* (29), 7410–7414.

(138) Kalashnyk, N.; Ganesh Nagaswaran, P.; Kervyn, S.; Riello, M.; Moreton, B.; Jones, T. S.; De Vita, A.; Bonifazi, D.; Costantini, G. *Chem. Eur. J.* **2014**, *20* (37), 11856–11862.

(139) Sánchez-Sánchez, C.; Sachdev, H.; Brüller, S.; Müllen, K.; Krieg, M.; Bettinger, H. F.; Nicolaï, A.; Meunier, V.; Talirz, L.; Fasel, R.; Ruffieux, P. *ACS Nano* **2015**, *9* (9), 9228–9235.

(140) Ciccullo, F.; Calzolari, A.; Píš, I.; Savu, S.-A.; Krieg, M.; Bettinger, H. F.; Magnano, E.; Chassé, T.; Casu, M. B. *J. Phys. Chem. C* **2016**, *120* (31), 17645–17651.

(141) Winsche, W. E.; Hoffman, K. C.; Salzano, F. J. *Science* **1973**, *180* (4093), 1325–1332.

(142) Schlapbach, L.; Züttel, A. *Nature* **2001**, *414* (6861), 353–358.

(143) Hirscher, M. *Handbook of hydrogen storage : new materials for future energy storage*; Wiley-VCH Verlag & Co: Weinheim, 2010.

(144) McKeown, N. B.; Budd, P. M. *Macromolecules* **2010**, *43* (12), 5163–5176.

(145) Jaska, C. A.; Emslie, D. J. H.; Bosdet, M. J. D.; Piers, W. E.; Sorensen, T. S.; Parvez, M. *J. Am. Chem. Soc.* **2006**, *128* (33), 10885–10896.

(146) Bonifazi, D.; Fasano, F.; Lorenzo-Garcia, M. M. M.; Marinelli, D.; Oubaha, H.; Tasseroul, J. *Chem. Commun.* **2015**, *51* (83), 15222–15236.

(147) Otero, N.; El-kelany, K. E.; Pouchan, C.; Rérat, M.; Karamanis, P. *Phys. Chem. Chem. Phys.* **2016**, *18* (36), 25315–25328.

(148) Otero, N.; Karamanis, P.; El-Kelany, K. E.; Rérat, M.; Maschio, L.; Civalleri, B.; Kirtman, B. *J. Phys. Chem. C* **2017**, *121* (1), 709–722.

(149) Kervyn, S.; Nakanishi, T.; Aimi, J.; Saeki, A.; Seki, S.; Champagne, B.; Bonifazi, D. *Chem. Lett.* **2012**, *41* (10), 1210–1212.

(150) Narita, A.; Wang, X.-Y.; Feng, X.; Müllen, K. *Chem. Soc. Rev.* **2015**, *44* (18), 6616–6643.

(151) Wang, X.-Y.; Wang, J.-Y.; Pei, J. *Chem. Eur. J.* **2015**, *21* (9), 3528–3539.

(152) Helten, H. *Chem. Eur. J.* **2016**, *22* (37), 12972–12982.

(153) Xie, W.; Yanase, T.; Nagahama, T.; Shimada, T. *C* **2016**, *2* (1), 2.

(154) Lorenzo-García, M. M.; Bonifazi, D. *Chim. Int. J. Chem.* **2017**, *71* (9), 550–557.

(155) Lorenz, T.; Lik, A.; Plamper, F. A.; Helten, H. *Angew. Chem., Int. Ed.* **2016**, *55* (25), 7236–7241.

(156) Ayhan, O.; Eckert, T.; Plamper, F. A.; Helten, H. *Angew. Chem., Int. Ed.* **2016**, *55* (42), 13321–13325.

(157) Lorenz, T.; Crumbach, M.; Eckert, T.; Lik, A.; Helten, H. *Angew. Chem., Int. Ed.* **2017**, *56* (10), 2780–2784.

(158) Li, G.; Xiong, W.-W.; Gu, P.-Y.; Cao, J.; Zhu, J.; Ganguly, R.; Li, Y.; Grimsdale, A. C.; Zhang, Q. *Org. Lett.* **2015**, *17* (3), 560–563.

(159) Wang, X.-Y.; Zhuang, F.-D.; Wang, R.-B.; Wang, X.-C.; Cao, X.-Y.; Wang, J.-Y.; Pei, J. *J. Am. Chem. Soc.* **2014**, *136* (10), 3764–3767.

(160) Davies, K. M.; Dewar, M. J. S.; Rona, P. *J. Am. Chem. Soc.* **1967**, *89* (24), 6294–6297.

(161) Emslie, D. J. H.; Piers, W. E.; Parvez, M. *Angew. Chem., Int. Ed.* **2003**, *42* (11), 1252–1255.

(162) Liu, Z.; Ma, L.; Shi, G.; Zhou, W.; Gong, Y.; Lei, S.; Yang, X.; Zhang, J.; Yu, J.; Hackenberg, K. P.; Babakhani, A.; Idrobo, J.-C.; Vajtai, R.; Lou, J.; Ajayan, P. M. *Nat. Nanotechnol.* **2013**, *8* (2), 119–124.

(163) Gao, Y.; Zhang, Y.; Chen, P.; Li, Y.; Liu, M.; Gao, T.; Ma, D.; Chen, Y.; Cheng, Z.; Qiu, X.; Duan, W.; Liu, Z. *Nano Lett.* **2013**, *13* (7), 3439–3443.

(164) Levendorf, M. P.; Kim, C.-J.; Brown, L.; Huang, P. Y.; Havener, R. W.; Muller, D. A.; Park, J. *Nature* **2012**, *488* (7413), 627–632.

(165) Beniwal, S.; Hooper, J.; Miller, D. P.; Costa, P. S.; Chen, G.; Liu, S.-Y.; Dowben, P. A.; Sykes, E. C. H.; Zurek, E.; Enders, A. *ACS Nano* **2017**, *11* (3), 2486–2493.

(166) Allemann, O.; Duttwyler, S.; Romanato, P.; Baldridge, K. K.; Siegel, J. S. *Science* **2011**, *332* (6029), 574–577.

(167) Watson, M. D.; Fechtenkötter, A.; Müllen, K. *Chem. Rev.* **2001**, *101* (5), 1267–1300.

(168) Hammer, B. A. G.; Müllen, K. *Chem. Rev.* **2016**, *116* (4), 2103–2140.

(169) Grimsdale, A. C.; Müllen, K. *Macromol. Rapid Commun.* **2007**, *28* (17), 1676–1702.

(170) Park, K. C.; Dodd, L. R.; Levon, K.; Kwei, T. K. *Macromolecules* **1996**, *29* (22), 7149–7154.

(171) Bohnen, A.; Heitz, W.; Müllen, K.; Räder, H.-J.; Schenk, R. *Die Makromol. Chemie* **1991**, *192* (8), 1679–1693.

(172) Grem, G.; Leditzky, G.; Ullrich, B.; Leising, G. *Adv. Mater.* **1992**, *4* (1), 36–37.

(173) Ried, W.; Freitag, D. *Angew. Chem., Int. Ed.* **1968**, *7* (11), 835–844.

(174) Grem, G.; Leising, G. *Synth. Met.* **1993**, *57* (1), 4105–4110.

(175) Grem, G.; Martin, V.; Meghdadi, F.; Paar, C.; Stampfl, J.; Sturm, J.; Tasch, S.; Leising, G. *Synth. Met.* **1995**, *71* (1), 2193–2194.

(176) Gregorius, H.; Heitz, W.; Müllen, K. *Adv. Mater.* **1993**, *5* (4), 279–281.

(177) Kovacic, P.; Kyriakis, A. *J. Am. Chem. Soc.* **1963**, *85* (4), 454–458.

(178) Scholl, R.; Seer, C.; Weitzenböck, R. *Ber. Deut. Chem. Gesell.* **1910**, *43* (2), 2202–2209.

(179) Carey, F. A.; Sundberg, R. J. In *Advanced Organic Chemistry*; Springer US: Boston, MA, 2007; pp 675–782.

(180) Fanta, P. E. *Synthesis* **1974**, *1974* (1), 9–21.

(181) Espinet, P.; Echavarren, A. M. *Angew. Chem., Int. Ed.* **2004**, *43* (36), 4704–4734.

(182) Gin, D. L.; Conticello, V. P.; Grubbs, R. H. *J. Am. Chem. Soc.* **1992**, *114* (8), 3167–3169.

(183) Yamamoto, T.; Hayashi, Y.; Yamamoto, A. *Bull. Chem. Soc. Jpn.* **1978**, *51* (7), 2091–2097.

(184) Rehahn, M.; Schlüter, A.-D.; Wegner, G.; Feast, W. J. *Polymer* **1989**, *30* (6), 1054–1059.

(185) Miyaura, N.; Yanagi, T.; Suzuki, A. *Synth. Commun.* **1981**, *11* (7), 513–519.

(186) Miller, R. B.; Dugar, S. *Organometallics* **1984**, *3* (8), 1261–1263.

(187) Mathew, S.; Crandall, L. A.; Ziegler, C. J.; Hartley, C. S. *J. Am. Chem. Soc.* **2014**, *136* (47), 16666–16675.

(188) Mathew, S. M.; Hartley, C. S. *Macromolecules* **2011**, *44* (21), 8425–8432.

(189) Liu, J.; Li, L.; Gong, C.; Yu, Z.; Pei, Q. *J. Mater. Chem.* **2011**, *21* (26), 9772–9777.

(190) Kandre, R.; Feldman, K.; Meijer, H. E. H.; Smith, P.; Schlüter, A. D. *Angew. Chem., Int. Ed.* **2007**, *46* (26), 4956–4959.

(191) Keegstra, M. A.; Müllen, K.; De Feyter, S.; De Schryver, F. C. *Angew. Chem., Int. Ed.* **1996**, *35* (7), 774–776.

(192) Miller, T. M.; Neenan, T. X. *Chem. Mater.* **1990**, *2* (4), 346–349.

(193) Miller, T. M.; Neenan, T. X.; Zayas, R.; Bair, H. E. *J. Am. Chem. Soc.* **1992**, *114* (3), 1018–1025.

(194) Hyatt, J. A. *Org. Prep. Proced. Int.* **1991**, *23* (4), 460–463.

(195) Vollhardt, K. P. C. *Acc. Chem. Res.* **1977**, *10* (1), 1–8.

(196) Vollhardt, K. P. C. *Angew. Chem., Int. Ed.* **1984**, *23* (8), 539–556.

(197) Pugh, C.; Percec, V. *J. Mater. Chem.* **1991**, *1* (5), 765–773.

(198) Ogliaruso, M. A.; Becker, E. I. *J. Org. Chem.* **1965**, *30* (10), 3354–3360.

(199) Ried, W.; Bönnighausen, K. H. *Chem. Ber.* **1960**, *93* (8), 1769–1773.

(200) Ogliaruso, M. A.; Shadoff, L. A.; Becker, E. I. *J. Org. Chem.* **1963**, *28* (10), 2725–2728.

(201) Johnson, J. R.; Grummitt, O. *Org. Synth.* **1943**, *23*, 92.

(202) Ogliaruso, M. A.; Romanelli, M. G.; Becker, E. I. *Chem. Rev.* **1965**, *65* (3), 261–367.

(203) Stille, J. K.; Harris, F. W.; Rakutis, R. O.; Mukamal, H. *J. Polym. Sci. Part B Polym. Lett.* **1966**, *4* (10), 791–793.

(204) Mukamal, H.; Harris, F. W.; Stille, J. K. *J. Polym. Sci. Part A-1 Polym. Chem.* **1967**, *5* (11), 2721–2729.

(205) Ried, W.; Saxena, V. B. *Angew. Chem., Int. Ed.* **1968**, *7* (5), 378–379.

(206) Stille, J. K.; Rakutis, R. O.; Mukamal, H.; Harris, F. W. *Macromolecules* **1968**, *1* (5), 431–436.

(207) Noren, G. K.; Stille, J. K. *J. Polym. Sci. Macromol. Rev.* **1971**, *5* (1), 385–430.

(208) Stille, J. K.; Noren, G. K. *J. Polym. Sci. Part B Polym. Lett.* **1969**, *7* (7), 525–527.

(209) Berresheim, A. J.; Müller, M.; Müllen, K. *Chem. Rev.* **1999**, *99* (7), 1747–1785.

(210) Li, C.; Liu, M.; Pschirer, N. G.; Baumgarten, M.; Müllen, K. *Chem. Rev.* **2010**, *110* (11), 6817–6855.

(211) Iyer, V. S.; Yoshimura, K.; Enkelmann, V.; Epsch, R.; Rabe, J. P.; Müllen, K. *Angew. Chem., Int. Ed.* **1998**, *37* (19), 2696–2699.

(212) Iyer, V. S.; Wehmeier, M.; Brand, J. D.; Keegstra, M. A.; Müllen, K. *Angew. Chem., Int. Ed.* **1997**, *36* (15), 1604–1607.

(213) Müller, M.; Iyer, V. S.; Kübel, C.; Enkelmann, V.; Müllen, K. *Angew. Chem., Int. Ed.* **1997**, *36* (15), 1607–1610.

(214) Andreitchenko, E. V.; Clark, C. G.; Bauer, R. E.; Lieser, G.; Müllen, K. *Angew. Chem., Int. Ed.* **2005**, *44* (39), 6348–6354.

(215) Wiesler, U.-M. M.; Berresheim, A. J.; Morgenroth, F.; Lieser, G.; Müllen, K. *Macromolecules* **2001**, *34* (2), 187–199.

(216) Teraoka, F.; Takahashi, T. *J. Macromol. Sci. Part B* **1980**, *18* (1), 73–82.

(217) Schlüter, A. D.; Rabe, J. P. *Angew. Chem., Int. Ed.* **2000**, *39* (5), 864–883.

(218) Zhang, H.; Grim, P. C. M.; Foubert, P.; Vosch, T.; Vanoppen, P.; Wiesler, U. M.; Berresheim, A. J.; Müllen, K.; De Schryver, F. C. *Langmuir* **2000**, *16* (23), 9009–9014.

(219) Zhang, H.; Grim, P. C. M.; Vosch, T.; Wiesler, U.-M.; Berresheim, A. J.; Müllen, K.; De Schryver, F. C. *Langmuir* **2000**, *16* (24), 9294–9298.

(220) Wiesler, U.-M. M.; Berresheim, A. J.; Morgenroth, F.; Lieser, G.; Müllen, K. *Macromolecules* **2001**, *34* (2), 187–199.

(221) Türp, D.; Wagner, M.; Enkelmann, V.; Müllen, K. *Angew. Chemie Int. Ed.* **2011**, *50* (21), 4962–4965.

(222) Moritz, R.; Zardalidis, G.; Butt, H.-J.; Wagner, M.; Müllen, K.; Floudas, G. *Macromolecules* **2014**, *47* (1), 191–196.

(223) Nguyen, T.-T.-T.; Türp, D.; Wagner, M.; Müllen, K. *Angew. Chem., Int. Ed.* **2013**, *52* (2), 669–673.

(224) Issberner, J.; Vögtle, F.; Cola, L. De; Balzani, V. *Chem. Eur. J.* **1997**, *3* (5), 706–712.

(225) Vögtle, F.; Plevoets, M.; Nieger, M.; Azzellini, G. C.; Credi, A.; De Cola, L.; De Marchis, V.; Venturi, M.; Balzani, V. *J. Am. Chem. Soc.* **1999**, *121* (26), 6290–6298.

(226) Haberecht, M. C.; Schnorr, J. M.; Andreitchenko, E. V.; Clark, C. G.; Wagner, M.; Müllen, K. *Angew. Chem., Int. Ed.* **2008**, *47* (9), 1662–1667.

(227) Iwasawa, T.; Tokunaga, M.; Obora, Y.; Tsuji, Y. *J. Am. Chem. Soc.* **2004**, *126* (21), 6554–6555.

(228) Komano, T.; Iwasawa, T.; Tokunaga, M.; Obora, Y.; Tsuji, Y. *Org. Lett.* **2005**, *7* (21), 4677–4679.

(229) Sato, H.; Fujihara, T.; Obora, Y.; Tokunaga, M.; Kiyosu, J.; Tsuji, Y. *Chem. Commun.* **2007**, No. 3, 269–271.

(230) Waybright, S. M.; McAlpine, K.; Laskoski, M.; Smith, M. D.; Bunz, U. H. F. *J. Am. Chem. Soc.* **2002**, *124* (29), 8661–8666.

(231) Kimura, M.; Sakaguchi, A.; Ohta, K.; Hanabusa, K.; Shirai, H.; Kobayashi, N. *Inorg. Chem.* **2003**, *42* (9), 2821–2823.

(232) Qin, T.; Ding, J.; Baumgarten, M.; Wang, L.; Müllen, K. *Macromol. Rapid Commun.* **2012**, *33* (12), 1036–1041.

(233) Qin, T.; Ding, J.; Wang, L.; Baumgarten, M.; Zhou, G.; Müllen, K. *J. Am. Chem. Soc.* **2009**, *131* (40), 14329–14336.

(234) Liu, D.; De Feyter, S.; Cotlet, M.; Stefan, A.; Wiesler, U.-M.; Herrmann, A.; Grebel-Koehler, D.; Qu, J.; Müllen, K.; De Schryver, F. C. *Macromolecules* **2003**, *36* (16), 5918–5925.

(235) Kühlbrandt, W.; Wang, D. N.; Fujiyoshi, Y. *Nature* **1994**, *367* (6464), 614–621.

(236) Hu, X.; Damjanovi, A.; Ritz, T.; Schulten, K. *Proc. Natl. Acad. Sci.* **1998**, *95* (11), 5935–5941.

(237) Hu, X.; Schulten, K. *Phys. Today* **1997**, *50* (8), 28–34.

(238) Krauß, N.; Schubert, W.-D.; Klukas, O.; Fromme, P.; Witt, H. T.; Saenger, W. *Nat. Struct. Biol.* **1996**, *3* (11), 965–973.

(239) Adronov, A.; Fréchet, J. M. J. *Chem. Commun.* **2000**, *33* (18), 1701–1710.

(240) Hoeben, F. J. M.; Jonkheijm, P.; Meijer, E. W.; Schenning, A. P. H. J. *Chem. Rev.* **2005**, *105* (4), 1491–1546.

(241) Kawa, M.; Fréchet, J. M. J. *Chem. Mater.* **1998**, *10* (1), 286–296.

(242) Kawa, M.; M.J. Fréchet, J. *Thin Solid Films* **1998**, *331* (1–2), 259–263.

(243) Gronheid, R.; Hofkens, J.; Köhn, F.; Weil, T.; Reuther, E.; Müllen, K.; De Schryver, F. C. *J. Am. Chem. Soc.* **2002**, *124* (11), 2418–2419.

(244) Weil, T.; Wiesler, U. M.; Herrmann, A.; Bauer, R.; Hofkens, J.; De Schryver, F. C.; Müllen, K. *J. Am. Chem. Soc.* **2001**, *123* (33), 8101–8108.

(245) Desurvire, E. *Erbium-doped fiber amplifiers : principles and applications*; Wiley: New York, 1994.

(246) Miniscalco, W. J. *J. Light. Technol.* **1991**, *9* (2), 234–250.

(247) Jiang, D.-L.; Aida, T. *J. Am. Chem. Soc.* **1998**, *120* (42), 10895–10901.

(248) Xu, Z.; Moore, J. S. *Angew. Chem., Int. Ed.* **1993**, *32* (9), 1354–1357.

(249) Xu, Z.; Moore, J. S. *Angew. Chem., Int. Ed.* **1993**, *32* (2), 246–248.

(250) Xu, Z.; Moore, J. S. *Acta Polym.* **1994**, *45* (2), 83–87.

(251) Devadoss, C.; Bharathi, P.; Moore, J. S. *J. Am. Chem. Soc.* **1996**, *118* (40), 9635–9644.

(252) Shortreed, M. R.; Swallen, S. F.; Shi, Z.-Y.; Tan, W.; Xu, Z.; Devadoss, C.; Moore, J. S.; Kopelman, R. *J. Phys. Chem. B* **1997**, *101* (33), 6318–6322.

(253) Swallen, S. F.; Shi, Z.-Y.; Tan, W.; Xu, Z.; Moore, J. S.; Kopelman, R. *J. Lumin.* **1998**, *76–77*, 193–196.

(254) Weil, T.; Vosch, T.; Hofkens, J.; Peneva, K.; Müllen, K. *Angew. Chem., Int. Ed.* **2010**, *49* (48), 9068–9093.

(255) Grimsdale, A. C.; Vosch, T.; Lor, M.; Cotlet, M.; Habuchi, S.; Hofkens, J.; De Schryver, F. C.; Müllen, K. *J. Lumin.* **2005**, *111* (4), 239–253.

(256) Maus, M.; De, R.; Lor, M.; Weil, T.; Mitra, S.; Wiesler, U.-M.; Herrmann, A.; Hofkens, J.; Vosch, T.; Müllen, K.; De Schryver, F. C. *J. Am. Chem. Soc.* **2001**, *123* (31), 7668–7676.

(257) Herrmann, A.; Weil, T.; Sinigersky, V.; Wiesler, U.-M.; Vosch, T.; Hofkens, J.; De Schryver, F. C.; Müllen, K. *Chem. Eur. J.* **2001**, *7* (22), 4844–4853.

(258) Bernhardt, S.; Kastler, M.; Enkelmann, V.; Baumgarten, M.; Müllen, K. *Chem. - A Eur. J.* **2006**, *12* (23), 6117–6128.

(259) Qu, J.; Zhang, J.; Grimsdale, A. C.; Müllen, K.; Jaiser, F.; Yang, X.; Neher, D. *Macromolecules* **2004**, *37* (22), 8297–8306.

(260) Nguyen, T.-T.-T.; Baumgarten, M.; Rouhanipour, A.; Räder, H. J.; Lieberwirth, I.; Müllen, K. *J. Am. Chem. Soc.* **2013**, *135* (11), 4183–4186.

(261) Tinnefeld, P.; Weston, K. D.; Vosch, T.; Cotlet, M.; Weil, T.; Hofkens, J.; Müllen, K.; De Schryver, F. C.; Sauer, M. *J. Am. Chem. Soc.* **2002**, *124* (48), 14310–14311.

(262) Gensch, T.; Hofkens, J.; Heirmann, A.; Tsuda, K.; Verheijen, W.; Vosch, T.; Christ, T.; Basché, T.; Müllen, K.; De Schryver, F. C. *Angew. Chem., Int. Ed.* **1999**, *38* (24), 3752–3756.

(263) Hofkens, J.; Latterini, L.; De Belder, G.; Gensch, T.; Maus, M.; Vosch, T.; Karni, Y.; Schweitzer, G.; De Schryver, F. C.; Hermann, A.; Müllen, K. *Chem. Phys. Lett.* **1999**, *304* (1), 1–9.

(264) Hofkens, J.; Maus, M.; Gensch, T.; Vosch, T.; Cotlet, M.; Köhn, F.; Herrmann, A.; Müllen, K.; De Schryver, F. *J. Am. Chem. Soc.* **2000**, *122* (38), 9278–9288.

(265) Vosch, T.; Hofkens, J.; Cotlet, M.; Köhn, F.; Fujiwara, H.; Gronheid, R.; Van Der Biest, K.; Weil, T.; Herrmann, A.; Müllen, K.; Mukamel, S.; Van der Auweraer, M.; De Schryver, F. C. *Angew. Chem., Int. Ed.* **2001**, *40* (24), 4643–4648.

(266) Vosch, T.; Cotlet, M.; Hofkens, J.; Van Der Biest, K.; Lor, M.; Weston, K.; Tinnefeld, P.; Sauer, M.; Latterini, L.; Müllen, K.; De Schryver, F. C. *J. Phys. Chem. A* **2003**, *107* (36), 6920–6931.

(267) Masuo, S.; Vosch, T.; Cotlet, M.; Tinnefeld, P.; Habuchi, S.; Bell, T. D. M.; Oesterling, I.; Beljonne, D.; Champagne, B.; Müllen, K.; Sauer, M.; Hofkens, J.; De Schryver, F. C. *J. Phys. Chem. B* **2004**, *108* (43), 16686–16696.

(268) Schroeyers, W.; Vallée, R.; Patra, D.; Hofkens, J.; Habuchi, S.; Vosch, T.; Cotlet, M.; Müllen, K.; Enderlein, J.; De Schryver, F. C. *J. Am. Chem. Soc.* **2004**, *126* (44), 14310–14311.

(269) Tinnefeld, P.; Hofkens, J.; Herten, D.-P.; Masuo, S.; Vosch, T.; Cotlet, M.; Habuchi, S.; Müllen, K.; De Schryver, F. C.; Sauer, M. *ChemPhysChem* **2004**, *5*

(11), 1786–1790.

(270) Jansson, S. In *Encyclopedia of Biological Chemistry*; Elsevier, 2004; pp 567–570.

(271) Horton, P.; Ruban, A. V.; Walters, R. G. *Annu. Rev. Plant Physiol. Plant Mol. Biol.* **1996**, *47* (1), 655–684.

(272) MacColl, R. *J. Struct. Biol.* **1998**, *124* (2–3), 311–334.

(273) Weil, T.; Reuther, E.; Beer, C.; Müllen, K. *Chem. Eur. J.* **2004**, *10* (6), 1398–1414.

(274) Weil, T.; Reuther, E.; Müllen, K. *Angew. Chem., Int. Ed.* **2002**, *41* (11), 1900–1904.

(275) Qin, T.; Wiedemair, W.; Nau, S.; Trattnig, R.; Sax, S.; Winkler, S.; Vollmer, A.; Koch, N.; Baumgarten, M.; List, E. J. W.; Müllen, K. *J. Am. Chem. Soc.* **2011**, *133* (5), 1301–1303.

(276) Zhang, G.; Baumgarten, M.; Auer, M.; Trattnig, R.; List-Kratochvil, E. J. W.; Müllen, K. *Macromol. Rapid Commun.* **2014**, *35* (22), 1931–1936.

(277) Fechtenkötter, A.; Saalwächter, K.; Harbison, M. A.; Müllen, K.; Spiess, H. W. *Angew. Chemie Int. Ed.* **1999**, *38* (20), 3039–3042.

(278) Dötz, F.; Brand, J. D.; Ito, S.; Gherghel, L.; Müllen, K. *J. Am. Chem. Soc.* **2000**, *122* (32), 7707–7717.

(279) Naomi Sakai; Jiri Mareda; Eric Vauthey; Stefan Matile; Sakai, N.; Mareda, J.; Vauthey, E.; Matile, S. *Chem. Commun.* **2010**, *46* (24), 4225–4237.

(280) Würthner, F.; Ahmed, S.; Thalacker, C.; Debaerdemaeker, T. *Chem. Eur. J.* **2002**, *8* (20), 4742–4750.

(281) Kishore, R. S. K.; Kel, O.; Banerji, N.; Emery, D.; Bollot, G.; Mareda, J.; Gomez-Casado, A.; Jonkheijm, P.; Huskens, J.; Maroni, P.; Borkovec, M.; Vauthey, E.; Sakai, N.; Matile, S. *J. Am. Chem. Soc.* **2009**, *131* (31), 11106–11116.

(282) Hatakeyama, T.; Hashimoto, S.; Seki, S.; Nakamura, M. *J. Am. Chem. Soc.* **2011**, *133* (46), 18614–18617.

(283) Lepeltier, M.; Lukoyanova, O.; Jacobson, A.; Jeeva, S.; Perepichka, D. F. *Chem. Commun.* **2010**, *46* (37), 7007.

(284) Bosdet, M. J. D.; Piers, W. E. *Can. J. Chem.* **2009**, *87* (1), 8–29.

(285) Noda, H.; Furutachi, M.; Asada, Y.; Shibasaki, M.; Kumagai, N. *Nat. Chem.* **2017**, *9* (6), 571–577.

(286) Tönshoff, C.; Müller, M.; Kar, T.; Latteyer, F.; Chassé, T.; Eichele, K.; Bettinger, H. F. *ChemPhysChem* **2012**, *13* (5), 1173–1181.

(287) Müller, M.; Petersen, J.; Strohmaier, R.; Günther, C.; Karl, N.; Müllen, K. *Angew. Chem., Int. Ed.* **1996**, *35* (8), 886–888.

(288) Stabel, A.; Herwig, P.; Müllen, K.; Rabe, J. P. *Angew. Chem., Int. Ed.* **1995**, *34* (15), 1609–1611.

(289) Chen, L.; Hernandez, Y.; Feng, X.; Müllen, K. *Angew. Chem., Int. Ed.* **2012**, *51*

(31), 7640–7654.

(290) Wolfe, J. P.; Singer, R. A.; Yang, B. H.; Buchwald, S. L. *J. Am. Chem. Soc.* **1999**, *121* (41), 9550–9561.

(291) Köhn, F.; Hofkens, J.; Wiesler, U.-M.; Cotlet, M.; van der Auweraer, M.; Müllen, K.; De Schryver, F. C. *Chem. Eur. J.* **2001**, *7* (19), 4126–4133.

(292) Morgenroth, F.; Kübel, C.; Müllen, K. *J. Mater. Chem.* **1997**, *7* (7), 1207–1211.

(293) Pauling, L. *Proc. Natl. Acad. Sci.* **1966**, *56* (6), 1646–1652.

(294) Pauling, L. *The Nature of the Chemical Bond*; Cornell University Press: New York, 1960.

(295) Proń, A.; Baumgarten, M.; Müllen, K. *Org. Lett.* **2010**, *12* (19), 4236–4239.

(296) Kurata, R.; Kaneda, K.; Ito, A. *Org. Lett.* **2017**, *19* (2), 392–395.

(297) Steeger, M.; Holzapfel, M.; Schmiedel, A.; Lambert, C. *Phys. Chem. Chem. Phys.* **2016**, *18* (19), 13403–13412.

(298) Ji, L.; Griesbeck, S.; Marder, T. B. *Chem. Sci.* **2017**, *8* (2), 846–863.

(299) Rostovtsev, V. V.; Green, L. G.; Fokin, V. V.; Sharpless, K. B. *Angew. Chem., Int. Ed.* **2002**, *41* (14), 2596–2599.

(300) Berezin, A. A.; Sciutto, A.; Demitri, N.; Bonifazi, D. *Org. Lett.* **2015**, *17* (8), 1870–1873.

(301) Sagar Reddy, G. V.; Rao, G. V.; Subramanyam, R. V. K.; Iyengar, D. S. *Synth. Commun.* **2000**, *30* (12), 2233–2237.

(302) Seybold, G.; Wagenblast G. *Dye. Pigment.* **1989**, *11* (4), 303–317.

(303) Stepanenko, V.; Stocker, M.; Müller, P.; Büchner, M.; Würthner, F. *J. Mater. Chem.* **2009**, *19* (37), 6816–6826.

(304) Melinger, J. J. S.; Pan, Y.; Kleiman, V. V. D.; Peng, Z.; Davis, B. L.; McMorrow, D.; Lu, M. *J. Am. Chem. Soc.* **2002**, *124* (40), 12002–12012.

(305) Qu, J.; Pschirer, N. G.; Liu, D.; Stefan, A.; De Schryver, F. C.; Müllen, K. *Chem. Eur. J.* **2004**, *10* (2), 528–537.

(306) Dössel, L.; Gherghel, L.; Feng, X.; Müllen, K. *Angew. Chem., Int. Ed.* **2011**, *50* (11), 2540–2543.

(307) Swamy, K. C. K.; Kumar, N. N. B.; Balaraman, E.; Kumar, K. V. P. P. *Chem. Rev.* **2009**, *109* (6), 2551–2651.

(308) Mitsunobu, O. *Synthesis* **1981**, *1981* (1), 1–28.

(309) Appel, R. *Angew. Chem., Int. Ed.* **1975**, *14* (12), 801–811.

(310) Panisch, R.; Bolte, M.; Müller, T. *J. Am. Chem. Soc.* **2006**, *128* (30), 9676–9682.

(311) Moussa, Z. *ARKIVOC* **2012**, 432–490.

(312) Hendrickson, J. B.; Hussoin, M. S. *J. Org. Chem.* **1987**, *52* (18), 4137–4139.

(313) Hendrickson, J. B.; Hussoin, M. S. *J. Org. Chem.* **1989**, *54* (5), 1144–1149.

(314) Hendrickson, J. B.; Hussoin, M. S. *Synthesis* **1989**, *3*, 217–218.

(315)   Hendrickson, J. B.; Hussoin, M. S. *Synlett* **1990**, *7*, 423–424.

(316)   Evans, P. R.; Murshudov, G. N. *Acta Crystallogr. Sect. D Biol. Crystallogr.* **2013**, *69* (7), 1204–1214.

(317)   Winn, M. D.; Ballard, C. C.; Cowtan, K. D.; Dodson, E. J.; Emsley, P.; Evans, P. R.; Keegan, R. M.; Krissinel, E. B.; Leslie, A. G. W.; McCoy, A.; McNicholas, S. J.; Murshudov, G. N.; Pannu, N. S.; Potterton, E. A.; Powell, H. R.; Read, R. J.; Vagin, A.; Wilson, K. S.; IUCr. *Acta Crystallogr. Sect. D Biol. Crystallogr.* **2011**, *67* (4), 235–242.

(318)   Kabsch, W. *Acta Crystallogr. Sect. D Biol. Crystallogr.* **2010**, *66* (2), 125–132.

(319)   Burla, M. C.; Caliandro, R.; Carrozzini, B.; Cascarano, G. L.; Cuocci, C.; Giacovazzo, C.; Mallamo, M.; Mazzone, A.; Polidori, G. *J. Appl. Cryst.* **2015**, *48* (1), 306–309.

(320)   Sheldrick, G. M. *Acta Cryst. A* **2008**, *64* (1), 112–122.

(321)   Emsley, P.; Cowtan, K. *Acta Crystallogr. Sect. D Biol. Crystallogr.* **2004**, *60* (12), 2126–2132.

(322)   Farrugia, L. J. *J. Appl. Crystallogr.* **2012**, *45* (4), 849–854.

(323)   Schrodinger, L. *PYMOL Mol. Graph. Syst. Ver. 1.3 r1, http//www.pymol.org* **2015**.